The Origin of High–SiO_2 Rhyolites at Long Valley and Benton Range, CA: Temperatures, Timescales, and Tectonic Implications

by

Bryanne Michelle Gordon

A dissertation submitted in partial fulfillment
of the requirements for the degree of
Doctor of Philosophy
(Earth and Environmental Sciences)
in the University of Michigan
2026

Doctoral Committee:

Professor Rebecca A. Lange, Chair
Assistant Professor Robert M. Holder
Professor Jie Li
Associate Professor Keren Sharon
Professor Adam C. Simon

Bryanne Michelle Gordon

bmgordon@umich.edu

ORCID iD: 0009–0008–8172–3628

© Bryanne Michelle Gordon 2026

Dedication

I dedicate this dissertation to my younger self whose incessant questions, curiosity, and obsession with knowledge and science has led me down a path I could have never dreamed of for myself. That child would be in awe of the people I have met, the places I have been, and the things I have accomplished.

Acknowledgements

There are many people who have made this work possible. Firstly, I thank my advisor, Becky Lange, for her continued patience, persistence, excitement, and support. I have learned more than seems possible about high-SiO_2 rhyolites and a whole myriad of topics beyond; not all in the great field of geology. Your guidance in the field, at conferences, in the classroom, and beyond has been invaluable and I treasure the time I have spent in your tutelage. You pushed me to academically succeed beyond what I thought was possible and I am forever grateful.

I thank my committee members, Robert Holder, Jackie Li, Keren Sharon, and Adam Simon, for excellent feedback, advice, and patience. Your feedback and perspectives over the years have been essential in shaping my dissertation. Robert, your extensive advice and the use of your MI-Chron lab have been foundational for the formulation of Chapter 4 of this dissertation. Jackie, from the time I was an undergraduate student, your expertise and classes have been foundational for my graduate career. Keren, your perspective from outside the Earth and Environmental Science Department was essential for me to learn the art of presenting my research in a digestible way. Adam, I appreciate the time that you have spent on every committee of mine over the years, including my M.S. thesis, qualifying exam, and now my dissertation committee. Your insight, questions, and knowledge have been crucial.

I would like to thank all the collaborators and laboratory experts who have been a part of my graduate work such as Owen Neill, Laura Waters, and Jameson Jolles. Owen, thank you for your never-ending advice, knowledge, and help with the microprobe and SEM over the years. I have spent more hours in EMAL since 2019 then I can count and have asked you more questions about analyses, polishing, and everything in between than I could ever remember. Laura, thank you for teaching me incredible experimental skills and sharing your lab and knowledge with me. My understanding and abilities as a scientist have been greatly expanded from the work and time spent with you. Jameson, I cannot thank you enough for all your training, advice, help, and encouragement. I have pursued this graduate experience following closely in your footsteps and have found help from you at every turn. You showed me the first step in almost every lab

endeavor I began starting all the way back in 2018 and you have continued to offer advice and help 8 years later.

This time at the University of Michigan has been made especially meaningful and successful due to the support, advice, and shared experiences of my lab mates: Jameson Jolles, Sarah Brehm, Juliana Mesa, Meredith Calogero, Mack Taylor, Madeline Frank, Amanada Florea, Benjamin Colding, and Christine Meiselback. I would especially like to thank Mack Taylor for being the best graduate school twin I could ask for. Joining in the same pandemic cohort, taking classes together, passing qualifying exams in the same semester, GSI-ing together, attending conferences, and sampling on so many field trips have all created so many wonderful memories with you. Beyond this, I am grateful for all your thoughtful advice, academic rigor, and kindness throughout the years.

Other fellow students and faculty of the EARTH community who have had a great impact on me include Elena Lee, Hannah Schroeder, Cecilia Howard, Sydney Gable, Jamie Gleason, Naomi Levin, Jeroen Ritsema, and every student that I have had the honor of teaching over the years.

Lastly, I would like to thank all the friends and family who supported me and listened to me talk repeatedly about high-SiO_2 rhyolite during my time at the University of Michigan. I would especially like to thank my dearest siblings, Kimberly and Rei, who have been my greatest support and encouragement throughout this journey. You both have seen more than your fair share of volcanoes, practice talks, and geology. Kimberly, thank you for spending so much of your time to join me in my wild adventures, traveling with me to nearly every field site and U.S. supervolcano that I have been to. Rei, thank you for your constant dedication to my science education from my earliest memories to now. You are, in no small way, the person who has made me most able to pursue this degree and I cannot thank you enough for your unwavering support through this all. You are very precious to me.

Thank you all.

Table of Contents

Dedication ii

Acknowledgements iii

List of Tables x

List of Figures xii

List of Appendices xviii

Abstract xix

Chapter 1 Introduction 1

1.1 References 10

Chapter 2 A New Biotite–liquid Thermometer Applicable to High–SiO_2 Rhyolites 13

2.1 Abstract: 13

2.2 Introduction 14

2.3 Experimental Methods 18

2.3.1 Synthesis of starting glass materials 18

2.3.2 Experimental design: T–P conditions and technique to grow large biotite crystals 19

2.4 Electron microprobe analytical methods 22

2.4.1 Analysis of Biotite 23

2.4.2 Analysis of Glass 23

2.5 Experimental Results 24

2.6 Analytical Results 25

2.6.1 Biotite compositions in Glass Mountain and Benton Range samples 25

2.6.2 Biotite compositions in experimental run products 29

2.6.3 Experimental glass compositions 31

2.7 Calibration of a new biotite–liquid thermometer 32

2.7.1 Construction of D_{TiO2} (bte-liq) values from Glass Mountain natural samples 32

2.7.2 Plot of D_{TiO2} (bte-liq) vs Fe–Ti oxide temperature for Glass Mountain samples 34

2.7.3 Construction of D_{TiO2} (bte-liq) values from experimental run products 36

2.7.4 Plot of D_{TiO2} (bte-liq) vs experimental pressure under isothermal conditions 36

2.7.5 Plot of D_{TiO2} (bte-liq) vs experimental temperature 38

2.7.6 Calibration of a new thermometer based on natural and experimental HSR samples 39

2.8 Test of new thermometer applied to Jurassic HSR dikes 41

2.9 Conclusions 42

2.10 References 44

Chapter 3 Phenocryst Compositions, Textures, and Abundances in Glass Mountain, CA High–SiO_2 Rhyolites and Experimental Constraints: Evidence for Rapid Crystal Growth During Ascent 49

Abstract: 49

3.1 Introduction 50

3.1.1 Tectonic setting and previous work 55

3.1.2 Sample locations and petrography 58

3.2 Experimental methods 59

3.2.1 Synthesis of starting glass materials 59

3.2.2 Experimental set–up 60

3.2.3 Experimental design: Two temperature–path trajectories 61

3.3 Imaging methods 63

3.4 Analytical methods 63

3.5 Imaging results 64

3.5.1 Experimental run products 64
3.5.2 Constraints on crystal growth rates 68
3.5.3 Granophyric intergrowths in natural samples 69
3.5.4 Quartz phenocrysts in natural samples 70
3.5.5 Sanidine phenocrysts in natural samples 71
3.5.6 Plagioclase phenocrysts in natural samples 74
3.5.7 Biotite phenocrysts in natural samples 74
3.6 Analytical results 76
3.6.1 Plagioclase 76
3.6.2 Sanidine 76
3.6.3 Biotite 79
3.7 Thermometry 81
3.7.1 Fe–Ti two–oxide thermometry 81
3.7.2 Biotite–Liquid Thermometry 81
3.8 Hygrometry 84
3.8.1 Sanidine–liquid hygrometry calibrated on high–SiO_2 rhyolite 84
3.9 Discussion 86
3.9.1 Do Glass Mountain phenocryst abundances reflect equilibrium T–P_{H2O} conditions? 87
3.9.2 A comparison of four GM units (YO, YG, OB, OL) at ~700°C 87
3.9.3 A comparison of units OD and OC 88
3.9.4 Do Glass Mountain phenocryst abundances reflect a lower water–saturated granitic solidus? 89
3.9.5 Do Glass Mountain phenocryst abundances reflect kinetic effects during rapid phenocryst growth during dike ascent? 90
3.9.6 Evidence of direct dike ascent between melt segregation and eruption: unit OC and OL 93

3.10 Conclusions 95

3.11 References: 98

Chapter 4 New Age Constraints on the High–SiO_2 Rhyolite Dike Swarm of the Benton Range, CA: Clues to the Tectonic Relationship between Coast Range Ophiolite Formation and Extension in the Jurassic Sierran Arc 103

4.1 Abstract: 103

4.2 Introduction 104

4.3 Benton Range dike swarm 109

4.3.1 Geological Setting 109

4.3.2 Sample Locations and Descriptions 109

4.4 Geochronology methods 110

4.5 Zircon geochronology results: 112

4.5.1 Zircon imaging and characterization 112

4.5.2 U concentrations and Th/U ratios in zircon 114

4.5.3 Zircon crystallization ages 114

4.5.4 Analysis of large age uncertainties 118

4.6 Discussion 118

4.6.1 Comparison of Benton Range dike zircon crystallization ages to previous constraints 118

4.6.2 Evidence of extension versus compression in the main Sierra arc between ~160–170 Ma 120

4.6.3 Evidence of crustal thickness in the Jurassic Sierran arc 122

4.6.4 Relationship between formation of the CRO and extension in the Sierra Nevada? 123

4.7 Conclusion 124

4.8 References 126

Chapter 5 Conclusions 132

5.1 Concluding remarks 132

5.2 Future Work 133

5.2.1 Deployment of biotite–liquid thermometer 133

5.2.2 Expanded calibrations of D_{TiO2}(bte-liq) thermometer to low–SiO_2 rhyolites 134

5.2.3 Establish an expanded phase diagram for high–SiO_2 rhyolite 135

5.2.4 Experimental investigation of timescales for phenocryst growth in high–SiO_2 rhyolites during dike ascent (i.e., at various undercoolings) 137

5.3 References 139

Appendices 141

List of Tables

Table 2-1:Experimental samples, run conditions, and run products. 20

Table 2-2: Averaged analyses for natural biotite grains (wt%) 28

Table 2-3: Averaged analyses experimental biotite grains (wt%) 30

Table 2-4: Averaged analyses experimental glass (wt%) 32

Table 2-5 Calculated values of D_{TiO2} (bte-liq) for natural and experimental samples 34

Table 2-6: Calculated values of D_{TiO2} (bte-liq) and temperature for natural samples 41

Table 3-1 Whole–rock major and minor element concentrations (wt%) Glass Mountain samples 59

Table 3-2: Experimental samples, run conditions, and run products 62

Table 3-3: Average composition (wt%) of plagioclase and sanidine in experimental and Older and Younger Glass Mountain samples 77

Table 3-4: Averaged analyses natural biotite grains (wt%) 80

Table 3-5: Calculated temperatures for GM units 83

Table 4-1:Whole–rock major–element (wt%) composition of the Benton Range dike swarm .. 111

Table 4-2 :Zircon crystallization ages for 6 HSR dikes from the Benton Range, CA 115

Table A-0-1 Electron microprobe standards and conditions of analysis 141

Table A-0-2 Natural individual biotite analyses (wt%) 142

Table A-0-3 Whole-rock major and minor element concentrations (wt%) for previously published samples from Glass Mountain (Gordon et al., 2026), Bishop Tuff (Jolles and Lange, 2019), and the Benton Range (Mesa, 2021) 171

Table A-0-4 Experimental individual biotite analyses (wt%) 172

Table A-0-5 Experimental individual glass analyses (wt%) 201

Table A-0-6 Natural individual biotite analyses (wt%) for previously published samples from the Bishop Tuff (Jolles and Lange, 2019)..... 225

Table A-0-7 Average compositions (wt%) of titanomagnetite and ilmenite for previously published samples from Glass Mountain (Gordon, 2022)..... 239

Table A-0-8 Calculated values of D_{TiO2} (bte-liq) for previously published samples (Jolles and Lange, 2019; Bolte et al., 2015)..... 240

Table B-0-9 Electron microprobe standards and conditions of analysis 244

Table B-0-10 Natural individual plagioclase analyses (wt%) 245

Table B-0-11 Natural individual sanidine analyses (wt%)..... 263

Table B-0-12 Natural individual biotite analysese (wt%) 290

Table B-0-13 Experimental individual plagioclase analyses (wt%)..... 306

Table B-0-14 Experimental individual sanidine analyses (wt%) 307

Table C-0-15 Analytical settings for Laser ablation and ICP-MS..... 313

Table C-0-16 Individual zircon spot analyses for samples analyzed by LaserChron..... 314

Table C-0-17 Individual zircon spot analyses for samples analyzed by MI-Chron 319

List of Figures

Figure 1-1: Google Earth map of western United States, depicting locations of recent (< 800 ka), voluminous eruptions of high–SiO_2 rhyolite (Long Valley, CA and Yellowstone, WY). For reference, other features are shown, including the Cascade arc and Sierra Nevada Batholith, along with the Basin and Range extensional province. 2

Figure 1-2: Study area location map of Long Valley Caldera and the Benton Range, CA modified from Chamberlin et al. (2015). The Benton Range is shown in a grey box just southeast of the Long Valley Caldera (topographic rim shown by dashed line). Glass Mountain is shown in light gray, and the Bishop Tuff (BT) is shown in dark gray..... 3

Figure 2-1: Plot of experimental or Fe–Ti two–oxide temperature (°C) vs D_{TiO2} (bte-liq). The data for the Early– and Late–type Bishop Tuff high–SiO_2 rhyolites are from Jolles and Lange (2019). A linear fit to these natural data is shown ($R^2 = 0.95$) and the only available experiments on biotite–bearing high–SiO_2 rhyolite (Bolte et al., 2015) match the trend line. In contrast, the experimental results from Wark et al. (2021) on a melt composition with a lower SiO_2 content (68 wt%) has a different trend. Error bars represent propagated 1 SD. 17

Figure 2-2 **:** A simplified phase–equilibrium diagram for a representative high–SiO_2 rhyolite under water–saturated conditions modified from Waters and Andrews (2016), which indicates the stability field of biotite relative to the tectosilicates. mineral in–curves. Pressure (MPa) = P_{H2O} is shown on the y–axis and temperature (°C) is shown on the x–axis. Dashed lines show concentrations of dissolved H_2O in the melt (Zhang et al., 2007). Superimposed on this diagram are the numbered experimental runs (inside boxes) from this study, illustrating the final temperature and P_{H2O} run conditions (Table 2–1). 19

Figure 2-3: Representative BSE images of experimental biotite phenocrysts from resulting experimental runs of both the MC–24 and BT–3B starting material (e.g., MC:2 refers to the MC–24 starting material and run #2). Biotite crystals frequently exceed 100 (and can reach >300) µm in length. Scale bars are shown in red..... 25

Figure 2-4 :Representative BSE images of biotite phenocrysts in natural high–SiO_2 rhyolite samples from the Benton Range dike swarm (a–b) and the Glass Mountain volcanic complex (c–d). 27

Figure 2-5: Plot of Fe–Ti oxide temperature (°C) vs D_{TiO2} (bte-liq) for natural samples from the Bishop Tuff and new data for the Glass Mountain high–SiO_2 rhyolites. The linear fit solely to the Bishop Tuff samples (R^2=0.95) is extrapolated (dashed line) to lower temperatures, and the new Glass Mountain results fall along the same trend. Error bars represent propagated 1SD..... 35

Figure 2-6: Plot of D_{TiO2} (bte-liq) vs. experimental P_{H2O} (MPa) for a set of isothermal 750 °C experiments conducted in this study on two different starting glass materials (MC–24 and BT–3B) of high–SiO_2 rhyolite composition. The average D_{TiO2} (bte-liq) (36.7 ± 6.6) at 750°C is shown as a black line. The results from all experiments fall within error of the average and show no systematic variation with experimental pressure. Error bars represent propagated 1SD. 37

Figure 2-7**:** Plot of temperature (°C) vs D_{TiO2} (bte-liq) for all natural high–SiO_2 rhyolite samples and experiments on high–SiO_2 rhyolite composition. A linear fit through all the data is shown (R^2 = 0.90). The experimental results confirm the trend observed in the natural data, which is based on Fe–Ti two–oxide thermometry. Note that large error bars of experimental data points at lower temperature is due to the relative error of low TiO_2 in the glass (see text for more). The linear fit can be used as a biotite–liquid thermometer for high–SiO_2 rhyolite melts: $T(°C) = 846\ (\pm 7) - 2.32\ (\pm 0.15) * DTiO2bte - liq$. Error bars represent propagated 1SD. 40

Figure 3-1**:** Location map of the Glass Mountain volcanic complex and Long Valley Caldera, California modified from Chamberlin et al. (2015). The current topographic expression of the caldera rim is shown by the outer dashed line, whereas the estimated ring fracture is shown by dotted line. Glass Mountain is shown in light gray, and the Bishop Tuff (BT) is shown in dark gray. 51

Figure 3-2**:** Simplified geologic map of the Glass Mountain (GM) eruptive units modified from Metz and Bailey (1993). Older GM units are shown in pink and Younger GM units are shown in green..... 56

Figure 3-3: A schematic diagram illustrating rate of crystal growth (dashed line) and nucleation (solid line) vs. effective undercooling ($\Delta T = T_{liquidus} - T_{melt}$) for supercooled liquids (modified from Pu et al., 2021). Arrows at the top of diagram represent the two experimental temperature–path trajectories in this study. Starting from the right side of the diagram, the 100% glass starting material in the bottom–up experiments were heated to temperatures above the glass transition and transited a region of undercooling characterized by high nucleation rates. When this experimental run reached its final equilibration temperature, it is expected to have numerous small nuclei and no kinetic delay to nucleation. Starting from the left side of the diagram, the 100% glass starting material in the top–down experiments were first taken to a superliquidus temperature for 2 h and then abruptly dropped to the final equilibration temperature, leading to a kinetic delay in nucleation and enabling crystallization to occur under conditions of relatively low nucleation rates and high crystal growth rates. 63

Figure 3-4**:** Representative BSE images of the bottom–up experimental charge from run 8–1 showing (a) zoomed–out image of the vesicular, crystallized run product in the capsule, and (b) zoomed–in image of the microcrystalline run product. Scale bars are shown in red. (a) Visible ilmenite and titanomagnetite "nucleation seeds" can be seen on the left edge of the charge. (b) No glass was found in the microcrystalline run product. Crystal phases are labeled: san (sanidine), plag (plagioclase) and qtz (quartz) and typically ≤ 10 μm in size. The results indicate complete crystallization at 650 °C and P_{H2O} = 200 MPa. 65

Figure 3-5**:** Representative BSE images of the top–down experimental charge from run 9–2 showing (a) zoomed–out image of the run product with crystals on the edges of the capsule and an interior pool of glass, and (b) zoomed–in image of (a). Scale bars are shown in red. (a) Clear evidence of abundant glass (~40%) is seen in the interior of the capsule, and it appears that quartz preferentially nucleated on the capsule walls, and that sanidine nucleated on quartz. Around the sanidine crystals can sometimes be seen a halo of glass depleted in K_2O. (b) Close up of quartz and sanidine crystals, the latter with hopper and swallow–tail textures. Crystals in (b) are ≤ 100 μm and are labelled as in Fig. 3–4. It is estimated that crystal growth occurred at an undercooling of ~50 °C (see text for details) for a duration ≤ 548 h. 66

Figure 3-6: More representative BSE images of the top–down experimental charges from (a) run 9–2 and (b) run 9–1. Labels of crystal phases are as in Fig. 3–4, and scale bars are shown in red. (a) Clear intergrowth of sanidine and quartz is seen, similar to granophyric textures seen in the natural GM samples. Sanidine crystals display rapid growth textures (i.e., skeletal and hopper) and reach ~300 μm in length. Quartz crystals reach ~200 μm in length. Plagioclase is seen growing in the interior hollows of hopper–textured sanidine. (b) Quartz crystals exceed 200 μm and display hopper textures (two grains to the right of image). It is estimated that crystal growth occurred at an undercooling of ~50 °C (see text for details) for a duration ≤ 548 h..... 67

Figure 3-7**:** BSE images from the top–down experimental charge from run 3 showing: (a) a euhedral, faceted sanidine crystal of ~ 80 μm length and (b) a partially faceted quartz crystal of ~60 μm in length. Lettering for crystal phases and scale bars are shown in red. It is estimated that crystal growth occurred at an undercooling of ~5 °C (see text for details) for a duration < 182 h..... 68

Figure 3-8**:** Representative granophyre images from four GM units that feature intergrowths of quartz and sanidine. Lettering for crystal phases and scale bars are shown in red. (a–b) Photomicrographs of granophyres (≤ 3 mm in length) from GM unit OD, where individual crystals of quartz and sanidine approach 500 μm and display rapid–growth hopper textures. (c–d) BSE images of finer–grained granophyric intergrowths of quartz and sanidine in GM units (c) YA/YB and (d) YO. Similar granophyres are seen in units OB, OC, YE, and YG, as well, in addition to the nine–day decompression experiments of Waters and Andrews (2016) on a GM high–SiO_2 rhyolite. 70

Figure 3-9**:** Representative monochromatic cathodoluminescence (CL) images of euhedral quartz crystals (< 1 mm) in several GM units, displaying subtle Ti zonation patterns. Scale bars are shown in red. 71

Figure 3-10: Representative CL and photomicrograph images of large (>1mm) quartz crystals in several GM units, featuring hopper textures that include protuberances, growth embayments, melt inclusions and hollow faces. These textures are consistent with diffusion–limited rapid growth (e.g. Barbee et al., 2020). Quartz phenocrysts with these textures are seen throughout the GM units. Scale bars are shown in red..... 72

Figure 3-11: Representative BSE images of plagioclase and sanidine (≤ 1 mm) in several GM units. Lettering for crystal phases and scale bars are shown in red. (a) euhedral plagioclase

crystal in unit OC with faceted edges; (b) Euhedral sanidine (light colored) with alteration rims, with euhedral crystals of plagioclase that appear to have nucleated against sanidine; unit OC. (c) euhedral sanidine with alteration rims in unit OL; (d) growth of euhedral plagioclase around altered sanidine in unit OL; (e) another example of plagioclase nucleated against altered sanidine; unit YE; (f) extensively altered in unit YG; (g) euhedral crystals of plagioclase in unit YO, with small melt inclusions; (h) euhedral, but altered sanidine with two plagioclase crystals that nucleated on its two sides in unit YO. Note that all sanidine crystals displayed show darker zones around edge cracks and interior cracks of crystals, which is alteration of the sanidine to albite (i.e., albitization), and is variably seen mostly along rims in some units (e.g., OC and OL) or throughout entire crystals (e.g., YE and YG). Plagioclase is pristine and unaltered in all units. 73

Figure 3-12:(a–f) Representative BSE images of biotite phenocrysts (≤ 800 μm) in several GM units, illustrating examples of rapid–growth textures (e.g., hopper and swallow tail) leading to partially enclosed melt embayments and inclusions. Scale bars are shown in red. 75

Figure 3-13: A comparison of all thermometry results for Older (pink circles) and Younger (green squares) GM units. The top and middle rows show temperatures calculated with the Ghiorso and Evans (2008) Fe–Ti two–oxide thermometer, using titanomagnetite and ilmenite analyses from Gordon (2022) and Metz and Mahood (1991), respectively. Collectively, the results show that the Older GM units span a wide range of temperature (660–724 °C), whereas the Younger GM units span the upper half of this interval (695–725°C). The third row shows results from the biotite–liquid thermometer from Chapter 2 based on biotite analyses reported in Table 3–4. The two thermometers provide broadly consistent results, indicating a range of temperatures between ~660 and ~725 °C for the GM units. Error is 1SD. 82

Figure 3-14: A 1:1 plot comparing Fe–Ti two–oxide temperatures, using the Ghiorso and Evans (2008) thermometer, with Chapter 2 biotite–liquid temperatures on samples where both were obtained. Older GM units are shown as pink circles while Younger GM units are shown as green squares. There is good agreement within error between the two thermometers. Note that the Fe–Ti oxide temperature for unit YG is based on oxide analyses reported in Metz and Mahood (1991). Error bars represent propagated 1SD. 84

Figure 3-15:A simplified water–saturated phase equilibrium diagram for a representative GM unit (YE) modified from Waters and Andrews (2016) based on their experimental results. Pressure (MPa) is shown on the y–axis and temperature (°C) is shown on the x–axis. Dashed lines show isopleths of dissolved H_2O contents in the melt (Zhang et al., 2007) and solid lines show approximate mineral in–curves for tectosilicate phases. Select experiment runs by Waters and Andrews (2016) are shown as a black circle and the bottom–up experiment run in this study is shown as an open circle. The mol% Or in sanidine is above the circle, and the total % crystals is below the circle for the run products reported in Waters and Andrews (2016). Two red bands are superimposed on the diagram showing the approximate temperature of several GM units (denoted at the top of each band). See text for details. 86

Figure 3-16: A schematic illustration of the ascent path for GM units YO (green squares) and OL (pink circles), which both have pre–eruptive temperatures of ~700 °C, superimposed on the simplified experimental phase diagram of Waters and Andrews (2016). A grey band and arrow

show the ascent path of these high–SiO_2 rhyolites in a dike. The highest sanidine composition (Or_{66}) in unit YO records the onset of sanidine growth at an undercooling of ~25 °C, indicative of a kinetic delay to nucleation. Plagioclase is present in unit YO and thus it continued to grow phenocrysts during ascent to conditions below plagioclase in–curve. Similarly, the highest sanidine composition (Or_{60}) in unit OL indicates the onset of sanidine growth in that sample at an undercooling of ~40 °C, perhaps indicating a longer kinetic delay to nucleation and/or a faster ascent rate than in unit YO. 91

Figure 3-17: A schematic diagram of magma ascent through the crust demonstrating how phenocryst growth during an undercooling develops, following a kinetic delay to crystal nucleation. The x–axis (top) tracks temperature increasing from left to right, while the y–axis (left) tracks pressure (increasing downward with depth). The black solid line shows the temperature change of the liquidus of the melt while the red solid line shows the actual temperature of the melt. If the magma segregates fluid undersaturated, then rapid ascent in a dike will cause the liquidus temperature to decrease due to decompression. This will lead to an interval during ascent when the melt is superliquidus, eliminating the presence of any nuclei. However, after continued ascent, fluid saturation will eventually occur, causing water to be exsolved from the melt, which will lead to an increase in the liquidus temperature during continued magma ascent. Eventually, the temperature of the melt will cross the liquidus, but because there are no nuclei present, a kinetic delay to nucleation is likely, leading to the development of an undercooling (where the temperature of the melt is lower than the liquidus temperature). From Figure 3–3, it is seen that moderate undercoolings lead to relatively high crystal growth rates at low nucleation rates, enabling the growth of large, sparse phenocrysts, which is observed in the GM high–SiO_2 rhyolites. 94

Figure 4-1: Simplified geologic map of California modified from Irwin (1990) with the location of the Benton Range shown in a black box. A simplified location of outcrops of the Coast Range Ophiolite (purple) are superimposed from the geologic map from Cisneros et al. (2022). Mapped are Precambrian (grey), Mesozoic granitoid (red), Franciscan assemblage (blue), Great Valley sequence (green), and Cenozoic fill of Great Valley. 105

Figure 4-2**:** A compilation of plutonic (dark green) and volcanic (light green) zircon ages from Paterson and Ducea (2015) from the Sierra Nevada. The results show three magmatic flare ups (Triassic, Jurassic, and Cretaceous) with intervening lulls. Also shown are the age intervals for the emplacement of the Benton Range dike swarm (K–Ar dates; Renne and Turrin, 1987), the formation of the CRO (Shervais et al., 2005), and dated Jurassic dike swarms (Independence, Owens Mountain, Sonora and King Creek; Chen and Moore, 1979; Wolf and Saleeby, 1992; Wesley et al., 2019). 106

Figure 4-3: Study area location map of Long Valley Caldera and the Benton Range, CA modified from Chamberlin et al. (2015). The Benton Range is shown in a red box just southeast of the Long Valley Caldera (topographic rim shown by dashed line). Glass Mountain is shown in light gray, and the Bishop Tuff (BT) is shown in dark gray. 108

Figure 4-4**:** Google Earth image showing the location of individual dikes (red) in the Benton Range along Banner Ridge as mapped by Rinehart and Ross (1957); modified from Mesa (2021). (A) Images showing all the dikes, with a yellow inset box. (B) Inset box from (A)

showing sample locations from Mesa (2021) in yellow circles. Samples targeted for U–Pb dating in this study are shown in blue boxes. 110

Figure 4-5 Representative cathodoluminescence images of zircon grains from sample CD–18–06, which were analyzed in this study by the LaserChron facility at the University of Arizona. (a–c) Zircon grains show oscillatory– and sector–zoning typical of original igneous growth textures. (d) Zircon crystal shows a bright rim indicative of low Th and U. (e–f) Zircon shows possible spongy textures, which may have formed during hydrothermal alteration. 113

Figure 4-6**:** Representative cathodoluminescence images of zircon grains from sample CD–18–13, which were analyzed in this study by the LaserChron facility at the University of Arizona. (a–d) Zircon grains show oscillatory– and sector–zoning typical of original igneous growth textures. 113

Figure 4-7**:** Histograms of individual zircon ages in each of six dikes targeted in this study. The weighted mean age is reported for each sample, together with the weighted 2–standard deviation as error bars. Ages range from 162 (± 9) to 169 (± 11) Ma. 116

Figure 4-8**:** A single histogram for individual zircon ages from all six dikes in this study. The combined weighted mean age (± 2–standard deviation; error bars) is 165 (± 11) Ma. 117

Figure A-0-1An SE image of allanite from a previously published sample from the Benton Range (Mesa, 2021) 241

Figure A-0-2 Plot of average $\log(Mg/Mn)^{titanomagnetite}$ versus $\log(Mg/Mn)^{ilmenite}$ obtained from Fe-Ti oxide analyses. Data from this study are shown in pink circles (Older GM) and green squares (Younger GM). Also shown are data from Metz and Mahood (1991) as open circles (Older GM) and open squares (Younger GM). The solid line is the Bacon and Hirschmann (1988) equilibrium relationship, and the dashed lines show the ±2 SD error envelope. 243

Figure C-0-3 Scatter diagrams of 206Pb/238U age (Ma) vs U (ppm) concentration for samples analyzed by LaserChron 320

Figure C-0-4 Scatter diagrams of 206Pb/238U age (Ma) vs. Th/U for samples analyzed by LaserChron 321

Figure C-0-5 Concordia diagrams for all samples plotted with IsoplotR 322

List of Appendices

Appendix A: Supplemental Material for Chapter 2 141

Text A.1 Fe-Ti Two-Oxide thermometry and oxybarometry from Gordon (2022) 242

Appendix B: Supplemental Material for Chapter 3 244

Appendix C: Supplemental Material for Chapter 4 313

Abstract

High–SiO_2 (>75 wt%) rhyolites are the most differentiated silicate magmas on Earth and are sparse in the rock record, especially at subduction zones. This may be due to their narrow liquidus–solidus interval(<50°C), which promotes extensive crystallization over small drops in temperature, preventing eruption. However, high–SiO_2 rhyolites do erupt, sometimes in supervolcano quantities (≤1000 km^3), in regions of continental extension (e.g., Yellowstone, WY and Long Valley, CA). Therefore, understanding the magmatic conditions (i.e., temperature/pressure) and processes that enable successful eruption of high–SiO_2 rhyolite are critical. A great challenge in studying high–SiO_2 rhyolites is the paucity of mineral–melt thermometers, barometers, and hygrometers that can be accurately applied to them. This leads to conflicting results when thermometers and hygrometers calibrated on different magma compositions are applied to high–SiO_2 rhyolites. Also, it is often not possible to use one of the only reliable thermometers, which is based on the equilibrium between two Fe–Ti oxides, because of post–eruptive alteration. In Chapter 2, a new biotite–liquid thermometer is presented. Biotite–liquid equilibrium experiments were conducted on high–SiO_2 rhyolite at 675–800 °C and P_{H2O} = 225–125 MPa. These experimental data were combined with biotite analyses of natural high–SiO_2 rhyolites, for which high–quality Fe–Ti two–oxide temperatures are available (660–800 °C), to calibrate the new $D_{TiO2}^{bte-liq}$ thermometer. It was successfully deployed on Jurassic high–SiO_2 rhyolite dikes, which contained biotite, demonstrating its utility on samples for which Fe–Ti two–oxide thermometry is not applicable. In Chapter 3, the $D_{TiO2}^{bte-liq}$ and Fe–Ti two–oxide

thermometers were applied to a suite of high–SiO_2 rhyolite (from Glass Mountain, CA,), which preceded a climactic, supervolcano eruption. A puzzling feature of these rhyolites is their highly variable phenocryst abundances (<1 to 20%), despite little change in their major–element compositions. One sample contains ~8% phenocrysts at a remarkably low temperature (660 ± 10 °C), which is below the water–saturated solidus at upper crustal conditions (≤300 MPa). Three hypotheses were tested to explain the variable phenocryst abundances: (1) they reflect equilibrium temperature, pressure, and melt H_2O contents during crystal growth in magmatic reservoir(s), (2) the H_2O–saturated granitic solidus is lower than previously documented, or (3) rapid phenocryst growth, following a kinetic delay to nucleation, occurred during magma ascent. Experiments, phenocryst compositions and textures presented in this chapter supply evidence that phenocrysts in the Glass Mountain high–SiO_2 rhyolites grew during dike transport to the surface. In Chapter 4, U–Pb zircon crystallization ages (162–169 Ma) were obtained on a high–SiO_2 rhyolite dike swarm in the Sierra Nevada, CA, which dates an episode of extension within the long–lived Mesozoic arc. These results are unexpected for two reasons: (1) this age range overlaps a magmatic flare–up Sierra Nevada arc (145–175 Ma), and (2) they differ from the previously established K–Ar age range for dike emplacement (168–209 Ma), which overlaps a lull in Sierran arc magmatism. However, the zircon ages for the dike swarm directly overlap the age (160–170 Ma) of the Coast Range Ophiolites, which formed in the forearc region due to trench–parallel spreading which may have induced shearing and extension in the main Sierran arc.

Chapter 1 Introduction

Over the last 1 million years, there have been two cataclysmic caldera–forming volcanic eruptions (100–1000's km^3 of erupted material) in the western U.S. (e.g., Long Valley, CA, Yellowstone, WY; Fig 1). The main composition of magma erupted in both cases is high–SiO_2 rhyolite (>75 wt% SiO_2) (Hildreth and Wilson, 2007, Christiansen, 2001). High–SiO_2 rhyolites (HSR) are the most differentiated magma on Earth and are the segregated interstitial liquid in granitic crystalline mushes (e.g., Bachmann and Bergantz 2004).

However, high–SiO_2 rhyolite is surprisingly sparse in the rock record. The parental source of high–SiO_2 rhyolite is the interstitial melt of a granitoid body; however, it rarely erupts at subduction zone settings (e.g., Hildreth, 2007) which are the birthplaces of continental crust through intermediate magma formation and emplacement of granitoid batholiths (e.g., De Silva and Grosnold, 2007). At subduction zones high–SiO_2 rhyolite is mostly found as thin (≤ 20 cm), scattered aplite dikes in granitoid batholiths (e.g., Glazner et al. 2008). These aplite dikes represent the late–stage, interstitial melts in granitoid bodies.

The failure of high–SiO_2 rhyolite eruption at subduction zones is unsurprising due to their extreme composition. High–SiO_2 rhyolite is a near eutectic melt in the quartz–plagioclase–orthoclase–H_2O system (Tuttle and Bowen, 1958; Johannes and Holtz, 1996). As such, it has a narrow liquidus–solidus interval (≤50 °C; e.g., Waters and Andrews, 2016) and a high viscosity (e.g., Zhang et al, 2003) that increases sharply with decreasing temperature, loss of dissolved H_2O, and crystal growth (e.g. Waters and Andrews, 2016). Understandably then, large–scale

transport, and extended storage in pre–eruptive magma chambers, while remaining above the solidus, is difficult for high–SiO_2 rhyolite in cool, upper crustal conditions.

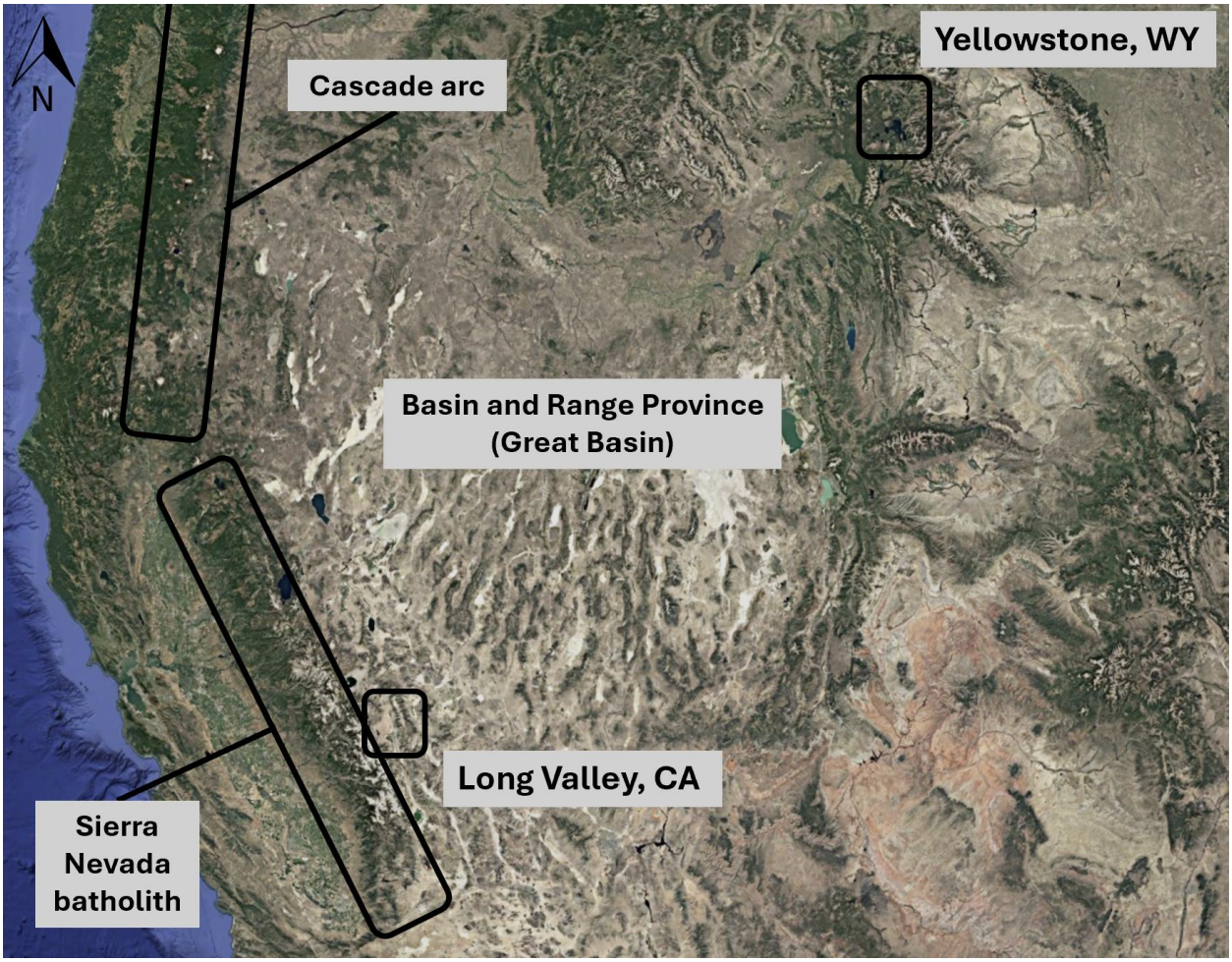


Figure 1-1: Google Earth map of western United States, depicting locations of recent (< 800 ka), voluminous eruptions of high–SiO_2 rhyolite (Long Valley, CA and Yellowstone, WY). For reference, other features are shown, including the Cascade arc and Sierra Nevada Batholith, along with the Basin and Range extensional province.

Perhaps the greatest factor controlling successful high–SiO_2 rhyolite eruption is tectonic setting. In both cases of the most recent supervolcano eruptions of high–SiO_2 rhyolite, the tectonic setting was continental lithospheric extension (e.g. the Basin and Range province; Fig 1). In both cases, the second most voluminous magma type that erupts is basalt (e.g., Hildreth, 2004; Christiansen, 2001). The bimodality of coeval basalt and high–SiO_2 rhyolite eruption signifies that substantial volumes of basalt have reached the upper granitoid crust instead of

being emplaced in the mafic, deep crust as is typically the case in subduction zones. The emplacement of basalt readily supplies heat and H_2O rich fluid to the upper granitoid layer which allows it to partially melt leading to an interstitial melt which is high–SiO_2 rhyolite in composition (Calegero, 2021; and continued work thereafter). Thus, this tectonic setting is unique in its potential to produce large scale accumulation and eruption of high–SiO_2 rhyolite.

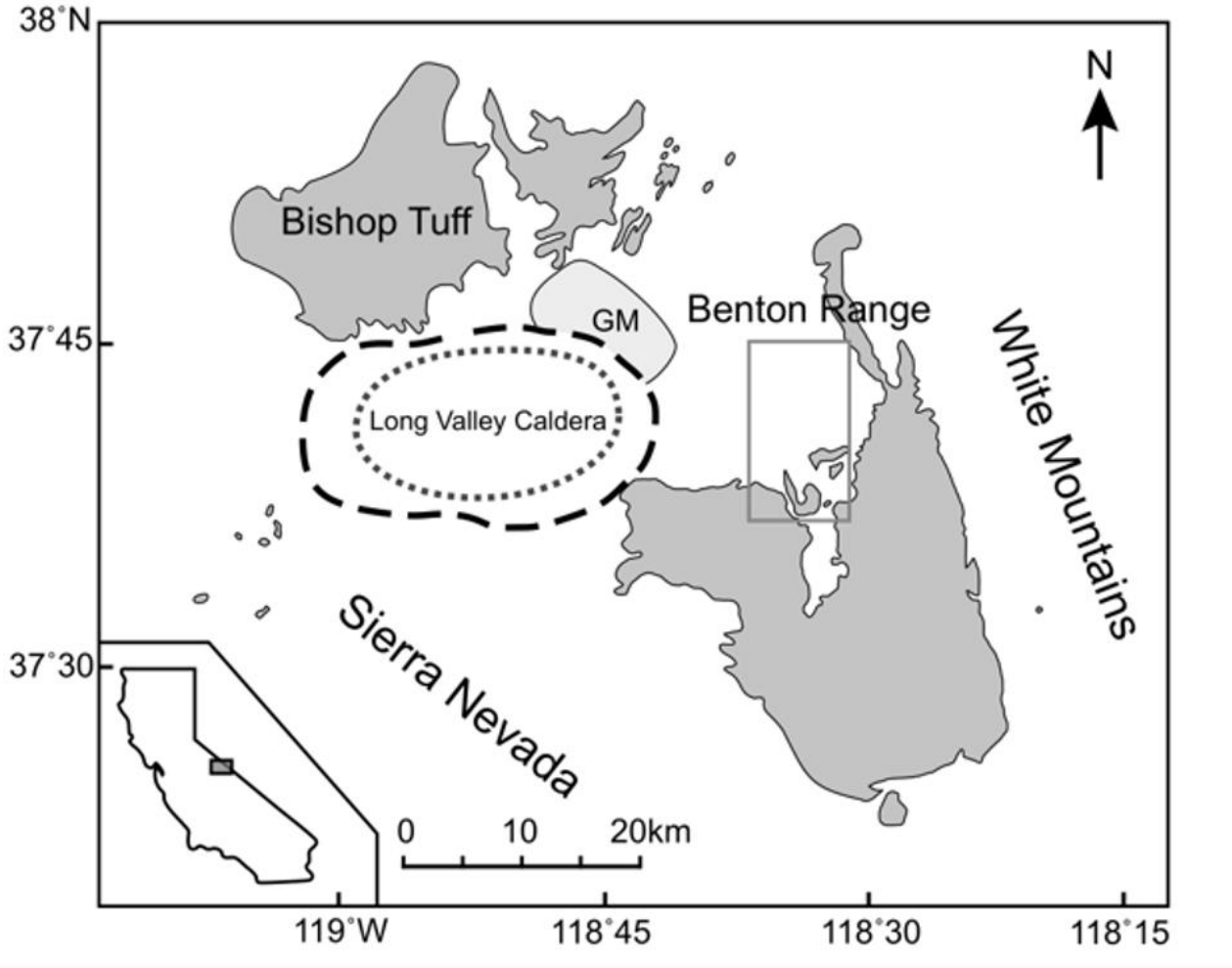


Figure 1-2: Study area location map of Long Valley Caldera and the Benton Range, CA modified from Chamberlin et al. (2015). The Benton Range is shown in a grey box just southeast of the Long Valley Caldera (topographic rim shown by dashed line). Glass Mountain is shown in light gray, and the Bishop Tuff (BT) is shown in dark gray.

However, the timescales, mechanisms, and conditions which allow high–SiO_2 rhyolite eruptions to occur, including in supervolcano quantities, are not yet well constrained. Thus, this dissertation investigates several topics, including: (1) the pre–eruptive temperature of phenocryst

growth, (2) the timescales and locations of phenocryst growth, (3) the true temperature of the H_2O–saturated granite solidus, and (4) tectonic implications regarding the timing of a Jurassic high–SiO_2 rhyolite dike swarm in the Mesozoic Sierra Nevada arc (Fig. 2).

In order to understand the mechanisms of magma accumulation and eruption, constraints on pre–eruptive temperatures, dissolved water contents in the melt, pressure, and fO_2 are necessary. Chapter 2 (to be submitted to *American Mineralogist*) of this dissertation presents a new mineral–melt thermometer specifically calibrated for high–SiO_2 rhyolites. There are an abundance of mineral–melt and mineral–mineral thermometers and barometers in the literature that have been developed to infer the conditions of phenocryst growth, which are often interpreted to be the conditions of storage in a magma chamber. These include the zircon saturation thermometer (Watson and Harrison, 1983; Boehnke et al., 2013), the Fe–Ti oxide thermometer/ oxybarometer (e.g., Ghiorso and Evans, 2008), the Ti–in–quartz thermobarometer (e.g., Wark and Watson, 2006; Thomas et al., 2010; Huang and Audétat, 2012; Thomas et al., 2015; Zhang et al., 2020), the Ti–in–zircon thermometer (e.g., Watson et al., 2006; Watson and Ferry, 2007; Crisp et al., 2023), the biotite thermobarometer (e.g., Li and Zhang, 2022), the two–feldspar thermometer (e.g., Elkins and Grove, 1990; Benisek et al., 2004; Putirka et al., 2008), the Rhyolite–MELTS geobarometer (e.g., Gualda et al., 2012; Gualda and Ghiorso, 2014) and many more. However, due to the scarcity and compositional challenges (i.e., high viscosity, narrow liquidus–solidus interval) of high–SiO_2 rhyolites, many of these thermometers and barometers are not calibrated on high–SiO_2 rhyolites. This has led to inconsistencies between the results of these thermometers when applied to well–characterized high–SiO_2 rhyolite volcanic deposits (e.g. the Bishop Tuff). Additionally, the longest standing thermometer applicable to high–SiO_2 rhyolites, the Fe–Ti oxide thermometer (Ghiorso and Evans, 2008), requires

equilibrium coexistence of unaltered ilmenite and titanomagnetite. This has presented a difficulty for its application in older, heavily altered, or phenocryst poor (>1 % crystallinity) high–SiO_2 rhyolite volcanic deposits. Therefore, this chapter presents a new biotite–liquid thermometer calibrated on experimental and natural samples of high–SiO_2 rhyolite. This thermometer is based on the partitioning of TiO_2 between biotite and high–SiO_2 rhyolite liquid ($D_{TiO_2}^{bte-liq}$). The idea for this thermometer is based on the strong linear relationship between $D_{TiO_2}^{bte-liq}$ and Fe–Ti oxide temperatures previously observed for the Bishop Tuff high–SiO_2 rhyolites from Long Valley, CA (Fig. 2; Hildreth 1977; Jolles and Lange 2019). This relationship is extended to lower eruptive temperatures by the addition of biotite analyses and Fe–Ti oxide temperatures from the Glass Mountain high SiO_2 rhyolites, which erupted directly before the caldera–forming eruption of the Bishop Tuff. A remarkably strong linear correlation ($R^2 = 0.95$) is established when $D_{TiO_2}^{bte-liq}$ is plotted against available Fe–Ti oxide temperatures for natural samples from Long Valley, CA (Glass Mountain and Bishop Tuff). To fully calibrate this thermometer, cold–seal pressure vessel experiments were performed on a high SiO_2 rhyolite glass starting material ranging from 125–225 MPa and temperatures from 675–800 °C, under water–saturated conditions. Resulting experimental biotite and glass were analyzed and the calculated $D_{TiO_2}^{bte-liq}$ plot within error of the natural trend. A final thermometer with a strong linear correlation ($R^2 = 0.90$) is established and returns Fe–Ti oxide and experimental temperatures used for calibration within ~ 30 °C. A test of this thermometer is performed on a Jurassic–aged high–SiO_2 rhyolite dike swarm in the Benton Range, CA, which has undergone significant weathering. The presence of allanite (experimentally determined stability limit of 770 °C in HSR; Vazquez et al., 2004) constrains expected temperature and the $D_{TiO_2}^{bte-liq}$ thermometer returns temperatures from 757 °C

–786 °C. Thus, this thermometer shows potential for deployment in older volcanic deposits of high–SiO_2 rhyolite composition, as well as leucogranite plutonic bodies such as those found in Miocene bimodal granite–diorite plutons along the Colorado River Extensional Corridor (e.g., Walker et al., 2007).

An accurate temperature of the H_2O–saturated granitic (high–SiO_2 rhyolite composition) solidus and understanding of the timescales and locations (i.e., magma chambers or dikes) of phenocryst growth in high–SiO_2 rhyolites is also needed for investigation of pre–eruptive magma evolution. Chapter 3 (to be submitted to *Contributions to Mineralogy and Petrology*) of this thesis investigates the location of the H_2O–saturated solidus at 200 MPa and evaluates evidence of kinetic delays to phenocryst growth in the Glass Mountain high–SiO_2 rhyolites from Long Valley Caldera, CA (Fig 1–2). The Glass Mountain high–SiO_2 rhyolites have highly variable phenocryst abundancies (>1–20 % crystals) across 39 erupted units, despite all having nearly the same major–element compositions and similar phenocryst growth temperatures. Additionally, a previously obtained Fe–Ti oxide temperature of 660 (± 10) °C for one Glass Mountain unit is below the accepted H_2O–saturated granitic solidus at upper crustal conditions (≤ 300 MPa; Ebadi and Johannes, 1991). In an effort to understand the highly variable crystal abundances and low temperatures of the GM rhyolites, three hypotheses are evaluated in Chapter 3: (1) phenocryst abundances in the GM units reflect equilibrium conditions (temperature, pressure, dissolved H_2O in the melt) during crystal growth in a magma chamber, (2) the H_2O–saturated granitic solidus is lower than previously documented, and (3) variable phenocryst abundances across the GM units reflect rapid phenocryst growth during ascent, following kinetic delays to nucleation. To evaluate these hypotheses, new experiments were conducted on a high–SiO_2 composition, together with a detailed characterization of several Glass Mountain units to document the textures and

compositions of plagioclase, sanidine, and biotite phenocrysts. Temperatures for Glass Mountain units were determined using the biotite–liquid thermometer (Chapter 2) and compared with temperatures from the Fe–Ti two–oxide thermometer (Ghiorso and Evans, 2008). The hypothesis that phenocryst abundances reflect equilibrium conditions in a magma chamber is ruled out by comparing data on the natural GM units to results from phase–equilibrium experiments on a high–SiO_2 rhyolite by Waters and Andrews (2016). These experiments also demonstrate that once all three tectosilicate phases are co–saturated in the melt, crystallinity in a high–SiO_2 rhyolite increases sharply to >50% with either decreasing temperature (~10°C) or degassing (~0.5 wt% H_2O). The hypothesis of a significantly lower H_2O–saturated granitic solidus at ≤ 200 MPa is also ruled out by experiments that were conducted in this study on a crystal–free high–SiO_2 rhyolite glass at 650 °C and 200 MPa with a hold time of ≤ 25 days to overcome kinetic delays to nucleation. At these conditions, the resulting experiment is completely crystallized and thus agrees with previous documentation of the water–saturated solidus at 200 MPa (≤ 670°C; Ebadi and Johannes, 1991). The final hypothesis was evaluated through analysis of natural phenocryst growth textures and abundances and an additional experiment. In this second water–saturated experimental run at 200 MPa, the high–SiO_2 rhyolite glass was taken to 850°C, well above the tectosilicate liquidus, and held for two hours before dropping the temperature abruptly to 650°C. Phenocryst–sized tectosilicates, with rapid growth textures (e.g, hopper, swallowtail) were found in the run products, along with granophyric intergrowths and ~40% glass. The crystal textures match those found among the phenocrysts in the GM natural samples. Overall, the results require that a kinetic delay to nucleation must have preceded phenocryst growth in the GM units. In Chapter 3, it is shown how a kinetic delay inevitably develops in melts that begin their ascent in dikes fluid undersaturated, which in turn enables an undercooling to develop after

fluid saturation. At moderate undercoolings, crystal growth rates are high and nucleation rates are low, producing large, sparse phenocrysts, similar to those seen in the GM units.

High–SiO_2 rhyolites primarily erupt in areas of continental extension and thus investigating the age of their emplacement in ancient arcs has tectonic implications. Chapter 4 of this thesis (to be submitted to *Geology*) presents new U–Pb zircon ages for the Benton Range high–SiO_2 rhyolite dike swarm (Mesa, 2021). The dike swarm is a Jurassic (168-209 Ma) extensional feature previously dated using K-Ar by Renne and Turin (1987) and located along the eastern margin of the Sierra Nevada batholith, near the Long Valley Caldera, CA (Fig. 2). The Sierra Nevada arc was formed in the Mesozoic primarily from three distinct magmatic flare ups in the Triassic, Jurassic and Cretaceous, each of which was separated by a magmatic lull (e.g. Paterson and Ducea, 2015). Overlapping the Jurassic magmatic flare up (~175–145 Ma; e.g., Paterson and Ducea, 2015), typically thought to be due to subduction, is the formation of the Coast Range Ophiolite (CRO) (~170–160 Ma; Shervais et al., 2005*),* which formed due to extension in the forearc (e.g., Shervais and Kimbrough, 1985; Arkula et al., 2023). To explain the tectonic models producing extension in the arc at this time, different models for plate kinematics have been proposed: (1) slab rollback (Saleeby, 1996) and more recently (2) trench parallel (N–S) spreading in the forearc (Arkula et al., 2023). Slab rollback can cause regional extension across the arc while trench parallel in the forearc spreading does not require this. New U–Pb zircon crystallization ages for the Benton Range dike swarm presented in Chapter 4 range from 162 ± 9 Ma to 169 ± 11Ma and add an improvement on the previous estimate for dike emplacement. This indicates that extension in the main Sierran arc occurred during formation of the CRO (~170–160 Ma). This matches other evidence that suggests a relatively thin crust in localities across the arc during the Jurassic (e.g., Tobisch et al., 2000). Given the evidence of

trench parallel spreading (N–S extension) in the forearc to form the CRO (Arkula et al., 2023), it is possible that this produced trans tensional shear stresses in the Sierra Nevada arc, including the formation of localized pull–apart basins (e.g., the Benton Range dike swarm). Moreover, slab rollback during this time is not precluded and widespread extension in the Sierran arc is possible but requires further field studies and geochronology to confirm.

1.1 References

Bachmann, O. (2004c). On the Origin of Crystal–poor Rhyolites: Extracted from Batholithic Crystal Mushes. *Journal of Petrology*, *45*(8), 1565–1582. https://doi.org/10.1093/petrology/egh019

Benisek, A., Kroll, H., & Cemič, L. (2004). New developments in two–feldspar thermometry. *American Mineralogist*, *89*(10), 1496–1504. https://doi.org/10.2138/am–2004–1018

Calogero, M. (2021). High–Resolution numerical thermal modeling of timescales and mechanisms of rhyolite genesis and transport as a consequence of basalt influx: Applications to the Long Valley Volcanic Field, CA. *Deep Blue (University of Michigan)*. https://doi.org/10.7302/1535

Christiansen, R.L. 2001. The Quaternary and Pliocene Yellowstone Plateau volcanic field of Wyoming, Idaho, and Montana. U.S. Geological Survey Professional Paper 729–G:145

Crisp, L. J., Berry, A. J., Burnham, A. D., Miller, L. A., & Newville, M. (2023). The Ti–in–zircon thermometer revised: The effect of pressure on the Ti site in zircon. *Geochimica Et Cosmochimica Acta*, *360*, 241–258. https://doi.org/10.1016/j.gca.2023.04.031

de Silva, S.L. & Grosnold, W.D. (2007) Episodic construction of batholiths: Insights from the spatiotemporal development of an ignimbrite flare–up. Journal of Volcanology and Geothermal Research 167:320–335.

Dickinson, W. R., Hopson, C. A., & Saleeby, J. (1996). Alternate origins of the Coast Range Ophiolite (California); introduction and implications. The Caltech Institute Archives (California Institute of Technology). https://authors.library.caltech.edu/49197/

Elkins, L. T., & Grove, T. L. (1990). Ternary feldspar experiments and thermodynamic models. *American Mineralogist*, *75*, 544–559.

Glazner, A.F., Colman, D.S., Bartley, J.M. 2008. The tenuous connection between high–silica rhyolites and granodiorite plutons. Geology 36:183–186

Gualda, G. a. R., Ghiorso, M. S., Lemons, R. V., & Carley, T. L. (2012). Rhyolite–MELTS: a Modified Calibration of MELTS Optimized for Silica–rich, Fluid–bearing Magmatic Systems. *Journal of Petrology*, *53*(5), 875–890. https://doi.org/10.1093/petrology/egr080

Hildreth, W. & Wilson, C.J. (2007) Compositional zoning of the Bishop Tuff. Journal of Petrology. 48:951–999.

Li, X., & Zhang, C. (2022). Machine Learning thermobarometry for Biotite-Bearing magmas. *Journal of Geophysical Research Solid Earth*, *127*(9). https://doi.org/10.1029/2022jb024137

Mesa, J. (2021). Evidence of Phenocryst Growth and Magma Mixing during Ascent along Fractures in Volcanic Rocks from Basalt to Rhyolite. *Deep Blue (University of Michigan)*. https://doi.org/10.7302/2876

Putirka KD (2008) Thermometers and barometers for volcanic systems. Rev Mineral Geochem 69:61–120

J.A. Wolff, F.C. Ramos, J.R. Boro, P.H. Olin, S. Self, R.L. Winters, D.C. Kuentz, C. Dimond, G.W. Cook, P.R. Kyle; Compositional zoning of the Otowi Member of the Bandelier Tuff, Valles caldera, New Mexico, USA. *Geosphere* 2024; 20 (2): 315–344. doi: https://doi.org/10.1130/GES02618.1

Shervais, J. W., Murchey, B., Kimbrough, D. L., Renne, P., & Hanan, B. B. (2005). Radioisotopic and biostratigraphic age relations in the coast range Ophiolite, northern California: Implications for the tectonic Evolution of the western Cordillera. Geological Society of America Bulletin, 117(5/6), 633–653.

Tobisch, O. T., Fiske, R. S., Saleeby, J. B., Holt, E., & Sorensen, S. S. (2000). Steep tilting of metavolcanic rocks by multiple mechanisms, central Sierra Nevada, California. Geological Society of America Bulletin, 112(7), 1043–1058. https://doi.org/10.1130/0016–7606(2000)112

Tuttle, O.F. and Bowen, N.L. (1958) Origin of granite in the light of experimental studies in the system NaAlSi3O8–KAlSi3O8–SiO2–H2O. Geological Society of America Memoir, v. 74.

Vazquez, J. A., Manning, C. E., & Reid, M. R. (2004). Experimental determination of allanite stability in High–Silica rhyolite. *AGU Fall Meeting Abstracts*, *2004*. http://ui.adsabs.harvard.edu/abs/2004AGUFM.V41C1407V/abstract

Walker, B., Miller, C., Claiborne, L. L., Wooden, J., & Miller, J. (2007). Geology and geochronology of the Spirit Mountain batholith, southern Nevada: Implications for timescales and physical processes of batholith construction. *Journal of Volcanology and Geothermal Research*, *167*(1–4), 239–262.

Watson EB, Wark DA, Thomas JB (2006) Crystallization thermometers for zircon and rutile. Contrib Mineral Petrol 151:413–433

Zhang, Y., Xu, Z., & Liu, Y. (2003). Viscosity of hydrous rhyolitic melts inferred from kinetic experiments, and a new viscosity model. *American Mineralogist*, *88*(11–12), 1741–1752. https://doi.org/10.2138/am–2003–11–1215

Zhang, C., Li, X., Almeev, R. R., Horn, I., Behrens, H., & Holtz, F. (2020). Ti–in–quartz thermobarometry and TiO2 solubility in rhyolitic melts: New experiments and parametrization. *Earth and Planetary Science Letters*, *538*, 116213. https://doi.org/10.1016/j.epsl.2020.116213

Chapter 2 A New Biotite–liquid Thermometer Applicable to High–SiO_2 Rhyolites

2.1 Abstract**:**

A new biotite–liquid thermometer for high–SiO_2 (>75 wt % SiO_2) rhyolites is presented in this study. The thermometer is based on the partitioning of TiO_2 between biotite phenocrysts and the high–SiO_2 rhyolite liquid ($D_{TiO_2}^{bte-liq}$). Data from the literature on the high–SiO_2 rhyolite portion of the Bishop Tuff (Long Valley, CA) show that $D_{TiO_2}^{bte-liq}$ varies linearly with Fe–Ti oxide temperature, from ~800 to 700°C. The only experimental study in the literature on a high–SiO_2 rhyolite (at 800–825 °C and 200 MPa), where $D_{TiO_2}^{bte-liq}$ could be obtained from published results produces results that plot along the extrapolation of the trend from natural Bishop Tuff samples to higher temperatures. New data obtained in this study on five Glass Mountain high–SiO_2 rhyolites (Long Valley, CA) extend the linear correlation between $D_{TiO_2}^{bte-liq}$ and Fe–Ti oxide temperature down to ~660 °C. In addition, several biotite–liquid equilibrium experiments were performed in this study under pure–H_2O fluid–saturated conditions on two high–SiO_2 rhyolite initial starting glasses with different concentrations TiO_2 (0.20 and 0.07 wt%). Experiments were conducted in cold–seal pressure vessels with an imposed oxygen fugacity of ΔNNO ~1.0 (± 0.5) over a range of temperatures (800–675°C) and pressures (225–125 MPa) for 182 h. A total of ten successful experiments produced biotite (≤ 200 μm in size) and glass (without tectosilicates) in the run product, which enabled $D_{TiO_2}^{bte-liq}$ values to be obtained. Six experiments were conducted under isothermal conditions (750°C) between 125 and 225 MPa and confirm no pressure dependence to $D_{TiO_2}^{bte-liq}$ over this interval. Two pairs of experiments were conducted under

identical run conditions (125 and 225 MPa; 750°C), but with different initial TiO_2 concentrations in the starting glass. The resulting $D_{TiO_2}^{bte-liq}$ values for each pair (i.e., two different initial starting glasses) provide a bracketed approach to the attainment of $D_{TiO_2}^{bte-liq}$ equilibrium. Overall, the results confirm the close approach to $D_{TiO_2}^{bte-liq}$ equilibrium over the 182 h duration of the experiments in this study. The new data obtained in this study (both experimental and natural) were combined with those from the literature on high–SiO_2 rhyolites to fit a linear relationship between temperature and $D_{TiO_2}^{bte-liq}$, with a standard error of the estimate of 14 °C (and $R^2 = 0.90$). The resulting equation, T(°C) = 846 (±7) – 2.32 (±0.15)*$D_{TiO_2}^{bte-liq}$, can be used as a biotite–liquid thermometer for high–SiO_2 rhyolite melts. A test of this thermometer is made by applying it to a suite of high–SiO_2 rhyolite dikes of Jurassic age, some of which contain allanite (stable at ≤ 770°C in HSR). Pristine biotite could be found and analyzed in four of these dikes, and calculated temperatures range from 757 (±16) to 786 (±10) °C. These temperatures (within propagated analytical errors) are close to the stability limit of allanite, which confirms the accuracy of the new $D_{TiO_2}^{bte-liq}$thermometer.

2.2 Introduction

High–SiO_2 rhyolite (75–78 wt% SiO_2) is the most evolved silicate magma type on Earth and is characterized by an extreme, end-member composition with high liquid viscosities and a narrow liquidus–interval which make the collection and eruption of this magma unlikely. It is the dominant composition, however, of some of the largest (100's–1000's km^3) explosive volcanic events over the last 1.2 Myr (e.g., Yellowstone, WY, Christensen, 2001; Long Valley caldera, CA, Hildreth, 1979; Valles caldera, Smith and Bailey, 1966). Therefore, understanding the

conditions (i.e. temperature, pressure, volatile content) of these magmatic systems prior to eruption is crucial.

Even at low crystallinities, high–SiO_2 rhyolites (HSR) can be multiply saturated with mineral phases which can be used to constrain pre–eruptive temperatures. This is accomplished with various mineral–melt and mineral–mineral thermometers such as the two Fe–Ti oxide thermometer (e.g., Ghiorso and Evans, 2008), the Ti–in–quartz thermobarometer (e.g., Wark and Watson, 2006; Thomas et al., 2010; Huang and Audétat, 2012; Thomas et al., 2015; Zhang et al., 2020), the Ti–in–zircon thermometer (e.g., Watson et al., 2006; Watson and Ferry, 2007; Crisp et al., 2023), the zircon saturation thermometer (Watson and Harrison, 1983; Boehnke et al., 2013), the two–feldspar thermometer (e.g., Elkins and Grove, 1990; Benisek et al., 2004; Putirka et al., 2008), and the biotite thermobarometer (e.g., Li and Zhang, 2022).

Unfortunately, many of these thermometers are not calibrated specifically on high–SiO_2 rhyolites and thus, when applied, their results are often inconsistent with one another. This is issue is demonstrated through debate surrounding the pre-eruptive temperature of the Bishop Tuff, which erupted ~766.5 ± 0.5 ka (Mark et al., 2017) to form the Long Valley caldera (Figure 2–1) in eastern California (e.g., Wilson and Hildreth, 1997). Thermometers used in some studies (e.g., Fe-Ti oxide: Hildreth, 1977, Hildreth and Wilson, 2007; Jolles and Lange, 2019) suggest that the magmatic system was thermally zoned (~700-800°C) however others (e.g., zircon–saturation: Watson and Harrison, 1983; Boehnke et al., 2013) suggest less variable and cooler temperatures (e.g., ≤730°C; Gualda and Ghiorso, 2022). A biotite thermobarometer was also applied to the deposit and the results range to much hotter values (e.g., 750–875°C; Li and Zhang, 2022) which led to the conclusion that biotite was not in equilibrium with the Fe–Ti oxides. This conclusion however is surprising given the strong linear correlations ($R^2 \geq 0.95$) that

Jolles and Lange (2019) documented between biotite compositional components and determined Fe–Ti oxide temperatures Bishop Tuff deposit.

The goal of this study is to re–examine the viability of using biotite as a thermometer applicable to high–SiO_2 rhyolite melts, and to re–evaluate its internal consistency with the Fe–Ti two–oxide thermometer (e.g., Ghiorso and Evans, 2008). A possible explanation for the discrepancy between the biotite thermometer of Li and Zhang (2022) and Fe–Ti oxide thermometry may be the scarcity of biotite–bearing experiments on natural high–SiO_2 rhyolite starting material that was available for the calibration of the Li and Zhang (2022) biotite model. In published hydrous phase–equilibrium studies where natural high–SiO_2 rhyolite was the starting composition and biotite is found in the run products (e.g., Gardner et al., 2014; Bolte et al., 2015; Waters and Andrews, 2016; Meszaros et al., 2024) only Bolte et al. (2015) reports biotite compositions.

Therefore, this study aims to fill this gap in the literature by presenting biotite–liquid equilibrium experiments on high–SiO_2 rhyolite glass starting material. Experiments in this study are motivated by evidence that the partition coefficient for TiO_2 between biotite and liquid (whole rock), $D_{TiO_2}^{bte-liq} = \frac{\text{wt\%TiO}_2\text{ (biotite)}}{\text{wt\%TiO}_2\text{ (liquid)}}$, has a strong, linear correlation ($R^2 = 0.95$) with Fe–Ti two–oxide temperature (Fig. 2–1; Jolles and Lange, 2019).

Also shown in Figure 2–1 are the data from the Bolte et al. (2015) experiments which were conducted at 200 MPa (H_2O fluid-saturated) on a 100% glass starting material (75 wt% SiO_2) fused from the Blacktail Creek Tuff from the Heise volcanic field, Yellowstone hotspot system. Biotite was found and analyzed in four experimental run products, but the analyzed biotite from one experiment (run JI21) is anomalous and has large errors (e.g., 56 ± 7.8 wt% SiO_2). When the three experimentally obtained $D_{TiO_2}^{bte-liq}$ values from Bolte et al. (2015) are

added to Figure 2–1 they fall near the extrapolated linear trend established by the natural data from the Bishop Tuff.

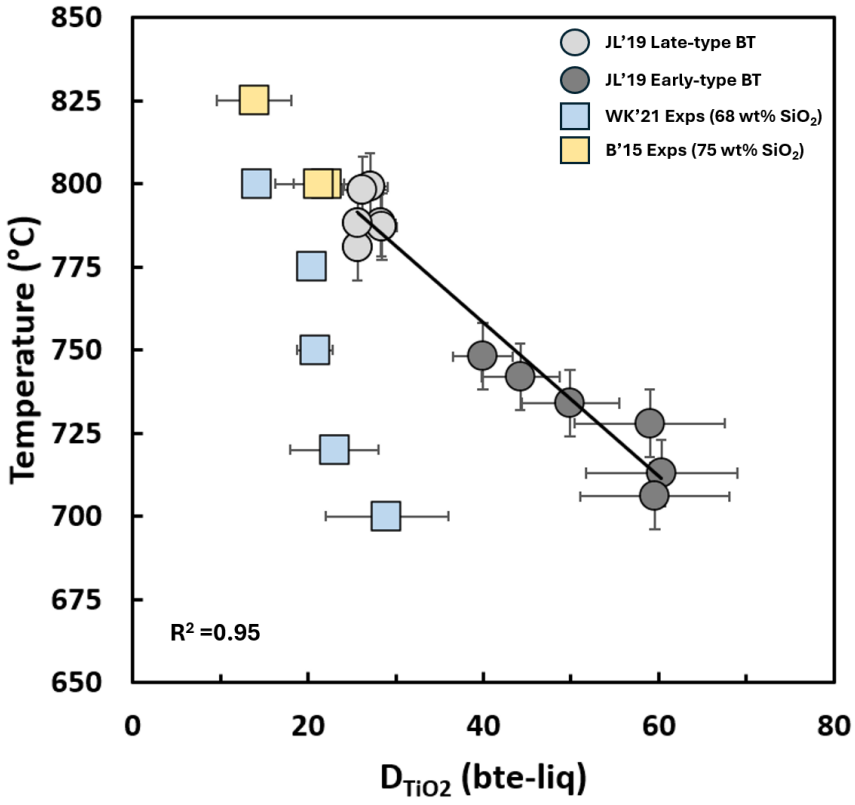


Figure 2-1: Plot of experimental or Fe–Ti two–oxide temperature (°C) vs D_{TiO2} (bte-liq). The data for the Early– and Late–type Bishop Tuff high–SiO_2 rhyolites are from Jolles and Lange (2019). A linear fit to these natural data is shown (R^2 = 0.95) and the only available experiments on biotite–bearing high–SiO_2 rhyolite (Bolte et al., 2015) match the trend line. In contrast, the experimental results from Wark et al. (2021) on a melt composition with a lower SiO_2 content (68 wt%) has a different trend. Error bars represent propagated 1 SD.

In Figure 2–1 another experimental data set is shown from partitioning experiments conducted by Were and Keppler (2021) on an initial starting glass with 68 wt% SiO_2. Note that the $D_{TiO_2}^{bte-liq}$ trend is systematically shifted to lower values compared to those for the high–SiO_2 rhyolites. This shift is not surprising since mineral–melt partition coefficients of trace–elements are known to be significantly different between high–SiO_2 versus low–SiO_2 rhyolites (e.g., Mahood and Hildreth, 1983; Ewart and Griffin, 1994; Davies et al., 1994) and only underscores

the need for a calibrated trend specifically for high-SiO_2 rhyolites. Moreover, if the coordination of Ti^{4+} shifts between high–SiO_2 vs low–SiO_2 rhyolites (e.g., Farges and Brown, 1997), this could also account for the difference.

In this study, hydrous phase–equilibrium experiments are conducted on two different natural starting glass materials, both of high–SiO_2 rhyolite composition, but differing TiO_2 contents and Mg# values. Additionally, new biotite analyses on five natural high–SiO_2 rhyolite samples from Glass Mountain, CA (precursor to the Bishop Tuff), for which Fe–Ti oxide temperatures are known (Gordon, 2022), are also obtained in this study. These enable the trend seen in the natural data in Fig. 2–1 to be extrapolated down to temperatures ≥ 660 °C. The overall goal is to calibrate a new Ti–based biotite–liquid thermometer applicable to high–SiO_2 rhyolites. Finally, unaltered biotite in four Jurassic high–SiO_2 rhyolite dikes (Benton Range dikes from eastern California; Mesa, 2021), which also contain evidence of allanite as a near–liquidus phase (only stable ≤ 770°C in HSR; Vasquez et al., 2004), are also analyzed to test the application of the newly calibrated thermometer.

2.3 Experimental Methods

2.3.1 Synthesis of starting glass materials

Two high–SiO_2 rhyolite compositions were selected with different initial whole rock TiO_2 concentrations. One is a single–clast sample from the Bishop Tuff (BT–3B; Jolles and Lange, 2019), with 0.20 wt% TiO_2. The second is from the Mono Craters (MC–24), analyzed by Mack Taylor (personal communication), with ~0.07 wt%TiO_2. Unaltered, interior portions of each sample were crushed and powdered in a tungsten carbide shatter box for homogenization and then melted in a box furnace at the University of Michigan. Each powdered sample was placed into a platinum crucible and then held in a box furnace for ≥ 14 hr at 1200°C, followed by

an additional 4 h at 1450°C to fully melt any crystals that may still be present. Each Pt crucible was then removed from the furnace and plunged into cold water to quench the molten sample into crystal–free 100% glass. The glass was removed from each Pt crucible and powdered in a tungsten carbide shatter box for further homogenization. Powdered glass was the starting material for each of the experiments.

2.3.2 Experimental design: T–P conditions and technique to grow large biotite crystals

Hydrous phase–equilibrium experiments were conducted in a cold–seal pressure vessel at the New Mexico Institute for Mining and Technology. Utilizing the schematic phase diagram in Figure 2–2, which is based on the pure–H_2O fluid–saturated experiments of Waters and Andrews (2016) on a high–SiO_2 rhyolite melt composition, a series of temperature and pressure conditions were chosen for the biotite–liquid equilibrations in this study.

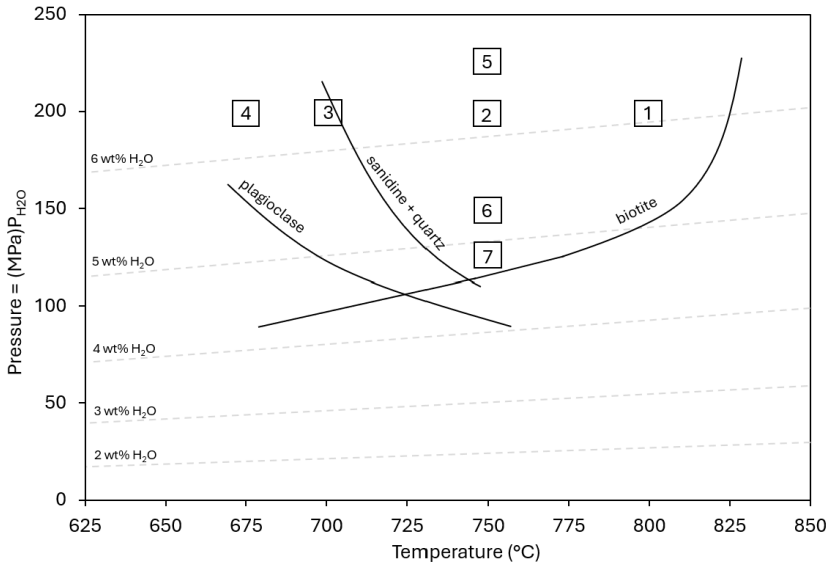


Figure 2-2 **:** A simplified phase–equilibrium diagram for a representative high–SiO_2 rhyolite under water–saturated conditions modified from Waters and Andrews (2016), which indicates the stability field of biotite relative to the tectosilicates. mineral in–curves. Pressure (MPa) = P_{H2O} is shown on the y–axis and temperature (°C) is shown on the x–axis. Dashed lines show concentrations of dissolved H_2O in the melt (Zhang et al., 2007). Superimposed on this diagram are the numbered experimental runs (inside boxes) from this study, illustrating the final temperature and P_{H2O} run conditions (Table 2–1).

The phase diagram shows the expected stability field of biotite, which guided the choice of experimental *T–P* (temperature–pressure) conditions (Table 2–1). The targeted *T–P* equilibrations will allow a test of whether $D_{TiO_2}^{bte-liq}$ varies as a function of temperature between 675–800°C at constant P_{H2O} (= 200 MPa) and/or as a function of pressure between 225–150 MPa at constant temperature (~750°C).

Table 2-1:Experimental samples, run conditions, and run products.

Run #	BT–3B sample #	T final (°C)	P (MPa)	Duration (h)	Phases present
1	25BT3B_OX_1	800	200	182	Bte, glass, tmte
2	25BT3B_OX_6	750	200	182	Bte, glass, tmte
3	25BT3B_OX_4	700	200	182	Bte, glass, tmte
4	25BT3B_OX_2	675	200	182	failed run (capsule failure)
5	25BT3B_OX_7	750	225	182	glass, tmte
6	25BT3B_OX_8	750	150	182	glass, tmte
7	25BT3B_OX_9	750	125	182	Bte, glass, tmte
Run #	**MC–24 sample #**	**T final (°C)**	**P (MPa)**	**Duration (h)**	**Phases present**
1	not run	800	200	182	Bte, glass, tmte
2	25MC24_OX_3	750	200	182	Bte, glass, tmte
3	25MC24_OX_2	700	200	182	Bte, glass, tmte, san, qtz
4	25MC24_OX_1	675	200	182	Bte, glass, tmte
5	25MC24_OX_4	750	225	182	Bte, glass, tmte
6	25MC24_OX_5	750	150	182	Bte, glass, tmte
7	25MC24_OX_6	750	125	182	Bte, glass, tmte

Experimental capsules were made of 3–mm OD gold tubing and packed with 25–50 mg of powdered glass (starting material) followed by a mixture of titanomagnetite and ilmenite (~15% of total mass). The Fe–Ti oxides were obtained by mineral separation from a single–clast pumice sample from the Bishop Tuff (BT–3B; Jolles and Lange, 2019). Then, a sufficient mass of deionized water was added (~10% of total mass) to ensure fluid saturation during each experimental run. A Lampert PUK high precision TIG welder was used to seal the experimental Au capsules. Capsules were then welded shut and the seals tested by placing capsules on a hot plate (~100 °C) for at least 2 min to check for weight loss, which would indicate an incomplete

seal. At the end of each experimental run (described below), the Au capsules were weighed again to test for any loss of fluid during the experiment, which would indicate a failed run. The reason for adding the Fe–Ti oxides at one end of each experimental capsule is to enable biotite crystallization through a reaction relationship with ilmenite and multicomponent silicate melt (Professor Waters, personal communication).

For each experimental run (1–7; Table 2–1), two sealed Au capsules containing the starting glass material were loaded into the hotspot of Waspaloy (nickel alloy) cold–seal pressure vessels followed by nickel–filler rods for each experimental run. In most experimental runs, one capsule contained the BT–3B starting glass and the other capsule contained the MC–24 starting glass. Water was the high–pressure medium for the experimental set up, with uncertainties in pressure < ±10 MPa. Loaded pressure vessels were heated in Thermo–scientific Linberg Blue tube furnaces, and temperature was monitored by a *K*–type thermocouple, within ± 3 °C.

During each experiment, samples were brought to a pressure of 200 MPa first and then heated to their target temperatures. As temperature increased, the pressure was manually adjusted (every 2–5 minutes) to remain isobaric at 200 MPa until the target temperature was reached.

Due to the composition of the pressure vessels and nickel filler rods, an intrinsic fO_2 close to the Ni–NiO buffer was imposed. Because the fO_2 increases with degree of oxidation of the filler rod (e.g., Venezky and Rutherford, 1999), care was taken between each run to remove the nickel filler rods and file off the oxidized surface to expose the metal in an effort to ensure that the imposed fO_2 approached that of the Ni–NiO buffer. A best estimate of the ΔNNO during each run is ~+0.5 (± 0.5).

Due to the composition of the pressure vessels and nickel filler rods, an intrinsic fO_2 close to the Ni–NiO buffer was imposed. Because the fO_2 increases with degree of oxidation of the

filler rod (e.g., Venezky and Rutherford, 1999), care was taken between each run to remove the nickel filler rods and file off the oxidized surface to expose the metal in an effort to ensure that the imposed fO_2 approached that of the Ni–NiO buffer. A best estimate of the ΔNNO during each run is ~+0.5 (± 0.5).

All experiments were set to an initial hold temperature of 850°C, above the liquidus, for 2 hours, at their designated experimental pressure. Temperature in the experimental runs is measured with a *K*–type thermocouple and is known to within ± 3 °C. After this initial hold (to ensure 100% rhyolite melt starting conditions), the temperature was dropped to 825°C (immediately below biotite liquidus) and held for 2 hours, before taking each experiment to their final run temperature condition. The purpose of the second hold at ~825°C is to promote formation of biotite nuclei. After these two holds, each experiment was dropped to its final temperature and held for 182 h (~7.6 days) at a consistent, unchanging pressure. At the end of each experiment, the Waspaloy vessels were removed from the furnace and immediately quenched to room temperature under isobaric conditions. All successful experimental *T–P* conditions for both starting glass samples are shown in Table 2–1 and range from 125–225 MPa (pure–H_2O fluid saturated) and from 675–800°C.

2.4 Electron microprobe analytical methods

The biotite crystals and quenched glass in all experimental run products, as well as biotite crystals in the natural samples (five Glass Mountain obsidian flows and four Benton Range dikes), were analyzed with a Cameca SX–100 Electron Microprobe in the Robert Mitchell Laboratory at the University of Michigan. A compilation of all microprobe standards used for both biotite and glass analyses for each element is presented in Supplemental Table A-0-1.

2.4.1 Analysis of Biotite

Analyses of biotite from the natural samples were made on thin sections and mineral separates in epoxy mounts. For the analysis of biotite in the experimental run products, the material inside the run capsules were placed in epoxy mounts. Analyses were made with a defocused beam of 2 μm, a beam current of 20 nA and an accelerating voltage of 15 kV. Ten elements were analyzed (Si, Ti, Al, Fe, Mn, Mg, Ba, Ca, Na, and K) with peak and background count times of 20 s, except for Fe (10 s) and Ba (30 s). The average 3 SD uncertainties on the oxide components, based on counting statistics, are ±0.49 wt% SiO_2, ±0.09 wt% TiO_2, ±0.28 wt% Al_2O_3, ±0.54 wt% FeO^T, ±0.04 wt% MnO, ±0.20 wt% MgO, ±0.27 wt% K_2O, ±0.08 wt% BaO., Prior to biotite formula calculations, only biotite analyses with original totals ≥ 93 wt % (set to account for volatile components up to 4.5 wt%) were considered successful. Back–scattered electron (BSE) images were taken of all analyzed biotite crystals. In the natural samples, care was taken to analyze fresh, unaltered biotite.

2.4.2 Analysis of Glass

Glass in each experimental run product was embedded in epoxy mounts and analyzed. The elements analyzed were Na, Mg, Si, Al, K, Ca, Ti, Mn, and Fe. The peak and background counting time was 10 s for Na, Si, Al, K and 20 s for Mg, Ca, Ti and Fe. The average 3 SD uncertainties on the oxide components, based on counting statistics, are ±1.53 wt% for SiO_2, 0.07 wt% for TiO_2, 0.10 wt% for FeO^T, 0.05 wt% for MnO, 0.02 wt% for MgO, 0.09 wt% for CaO, 0.30 wt% for Na_2O and 0.18 wt% for K_2O. For analysis of glass, a defocused beam was used to minimize element migration (e.g., Morgan and London, 1996), the beam current was 10 nA, and the accelerating voltage was 15 kV. In addition, a time–dependent intensity correction was applied to measurements of Na Ka X–rays, similar to the method described in Nielsen and Sigurdsson (1981). Since all phase–equilibrium experiments were conducted under pure–H_2O

fluid–saturated conditions, the concentration of dissolved water in each experimental liquid at the *T–P* run condition were calculated using the water solubility model of Zhang et al. (2007). Only analyses with totals (including calculated dissolved water contents) between 97–101 wt% were used in this study. Additional filters were applied to glass analyses that signaled contamination from a mineral phase (e.g., FeO^T > 1.4 wt% indicated that the defocused beam included a small portion of Fe–Ti oxide and not 100% glass).

2.5 Experimental Results

The list of successful runs is shown in Table 2–1. One experiment failed due to capsule rupture (BT–3B during run #4). Biotite crystallized in all but two of the successful runs (sample BT–3B; runs 5 and 6), with crystals sizes that range from ~20 to ~200 μm. Given run durations of 182 h, this yields an estimated growth rate of ≥1 μm/h for the larger (200 μm) biotite phenocrysts. Biotite growth largely occurred at the interface between the high–SiO_2 rhyolite melt and the Fe–Ti oxides at the end of the capsule. In most experimental runs, ilmenite is absent (i.e., it appears to have been completely consumed during crystallization of biotite from the melt and ilmenite), whereas titanomagnetite grains at the end of the capsule remain. It is possible that biotite did not grow in two experiments (BT–3B in runs 5 and 6), despite the *P–T* conditions in the stability field of biotite, due to an insufficient amount of ilmenite in the Fe–Ti oxides that were added to those capsules. Select BSE images of experimental biotite crystals from experimental runs of both BT–3B and MC–24 starting composition are shown in Figure 2–3.

Quenched glass is present in all run products. In one of the MC–24 experimental run products (run #3 at 700°C, 200 MPa), one quartz crystal and one sanidine crystal were found (Table 2–1). Their rapid growth (~80 μm each in ≤ 7 days) created gradients in the TiO_2 content in the glass, and so this experiment was not included in the calibration of the new biotite–liquid

thermometer in this study. Note that the experiments run at 700 and 675°C are expected to be within the stability field of quartz and sanidine at $P_{H2O} \leq 200$ MPa but they are only found in one experiment. The absence of quartz and sanidine in the other runs is likely due to the kinetic delay of their nucleation.

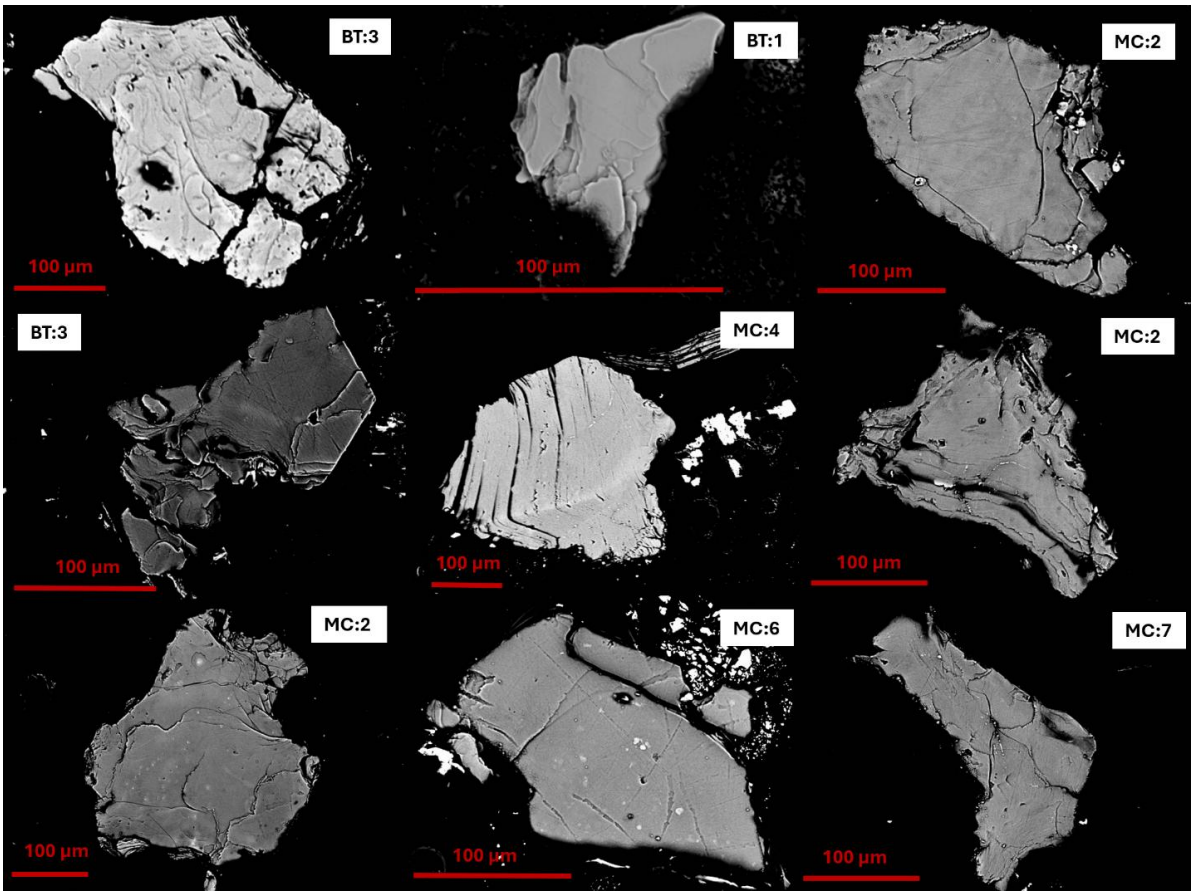


Figure 2-3: Representative BSE images of experimental biotite phenocrysts from resulting experimental runs of both the MC–24 and BT–3B starting material (e.g., MC:2 refers to the MC–24 starting material and run #2). Biotite crystals frequently exceed 100 (and can reach >300) µm in length. Scale bars are shown in red.

2.6 Analytical Results

2.6.1 Biotite compositions in Glass Mountain and Benton Range samples

Individual analyses of biotite crystals in the Glass Mountain obsidian samples and the Benton Range dike samples are found in Supplemental Table A-0-2. The average of the biotite analyses from each sample is reported in Table 2–2. For each average composition, the number

of biotite crystals that were analyzed (N) and the total number of analyses (n) are reported. On the basis of stoichiometry, FeO, Fe_2O_3, and H_2O contents were calculated using the model of Li et al. (2020), and updated totals range from 99–100 wt%. The full stoichiometry results are also shown in Table 2–2 and provide supporting evidence that the biotite analyses are accurate, consistent with the pristine character of analyzed biotite. Calculated H_2O contents are ~2.7 and ~3.1 wt% in the Glass Mountain and Benton Range biotites, respectively. Calculated Fe^{3+}/Fe^{T} ratios range from ~0.23–0.29 and ~0.15–0.19 in the Glass Mountain and Benton Rnage biotites, respectively. It is possible that the Benton Range high–SiO_2 rhyolites crystallized biotite under slightly more reducing conditions than the Glass Mountain high–SiO_2 rhyolites.

The average biotite compositions for both the Glass Mountain and Benton Range samples are similar in terms of their SiO_2 contents (35–36 wt%) and Mg# (=100 x moles MgO/[moles MgO+MnO+ FeO^{T}]) values, which largely range from 37–42. One Glass Mountain sample, GM–01, has a much lower biotite Mg# of 25. The TiO_2 contents in the Glass Mountain biotites (3.7–4.6 wt%) are systematically higher than those in the Benton Range biotites (3.0–3.2 wt%), despite the fact that the whole–rock TiO_2 contents in the Glass Mountain high–SiO_2 rhyolites (0.06–0.07 wt%, Gordon et al., 2026; Supplemental Table A-0-3) are lower than those in the Benton Range high–SiO_2 rhyolites (0.08–0.12 wt%, Mesa, 2021; Supplemental Table A-0-3). The Glass Mountain biotites have Na_2O contents of ~0.5 wt%, similar to those seen in the Bishop Tuff biotites (e.g., Jolles and Lange, 2019), whereas the Benton Range biotites contain little Na_2O. It is likely that this reflects K–Na ionic exchange during alteration, which also affected the K–feldspars in the Benton Range dikes (Mesa, 2021) but did not otherwise affect the composition of biotite. Another notable difference is the much lower BaO contents in the Glass Mountain biotites compared to those in the Benton Range biotites, which may be explained by

the significantly lower whole–rock Ba contents in the Glass Mountain samples (<2–4 ppm, Gordon et al, 2026; Supplemental Table A-0-3) compared to those in the Benton Range samples (221–1237 ppm, Mesa, 2021; Supplemental Table A-0-3).

Representative BSE images of analyzed biotite from the Glass Mountain and Benton Range rhyolites are shown in Figure 2–4 and illustrate the ability to find unaltered biotite, even in the Benton Range dikes of Jurassic age (e.g., Renne and Turrin, 1987). Some analyses of the Benton Range samples were obtained on chloritized biotite, which are readily identified by low totals (84–87 %), due to the high–water content (>13 wt%) of chlorite, and low K_2O contents (0.1–0.7 wt%). Representative analyses of chloritized biotite are reported in Table A.2, although none of which were used in this study.

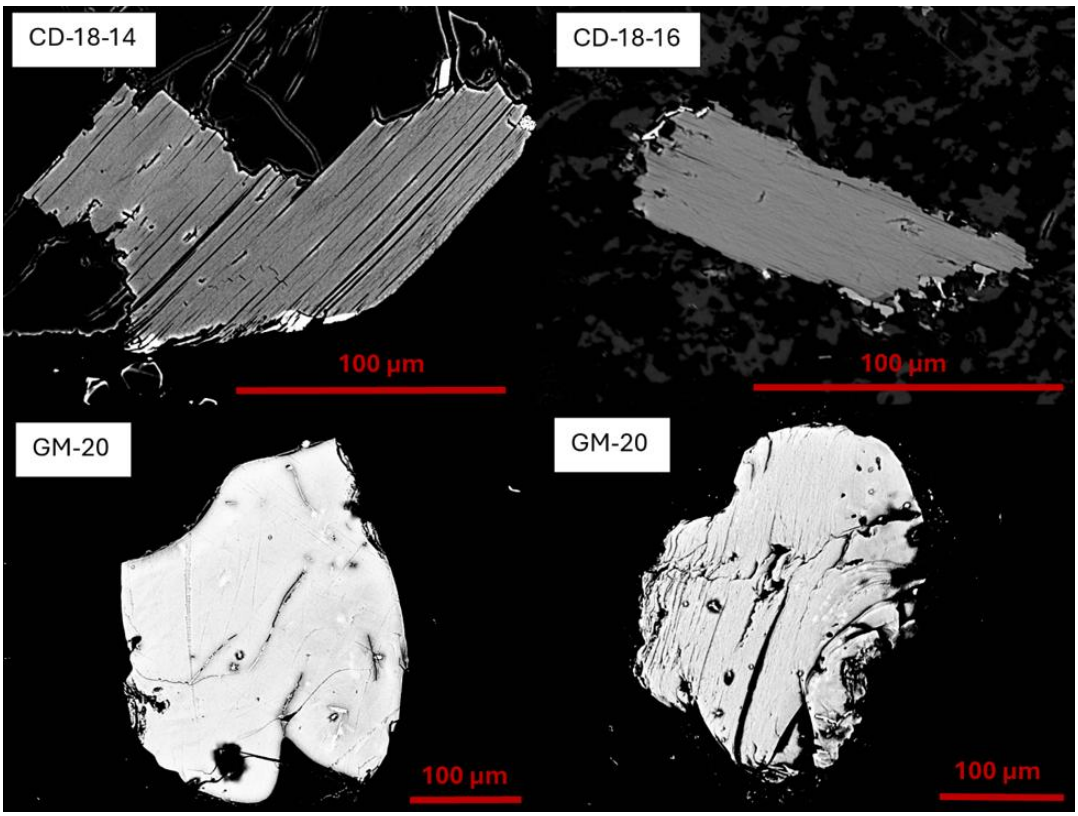


Figure 2-4 :Representative BSE images of biotite phenocrysts in natural high–SiO_2 rhyolite samples from the Benton Range dike swarm (a–b) and the Glass Mountain volcanic complex (c–d).

Table 2-2: Averaged analyses for natural biotite grains (wt%)

Sample N;n	GM–01 1;6	GM–07 8;55	GM–10 10;56	GM– 18 9;45	GM–20 2;71	CD–18–09 7;188	CD–18–12 6;71	CD–18–14 6;57	CD–18–16 3;48
SiO_2	35.43 (44)	36.54 (59)	36.33 (60)	35.97 (59)	36.13 (32)	35.62 (54)	35.94 (63)	35.78 (40)	35.69 (21)
TiO_2	4.57 (06)	3.72 (19)	4.27 (07)	3.74 (22)	4.40 (11)	3.25 (51)	3.07 (53)	3.11 (32)	3.03 (31)
Al_2O_3	12.69 (19)	12.26 (26)	12.53 (23)	12.28 (22)	12.67 (41)	15.36 (55)	15.31 (73)	14.5 (58)	14.60 (43)
FeO^T	28.55 (31)	24.25 (83)	23.43 (67)	25.49 (77)	23.79 (91)	22.26 (1.50)	23.08 (55)	23.02 (88)	23.40 (41)
MnO	0.30 (01)	0.69 (06)	0.33 (02)	0.55 (02)	0.40 (02)	0.57 (04)	0.52 (08)	0.48 (10)	0.40 (17)
MgO	5.28 (09)	9.02 (41)	9.57 (27)	8.44 (35)	9.53 (53)	8.47 (1.27)	7.85 (60)	8.90 (68)	9.20 (43)
CaO	0.0 (00)	0.00 (01)	0.00 (01)	0.00 (01)	0.01 (00)	0.02 (02)	0.01 (01)	0.01 (02)	0.01 (01)
Na_2O	0.40 (02)	0.54 (02)	0.54 (02)	0.52 (02)	0.55 (04)	0.05 (02)	0.05 (02)	0.05 (02)	0.04 (01)
K_2O	9.15 (07)	9.21 (12)	9.35 (10)	9.26 (11)	9.50 (18)	9.99 (20)	10.07 (26)	10.01 (17)	10.10 (11)
BaO	0.09 (02)	0.03 (02)	0.03 (02)	0.03 (02)	0.02 (02)	0.64(23)	0.54(32)	0.30 (18)	0.09 (14)
Fe_2O_{3calc}	7.63	8.00	6.99	8.13	6.97	4.95	4.86	5.26	5.00
FeO_{calc}	21.68	17.05	17.14	18.18	17.52	17.81	18.70	18.29	18.90
H_2O_{calc}	2.66	2.70	2.68	2.75	2.67	3.07	3.12	3.12	3.19
$Total_{calc}$	99.88	99.77	99.76	99.84	100.37	99.80	100.05	99.81	100.25
[1]Mg#	25	40	42	37	42	40	38	41	41
Fe^{3+}/Fe^T	0.24	0.30	0.27	0.29	0.26	0.20	0.19	0.21	0.19
T. Si	2.84	2.86	2.84	2.84	2.83	2.78	2.80	2.80	2.78
T.Al	0.86	0.86	0.90	0.87	0.93	1.05	1.01	1.00	1.01
T.Fe^{3+}	0.30	0.27	0.25	0.29	0.24	0.17	0.19	0.21	0.21
sum Tet	4.00	4.00	4.00	4.00	4.00	4.00	4.00	4.00	4.00
M.Al	0.34	0.27	0.25	0.27	0.24	0.36	0.40	0.34	0.33
M.Mg	0.69	1.08	1.13	1.02	1.13	1.01	0.94	1.06	1.08
M.Fe^{2+}	1.45	1.12	1.12	1.20	1.15	1.16	1.22	1.19	1.23
M.Fe^{3+}	0.16	0.20	0.16	0.19	0.17	0.12	0.10	0.10	0.08
M.Ti	0.27	0.22	0.25	0.22	0.25	0.19	0.18	0.18	0.17
M.Cr	0.00	0.00	0.00	0.00	0.00	0.00	0.00	0.00	0.00
M.Mn	0.02	0.05	0.02	0.04	0.03	0.04	0.03	0.03	0.03
M.Ni	0.00	0.00	0.00	0.00	0.00	0.00	0.00	0.00	0.00
M.Li	0.00	0.00	0.00	0.00	0.00	0.00	0.00	0.00	0.00
sum oct	2.93	2.92	2.94	2.94	2.95	2.88	2.87	2.91	2.93
Oct Vacancy	0.07	0.08	0.06	0.06	0.05	0.12	0.13	0.09	0.07
A.K	0.92	0.92	0.92	0.92	0.94	0.98	0.99	0.99	0.99
A.Na	0.06	0.08	0.08	0.08	0.08	0.01	0.01	0.01	0.01
A.Ba	0.00	0.00	0.00	0.00	0.00	0.02	0.02	0.01	0.00
A.Ca	0.00	0.00	0.00	0.00	0.00	0.00	0.00	0.00	0.00
sum inter	0.99	1.00	1.01	1.01	1.02	1.01	1.01	1.00	1.00
Inter Vacancy	0.01	0.00	0.00	0.00	0.00	0.00	0.00	0.00	0.00
W.F	0.00	0.00	0.00	0.00	0.00	0.00	0.00	0.00	0.00
W.Cl	0.00	0.00	0.00	0.00	0.00	0.00	0.00	0.00	0.00
W.OH	1.42	1.41	1.40	1.45	1.39	1.60	1.62	1.63	1.66
W.O^{2-}	0.58	0.59	0.60	0.55	0.61	0.40	0.38	0.37	0.34

Biotite formula calculation using Li et al., 2020

[1]Mg# = molar MgO/(MgO +FeO^T) x100

Parentheses values represent the sample population 1 SD on the last digits

2.6.2 Biotite compositions in experimental run products

Individual analyses of biotite crystals in the experimental run products are found in Supplemental Table A-0-4. The average of the biotite analyses from each experimental run is reported in Table 2–3. For each average composition, the number of biotite crystals that were analyzed (N) and the total number of analyses (n) are reported. On the basis of stoichiometry, FeO, Fe_2O_3, and H_2O contents were calculated using the model of Li et al. (2020), and updated totals range from 97.6–99.7 wt%. The full stoichiometry results are also shown in Table 2–3 and provide evidence that the biotite analyses are accurate, consistent with the presence of biotite crystals ≥ 100 μm in most of the experimental charges. Calculated H_2O contents are all ~2.6 wt%, and calculated Fe^{3+}/Fe^{T} ratios span a narrow range (0.22–0.25).

The average biotite compositions for all the BT–3B and MC–24 experimental runs are remarkably similar, and they broadly overlap those analyzed in the Glass Mountain natural samples (Table 2–2) and the biotite phenocrysts analyzed in Bishop Tuff samples (Jolles and Lange, 2019). However, all the experimental biotites have slightly higher Mg# (=100 x moles MgO/[moles MgO+MnO+ FeO^{T}]) values (52–56) than those found in the Glass Mountain and Benton Range biotites (mostly 37–42). Interestingly, there is no systematic difference between the Mg# or TiO_2 concentration in the experimental biotite crystals that grew over the range of *T*–*P* experimental run conditions (Table 2–1).

Table 2-3: Averaged analyses experimental biotite grains (wt%)

Sample: Run	BT:1	BT:2	BT:3	BT:7	MC:2	MC:4	MC:5	MC:6	MC:7
Temperature (°C)	800	750	700	750	750	675	750	750	750
Pressure (MPa)	200	200	200	125	200	200	225	150	125
N;n	5;33	2;27	3;54	3;61	3;121	3;129	3;37	2;91	2;66
SiO_2	36.80(1.02)	36.86(54)	36.77(85)	36.61(1.02)	36.86(65)	36.93(73)	36.91(51)	36.25(42)	36.48(59)
TiO_2	4.80(11)	4.76(17)	4.85(08)	4.76(12)	4.90(08)	4.80(29)	4.87(08)	4.96(05)	4.89(09)
Al_2O_3	13.00(59)	13.32(42)	13.17(32)	13.23(77)	13.07(82)	13.03(51)	13.29(80)	12.81(32)	13.25(66)
FeO^T	17.45(1.01)	18.40(98)	19.54(23)	17.88(1.37)	18.14(93)	19.62(1.00)	17.77(38)	18.69(76)	18.02(41)
MnO	0.15(01)	0.19(04)	0.15(01)	0.15(01)	0.18(0.01)	0.18(05)	0.13(02)	0.15(01)	0.13(02)
MgO	12.57(95)	12.12(61)	11.79(40)	12.52(69)	12.72(1.10)	11.95(62)	12.69(20)	12.19(59)	12.67(55)
CaO	0.01(02)	0.05(10)	0.01(06)	0.00(02)	0.00(03)	0.02(07)	0.00(01)	0.02(03)	0.00(01)
Na_2O	0.41(04)	0.44(04)	0.48(03)	0.43(03)	0.54(10)	0.44(09)	0.44(02)	0.46(03)	0.46(03)
K_2O	9.14(29)	9.43(15)	9.31(013)	9.35(19)	9.38(15)	9.48(34)	9.28(11)	9.33(14)	9.33(16)
BaO	0.14 (03)	0.11 (11)	0.14 (03)	0.13 (02)	0.19 (06)	0.09 (07)	0.12 (03)	0.19 (04)	0.03 (02)
Fe_2O_{3calc}	4.94	4.81	5.53	4.87	5.45	5.45	4.92	5.36	4.81
FeO_{calc}	13.01	14.08	14.56	13.50	13.24	14.72	13.35	13.86	13.69
H_2O_{calc}	2.59	2.62	2.62	2.63	2.58	2.64	2.62	2.57	2.62
$Total_{calc}$	97.55	98.78	99.38	98.18	99.10	99.73	98.61	98.16	98.36
[1]Mg#	56	54	52	56	55	52	56	54	56
Fe^{3+}/Fe^T	0.25	0.23	0.25	0.24	0.27	0.25	0.25	0.26	0.24
T. Si	2.86	2.85	2.84	2.84	2.84	2.84	2.84	2.83	2.83
T.Al	0.99	1.01	0.99	1.01	1.00	0.98	1.01	1.00	1.02
$T.Fe^{3+}$	0.16	0.15	0.17	0.16	0.16	0.18	0.15	0.17	0.15
sum Tet	4.00	4.00	4.00	4.00	4.00	4.00	4.00	4.00	4.00
M.Al	0.20	0.21	0.21	0.20	0.19	0.20	0.20	0.18	0.19
M.Mg	1.46	1.39	1.35	1.45	1.46	1.37	1.46	1.42	1.46
$M.Fe^{2+}$	0.84	0.91	0.94	0.88	0.85	0.95	0.86	0.90	0.89
$M.Fe^{3+}$	0.13	0.13	0.15	0.13	0.16	0.14	0.14	0.14	0.13
M.Ti	0.28	0.27	0.28	0.27	0.28	0.27	0.28	0.28	0.28
M.Cr	0.00	0.00	0.00	0.00	0.00	0.00	0.00	0.00	0.00
M.Mn	0.01	0.01	0.01	0.01	0.01	0.01	0.01	0.01	0.01
M.Ni	0.00	0.00	0.00	0.00	0.00	0.00	0.00	0.00	0.00
M.Li	0.00	0.00	0.00	0.00	0.00	0.00	0.00	0.00	0.00
sum oct	2.92	2.92	2.94	2.94	2.95	2.94	2.94	2.94	2.95
Oct Vacancy	0.08	0.08	0.06	0.06	0.05	0.06	0.06	0.06	0.05
A.K	0.91	0.93	0.91	0.92	0.91	0.92	0.91	0.92	0.92
A.Na	0.06	0.07	0.07	0.06	0.08	0.07	0.07	0.07	0.07
A.Ba	0.00	0.00	0.00	0.00	0.01	0.00	0.00	0.01	0.00
A.Ca	0.00	0.00	0.00	0.00	0.00	0.00	0.00	0.00	0.00
sum inter	0.97	1.00	0.99	0.99	1.00	0.99	0.98	1.00	0.99
Inter Vacancy	0.03	0.00	0.01	0.01	0.00	0.01	0.02	0.00	0.01
W.F	0.00	0.00	0.00	0.00	0.00	0.00	0.00	0.00	0.00
W.Cl	0.00	0.00	0.00	0.00	0.00	0.00	0.00	0.00	0.00
W.OH	1.34	1.35	1.35	1.36	1.33	1.36	1.35	1.34	1.35
$W.O^{2-}$	0.66	0.65	0.65	0.64	0.67	0.64	0.65	0.66	0.65

All calculated values and biotite formula are for the average biotite value for each sample using Li et al., 2020

[1]Mg# = molar MgO/(MgO +FeO^T) x100

Parentheses values represent the sample population 1 SD on the last digits

2.6.3 Experimental glass compositions

The average glass composition analyzed in each experimental charge is shown in Table 2–4 and individual spot analyses are shown in Supplemental Table A-0-5. Calculated water contents range from 4.7–6.4 wt% (Zhang et al., 2007), reflecting the P_{H2O} of their experimental calibration (125–225 MPa); the 1SD model uncertainties on the calculated water contents are ± 0.34 wt% (Table 2–4). When these water contents are included, the glass compositional totals range from 98.8–100.2 wt%. The MC–24 experimental glasses have average TiO_2 concentrations that range from 0.06 (±0.03) to 0.14 (± 0.03) wt% across the six experiments, which are generally ≥ the TiO_2 content in the original starting material (0.07 wt%; Supplemental Table A-0-3). In contrast, the average TiO_2 content in each of the BT–3B experimental glasses ranges from 0.10 (± 0.07) to 0.19 (± 0.05) and are generally ≤ the TiO_2 content in the original starting material (0.20 wt%; Supplemental Table A-0-3; Jolles and Lange, 2019). Thus, the glass data appear to show a change in the melt TiO_2 concentration during biotite growth and equilibration in each experimental run.

Table 2-4: Averaged analyses experimental glass (wt%)

Sample: Run	BT:1	BT:2	BT:3	BT:7
Temperature (°C)	800	750	700	750
Pressure (MPa)	200	200	200	125
N;n	N;47	N; 85	N;76	N;99
SiO_2	76.14(74)	77.42(61)	78.09(1.11)	77.18(80)
TiO_2	0.16(03)	0.14(05)	0.10(07)	0.19(05)
Al_2O_3	13.87(25)	12.94(28)	12.37(36)	12.75(26)
FeO^T	0.89(22)	0.65(16)	0.69(27)	0.82(19)
MnO	0.03(02)	0.02(02)	0.02(02)	0.02(02)
MgO	0.08(01)	0.11(14)	0.09(09)	0.16(14)
CaO	1.03(06)	0.76(10)	0.71(09)	0.74(04)
Na_2O	2.99(60)	3.21(37)	3.05(45)	3.03(72)
K_2O	4.82(27)	4.75(19)	4.88(11)	5.10(13)
[1]H_2O	5.86(34)	6.06(34)	6.21(34)	4.74(34)
[1]Total	99.17	100.22	99.18	98.78

Sample: Run	MC:2	MC:4	MC:5	MC:6	MC:7
Temperature (°C)	750	675	750	750	750
Pressure (MPa)	200	200	225	150	125
N;n	N;69	N; 117	N;147	N:31	N;79
SiO_2	78.12(95)	77.77(57)	77.82(72)	78.10(88)	77.85(88)
TiO_2	0.12(03)	0.06(03)	0.12(04)	0.14(03)	0.11(05)
Al_2O_3	12.68(45)	12.66(21)	12.71(21)	12.93(43)	12.74(68)
FeO^T	1.04(28)	0.55(20)	0.87(19)	1.13(13)	0.81(21)
MnO	0.03(02)	0.03(02)	0.02(02)	0.03(02)	0.02(02)
MgO	0.05(01)	0.05(04)	0.06(01)	0.06(01)	0.05(01)
CaO	0.68(06)	0.69(04)	0.70(05)	0.76(06)	0.70(13)
Na_2O	2.74(85)	3.36(46)	2.87(64)	2.35(93)	3.01(74)
K_2O	4.53(21)	4.82(09)	4.81(11)	4.49(24)	4.70(15)
[1]H_2O	6.01(34)	6.3(34)	6.43(34)	5.1(34)	4.71(34)
[1]Total	99.52	99.75	99.61	99.31	99.04

[1]Total + H_2O for given experimental pressure calculated from Zhang et al., 2007

Parentheses values represent the sample population 1 SD on the last digits

2.7 Calibration of a new biotite–liquid thermometer

2.7.1 Construction of D_{TiO2} (bte-liq) values from Glass Mountain natural samples

From the average wt% TiO_2 in biotite for each of the Glass Mountain samples (Table 2–2), together with their respective whole–rock TiO_2 contents (Table A.3), values of $D_{TiO2}^{bte-liq}$ can

be calculated. The resulting $D_{TiO2}^{bte-liq}$ values (61–76) and propagated 1 SD (±8–15) are reported in Table 2–5a. The uncertainties in $D_{TiO2}^{bte-liq}$ are highest for the whole–rock samples with the lowest TiO_2 contents (e.g., 0.06 wt% in GM–01), since the uncertainty of ± 0.01 wt% is independent of total wt% TiO_2.

In the construction of $D_{TiO2}^{bte-liq}$ above, it is assumed that whole–rock concentration of TiO_2 (Table 2–5a) can be used to accurately represent wt% TiO_2 in the coexisting liquid during biotite crystallization in the natural rhyolites. There are three main reasons why this assumption can be made. First, biotite is a near–liquidus phase in high–SiO_2 rhyolite melts and begins to crystallize prior to the tectosilicates (e.g., Fig. 2–2). Therefore, the whole–rock composition represents the liquid composition at the onset of biotite crystallization. Second, the Glass Mountain samples in this study are all are crystal–poor (~1–8%; Gordon et al., 2026), with the tectosilicates accounting for the vast majority (>95%) of the crystals present. The abundance of biotite in each Glass Mountain sample in this study is <1% (Gordon et al., 2026). Third, concentration of TiO_2 in high–SiO_2 rhyolite liquids (X_{TiO2}^{liq}) is related to its activity (a_{TiO2}^{liq}) through the relation, $a_{TiO2}^{liq} = X_{TiO2}^{liq}\gamma_{TiO2}^{liq}$, where γ_{TiO2}^{liq} is a function of melt composition. Ghiorso and Gualda (2013) show that a_{TiO2}^{liq} is buffered during co–crystallization of titanomagnetite and ilmenite, which are both near–liquidus phases with biotite in high–SiO_2 rhyolite melts, through the reaction:

$$Fe_2TiO_4 \text{ (titanomagnetite)} + TiO_2 \text{ (liquid)} = 2FeTiO_3 \text{ (ilmenite)}. \quad (1)$$

Therefore, the initial a_{TiO2}^{liq} at the liquidus (determined by X_{TiO2}^{liq} of the whole–rock liquid) is not expected to change during crystallization. Note also that construction of the $D_{TiO2}^{bte-liq}$ values for the single–clast Bishop Tuff pumice samples from the data of Jolles and Lange (2019),

shown in Figure 2–1, are based on average biotite wt% TiO_2 (Table A.6) and whole–rock wt% TiO_2 values to represent the liquid concentration (Table A.3) for the same three reasons.

Table 2-5 Calculated values of D_{TiO2} (bte-liq) for natural and experimental samples

Sample	GM–01	GM–07	GM–10	GM–18	GM–20
Avg Bte wt% TiO_2	4.57	3.72	4.27	3.74	4.40
± 1 SD	0.06	0.19	0.07	0.22	0.11
WR wt% TiO_2	0.06	0.06	0.07	0.06	0.07
± 1 SD	0.01	0.01	0.01	0.01	0.01
Calculated D_{TiO_2}	76	62	61	62	63
± 1 SD	15	10	8	11	9
$D_{TiO_2}^{bte-liq}$ Temperature (°C)	669	702	704	701	700
± 1 SD (model error)	31	27	22	27	23
Fe–Ti Oxide Temperature (°C)	660	700	695	698	716
Residuals	–9	–2	–9	–3	16

Sample: Run	BT: 1	BT: 2	BT: 3	BT: 7	MC: 2	MC: 4	MC: 5	MC: 6	MC: 7
Avg Bte wt% TiO_2	4.80	4.76	4.85	4.76	4.90	4.80	4.87	4.96	4.89
± 1 SD	0.11	0.17	0.08	0.12	0.08	0.29	0.08	0.05	0.09
Avg Gl wt% TiO_2	0.16	0.14	0.10	0.19	0.12	0.06	0.12	0.14	0.11
± 1 SD	0.03	0.05	0.07	0.05	0.03	0.03	0.04	0.03	0.05
Calculated D_{TiO_2}	30	34	49	25	41	80	41	35	44
± 1 SD	6	12	36	7	10	40	14	8	20
$D_{TiO_2}^{bte-liq}$ Temperature (°C)	776	766	733	788	751	660	752	764	743
± 1 SD (model error)	15	29	77	17	25	92	32	19	47
Exp. set Temperature (°C)	800	750	700	750	750	675	750	750	750
Residuals	24	–16	–33	–38	–1	15	–2	–14	7

2.7.2 Plot of D_{TiO2} (bte-liq) vs Fe–Ti oxide temperature for Glass Mountain samples

Fe–Ti two oxide temperatures are available for the five Glass Mountain samples from the study of Gordon (2022) and reported in Table 2–5a. Average ilmenite and titanomagnetite compositions in each sample are shown in Supplemental Table A-0-7, along with calculated temperatures and oxygen fugacity values (relative to the Ni–NiO buffer) from the thermometer/oxybarometer model of Ghiorso and Evans (2008). All ilmenite and titanomagnetite pairs for the samples in Supplemental Table A-0-7 pass the Mn–Mg equilibrium test of Bacon and Hirschmann (1988) (supplemental discussion in Text A.1). Uncertainties in the

calculated temperatures are ± ≤10°C (based on the number of analyses obtained on titanomagnetite and ilmenite in each sample; see explanation in Gordon, 2022 and Jolles and Lange, 2019).

The calculated values for $D_{TiO2}^{bte-liq}$ for the Glass Mountain samples are plotted as a function of temperature together with those for the natural Bishop Tuff samples from Jolles and Lange (2019) in Figure 2–5. The results show that the linear relationship defined by the Bishop Tuff data (Fig. 2–1) are consistent with the new Glass Mountain data, which extend the linear relationship down to ~660 °C. The next step is to test whether the linear relationship (between $D_{TiO2}^{bte-liq}$ and temperature) defined by the natural samples can be verified by the experimental results obtained in this study.

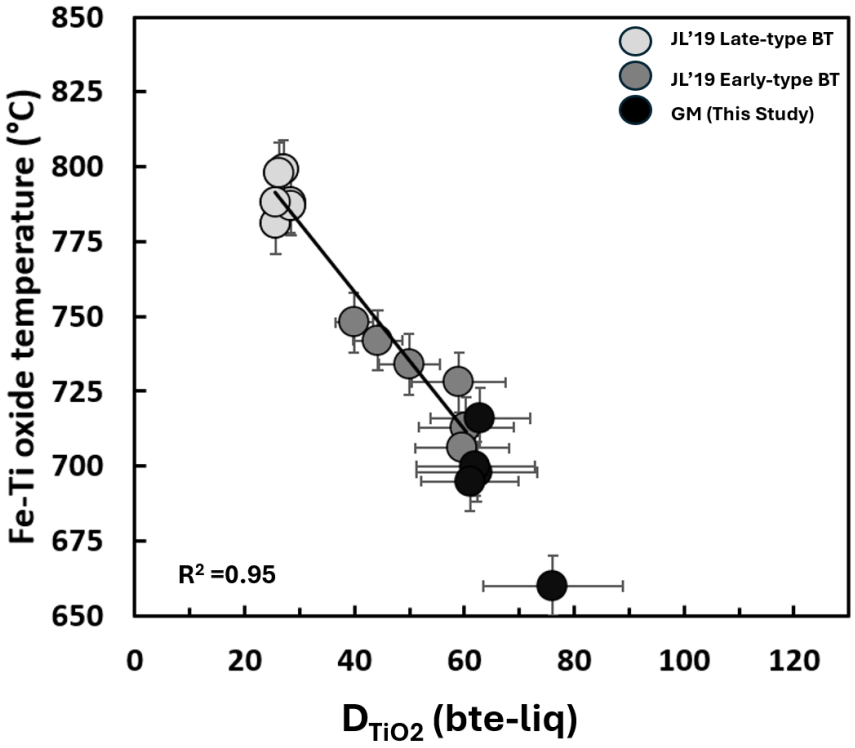


Figure 2-5: Plot of Fe–Ti oxide temperature (°C) vs D_{TiO2} (bte-liq) for natural samples from the Bishop Tuff and new data for the Glass Mountain high–SiO_2 rhyolites. The linear fit solely to the Bishop Tuff samples (R^2=0.95) is extrapolated (dashed line) to lower temperatures, and the new Glass Mountain results fall along the same trend. Error bars represent propagated 1SD.

2.7.3 Construction of D_{TiO2} (bte-liq) values from experimental run products

The average wt% TiO_2 (± 1 SD) in the biotite and glass of each experimental run is summarized in Table 2–5b, together with calculated $D_{TiO2}^{bte-liq}$ values (25–80) and propagated 1SD uncertainties (±6–40) from the analytical uncertainties. The uncertainties in $D_{TiO2}^{bte-liq}$ are highest for runs with experimental glass compositions with the lowest TiO_2 content (i.e., 0.06 ± 0.03 wt% in MC–24 run #4) and the highest variability in the glass compositions (i.e., 0.10 ± 0.07 wt% TiO_2 in BT–3B run #3), as seen in Table 2–5b. The large uncertainty at lower TiO_2 content is due to a larger relative error with EMPA analysis. An improvement on this error at lower TiO_2 contents could be achieved through replications or a more precise method (e.g. TIMS).

2.7.4 Plot of D_{TiO2} (bte-liq) vs experimental pressure under isothermal conditions

For sample MC–24, successful runs were conducted under isothermal conditions (750°C) at four different pressures (225–125 MPa). A plot of $D_{TiO2}^{bte-liq}$ vs pressure is shown in Figure 2–6. There is no resolvable effect of pressure on the $D_{TiO2}^{bte-liq}$ values for sample MC–24. For sample BT–3B, only two successful runs were completed at 750°C (at 200 MPa). When they are plotted with the MC–24 experiments, there is no discernable difference within the propagated uncertainties (± 1 SD.).

Interestingly, the $D_{TiO2}^{bte-liq}$ values for the BT–3B runs are consistently below those for the MC–24 runs at the same experimental pressure (200 and 125 MPa; Fig. 2–6). It is possible that this reflects the approach to biotite–liquid equilibrium (for the partitioning of TiO_2) from two different directions for the BT–3B and MC–24 runs, respectively.

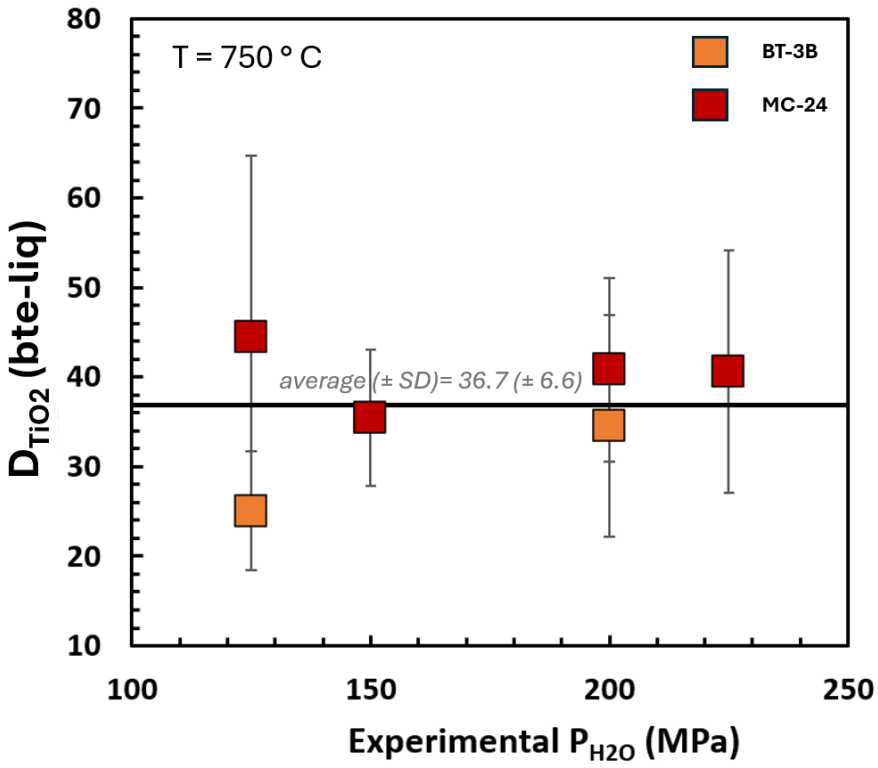


Figure 2-6: Plot of D_{TiO2} (bte-liq) vs. experimental P_{H2O} (MPa) for a set of isothermal 750 °C experiments conducted in this study on two different starting glass materials (MC–24 and BT–3B) of high–SiO_2 rhyolite composition. The average D_{TiO2} (bte-liq) (36.7 ± 6.6) at 750°C is shown as a black line. The results from all experiments fall within error of the average and show no systematic variation with experimental pressure. Error bars represent propagated 1SD.

In the BT–3B runs, the initial liquid TiO_2 concentration was ~0.20 wt%, which changed to lower values in these two runs (Table 2–4) in an approach to equilibrium with the TiO_2 concentration in biotite, which is remarkably similar across all experiments (Table 2–3).

Conversely, in the MC–24 runs, the initial liquid TiO_2 concentration was ~0.07 wt%, which changed to higher values (Table 2–4) in an approach to equilibrium with biotite. If this interpretation is correct, then the two pairs of experiments (one starting with BT–3B and the other with MC–24) present a bracketed approach to equilibrium. Therefore, taking the average of these two pairs of experiments likely provides the best determination of the equilibrium value of $D_{TiO2}^{bte-liq}$ during the 750°C runs at 125 and 200 MPa. The fact that the average (± 1 SD)

$D_{TiO2}^{bte-liq}$ of all six experimental runs (36.7 ± 6.6), shown as the horizontal line in Figure 2–6, runs through the mid–point of the two pairs at 125 and 200 MPa, suggests that it closely matches the equilibrium value of $D_{TiO2}^{bte-liq}$ at 750°C.

The results in Figure 2–6 for both MC–24 and BT–3B confirm there is no resolvable pressure dependence between 125–225 MPa. This interval overlaps that pressure interval of crystallization of the Bishop Tuff high–SiO_2 rhyolites (~100–250 MPa) on the basis of calculations from fluid–saturated melt entrapped in quartz (Wallace et al., 1999; Anderson et al., 2000; Roberge et al., 2013) and geobarometry results from Rhyolite–MELTS (Ghiorso and Gualda, 2013; Gualda et al., 2022).

2.7.5 Plot of D_{TiO2} (bte-liq) vs experimental temperature

Since there is no evidence that there is a resolvable pressure dependence to $D_{TiO2}^{bte-liq}$ between 225 and 125 MPa, the experimental results can be evaluated for a temperature dependence. The calculated values for $D_{TiO2}^{bte-liq}$ from the experimental runs are plotted as a function of experimental temperature together with those for the natural Glass Mountain and Bishop Tuff data (plotted against Fe–Ti oxide temperatures) in Figure 2–7. Also shown on this plot are the experimental results from Bolte et al. (2015), which were previously shown in Figure 2–1. Collectively, the experimental results are consistent with those for the natural data, despite relatively large experimental uncertainties in $D_{TiO2}^{bte-liq}$ due to low TiO_2 wt% in the glass at the lowest temperatures (700 and 675 °C) compared to those for the natural data. Although more replicate experiments are needed at 800, 700 and 675 °C for both BT–3B and MC–24, the experimental results from this study corroborate the results from the natural data.

2.7.6 Calibration of a new thermometer based on natural and experimental HSR samples

The experimental results in Figure 2–6 for both MC–24 and BT–3B confirm there is no resolvable pressure dependence between 125–225 MPa. This interval overlaps that pressure interval of crystallization of the Bishop Tuff high–SiO_2 rhyolites (~100–250 MPa) on the basis of calculations from fluid–saturated melt entrapped in quartz (Wallace et al., 1999; Anderson et al., 2000; Roberge et al., 2013) and geobarometry results from Rhyolite–MELTS (Ghiorso and Gualda, 2013; Gualda et al., 2022). Therefore, the data obtained in this study can be used to calibrate a new biotite–liquid thermometer applicable to high–SiO_2 rhyolites that crystallized at upper crustal conditions.

In Figure 2–7, the natural data from the Bishop Tuff (Jolles and Lange, 2019;Table A.8) and Glass Mountain (this study; Table 2–5a) are combined with the experimental results of Bolte et al. (2015; Supplemental Table A-0-8) and this study (Table 2–5). A linear fit to all data leads to the following equation:

$$T\,(^{\circ}\mathrm{C}) = 846\ (\pm 7) - 2.32(\pm 0.15) * D_{TiO2}^{bte-liq} \qquad (2)$$

The linear fit in Eq. 2 has a standard error on the estimate of ± 14 °C and a R^2 value of 0.90. Among the natural samples in Figure 2–7, calculated temperatures (via Eq. 2) deviate from Fe–Ti two–oxide temperatures by values that range from +19 to –9 °C, with an average deviation of 8°C. Among the experimental results, calculated temperatures differ from experimental temperatures by +24 to –38 °C, with an average deviation of 14°C. The largest experimental residuals are from the BT–3B runs (+ 24 to –38°C), whereas the residuals from the MC–24 runs (+15 to –14°C) and the Bolte et al. (2015) runs (+11 to +3 °C) are significantly lower. Additional experiments are needed to test whether it takes longer to approach equilibrium in experiments with a starting glass material that has a higher initial TiO_2 concentration than equilibrium values (e.g., the case for the BT–3B runs in this study).

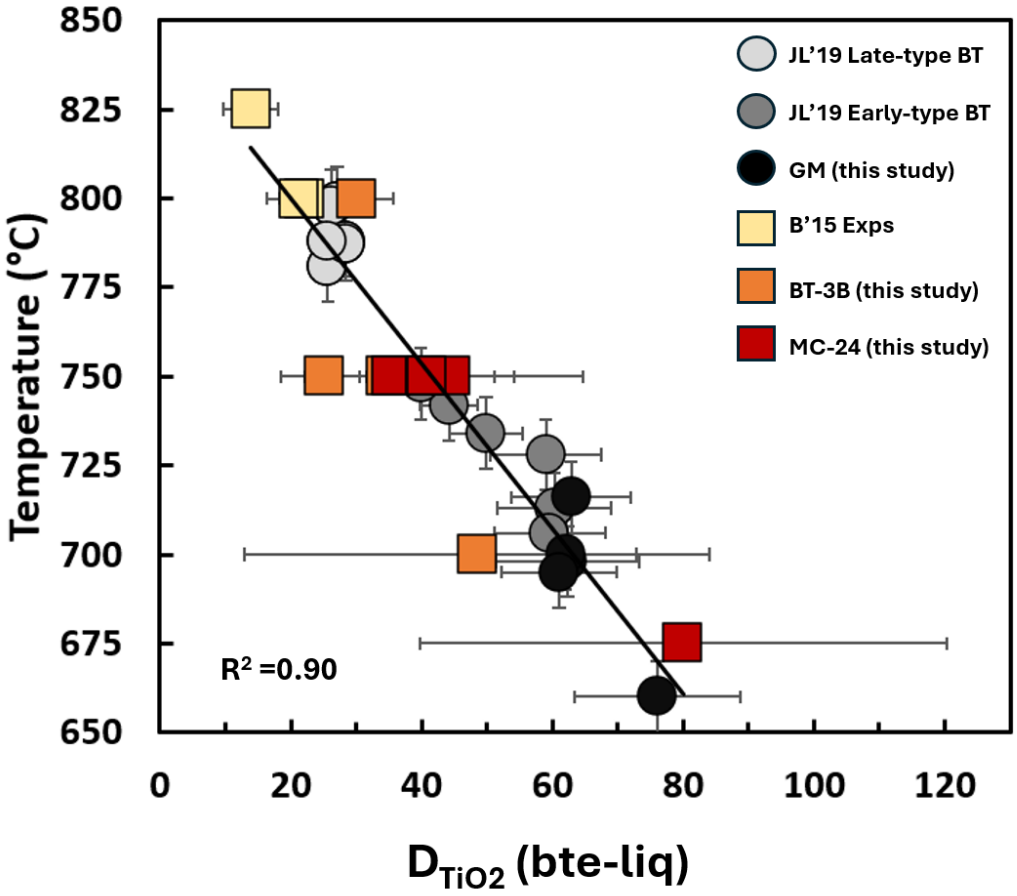


Figure 2-7**:** Plot of temperature (°C) vs D_{TiO2} (bte-liq) for all natural high–SiO_2 rhyolite samples and experiments on high–SiO_2 rhyolite composition. A linear fit through all the data is shown (R^2 = 0.90). The experimental results confirm the trend observed in the natural data, which is based on Fe–Ti two–oxide thermometry. Note that large error bars of experimental data points at lower temperature is due to the relative error of low TiO_2 in the glass (see text for more). The linear fit can be used as a biotite–liquid thermometer for high–SiO_2 rhyolite melts: T(°C) = 846 (±7) – 2.32 (±0.15)*$D_{TiO_2}^{bte-liq}$. Error bars represent propagated 1SD.

Overall, the linear fit to the combined data in Figure 2–7 closely recovers both the Fe–Ti two–oxide temperatures obtained for the natural samples and the experimental temperatures. This result provides strong evidence that the Fe–Ti two–oxide thermometer of Ghiorso and Evans (2008), when applied to pristine ilmenite and titanomagnetite (following analytical protocols outlined in Jolles and Lange, 2019) in high–SiO_2 rhyolite melts leads to calculated temperatures that are consistent with experimental temperatures (measured with a K–type thermocouple) during cold–seal pressure vessel runs.

2.8 Test of new thermometer applied to Jurassic HSR dikes

The new Ti–based biotite–liquid thermometer in Eq. 2 can be tested through application to the Benton Range suite of high–SiO_2 rhyolite dikes of Jurassic age (Renne and Turrin, 1987). These porphyritic dikes were previously studied by Mesa (2021), where whole–rock analyses are reported and the presence of allanite noted in several samples. A photomicrograph of allanite in sample CD–18–09 is shown in Figure A-0-1. The significance of allanite is that it has an experimentally demonstrated thermal stability limit of ≤ 770 °C in high-SiO_2 rhyolite compositions (Vasquez et al., 2004), and thus application of Eq. 2 to the Benton Range dikes permits a test of the accuracy of the new Ti–based biotite–liquid thermometer.

Table 2-6: Calculated values of D_{TiO2} (bte-liq) and temperature for natural samples

Sample	CD–18–09	CD–18–12	CD–18–14–2	CD–18–16
Avg Bte wt% TiO_2	3.25	3.08	3.11	3.07
± 1 SD	0.51	0.53	0.32	0.31
WR wt% TiO_2	0.11	0.11	0.12	0.08
± 1 SD	0.01	0.01	0.01	0.01
Calculated D_{TiO_2}	30	28	26	38
± 1 SD	5	5	3	6
$D_{TiO_2}^{bte-liq}$ Temperature (°C)	777	781	786	757
± 1 SD (model error)	14	14	10	16

From the average wt% TiO_2 in biotite for each of four Benton Range dike samples (Table 2–2), together with their respective whole–rock TiO_2 content (Mesa, 2021;Table A.3), $D_{TiO2}^{bte-liq}$ can be calculated. The resulting $D_{TiO2}^{bte-liq}$ values (26–38) and propagated uncertainties (±3–6) are reported in Table 2–6. Input of these values into Eq. 2 leads to calculated temperatures of 757–786 °C, with propagated uncertainties (from both analytical and model errors) of ±10–16 °C. Specifically, the calculated biotite crystallization temperature for sample CD–18–09 is 778 ± 14

°C, which is within error of the thermal stability limit of allanite (≤ 770 °C) and thus confirms its accuracy.

It is noteworthy that the new Ti–based biotite–liquid thermometer (Eq. 2) can be successfully applied to a high–SiO_2 rhyolite dike of Jurassic age. Typically, it is difficult to obtain magmatic temperatures for rhyolites of this age owing to the effects of alteration, especially of the Fe–Ti oxides, which precludes application of the Ghiorso and Evans (2008) thermometer. This study shows that if pristine portions of biotite can be analyzed in older high–SiO_2 rhyolite samples, even those of Jurassic age, then accurate temperatures can be obtained.

2.9 Conclusions

There are several key conclusions that can be drawn from this study. First, when $D_{TiO2}^{bte-liq}$ values are obtained on natural high–SiO_2 rhyolite samples from the Bishop Tuff (Jolles and Lange, 2019) and Glass Mountain (this study), by pairing the average wt% TiO_2 in biotite phenocrysts with the whole–rock TiO_2 content, they form a strong linear correlation with temperatures obtained for each sample using the Fe–Ti two–oxide thermometer (Ghiorso and Evans, 2008) over a temperature interval of ~800–660°C (Fig. 2–5).

Second, a series of biotite–liquid equilibrium experiments conducted on two high–SiO_2 rhyolite 100% glasses with different initial TiO_2 contents (0.20 and 0.07 wt%), under pure–H_2O fluid–saturated conditions, enabled experimental values of $D_{TiO2}^{bte-liq}$ to be obtained over temperatures and pressures of 675–800 °C and 125–225 MPa. The results on six isothermal runs at 750 °C show there is no pressure dependence to $D_{TiO2}^{bte-liq}$ for high–SiO_2 rhyolite melts between 125 and 225 MPa (Fig. 2–6), which overlaps the pressure interval for phenocryst growth in the high–SiO_2 rhyolite portion of the Bishop Tuff (e.g., Roberge et al., 2013; Gualda et al., 2022). Additionally, experimental results on starting glasses with different initial TiO_2 contents, but

identical run conditions at 750°C, enabled a bracketed approach to biotite–liquid equilibrium (in terms of the partitioning of TiO_2) at 125 and 200 MPa. The results strongly support a close approach to biotite–liquid equilibrium, within analytical error, over the duration of the experiments (182 h) in this study.

Third, when the $D_{TiO2}^{bte-liq}$ experimental values from this study are combined with those from Bolte et al. (2015) and plotted versus experimental temperature, the results overlap $D_{TiO2}^{bte-liq}$ values obtained on the natural high–SiO_2 rhyolites (Bishop Tuff and Glass Mountain, CA) when plotted against temperature. A linear fit to the combined experimental and natural data (Fig. 2–1), with a SEE of ± 14 °C and R^2 of 0.90, provides the calibration for a new biotite–liquid thermometer (Eq. 2), which recovers the experimental temperatures within 12 degrees, on average, and the natural Fe–Ti oxide temperatures within 8 degrees, on average. Thus, the data obtained from this study demonstrate the internal consistency between Fe–Ti two–oxide thermometry applied to high–SiO_2 rhyolites and experimental temperatures (K–type thermocouple) in cold–seal pressure vessels.

Fourth, application of the new biotite–liquid thermometer (Eq. 2) to the Benton Range high–SiO_2 rhyolite dikes (from eastern CA) of Jurassic age led to temperatures that range from 757–786 °C, with propagated 1SD errors of ± 10–16 °C. These results are consistent with the presence of allanite in several of these dikes, which has a thermal stability limit of ≤ 770 °C in high-SiO_2 rhyolite (Vasquez et al., 2004). It is therefore possible to apply this new biotite–liquid thermometer to numerous high–SiO_2 rhyolite samples of varying age, both volcanic and plutonic, which have been otherwise intractable to Fe–Ti two–oxide thermometry owing to alteration.

2.10 References

Anderson AT, Davis AM, Lu F (2000) Evolution of Bishop Tuff rhyolitic magma based on melt and magnetite inclusions and zoned phenocrysts. J Petrol 41:449–473

Bacon CR, Hirschmann MM (1988) Mg/Mn partitioning as a test for equilibrium between coexisting Fe–Ti oxides. Am Mineral 73:57–61

Benisek, A., Kroll, H., & Cemič, L. (2004). New developments in two–feldspar thermometry. *American Mineralogist*, *89*(10), 1496–1504. https://doi.org/10.2138/am–2004–1018

Bindeman IN, Valley JW (2002) Oxygen isotope study of the Long Valley magmatic system, California: isotope thermometry and convection in large silicic magma bodies. Contrib Mineral Petrol 144:185–205

Boehnke P, Watson EB, Trail D, Harrison TM, Schmitt AK (2013) Zircon saturation re–visited. Chemical Geology 351:324–334

Bolte, T., Holtz, F., Almeev, R., & Nash, B. (2015). The Blacktail Creek Tuff: an analytical and experimental study of rhyolites from the Heise volcanic field, Yellowstone hotspot system. *Contributions to Mineralogy and Petrology*, *169*(2). https://doi.org/10.1007/s00410–015–1112–0

Chamberlain, K.J., Wilson, C.J.N., Wooden, J.L, Charlier, B.L.A. & Ireland, T.R. (2014) New perspectives on the Bishop Tuff from zircon textures, ages and trace elements. Journal of Petrology, 55, 395–426.

Charles H. Nielsen, Haraldur Sigurdsson; Quantitative methods for electron microprobe analysis of sodium in natural and synthetic glasses. American Mineralogist 1981;; 66 (5–6): 547–552. Doi

Christiansen, R.L. 2001. The Quaternary and Pliocene Yellowstone Plateau volcanic field of Wyoming, Idaho, and Montana. U.S. Geological Survey Professional Paper 729–G:145

Crisp, L. J., Berry, A. J., Burnham, A. D., Miller, L. A., & Newville, M. (2023). The Ti–in–zircon thermometer revised: The effect of pressure on the Ti site in zircon. *Geochimica Et Cosmochimica Acta*, *360*, 241–258. https://doi.org/10.1016/j.gca.2023.04.031

Davies, G.R., Halliday, A.N., Mahood, G.A. & Hall, C.M. (1994). Isotopic constraints on the production rates, crystallization histories and residence times of pre–caldera silicic magmas, Long Valley, California. Earth and Planetary Science Letters, 125(4), 17–37

Douce, A. E. P., & Beard, J. S. (1995). Dehydration–melting of Biotite Gneiss and Quartz Amphibolite from 3 to 15 kbar. *Journal of Petrology*, *36*(3), 707–738. https://doi.org/10.1093/petrology/36.3.707

Douce, A. E. P., & Beard, J. S. (1996). Effects of P , f (O2) and Mg/Fe Ratio on Dehydration Melting of Model Metagreywackes. *Journal of Petrology*, *37*(5), 999–1024. https://doi.org/10.1093/petrology/37.5.999

Elkins, L. T., & Grove, T. L. (1990). Ternary feldspar experiments and thermodynamic models. *American Mineralogist*, *75*, 544–559. https://asu.pure.elsevier.com/en/publications/ternary–feldspar–experiments–and–thermodynamic–models

Ewart, A., & Griffin, W. (1994). Application of proton–microprobe data to trace–element partitioning in volcanic rocks. *Chemical Geology*, *117*(1–4), 251–284. https://doi.org/10.1016/0009–2541(94)90131–7

Farges, F., Brown, G. E., & Rehr, J. J. (1997). TiK–edge XANES studies of Ti coordination and disorder in oxide compounds: Comparison between theory and experiment. *Physical Review. B, Condensed Matter*, *56*(4), 1809–1819. https://doi.org/10.1103/physrevb.56.1809

Ferry, J.M., and Watson, E.B., 2007, New thermodynamic models and revised calibrations for the Ti–in–zircon and Zr–in–rutile thermometers: Contributions to Mineralogy and Petrology, v. 154, p. 429–437, doi:10.1007/s00410 –007–0201–0.

Gardner JE, Befus KS, Gualda GAR, Ghiorso MS (2014) Experimental constraints on rhyoliteMELTS and the Late Bishop Tuff magma body. Contrib Mineral Petrol 168:1051

Geschwind CH, Rutherford M (1995) Crystallization of microlites during magma ascent: the flui mechanics of 1980–1986 erup– tions at Mount St Helens. Bull Volc 57:356–370

Ghiorso, M.S. & Evans, B.W. (2008) Thermodynamics of rhombohedral oxide solutions and revision of the Fe–Ti two–oxide geothermometer and oxygen barometer. American Journal of Science, 308, 957–1039.

Ghiorso MS, Gualda GAR (2013) A method for estimating the activity of titania in magmatic liquids from the compositions of coexisting rhombohedral and cubic iron–titanium oxides. Contrib Mineral Petrol 165:73–81

Gordon, B. (2022). The generation of geochemical gradients in the pre–caldera Glass Mountain high–SiO2 rhyolites of Long Valley, CA: clues to the origin and preservation of Rb–Sr isochrons. Deep Blue (University of Michigan). https://doi.org/10.7302/6563

Gualda, G. a. R., Ghiorso, M. S., Hurst, A. A., Allen, M. C., & Bradshaw, R. W. (2022). A complex patchwork of magma bodies that fed the Bishop Tuff supereruption (Long Valley Caldera, CA, United States): Evidence from matrix glass major and trace–element compositions. *Frontiers in Earth Science*, *10*. https://doi.org/10.3389/feart.2022.798387

Hildreth EW (1977) The magma chamber of the Bishop Tuff: gradients in temperature, pressure, and composition. PhD thesis. University of California, Berkeley, California

Hildreth, W. (1979) The Bishop Tuff: evidence for the origin of compositional zonation in silicic magma chambers. In: Chapin, C.E. & Elston, W.E. (eds) Ash–flow tuffs. Geological Society of America Special Paper, 180, 43–75.

Hildreth, W. & Wilson, C.J. (2007) Compositional zoning of the Bishop Tuff. Journal of Petrology. 48:951–999.

Holtz, F. O., & Johannes, W. (1991). Genesis of Peraluminous Granites I. Experimental Investigation of Melt Compositions at 3 and 5 kb and Various H2O Activities. *Journal of Petrology*, *32*(5), 935–958. https://doi.org/10.1093/petrology/32.5.935

Huang R, Audétat A (2012) The titanium–in–quartz (TitaniQ) thermobarometer: a critical examination and re–calibration. Geochim Cosmochim Acta 84:75–89

Jolles, J. S. R., & Lange, R. A. (2019). High–resolution Fe–Ti oxide thermometry applied to single–clast pumices from the Bishop Tuff: a re–examination of compositional variations in phenocryst phases with temperature. Contributions to Mineralogy and Petrology, 174(8). https://doi.org/10.1007/s00410–019–1597–z

Li, X., & Zhang, C. (2022). Machine Learning thermobarometry for Biotite-Bearing magmas. *Journal of Geophysical Research Solid Earth*, *127*(9). https://doi.org/10.1029/2022jb024137

Li, X., Zhang, C., Behrens, H., & Holtz, F. (2020). Calculating biotite formula from electron microprobe analysis data using a machine learning method based on principal components regression. Lithos, 356–357, 105371. https://doi.org/10.1016/j.lithos.2020.105371

Putirka KD (2008) Thermometers and barometers for volcanic systems. Rev Mineral Geochem 69:61–120

Mahood G, Hildreth W (1983) Large partition coefficients for trace elements in high–silica rhyolites. Geochim Cosmochim Acta 47:11–30

Meszaros, N. F., Zimmerer, M. J., & Gardner, J. E. (2024). Evolution of eruption rate between two caldera–forming eruptions in the Jemez Mountains volcanic field, New Mexico, USA. *Journal of Volcanology and Geothermal Research*, *457*, 108216. https://doi.org/10.1016/j.jvolgeores.2024.108216

Mesa, J. (2021). Evidence of Phenocryst Growth and Magma Mixing during Ascent along Fractures in Volcanic Rocks from Basalt to Rhyolite. *Deep Blue (University of Michigan)*. https://doi.org/10.7302/2876

Morgan, G. B., & London, D. (1996). Optimizing the electron microprobe analysis of hydrous alkali aluminosilicate glasses. American Mineralogist, 81(9–10), 1176–1185. https://doi.org/10.2138/am–1996–9–1016

Putirka, K. D., Perfit, M., Ryerson, F. J., & Jackson, M. G. (2007). Ambient and excess mantle temperatures, olivine thermometry, and active vs. passive upwelling. Chemical Geology, 241(3–4), 177–206

Renne, P.R., and Turrin, B.D. (1987) Constraints on timing of deformation in the Benton Range, southeastern California, and implications to Nevadan orogenesis: Geology, 15, 1031–1034.

Roberge J, Wallace PJ, Kent AJR (2013) Magmatic processes in the Bishop Tuff rhyolitic magma based on trace elements in melt inclusions and pumice matrix glass. Contrib Mineral Petrol 165:237–257

Scaillet, B. (2003). Experimental Constraints on the Relationships between Peralkaline Rhyolites of the Kenya Rift Valley. *Journal of Petrology*, *44*(10), 1867–1894. https://doi.org/10.1093/petrology/egg062

Thomas JB, Watson EB, Spear FS, Shemella FS, Nayak SK, Lanzirotti A (2010) TitaniQ under pressure: the effect of pressure and temperature on the solubility of Ti in quartz. Contributions to Mineralogy and Petrology 160:743–759

Thomas JB, Watson EB, Spear FS, Wark DA (2015) TitaniQ recrystallized: experimental confirmation of the Ti–in–quartz calibrations. Contrib Mineral Petrol 169:27

Vazquez, J. A., Manning, C. E., & Reid, M. R. (2004). Experimental determination of allanite stability in High–Silica rhyolite. *AGU Fall Meeting Abstracts*, *2004*. http://ui.adsabs.harvard.edu/abs/2004AGUFM.V41C1407V/abstract

Venezky, D. Y., & Rutherford, M. J. (1999). Petrology and Fe–Ti oxide reequilibration of the 1991 Mount Unzen mixed magma. *Journal of Volcanology and Geothermal Research*, *89*(1–4), 213–230. https://doi.org/10.1016/s0377–0273(98)00133–4

Wallace, P.J., Anderson, A.T, and Davis, A. M. (1999) Gradients in H2O, CO2, and exsolved gas in a large–volume silicic magma system: Interpreting the record preserved in melt inclusions from the Bishop Tuff. Journal of Geophysical Research, v. 104, p. 20097–20122.

Wark DA, Watson EB (2006) The TitaniQ: a titanium–in–quartz geothermometer. Contrib Mineral Petrol 152:743–754

Waters, L.E. & Andrews, B.J. (2016) The role of superheating in the formation of Glass Mountain obsidians (Long Valley, CA) inferred through crystallization of sanidine. Contributions to Mineralogy and Petrology, 171, 79.

Watson EB, Wark DA, Thomas JB (2006) Crystallization thermometers for zircon and rutile. Contrib Mineral Petrol 151:413–433

Watson EB, Harrison TM (1983) Zircon saturation revisited: temperature and composition effects in a variety of crustal magma types. Earth Planet Sci Lett 64:295–304

Were, P., & Keppler, H. (2021). Trace element fractionation between biotite, allanite, and granitic melt. *Contributions to Mineralogy and Petrology*, *176*(9). https://doi.org/10.1007/s00410–021–01831–3

Wilson CJN, Hildreth W (1997) The Bishop Tuff: new insights from eruptive stratigraphy. J Geol 105: 407:439

Zhang, Y., Xu, Z., Zhu, M., & Wang, H. (2007). Silicate melt properties and volcanic eruptions. *Reviews of Geophysics*, *45*(4). https://doi.org/10.1029/2006rg000216

Zhang, C., Li, X., Almeev, R. R., Horn, I., Behrens, H., & Holtz, F. (2020). Ti–in–quartz thermobarometry and TiO2 solubility in rhyolitic melts: New experiments and parametrization. *Earth and Planetary Science Letters*, *538*, 116213. https://doi.org/10.1016/j.epsl.2020.11621

Chapter 3 Phenocryst Compositions, Textures, and Abundances in Glass Mountain, CA High–SiO_2 Rhyolites and Experimental Constraints: Evidence for Rapid Crystal Growth During Ascent

Abstract:

The Glass Mountain (GM) volcanic complex in Long Valley, CA erupted ~100 km^3 of high–SiO_2 rhyolite between 2.1 and 0.8 Ma, directly preceding the climactic eruption (>600 km^3) of the Bishop Tuff (BT). A notable feature of the GM rhyolites, which are all near–eutectic melts with little variation in their major–element compositions, is their highly variable crystal contents (<1 to 20%). At least one eruptive unit (OC), with 8% phenocrysts, has a previously determined Fe–Ti two–oxide temperature of 660 (±10) °C, which is below the water–saturated granitic solidus at $P_{H2O} \leq 300$ MPa (Johannes and Holz, 1996). In this study, we test three different hypotheses to explain the variable phenocryst abundances in the GM units, including unit OC: (1) they reflect equilibrium T–P_{H2O} conditions in a magmatic reservoir prior to eruption; (2) the water–saturated granitic solidus is lower than previously documented, or (3) phenocryst growth in the GM units occurred rapidly during ascent after an initial kinetic delay to nucleation. To investigate these hypotheses, a pair of water–saturated experiments were performed in this study at 650 °C and 200 MPa on a representative high–SiO_2 rhyolite (using two temperature–path trajectories: bottom–up and top–down) and combined with previously published water–saturated phase–equilibrium and decompression experiments at 700–850 °C and 75–225 MPa. In addition, the textures and compositions of plagioclase, sanidine, and biotite in several GM units were obtained, enabling biotite–liquid thermometry and sanidine hygrometry to be combined with

previously published Fe–Ti oxide thermometry. The results (660–725 °C; 4.8–5.3 wt% H_2O) lead to several inconsistencies in the predicted phenocryst assemblages and abundances when compared to equilibrium experimental results, which eliminates the first hypothesis. The second hypothesis was tested through the bottom–up experiment, which confirmed complete crystallization under water–saturated conditions at 650 °C at 200 MPa. Thus, the low (8%) phenocryst abundance in unit OC, which is expected to exceed 20% based on thermometry and hygrometry results, is not explained by a mislocated water–saturated solidus. The third hypothesis was tested by the top–down experiment conducted in this study, which induced a kinetic delay and thus an undercooling of ~50°C at the onset of crystal growth in the experimental run at 650 °C and P_{H2O} = 200 MPa. Phenocryst–sized (~200–300 μm) quartz and sanidine, with rapid growth textures (e.g, hopper, swallowtail) were found in the run products, along with granophyric intergrowths and ~40% glass. The crystal textures match those found among the phenocrysts in the GM natural samples. Therefore, the only viable hypothesis that explains the phenocryst abundances and textures in the GM eruptive units is that crystal growth occurred rapidly, during dike ascent to the surface, and not slowly within a stalled magma chamber.

3.1 Introduction

The Glass Mountain (GM) high–SiO_2 (77–78 wt%) rhyolites in Long Valley, California (Figure 3–1) are among the most differentiated silicate magmas on Earth (Metz and Mahood, 1991) and thus closely match eutectic melt compositions in the quartz–plagioclase–orthoclase–H_2O system (Tuttle and Bowen, 1955; Johannes and Holtz, 1996). The GM volcanic complex erupted ~100 km^3 of high–SiO_2 rhyolite between 2.2 and 0.8 Ma (Metz and Mahood, 1985; Hildreth, 2004), directly proceeding the climactic eruption of the Bishop Tuff at ~766.5 ± 0.5 ka

(Mark et al., 2017). The GM units are divided into two groups based on age (Figure 3–2), with eruption of the Older GM units (~25 km^3) prior to 1.2 Ma and the Younger GM units (~75 km^3) after 1.2 Ma (Metz and Mahood, 1985; Davies et al., 1994; Hildreth, 2004; Simon et al., 2014).

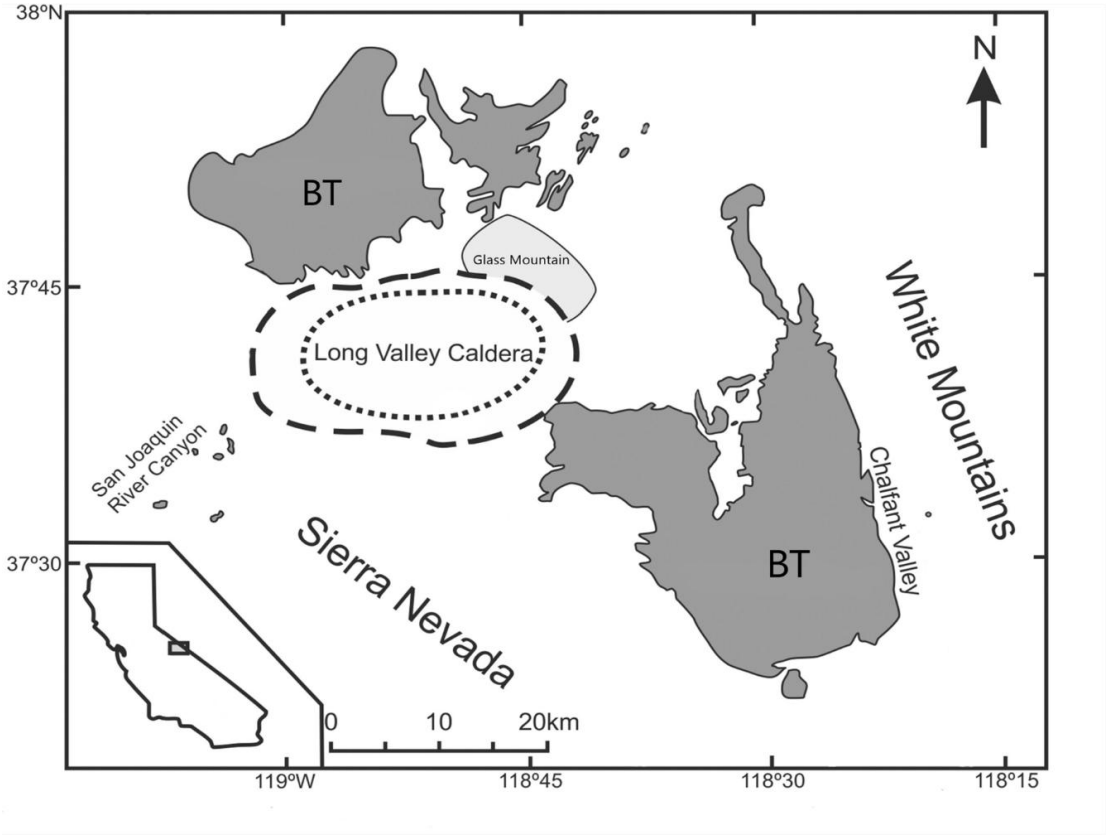


Figure 3-1**:** Location map of the Glass Mountain volcanic complex and Long Valley Caldera, California modified from Chamberlin et al. (2015). The current topographic expression of the caldera rim is shown by the outer dashed line, whereas the estimated ring fracture is shown by dotted line. Glass Mountain is shown in light gray, and the Bishop Tuff (BT) is shown in dark gray.

In a petrological study of the GM suite, Metz and Mahood (1991) found that despite little variation in the major–element compositions of the high–SiO_2 rhyolites, they contain a wide range of phenocryst abundances (<1 to 20%), dominated by quartz, sanidine and plagioclase, with subordinate biotite, titanomagnetite, ilmenite, zircon, apatite and allanite commonly present. Among the 38 eruptive GM units described by Metz and Mahood (1991), 31 (78%) contain <1 to 3% phenocrysts, seven (18%) contain 6–8% phenocrysts, and a single unit contains 20%

phenocrysts. Although the unit with the highest phenocryst abundance is from the Older GM suite (unit OD), both the Older and Younger GM units have phenocryst abundances that range from <1 to 7%. Available Fe–Ti oxide thermometry applied to various GM units (Metz and Mahood, 1991; Gordon, 2022) show that there is no clear correlation between temperature and phenocryst abundance. Moreover, at least one Older GM unit (OC with 8% phenocrysts) has an Fe–Ti oxide temperature of 660 (± 10) °C (Gordon, 2022), which is below the water–saturated solidus temperature of 680 °C at P_{H2O} = 200 MPa for the minimum/eutectic melt in the quartz–albite–orthocase–H_2O system, determined experimentally in reversed experiments by Ebadi and Johannes (1991). This implies that either the unit OC melt crystallized at relatively high P_{H2O} conditions (≥300 MPa) or the water–saturated granite solidus is lower than previously understood (e.g., Thompson et al., 2026). A third possibility is that phenocryst growth in the unit OC melt occurred during ascent, driven by degassing, following a kinetic delay to nucleation (e.g., Waters and Lange, 2017). Given these different explanations, the primary goal of this study is to evaluate three distinct hypotheses to understand the cause for the observed (and highly variable) phenocryst abundances in the different GM units with very similar major–element compositions.

The first hypothesis is the most straightforward: that the phenocryst content in each GM sample reflects the equilibrium abundance, which varies between units due to differences in the temperature and melt water content during phenocryst growth in a magmatic reservoir prior to eruption. To explore this explanation, it is necessary to obtain as much information as possible on the temperature and H_2O concentration in the melt at the time of phenocryst growth in various GM units that span a range of crystallinity. The next step is to compare the results with available phase–equilibrium experiments that have been conducted on a GM high–SiO_2 rhyolite over

relevant $T–P_{H2O}$ conditions with reported crystal phases and abundances (i.e., Waters and Andrews, 2016). As noted above, Fe–Ti two–oxide thermometry has previously been applied to the GM suite (Metz and Mahood, 1991; Gordon, 2022). In this study, we additionally deploy the new biotite–liquid thermometer from Chapter 2. This enables thermometry to be obtained on GM units where ilmenite is absent (due to exceptionally low crystallinities) or where Fe–Ti oxides are altered. Other thermometers (e.g., zircon–saturation; two–feldspar) are not deployed because they have not been directly calibrated on high–SiO_2 rhyolites, with the potential for systematic errors. To constrain H_2O melt concentrations at the time of phenocryst growth, we utilize the sanidine hygrometer from Waters and Andrews (2016). Collectively, these data will allow each GM unit to be placed on the equilibrium phase diagram constructed by Waters and Andrews (2016) for high–SiO_2 rhyolite, enabling a comparison between the observed abundance and composition of tectosilicates in each natural sample to those obtained under equilibrium conditions.

The second hypothesis is that the water–saturated solidus of high–SiO_2 rhyolite (leucogranite) is lower than that previously documented by Ebadi and Johannes (1991). In a recent paper, Thompson et al. (2026) present crystallization experiments on a high–SiO_2 rhyolite under water–saturated conditions at 200 MPa. Their quenched run products from experiments held for five days at 625 and 640 °C contained ~4% and ~20% melt, respectively. This result led Thompson et al. (2026) to place the water–saturated solidus at ~620–625 °C, which contradicts the water–saturated solidus of 680 °C at a P_{H2O} = 200 MPa of Ebadi and Johannes (1991). It is noteworthy that Ebadi and Johannes (1991) report complete crystallization at 670°C and significant melt present at 690 °C, and thus estimate the location of the solidus at the midpoint of 680 °C. Therefore, it may be more accurate to report a water–saturated minimum–melt solidus

temperature of ≥ 670 °C at 200 MPa from the experiments of Ebadi and Johannes (1991), which is still ~50 degrees higher than indicated by the experiments of Thompson et al. (2026). To help resolve the difference between these results, and to provide an inter–laboratory comparison, one of the objectives of this study is to perform a pair of crystallization experiments on a water–saturated, high–SiO_2 rhyolite glass powder at 650 °C and P_{H2O} = 200 MPa in a cold–seal pressure vessel for 30 and 25 days. The goal of this study is to evaluate whether results are consistent with those of Thompson et al. (2026) or Ebadi and Johannes (1991), and what implications there may be for the GM unit (OC) which has a Fe–Ti two–oxide temperature of 660 (±10) °C and only 8% phenocrysts.

The third hypothesis is that phenocryst growth in the GM high–SiO_2 rhyolites occurred during ascent, due to degassing, following a kinetic delay to nucleation. As noted in previous studies (e.g., Waters and Andrews, 2016; Waters and Lange, 2017), if a high–SiO_2 rhyolite melt segregates from its source region under fluid–undersaturated conditions, its liquidus temperature will decrease during ascent along a dike (due to decreasing pressure), leading to super–liquidus (nuclei–free) conditions. Eventually, due to the presence of dissolved water (± CO_2) in the ascending melts, saturation with a fluid phase will occur. At this point, the liquidus temperature will begin to increase with continued ascent (due to loss of dissolved water in the melt) until the temperature of the ascending rhyolite crosses below its liquidus temperature. However, a kinetic delay to nucleation is expected, which will cause an undercooling ($\Delta T = T_{liquidus} - T_{melt}$) to develop where nucleation rates are low (but non–zero) and crystal growth rates are high (e.g., Lofgren et al., 1974). This will lead to the crystallization of large, sparse tectosilicate phenocrysts, as observed in the Glass Mountain rhyolites (Metz and Mahood, 1991). This third hypothesis can be tested by evaluating if there is evidence of: (1) a kinetic delay to nucleation

(i.e., phenocryst contents are below equilibrium abundances) and/or (2) diffusion–limited (i.e., rapid) growth textures in phenocrysts (e.g., hopper, swallowtail, etc.) and granophyric intergrowths of quartz/sanidine. A comparison can be made between the textures of tectosilicate phenocrysts and granophyric intergrowths in the natural GM samples to those in the run products from a subset of experiments (which were designed to produce a kinetic delay prior to tectosilicate growth) from Waters and Andrews (2016), Chapter 2, and this study.

3.1.1 Tectonic setting and previous work

The Glass Mountain (GM) volcanic complex is series of domes and flows of high–SiO_2 rhyolite, which was mapped by Bailey et al. (1976) and Metz and Bailey (1993) (Figure 3–2). It is located along the northeastern rim of the Long Valley Caldera (LVC), which was produced during the climactic eruption of the Bishop Tuff. The GM complex and LVC are located on the eastern side of the Sierra Nevada and western edge of the Basin and Range extensional province (Figure 3–1).

Metz and Mahood (1991) undertook a comprehensive petrologic study of the GM high–SiO_2 rhyolites, including whole–rock major and trace–element analyses, as well as detailed characterization of phenocryst abundances and compositions. Although a majority of both Older and Younger GM units are crystal–poor, they report that sparse phenocrysts of quartz, sanidine and plagioclase range in size from 0.5–2.0 mm, with some feldspars reaching 7 mm in length. They additionally analyzed unaltered pairs of titanomagnetite and ilmenite, which passed the Bacon and Hirschmann (1988) equilibrium test, in four Older and three Younger GM units. Temperatures were calculated using the Fe–Ti two–oxide thermometers of Buddington and Lindsley (1964) and Andersen and Lindsley (1988), resulting in temperatures of 705–718 °C and

766–788 °C, respectively, for the Older GM units and 695–720 °C and 751–778 °C, respectively, for the Younger GM units.

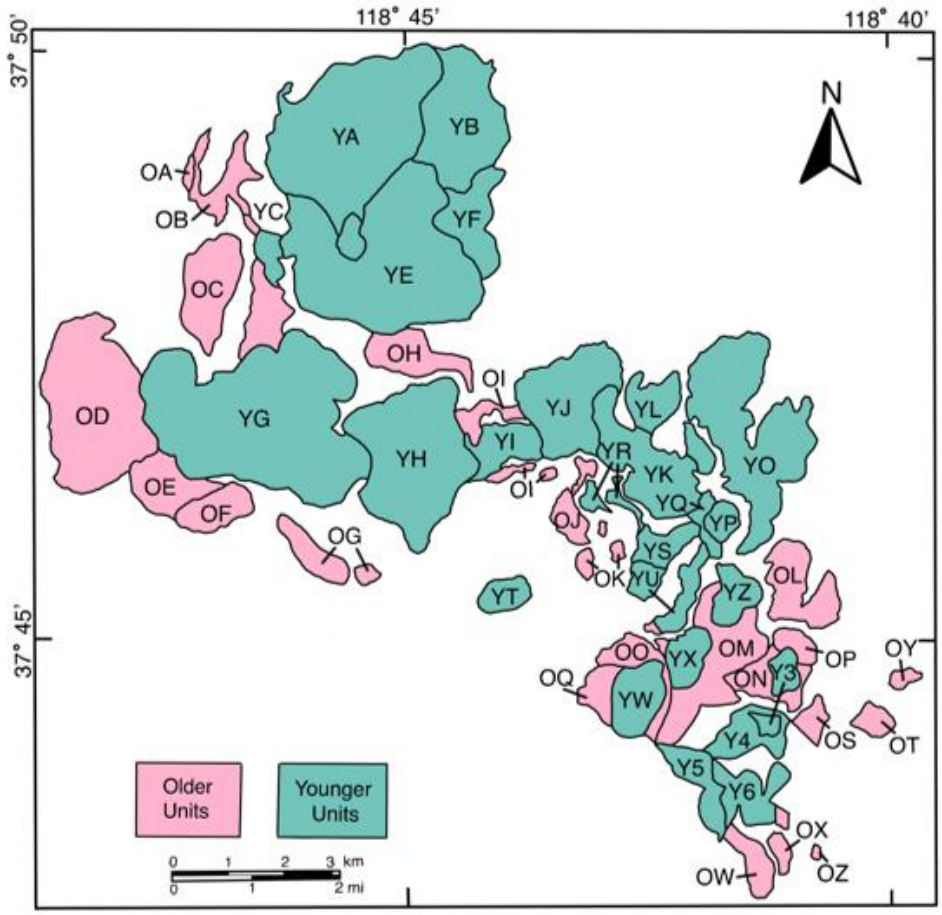


Figure 3-2**:** Simplified geologic map of the Glass Mountain (GM) eruptive units modified from Metz and Bailey (1993). Older GM units are shown in pink and Younger GM units are shown in green.

In Gordon (2022), these Fe–Ti oxide temperatures were recalculated from the updated thermometer of Ghiorso and Evans (2008). The revised temperatures are 698–724 °C for the Older GM samples and 701–725°C for the Younger GM samples, with no resolved, systematic difference in temperature between them. Metz and Mahood (1991) also utilized the two–feldspar thermometer of Fuhrman and Lindsley (1988) at 200 MPa and obtained temperatures of 667–735°C for Older GM units and 673–774°C for Younger GM units, indicative of overlap but a shift to higher temperatures among the Younger GM units. Metz and Mahood (1991) report their

analyzed feldspar and biotite compositions graphically (instead of in tables). In several samples, a surprising compositional variation is found in plagioclase (e.g., bimodal population of ~An_{20} and ~An_{15} in unit YK) and sanidine (a continuous variation from ~$Or_{65–31}$ in unit YO). Metz and Mahood (1991) additionally report a wide range in the Mg# of biotite in individual GM units (e.g., YG and YT).

Waters and Andrews (2016) conducted phase–equilibrium and decompression experiments on a sample from GM unit YE under H_2O–saturated conditions from 75–225 MPa and 700–850 °C. Their phase–equilibrium experiments started with crystal–free glass that was taken directly up to the final equilibration temperature and held for durations of 48, 72 and 120 hours. Their results constrain the location of the liquidus (sanidine and quartz cotectic) in $T–P_{H2O}$ space. At P_{H2O} = 200 MPa, the liquidus is at ~700°C (99% liquid), and the water–saturated melt contains ~6.3 wt% H_2O (Zhang et al., 2007). The plagioclase–in curve is located below the sanidine + quartz liquidus. One of the key findings of their experiments is that once plagioclase joins the crystallizing assemblage of quartz and sanidine (at P_{H2O} = 80 MPa), the percentage of melt drops from ~90% at 725 °C to 0 % (i.e., below the solidus) at 700 °C within ~25 °C of cooling. Waters and Andrews (2016) also conducted an isothermal (700 °C) single–step decompression (i.e., degassing) experiment initiated at 225 MPa and then held at 100 MPa for nine days. The resulting run product contained granophyric intergrowths of quartz and sanidine.

Gordon (2022) presented microprobe analyses of unaltered ilmenite and titanomagnetite in five GM units (OB, OC, OL, OT, YO), which passed the Bacon and Hirschmann (1988) equilibrium test. Care was taken to follow the procedures outlined in Jolles and Lange (2019) to minimize the effects of analytical errors. These data were used to calculate temperatures of 660–716 °C (± 10°C) for the four Older GM units and 695 °C for the YO unit, utilizing the Fe–Ti

two–oxide thermometer of Ghiorso and Evans (2008). These temperatures were used, in combination with analyzed biotite in these five GM units, to help calibrate the TiO_2–based biotite–liquid thermometer applicable to high–SiO_2 rhyolites from Chapter 2.

Gordon et al. (2026) analyzed 19 samples from five Older and seven Younger GM units for whole–rock major– and trace–element compositions using ICP–MS and ICP–OES. These data were used to investigate the origin of the observed 2–fold variation in trace–element concentrations in the GM rhyolites. This was explained through segregation of variable melt fractions during partial melting of their granitic parental source. Gordon et al. (2026) proposed that the four Rb/Sr isochrons documented by Davies et al. (1994) and Davies and Halliday (1998) record the ages of four discrete partial melting episodes, and they draw attention to the fact that the $^{40}Ar/^{39}Ar$ eruption age for unit OC (2.059 ± 0.020 Ma; Simon et al., 2014) and unit OL (1.867 ± 0.005 Ma, Davies et al, 1994; 1.939 ± 0.026 Ma; Simon et al., 2014) cannot be resolved from the age of their respective isochrons (2.047 ± 0.013 Ma and 1.894 ± 0.014 Ma, respectively; Davies et al., 1994). Gordon et al. (2026) therefore suggest that these two erupted units may have ascended directly to the surface after their formation by partial melting, with no intervening period of storage.

3.1.2 Sample locations and petrography

In this study, 10 samples from nine eruptive units of the Glass Mountain complex were chosen for phenocryst analyses. Five are from the Older GM units (OB, OC, OD, OL, OT) and four are from the Younger GM units (YA/YB, YE, YG, YO) (Figure 3–2). Their whole–rock major–element compositions and location coordinates are reported in Table 3–1, which were previously reported in Gordon et al. (2026). Therefore, sample and unit numbers in this study

correspond to those referenced in that study. All samples are glassy obsidians and range from >1% to 20% phenocrysts (Table 3–1).

Table 3-1 Whole–rock major and minor element concentrations (wt%) Glass Mountain samples

Sample	GM–18	GM–01	GM–JJ–10	GM–07	GM–20	GM–28	GM–16	GM–13	GM–09	GM–10
Eruptive Unit	OB	OC	OD	OL	OT	YA/YB	YE	YG	YO	YO
Age (Ma)	1.74	[1]1.999/2.045	[1]1.691/1.687	[1]1.867/1.926			0.96	0.90	1.06	1.06
% Pheno.	3	8	20	<1	1	<1	2	6	3	3
Lat. (37)	.81381°	.80224°	.78450°	.76461°	.74133°	.82726°	.79483°	.78945°	.76460°	.76472°
Long. (–118)	.78604°	.79119°	.81683°	.68333°	.67166°	.75620°	.74294°	.79164°	.69012°	.68970°
SiO_2	77.87	77.44	77.45	76.94	77.75	77.20	77.62	77.68	77.36	77.43
TiO_2	0.06	0.06	0.06	0.06	0.07	0.08	0.08	0.08	0.07	0.07
Al_2O_3	12.37	12.55	12.73	13.04	12.48	12.67	12.48	12.47	12.62	12.50
FeO^T	0.86	0.68	0.67	0.76	0.87	0.82	0.89	0.83	0.78	0.78
MnO	0.06	0.09	0.06	0.07	0.04	0.03	0.04	0.03	0.04	0.04
MgO	0.03	0.04	0.04	0.03	0.04	0.04	0.04	0.04	0.04	0.06
CaO	0.37	0.34	0.42	0.36	0.40	0.49	0.47	0.48	0.48	0.49
Na_2O	4.00	4.28	4.04	4.27	3.85	3.84	3.64	3.65	3.91	3.92
K_2O	4.28	4.44	4.46	4.38	4.41	4.82	4.63	4.64	4.61	4.60
LOI	0.28	0.85	2.68	0.38	0.46	1.10	0.26	0.27	0.32	0.38
Total	99.2	99.9	99.2	98.7	100.6	98.6	99.4	100.7	98.5	99.9

OB, OC, OD, OL, OT, YE, YG, YO previously reported in Gordon et al. (2026)

Major element analyses normalized to 100%. LOI and original totals also shown.

K–Ar ages from Metz and Mahood (1985)

[1] $^{40}Ar/^{39}Ar$ ages from Davies et al., (1994), Simon et al., (2014)

[2] glass analyses reported in Chapter 2

Most units contain 9 mineral phases: quartz, sanidine, plagioclase, biotite, titanomagnetite, ilmenite, allanite, apatite, and zircon. However, owing to a low overall crystal abundance (<1%), neither ilmenite nor biotite were found in sample YA/YB. As previously described by Metz and Mahood (1991), the tectosilicates dominate the phenocryst abundances. However, whereas they report a higher proportion of plagioclase relative to sanidine in their GM samples, those in this study show a dominance of quartz and sanidine relative to plagioclase.

3.2 Experimental methods

3.2.1 Synthesis of starting glass materials

A sample of high–SiO_2 rhyolite composition from Mono Craters, CA (MC–24) was chosen as the starting material for experiments. Unaltered, interior portions of the sample were

crushed and powdered in a tungsten carbide shatter box for homogenization. The powdered sample was then placed in a platinum crucible and loaded into a box furnace where it was held for ≥ 14 hr at 1200°C before it was raised to 1450°C for an additional 4 h to fully melt it and eliminate all crystals. The Pt crucible was then removed from the furnace and immediately plunged into cold water to quench the molten sample into 100% crystal–free glass. The resulting glass was removed from the Pt crucible and powdered in a tungsten carbide shatter box for further homogenization. This powdered glass was used as the starting material for the experiments in this study.

3.2.2 Experimental set–up

Pure–H_2O fluid–saturated crystallization experiments were conducted in a Waspaloy (nickel alloy) cold–seal pressure vessel at New Mexico Tech (NMT) at 200 MPa and 650°C. For each experiment, two capsules were made of 3–mm OD gold tubing and welded with a Lampert PUK high precision TIG welder. The two capsules were then packed with 25–50 mg of powdered glass (crystal–free) starting material (MC–24) together with Fe–Ti oxide separates (~15% of total mass; as nucleation sites) and a sufficient mass of deionized H_2O (at least 10% of total mass) to ensure fluid saturation during each experimental run (estimated from the water solubility model of Zhang et al., 2007). Capsules were then welded shut and the seals tested by placing capsules on a hot plate (~100 °C) for at least 2 min to check for weight loss, which would indicate an incomplete seal. At the end of each experimental run (described below), the Au capsules were weighed again to test for any loss of fluid during the experiment, which would indicate a failed run.

Two sealed Au capsules containing the starting glass material were loaded into the hotspot of Waspaloy (nickel alloy) cold–seal pressure vessels followed by nickel–filler rods for

each experimental run. Water was the high–pressure medium for the experimental set up, with uncertainties in pressure < ±10 MPa. Loaded pressure vessels were heated in Thermo–scientific Linberg Blue tube furnaces, and temperature was monitored by a *K*–type thermocouple, within ± 3 °C. During each experiment, samples were brought to a pressure of 200 MPa first and then heated to their target temperatures. As temperature increased, the pressure was manually adjusted (every 2–5 minutes) to remain isobaric at 200 MPa until the target temperature was reached. Due to the composition of the pressure vessels and nickel filler rods, an intrinsic fO_2 close to the Ni–NiO buffer was imposed. Because the fO_2 increases with degree of oxidation of the filler rod (e.g., Venezky and Rutherford, 1999), care was taken between each run to remove the nickel filler rods and file off the oxidized surface to expose the metal in an effort to ensure that the imposed fO_2 approached that of the Ni–NiO buffer. A best estimate of the ΔNNO during each run is ~+0.5 (± 0.5).

3.2.3 Experimental design: Two temperature–path trajectories

Two types of crystallization experiments were performed, each with a different temperature–path trajectory (bottom–up vs. top–down) (Table 3–2). The difference in the temperature paths between each experiment was that the final temperature (650 °C) was reached from lower vs. higher temperatures. For the "bottom–up" experiment, the glass starting material was heated from room temperature up to 650°C, and thus briefly passed through a region of supercooled liquid between the glass transition and final equilibration temperature. This pathway causes the sample to transit through a region of undercooling ($\Delta T = T_{liquidus} - T_{supercooled\ liquid}$) that is characterized by high nucleation rates and low crystal growth rates (Figure 3–3) before reaching its final equilibration temperature of 650 °C. The presence of numerous nuclei minimizes kinetic delays to nucleation and facilitates crystallization. The sample was held at 650

°C for 596.5 h (~25 days) and then quenched in room–temperature water under isobaric conditions in ~30 s.

Table 3-2: Experimental samples, run conditions, and run products

T–path	Run #	MC–24 sample #	T1 hold (°C)	T2 hold (°C)	T final (°C)	P (MPa)	Duration (h)	Phases present
Bottom up	8–1 8–2	25MC24_OX_9 25MC24_OX_12			650	200	596.5	qtz, san, plag
Top down	9–1 9–2	25MC24_OX_7 25MC24_OX_10	850		650	200	730.5	qtz, san, plag, glass
Top down	3	25MC24_OX_2	850	825	700	200	182	bte, glass, san, qtz

For the "top–down" experiment, the starting glass was initially brought to a temperature of 850 °C, well above the tectosilicate liquidus, and held there for two hours to eliminate any nuclei that may have formed during heating. After this initial hold, the temperature was abruptly dropped to the final equilibration temperature of 650°C and then held there for 730.5 h (~30 days), while maintaining pressure at 200 MPa, before quenching into water. Owing to a kinetic delay in nucleation, this abrupt drop in temperature induced an undercooling of ~50 °C (ΔT = 700 – 650 °C), assuming the tectosilicate liquidus is at ~700 °C (Waters and Andrews, 2016) at a P_{H2O} = 200 MPa. At this undercooling, crystal growth rates are expected to be higher than nucleation rates (Figure 3–3), enabling the experimental growth of large, sparse crystals (e.g., Lofgren et al., 1974).

An additional top–down experiment (with the same MC–24 starting material in the capsule) is included in this study, which was previously undertaken in Chapter 2 and labeled run#3. In that experiment, conducted at P_{H2O} = 200 MPa, the sample was first taken to 850 °C for two hours, then dropped to 825°C for another two–hour hold (to facilitate the nucleation of biotite), and then rapidly dropped to 700°C and held for 182 h.

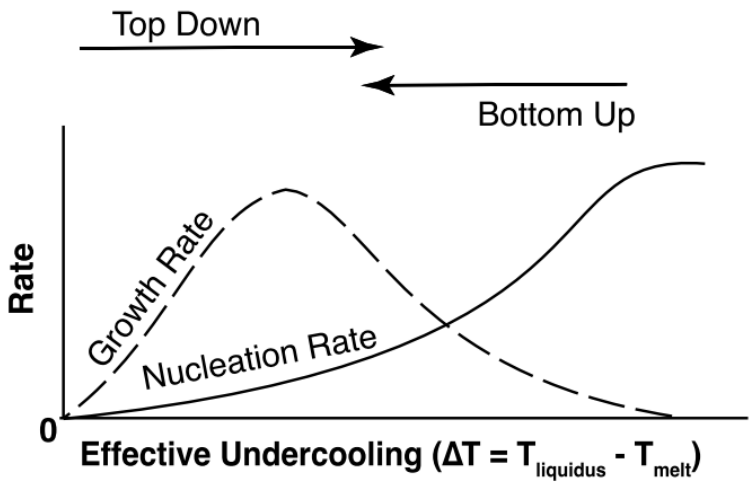


Figure 3-3: A schematic diagram illustrating rate of crystal growth (dashed line) and nucleation (solid line) vs. effective undercooling ($\Delta T=T_{liquidus}–T_{melt}$) for supercooled liquids (modified from Pu et al., 2021). Arrows at the top of diagram represent the two experimental temperature–path trajectories in this study. Starting from the right side of the diagram, the 100% glass starting material in the bottom–up experiments were heated to temperatures above the glass transition and transited a region of undercooling characterized by high nucleation rates. When this experimental run reached its final equilibration temperature, it is expected to have numerous small nuclei and no kinetic delay to nucleation. Starting from the left side of the diagram, the 100% glass starting material in the top–down experiments were first taken to a superliquidus temperature for 2 h and then abruptly dropped to the final equilibration temperature, leading to a kinetic delay in nucleation and enabling crystallization to occur under conditions of relatively low nucleation rates and high crystal growth rates.

3.3 Imaging methods

Back–scattered electron (BSE) images were taken of all experimental run products and analyzed crystals in the natural samples using both the Cameca SX100 Electron Microprobe and the JEOL JSM–7800FLV field–emission scanning electron microscope (SEM) in the Robert Mitchell Laboratory at the University of Michigan. Cathodoluminescence images of quartz phenocrysts in experimental runs were acquired from a mounted monochromatic cathodoluminescence (CL) detector on the JEOL SEM. Photomicrographs of representative phenocryst textures in GM units OC, OD, OT, YA, and YO were also obtained using a petrographic microscope.

3.4 Analytical methods

All mineral analyses were obtained with the Cameca SX100 Electron Microprobe at the University of Michigan. A compilation of all microprobe standards used for plagioclase, sanidine

and biotite analyses is presented in Supplemental Table B-0-9. Experimental capsules were opened and mounted in 1" epoxy–mounts for analysis of crystals and glass in the run products. Phenocrysts in natural samples were analyzed in both thin sections and 1" epoxy–mounted mineral separates.

Plagioclase and sanidine analyses were made with a defocused beam of 2 μm, a beam current of 20 nA, and an accelerating voltage of 15 kV. Nine elements were analyzed (Mg, Na, Si, Al, Ti, Fe, Mn, Ca, and K) at a peak and background counting time of 20 s each. The average 3 SD uncertainties on the oxide components, based on counting statistics, are 0.67 wt% for SiO_2, 0.02 wt% for TiO_2, 0.38 wt% for Al_2O_3, 0.04 wt% for FeO^T, 0.03 wt% for MnO, 0.02 wt% for MgO, 0.05 wt% for CaO, 0.15 wt% for Na_2O and 0.15 wt% for K_2O. Only analyses with $SiO_2 <$ 70% (to avoid analyses where the electron beam may have partially hit glass) and oxide totals between 98.5 and 101.5 wt% were used.

Biotite analyses were made with a defocused beam of 2 μm, a beam current of 20 nA and an accelerating voltage of 15 kV. Ten elements were analyzed (Si, Ti, Al, Fe, Mn, Mg, Ca, Na, K and Ba) at a peak and background counting time of 20 s each except for Fe (10 s) and Ba (30 s). The average 3 SD uncertainties on the oxide components, based on counting statistics, are 0.47 wt% for SiO_2, 0.09 wt% for TiO_2, 0.26 wt% Al_2O_3, 0.54 wt% for FeO^T, 0.04 wt% for MnO, 0.19 wt% for MgO, 0.06 wt% for BaO, 0.04 wt% for CaO, 0.04 wt% for Na_2O and 0.25 wt% for K_2O. Only analyses with totals ≥ 93 wt% were used.

3.5 Imaging results

3.5.1 Experimental run products

All four capsules from the two experiments at 650°C and 200 MPa (runs #8 and #9; Table 3–2) experienced no loss of fluid after their quench, and thus all runs were successful.

Images of the run products from the "bottom–up" experiments (run #8–1; Figure 3–4) illustrate the microcrystalline presence of quartz, sanidine, and plagioclase, with no glass detected. Thus, these experimental run products were completely crystallized. This result places the water–saturated solidus at 200 MPa for the high–SiO_2 rhyolite composition at a temperature ≥ 650°C.

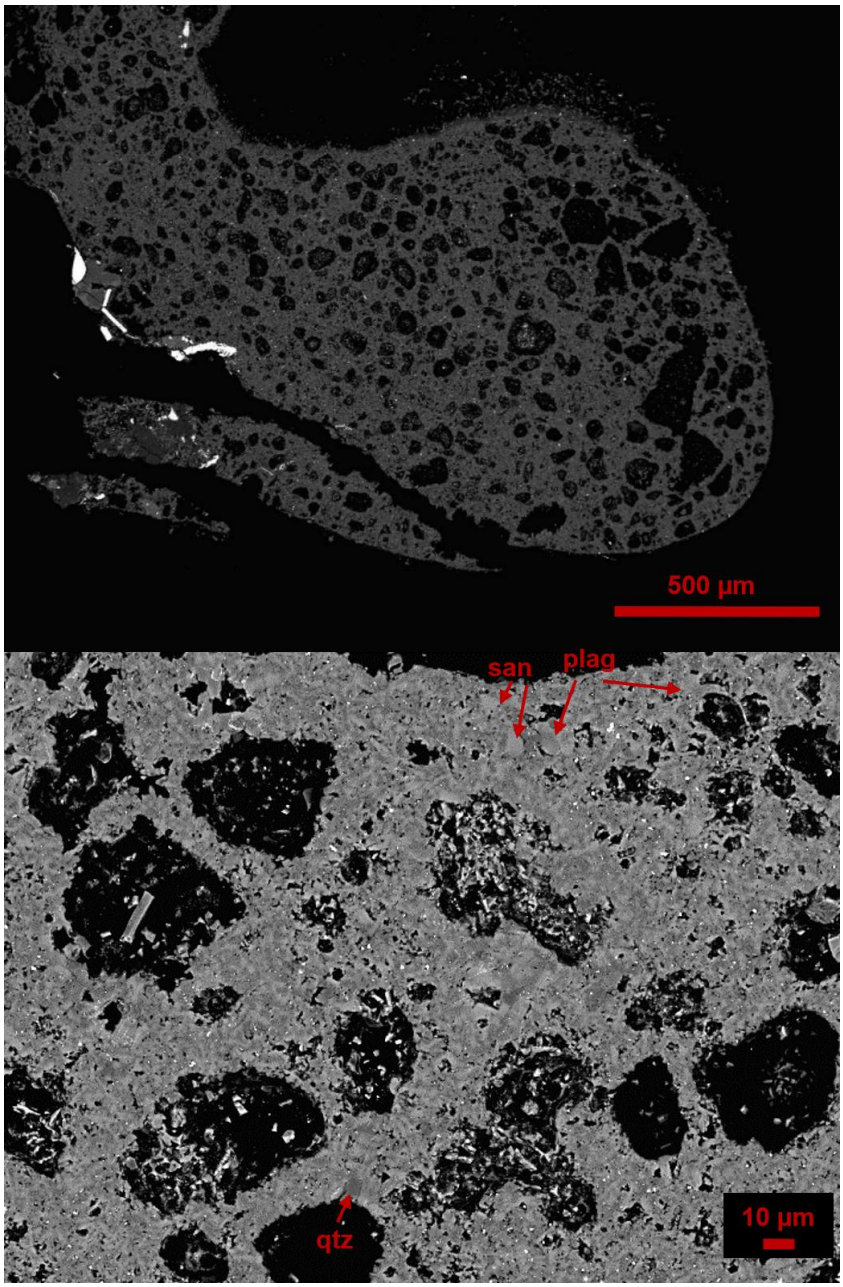


Figure 3-4**:** Representative BSE images of the bottom–up experimental charge from run 8–1 showing (a) zoomed–out image of the vesicular, crystallized run product in the capsule, and (b) zoomed–in image of the microcrystalline run product. Scale bars are shown in red. (a) Visible ilmenite and titanomagnetite "nucleation seeds" can be seen on the left edge of the charge. (b) No glass was found in the microcrystalline run product. Crystal phases are labeled:

san (sanidine), plag (plagioclase) and qtz (quartz) and typically ≤ 10 μm in size. The results indicate complete crystallization at 650 °C and P_{H2O} = 200 MPa.

Images of the run products from the "top–down" experiment (Figures 3–5 and 3–6) are distinctly different from the "bottom–up" runs. Most notably, they contain significant amounts of glass (~40%), as well as significantly larger crystals of sanidine and quartz, and smaller, sparser crystals of plagioclase (Figure 3–5; run #9–1).

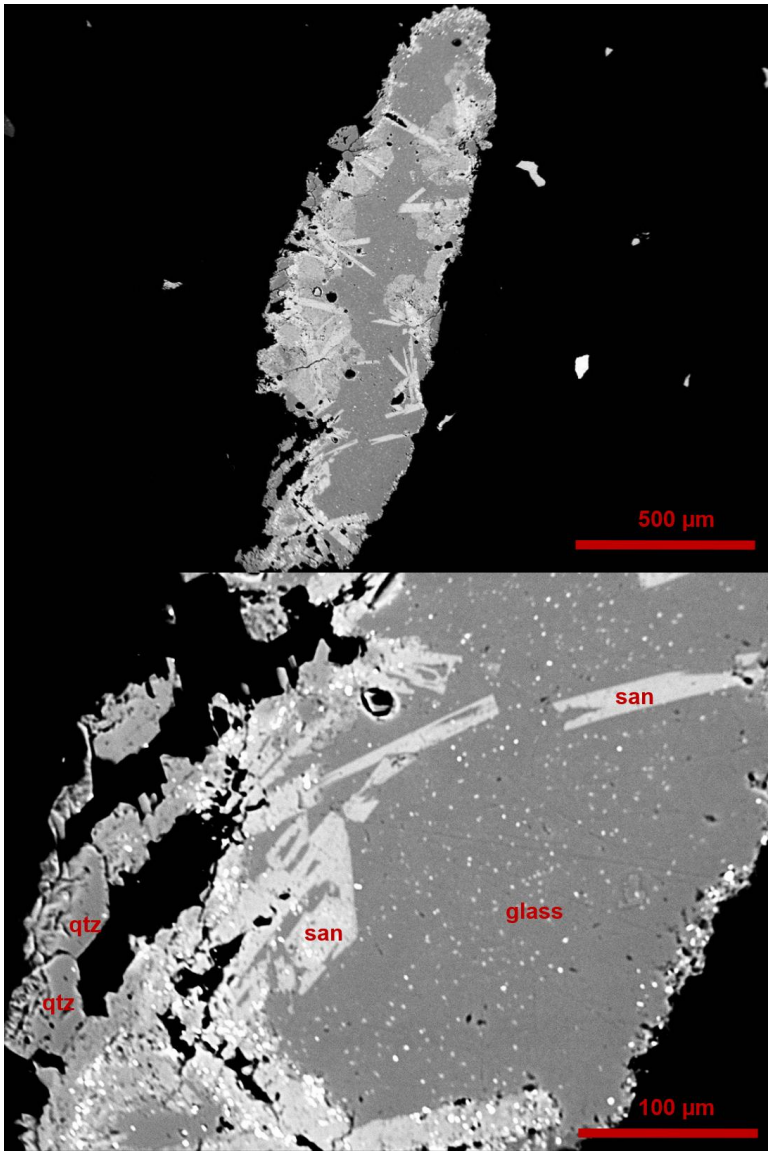


Figure 3-5**:** Representative BSE images of the top–down experimental charge from run 9–2 showing (a) zoomed–out image of the run product with crystals on the edges of the capsule and an interior pool of glass, and (b) zoomed–in image of (a). Scale bars are shown in red. (a) Clear evidence of abundant glass (~40%) is seen in the interior of the capsule, and it appears that quartz preferentially nucleated on the capsule walls, and that sanidine nucleated on quartz. Around the sanidine crystals can sometimes be seen a halo of glass depleted in K_2O. (b) Close up of quartz

and sanidine crystals, the latter with hopper and swallow–tail textures. Crystals in (b) are ≤ 100 μm and are labelled as in Fig. 3–4. It is estimated that crystal growth occurred at an undercooling of ~50 °C (see text for details) for a duration ≤ 548 h.

The presence of abundant glass, despite an experimental duration of 30 days, reflects the effects of a kinetic delay to nucleation. This kinetic delay enabled an undercooling to develop, which facilitated conditions of relatively high crystal growth rate in the top–down experimental run, compared to the bottom–up run (Figure 3–3). It appears that quartz preferentially nucleated along the margins of the capsule and that sanidine then preferentially nucleated on the quartz grains in a halo of depleted glass owing to the rapid growth of crystals (Figure 3–5). Sanidine crystals display swallow tail and hopper textures, as well as intergrowth with quartz (Figure 3–5).

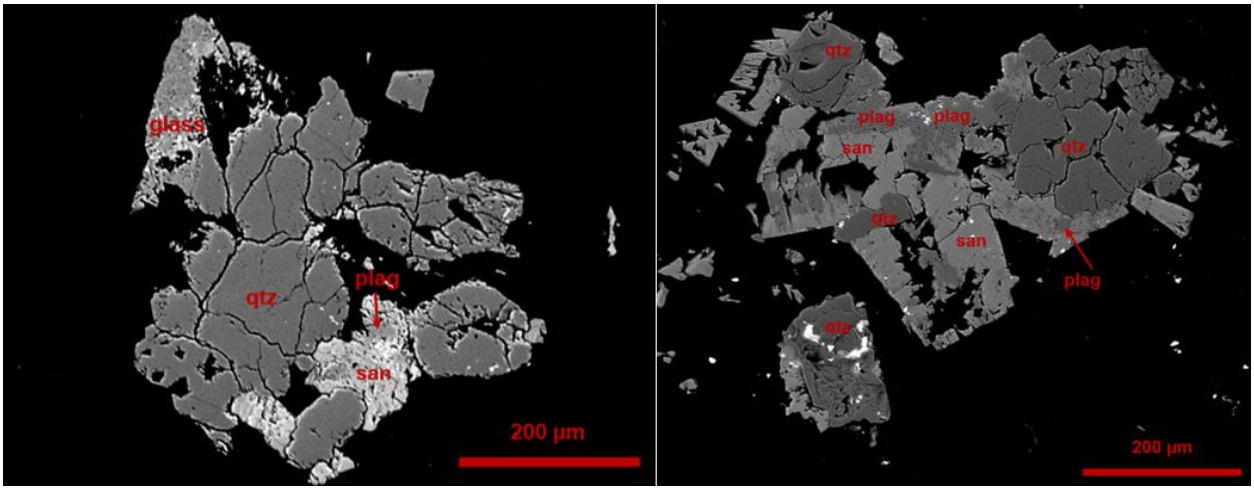


Figure 3-6: More representative BSE images of the top–down experimental charges from (a) run 9–2 and (b) run 9–1. Labels of crystal phases are as in Fig. 3–4, and scale bars are shown in red. (a) Clear intergrowth of sanidine and quartz is seen, similar to granophyric textures seen in the natural GM samples. Sanidine crystals display rapid growth textures (i.e., skeletal and hopper) and reach ~300 μm in length. Quartz crystals reach ~200 μm in length. Plagioclase is seen growing in the interior hollows of hopper–textured sanidine. (b) Quartz crystals exceed 200 μm and display hopper textures (two grains to the right of image). It is estimated that crystal growth occurred at an undercooling of ~50 °C (see text for details) for a duration ≤ 548 h.

In Figure 3–6, an image of a clot of quartz and sanidine crystals (from top–down run #9–2), shows that phenocryst–sized (~200+ μm) tectosilicates can grow in a high–SiO_2 rhyolite melt

at P_{H2O} = 200 MPa and 650 °C within < 30 days. At this T–P_{H2O} condition, the solubility of water in the melt is 6.4 wt% H_2O (Zhang et al., 2007), and the calculated melt viscosity is 5.6 $\log_{10}$ Pa–s (Hui and Zhang, 2007).

The sanidine crystals display diffusion–limited textures (skeletal, hopper, swallowtail), all characteristic of rapid growth conditions. Some of the sanidine crystals are partly intergrown with quartz crystals, similar to a granophyric texture. In addition, plagioclase patches are seen within the sanidine crystals. This may reflect initial crystallization of quartz and sanidine, followed by subsequent growth of plagioclase filling in melt hollows within sanidine.

In Figure 3–7, BSE images of a single sanidine and a single quartz grain are shown from the top–down experiment (run#3 for MC–24 starting material) from Chapter 2. The final equilibration temperature (held for 182 h) was 700 °C at P_{H2O} = 200 MPa. Both the sanidine and quartz crystals are euhedral and approximately 80 and 65 µm, respectively, in length.

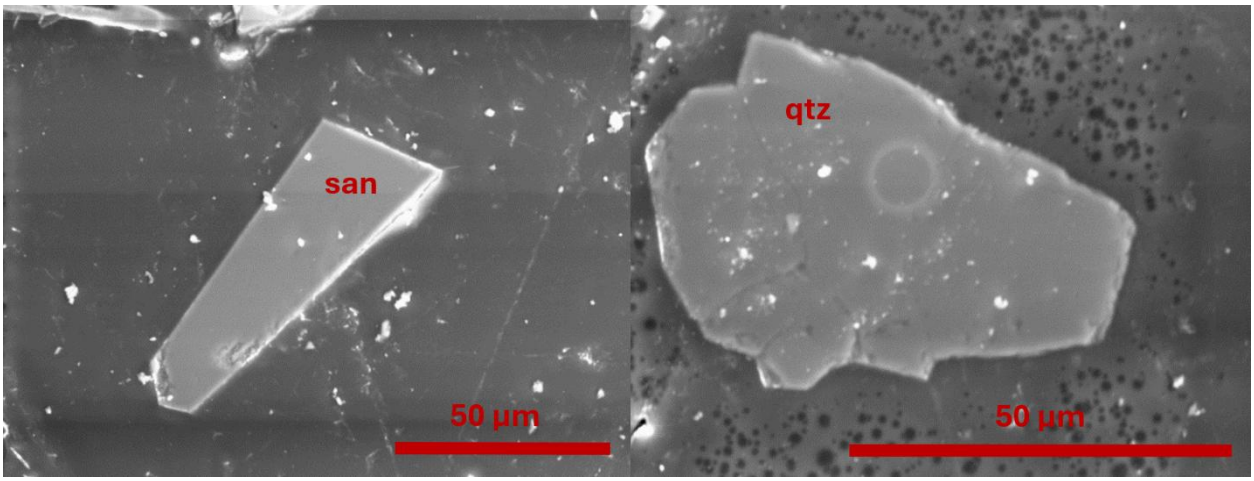


Figure 3-7**:** BSE images from the top–down experimental charge from run 3 showing: (a) a euhedral, faceted sanidine crystal of ~ 80 µm length and (b) a partially faceted quartz crystal of ~60 µm in length. Lettering for crystal phases and scale bars are shown in red. It is estimated that crystal growth occurred at an undercooling of ~5 °C (see text for details) for a duration < 182 h.

3.5.2 Constraints on crystal growth rates

Broad constraints on minimum crystal growth rates can be obtained from the top–down experimental images in Figures 3–6 and 3–7. The time durations for crystal growth during run #9

(this study) and run #3 (Chapter 2) are not precisely known, because of the unknown durations of any kinetic delay to nucleation. However, because Chapter 2 of this thesis documents kinetic delays of >182 h for nucleation of tectosilicates in top–down experiments at 675°C and P_{H2O} = 200°C, it is likely that a similar kinetic delay (182 h) occurred in the top–down experiment in this study at 650°C and P_{H2O} = 200 MPa. Thus, it is estimated that the quartz and sanidine crystals of ~300 and ~200 μm, respectively, in the run #9 experiments (Fig. 3–6) grew over time durations of ≤548 (730–182) h, which translate to crystal growth rates of ≥1.5 and ≥1.0 x 10^{-8} cm/s, respectively, at an undercooling (ΔT_{UC}) of ~50 °C. For the quartz (~65 μm) and sanidine (~80 μm) in the top–down run #3 experiment held for 182 h at 700°C and P_{H2O} = 200 MPa (Fig. 3–7), minimum crystal growth rates are ≥1.0 and ≥1.2 x 10^{-8} cm/s, respectively, at an undercooling of ~5°C. These minimum crystal growth rates are within an order of magnitude of the highest crystal growth rate (7 x 10^{-8} cm/s) experimentally documented by Swanson and Fenn (1986) for quartz in a low–SiO_2 rhyolite (Harding Pegmatite) with 4.5 wt% H_2O at 500 MPa and 750 °C (at an estimated undercooling of 186 °C).

3.5.3 Granophyric intergrowths in natural samples

Granophyric intergrowths of quartz and sanidine have been identified in at least seven of the nine eruptive units examined in this study (OB, OC, OD, YA, YE, YG, YO). Representative BSE and petrographic images of granophyres from units OC, OD, YA and YO are shown in Figure 3–8. They range in size from ~200 μm up to ~3 mm. Note that some of the sanidine crystals in these granophyric intergrowths in unit OD display hopper textures (interior melt hollows). Additionally, Waters and Andrews (2016) present BSE images of granophyric intergrowths (≤200 μm) from unit YE.

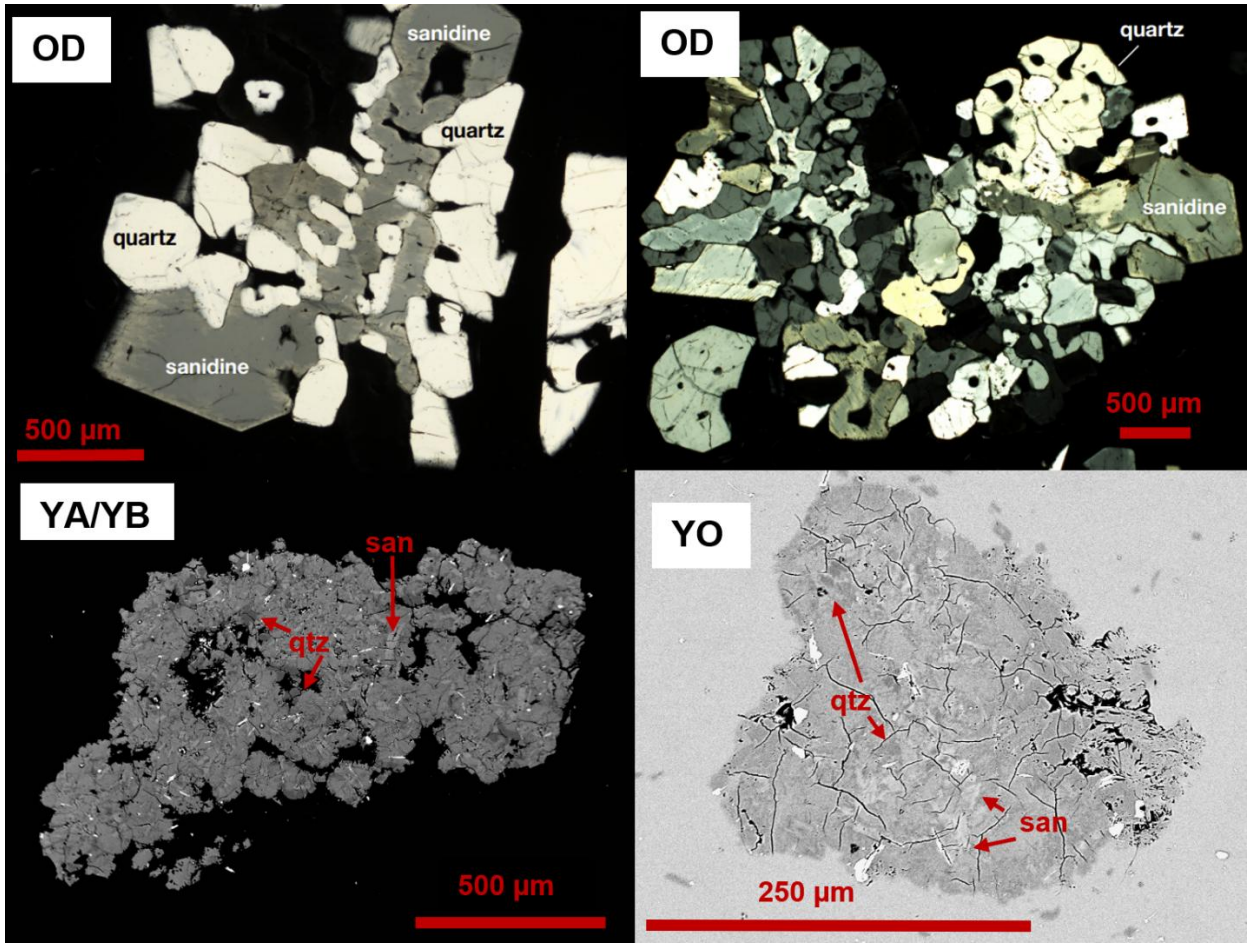


Figure 3-8**:** Representative granophyre images from four GM units that feature intergrowths of quartz and sanidine. Lettering for crystal phases and scale bars are shown in red. (a–b) Photomicrographs of granophyres (≤ 3 mm in length) from GM unit OD, where individual crystals of quartz and sanidine approach 500 µm and display rapid–growth hopper textures. (c–d) BSE images of finer–grained granophyric intergrowths of quartz and sanidine in GM units (c) YA/YB and (d) YO. Similar granophyres are seen in units OB, OC, YE, and YG, as well, in addition to the nine–day decompression experiments of Waters and Andrews (2016) on a GM high–SiO_2 rhyolite.

3.5.4 Quartz phenocrysts in natural samples

A wide range of quartz phenocryst sizes (≤ 3 mm) and textures are found in the various GM units. Photomicrograph, BSE and CL images of quartz in unit OD (Fig. 3–9a–f) display rapid–growth textures, including hopper cavities and embayments (Barbee et al., 2020). In the same samples, quartz phenocrysts with faceted crystal rims are also seen (Fig. 3–10a–d).

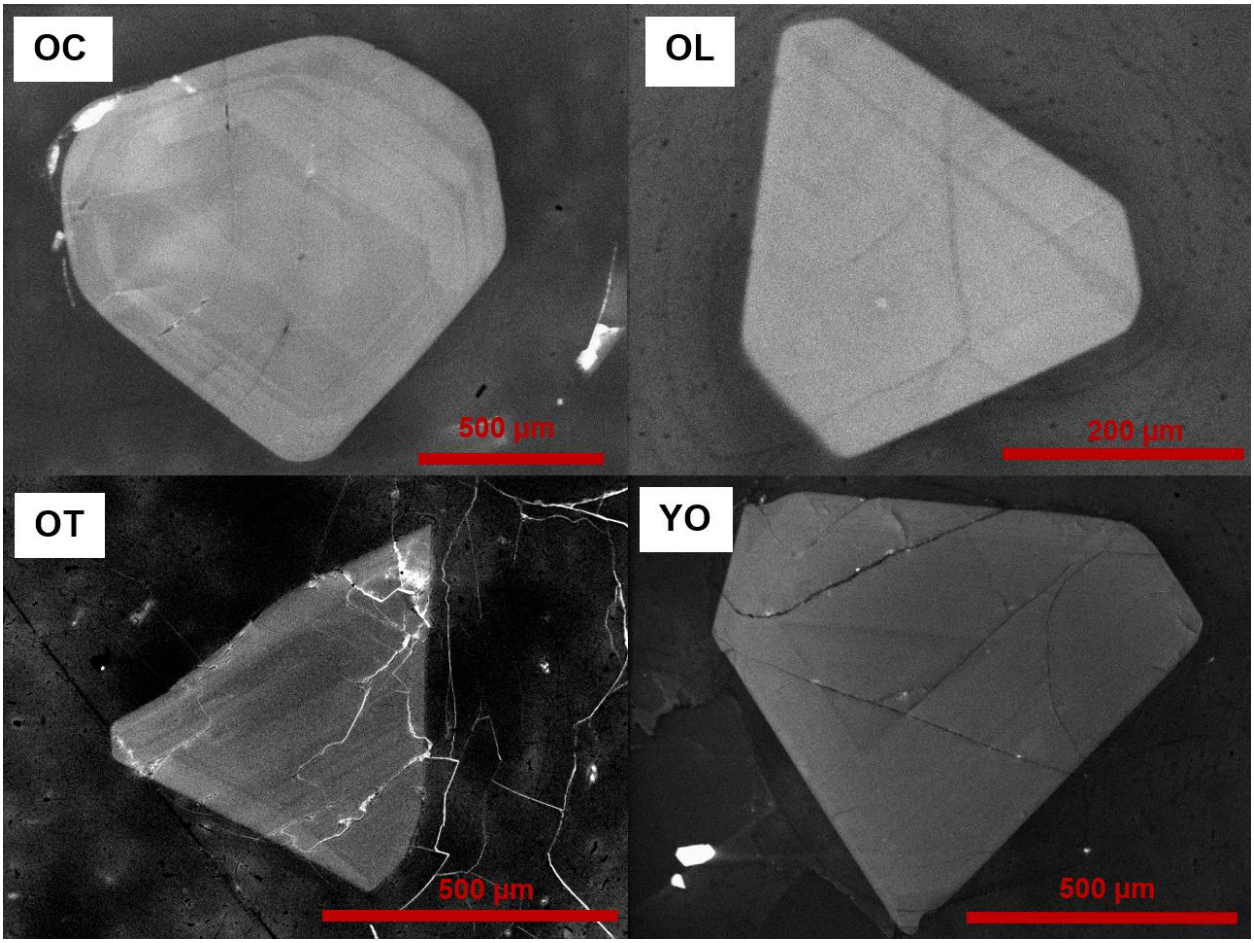


Figure 3-9**:** Representative monochromatic cathodoluminescence (CL) images of euhedral quartz crystals (< 1 mm) in several GM units, displaying subtle Ti zonation patterns. Scale bars are shown in red.

3.5.5 Sanidine phenocrysts in natural samples

BSE images of sanidine phenocrysts reveal a wide range of sizes and textures (Fig. 3–11). However, in nearly all cases, there is evidence of alteration along rims and cracks, even in crystals with euhedral, faceted rims. This ubiquitous alteration of sanidine occurs in GM samples with pristine, unaltered titanomagnetite and ilmenite (e.g., units OC, OB, OL, OT, YO; Gordon, 2022). Sanidine is sometimes intergrown with plagioclase (Fig. 3–11b, d, e). and the juxtaposition of altered sanidine and pristine plagioclase is striking. Individual sanidine phenocrysts are typically ~200–400 µm in size, but some reach >1 mm in length.

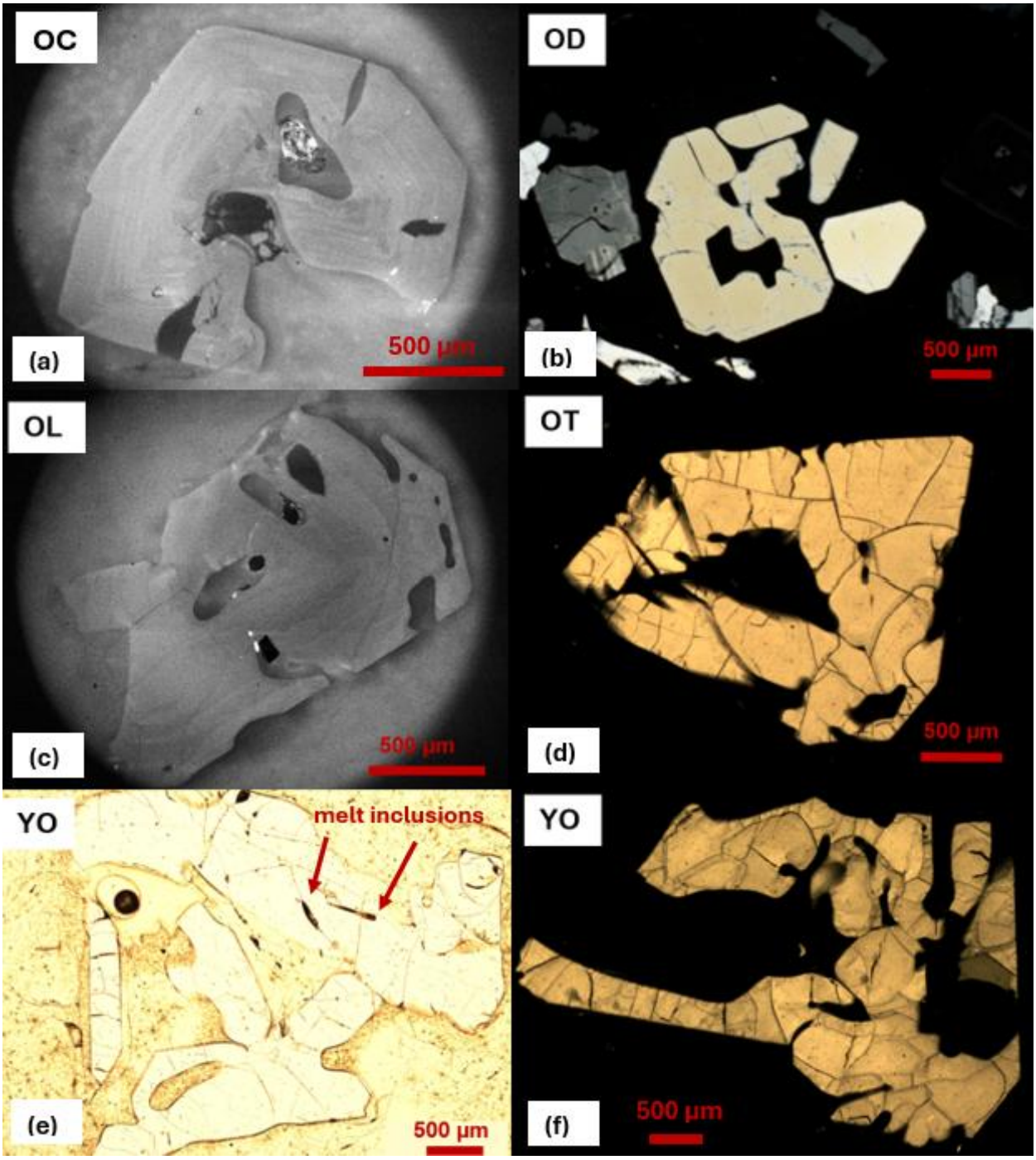


Figure 3-10: Representative CL and photomicrograph images of large (>1mm) quartz crystals in several GM units, featuring hopper textures that include protuberances, growth embayments, melt inclusions and hollow faces. These textures are consistent with diffusion–limited rapid growth (e.g. Barbee et al., 2020). Quartz phenocrysts with these textures are seen throughout the GM units. Scale bars are shown in red.

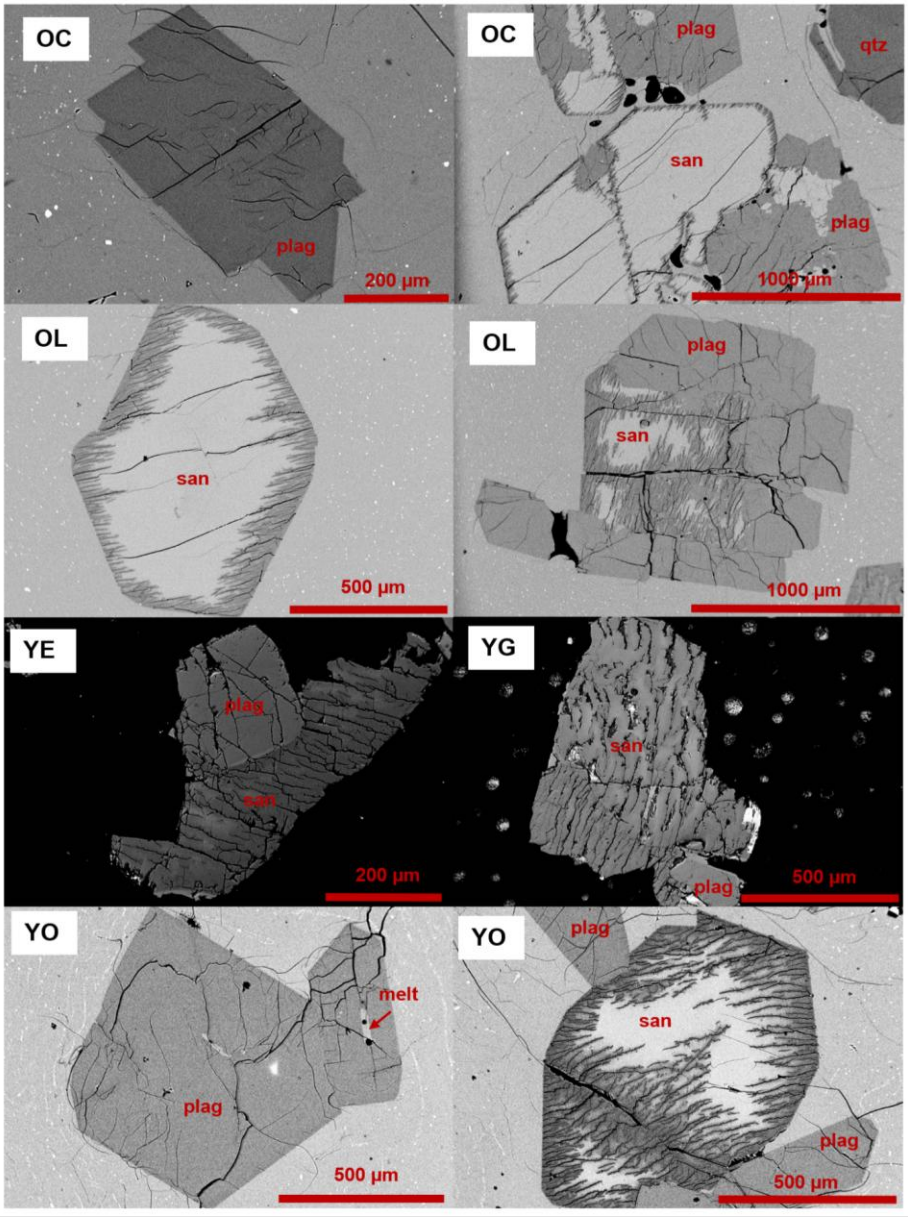


Figure 3-11: Representative BSE images of plagioclase and sanidine (≤ 1 mm) in several GM units. Lettering for crystal phases and scale bars are shown in red. (a) euhedral plagioclase crystal in unit OC with faceted edges; (b) Euhedral sanidine (light colored) with alteration rims, with euhedral crystals of plagioclase that appear to have nucleated against sanidine; unit OC. (c) euhedral sanidine with alteration rims in unit OL; (d) growth of euhedral plagioclase around altered sanidine in unit OL; (e) another example of plagioclase nucleated against altered sanidine; unit YE; (f) extensively altered in unit YG; (g) euhedral crystals of plagioclase in unit YO, with small melt inclusions; (h) euhedral, but altered sanidine with two plagioclase crystals that nucleated on its two sides in unit YO. Note that all sanidine crystals displayed show darker zones around edge cracks and interior cracks of crystals, which is alteration of the sanidine to albite (i.e., albitization), and is variably seen mostly along rims in some units (e.g., OC and OL) or throughout entire crystals (e.g., YE and YG). Plagioclase is pristine and unaltered in all units.

3.5.6 Plagioclase phenocrysts in natural samples

Plagioclase is found in all GM units from this study, and representative BSE images are shown in Figure 3–11 (a and g), including examples of intergrowth with sanidine (Fig. 3–11b, d, e). Unlike sanidine, there is no evidence of any alteration of plagioclase. Most plagioclase phenocrysts display faceted, euhedral crystal rims. Individual crystals are typically ~100–200 μm in size, but some reach >800 μm in length. In any eruptive GM unit, the plagioclase phenocrysts are less abundant compared to sanidine and quartz phenocrysts.

3.5.7 Biotite phenocrysts in natural samples

Biotite was found in eight of the nine eruptive units in this study; it is only absent in unit YA/YB owing to its exceptionally low crystallinity (<1%). Representative BSE images of biotite crystals in units OD, YE and YG (Figure 3–12) show individual crystals with hopper cavities and embayments, indicative of rapid growth. These same crystals also have edges with faceted rims. Among all eight eruptive units, individual biotite phenocrysts are typically around 200–400 μm but some reach >600 μm in size.

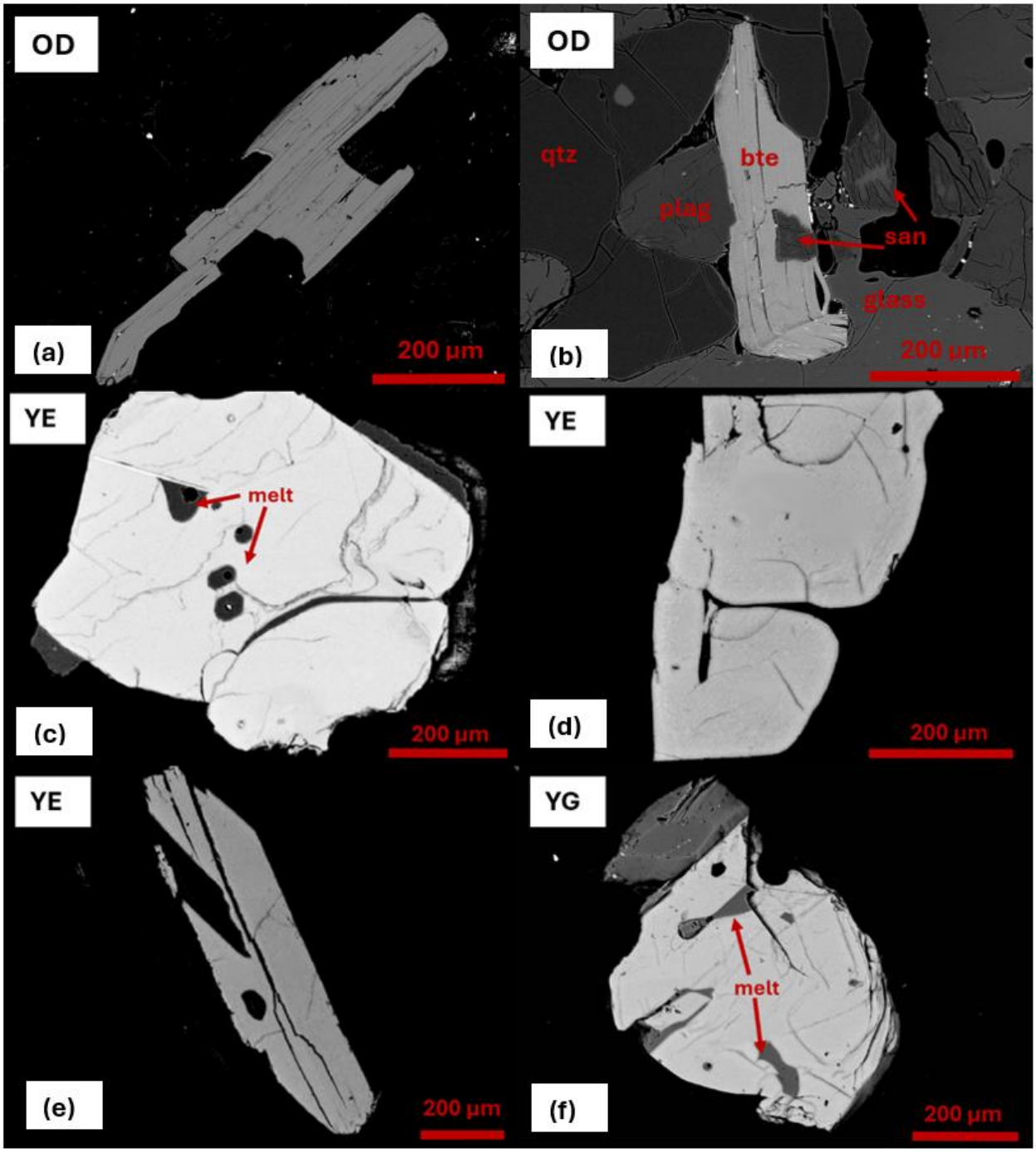


Figure 3-12:(a–f) Representative BSE images of biotite phenocrysts (≤ 800 µm) in several GM units, illustrating examples of rapid–growth textures (e.g., hopper and swallow tail) leading to partially enclosed melt embayments and inclusions. Scale bars are shown in red.

3.6 Analytical results

3.6.1 Plagioclase

Individual analyses of plagioclase crystals in the experimental run products and natural samples are available in Supplemental Table B-0-10. The average composition in each run/sample is reported in Table 3–3 along with the number of plagioclase crystals that were analyzed (N) and the total number of analyses (n) for that run/sample. Average molar % anorthite for each sample is reported (Table 3–3), where An% (=100 x moles CaO/[moles $CaO+Na_2O+ K_2O$]). In the bottom–up experimental run, plagioclase crystals were too small for analysis, whereas the average plagioclase compositions are both ~An_8 in the two capsules in the top–down experiment at 650°C (run #9; Table 3–2). In the natural samples, the average plagioclase compositions range from $An_{7–10}$ in the five Older GM units and from $An_{14–16}$ in the four Younger GM units.

3.6.2 Sanidine

Individual analyses of sanidine phenocrysts in the experimental run products and natural samples are available in Supplemental Table B-0-11. The average composition in each run/sample is reported in Table 3–3 along with the number of sanidine crystals that were analyzed (N) and the total number of analyses (n) for that sample. Average molar % orthoclase for each sample is reported (Table 3–3), where Or% (=100 x moles K_2O/[moles $Na_2O+ K_2O$]). In the bottom–up experimental run, sanidine crystals were too small for analysis, whereas the average sanidine compositions are Or_{72} and Or_{75} in the two capsules in the top–down experiment at 650 °C (run #9; Table 3–2). In the top–down experiment at 700 °C (run #3; Table 3–2), the average sanidine composition is Or_{77}. In the natural samples, the average sanidine compositions (for pristine cores) range from $Or_{57–61}$ in the five Older GM units and from $Or_{61–65}$ in the four Younger GM units (Table 3–3).

Table 3-3: Average composition (wt%) of plagioclase and sanidine in experimental and Older and Younger Glass Mountain samples

Sample/Run Eruptive Unit	GM–18 OB	GM–01 OC	GM–JJ–10 OD	GM–07 OL	GM–20 OT	GM–16 YE	GM–13 YG	GM–09 YO	GM–10 YO
Plag, *N;n*	8;19	12;34	14;45	1;4	3;98	3;85	3;101	10;48	14;42
SiO_2	66.64 (38)	67.14 (41)	66.28 (39)	67.16 (42)	65.32 (33)	63.67 (27)	64.22 (33)	64.87 272)	65.31 (46)
TiO_2	0.00	0.00	0.00 (01)	0.00				0.00	0.00
Al_2O_3	20.95 (34)	20.39 (20)	20.86 (17)	20.91 (33)	21.06 (22)	21.95 (19)	21.85 (25)	21.78 (18)	21.78 (25)
FeO^T	0.12 (02)	0.13 (02)	0.11 (02)	0.13 (01)	0.13 (02)	0.14 (01)	0.14 (02)	0.13 (01)	0.13 (02)
MnO	0.00 (01)	0.00 (01)	0.02 (04)	0.00	0.00 (01)	0.00 (01)	0.00 (01)	0.00 (01)	0.00 (01)
MgO	0.00	0.00	0.00	0.00	0.00	0.00	0.00	0.00	0.00
CaO	2.05 (17)	1.55 (11)	1.91 (14)	1.82 (04)	2.41 (16)	3.58 (09)	3.35 (19)	3.13 (14)	3.02 (20)
Na_2O	9.42 (18)	9.65 (15)	9.65 (08)	9.53 (16)	9.38 (11)	8.92 (07)	8.87 (11)	9.00 (06)	9.00 (11)
K_2O	1.56 (14)	1.72 (17)	1.40 (15)	1.76 (06)	1.56 (17)	1.21 (08)	1.36 (10)	1.37 (07)	1.41 (07)
Total	100.74	100.58	100.21	101.32	99.85	99.48	99.80	100.29	100.66
[1]Avg. mol% An	9.8 (8)	7.3(5)	9.1(7)	8.6(3)	11.34 (8)	16.9 (4)	16.0 (9)	14.9 (6)	14.4 (9)
min. mol% An	7.9	6.1	7.7	8.2	9.5	16.0	13.8	13.2	11.9
max. mol% An	11.5	8.2	10.3	8.9	12.6	18.0	18.0	16.3	16.4
San, *N;n*	10;24	32;93	22;302	14;35	1;34	1;54	2;34	2;7	15;39
SiO_2	66.68 (14)	66.43 (33)	65.82 (27)	66.36 (49)	65.48 (28)	65.33 (28)	65.39 (28)	65.85 (12)	66.05 (40)
TiO_2	0.00	0.00 (01)	0.00	0.00 (01)				0.01 (01)	0.00 (01)
Al_2O_3	18.79 (10)	18.81 (21)	18.79 (10)	18.85 (26)	18.57 (13)	18.51 (15)	18.60 (14)	18.65 (05)	18.75 (17)
FeO^T	0.09 (01)	0.10 (01)	0.08 (01)	0.09 (01)	0.09 (01)	0.08 (01)	0.08 (02)	0.08 (01)	0.08 (01)
MnO	0.00 (01)	0.00 (01)	0.01 (03)	0.00 (01)	0.00 (01)	0.00 (01)	0.00 (01)	0.01 (01)	0.00
MgO	0.00	0.00	0.00	0.00	0.00	0.00	0.00	0.00	0.00
CaO	0.16 (02)	0.17 (02)	0.14 (02)	0.16 (02)	0.17 (02)	0.17 (01)	0.18 (01)	0.18 (01)	0.19 (02)
Na_2O	4.6 (08)	5.00 (12)	4.51 (08)	4.76 (13)	4.33 (14)	3.87 (08)	3.86 (09)	3.99 (04)	3.97 (07)
K_2O	10.86 (15)	10.17 (16)	10.88 (13)	10.51 (13)	11.31 (22)	11.95 (16)	12.09 (33)	11.69 (12)	11.68 (15)
Total	101.16	100.67	100.22	100.74	99.95	99.91	100.20	100.43	100.73
[2]Avg. mol% Or	60.4 (7)	56.8 (9)	61.0 (7)	58.8 (8)	62.7 (1.2)	66.5 (7)	66.8 (1.05)	65.3 (4)	65.3 (5)
min. mol% Or	58.9	54.5	58.2	57.0	60.1	64.6	64.0	65.0	64.4
max. mol% Or	61.7	59.0	62.8	60.4	64.6	67.8	68.0	66.0	66.7

[1] An # (=100 x moles CaO/[moles CaO+Na_2O+ K_2O])

[2] Or # (=100 x moles K_2O/[moles Na_2O+ K_2O]

Parentheses values represent the sample population 1 SD on the last digits

Table 3–3 continued

Sample/Run *T*–Path	9–1 Top Down	9–2 Top Down	3 Top Down
Plag, *N;n*	4;9	4;4	
SiO_2	66.64 (1.06)	66.70 (68)	
TiO_2	0.01 (01)	0.00	
Al_2O_3	20.84 (42)	20.92(21)	
FeO^T	0.20 (07)	0.10 (01)	
MnO	0.01 (01)	0.00	
MgO	0.01 (02)	0.00	
CaO	1.70 (36)	1.55 (21)	
Na_2O	9.54 (58)	9.44 (25)	
K_2O	1.63 (50)	1.26 (46)	
Total	100.56	99.96	
[1]Avg. mol% An	8.1(1.8)	7.7 (1.01)	
min. mol% An	5.5	6.8	
max. mol% An	10.6	8.6	
San, *N;n*	4;33	6;50	1;13
SiO_2	65.29 (85)	65.60 (85)	66.64 (84)
TiO_2	0.00 (01)	0.00 (01)	0.00 (02)
Al_2O_3	18.14 (37)	18.07 (49)	18.27 (33)
FeO^T	0.15 (05)	0.15 (06)	0.44 (06)
MnO	0.00	0.00	0.01 (01)
MgO	0.00	0.00	0.00
CaO	0.10 (09)	0.09 (11)	0.10 (05)
Na_2O	2.87 (40)	2.60 (42)	2.43 (14)
K_2O	12.97 (65)	12.87 (64)	12.81 (16)
Total	99.52	99.38	100.72
[2]Avg. mol% Or	74.5(3.5)	76.2 (3.8)	77.3 (1.2)
min. mol% Or	69.2	69.8	75.7
max. mol% Or	80.8	80.4	79.4

A large change in composition is found between the pristine cores of sanidine crystals and their altered rims. The rims, which appear dark in BSE images (Fig. 3–10), have compositions that often range from $Or_{10–20}$ and sometimes as low as Or_5. Thus, the altered rims appear to the be the result of albitization (i.e., ion exchange of Na+ for K+), perhaps through deuteric alteration after exsolution of a late–stage sodium–rich aqueous fluid phase (e.g., Wilshire, 1959). Its ubiquity in the GM units and absence in sanidine crystals in the Bishop Tuff is notable. Note that similarly low Or contents in sanidine were reported in Metz and Mahood (1991) but assumed to be xenocrystic. From the BSE images in Figure 3–10, it is likely that albitized portions of sanidine were unintentionally analyzed in that study, since the alteration is difficult to detect without BSE imaging.

3.6.3 Biotite

As noted previously, biotite is found in eight of the nine eruptive units in this study. The average composition of biotite in five of the GM units (OB, OC, OL, OT and YO) were previously reported in Chapter 2. For the remaining three GM units (OD, YE, YG), individual analyses of biotite phenocrysts are available in Supplemental Table B-0-12. The average biotite composition from all eight GM units are reported in Table 3–4, along with the number of biotite crystals that were analyzed (N) and the total number of analyses (n) for that sample. Concentrations of FeO, Fe_2O_3, and H_2O were calculated on the basis of stoichiometry (model of Li et al. (2020) and only analyses with totals from 97–101 wt% are used. Calculated water contents in biotite are all ~2.7 wt%, and calculated Fe^{3+}/Fe^{T} ratios range from 0.24–0.30. Average concentrations of TiO_2 range from 3.7–4.6 wt%.

Table 3-4: Averaged analyses natural biotite grains (wt%)

Sample	GM– 18	GM–01	GM_JJ_10	GM–07	GM–20	GM_16	GM_13	GM–10
Unit	OB	OC	OD	OL	OT	YE	YG	YO
N;n	9;45	1;6	13;163	8;55	2;71	33;119	39;107	10;56
SiO_2	35.97 (59)	35.43 (44)	35.02(41)	36.54 (59)	36.13 (32)	35.99(21)	36.28(34)	36.33 (60)
TiO_2	3.74 (22)	4.57 (06)	3.88(10)	3.72 (19)	4.40 (11)	4.31(12)	4.34(14)	4.27 (07)
Al_2O_3	12.28 (22)	12.69 (19)	12.39(33)	12.26 (26)	12.67 (41)	12.71(11)	12.79(14)	12.53 (23)
FeO^T	25.49 (77)	28.55 (31)	27.92(61)	24.25 (83)	23.79 (91)	22.77(49)	22.75(98)	23.43 (67)
MnO	0.55 (02)	0.30 (01)	0.89(05)	0.69 (06)	0.40 (02)	0.28(01)	0.28(02)	0.33 (02)
MgO	8.44 (35)	5.28 (09)	6.41(32)	9.02 (41)	9.53 (53)	10.19 (15)	10.30(46)	9.57 (27)
CaO	0.00 (01)	0.0 (00)	0.04(12)	0.00 (01)	0.01 (00)	0.00 (01)	0.00(01)	0.00 (01)
Na_2O	0.52 (02)	0.40 (02)	0.47(05)	0.54 (02)	0.55 (04)	0.54(02)	0.55(03)	0.54 (02)
K_2O	9.26 (11)	9.15 (07)	9.34(17)	9.21 (12)	9.50 (18)	9.44(09)	9.51(08)	9.35 (10)
BaO	0.03 (02)	0.09 (02)	0.03 (02)	0.03 (02)	0.02 (02)	0.03(02)	0.04(04)	0.03 (02)
Fe_2O_{3calc}	8.13	7.63	8.56	8.00	6.97	6.69	6.67	6.99
FeO_{calc}	18.18	21.68	20.22	17.05	17.52	16.75	16.75	17.14
H_2O_{calc}	2.75	2.66	2.67	2.70	2.67	2.70	2.71	2.68
$Total_{calc}$	99.84	99.88	99.92	99.77	100.37	99.63	100.22	99.76
[1]Mg#	37	25	29	40	42	44	45	42
Fe^{3+}/Fe^T	0.29	0.24	0.28	0.30	0.26	0.26	0.26	0.27
T. Si	2.84	2.84	2.81	2.86	2.83	2.82	2.83	2.84
T.Al	0.87	0.86	0.90	0.86	0.93	0.94	0.94	0.90
T.Fe^{3+}	0.29	0.30	0.29	0.27	0.24	0.24	0.23	0.25
sum Tet	4.00	4.00	4.00	4.00	4.00	4.00	4.00	4.00
M.Al	0.27	0.34	0.27	0.27	0.24	0.23	0.23	0.25
M.Mg	1.02	0.69	0.82	1.08	1.13	1.20	1.20	1.13
M.Fe^{2+}	1.20	1.45	1.36	1.12	1.15	1.10	1.09	1.12
M.Fe^{3+}	0.19	0.16	0.23	0.20	0.17	0.16	0.16	0.16
M.Ti	0.22	0.27	0.23	0.22	0.25	0.25	0.25	0.25
M.Cr	0.00	0.00	0.00	0.00	0.00	0.00	0.00	0.00
M.Mn	0.04	0.02	0.06	0.05	0.03	0.02	0.02	0.02
M.Ni	0.00	0.00	0.00	0.00	0.00	0.00	0.00	0.00
M.Li	0.00	0.00	0.00	0.00	0.00	0.00	0.00	0.00
sum oct	2.94	2.93	2.96	2.92	2.95	2.96	2.95	2.94
Oct Vacancy	0.06	0.07	0.04	0.08	0.05	0.04	0.05	0.06
A.K	0.92	0.92	0.95	0.92	0.94	0.93	0.93	0.92
A.Na	0.08	0.06	0.07	0.08	0.08	0.08	0.08	0.08
A.Ba	0.00	0.00	0.00	0.00	0.00	0.00	0.00	0.00
A.Ca	0.00	0.00	0.00	0.00	0.00	0.00	0.00	0.00
sum inter	1.01	0.99	1.03	1.00	1.02	1.01	1.01	1.01
Inter Vacancy	0.00	0.01	0.00	0.00	0.00	0.00	0.00	0.00
W.F	0.00	0.00	0.00	0.00	0.00	0.00	0.00	0.00
W.Cl	0.00	0.00	0.00	0.00	0.00	0.00	0.00	0.00
W.OH	1.45	1.42	1.43	1.41	1.39	1.41	1.41	1.40
W.O^{2-}	0.55	0.58	0.57	0.59	0.61	0.59	0.59	0.60

OB, OC, OL, OT, YO previously reported in Chapter 2
Parentheses values represent the sample population 1 SD on the last digits
Biotite formula calculated using Li et al., 2020
[1]Mg# = molar MgO/(MgO +FeO^T) x100

3.7 Thermometry

3.7.1 Fe–Ti two–oxide thermometry

As noted in the Previous Work section, Fe–Ti two–oxide thermometry, using the model of Ghiorso and Evans (2008), was previously obtained on five of the eight eruptive units (OB, OC, OL, OT, YO) by Gordon (2022). In addition, Gordon (2022) recalculated Fe–Ti two–oxide temperatures from the oxide analyses reported in Metz and Mahood (1991) for seven units (OL, ON, OT, OX, YG, YJ and YK). Both Metz and Mahood (1991) and Gordon (2022) report Fe–Ti oxide analyses for units OL and OT. A comparison of recalculated temperatures from the two sets of analyses shows agreement (698 vs 703 °C, unit OL; 724 vs 716 °C, unit OT) (Table 3–5), within the propagated uncertainty of < ±10°C (Further explanation in Text A.1). This close agreement suggests that all recalculated Fe–Ti two–oxide temperatures (using the model of Ghiorso and Evans, 2008) from the data of Metz and Mahood (1991) can be used in this study. The combined Fe–Ti two–oxide temperatures are illustrated in Figure 3–13. They show that the Older GM units span a wide temperature interval of 660–724 °C, whereas the Younger GM units have temperatures that only overlap the upper half of this interval (695–725 °C).

3.7.2 Biotite–Liquid Thermometry

The biotite thermometer that is used in this study is one that is based on the partitioning of TiO_2 between biotite and liquid ($D_{TiO2}^{bte-liq} = \frac{wt\%\ TiO2^{bte}}{wt\%\ TiO2^{liq}}$), and it has been specifically calibrated on high–SiO_2 rhyolites (Chapter 2). The simple, calibrated model is:

$$T(°C) = 846\ (\pm 7) - 2.32\ (\pm 0.15)^{*}\ D_{TiO2}^{bte-liq} \quad (1)$$

Application of this thermometer enables temperature to be determined in GM units where ilmenite is absent and/or the Fe–Ti oxides are altered, which precludes application of Fe–Ti oxide thermometry.

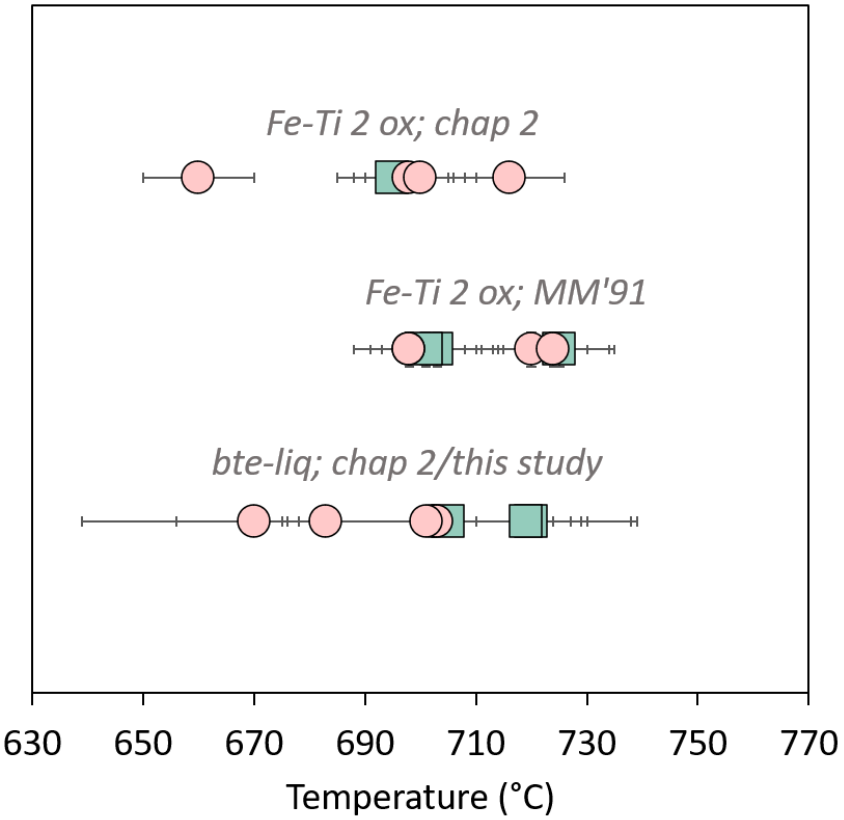


Figure 3-13: A comparison of all thermometry results for Older (pink circles) and Younger (green squares) GM units. The top and middle rows show temperatures calculated with the Ghiorso and Evans (2008) Fe–Ti two–oxide thermometer, using titanomagnetite and ilmenite analyses from Gordon (2022) and Metz and Mahood (1991), respectively. Collectively, the results show that the Older GM units span a wide range of temperature (660–724 °C), whereas the Younger GM units span the upper half of this interval (695–725°C). The third row shows results from the biotite–liquid thermometer from Chapter 2 based on biotite analyses reported in Table 3–4. The two thermometers provide broadly consistent results, indicating a range of temperatures between ~660 and ~725 °C for the GM units. Error is 1SD.

To calculate temperature, the value of $D_{TiO2}^{bte-liq}$ must be determined for each sample. Since biotite crystallizes close to the liquidus of HSR under hydrous conditions (e.g., Waters and Andrews, 2016), $D_{TiO2}^{bte-liq}$ values for the eight GM units with biotite are based upon the ratio of wt% TiO_2 in biotite (Table 3–4) over the wt% TiO_2 in the whole–rock composition (Table 3–1). In other words, the assumption made in this study is that biotite was one of the first phases to crystallize from a liquid composition that matches that of each whole–rock sample.

Table 3-5: Calculated temperatures for GM units

Sample	GM–18	GM–01	GM–07	GM–20	GM–10	GM–JJ–10	GM–16	GM–13
Eruptive unit	OB	OC	OL	OT	YO	OD	YE	[3]YG
Avg Bte wt% TiO_2	3.74	4.57	3.72	4.40	4.27	3.88	4.31	4.34
± 1 SD	0.22	0.06	0.19	0.11	0.07	0.1	0.12	0.14
WR wt% TiO_2	0.06	0.06	0.06	0.07	0.07	0.06	0.08	0.08
± 1 SD	0.01	0.01	0.01	0.01	0.01	0.01	0.01	0.01
Calculated D_{TiO_2}	62.3	76.1	62.0	62.9	61.0	64.7	53.9	54.3
± 1 SD	11.4	15.1	10.5	9.9	8.3	13.0	7.1	7.2
[1]$D_{TiO_2}^{bte-liq}$ Temperature (°C)	702	670	703	701	705	697	722	721
± 1 SD (model error)	27	31	27	23	22	27	19	19
[2]Fe–Ti Oxide Temperature (°C)	698	660	700	716	695			703
Difference	–4	–10	–3	15	–10			–18

OB, OC, OL, OT, YO previously reported in Chapter 2

[1] $D_{TiO_2}^{bte-liq}$ thermometer from Chapter 2

[2] thermometer of Ghiorso and Evans (2008)

[3] temperature from ilmenite and titanomagnetite analyzed by Metz and Mahood (1991) and recalculated using Ghiorso and Evans (2008)

The resulting $D_{TiO2}^{bte-liq}$ ratios are reported in Table 3–5, along with propagated 1s errors from the analysis of TiO_2 in biotite (Table 3–4) and in the whole–rock (± 0.01 wt%). $D_{TiO2}^{bte-liq}$ values (based on the average biotite composition in each sample) range from 53.9–76.1, with 1SD uncertainties that range from ± 7.1–15.1. The temperatures calculated for the GM samples, using Eq. 1 from Gordon (2022), range from 670–722°C. There are two primary sources of error in these temperatures: (1) the uncertainty in $D_{TiO2}^{bte-liq}$ and (2) the uncertainty in the model. In Table 3–5, the 1s propagated error from these two sources on the calculated temperature for each sample is shown, and ranges from ± 19–31 °C. The relatively large errors are primarily due to the low whole–rock concentrations of TiO_2 (~0.06–0.07 wt%) in the GM samples, combined with their analytical uncertainty (± 0.01 wt%) (Gordon et al., 2026). A summary of the biotite–liquid thermometry results suggest that the Older GM units crystallized at systematically cooler temperatures (670–703°C) compared to the Younger GM units (705–722°C).

A comparison of the biotite and Fe–Ti two–oxide temperatures is illustrated in Figure 3–13, and also in a 1:1 plot for samples where a direct comparison can be made (Figure 3–14). Overall, the agreement is within reported 1SD uncertainties.

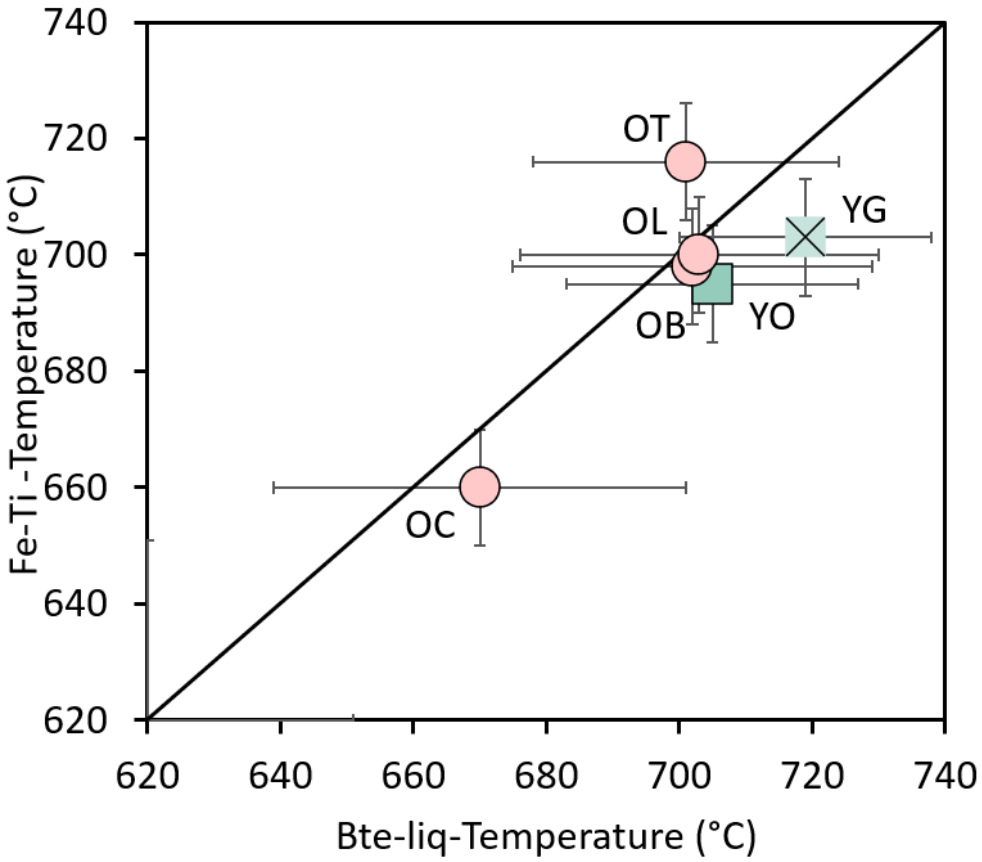


Figure 3-14: A 1:1 plot comparing Fe–Ti two–oxide temperatures, using the Ghiorso and Evans (2008) thermometer, with Chapter 2 biotite–liquid temperatures on samples where both were obtained. Older GM units are shown as pink circles while Younger GM units are shown as green squares. There is good agreement within error between the two thermometers. Note that the Fe–Ti oxide temperature for unit YG is based on oxide analyses reported in Metz and Mahood (1991). Error bars represent propagated 1SD.

3.8 Hygrometry

3.8.1 Sanidine–liquid hygrometry calibrated on high–SiO_2 rhyolite

As noted in the Previous Work section, Waters and Andrews (2016) conducted hydrous phase–equilibrium experiments on a high–SiO_2 rhyolite from the Glass Mountain complex (unit YE). One of the most striking findings in their study is that the composition of sanidine (i.e., Or

content) varies with temperature and the dissolved water content in the coexisting melt. Specifically, the Or content in sanidine increases with increasing temperature and/or increasing water in the melt. The effect of dissolved water in the melt is clearly seen in the experiments conducted over a range of P_{H2O}, but at isothermal conditions at 700 °C (Fig. 3–15). As dissolved hydroxyl groups in the melt increase, they preferentially complex with Na^+ relative to K^+, which reduces the availability of Na to form the albite component (i.e., it reduces the activity of the albite component in the melt; Waters and Andrews, 2016). This, in turn, leads to higher Or contents in sanidine phenocrysts at higher melt water contents. An advantage of using sanidine (vs plagioclase) compositions for hygrometry in high–SiO_2 rhyolite melts is because of the relatively rapid Na–K ionic exchange between sanidine and melt, which enables the Or content in sanidine to reach equilibrium relatively quickly. In contrast, the NaSi–CaAl exchange between plagioclase and melt (the basis of the plagioclase–melt hygrometer; Waters and Lange, 2015) involves slow diffusion of covalently bonded Si and Al in both plagioclase and melt.

With independent constraints on temperature in hand (from Fe–Ti two–oxide and biotite–liquid thermometry), the analyzed sanidine compositions in Table 3–3 were compared to those in the phase–diagram of Waters and Andrews (2016). This enabled broad constraints to be placed on the water contents at the time of sanidine crystallization in the GM high–SiO_2 rhyolites. For the four eruptive units (OB, OL, YG, YO) with Fe–Ti two–oxide temperatures that cluster ~700 °C (695–703 °C), their collective range in average sanidine composition (Or_{59} – Or_{65}) indicate a range in water contents of ~4.8 to ~5.3 wt%. Unit OD has a biotite crystallization temperature that is also close to ~700 °C (697 ± 31 °C; Table 3–5) and an average sanidine composition of Or_{61}, which suggests an average water content of ~5 wt%. Finally, unit YE has a higher biotite

crystallization temperature of ~722 (± 19) °C, and its average sanidine composition of Or_{65} suggests a melt water content of ~5 wt %.

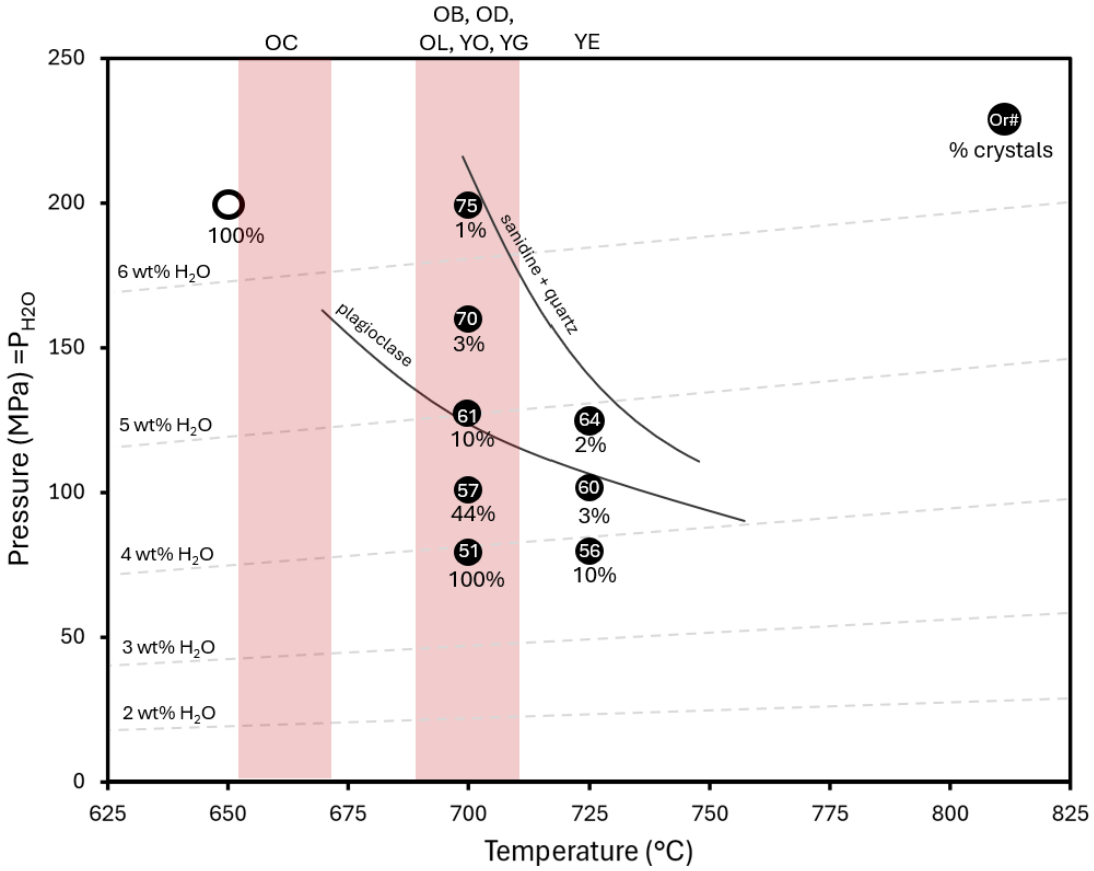


Figure 3-15:A simplified water–saturated phase equilibrium diagram for a representative GM unit (YE) modified from Waters and Andrews (2016) based on their experimental results. Pressure (MPa) is shown on the y–axis and temperature (°C) is shown on the x–axis. Dashed lines show isopleths of dissolved H_2O contents in the melt (Zhang et al., 2007) and solid lines show approximate mineral in–curves for tectosilicate phases. Select experiment runs by Waters and Andrews (2016) are shown as a black circle and the bottom–up experiment run in this study is shown as an open circle. The mol% Or in sanidine is above the circle, and the total % crystals is below the circle for the run products reported in Waters and Andrews (2016). Two red bands are superimposed on the diagram showing the approximate temperature of several GM units (denoted at the top of each band). See text for details.

3.9 Discussion

The primary goal of this study is to understand the cause for the large variation in the abundance of phenocrysts in the Glass Mountain high–SiO_2 rhyolites, given their near–eutectic melt compositions. With constraints on the temperature and amount of dissolved water in the GM melts at the time of phenocryst growth in hand, together with documentation of phenocryst

textures and new experimental constraints on the location of the water–saturated solidus at 200 MPa, three different hypotheses to explain the phenocryst variability can be evaluated.

3.9.1 Do Glass Mountain phenocryst abundances reflect equilibrium T–P_{H2O} conditions?

The first hypothesis to consider is that the variability of phenocryst contents in the different GM units reflects equilibrium conditions in pre–eruptive magmatic reservoir(s). If so, it is expected that the large differences in phenocryst abundances (<1 to 20%) must reflect variations in the temperature and melt water content during crystal growth. This hypothesis is readily evaluated with the new thermometry results obtained in this study, together with the phase–equilibrium data (Figure 3–15) from Waters and Andrews (2016).

3.9.2 A comparison of four GM units (YO, YG, OB, OL) at ~700°C

Two Younger GM units (YO and YG) have Fe–Ti two–oxide temperatures close to 700 °C (695 and 703 °C; Table 3–5), and sanidine compositions that span $Or_{67–64}$ and $Or_{68–64}$, respectively. According to the phase–equilibrium experiments of Waters and Andrew (2016), for these temperatures and sanidine compositions, water contents are >5 wt% and phenocryst abundances are expected to be <10%, which is the case for both YO (~3%) and YG (~6%). However, the *T–*P_{H2O} conditions during phenocryst growth in YO and YG are above the plagioclase–in curve, and yet both units contain euhedral phenocrysts of plagioclase, which is not explained by the phase–equilibrium experimental data (Fig. 3–15).

Two Older GM units (OB, OL) also have Fe–Ti oxide temperatures close to 700 °C (698 and 700 °C; Table 3–5). For these two units, the range in their sanidine compositions ($Or_{62–59}$ and $Or_{60–57}$, respectively) places phenocryst growth at melt water contents ≤5 wt% and thus below the plagioclase–in curve, consistent with the presence of plagioclase in both units. What is contradictory, however, is that the equilibrium phenocryst abundances in both units are expected

to be ≥ 10% below the plagioclase–in curve at 700 °C (Fig. 3–15), and yet both OB and OL have very low (1–3%) phenocryst abundances.

3.9.3 A comparison of units OD and OC

Unit OD has a biotite crystallization temperature that is also close to ~700 °C, albeit with a larger uncertainty (697 ± 27 °C). The range in sanidine composition in this sample ($Or_{63–58}$) places most of its crystallization below the plagioclase–in curve, consistent with plagioclase in this sample. Moreover, the overall phenocryst abundance of ~20% is broadly consistent with the bounds between ~10% and ~44% over this range of sanidine composition at ~700°C (Fig. 3–15). Thus, within uncertainties, unit OD has an overall phenocryst abundance and assemblage (i.e., quartz + sanidine + plagioclase) that is consistent with the phase–equilibrium experiments of Waters and Andrews (2016).

However, it is a comparison of unit OC with unit OD that leads to a significant discrepancy with the equilibrium data in Figure 3–15. Unit OC has an Fe–Ti oxide temperature of 660 (±10) °C and a biotite temperature of ~670 (±31) °C, and thus the evidence strongly indicates it grew its phenocrysts at a temperature below (or, within error of) that for unit OD. Moreover, the orthoclase content in its sanidine phenocrysts ranges to lower values ($Or_{59–55}$) than found in unit OD ($Or_{63–58}$), which indicates lower water contents. Thus, unit OC grew its phenocrysts at lower temperatures and/or lower water contents compared to unit OD, which should lead to a higher phenocryst abundance in unit OC relative to unit OD. However, the abundance of phenocrysts in unit OC is only ~8% compared to ~20% in unit OD, which cannot be explained by equilibrium phenocryst abundances.

In fact, the overall observation that the vast majority (~78%) of GM units contain all three tectosilicate phases and yet have overall phenocryst abundances that are exceptionally low

(<1–3%) is inconsistent with available phase–equilibrium experiments on high–SiO_2 rhyolite (e.g., Waters and Andrews, 2016; Scaillet and Hildreth, 2001). These studies demonstrate that once all three tectosilicates (quartz, sanidine, plagioclase) are co–crystallizing under equilibrium conditions, it only takes a very small drop in temperature (~20 degrees) and/or decrease in P_{H2O} (loss of < 0.5 wt% dissolved water) to induce a massive (i.e., ≥50%) increase in crystallinity, which will dramatically increase magma viscosity and preclude eruption. For unit OC, with a phenocryst growth temperature of ~660°C and the presence of all three tectosilicate phases present, it surprising that it only contains ~8% phenocrysts, especially given the water–saturated granite solidus of Ebadi and Johannes (1991) at P_{H2O} = 200 MPa of ≥ 670 °C.

3.9.4 Do Glass Mountain phenocryst abundances reflect a lower water–saturated granitic solidus?

The second hypothesis to evaluate is that the water–saturated granitic (i.e., high–SiO_2 rhyolite composition) solidus is lower than previously understood (e.g., Johannes and Holtz, 1996). Recent experiments of Thompson et al. (2026) suggest that the water–saturated solidus at 200 MPa is~620–625 °C, which contradicts the experimentally determined water–saturated solidus at 200 MPa of ≥ 670 °C reported by Ebadi and Johannes (1991). The results from the bottom–up experiments conducted in this study at P_{H2O} = 200 MPa (Figure 3–15) show that complete crystallization of water–saturated high–SiO_2 rhyolite occurred at 650 °C, which indicates a water–saturated solidus at ≥ 650 °C at this pressure. This result is consistent with the experimental results of Ebadi and Johannes (1991), but it is ~30 degrees hotter than the temperature reported by Thompson et al. (2026). Since their experimental procedure most closely follows the bottom–up trajectory (i.e., their starting glass was taken directly up to the experimental final temperature), the only key difference between the two experimental studies is the duration of the runs. Thompson et al. (2026) held their experiment for 5 days, whereas ours

was held for 25 days (Table 3–2). Thus, it is possible that the difference in results is due to kinetic effects and durations longer than five days are needed for complete crystallization at these temperatures. In summary, given the experimental results from this study, where complete crystallization occurs at 650 °C and P_{H2O} = 200 MPa, the phenocryst abundance of only ~8% for unit OC with an Fe–Ti oxide temperature of ~660 (±10) °C remains unexplained.

3.9.5 Do Glass Mountain phenocryst abundances reflect kinetic effects during rapid phenocryst growth during dike ascent?

The third hypothesis considered in this study is that the variable (and often, surprisingly low) phenocryst abundances in the GM units reflects kinetic effects that develop when phenocrysts grow rapidly during dike ascent to the surface, as schematically illustrated in Figure 3–16. Here, the decompression path for a high–SiO_2 rhyolite melt at ~700°C (e.g., units YO, YG, OB, OL) is shown. According to this diagram, an ascending melt at ~700 °C will cross the liquidus at a P_{H2O} = ~200 MPa (at a melt water content of ~6.3 wt%). However, because sanidine phenocrysts with Or contents ≥ 70 are not found in any of the natural GM samples, including those with Fe–Ti oxide temperatures close to ~700°C, a kinetic delay to nucleation must have occurred. The proposed paths of two specific samples (unit YO and unit OL) are described below.

For unit YO, it appears that phenocrysts of sanidine ($Or_{67–64}$) did not grow until a P_{H2O} = ~140 MPa was reached (melt water contents of ~5.5 wt %), where the corresponding liquidus temperature is 725°C (Fig. 3–16). Therefore, the onset of cotectic phenocryst growth in unit YO appears to have occurred at an effective undercooling (ΔT_{UC}) of ~25 °C ($\Delta T_{UC} = T_{liquidus}–T_{melt}$ = 725–700 °C). As the YO melt continued to ascend, it crossed into the plagioclase stability field and grew a sparse amount of large plagioclase crystals, some of them preferentially nucleating

on sanidine (e.g., Fig. 3–10h). Owing to kinetic delays in crystallization during dike transport, only a total of 3% phenocrysts grew during its ascent to the surface.

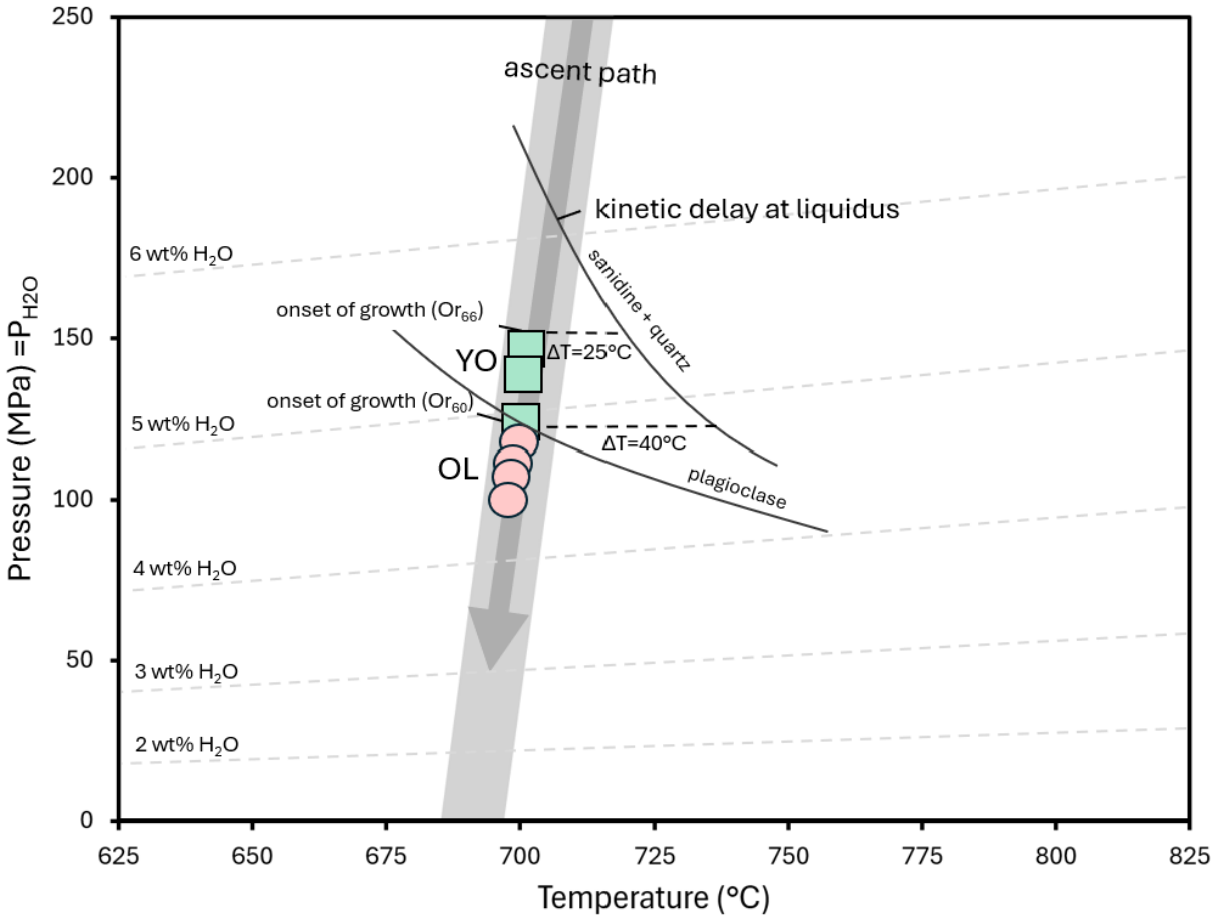


Figure 3-16: A schematic illustration of the ascent path for GM units YO (green squares) and OL (pink circles), which both have pre–eruptive temperatures of ~700 °C, superimposed on the simplified experimental phase diagram of Waters and Andrews (2016). A grey band and arrow show the ascent path of these high–SiO_2 rhyolites in a dike. The highest sanidine composition (Or_{66}) in unit YO records the onset of sanidine growth at an undercooling of ~25 °C, indicative of a kinetic delay to nucleation. Plagioclase is present in unit YO and thus it continued to grow phenocrysts during ascent to conditions below plagioclase in–curve. Similarly, the highest sanidine composition (Or_{60}) in unit OL indicates the onset of sanidine growth in that sample at an undercooling of ~40 °C, perhaps indicating a longer kinetic delay to nucleation and/or a faster ascent rate than in unit YO.

Similarly, for unit OL, it appears that phenocrysts of sanidine ($Or_{60–57}$) did not grow until a P_{H2O} = ~120 MPa was reached (melt water contents of ~4.8 wt %), where the corresponding liquidus temperature is ~745°C (Fig. 3–16). Therefore, the onset of cotectic phenocryst growth in unit OL appears to have occurred at an effective undercooling (ΔT_{UC}) of ~40 °C ($\Delta T_{UC} = T_{liquidus}–T_{melt}$ = 740–700 °C). At this $T–P_{H2O}$ condition, OL is in the plagioclase stability field and so all three tectosilicates are expected to grow. Once again, owing to kinetic delays, only a total of 3% phenocrysts (quartz, sanidine and plagioclase) grew during the rapid ascent of unit OL, via dike transport, to the surface.

It is proposed that a similar path was followed by all GM units, where phenocryst growth occurred during dike transport to the surface. Support for this hypothesis is found also in the abundant rapid–growth textures (e.g., hopper) in sanidine and quartz from numerous GM units (Figs. 8 and 9). Barbee et al. (2020) demonstrate that textural features in quartz such as embayments, hopper cavities, melt inclusions and hollow faces are due to rapid crystallization at various degrees of undercooling over short timescales. Similar rapid–growth, hopper textures are documented in the top–down experimental run (#9) conducted in this study (e.g., Figs. 6 and 7), where phenocryst–sized crystals (≤ 200–300 μm) grew within ~3 weeks duration (Fig. 3–6), in viscous high–SiO_2 rhyolite melt (~5.6 $\log_{10}$ Pa–s). Biotite phenocrysts in the GM units (Fig. 3–12) also show rapid–growth textures (i.e. melt hollows, rounded and nubby corners). Granophyric textures are also visibly present in seven GM units (OB, OC, OD, OT, YA/YB, YE and YO), as seen in Figure 3–8. In an H_2O–saturated decompression experiment, which mimics H_2O degassing during ascent, Waters and Andrews (2016) grew granophyric intergrowths of quartz and sanidine in ≤ 9 days.

In summary, the available evidence strongly supports the hypothesis that rapid phenocryst growth occurred in the GM melts during dike transport to the surface. The abundance of phenocrysts most likely reflects the effects of kinetics and available time scales for their growth (i.e., the speed of their ascent in dikes) rather than $T–P_{H2O}$ conditions in a pre–eruptive magmatic reservoir.

3.9.6 Evidence of direct dike ascent between melt segregation and eruption: unit OC and OL

As noted earlier in the Previous Work section, Gordon et al. (2026) point out that the $^{40}Ar/^{39}Ar$ eruption age for unit OC (2.059 ± 0.020 Ma; Simon et al., 2014) and unit OL (1.867 ± 0.005 Ma, Davies et al, 1994; 1.939 ± 0.026 Ma; Simon et al., 2014) cannot be resolved from the age of their respective Rb/Sr isochrons (2.047 ± 0.013 Ma and 1.894 ± 0.014 Ma, respectively; Davies et al., 1994). Each of the four Glass Mountain Rb/Sr isochrons (Davies et al., 1994; Davies and Halliday, 1998) dates the age at which each of the GM melts segregated from their granitic parent. Because units OC and OL have eruption ages that are indistinguishable from their melt segregation ages, it is plausible that they ascended directly to the surface, via dike transport, immediately following segregation from their parental source region.

A schematic illustration of how an undercooling develops during dike transport to the surface is shown in Figure 3–17, enabling the growth of large, sparse phenocrysts as seen in units OC and OL (and most GM units). As noted in Waters and Lange (2017), it is necessary (for successful eruption) that high–SiO_2 rhyolite melts segregate from their source regions fluid undersaturated, which causes their liquidus temperature to decrease as they ascend (along a dike)

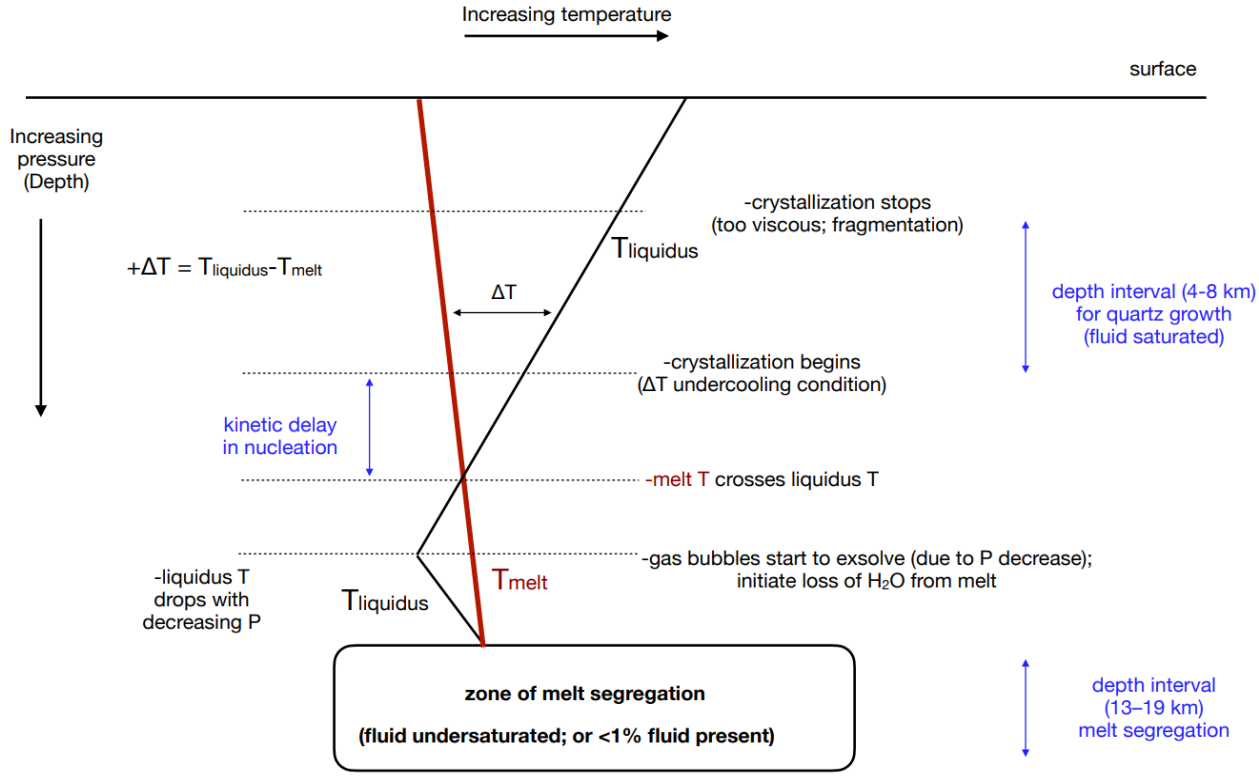


Figure 3-17: A schematic diagram of magma ascent through the crust demonstrating how phenocryst growth during an undercooling develops, following a kinetic delay to crystal nucleation. The x–axis (top) tracks temperature increasing from left to right, while the y–axis (left) tracks pressure (increasing downward with depth). The black solid line shows the temperature change of the liquidus of the melt while the red solid line shows the actual temperature of the melt. If the magma segregates fluid undersaturated, then rapid ascent in a dike will cause the liquidus temperature to decrease due to decompression. This will lead to an interval during ascent when the melt is superliquidus, eliminating the presence of any nuclei. However, after continued ascent, fluid saturation will eventually occur, causing water to be exsolved from the melt, which will lead to an increase in the liquidus temperature during continued magma ascent. Eventually, the temperature of the melt will cross the liquidus, but because there are no nuclei present, a kinetic delay to nucleation is likely, leading to the development of an undercooling (where the temperature of the melt is lower than the liquidus temperature). From Figure 3–3, it is seen that moderate undercoolings lead to relatively high crystal growth rates at low nucleation rates, enabling the growth of large, sparse phenocrysts, which is observed in the GM high–SiO_2 rhyolites.

due to decompression (Fig. 3–17). If the rate of cooling during dike transport is less than the drop in the liquidus temperature, the melt will attain super–liquidus conditions (Waters and Andrews, 2016; Waters and Lange, 2017) and any existing nuclei will melt. However, with continued ascent (i.e., decompression), the melt will eventually become saturated with H_2O–rich fluid, and thus the liquidus temperature will begin to increase due to loss of dissolved H_2O from the melt during continued ascent (Fig. 3–17). The temperature of the ascending melt will

eventually cross its own liquidus. At equilibrium conditions (i.e., those in a magma chamber), crystallization commences immediately at the liquidus (by definition). However, within the ascending melt, there is a kinetic delay to nucleation due to the elimination of nuclei during its earlier super–liquidus condition (Fig. 3–17). This kinetic delay leads to an undercooling ($\Delta T = T_{liquidus} - T_{melt}$), where the temperature of the melt is below its own liquidus. Figure 3–3 illustrates that, at modest undercoolings, crystallization rates are expected to be high while nucleation rates are low, leading to the growth of large, sparse crystals (a characteristic of GM units).

In this study, we propose that units OC and OL ascended directly to the surface after they segregated from their granitic parental source, leading to phenocryst growth en route. For the other GM units, Gordon et al. (2026) proposed that they crystallized into a sill/dike complex after their segregation from their parental source and were later fully re–melted (owing to their eutectic melt compositions) due to the influx of hot, H_2O–rich fluids (from degassed basalts at depth), enabling their subsequent ascent to the surface. The primary conclusion drawn in this study is that all of the high–SiO_2 rhyolites that successfully erupted to form the Glass Mountain volcanic complex (Fig. 3–2) grew their phenocryst during ascent to the surface and not in long–lived magmatic reservoirs.

3.10 Conclusions

This study evaluated three hypotheses to explain the cause of the highly variable phenocryst abundances in the different GM units despite their nearly unchanging major–element compositions. The three hypotheses evaluated in this study were: (1) the large differences observed in phenocryst abundances (<1–20%) reflected variations in the temperature and melt water content during phenocryst growth, (2) the water–saturated granite solidus is lower than

previously understood, or (3) phenocryst growth occurred during ascent, driven by degassing, following a kinetic delay to nucleation.

Sanidine compositions, thermometry and hygrometry results from GM units with largely the same calculated temperature (~ 700 °C) allowed for the first hypothesis to be evaluated against phase equilibrium experiments conducted on a GM unit (Waters and Andrews, 2016). Both Younger GM units have sanidine compositions which suggest they grew their phenocrysts above the plagioclase in–curve and yet, both units contain euhedral plagioclase. Additionally, Older GM units contain vastly different phenocryst abundance despite the same P_{H2O} and temperature conditions. Only one GM unit (OD) has a phenocryst abundance that is expected for the presence of plagioclase in the unit while the other 2 have phenocryst abundances that are too low (1–3 %) for the expected crystallization of plagioclase (> 10% crystallinity). Moreover, the presence of all three tectosilicates across all the GM units, 78% of which have crystallinities of <1–3%, is inconsistent with phase–equilibrium experiments on high–SiO_2 rhyolite (e.g., Waters and Andrews, 2016; Scaillet and Hildreth, 2001).

Experimental results from the "bottom–up" trajectory in this study indicate that the water–saturated solidus is ≥ 650 °C at 200 MPa and is consistent with the experimentally determined water–saturated solidus of ≥ 670 °C at this pressure reported by Ebadi and Johannes (1991). This contrasts with a water–saturated solidus of ~620–625 °C at the same pressure suggested by experiments performed by Thompson et al. (2026). Therefore, hypothesis two, a reduced water–saturated granitic solidus, is not a likely explanation for the variable phenocryst abundances observed in the GM units.

The third hypothesis to explain the difference in phenocryst abundance across GM units was phenocryst growth during ascent, driven by degassing, and following a kinetic delay to

nucleation. If the GM units segregated initially fluid undersaturated, the liquidus temperature would immediately decrease. During continued ascent however, the melts would reach fluid saturation and degassing of dissolved H_2O would cause the liquidus temperature to rise, eventually crossing the melt temperature. A kinetic delay to nucleation due to a lack of crystal nuclei present from its high viscosity and generation at a super–liquidus condition will cause an initial undercooling to develop which promotes low nucleation rates high crystal growth rates. This will lead to the rapid growth of large, sparse crystals with diffusion–limited textures like those seen ubiquitously across GM units and in the "top–down" experiments for this study. Additionally experiments aimed at discovering the timescales of the kinetic lag to nucleation are needed, however, the explanation that phenocryst growth in the GM units reflects rapid phenocryst growth during ascent remains a viable hypothesis.

3.11 References:

Andersen, D. J., & Lindsley, D. H. (1988). Internally consistent solution models for Fe-Mg-Mn-Ti oxides; Fe-Ti oxides. *American Mineralogist*, *73*, 714–726. https://pubs.geoscienceworld.org/msa/ammin/article-abstract/73/7-8/714/42110/

Andersen NL, Jicha BR, Singer BS, Hildreth W (2017) Incremental heating of Bishop Tuff sanidine reveals preeruptive radiogenic Ar and rapid remobilization from cold storage. Proceedings of the National Academy of Science of the USA 114(47):12407–12412

Bacon CR, Hirschmann MM (1988) Mg/Mn partitioning as a test for equilibrium between coexisting Fe–Ti oxides. American Mineralogist 73:57–61

Bailey RA, Dalrymple GB, Lanphere MA (1976) Volcanism, structure, and geochronology of Long Valley caldera, Mono County, California. J Geophys Res 81 : 725–744

Bailey RA (1989) Geologic map of the Long Valley caldera, Mono–Inyo Craters volcanic chain, and vicinity, eastern California. United States Geological Survey Map I–1933, scale 1:62,500; pamphlet

Barbee O, Chesner C, Deering C (2020) Quartz crystals in Toba rhyolite show textures symptomatic of rapid crystallization. American Mineralogist 105:194–226

Buddington, A. F., & Lindsley, D. H. (1964). Iron–Titanium oxide minerals and synthetic equivalents. *Journal of Petrology*, *5*(2), 310–357. https://doi.org/10.1093/petrology/5.2.310

Chamberlain KJ, Wilson CJN, Wallace PJ, Millet MA (2015) Micro–analytical perspectives on the Bishop Tuff and its magma chamber. Journal of Petrology 56:605–640

Couch S, Sparks RSJ, Carroll MR (2003) The kinetics of degassing–induced crystallization at Soufriere Hills Volcano, Montserrat. Journal of Petrology 44:1477–1502

Cousens, BL (1996) Magmatic evolution of Quaternary mafic magmas at Long Valley Caldera and the Devil's Postpile, California: Effects of crustal contamination on lithospheric mantle–derived magmas. Journal of Geophysical Research 101: 27673–27689

Crabtree SM, Lange RA (2011) Complex Phenocryst Textures and Zoning Patterns in Andesites and Dacites: Evidence of Degassing–Induced Rapid Crystallization? Journal of Petrology 52(1):3–38

Davies GR, Halliday AN (1998) Development of the Long Valley rhyolitic magma system: Strontium and neodymium isotope evidence from glasses and individual phenocrysts. Geochim Cosmochim Acta 62:3561–3574

Davies GR, Halliday AN, Mahood GA, Hall CM, (1994) Isotopic constraints on the production rates, crystallization histories and residence times of pre–caldera silicic magmas, Long Valley, California. Earth and Planetary Science Letters 125: 17–37

Du Bray EA, John DA, Cousens BL, Hayden LA, Vikre PG (2016) Geochemistry, petrologic evolution, and ore deposits of the Miocene Bodie Hills volcanic field, California and Nevada. American Mineralogist 101(3):644–677

Ebadi A, Johannes W (1991) Beginning of melting and composition of first melts in the system Qz–Ab–Or–H2O–CO2. Contrib Mineral Petrol 106:286–295

Fenn PM (1977) The nucleation and growth of alkali feldspars from hydrous melts. Canadian Mineralogist 15:135–161

Fliedner MM, Klemperer SL, Christensen NI (2000) Three–dimensional seismic model of the Sierra Nevada arc, California, and implications for crustal and mantle composition. Journal of Geophysical Research 105(B5): 10899–10922

Frey HM, Lange RA (2011) Phenocryst complexity in andesites from the Tequila volcanic field, Mexico: resolving the effects of degassing vs. magma mixing. Contributions to Minerology and Petrology 162:415–445

Fuhrman, M., & Lindsley, D. H. (1988). Ternary–feldspar modeling and thermometry. *American Mineralogist*, *73*, 201–215. https://pubs.geoscienceworld.org/msa/ammin/article/73/3–4/201/42101/Ternary–feldspar–modeling–and–thermometry

Ghiorso M, Evans BW (2008) Thermodynamics of rhombohedral oxide solutions and revision of the Fe–Ti two–oxide geothermometer and oxygen barometer. American Journal of Science 308:957–1039

Gordon BM (2022) The generation of geochemical gradients in the pre–caldera Glass Mountain high–SiO_2 rhyolites of Long Valley, CA: clues to the origin and preservation of Rb–Sr isochrons. University of Michigan, Ann Arbor

Gordon, B., Jolles, J., & Lange, R. (2026). The generation of geochemical gradients in the pre–caldera Glass Mountain high–SiO2 rhyolites of Long Valley, CA: Clues to the preservation of Rb–Sr isochrons. *Journal of Volcanology and Geothermal Research*, *476*, 108638. https://doi.org/10.1016/j.jvolgeores.2026.108638

Halliday AN, Mahood GA, Holden P, Metz JM, Dempster TJ, Davidson JP (1989) Evidence for long residence times of rhyolitic magma in the Long Valley magmatic system: the isotopic record in precaldera lavas of Glass Mountain. Earth and Planetary Science Letters 94:274–290

Hildreth W (2004) Volcanological perspectives on Long Valley, Mammoth Mountain, and Mono Craters: several contiguous but discrete systems. Journal of Volcanology and Geothermal Research 136:169–198

Hildreth W (1981) Gradients in silicic magma chambers: implications for lithospheric magmatism. Journal of Geophysical Research 86:10153– 10192

Hildreth W (1979) The Bishop Tuff: evidence for the origin of com–positional zonation in silicic magma chambers. In: Chapin CE, Elston WE (eds) Ash–flow tuffs. Geological Society of America Special Papers 180: 43–75

Hodge K, Miller CF, Miller JS, Faulds J (2006) Dike emplacement at the Searchlight, NV, volcano–plutonic complex. GSA

Hui H, Zhang Y (2007) Toward a general viscosity equation for natural anhydrous and hydrous silicate melts. Geochimica et Cosmochimica Acta 71:403–416

James RS, Hamilton DL (1969) Phase relations in the system $NaA1Si_3O_8$–$KA1Si_2O_8$–$CaAl_2Si_2O_8$ at 1 kilobar water vapor pressure. Contributions to Mineralogy and Petrology 21:111–141

Johannes W, Holtz F (1996) Petrogenesis and Experimental Petrology of Granitic Rocks: Minerals and Rock Series, volume 22: Berlin: Springer–Verlag, 335 p.

Jolles JSR, Lange RA (2019) High–resolution Fe–Ti oxide thermometry applied to single–clast pumices from the Bishop Tuff: a re–examination of compositional variations in phenocryst phases with temperature. Contributions to Minerology and Petrology 174 (70):1–43

Lange RA, Frey HM, Hector J (2009) A thermodynamic model for the plagioclase–liquid hygrometer/thermometer. American Mineralogist 94: 494–506

Li, X., Zhang, C., Behrens, H., & Holtz, F. (2020). Calculating biotite formula from electron microprobe analysis data using a machine learning method based on principal components regression. Lithos, 356–357, 105371. https://doi.org/10.1016/j.lithos.2020.105371

Lofgren G (1974) An experimental study of plagioclase crystal morphology: Isothermal crystallization. American Journal of Science 274: 243–273

Loomis TP (1981) An investigation of disequilibrium growth processes of plagioclase in the system anorthite–albite–water by methods of numerical simulation. Contributions to Minerology and Petrology 81:230–239

Mark, D. F., Renne, P. R., Dymock, R. C., Smith, V. C., Simon, J. I., Morgan, L. E., Staff, R. A., Ellis, B. S., & Pearce, N. J. (2017b). High–precision 40Ar/39Ar dating of pleistocene tuffs and temporal anchoring of the Matuyama–Brunhes boundary. *Quaternary Geochronology*, *39*, 1–23. https://doi.org/10.1016/j.quageo.2017.01.002

Meiling GS, Uhlmann DR (1967) Crystallization and melting kinetics of sodium disilicate. American Ceramic Society Bulletin 46(4):397

Metz JM, Bailey RA (1993) Geologic map of Glass Mountain, Mono County, California. Geological Survey, Miscellaneous Investigations Series Map I–1995, scale 1:24,00

Metz JM, Mahood GA (1985) Precursors to the Bishop Tuff Eruption: Glass Mountain, Long Valley, California. Journal of Geophysical Research 90: 121–126

Metz JM, Mahood GA (1991) Development of the Long Valley, California, magma chamber recorded in precaldera rhyolite lavas of Glass Mountain. Contributions to Minerology and Petrology 106:379–397

Miller CF, Furbish DJ, Walker BA, Claiborne LI, Koteas GC, Bleick HA, Miller JS (2011) Growth of plutons by incremental emplacement of sheets in crystal–rich host: Evidence from Miocene intrusions of the Colorado River region, Nevada, USA. Tectonophysics 500:65–77

Petford N, Kerr RC, Lister JR (1993) Dike transport of granitoid magmas. Geology 21(9): 845–848

Scaillet B, Hildreth W (2001) Experimental constraints on the origin and evolution of the Bishop Tuff. Penrose conference, 2001, Mammoth, United States. 2001, 07–12 June 2001

Simon, J.I., Weis, D., DePaolo, D.J., Renne, P.R., Mundil, R. & Schmitt, A.K. (2014). Assimilation of preexisting Pleistocene intrusions at Long Valley by periodic magma recharge accelerates rhyolite generation: rethinking the remelting model. Contributions to Mineralogy and Petrology, 167, 955

Swanson, S. E., & Fenn, P. M. (1986). Quartz crystallization in igneous rocks. *American Mineralogist*, *71*, 331–342. https://pubs.geoscienceworld.org/msa/ammin/article–abstract/71/3–4/331/41821/Quartz–crystallization–in–igneous–rocks

Thompson, G. T., Rufledt, C. J., & Thomas, J. B. (2026). The transition from magmatic to hydrothermal crystallization conditions of a shallow–level granitic pluton. *Contributions to Mineralogy and Petrology*, *181*(1). https://doi.org/10.1007/s00410–025–02280–y

Tuttle, O.F. and Bowen, N.L. (1958) Origin of granite in the light of experimental studies in the system NaAlSi3O8–KAlSi3O8–SiO2–H2O. Geological Society of America Memoir, v.74.

Waters LE, Andrews BJ (2016) The role of superheating in the formation of Glass Mountain obsidians (Long Valley, CA) inferred through crystallization of sanidine. Contributions to Mineralogy and Petrology 171: 79

Waters LE, Lange RA (2013) Crystal–poor, multiply saturated rhyolites(obsidians) from the Cascade and Mexican arcs: evidence of degassing–induced crystallization of phenocrysts. Contributions to Minerology and Petrology 166 (3) 731–754

Waters LE, Lange RA (2015) An updated calibration of the plagioclase–liquid hygrometer–thermometer applicable to basalts through rhyolites. The American Mineralogist 100:2172–2184

Waters LE, Lange RA (2017) Why aplites freeze and rhyolites erupt: Controls on the accumulation and eruption of high–SiO_2 (eutectic) melts). Geology 45(11): 1019–1022

Waters LE, Andrews BJ, Lange RA (2015) Rapid crystallization of plagioclase phenocrysts in silicic melts during fluid–saturated ascent: Phase equilibrium and decompression experiments. Journal of Petrology 56:981–1006

Wilson CJN, Hildreth W (1997) The Bishop Tuff: new insights from eruptive stratigraphy. The Journal of Geology 105:407–439

Venezky, D. Y., & Rutherford, M. J. (1999). Petrology and Fe–Ti oxide reequilibration of the 1991 Mount Unzen mixed magma. *Journal of Volcanology and Geothermal Research*, *89*(1–4), 213–230. https://doi.org/10.1016/s0377–0273(98)00133–4

Vetere F, Iezzi G, Behrens H, Cavallo A, Misiti V, Dietrich M, Knip–ping J, Ventura G, Mollo S (2013) Intrinsic solidification behavior of basaltic to rhyolitic melts: a cooling rate experimental study. Chemical Geology 354:233–242

Zhang, Y., Xu, Z., Zhu, M., & Wang, H. (2007). Silicate melt properties and volcanic eruptions. *Reviews of Geophysics*, *45*(4). https://doi.org/10.1029/2006rg000216

Chapter 4 New Age Constraints on the High–SiO_2 Rhyolite Dike Swarm of the Benton Range, CA: Clues to the Tectonic Relationship between Coast Range Ophiolite Formation and Extension in the Jurassic Sierran Arc

4.1 Abstract:

The long–lived Mesozoic Sierra Nevada arc, which formed in response to subduction of Pacific basin lithosphere beneath North America, is characterized by three magmatic flare–ups, separated by lulls, in the Triassic, Jurassic and Cretaceous. Numerous hypotheses have been proposed in the literature to explain the waxing and waning of magmatic activity, including changes in plate kinematics. One hypothesis is that formation of the Jurassic Coast Range Ophiolite (CRO) is related to slab rollback, which also led to extension within the main Sierran arc. The occurrence of Jurassic dike swarms has been pointed to as evidence to support this hypothesis, although their ages (148–153 Ma) all postdate the time interval of CRO formation (160–170 Ma), which instead corresponds to the peak Jurassic flare–up in the Sierran arc. Moreover, there is debate in the literature regarding Sierran crustal thickness in the Jurassic, with geochemical proxies indicating thick crust (40–60 km) in the main arc, despite widespread field evidence of Jurassic arc volcanic deposits in a marine setting (i.e., low elevations). In this study, new U–Pb zircon ages are obtained on a unique dike swarm of bimodal composition, mostly high–SiO_2 rhyolite (76–77 wt% SiO_2) with minor high–MgO basalt, in the Benton Range (BR), located along the eastern margin of the Sierra Nevada, CA. The dikes span an area of ~27 x 7 km and are oriented ~N°5–15, indicating their emplacement in an E–W extensional environment.

Previous K–Ar dates from the literature constrain the age of their emplacement between 168 and 209 Ma, which corresponds to the lull between the Triassic and Jurassic flare–ups. However, the weighted mean zircon ages obtained in this study range from 162–169 Ma, which directly overlaps the time of CRO formation. New evidence in the literature shows that the CRO formed through trench–parallel (N–S) extension, which is inconsistent with E–W extension associated with slab rollback. Instead, CRO formation may have induced trans–tensional shear stress and strike–slip deformation along the margins of the Sierran arc (consistent with shearing in Late Jurassic dikes along the eastern and western margins) and the formation of pull–apart basins within the main arc, leading to the bimodal Benton Range dike swarm.

4.2 Introduction

The Sierra Nevada batholith in eastern CA (Fig. 4–1) provides a record of the long–lived, Mesozoic continental arc that formed in response to subduction of Pacific basin oceanic lithosphere beneath North America. A key characteristic of the Sierran arc is the episodic nature of its magmatic flux (Fig. 4–2), which is revealed by a histogram of volcanic and plutonic U–Pb zircon ages (Paterson and Ducea, 2015). The histogram reveals three flare–ups: (1) in the Triassic (~240–210 Ma), (2) in the Jurassic (~175–145 Ma) and (3) in the Cretaceous (~120–85 Ma), which are separated by lulls of ~25–35 Myr duration (Armstrong and Ward, 1993; Ducea, 2001; DeCelles et al., 2009; Paterson and Ducea, 2015; Cao et al., 2015). By far, the Cretaceous flare–up was the most voluminous (Ducea, 2001), although it is unclear whether the magnitude of the Jurassic flare–up is fully captured by exposed plutonic and volcanic rocks, owing to overprinting by the Cretaceous flare–up event (e.g., Ardill et al., 2024).

Numerous hypotheses have been proposed to explain the occurrence of both the magmatic flare–ups and the lulls in the Sierran arc (Fig. 4– 2), including variations in plate

motions and kinematics (e.g., highly oblique subduction, transition to transform faulting, slab rollback, flat–slab subduction, slab tearing, subduction of buoyant features, changes in plate velocity), as well as processes that either enhance or deplete the fertility of the lower crust and/or mantle (e.g., Ardill et al., 2018, 2024; Barth et al., 2013; Chapman et al., 2021; DeCelles et al., 2009; Dumitru et al., 2010). In this study, we focus on the relationship between the formation of the Coast Range Ophiolite (CRO) in the forearc and the main Sierran arc during the Jurassic.

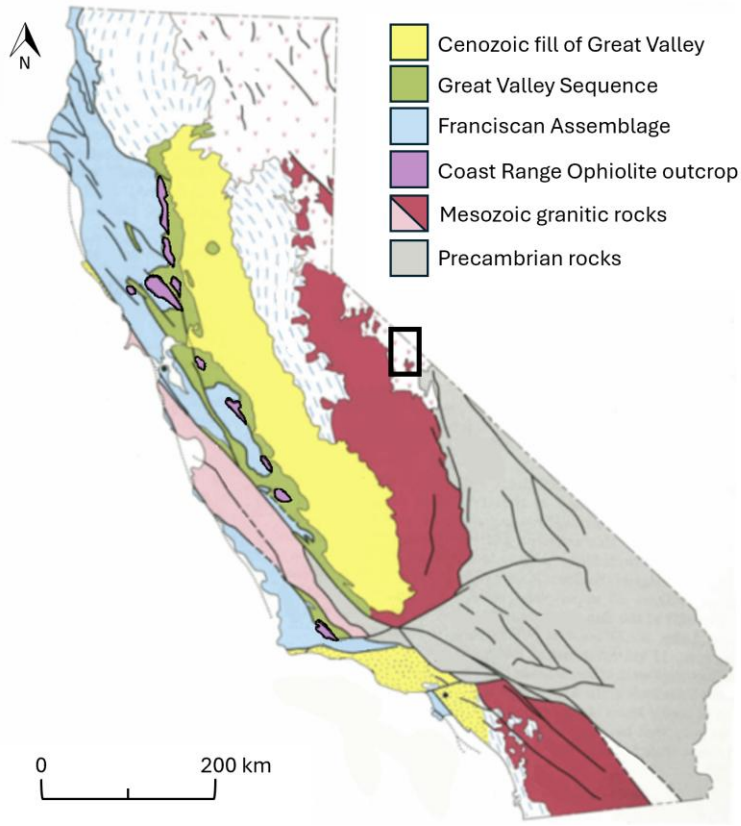


Figure 4-1: Simplified geologic map of California modified from Irwin (1990) with the location of the Benton Range shown in a black box. A simplified location of outcrops of the Coast Range Ophiolite (purple) are superimposed from the geologic map from Cisneros et al. (2022). Mapped are Precambrian (grey), Mesozoic granitoid (red), Franciscan assemblage (blue), Great Valley sequence (green), and Cenozoic fill of Great Valley

There is abundant geochemical and field evidence that the CRO formed between ~160 and 170 Ma (overlapping in time with the Jurassic flare–up; Shervais et al., 2005; Fig. 4–2) in a forearc setting when subduction was being initiated or reestablishing itself (e.g., Choi et al.,

2008; Harper, 2003; Shervais and Kimbrough, 1985; Sportum and Day, 2020), possibly following a collisional event of an exotic or fringing arc against the western margin of North America between 206–180 Ma (e.g., Shervais et al., 2005), which overlaps a lull in Sierran magmatism (Fig. 4–2).

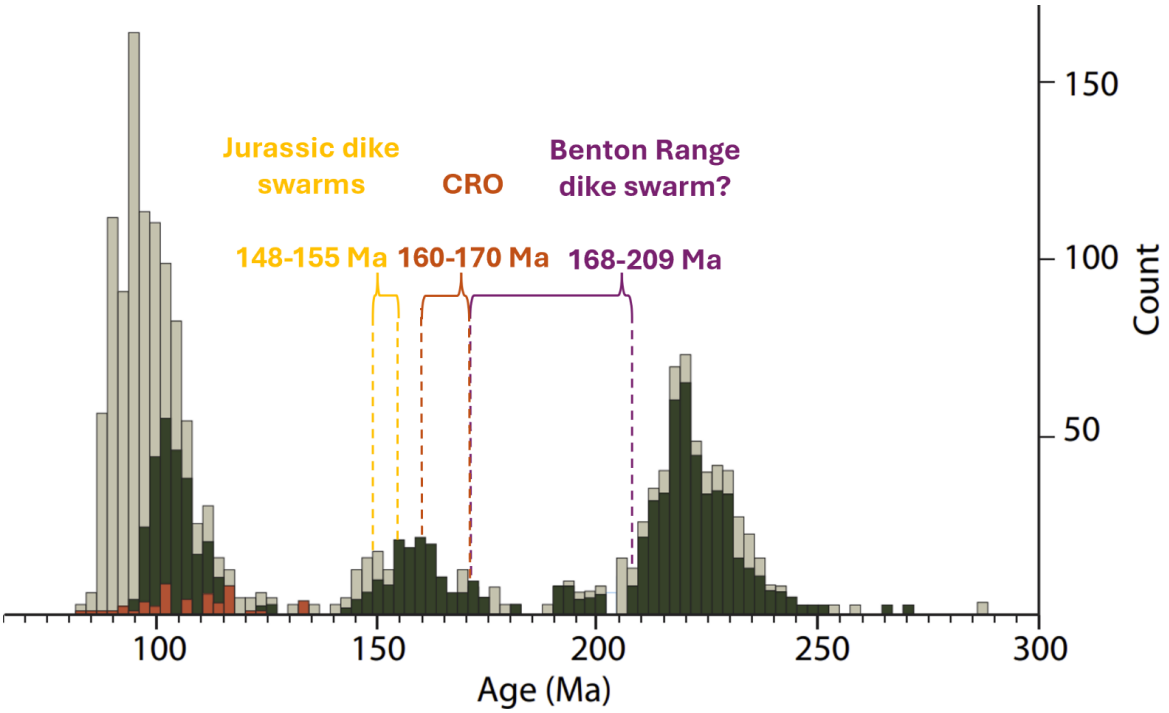


Figure 4-2**:** A compilation of plutonic (dark green) and volcanic (light green) zircon ages from Paterson and Ducea (2015) from the Sierra Nevada. The results show three magmatic flare ups (Triassic, Jurassic, and Cretaceous) with intervening lulls. Also shown are the age intervals for the emplacement of the Benton Range dike swarm (K–Ar dates; Renne and Turrin, 1987), the formation of the CRO (Shervais et al., 2005), and dated Jurassic dike swarms (Independence, Owens Mountain, Sonora and King Creek; Chen and Moore, 1979; Wolf and Saleeby, 1992; Wesley et al., 2019).

Although there is broad consensus that CRO formation occurred in an extensional forearc setting in a supra–subduction zone (e.g., Saleeby, 1996; Sharvais et al., 2005; Arkula et al., 2023), there are disagreements in various models about whether CRO formation (~170–160 Ma) is associated with widespread extension (e.g., Chen et al., 1982; Cao et al., 2015; Saleeby and Dunne, 2015; Ryan–Davis et al., 2026) or compression and crustal thickening (i.e. the Nevadan

Orogeny) (e.g., Dunne and Walker, 2004; Profeta et al., 2015; Tang et al., 2024) within the Jurassic Sierran arc.

Saleeby (1996) proposed a direct link between CRO formation and co–eval extension in the main Sierran arc, due to the combination of slab rollback and highly oblique plate convergence, which would have produced widespread trans–tension (a combination of both extension and strike–slip shearing) both within the oceanic forearc crust to produce the CRO and within the main Sierran arc. However, most of the evidence for Jurassic extension in the main arc is from dike swarms (Independence; Owens Mountain; Sonora and King Creek) with ages (148–155 Ma; Chen and Moore, 1979; Wolf and Saleeby, 1992; Wesley et al., 2019) that are younger than the CRO (~160–170 Ma) (Fig. 4–2). Although numerous models propose that slab rollback was the driving force for forearc extension, leading to the formation of the CRO (e.g., Saleeby, 1996; Snow and Shervais, 2015), new evidence provided by Arkula et al. (2023) shows that the CRO was formed in the forearc during trench–parallel spreading, where the axis of the spreading ridge was perpendicular to the trench. Although this tectonic configuration for CRO formation does not require or predict extension in the main magmatic arc of the Sierra Nevada, it does not preclude it.

In this study, we propose to test whether there is a link between CRO formation (~160–170 Ma) and concurrent extension in the main Sierran arc by obtaining zircon crystallization ages on a felsic dike swarm located in the east–central portion of the Sierra Nevada, namely the Benton Range, an uplifted fault block immediately southeast of the Long Valley Caldera, CA (Fig. 4–3). The Benton Range dikes span an area of ~27 x 7 km (Fig. 4–4a), and most dikes are oriented ~N°5–15W (Rinehart and Ross, 1957), consistent with east–west extension during their emplacement. There are broad constraints on the age of the Benton Range dike swarm (209–168

Ma) based on K–Ar dates presented by Renne and Turin (1987). This wide age interval overlaps the lull in magmatism between the Triassic and Jurassic flare–ups (Fig. 4– 2) and just barely overlaps the age range of the CRO. The goal of this study is to obtain new U–Pb zircon crystallization ages on the Benton Range dikes to test whether formation of the CRO directly coincides with extension within the main Sierran arc.

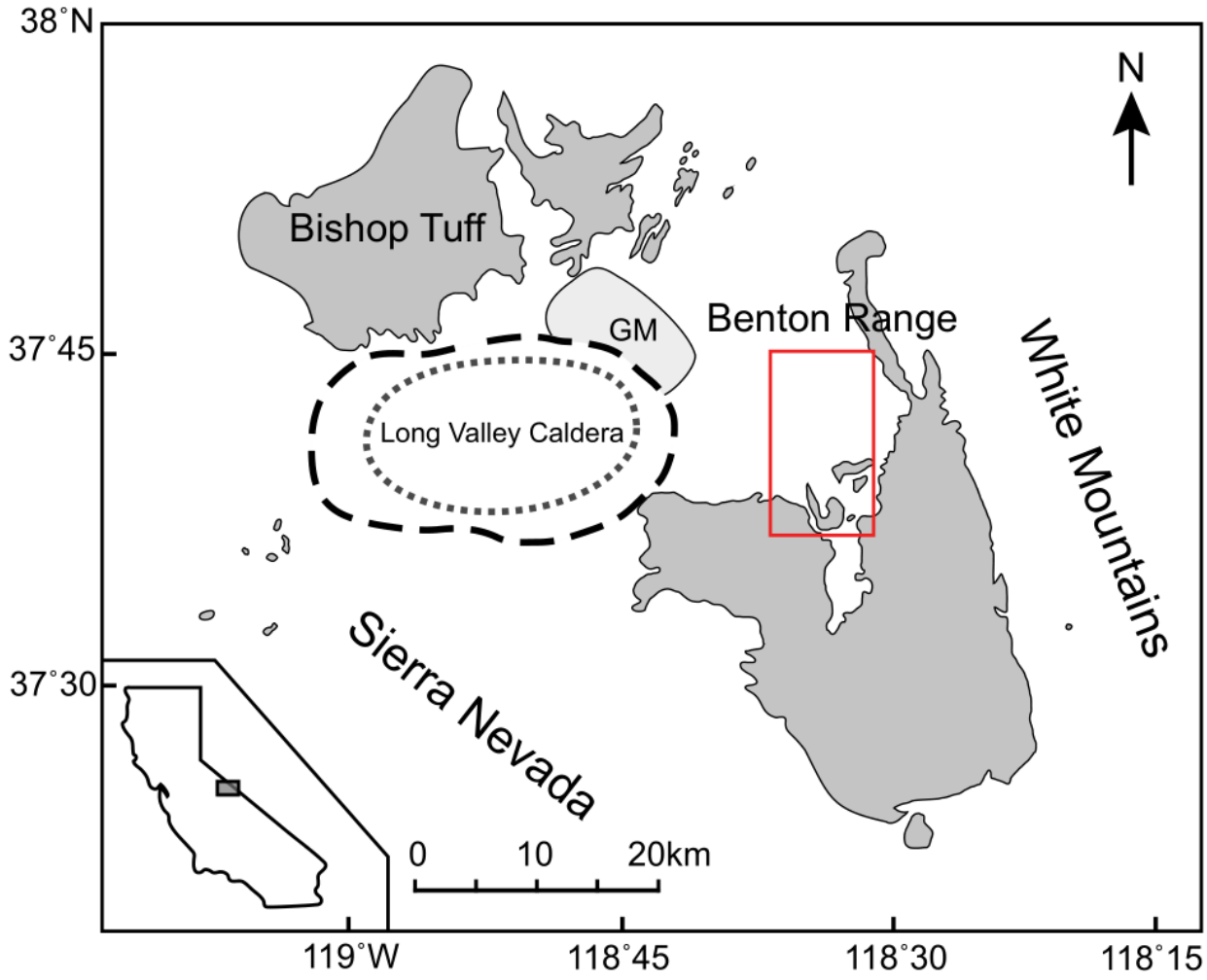


Figure 4-3: Study area location map of Long Valley Caldera and the Benton Range, CA modified from Chamberlin et al. (2015). The Benton Range is shown in a red box just southeast of the Long Valley Caldera (topographic rim shown by dashed line). Glass Mountain is shown in light gray, and the Bishop Tuff (BT) is shown in dark gray.

4.3 Benton Range dike swarm

4.3.1 Geological Setting

The felsic dike swarm of the Benton Range in eastern California was first described by Lemmon (1940) and Gilbert (1941) and mapped in detail by Rinehart and Ross (1957). Individual dikes are mostly 2–9 m wide (some range up to 19 m), with an average width of ~4–6 m. Some dikes can be individually traced for up to 4 km and none are structurally deformed (Renne and Turrin, 1987). The dikes intrude shallow, Paleozoic, low–grade metasedimentary rocks (i.e., andalusite hornfels), and they both cut and are cut by Mesozoic magmatic bodies (calc–alkaline granitoids; two–mica granites; hornblende gabbros) (Rinehart and Ross, 1957; Renne and Turrin, 1987). The dikes were analyzed for their whole–rock compositions by Mesa (2021) and shown to be predominantly made of high–SiO_2 (76–77 wt%) rhyolite, with a small subset made of high–MgO (7–11 wt%) basalt (with an arc geochemical signature). Thus, they are bimodal, which is consistent with an extensional tectonic setting (e.g., Ahmad et al., 2009; Barbarin, 1999; Cox, 1988; Rudnick, 1990; Terentiev et al., 2017).

4.3.2 Sample Locations and Descriptions

Interior, fresh samples from six separate dikes in the Benton Range (Fig. 4–4b) were selected to broadly represent the range of samples previously collected and analyzed by Mesa (2021). Samples were chosen to cover a wide geographical area to assess any spatial variation in emplacement age. Their major–element whole–rock compositions were obtained by ICP–OES (inductively coupled plasma optical emission spectroscopy) at Activation Laboratories, Ltd., Ontario, Canada and are reported in Table 4–1. All are high–SiO_2 rhyolites, with phenocrysts of quartz, sanidine, plagioclase, biotite, and Fe–Ti oxides, and accessory apatite, zircon and allanite also present.

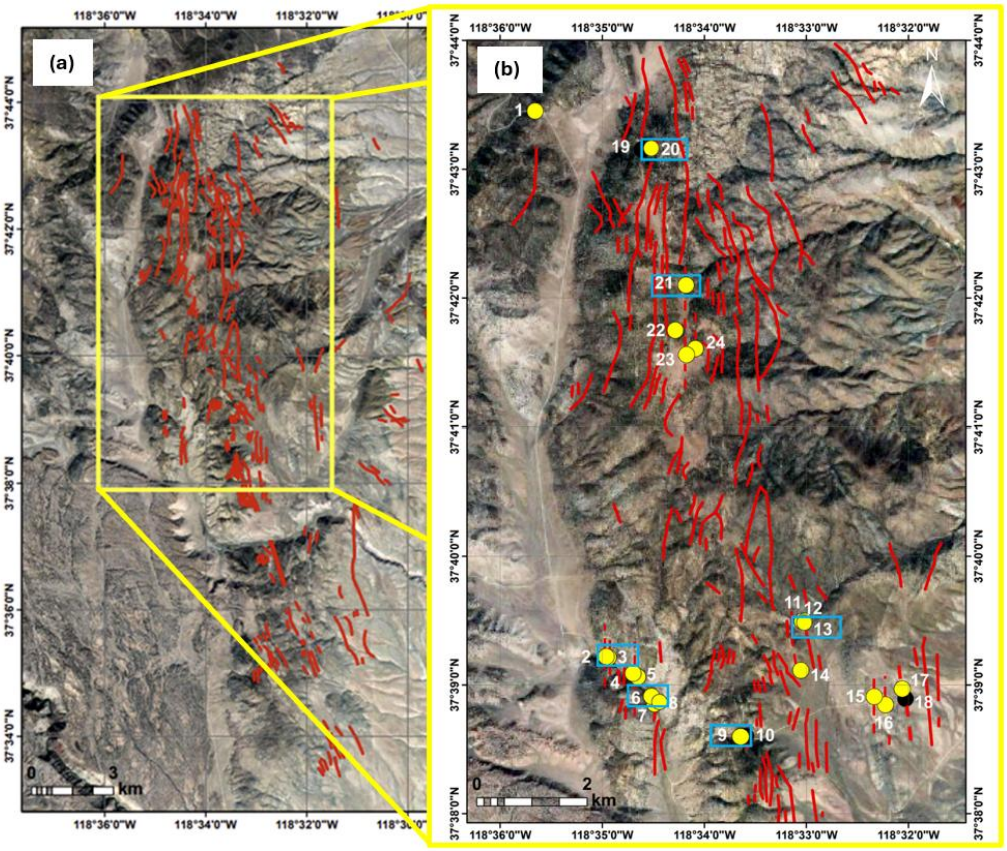


Figure 4-4**:** Google Earth image showing the location of individual dikes (red) in the Benton Range along Banner Ridge as mapped by Rinehart and Ross (1957); modified from Mesa (2021). (A) Images showing all the dikes, with a yellow inset box. (B) Inset box from (A) showing sample locations from Mesa (2021) in yellow circles. Samples targeted for U–Pb dating in this study are shown in blue boxes.

4.4 Geochronology methods

Zircons were separated using standard procedures (i.e., heavy liquids, a Franz magnet and water table) at Zirchron, LLC. Zircon separates from each sample were then annealed at the University of Michigan in alumina crucibles in a benchtop box furnace for three days at 1000 °C. All samples were analyzed for isotopes of U and Pb using LA–ICP–MS (laser ablation inductively coupled plasma mass spectrometry) at two laboratories. One sample (CD–18–03a) was analyzed at the MI–Chron facility at the University of Michigan and the remaining five samples were analyzed at the LaserChron facility at the University of Arizona. In addition, concentrations of U and Th were obtained on five samples at LaserChron. Prior to analyses,

zircon separates were mounted in 1" epoxy mounts for cathodoluminescence imaging: with a JEOL JSM–7800FLV scanning electron microscope (SEM) at the University of Michigan and with a Hitachi S–3400N variable–pressure SEM at the University of Arizona (using a Gatan ChromaCL2 cathodoluminescence system with Gatan Digital Micrograph microscopy software).

Table 4-1:Whole–rock major–element (wt%) composition of the Benton Range dike swarm

Sample	CD–18–03	CD–18–06	CD–18–09	CD–18–13	CD–18–20	CD–18–21
Lat. (N 37)	.653617°	.648542°	.643408°	.658297°	.719258°	.701689°
Long. (W –118)	.565678°	.5753°	.560617°	.550681°	.576808°	.569633°
SiO_2	76.60	75.30	75.80	77.30	76.00	77.10
TiO_2	0.090	0.150	0.110	0.100	0.110	0.070
Al_2O_3	13.00	13.80	13.30	12.60	13.70	12.80
FeO^T	0.97	1.11	1.20	0.82	0.83	0.79
MnO	0.01	0.03	0.04	0.02	0.04	0.06
MgO	0.11	0.20	0.12	0.13	0.11	0.08
CaO	0.76	1.08	0.88	0.89	0.89	0.78
Na_2O	3.51	3.30	3.34	3.16	3.31	3.37
K_2O	4.86	4.92	5.14	4.88	4.92	4.86
P_2O_5	0.02	0.05	0.02	0.05	0.02	0.01
LOI	0.61	0.59	0.33	0.50	0.43	0.38
Total	98.8	98.8	98.5	98.8	98.5	98.5

Whole rock compositions previously reported by Mesa (2021)

At MI–Chron, both annealed and unannealed zircon grains were analyzed using an ESI NWR 193 EXCIMER laser with a TwoV612 sample chamber and connected to an Agilent 7900 ICP–MS. A spot size of 20 μm with a fluence of 1.7 J/cm^2, was used with a 50 Hz repetition rate and a 4 second analysis time. The duty cycle was 0.1 second with 20 milliseconds for Pb206, 30 milliseconds for Pb207 and 10 milliseconds for Pb208, Th232, U235, and U238. Prior to each analysis, 4 cleaning shots were fired with a 3 second wash out delay. The He carrier gas flow rate was 0.8 L/min, the He collision cell rate was 3.5 mL/min, and the Ar carrier flow rate was 1 L/min.

At LaserChron, annealed zircon grains were analyzed using a Teledyne Iridia (500) laser and a Thermo Element2 HR ICP–MS. A spot size of 15–20 μm with a fluence of 4 J/cm^2 was used with an 8 Hz repetition rate and a 15 second ablation duration. Total scan time was 0.5 seconds, with dwell times for each mass of 0.081 seconds for Pb206, 0.150 seconds for Pb207 and U235, and 0.010 seconds Pb208 and Th232. Prior to each analysis, a 3 burst cleaning shot with a spot size of 40 μm was fired. The He carrier gas flow rate was 0.19 L/min in the cobalt cell and 0.17 L/min in the z–prime cup. A common Pb correction based on measured 206 Pb /204 Pb and the assumed composition of common Pb was applied (Stacey and Kramers, 1975). A collection of standards and method specifications can be found in Supplemental Table C-0-15.

4.5 Zircon geochronology results:

4.5.1 Zircon imaging and characterization

Cathodoluminescence (CL) images of select zircon grains are shown for two representative samples, CD–18–06 (Fig. 4–5) and CD–18–13 (Fig. 4–6). Grain sizes predominantly range from ~ 50–200 μm. Most grains are euhedral and show oscillatory– and sector–zoning growth patterns (Figures 4–5 and 4–6). Some grains in CD–18–06 appear to have antecrystic or xenocrystic cores and/or thin, bright outer rims (Fig. 4–5). The bright CL rims reflect lower concentrations of U and Th, which may reflect the effects of either magma mixing (e.g., intersection of two dikes at depth) and/or hydrothermal alteration. A hallmark of hydrothermal alteration of zircons is the formation of speckled and spongy textures (Jiang et al., 2019; Han et al., 2023), which has also been attributed to metamictization. A few grains that possibly have this texture are seen in sample CD–18–06 (Fig. 4–5). However, most zircon grains in all six Benton Range samples have pristine growth textures, devoid of evidence of alteration.

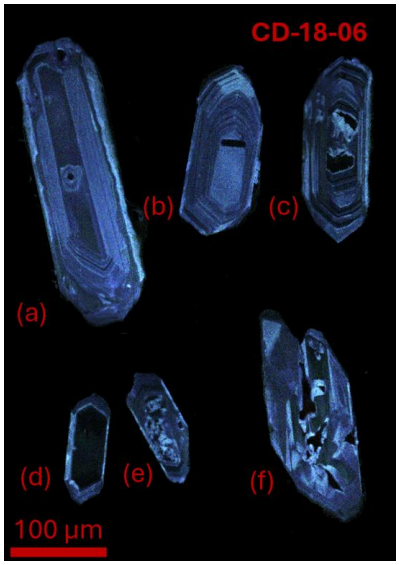


Figure 4-5 Representative cathodoluminescence images of zircon grains from sample CD–18–06, which were analyzed in this study by the LaserChron facility at the University of Arizona. (a–c) Zircon grains show oscillatory– and sector–zoning typical of original igneous growth textures. (d) Zircon crystal shows a bright rim indicative of low Th and U. (e–f) Zircon shows possible spongy textures, which may have formed during hydrothermal alteration.

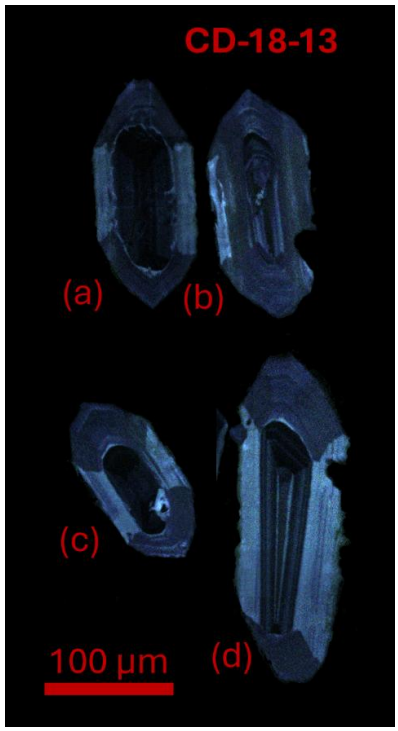


Figure 4-6**:** Representative cathodoluminescence images of zircon grains from sample CD–18–13, which were analyzed in this study by the LaserChron facility at the University of Arizona. (a–d) Zircon grains show oscillatory– and sector–zoning typical of original igneous growth textures.

4.5.2 U concentrations and Th/U ratios in zircon

For the zircon separates from five samples analyzed at LaserChron, U concentrations and Th/U ratios were obtained (Supplemental Table C-0-16). Scatter diagrams of U concentrations and Th/U ratios and vs. $^{238}U/^{206}Pb$ age (Ma) are available in Figure C-0-2 and Figure C-0-3, respectively. All samples have zircons with U concentrations ≥2,000 ppm and Th/U ratios primarily between ~0.5–2.1. The latter overlap the expected average Th/U ratio for zircon from a felsic magmatic source of ~ 0.5–0.9 (e.g. Wang et al., 2011; Kirkland et al., 2015).

The zircons in sample CD–18–6 have U concentrations that approach 10,000 ppm and Th/U ratios that range from 0 to 2.7. The elevated U ppm concentrations in sample CD–18–06 may reflect the effects of hydrothermal alteration (Han et al., 2023), high levels of metamictization, and/or crystallization in disequilibrium (i.e., rapid growth) with the melt (Wang et al., 2011). CD–18–06 is the only sample that has a significant number of zircons with Th/U ratios below 0.5 (generally accepted to be the minimum for primary igneous crystallization; Hoskin and Schaltegger, 2003), which is potentially evidence of hydrothermal alteration. It should be noted, however, that the co–crystallization of allanite, which is present in these samples (Mesa, 2021), can affect available Th in the melt at the time of crystal growth and skew the Th/U ratios in zircons to lower values (e.g. Maraszewska et al., 2023).

4.5.3 Zircon crystallization ages

Individual spot analyses of zircon $^{206}Pb/^{238}U$ ages and their two standard errors (±2 SE) for all six samples are reported in Supplemental Table C-0-17. For the five samples analyzed at LaserChron, a filter for discordant ages was applied and all points with >10% discordance between $^{238}U/^{206}Pb$ vs. $^{235}U/^{207}Pb$ were removed before sample ages were calculated (but are available in Supplemental Table C-0-16). A small number of outliers were observed in the data

that are not discordant but do show anonymously high or low ages (possibly reflecting xenocrysts or alteration, respectively). Concordia plots of $^{206}Pb/^{238}U$ versus $^{207}Pb/^{234}U$ are shown for all six samples in Figure C-0-4.

Table 4-2 :Zircon crystallization ages for 6 HSR dikes from the Benton Range, CA

	Total sample weighted mean age					
Sample	Age (Ma)	± 2SE	± weighted 2SD	Analyses (n)	MSWD	$MSWD_{Max}$
[1]CD–18–03	161.6	0.9	9.1	26	3.6	1.6
CD–18–06	168.6	0.8	11.2	26	7.9	1.6
CD–18–09	163.1	0.9	7.2	28	1.0	1.5
CD–18–13	164.9	0.9	6.3	25	2.1	1.6
CD–18–20	167.6	0.8	13.0	29	9.9	1.5
CD–18–21	164.5	0.8	9.3	29	4.8	1.5

	Sample minimum and maximum age, n=10					
Sample	Min age (Ma)	±2SE; weighted 2SD	MSWD	Max age (Ma)	±2SE; weighted 2SD	MSWD
[1]CD–18–03	157.8	1.5; 4.8	1.0	165.9	1.6; 8.2	2.8
CD–18–06	161.7	1.4; 3.6	0.6	173.5	1.1; 3.8	1.2
CD–18–09	160.1	1.5;3.6	0.6	166.7	1.5; 7.3	2.3
CD–18–13	161.6	1.5;2.6	0.3	167.8	1.3; 3.8	0.9
CD–18–20	161.1	1.3; 5.3	1.7	175.6	1.2; 4.8	1.2
CD–18–21	160.3	1.3; 4.9	1.4	170.3	1.5; 6.1	1.7

Samples analyzed at LaserChron at the University of Arizona

[1] analyzed at Mi–Chron at the University of Michigan

$MSWD_{Max}$ is the highest value expected at the 95% confidence interval for normal scatter associated with a single age population

All ages are $^{206}Pb/^{238}U$

The weighted mean zircon crystallization $^{206}Pb/^{238}U$ ages and both their two–standard error (± 2 SE) and weighted two–standard deviation (± 2 SD) are reported in Table 4–2 for all six Benton Range dike samples, along with MSWD values. For the number of analyses in each sample, MSWD values of ~1.5 are expected for a single zircon age population. Four samples (CD–18–03, CD–18–09, CD–18–13, CD–18–21) have calculated MSWD values that range from 1.0–4.8 and thus approach the criteria for a single population.

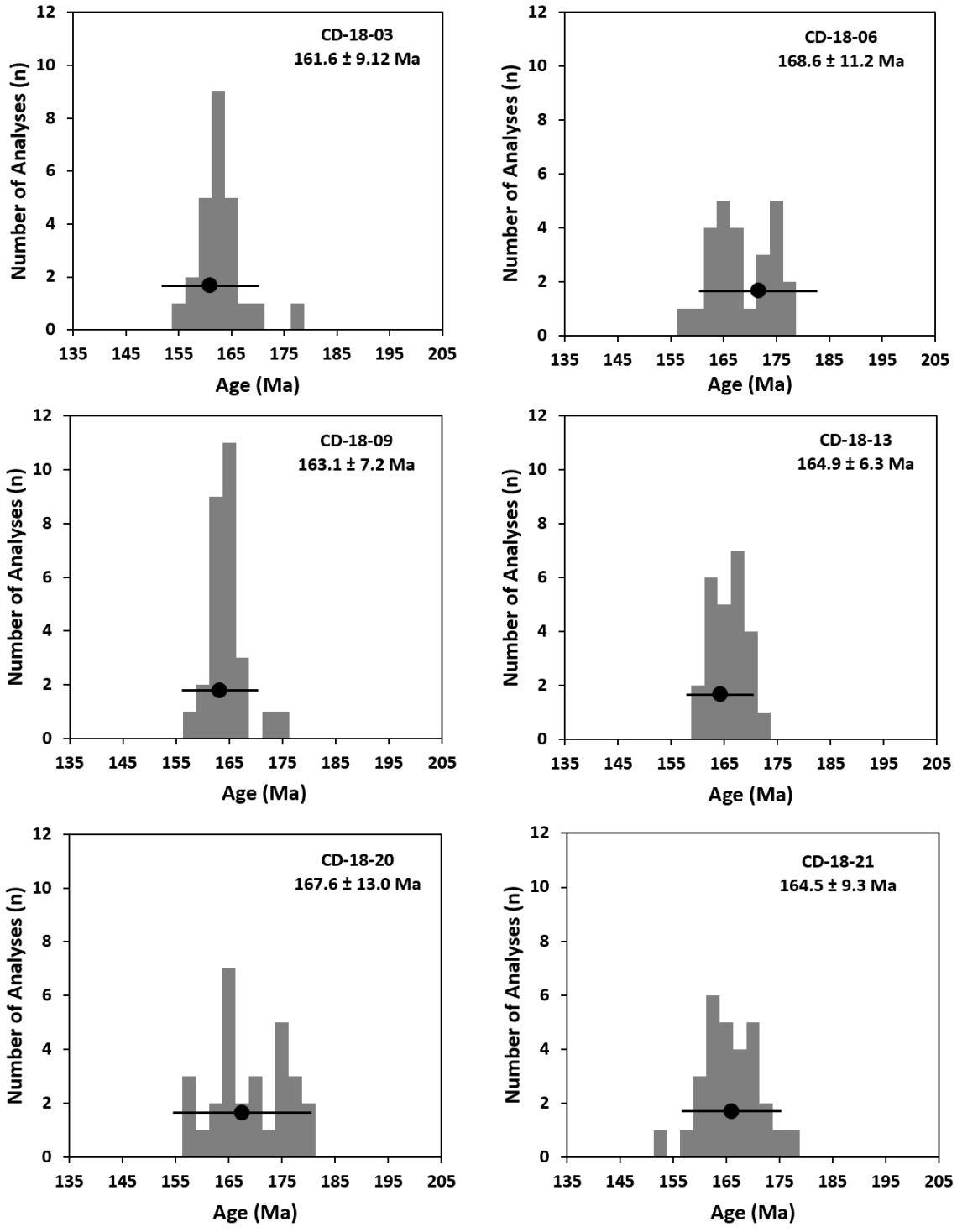


Figure 4-7**:** Histograms of individual zircon ages in each of six dikes targeted in this study. The weighted mean age is reported for each sample, together with the weighted 2–standard deviation as error bars. Ages range from 162 (± 9) to 169 (± 11) Ma.

However, the other two samples (CD–18–06 and CD–18–20) have much larger MSWD values (8–10) and thus may have multiple zircon age populations. Therefore, both minimum and maximum ages were calculated for all six samples by using their respective 10 lowest and 10 highest ages (n = 10). These maximum and minimum ages are an effort to conservatively estimate the zircon age range in each sample, and they are reported in Table 4–1 along with their errors and MSWD values.

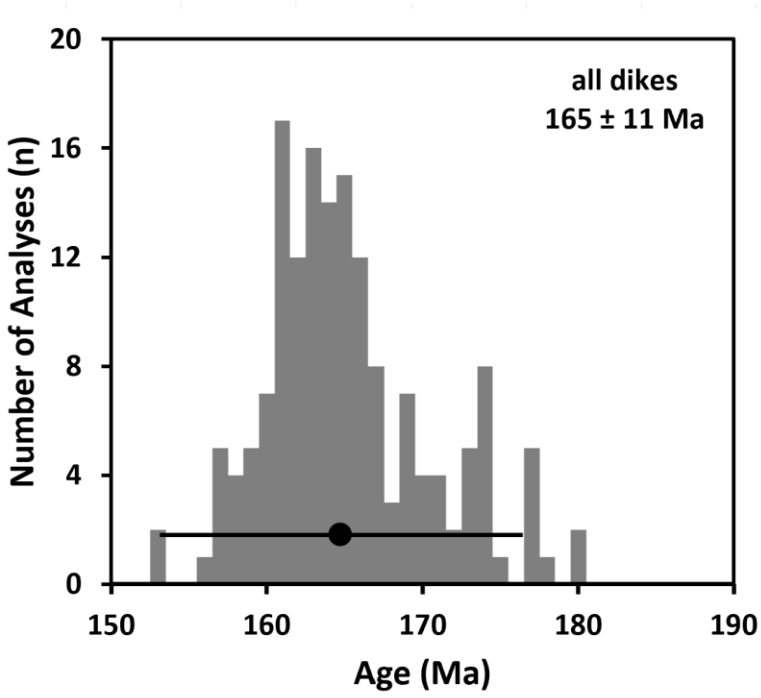


Figure 4-8**:** A single histogram for individual zircon ages from all six dikes in this study. The combined weighted mean age (± 2–standard deviation; error bars) is 165 (± 11) Ma.

Histograms of the individual ages for each sample are shown in Figure 4–7 together with the weighted mean zircon crystallization age and weighted two–standard deviation. All weighted mean ages ± 2SD for the six samples fall in a narrow range between 161.6 ± 9.1 Ma and 168.6 ± 11.2 Ma. There is no relationship between calculated age and dike location (Fig. 4–4). The youngest and oldest dated dikes are CD–18–03 and CD–18–06, respectively, and they are

spatially the closest. The range in minimum and maximum ages ± 2 SD among all six samples is 157.8 (± 4.8) and 175.6 (± 4.8) Ma. When all ages across all samples are used to find a single weighted mean age, the result is shown in Figure 4–8 and produces an age of 165 Ma with a weighted standard deviation of ± 11 Ma which nearly covers the range of the maximum and minimum ages.

4.5.4 Analysis of large age uncertainties

In addition to the possibility of more than one zircon population in individual dike samples (i.e., those with large MSWD values), another potential cause of large standard deviations could be because of hydrothermal alteration, leading to heterogeneity in U concentrations (e.g., grains with markedly bright rims versus their interiors). Since all samples have elevated U concentrations (>2,000 ppm), radiation damage is possible, which will produce irregular signals during laser ablation and lead to large errors. Although annealing of the grains prior to analysis can repair the zircon lattice, it cannot account for potential natural disturbances to the U and Pb prior to analysis. Irregular signals could also occur from the ablation (spot diameter 15–20 μm) of relatively small zircon grains (≤ 20 μm in width).

4.6 Discussion

4.6.1 Comparison of Benton Range dike zircon crystallization ages to previous constraints

For the six Benton Range dikes dated in this study, the weighted mean U–Pb zircon ages span a narrow interval of 162–169 Ma, which only overlaps the lower bound of the 168–209 Ma constraint provided by Renne and Turrin (1987). However, a detailed examination of their K–Ar ages reveals broad agreement with the U–Pb zircon ages from this study. First, the upper bound of 209 Ma is based on a cross–cutting relationship, where a Benton Range dike is observed to cut an older hornblende gabbro dated by Renne and Turrin (1987) at 209 ± 5 Ma (K–Ar age on

hornblende separate), which broadly matches (within error) the U–Pb zircon crystallization age of 214 Ma for the same hornblende gabbro (Stern et al., 1981). Thus, while the age of the gabbro provides an upper bound on the age of the Benton Range dikes it does not directly date them.

Renne and Turrin (1987) additionally report hornblende crystallization ages in two mafic Benton Range dikes (167 ± 3 Ma for each), which match the age range obtained for the high–SiO_2 rhyolite dikes in this study (162–169 Ma; Table 4–2). Renne and Turrin (1987) point out that hornblende is more reliable than biotite for K–Ar dating, owing to the difference in their respective Ar closure temperatures (~500 vs ~300°C, respectively; Harrison, 1981). This observation led them to be less confident regarding the K–Ar ages obtained on biotite separates in two felsic dikes of 160 ± 4 and 153 ± 4 Ma. Although it is possible that these ages are too low, reflecting some diffusive loss of Ar, they fall within the conservative age window of 158 (± 5) to 176 (± 5) Ma presented in this study, based on the ten lowest and ten highest zircon ages in each sample (Table 4–2).

Clear evidence of significant Ar loss in biotite was found by Renne and Turrin (1987) in their comparison of biotite and muscovite K–Ar ages obtained on two samples from a two–mica granite (which cuts several Benton Range dikes). However, because of the higher Ar closure temperature in muscovite (≥ 405 °C; Harrison et al., 2009) compared to biotite, the maximum K–Ar age they obtained on muscovite (168 ± 3 Ma) from this two–mica granite is more reliable. It forms the lower bound they report for the age range of the Benton Range dike swarm and matches, within error, the weighted mean of all zircon crystallization ages obtained in this study (165 ± 11 Ma; Fig. 4–8). In summary, both previous K-Ar dates (Renne and Turin, 1987) and updated U-Pb dates from this study are consistent with emplacement during the middle Jurassic. and therefore overlap the middle Jurassic flare up as well as the age range of the Coast Range

Ophiolites (~160–170 Ma; Shervais et al., 2005). We additionally note that the results from this study place minimum and maximum age limits on the Benton Range dike swarm at ~158–176 Ma.

4.6.2 Evidence of extension versus compression in the main Sierra arc between ~160–170 Ma

The Benton Range dike swarm is the only Jurassic dike swarm in the Sierran main arc that directly overlaps the 160–170 Ma age range of the CRO. As noted earlier, the other Jurassic dike swarms are younger, including: (1) the 148 Ma Independence dike swarm (mylonitized soon after emplacement) in eastern California (Chen and Moore, 1979), (2) the 148–155 Ma Owens Mountain dike swarm (mylonitized during emplacement) in the southwestern Sierran foothills near Fresno, California (Wolf and Saleeby, 1992), and (3) the ~153 Ma age of rhyolitic to basaltic dikes, which intrude ~168 Ma granodiorite in the southern Ritter Range of the Sierra Nevada in eastern California (Wesley et al., 2019). There is, however, indirect evidence of extension from the Jurassic Emigrant Gap intrusive mafic complex, owing to evidence of its upper–crustal emplacement, which requires an extensional setting (Ryan–Davis et al., 2026). Importantly, the Emigrant Gap mafic complex has an emplacement age of 168 ± 2 Ma (Girty et al., 1995), which overlaps the age range of the Benton Range dike swarm and the CRO. The Emigrant Gap mafic complex is located ~240 km north of the Benton Range, which may indicate that extension was not localized in the main Sierran arc during this time interval.

Further evidence of extension is found in the composition of the Benton Range dike swarm and their similarity to the Plio–Quaternary Long Valley high–SiO_2 rhyolites (Fig. 4–3). Successful eruption of high–SiO_2 rhyolites is not typical of active subduction zones, but instead largely occurs in regions of continental extension, since it requires emplacement of basalt into the upper granitoid crust to drive partial melting and successful segregation of high–SiO_2

rhyolite (e.g., Taylor et al., 2026). In Chapter 2 of this thesis, a new biotite–liquid thermometer was applied to four of the Benton Range dikes and obtained temperatures that range from 757–786 °C, which requires significant amounts of water (>5 wt%) for the Benton Range high–SiO_2 rhyolites to be molten at these temperatures. The source of water in the Benton Range rhyolites was likely associated basalts, represented by the coeval mafic dikes of high–MgO basalt composition (with arc geochemical signatures; Mesa, 2021), which crystallized primary hornblende. Similarly, the source of water for the Long Valley high–SiO_2 rhyolites was the associated Long Valley basalts (~4.3 wt% H_2O on average; Jolles and Lange, 2021), which were derived from subduction–modified mantle (Cousens, 1996). However, the overall tectonic setting that drove formation of the Plio–Quaternary Long Valley volcanism was Basin and Range lithospheric extension (in the absence of active subduction, despite the subduction signature of the Long Valley basalts). It is probable that a similar tectonic setting of extension, leading to thinning and partial melting of subduction–modified lithospheric mantle due to upwelling asthenosphere, drove formation of the Benton Range basalts and high–SiO_2 rhyolites between ~162–169 Ma.

Although field evidence of episodic compression during the Jurassic is found in the Eastern Sierra Thrust System (ESTS), which outcrops along the eastern Sierra Nevada in the southern part of Owens Valley, there is evidence that it also experienced an episode of extension that was possibly coeval with the Benton Range dike swarm. Dunne and Walker (2004) document up to ~9 km of shortening in the ESTS during three distinct episodes at: (1) >188 Ma, (2) 148–152 Ma, and (3) post Late Jurassic. Notably, sometime in the Middle Jurassic, the ESTS was quiescent and a thick sequence of flat–lying volcaniclastics were deposited. They were subsequently tilted 35°SW prior to ~152 Ma, which Dunne and Walker (2004) note could have

occurred during an extensional event. Additional field evidence of Jurassic compression is seen in magmatic foliations that formed in plutons during compressional strain, but date to periods >186 Ma (Cao et al., 2015).

4.6.3 Evidence of crustal thickness in the Jurassic Sierran arc

There is conflicting evidence in the literature regarding the thickness of the crust in the Sierran arc during the Jurassic. Ardill et al. (2024) compiled geochemical data for granitoids in the central Sierra Nevada and used the updated geochemical proxies (Sr/Y, La/Yb) from Luffi and Ducea (2022) to infer a bimodal distribution of Sierran crustal thickness in the Jurassic, ranging from ~24 ± 4 in the western foothills and ~40 ± 4 km in the main arc. Similarly, utilizing Eu anomaly ratios in zircons from Sierran granitoids, Tang et al. (2024) infer crustal thickening during the Jurassic and a thickness between 50–60 km. However, these results conflict with field evidence for relatively thin (and/or unusually dense) crust in the Jurassic based on widespread marine volcanic and sedimentary packages, which are not seen in the Triassic or Cretaceous (e.g., Tobisch et al., 2000; Barth et al., 2018; Attia et al., 2020, 2021). For example, roof pendants in the Ritter Range of the eastern Sierra Nevada (~65 km west of the Benton Range) record volcanics and volcaniclastics (dated at ~164–171 Ma; Barth et al., 2018) deposited in a marine setting (e.g., Tobisch et al., 2010; Attia et al., 2021), which again is suggestive of relatively thin crust (or at least low elevations) in this region at this time (Cao and Paterson, 2016). Additional evidence of Jurassic extension is found in roof pendants in the northern Sierra Nevada, which have been interpreted to be marine conglomeritic clasts (of which a subset is volcanic) deposited in syn–tectonic fault troughs formed during extension (Fisher, 1990). Similarly, there is evidence of Jurassic volcanics deposited in a long–lived marine basin in the northern Sierran arc (English Mountain; Templeton and Hanson, 2003), which adds to the

evidence of both marine environments and extensional tectonics in the Sierran arc during the Middle Jurassic (Fisher, 1990).

4.6.4 Relationship between formation of the CRO and extension in the Sierra Nevada?

An outstanding question is whether there is a relationship between the formation of the CRO (~160–170 Ma) and extension in the main Sierran arc, as proposed by Saleeby (1996) through the mechanism of slab rollback. The data presented in this study provides direct evidence of extension in the main Sierran arc at ~162–169 Ma (possibly ~158–176 Ma), through zircon crystallization ages of the Benton Range dike swarm. However, Arkula et al. (2023) provide compelling evidence that the CRO was formed by trench–parallel N–S spreading in the forearc region, which is inconsistent with extension driven by slab rollback, which predicts E–W spreading (e.g., Snow and Shervais, 2015). Although not discussed in Arkula et al. (2023), one possible outcome of the extreme, trench–parallel (N–S) extension in the supra–subduction forearc, enabling formation of the CRO, was the development of lateral forces, subjecting the eastern and western margins of the Jurassic Sierran arc to trans–tensional shear stress and strike–slip deformation, as documented in the Independence (148 Ma; Chen and Moore, 1979) and Owens Mountain (148–153 Ma; Wolf and Saleeby, 1992) dike swarms, respectively, although both post–date the CRO (160–170 Ma). It is also possible that the N–S extensional forces in the forearc region led to the development of pull–apart basins in the main Sierran arc, enabling localized regions of extension to develop (e.g., the Benton Range dike swarm, this study; the Emigrant Gap mafic complex; Ryan–Davis et al., 1996). Continued field work and geochronology of Jurassic–age rock suites in the Sierra Nevada are needed to further resolve whether extension in the main Jurassic arc was only localized or relatively widespread between ~160–170 Ma.

4.7 Conclusion

Several conclusions can be drawn from the updated U–Pb zircon crystallization ages of the Benton Range high–SiO_2 rhyolite dike swarm presented in this study. Firstly, the dikes are directly dated with U–Pb geochronology for the first time establishing a weighted mean of all zircon crystallization ages from all studied units of 165 ± 11 Ma. The weighted mean zircon crystallization ages of each dike define a range of 162 ± 9 Ma –169 ± 11 Ma with a most conservative estimate of dike emplacement ranging from 158 ± 5 –176 ± 5 Ma.

A comparison between the previous age constraints for the dikes (168–209 Ma) established by Renne and Turrin (1987) and the range established in this study (~162–169 Ma; conservatively ~158–176 Ma) reveal only partial overlap and shift the emplacement age of the dike swarm significantly younger. This additionally suggests that K–Ar ages (~153–160 Ma) obtained from biotite in the Benton Range dikes by Renne and Turrin (1987) fall within error of the conservative estimate of dike emplacement from this study and likely reflect more accurate dates than initially expected.

Another key take away is the evidence that the extensional feature of the Benton Range high–SiO_2 rhyolite dike swarm emplacement occurred simultaneously with the formation of the CRO (~160–170 Ma; Shervais et al., 2005) and also overlapped the Jurassic magmatic flare–up (~145–175 Ma; e.g. Paterson and Ducea, 2015) in the main Sierran arc. This places new tectonic constraints on the kinematics of western U.S. during the Jurassic and could be casually related.

The timing of the Benton Range emplacement adds to the abundant field evidence of extension and a thin crust in the surrounding area. Younger dike swarms (148–155 Ma; Independence; Owens Mountain; Sonora and King Creek; Chen and Moore, 1979; Wolf and Saleeby, 1992; Wesley et al., 2019), the Emigrant Gap intrusive mafic complex (168 ± 2 Ma; Girty et al., 1995), and Jurassic marine volcanics (Ritter Range, English Mountain, and roof

pendants in the norther Sierra Nevada; Tobisch et al., 2010; Attia et al., 2021; Fisher, 1990; Templeton and Hanson, 2003) all suggest local or regional extensional settings during this time.

Although many models suggest different tectonic explanations for the formation of the CRO, it's timing with the extensional Benton Range dike swarm indicates that, whether localized or regional, extension was occurring both in the forearc and back arc simultaneously. This could be a result of slab roll back (consistent with Saleeby, 1996) causing rifting in the fore arc and extension in the back arc that led to both the formation of the CRO and the emplacement of the Benton Range dike swarm. Or, alternatively, this could be due to the geometry of the subducting slab which caused trench–parallel (N–S) spreading (Arkula et al., 2023) in the forearc which gave rise to a series of localized pull–apart basins. Regardless of the tectonic model, new U–Pb ages (~162–169 Ma; conservatively ~158–176 Ma) established in this study provide constraints for the emplacement of the Benton Range high–SiO_2 dike swarm and confirm that either local or regional extensional was occurring during the Jurassic in the Long Valley area.

4.8 References

Ahmad, T., Longjam, K. C., Fouzdar, B., Bickle, M. J., & Chapman, H. J. (2009). Petrogenesis and tectonic setting of bimodal volcanism in the Sakoli Mobile Belt, Central Indian shield. *Island Arc*, *18*(1), 155–174. https://doi.org/10.1111/j.1440–1738.2008.00651.x

Ardill, K., Paterson, S., & Memeti, V. (2018). Spatiotemporal magmatic focusing in upper–mid crustal plutons of the Sierra Nevada arc. *Earth and Planetary Science Letters*, *498*, 88–100. https://doi.org/10.1016/j.epsl.2018.06.023

Ardill, K., Attia, S., Memeti, V., & Paterson, S. R. (2024). Fingerprinting the geochemical signals of episodic arc activity in the Sierra Nevada batholith in space and time. *Geological Society of America Bulletin*, *136*(9–10), 4321–4341. https://doi.org/10.1130/b37266.1

Armstrong, R. L., Ward, P. L., (1993). Late Triassic to Earliest Eocene magmatism in the North American Cordillera: Implications for the Western Interior Basin. In W. G. E. Caldwell & E. G. Kauffman (Eds.), *Evolution of the Western Interior Basin* (pp. 49–72). Geological Association of Canada. https://whyclimatechanges.com/pdf/Papers/Armstrong1993LateTriassicMagmatism.pdf

Arkula, C., Lom, N., Wakabayashi, J., Rea–Downing, G., Qayyum, A., Dekkers, M. J., Lippert, P. C., & Van Hinsbergen, D. J. (2023). The forearc ophiolites of California formed during trench–parallel spreading: Kinematic reconstruction of the western USA Cordillera since the Jurassic. Earth–Science Reviews, 237, 104275. https://doi.org/10.1016/j.earscirev.2022.104275

Attia, S., Cottle, J. M., & Paterson, S. R. (2020). Erupted zircon record of continental crust formation during mantle driven arc flare–ups. Geology, 48(5), 446–451. https://doi.org/10.1130/g46991.1

Attia, S., Paterson, S. R., che, J., & Cao, W. (2021). Detrital zircon provenance and depositional links of Mesozoic Sierra Nevada intra–arc strata. Geosphere, 17(5), 1422–1453. https://doi.org/10.1130/ges02296.1

Balázs, A., Faccenna, C., Gerya, T., Ueda, K., & Funiciello, F. (2022). The dynamics of ForEARC – Back-Arc basin subsidence: numerical models and observations from Mediterranean subduction zones. Tectonics, 41(5). https://doi.org/10.1029/2021tc007078

Barth, A. P., Wooden, J. L., Jacobson, C. E., & Economos, R. C. (2013). Detrital zircon as a proxy for 773 tracking the magmatic arc system: The California arc example. Geology, 41(2), 223–226.

Barth, A. P., Wooden, J. L., Riggs, N. R., Walker, J. D., Tani, K., Penniston-Dorland, S. C., Jacobson, C. E., Laughlin, J. A., & Hiramatsu, R. (2018). Marine Volcaniclastic record of early arc evolution in the Eastern Ritter Range Pendant, Central Sierra Nevada, California. Geochemistry Geophysics Geosystems, 19(8), 2543–2559. https://doi.org/10.1029/2018gc007456

Busby–Spera, C. J. (1988). Speculative tectonic model for the early Mesozoic arc of the southwest Cordilleran United States. Geology, 16(12), 1121. https://doi.org/10.1130/0091–7613(1988)016

Cao, W., & Paterson, S. (2016). A mass balance and isostasy model: Exploring the interplay between magmatism, deformation and surface erosion in continental arcs using central Sierra Nevada as a case study. Geochemistry Geophysics Geosystems, 17(6), 2194–2212. https://doi.org/10.1002/2015gc006229

Cao, W., Paterson, S., Saleeby, J., & Zalunardo, S. (2015). Bulk arc strain, crustal thickening, magma emplacement, and mass balances in the Mesozoic Sierra Nevada arc. *Journal of Structural Geology*, *84*, 14–30. https://doi.org/10.1016/j.jsg.2015.11.002

Chamberlain, K.J., Wilson, C.J.N., Wallace, P.J., and Millet, M.A. (2015) Micro–analytical perspectives on the Bishop Tuff and its magma chamber: Journal of Petrology, 56, 605–640.

Chapman, J. B., Shields, J. E., Ducea, M. N., Paterson, S. R., Attia, S., & Ardill, K. E. (2021). The causes of continental arc flare ups and drivers of episodic magmatic activity in Cordilleran orogenic systems. *Lithos*, *398–399*, 106307. https://doi.org/10.1016/j.lithos.2021.106307dec

Chen, J. H., & Moore, J. G. (1979). Late Jurassic Independence dike swarm in eastern California. *Geology*, *7*(3), 129. https://doi.org/10.1130/0091–7613(1979)7

Chen, J. H., & Moore, J. G. (1982). Uranium-lead isotopic ages from the Sierra Nevada Batholith, California. *Journal of Geophysical Research Atmospheres*, *87*(B6), 4761–4784. https://doi.org/10.1029/jb087ib06p04761

Choi, S. H., Mukasa, S. B., & Shervais, J. W. (2008). Initiation of Franciscan subduction along a large–offset fracture zone: Evidence from mantle peridotites, Stonyford, California. *Geology*, *36*(8), 595. https://doi.org/10.1130/g24993a.1

Cisneros, M., Behr, W. M., Platt, J. P., & Anczkiewicz, R. (2022). Quartz–in–garnet barometry constraints on formation pressures of eclogites from the Franciscan Complex, California. Contributions to Mineralogy and Petrology, 177(1). https://doi.org/10.1007/s00410–021–01876–4

Cousens, B.L. (1996). Magmatic evolution of Quaternary mafic magmas at Long Valley caldera and the Devils Postpile, California: Effects of crustal contamination on lithospheric mantle–derived magmas. Journal of Geophysical Research, 101(B12), 27673–27689

DeCelles, P. G., Ducea, M. N., Kapp, P., & Zandt, G. (2009). Cyclicity in Cordilleran orogenic systems. *Nature Geoscience*, *2*(4), 251–257. https://doi.org/10.1038/ngeo469

Dickinson, W. R., Hopson, C. A., & Saleeby, J. (1996). Alternate origins of the Coast Range Ophiolite (California); introduction and implications. The Caltech Institute Archives (California Institute of Technology). https://authors.library.caltech.edu/49197/

Ducea, M. (2001). The California Arc: thick granitic batholiths, eclogitic residues, Lithospheric–Scale thrusting, and magmatic Flare–Ups. In *GSA TODAY*. https://rock.geosociety.org/net/gsatoday/archive/11/11/pdf/i1052–5173–11–11–4.pdf

Dumitru, T.A., Wakabayashi, J., Wright, J.E., and Wooden, J.L., 2010, Early Cretaceous transition from nonaccretionary behavior to strongly accretionary behavior within the Franciscan subduction complex: Tectonics, v. 29, TC5001, doi:10.1029/2009TC002542.

Dunne, G. C., & Walker, J. D. (2004). Structure and evolution of the East Sierran thrust system, east central California. Tectonics, 23(4). https://doi.org/10.1029/2002tc001478

Gilbert, C. M. (1941). Late Tertiary geology southeast of Mono Lake, California. *Geological Society of America Bulletin*, *52*(6), 781–816. https://doi.org/10.1130/gsab–52–781

Godfrey, N.J. and S.L. Klemperer (1998) Ophiolite basement to a forearc basin and implications for continental growth: The Coast Range/Great Valley ophiolite, California. Tectonics, v. 17, pp. 558–570.

Girty, G. H., Hanson, R. E., Girty, M. S., Schweickert, R. A., Harwood, D. S., Yoshinobu, A. S., Bryan, K. A., Skinner, J. E., & Hill, C. A. (1995). Timing of emplacement of the Haypress Creek and Emigrant Gap plutons: Implications for the timing and controls of Jurassic orogenesis, northern Sierra Nevada, California. In *Geological Society of America Special Papers* (pp. 191–202). https://doi.org/10.1130/spe299–p191

Han, J., Hanchar, J. M., Pan, Y., Hollings, P., & Chen, H. (2023). Hydrothermal alteration, not metamictization, is the main trigger for modifying zircon in highly evolved granites. *Geological Society of America Bulletin*. https://doi.org/10.1130/b36996.1

Harper, G.D., 2003, Tectonic implications of boninite, arc tholeiite, and MORB magma types in the Josephine Ophiolite, California–Oregon, in Dilek, Y., and Robinson, P.T., eds., Ophiolites in Earth History: The Geological Society of London Special Publication 218, p. 207–230

Harrison, T. M., Célérier, J., Aikman, A. B., Hermann, J., & Heizler, M. T. (2009). Diffusion of 40Ar in muscovite. *Geochimica Et Cosmochimica Acta*, *73*(4), 1039–1051. https://doi.org/10.1016/j.gca.2008.09.038

Hoskin, P. W. O. (2003). The composition of zircon and igneous and metamorphic petrogenesis. *Reviews in Mineralogy and Geochemistry*, *53*(1), 27–62. https://doi.org/10.2113/0530027

Humphreys, E., Hessler, E., Dueker, K., Farmer, G. L., Erslev, E., & Atwater, T. (2003). How Laramide–Age hydration of North American lithosphere by the Farallon slab controlled subsequent activity in the Western United States. International Geology Review, 45(7), 575–595. https://doi.org/10.2747/0020–6814.45.7.575

Jiang, W., Li, H., Evans, N. J., & Wu, J. (2019). Zircon records multiple magmatic–hydrothermal processes at the giant Shizhuyuan W–Sn–Mo–Bi polymetallic deposit,

South China. *Ore Geology Reviews*, *115*, 103160. https://doi.org/10.1016/j.oregeorev.2019.103160

Kirkland, C., Smithies, R., Taylor, R., Evans, N., & McDonald, B. (2014). Zircon Th/U ratios in magmatic environs. *Lithos*, *212–215*, 397–414. https://doi.org/10.1016/j.lithos.2014.11.021

Lemmon, D. M., UNITED STATES DEPARTMENT OF THE INTERIOR, & GEOLOGICAL SURVEY. (1941). TUNGSTEN DEPOSITS OF THE BENTON RANGE, MONO COUNTY, CALIFORNIA. In *Strategic Minerals Investigations* (pp. 581–593). UNITED STATES GOVERNMENT PRINTING OFFICE. https://pubs.usgs.gov/bul/0922s/report.pdf

Luffi, P., & Ducea, M. N. (2022). Chemical mohometry: Assessing crustal thickness of ancient orogens using geochemical and isotopic data. Reviews of Geophysics, 60(2), e2021RG000753. https://doi.org/10.1029/2021rg000753

Maraszewska, M., Majka, J., Harlov, D. E., Manecki, M., Schneider, D. A., Broska, I., & Myhre, P. (2023). Multi–stage metamorphic and metasomatic imprints on apatite–monazite–xenotime assemblages in a set of small iron oxide–apatite (IOA) ore bodies, Prins Karls Forland, Svalbard. *Ore Geology Reviews*, *155*, 105344. https://doi.org/10.1016/j.oregeorev.2023.105344

Mesa, J. (2021). Evidence of Phenocryst Growth and Magma Mixing during Ascent along Fractures in Volcanic Rocks from Basalt to Rhyolite. *Deep Blue (University of Michigan)*. https://doi.org/10.7302/2876

Paterson, S. R., & Ducea, M. N. (2015). ArC Magmatic Tempos: Gathering the evidence. Elements, 11(2), 91–98. https://doi.org/10.2113/gselements.11.2.91

Profeta, L., Ducea, M. N., Chapman, J. B., Paterson, S. R., Gonzales, S. M. H., Kirsch, M., Petrescu, L., & DeCelles, P. G. (2015). Quantifying crustal thickness over time in magmatic arcs. Scientific Reports, 5(1), 17786. https://doi.org/10.1038/srep17786

Renne, P.R., and Turrin, B.D. (1987) Constraints on timing of deformation in the Benton Range, southeastern California, and implications to Nevadan orogenesis: Geology, 15, 1031–1034.

Rinehart, C.D., and Ross, D.C. (1957). Geologic map of the Benton Range Mountain quadrangle, California: U.S. Geological Survey GQ–99, 1:62,50.

Saleeby, J., Dickinson, W. R., Hopson, C. A., (1996). Alternate origins of the Coast Range Ophiolite (California); introduction and implications. *CaltechAUTHORS (California Institute of Technology)*. https://authors.library.caltech.edu/49197/

Shervais, J. W., & Kimbrough, D. L. (1985). Geochemical evidence for the tectonic setting of the Coast Range ophiolite: A composite island arc–oceanic crust terrane in western California. Geology, 13(1), 35. https://doi.org/10.1130/0091–7613(1985)13

Shervais, J. W., Murchey, B., Kimbrough, D. L., Renne, P., & Hanan, B. B. (2005). Radioisotopic and biostratigraphic age relations in the coast range Ophiolite, northern California: Implications for the tectonic Evolution of the western Cordillera. Geological Society of America Bulletin, 117(5/6), 633–653.

Snow, C. A., & Shervais, J. W. (2015). Cuesta Ridge ophiolite, San Luis Obispo, California: Implications for the origin of the Coast Range ophiolite. In *Geological Society of America Special Papers* (pp. 285–298). https://doi.org/10.1130/2015.2513(07)

Stacey, J., & Kramers, J. (1975). Approximation of terrestrial lead isotope evolution by a two–stage model. *Earth and Planetary Science Letters*, *26*(2), 207–221. https://doi.org/10.1016/0012–821x(75)90088–6

Stern, R. J., & Bloomer, S. H. (1992). Subduction zone infancy: Examples from the Eocene Izu–Bonin–Mariana and Jurassic California arcs. Geological Society of America Bulletin, 104(12), 1621–1636. https://doi.org/10.1130/0016–7606(1992)104

Tang, M., Guo, Z., Cao, W., & Chu, X. (2024). Revisiting zircon Eu anomaly as a proxy for crustal thickness: A case study of the Sierra Nevada Batholith. *Earth and Planetary Science Letters*, *643*, 118897. https://doi.org/10.1016/j.epsl.2024.118897

Templeton, J. H., & Hanson, R. E. (2003). Jurassic submarine arc–apron deposits and associated magma/wet–sediment interaction, northern Sierra Nevada, California. Journal of Volcanology and Geothermal Research, 128(4), 299–326. https://doi.org/10.1016/s0377–0273(03)00197–5

Terentiev, R. A., Savko, K. A., & Santosh, M. (2017). Paleoproterozoic evolution of the arc–back–arc system in the east Sarmatian Orogen (East European Craton): Zircon SHRIMP geochronology and geochemistry of the Losevo volcanic suite. *American Journal of Science*, *317*(6), 707–753. https://doi.org/10.2475/06.2017.03

Tobisch, O. T., Fiske, R. S., Saleeby, J. B., Holt, E., & Sorensen, S. S. (2000). Steep tilting of metavolcanic rocks by multiple mechanisms, central Sierra Nevada, California. Geological Society of America Bulletin, 112(7), 1043–1058. https://doi.org/10.1130/0016–7606(2000)112

Fisher, G. Reid 1990. "Middle Jurassic syntectonic conglomerate in the Mt. Tallac roof pendant, northern Sierra Nevada, California", Paleozoic and Early Mesozoic Paleogeographic Relations; Sierra Nevada, Klamath Mountains, and Related Terranes, David S. Harwood, M. Meghan Miller

Ryan–Davis, J., Bucholz, C. E., & Sisson, T. W. (2026). Shallow differentiation of primitive arc magmas at the Jurassic Emigrant Gap Mafic Complex, Sierra Nevada, California. *Journal of Petrology*, *67*(2). https://doi.org/10.1093/petrology/egag013

Saleeby, J., Dunne, G., 2015, Temporal and tectonic relations of early Mesozoic arc magmatism, southern Sierra Nevada, California, in Anderson, T.H.et al., eds., Late Jurassic margin of Laurasia—A record of faulting accommodating plate rotation: Geological Society of America Special Paper 513 , doi:10.1130/2015.2513(05)

Wesley, A. J., Paterson, S. R., Attia, S., & Memeti, V. (2019). THE JURASSIC KING CREEK PLUTON AND INDEPENDENCE DIKES, SOUTHERN RITTER RANGE, SIERRA NEVADA, CA: IMPLICATIONS FOR JURASSIC MAGMATISM AND TECTONICS. *Abstracts With Programs – Geological Society of America*. https://doi.org/10.1130/abs/2019am–339526

Wolf, M. B., & Saleeby, J. B. (n.d.). Jurassic Cordilleran dike swarm–shear zones: Implications for the Nevadan orogeny and North American plate motion. *Geology*, *20*(8), 745. https://doi.org/10.1130/0091–7613(1992)020

Wang, X., Griffin, W. L., Jie, C., Pinyun, H., & Xiang, L. (2011). U and TH contents and TH/U ratios of zircon in felsic and mafic magmatic rocks: Improved Zircon-Melt distribution coefficients. *Acta Geologica Sinica – English Edition*, *85*(1), 164–174. https://doi.org/10.1111/j.1755–6724.2011.00387.x

Chapter 5 Conclusions

5.1 Concluding remarks

Chapters from this dissertation have addressed various topics related to the timescales, mechanisms, and conditions of phenocryst growth in high–SiO_2 rhyolites that either successfully erupted or were emplaced in a dike swarm, including: (1) the pre–eruptive temperature of phenocryst growth, (2) the timescales and conditions of phenocryst growth (i.e., rapid growth during dike ascent vs slow growth in a magma chamber), (3) confirmation of the H_2O–saturated granite solidus, and (4) zircon crystallization ages in a Jurassic high–SiO_2 rhyolite dike swarm, with tectonic implication for the timing of extension in the Mesozoic Sierra Nevada arc.

Chapter 2 presented a new biotite–liquid thermometer calibrated specifically on high–SiO_2 rhyolites, using both natural samples and new experiments conducted in this thesis. This was pursued because many current thermometers in the literature are not calibrated on high–SiO_2 rhyolites, and those that are (e.g. Fe–Ti two–oxide thermometer) is sensitive to post–eruptive mineral alteration. The $D_{TiO_2}^{bte-liq}$ thermometer presented in this chapter allows for determination of pre–eruptive temperature in older and/or altered high–SiO_2 rhyolite samples (e.g. the Jurassic Benton Range high–SiO_2 rhyolite dike swarm) for which Fe–Ti two–oxide thermometry is not possible.

Chapter 3 explored three hypotheses to explain highly variable crystal abundances in the Glass Mountain high–SiO_2 rhyolite units, despite minimal difference in their major–element compositions: (1) equilibrium phenocryst growth under different temperature and P_{H2O} conditions during storage in a magma chamber; (2) the possibility that the water–saturated

granite solidus is much lower than previously documented, and (3) phenocryst growth during rapid ascent in dikes, following a kinetic delay to nucleation. Through a combination of new experiments and a detailed characterization of phenocryst compositions and textures, the first two hypotheses were ruled out, leading to the third hypothesis as the most viable.

Chapter 4 constrained a period of extension in the main Sierran arc by presenting new U–Pb zircon crystallization ages (162–169 Ma) for a high–SiO_2 rhyolite dike swarm. These ages are shown to overlap the formation of the Coast Range Ophiolites (160–170 Ma; Shervais et al., 2005) as well as the Jurassic magmatic flare up (145–175 Ma; Paterson and Ducea, 2015). To explain this, it is suggested that the formation of the Coast Range Ophiolites through trench–parallel spreading in the forearc likely induced shearing and extension across the main Sierran arc.

Although various topics and questions which were presented at the beginning of this dissertation were successfully addressed, new opportunities present themselves for future directions exploring the timescales, mechanisms, and conditions of successful high–SiO_2 rhyolite eruption.

5.2 Future Work

5.2.1 Deployment of biotite–liquid thermometer

The biotite–liquid thermometer presented in Chapter 2 provides an opportunity for its application to a wide variety of volcanic deposits, dikes and plutons of high–SiO_2 rhyolite composition, for which Fe–Ti oxide thermometry is not possible due to alteration/weathering, welding, or extremely low crystallinities where ilmenite is absent. Some potential target applications include:

(1) Numerous ignimbrite flows of the Bishop Tuff that have undergone welding. Most of the Bishop Tuff, deposited during the caldera–forming eruption (>600 km^3) that formed Long Valley Caldera, is welded (Wilson and Hildreth, 1997). Fe–Ti oxides are particularly susceptible to alteration, which has made deployment of the Fe–Ti two–oxide thermometer only possible to a small subset of the Bishop Tuff. Deployment of the $D_{TiO_2}^{bte-liq}$ thermometer could provide additional temperature constraints for parts of the Bishop Tuff deposit that has yet to be determined. This, in turn, would provide additional information on the extent to which the pre–eruptive magma body was thermally zoned.

(2) Determination of temperature for plutonic bodies of high–SiO_2 rhyolite composition. Chapter 2 demonstrated the applicability of the biotite–liquid thermometer to significantly older (Jurassic–age) dike samples. It could also be deployed on biotite–bearing plutonic bodies, namely leucogranites of high–SiO_2 rhyolite composition of varying ages. For example, leucogranites in Miocene–aged bimodal (granite–diorite) plutons found in the Colorado River Extensional Province (e.g., Miller et al., 2011), including the Spirit Mountain batholith (e.g., Walker et al., 2007) and the Searchlight pluton (e.g., Bachl et al., 2001), NV contain pristine biotite and the new thermometer provides an opportunity to constrain temperatures in these plutonic bodies for the first time.

5.2.2 Expanded calibrations of D_{TiO2}(bte-liq) thermometer to low–SiO_2 rhyolites

Additional future work surrounding the $D_{TiO_2}^{bte-liq}$ thermometer from Chapter 2 is to provide additional replications at specific temperatures (e.g., 675, 700, and 825 °C) as was done at 750 °C to improve the calibration. In my thesis, six successful replicated experiments were

conducted at 750° C between 125–225 MPa. This allowed for confirmation of the thermometer calibration at this temperature and allowed a more accurate determination of $D_{TiO_2}^{bte-liq}$ at 750°C to be determined for high–SiO_2 rhyolites. To improve the thermometer, additional replications at other temperatures would be helpful.

Another potential area of future work is to expand experimental calibration of the partitioning of TiO_2 between biotite and melt to low–SiO_2 rhyolites, which are more common in the volcanic rock record than high–SiO_2 rhyolites. This would be useful to determine pre–eruptive temperatures for low–SiO_2 rhyolites where extensive alteration has precluded application of the Fe–Ti oxide thermometer (Ghiorso and Evans, 2008). This would require a new set of experiments and a new natural dataset, focused exclusively on low–SiO_2 rhyolite, because Ti^{4+} undergoes composition–induced coordination change (Farges and Brown, 2007) and the partitioning behavior of elements between various mineral phases and melts is known to be very different between low– and high–SiO_2 rhyolites (e.g., Mahood and Hildreth, 1983). The key point is that it is essential that experiments be conducted on the same melt composition to which the biotite–liquid thermobarometer is applied. A potential suite of natural low–SiO_2 rhyolites that could be used for calibration is the post caldera rhyolites from Long Valley Caldera for which independent Fe–Ti oxide temperatures have been obtained (Hildreth et al., 2017).

5.2.3 Establish an expanded phase diagram for high–SiO_2 rhyolite

Another potential avenue of future work is to conduct additional phase–equilibrium experiments to significantly expand the water–saturated phase diagram for high–SiO_2 rhyolite (e.g. a Glass Mountain unit). The experiments reported by Waters and Andrews (2016) on a representative Glass Mountain unit established a phase diagram that has been used extensively in this work. However, additions to phenocrysts analyzed (e.g, plagioclase and biotite, in addition

to sanidine) and an expansion of the experimental conditions to lower temperatures (650–675 °C) and higher pressures (250–300 MPa) could be useful.

First, biotite–liquid temperatures of the Glass Mountain units from Chapter 3 of this study as well as Fe–Ti oxide temperatures reported by Gordon (2022) indicate that they grew their phenocrysts at ≤ 725 °C, with at least one (OC) at ~660°C. The lowest temperature investigated in Waters and Andrews (2016) was 700 °C, and thus an extension of H_2O–saturated experiments down to 650 °C at upper crustal pressures (≤300 MPa) would help to fully understand the phenocryst assemblage expected in low–temperature high–SiO_2 rhyolites under equilibrium conditions.

Another reason to extend experiments to lower temperatures is to fully map the location of the H_2O–saturated solidus at upper crustal conditions (≤ 300 MPa). In Chapter 3 of this dissertation, I provided a lower bound for the H_2O–saturated solidus of ≥650 °C at 200 MPa which is consistent with the ≥670 °C limit at that same pressure reported by Ebadi and Johannes (1991). However, considering the current controversy surrounding the location of the H_2O saturated solidus in the literature (e.g. Thompson et al., 2026), a detailed experimental determination of the H_2O–saturated solidus over a range of upper crustal pressures (~300–75 MPa) for a high–SiO_2 rhyolite starting composition would be beneficial.

Another benefit of both extending, and also redocumenting, phase equilibrium experiments for a H_2O–saturated high–SiO_2 rhyolite starting composition is to document and analyze all phases present in experimental run products. In the study of Waters and Andrews (2016), although the plagioclase in–curve was determined, compositional data for plagioclase in the run products is not reported. A thorough documentation of all mineral phases and their compositions at varying P_{H2O} and temperatures is needed for a fully characterized phase

diagram. This would also be particularly insightful for potential changes in plagioclase composition across an expanded phase diagram for high–SiO_2 rhyolites (e.g. 650°C– 850°C and 300 – 75 MPa). Also, a finer experimental grid of T–P_{H2O} run conditions, as well as additional lower temperature experiments, would also be insightful for the application of hygrometry to low–temperature high–SiO_2 rhyolites through the documentation of changes in sanidine compositions (Or#), which was discussed at length in Chapter 3.

5.2.4 Experimental investigation of timescales for phenocryst growth in high–SiO_2 rhyolites during dike ascent (i.e., at various undercoolings)

Following the abundant evidence from Chapter 3 that rapid phenocryst growth occurred in the Glass Mountain high–SiO_2 rhyolites during dike ascent to the surface, presumably over a period of several days or weeks, it is useful to conduct additional experiments to further verify this conclusion. The needed experiments are those that mimic the undercooling ($\Delta T = T_{liquidus}$–T_{melt}) conditions required for the growth of large, sparse phenocrysts, which in turn require a kinetic delay to nucleation. These undercooling experiments on 100% starting glass can be accomplished in two ways.

(1) Isobaric experiments can be conducted by bringing samples above the liquidus for a hold duration (to purge nuclei) before being rapidly dropped to their final hold temperature (e.g. 675°C) to produce an effective undercooling (e.g., similar to the "top–down" experiment in Chapter 3). This could be replicated multiple times with the same final hold temperature (e.g. 675°C), but over varying durations. By analyzing the various run products to see how long a duration is needed before crystals begin to grow, an estimate of the kinetic delay to nucleation can be deduced. This, in turn, enables the actual time over which crystal growth occurred to be determined, helping to constrain actual crystal growth rates. Similarly, experiments can be

conducted at different ΔT (undercooling) values (Chap 3; Fig 3), to determine at what ΔT in high–SiO_2 rhyolites do we find maximum crystal growth rates.

(2) Similar experiments can be conducted under isothermal conditions, but where an undercooling develops due to decompression (analogous to what occurs in an ascending melt during dike transport). In this case, experiments can be taken to superliquidus conditions at a P_{H2O} = 250 MPa and 700 °C and then decompressed (isothermally) abruptly to a P_{H2O} = 140 MPa, which will induce an undercooling of ~25 °C (as seen for unit YO in Fig. 3–16). By holding the experiment at the lower P_{H2O} for different durations, the length of the kinetic delay to nucleation can be determined, constraining the actual time for crystal growth and thus (with the size of crystals in the various run products) crystal growth rates. A similar set of experiments can be done where the decompression step is down to P_{H2O} = 120 MPa, which will induce an undercooling of ~40 °C (as seen for unit OL in Fig. 3–16). This will enable an evaluation of how crystal growth rates in high–SiO_2 rhyolites vary with ΔT values (as predicted in Fig. 3– 3).

5.3 References

Bachl, C. A., Miller, C. F., Miller, J. S., & Faulds, J. E. (2001). Construction of a pluton: Evidence from an exposed cross section of the Searchlight pluton, Eldorado Mountains, Nevada. Geological Society of America Bulletin, 113(9), 1213–1228. https://doi.org/10.1130/0016–7606(2001)113

Ebadi A, Johannes W (1991) Beginning of melting and composition of first melts in the system Qz–Ab–Or–H2O–CO2. Contrib Mineral Petrol 106:286–295

Gordon, B. (2022). The generation of geochemical gradients in the pre–caldera Glass Mountain high–SiO2 rhyolites of Long Valley, CA: clues to the origin and preservation of Rb–Sr isochrons. Deep Blue (University of Michigan). https://doi.org/10.7302/6563

Ghiorso, M.S. & Evans, B.W. (2008) Thermodynamics of rhombohedral oxide solutions and revision of the Fe–Ti two–oxide geothermometer and oxygen barometer. American Journal of Science, 308, 957–1039

Hildreth, W., Fierstein, J., & Calvert, A. (2017). Early postcaldera rhyolite and structural resurgence at Long Valley Caldera, California. Journal of Volcanology and Geothermal Research, 335, 1–34. https://doi.org/10.1016/j.jvolgeores.2017.01.005

Mahood G, Hildreth W (1983) Large partition coefficients for trace elements in high–silica rhyolites. Geochim Cosmochim Acta 47:11–30

Miller, C. F., Furbish, D. J., Walker, B. A., Claiborne, L. L., Koteas, G. C., Bleick, H. A., & Miller, J. S. (2011). Growth of plutons by incremental emplacement of sheets in crystal–rich host: Evidence from Miocene intrusions of the Colorado River region, Nevada, USA. Tectonophysics, 500(1–4), 65–77. https://doi.org/10.1016/j.tecto.2009.07.011

Paterson, S. R., & Ducea, M. N. (2015). ArC Magmatic Tempos: Gathering the evidence. Elements, 11(2), 91–98. https://doi.org/10.2113/gselements.11.2.91

Shervais, J. W., Murchey, B., Kimbrough, D. L., Renne, P., & Hanan, B. B. (2005). Radioisotopic and biostratigraphic age relations in the coast range Ophiolite, northern California: Implications for the tectonic Evolution of the western Cordillera. Geological Society of America Bulletin, 117(5/6), 633–653.

Thompson, G. T., Rufledt, C. J., & Thomas, J. B. (2026). The transition from magmatic to hydrothermal crystallization conditions of a shallow–level granitic pluton. Contributions to Mineralogy and Petrology, 181(1). https://doi.org/10.1007/s00410–025–02280–y

Walker, B., Miller, C., Claiborne, L. L., Wooden, J., & Miller, J. (2007b). Geology and geochronology of the Spirit Mountain batholith, southern Nevada: Implications for timescales and physical processes of batholith construction. Journal of Volcanology and Geothermal Research, 167(1–4), 239–262. https://doi.org/10.1016/j.jvolgeores.2006.12.008

Waters, L.E. & Andrews, B.J. (2016) The role of superheating in the formation of Glass Mountain obsidians (Long Valley, CA) inferred through crystallization of sanidine. Contributions to Mineralogy and Petrology, 171, 79.

Wilson CJN, Hildreth W (1997) The Bishop Tuff: new insights from eruptive stratigraphy. J Geol 105: 407:439

Appendices

Appendix A: Supplemental Material for Chapter 2

Table A-0-1 Electron microprobe standards and conditions of analysis

Instrument:			
Cameca SX100, EMAL/University of Michigan			
Phase: Glass			
Accelerating Voltage (kV)	**Beam Current (nA)**	**Beam Size (µm)**	**Peak Counting Time (s)**
15	10	10	10-30
Standard	**Elements Calibrated**		
Orthoclase OR-1, PSU	K		
Wollastonite	Ca		
Rutile, MTI Corp.	Ti		
SILL	Al	3SD uncertainty based on counting statistics for glass:±1.53 wt% SiO_2, ±0.41 wt% Al_2O_3, ±0.09 wt% CaO, ±0.30 wt% Na_2O, ±0.18 wt% K_2O	
Ferrosilite (synthetic)	Fe		
FOBO	Mg, Si		
Albite (Tiburon)	Na		
Rhodonite (Broken Hill)	Mn		
Phase: biotite			
Accelerating Voltage (kV)	**Beam Current (nA)**	**Beam Size (µm)**	**Peak Counting Time (s)**
15	20	2	10-30
Standard	**Elements Calibrated**		
Ferrosilite (synthetic)	Si, Fe		
Geikelite (synthetic)	Ti, Mg		
Tanzanite	Al		
Rhodonite (Broken Hill)	Mn	3SD uncertainty based on counting statistics for biotite: ±0.49 wt% SiO_2, ±0.09 wt% TiO_2, ±0.28 wt% Al_2O_3, ±0.54 wt% FeO^T, ±0.04 wt% MnO, ±0.20 wt% MgO, ±0.27 wt% K_2O, ±0.08 wt% BaO	
Wollastonite	Ca		
Albite (Tiburon)	Na		
Ba-Cl-Apatite	Ba		
Adularia (St. Gotthard)	K		

Table A-0-2 Natural individual biotite analyses (wt%)

Sample	Point	SiO_2	TiO_2	Al_2O_3	FeO^T	MnO	MgO	CaO	Na_2O	K_2O	BaO	Total	Mg#
GM-01 (OC)	GM-01_BTE_15_7	35.68	4.54	12.94	28.59	0.29	5.31	0.00	0.37	9.10	0.07	96.87	25
	GM-01_BTE_15_8	34.97	4.52	12.48	28.61	0.30	5.35	0.00	0.41	9.06	0.12	95.80	25
	GM-01_BTE_15_9	35.52	4.64	12.80	28.70	0.29	5.35	0.01	0.42	9.24	0.08	97.05	25
	GM-01_BTE_15_10	35.09	4.62	12.63	28.28	0.31	5.26	0.00	0.43	9.16	0.09	95.83	25
	GM-01_BTE_15_11	35.15	4.59	12.49	29.00	0.30	5.27	0.00	0.41	9.23	0.08	96.53	24
	GM-01_BTE_15_12	36.14	4.47	12.81	28.14	0.30	5.12	0.00	0.39	9.10	0.08	96.53	24
	Average	**35.43**	**4.57**	**12.69**	28.55	**0.30**	**5.28**	**0.00**	**0.40**	9.15	**0.09**	**96.44**	25
	Standard Deviation	**0.44**	**0.06**	**0.19**	0.31	**0.01**	**0.09**	**0.00**	**0.02**	0.07	**0.02**	**0.52**	0
GM-07 (OL)	GM-07_BTE_1_2	37.20	3.85	12.37	21.74	0.71	10.23	0.00	0.57	9.26	0.06	95.99	46
	GM-07_BTE_1_3	36.93	3.14	12.45	24.85	0.74	8.91	0.00	0.54	9.13	0.04	96.74	39
	GM-07_BTE_1_5	35.90	3.85	12.30	24.67	0.71	9.01	0.02	0.54	9.08	0.03	96.13	39
	GM-07_BTE_1_7	36.07	3.88	11.99	24.17	0.71	8.70	0.00	0.53	9.12	0.03	95.18	39
	GM-07_BTE_1_9	37.52	3.98	12.56	20.61	0.73	10.72	0.00	0.60	9.39	0.01	96.10	48
	GM-07_BTE_1_10	36.49	3.24	12.48	25.51	0.76	9.05	0.00	0.54	9.15	0.03	97.24	39
	GM-07_BTE_1_11	36.79	3.17	12.32	25.59	0.77	8.91	0.01	0.56	9.00	0.05	97.16	38
	GM-07_BTE_1_12	36.70	3.05	12.29	25.11	0.74	8.60	0.01	0.56	8.95	0.04	96.05	38
	GM-07_BTE_2_1	36.61	3.64	12.25	25.10	0.66	8.54	0.01	0.59	9.03	0.07	96.50	38
	GM-07_BTE_2_2	36.70	3.79	12.38	24.13	0.68	9.27	0.00	0.59	9.22	0.03	96.77	41
	GM-07_BTE_2_5	36.68	3.78	12.25	24.13	0.68	9.40	0.01	0.58	9.18	0.03	96.71	41
	GM-07_BTE_2_6	36.63	3.69	12.31	23.69	0.70	9.39	0.00	0.57	9.19	0.07	96.23	41
	GM-07_BTE_2_7	39.53	3.53	12.64	23.37	0.65	8.24	0.02	0.52	9.00	0.00	97.47	39
	GM-07_BTE_2_8	37.80	3.47	12.64	23.09	0.63	9.34	0.00	0.55	8.89	0.03	96.46	42

GM-07_BTE_4_1	35.77	3.83	12.37	25.14	0.76	9.20	0.00	0.55	9.35	0.06	97.00	39
GM-07_BTE_4_2	36.03	3.78	12.32	24.27	0.72	9.03	0.00	0.55	9.39	0.04	96.13	40
GM-07_BTE_4_3	36.73	3.79	11.97	23.68	0.69	8.91	0.00	0.51	9.20	0.02	95.48	40
GM-07_BTE_4_4	36.20	3.82	12.34	24.17	0.75	9.06	0.00	0.52	9.25	0.03	96.12	40
GM-07_BTE_4_5	36.71	3.84	12.52	24.28	0.70	9.10	0.00	0.53	9.39	0.05	97.11	40
GM-07_BTE_4_6	36.43	3.80	12.39	24.19	0.74	9.04	0.00	0.56	9.33	0.02	96.49	40
GM-07_BTE_4_7	35.87	3.81	12.18	25.89	0.70	7.77	0.00	0.55	9.27	0.00	96.03	35
GM-07_BTE_4_8	36.39	3.82	12.45	24.53	0.73	9.05	0.00	0.53	9.15	0.03	96.68	40
GM-07_BTE_4_9	36.13	3.80	12.45	24.27	0.71	8.95	0.00	0.54	9.40	0.02	96.27	40
GM-07_BTE_4_10	36.31	3.82	12.31	24.28	0.73	9.02	0.00	0.53	9.35	0.01	96.32	40
GM-07_BTE_4_13	36.76	3.78	12.27	23.88	0.70	8.99	0.00	0.51	9.14	0.03	96.04	40
GM-07_BTE_4_14	36.47	3.84	12.12	24.36	0.74	8.95	0.00	0.53	9.27	0.04	96.31	40
GM-07_BTE_5_1	36.46	3.65	12.35	24.71	0.71	9.27	0.00	0.53	9.24	0.02	96.95	40
GM-07_BTE_5_2	36.30	3.57	12.27	24.49	0.73	9.27	0.00	0.54	9.30	0.02	96.50	40
GM-07_BTE_5_3	36.42	3.58	12.28	24.91	0.70	8.94	0.01	0.55	9.22	0.03	96.64	39
GM-07_BTE_5_5	36.05	3.65	12.14	24.47	0.73	9.14	0.00	0.53	9.35	0.00	96.04	40
GM-07_BTE_5_6	36.43	3.55	12.29	24.45	0.72	9.09	0.00	0.53	9.19	0.04	96.28	40
GM-07_BTE_6_1	36.84	3.74	12.62	24.08	0.72	9.07	0.00	0.55	9.11	0.02	96.74	40
GM-07_BTE_6_3	36.65	3.75	12.42	23.96	0.70	8.87	0.00	0.53	9.11	0.02	96.01	40
GM-07_BTE_6_4	36.99	3.74	12.59	23.86	0.71	8.99	0.00	0.54	9.21	0.07	96.68	40
GM-07_BTE_6_5	36.90	3.65	12.69	23.51	0.70	8.88	0.00	0.53	8.92	0.02	95.80	40
GM-07_BTE_7_1	36.95	3.64	12.49	24.27	0.71	9.09	0.00	0.54	9.27	0.03	96.99	40
GM-07_BTE_7_2	36.11	3.82	11.91	24.49	0.74	8.57	0.00	0.50	9.28	0.04	95.44	38

	GM-07_BTE_7_3	36.98	3.83	12.22	24.18	0.73	9.22	0.00	0.53	9.31	0.07	97.06	40
	GM-07_BTE_7_4	36.79	3.69	12.20	24.31	0.72	9.06	0.00	0.53	9.28	0.03	96.59	40
	GM-07_BTE_7_5	36.40	3.61	12.44	24.30	0.71	9.06	0.01	0.53	9.19	0.02	96.28	40
	GM-07_BTE_7_8	36.24	3.65	12.17	24.23	0.70	8.88	0.00	0.52	9.21	0.04	95.64	40
	GM-07_BTE_7_9	35.62	3.74	11.86	24.70	0.72	8.78	0.01	0.52	9.22	0.03	95.20	39
	GM-07_BTE_7_11	36.55	3.87	12.19	24.71	0.71	8.74	0.00	0.54	9.24	0.02	96.56	39
	GM-07_BTE_7_12	36.68	3.77	11.91	24.22	0.72	9.18	0.00	0.55	9.25	0.01	96.29	40
	GM-07_BTE_8_1	36.79	3.70	11.70	23.29	0.71	9.31	0.01	0.56	9.17	0.05	95.28	42
	GM-07_BTE_8_2	36.74	3.65	11.70	23.32	0.71	9.35	0.00	0.58	9.04	0.02	95.10	42
	GM-07_BTE_8_3	36.79	3.66	11.71	23.55	0.68	9.33	0.00	0.56	9.12	0.04	95.44	41
	GM-07_BTE_8_5	35.93	3.79	11.75	24.43	0.69	8.70	0.00	0.57	9.26	0.04	95.14	39
	GM-07_BTE_8_6	36.04	3.79	12.43	24.28	0.72	8.62	0.00	0.53	9.13	0.05	95.57	39
	GM-07_BTE_8_8	36.35	3.76	11.62	24.33	0.71	8.75	0.00	0.56	9.26	0.00	95.34	39
	GM-07_BTE_9_1	36.10	3.93	12.43	24.40	0.53	8.80	0.00	0.50	9.21	0.03	95.91	39
	GM-07_BTE_9_2	36.12	3.91	12.41	24.33	0.54	9.00	0.01	0.53	9.29	0.01	96.14	40
	GM-07_BTE_9_3	35.90	3.91	12.47	24.60	0.55	8.82	0.00	0.48	9.37	0.02	96.12	39
	GM-07_BTE_9_4	36.34	3.93	12.34	24.69	0.54	9.05	0.00	0.51	9.49	0.02	96.91	40
	GM-07_BTE_9_5	35.99	3.88	11.96	25.55	0.55	9.32	0.01	0.55	9.27	0.06	97.14	39
	GM-07_BTE_9_6	36.48	3.89	12.01	24.82	0.50	8.42	0.01	0.54	9.13	0.00	95.81	38
	Average	**36.54**	**3.72**	**12.26**	24.25	**0.69**	**9.02**	**0.00**	**0.54**	9.21	**0.03**	**96.26**	40
	Standard Deviation	**0.59**	**0.19**	**0.26**	0.83	**0.06**	**0.41**	**0.01**	**0.02**	0.12	**0.02**	**0.60**	2
GM-10 (YO)	GM-10_BTE_1_1	36.21	4.29	12.54	24.11	0.34	9.07	0.01	0.51	9.54	0.02	96.63	40
	GM-10_BTE_1_2	36.41	4.28	12.61	24.79	0.35	9.13	0.00	0.57	9.36	0.02	97.51	40

GM-10_BTE_1_3	36.10	4.31	12.62	23.57	0.36	9.58	0.01	0.53	9.41	0.06	96.53	42
GM-10_BTE_1_4	36.01	4.28	12.32	23.04	0.36	9.62	0.01	0.54	9.21	0.05	95.43	43
GM-10_BTE_1_5	35.94	4.30	12.55	23.84	0.36	9.53	0.00	0.54	9.46	0.04	96.56	42
GM-10_BTE_1_6	35.89	4.31	12.59	23.52	0.31	9.59	0.00	0.52	9.37	0.00	96.10	42
GM-10_BTE_1_7	36.32	4.30	12.62	23.42	0.36	9.54	0.00	0.52	9.34	0.04	96.45	42
GM-10_BTE_1_8	36.35	4.30	12.57	23.84	0.30	9.61	0.00	0.56	9.44	0.04	97.00	42
GM-10_BTE_1_9	36.20	4.28	12.51	23.48	0.35	9.40	0.00	0.53	9.35	0.06	96.15	42
GM-10_BTE_1_10	36.02	4.24	12.41	23.45	0.34	9.53	0.00	0.50	9.27	0.05	95.81	42
GM-10_BTE_2_1	36.23	4.27	12.42	23.40	0.32	9.53	0.00	0.50	9.36	0.02	96.03	42
GM-10_BTE_2_2	36.03	4.24	12.59	23.66	0.33	9.69	0.01	0.52	9.49	0.02	96.58	42
GM-10_BTE_2_3	37.26	4.23	12.52	23.35	0.32	9.64	0.00	0.54	9.42	0.03	97.31	42
GM-10_BTE_2_4	36.26	4.18	12.52	24.01	0.35	9.21	0.01	0.56	9.37	0.04	96.50	41
GM-10_BTE_2_5	36.55	4.20	12.53	23.60	0.34	9.73	0.00	0.56	9.36	0.04	96.91	42
GM-10_BTE_2_8	35.90	4.11	12.34	23.54	0.33	9.18	0.00	0.54	9.23	0.02	95.20	41
GM-10_BTE_3_1	35.50	4.31	12.30	23.71	0.36	9.74	0.00	0.54	9.49	0.01	95.97	42
GM-10_BTE_3_2	36.09	4.34	12.51	23.50	0.33	9.63	0.00	0.54	9.30	0.07	96.31	42
GM-10_BTE_3_3	36.02	4.31	12.46	23.46	0.34	9.73	0.01	0.56	9.29	0.00	96.19	43
GM-10_BTE_3_4	36.16	4.20	12.66	23.80	0.31	9.54	0.00	0.54	9.31	0.01	96.52	42
GM-10_BTE_3_5	36.01	4.32	12.39	23.61	0.35	9.11	0.01	0.50	9.54	0.05	95.88	41
GM-10_BTE_4_1	35.54	4.35	12.15	23.83	0.35	8.96	0.00	0.49	9.49	0.01	95.16	40
GM-10_BTE_4_2	35.81	4.35	12.23	23.85	0.32	8.95	0.00	0.49	9.47	0.01	95.47	40
GM-10_BTE_4_3	36.60	4.29	12.59	23.41	0.32	9.48	0.00	0.51	9.55	0.03	96.77	42
GM-10_BTE_4_4	36.91	4.27	12.92	23.51	0.33	9.69	0.00	0.54	9.38	0.02	97.57	42

GM-10_BTE_4_6	36.61	4.30	12.58	23.23	0.32	9.72	0.01	0.55	9.40	0.03	96.75	43
GM-10_BTE_5_1	37.45	4.27	12.84	23.52	0.33	9.25	0.00	0.52	9.33	0.04	97.55	41
GM-10_BTE_5_3	36.23	4.25	12.58	23.70	0.31	9.54	0.00	0.51	9.24	0.01	96.36	42
GM-10_BTE_5_4	36.25	4.22	12.65	24.02	0.32	9.30	0.00	0.51	9.34	0.03	96.65	41
GM-10_BTE_5_5	36.51	4.22	12.41	24.51	0.33	8.79	0.02	0.51	9.37	0.01	96.69	39
GM-10_BTE_5_6	36.09	4.25	12.42	23.18	0.32	9.82	0.00	0.56	9.33	0.02	95.98	43
GM-10_BTE_5_7	36.45	4.26	12.42	23.35	0.31	9.62	0.00	0.53	9.41	0.03	96.39	42
GM-10_BTE_5_8	36.12	4.30	12.42	23.71	0.34	9.77	0.00	0.51	9.38	0.02	96.56	42
GM-10_BTE_6_1	36.56	4.23	12.47	22.87	0.34	9.56	0.00	0.53	9.29	0.01	95.84	43
GM-10_BTE_6_2	36.19	4.22	12.35	23.18	0.36	9.54	0.01	0.53	9.24	0.04	95.68	42
GM-10_BTE_6_3	36.32	4.34	12.37	23.49	0.34	9.59	0.01	0.55	9.44	0.03	96.49	42
GM-10_BTE_6_4	35.83	4.26	12.27	23.77	0.35	9.64	0.00	0.55	9.32	0.05	96.02	42
GM-10_BTE_6_5	38.07	4.55	12.89	20.40	0.32	9.95	0.02	0.58	9.43	0.06	96.27	47
GM-10_BTE_6_6	38.28	4.47	13.14	20.56	0.33	10.55	0.01	0.61	9.37	0.04	97.35	48
GM-10_BTE_6_7	36.19	4.25	12.36	23.01	0.32	9.59	0.00	0.55	9.16	0.03	95.47	43
GM-10_BTE_7_2	35.41	4.30	12.29	24.09	0.35	9.90	0.00	0.59	9.31	0.00	96.24	42
GM-10_BTE_7_4	35.86	4.33	12.36	23.58	0.34	9.54	0.00	0.52	9.50	0.03	96.04	42
GM-10_BTE_7_6	36.63	4.24	12.72	23.56	0.32	9.66	0.00	0.54	9.60	0.05	97.32	42
GM-10_BTE_8_1	37.30	4.28	12.92	23.16	0.33	9.72	0.00	0.55	9.30	0.01	97.57	43
GM-10_BTE_8_2	36.78	4.16	13.10	23.64	0.31	9.58	0.00	0.52	9.25	0.04	97.38	42
GM-10_BTE_8_3	36.71	4.30	12.65	23.30	0.35	9.72	0.00	0.56	9.32	0.07	96.98	43
GM-10_BTE_8_4	36.76	4.22	12.81	23.29	0.34	9.77	0.00	0.56	9.30	0.03	97.07	43
GM-10_BTE_8_5	37.06	4.27	12.91	23.29	0.35	9.74	0.00	0.55	9.22	0.05	97.43	43

	GM-10_BTE_9_3	37.44	4.14	12.99	22.96	0.31	9.65	0.02	0.55	9.29	0.02	97.38	43
	GM-10_BTE_9_4	37.06	4.21	12.85	23.19	0.33	9.66	0.00	0.53	9.38	0.00	97.19	43
	GM-10_BTE_10_1	35.36	4.23	12.19	23.37	0.34	9.73	0.00	0.52	9.31	0.03	95.10	43
	GM-10_BTE_10_2	36.12	4.21	12.50	23.17	0.33	9.68	0.00	0.56	9.17	0.01	95.75	43
	GM-10_BTE_10_3	36.00	4.22	12.38	23.50	0.33	9.66	0.00	0.53	9.26	0.03	95.90	42
	GM-10_BTE_10_5	35.82	4.20	12.25	23.22	0.36	9.60	0.00	0.53	9.17	0.03	95.17	42
	GM-10_BTE_10_6	35.65	4.20	12.44	23.29	0.31	9.62	0.00	0.54	9.18	0.00	95.21	42
	GM-10_BTE_10_7	35.71	4.17	12.23	23.38	0.32	9.69	0.00	0.50	9.31	0.04	95.37	42
	GM-10_BTE_10_8	35.61	4.22	12.23	23.51	0.34	9.69	0.00	0.54	9.26	0.00	95.40	42
	Average	**36.33**	**4.27**	**12.53**	23.43	**0.33**	**9.57**	**0.00**	**0.54**	9.35	**0.03**	**96.37**	42
	Standard Deviation	**0.60**	**0.07**	**0.23**	0.67	**0.02**	**0.27**	**0.01**	**0.02**	0.10	**0.02**	**0.72**	1
GM-18 (OB)	GM-18_BTE_2_2	34.34	3.54	11.86	28.82	0.60	8.45	0.01	0.52	8.82	0.01	96.96	34
	GM-18_BTE_2_3	36.27	3.68	12.37	25.12	0.55	8.58	0.00	0.53	9.21	0.05	96.35	38
	GM-18_BTE_2_5	36.10	3.85	12.26	25.23	0.56	8.65	0.00	0.55	9.17	0.03	96.37	38
	GM-18_BTE_3_1	36.20	3.86	12.77	25.88	0.52	7.40	0.00	0.53	9.06	0.05	96.25	34
	GM-18_BTE_4_2	35.71	4.04	12.10	25.06	0.57	8.41	0.00	0.51	9.35	0.08	95.81	37
	GM-18_BTE_4_3	35.93	4.03	12.34	25.16	0.56	8.48	0.02	0.51	9.31	0.04	96.37	38
	GM-18_BTE_4_4	36.32	3.74	12.14	25.25	0.56	8.67	0.00	0.50	9.21	0.02	96.40	38
	GM-18_BTE_4_5	36.54	3.87	12.16	24.85	0.54	8.67	0.01	0.52	9.23	0.05	96.45	38
	GM-18_BTE_4_6	36.18	3.78	11.99	25.05	0.56	8.56	0.00	0.51	9.28	0.07	95.97	38
	GM-18_BTE_4_7	36.79	3.83	12.41	25.12	0.56	8.63	0.00	0.51	9.17	0.04	97.07	38
	GM-18_BTE_4_8	36.62	3.73	12.38	24.79	0.54	8.62	0.01	0.52	9.38	0.05	96.64	38
	GM-18_BTE_4_9	35.67	3.88	12.40	25.27	0.55	8.27	0.01	0.52	9.21	0.03	95.81	37

GM-18_BTE_5_2	34.99	3.84	11.88	26.55	0.54	7.84	0.00	0.57	9.30	0.03	95.55	34
GM-18_BTE_5_3	34.90	3.80	11.96	26.23	0.55	8.06	0.00	0.55	9.14	0.01	95.17	35
GM-18_BTE_5_4	35.28	3.79	11.88	26.24	0.56	8.12	0.00	0.53	9.23	0.01	95.64	36
GM-18_BTE_5_6	35.42	3.80	11.94	25.67	0.57	8.11	0.01	0.54	9.29	0.01	95.36	36
GM-18_BTE_7_7	35.93	4.02	12.29	25.17	0.54	8.23	0.01	0.49	9.36	0.04	96.08	37
GM-18_BTE_8_1	35.39	4.06	12.36	25.15	0.58	8.32	0.00	0.53	9.26	0.01	95.64	37
GM-18_BTE_8_2	35.15	4.07	12.12	25.39	0.55	8.23	0.00	0.50	9.28	0.02	95.31	37
GM-18_BTE_8_3	35.95	4.01	12.49	25.26	0.55	8.48	0.02	0.54	9.18	0.03	96.50	37
GM-18_BTE_8_4	35.07	4.06	12.30	25.09	0.54	8.34	0.00	0.52	9.40	0.02	95.35	37
GM-18_BTE_8_5	35.99	3.96	12.38	25.13	0.56	8.24	0.00	0.50	9.25	0.01	96.03	37
GM-18_BTE_8_6	35.74	3.55	12.53	24.96	0.53	8.59	0.00	0.54	9.20	0.01	95.65	38
GM-18_BTE_9_1	35.54	3.21	11.71	26.18	0.59	9.00	0.00	0.53	9.36	0.06	96.17	38
GM-18_BTE_9_2	36.21	3.12	12.28	25.85	0.54	8.78	0.01	0.57	9.30	0.00	96.63	38
GM-18_BTE_9_7	35.17	3.78	12.26	27.87	0.62	7.30	0.01	0.50	9.12	0.01	96.63	32
GM-18_BTE_10_2	36.01	3.83	12.41	25.58	0.55	8.37	0.00	0.53	9.38	0.03	96.69	37
GM-18_BTE_10_3	36.38	3.69	12.51	25.43	0.58	8.52	0.02	0.50	9.28	0.04	96.96	37
GM-18_BTE_10_5	35.97	3.82	12.19	26.38	0.55	8.21	0.01	0.52	9.31	0.02	96.98	36
GM-18_BTE_10_6	35.72	3.80	12.21	25.49	0.54	8.25	0.00	0.50	9.35	0.00	95.86	37
GM-18_BTE_10_7	36.13	3.87	12.41	25.66	0.53	8.48	0.00	0.52	9.38	0.08	97.06	37
GM-18_BTE_10_8	36.67	3.63	12.46	25.49	0.56	8.62	0.01	0.51	9.37	0.02	97.33	38
GM-18_BTE_11_0	36.44	3.51	12.33	24.98	0.54	8.79	0.00	0.54	9.26	0.00	96.39	39
GM-18_BTE_11_1	35.59	3.63	12.29	25.46	0.53	8.31	0.00	0.52	9.24	0.05	95.61	37
GM-18_BTE_11_2	35.77	3.67	12.33	25.48	0.53	8.27	0.00	0.54	9.29	0.06	95.94	37

	GM-18_BTE_11_3	36.31	4.06	12.39	25.81	0.54	8.30	0.01	0.51	9.37	0.02	97.33	36
	GM-18_BTE_11_4	35.38	3.71	12.50	25.26	0.56	8.33	0.00	0.52	9.31	0.01	95.58	37
	GM-18_BTE_11_5	36.72	3.55	12.42	24.86	0.55	8.87	0.00	0.51	9.28	0.01	96.78	39
	GM-18_BTE_11_6	36.72	3.53	12.44	24.93	0.54	8.89	0.01	0.55	9.25	0.00	96.87	39
	GM-18_BTE_11_7	36.84	3.50	12.28	24.85	0.54	8.91	0.00	0.50	9.15	0.00	96.57	39
	GM-18_BTE_11_9	36.12	3.57	12.72	24.70	0.54	8.70	0.01	0.54	9.28	0.03	96.18	39
	GM-18_BTE_11_10	35.90	3.88	12.51	25.96	0.56	8.29	0.00	0.53	9.49	0.02	97.15	36
	GM-18_BTE_11_11	36.83	3.46	12.18	25.00	0.57	8.85	0.00	0.55	9.13	0.04	96.60	39
	GM-18_BTE_11_12	36.79	3.53	12.23	24.72	0.55	8.89	0.00	0.54	9.23	0.03	96.52	39
	GM-18_BTE_11_13	36.46	3.51	12.12	25.25	0.55	8.65	0.00	0.50	9.26	0.07	96.35	38
	GM-18_BTE_11_14	36.52	3.50	12.28	24.83	0.55	8.86	0.00	0.52	9.30	0.04	96.39	39
	Average	**35.97**	**3.74**	**12.28**	25.49	**0.55**	**8.44**	**0.00**	**0.52**	9.26	**0.03**	**96.29**	37
	Standard Deviation	**0.59**	**0.22**	**0.22**	0.77	**0.02**	**0.35**	**0.01**	**0.02**	0.11	**0.02**	**0.57**	1
GM-20 (OT)	GM-20_OT_BTE_1-18	35.77	4.03	13.46	22.62	0.39	9.65	0.00	0.55	9.01	0.01	95.47	43
	GM-20_OT_BTE_1-20	36.95	3.90	15.50	21.49	0.37	9.01	0.00	0.54	8.76	0.00	96.49	43
	GM-20_OT_BTE_1-21	36.58	3.92	13.52	23.09	0.37	10.11	0.01	0.65	8.83	0.02	97.10	44
	GM-20_OT_BTE_1-40	36.37	4.56	12.68	24.11	0.42	9.25	0.00	0.53	9.65	0.04	97.59	41
	GM-20_OT_BTE_1-43	36.19	4.47	12.69	24.10	0.43	9.60	0.00	0.55	9.49	0.01	97.51	42
	GM-20_OT_BTE_1-44	36.55	4.39	12.69	23.68	0.41	9.68	0.01	0.58	9.40	0.02	97.41	42
	GM-20_OT_BTE_1-48	36.14	4.39	12.63	24.20	0.39	9.60	0.00	0.55	9.58	0.02	97.46	41
	GM-20_OT_BTE_1-49	36.04	4.37	12.61	23.92	0.41	9.58	0.01	0.52	9.64	0.03	97.10	42
	GM-20_OT_BTE_1-50	36.11	4.36	12.59	24.16	0.40	9.68	0.00	0.54	9.62	0.04	97.49	42
	GM-20_OT_BTE_1-51	35.91	4.33	12.56	24.06	0.44	9.50	0.00	0.53	9.52	0.03	96.87	41

GM-20_OT_BTE_1-53	36.11	4.31	12.61	24.01	0.40	9.77	0.02	0.55	9.65	0.03	97.45	42
GM-20_OT_BTE_1-59	35.95	4.47	12.41	24.33	0.42	9.63	0.00	0.57	9.57	0.00	97.36	41
GM-20_OT_BTE_1-62	35.89	4.54	12.44	23.91	0.42	9.39	0.00	0.51	9.45	0.00	96.54	41
GM-20_OT_BTE_1-64	35.24	4.50	12.28	25.33	0.41	8.81	0.00	0.54	9.49	0.00	96.59	38
GM-20_OT_BTE_1-65	35.59	4.48	12.29	24.72	0.41	9.03	0.00	0.54	9.42	0.03	96.51	39
GM-20_OT_BTE_1-66	35.70	4.41	12.33	24.03	0.43	9.63	0.00	0.53	9.57	0.02	96.62	42
GM-20_OT_BTE_1-70	36.15	4.37	12.66	24.05	0.43	9.47	0.00	0.56	9.55	0.00	97.22	41
GM-20_OT_BTE_1-71	35.95	4.37	12.67	24.28	0.41	9.56	0.00	0.56	9.63	0.00	97.42	41
GM-20_OT_BTE_1-73	36.04	4.37	12.49	24.05	0.39	9.56	0.00	0.51	9.55	0.01	96.98	41
GM-20_OT_BTE_1-74	36.32	4.19	12.27	23.84	0.40	9.18	0.00	0.49	9.12	0.03	95.81	41
GM-20_OT_BTE_1-77	35.91	4.42	12.45	24.40	0.38	9.46	0.01	0.54	9.66	0.02	97.25	41
GM-20_OT_BTE_1-79	35.75	4.46	12.41	24.62	0.40	9.23	0.00	0.55	9.62	0.01	97.02	40
GM-20_OT_BTE_4-1	35.62	4.41	12.16	25.20	0.43	8.81	0.00	0.55	9.48	0.03	96.67	38
GM-20_OT_BTE_4-2	36.18	4.42	12.48	23.72	0.39	9.36	0.00	0.51	9.46	0.05	96.57	41
GM-20_OT_BTE_4-3	35.61	4.44	12.22	24.15	0.40	9.25	0.00	0.52	9.45	0.03	96.09	41
GM-20_OT_BTE_4-4	35.62	4.36	12.28	24.20	0.38	9.11	0.00	0.53	9.36	0.04	95.87	40
GM-20_OT_BTE_4-5	36.27	4.41	12.70	23.83	0.38	9.18	0.00	0.52	9.69	0.03	97.00	41
GM-20_OT_BTE_4-9	35.69	4.45	12.41	24.05	0.41	9.34	0.01	0.49	9.66	0.01	96.53	41
GM-20_OT_BTE_4-10	36.10	4.45	12.64	23.89	0.42	9.57	0.00	0.56	9.55	0.03	97.19	42
GM-20_OT_BTE_4-11	36.20	4.48	12.63	23.57	0.40	9.60	0.00	0.54	9.54	0.05	97.01	42
GM-20_OT_BTE_4-12	35.65	4.45	12.39	23.63	0.43	9.57	0.00	0.54	9.43	0.01	96.11	42
GM-20_OT_BTE_4-13	36.22	4.39	12.59	23.81	0.40	9.49	0.01	0.56	9.59	0.05	97.11	42
GM-20_OT_BTE_4-17	36.42	4.49	12.61	23.67	0.42	9.69	0.01	0.57	9.48	0.05	97.40	42

GM-20_OT_BTE_4-18	36.15	4.44	12.70	23.61	0.40	9.61	0.00	0.52	9.53	0.04	97.00	42
GM-20_OT_BTE_4-19	36.15	4.41	12.63	23.55	0.41	9.52	0.02	0.54	9.53	0.04	96.79	42
GM-20_OT_BTE_4-20	35.87	4.41	12.55	23.88	0.41	9.57	0.00	0.57	9.57	0.03	96.86	42
GM-20_OT_BTE_4-21	36.05	4.44	12.66	23.86	0.41	9.52	0.00	0.51	9.63	0.00	97.05	42
GM-20_OT_BTE_4-22	36.20	4.43	12.63	23.79	0.39	9.48	0.00	0.53	9.70	0.06	97.22	42
GM-20_OT_BTE_4-23	36.39	4.33	12.75	25.03	0.40	8.59	0.00	0.56	9.45	0.04	97.54	38
GM-20_OT_BTE_4-24	35.46	4.27	12.84	24.35	0.41	8.74	0.00	0.54	9.36	0.02	95.98	39
GM-20_OT_BTE_4-25	36.30	4.40	12.81	23.94	0.39	9.39	0.01	0.54	9.46	0.05	97.27	41
GM-20_OT_BTE_4-26	36.29	4.42	12.70	23.81	0.41	9.57	0.00	0.53	9.56	0.00	97.24	42
GM-20_OT_BTE_4-27	36.13	4.44	12.71	23.93	0.42	9.55	0.01	0.52	9.61	0.03	97.36	42
GM-20_OT_BTE_4-28	36.65	4.58	12.61	23.71	0.41	9.73	0.10	0.80	8.97	0.01	97.55	42
GM-20_OT_BTE_4-29	36.20	4.40	12.55	23.99	0.36	9.58	0.00	0.55	9.56	0.04	97.21	42
GM-20_OT_BTE_4-30	36.40	4.44	12.71	23.61	0.40	9.83	0.00	0.55	9.57	0.01	97.50	43
GM-20_OT_BTE_4-34	36.54	4.42	12.69	23.89	0.41	9.38	0.00	0.52	9.52	0.03	97.39	41
GM-20_OT_BTE_4-36	36.21	4.42	12.80	23.63	0.38	9.77	0.00	0.53	9.46	0.06	97.25	42
GM-20_OT_BTE_4-39	36.21	4.43	12.74	23.64	0.42	9.56	0.00	0.53	9.65	0.04	97.19	42
GM-20_OT_BTE_4-40	36.25	4.37	12.69	23.97	0.42	9.68	0.02	0.55	9.59	0.03	97.57	42
GM-20_OT_BTE_4-41	36.36	4.41	12.86	23.80	0.41	9.53	0.00	0.54	9.49	0.00	97.40	42
GM-20_OT_BTE_4-42	35.83	4.33	12.57	24.65	0.41	8.64	0.00	0.52	9.49	0.00	96.42	38
GM-20_OT_BTE_4-43	36.01	4.37	12.72	24.07	0.39	8.99	0.00	0.55	9.51	0.01	96.62	40
GM-20_OT_BTE_4-44	36.08	4.58	12.74	21.44	0.40	10.37	0.00	0.57	9.55	0.00	95.70	46
GM-20_OT_BTE_4-46	36.04	4.37	12.75	24.46	0.41	9.09	0.00	0.54	9.60	0.00	97.25	40
GM-20_OT_BTE_4-48	36.37	4.47	12.89	22.74	0.39	10.13	0.03	0.57	9.59	0.00	97.19	44

	GM-20_OT_BTE_4-49	35.86	4.41	12.47	23.70	0.36	9.47	0.02	0.57	9.55	0.03	96.43	42
	GM-20_OT_BTE_4-50	36.14	4.42	12.69	23.27	0.39	9.80	0.00	0.57	9.59	0.02	96.89	43
	GM-20_OT_BTE_4-52	36.32	4.41	12.60	23.72	0.40	9.76	0.01	0.54	9.45	0.00	97.20	42
	GM-20_OT_BTE_4-53	36.15	4.40	12.53	24.12	0.40	9.38	0.00	0.57	9.61	0.04	97.18	41
	GM-20_OT_BTE_4-54	36.13	4.42	12.54	24.51	0.40	9.19	0.01	0.52	9.49	0.05	97.26	40
	GM-20_OT_BTE_4-57	36.15	4.43	12.55	23.82	0.42	9.70	0.00	0.52	9.62	0.02	97.24	42
	GM-20_OT_BTE_4-58	36.41	4.42	12.72	23.58	0.39	9.83	0.01	0.54	9.60	0.02	97.51	43
	GM-20_OT_BTE_4-59	36.23	4.44	12.48	23.83	0.38	9.46	0.00	0.53	9.45	0.03	96.85	41
	GM-20_OT_BTE_4-60	36.60	4.50	13.00	21.84	0.34	10.67	0.00	0.64	9.55	0.00	97.13	47
	GM-20_OT_BTE_4-61	36.46	4.43	12.59	23.76	0.38	9.66	0.00	0.54	9.62	0.04	97.45	42
	GM-20_OT_BTE_4-63	36.96	4.49	13.22	20.08	0.39	12.15	0.02	0.64	9.58	0.04	97.56	52
	GM-20_OT_BTE_4-66	36.30	4.41	12.74	23.42	0.39	9.79	0.01	0.53	9.60	0.04	97.23	43
	GM-20_OT_BTE_4-73	36.01	4.42	12.50	25.32	0.40	8.68	0.02	0.56	9.44	0.02	97.37	38
	GM-20_OT_BTE_4-76	36.24	4.36	12.58	24.54	0.36	9.18	0.01	0.55	9.47	0.07	97.35	40
	GM-20_OT_BTE_4-79	36.55	4.48	12.96	20.50	0.38	11.30	0.01	0.62	9.56	0.04	96.41	50
	GM-20_OT_BTE_4-80	35.77	4.36	12.49	24.59	0.38	8.72	0.00	0.57	9.45	0.02	96.33	39
	Average	**36.13**	**4.40**	**12.67**	23.79	**0.40**	**9.53**	**0.01**	**0.55**	9.50	**0.02**	**96.98**	42
	Standard Deviation	**0.32**	**0.11**	**0.41**	0.91	**0.02**	**0.53**	**0.01**	**0.04**	0.18	**0.02**	**0.50**	2
CD-18-09	CD-18-09_BTE_1-3	35.38	3.19	15.60	22.65	0.56	8.30	0.02	0.06	9.82	0.55	96.12	40
	CD-18-09_BTE_1-10	35.84	2.46	16.25	22.11	0.55	8.53	0.01	0.03	9.79	0.57	96.13	41
	CD-18-09_BTE_1-13	35.06	2.67	15.67	22.00	0.56	9.02	0.04	0.03	9.81	0.61	95.46	42
	CD-18-09_BTE_2-1	35.63	2.56	15.92	22.09	0.66	8.27	0.00	0.03	10.15	0.63	95.94	40
	CD-18-09_BTE_2-2	35.39	3.05	15.89	22.65	0.62	7.82	0.00	0.03	10.23	0.77	96.44	38

CD-18-09_BTE_2-3	35.89	2.37	16.16	21.95	0.60	8.41	0.00	0.07	10.19	0.63	96.24	41
CD-18-09_BTE_2-5	36.05	2.14	16.14	21.87	0.62	8.68	0.07	0.02	9.91	0.83	96.33	41
CD-18-09_BTE_2-6	35.58	2.91	16.19	22.39	0.64	7.86	0.00	0.05	10.28	0.75	96.65	38
CD-18-09_BTE_2-7	35.65	2.56	15.96	22.18	0.63	8.33	0.00	0.02	10.30	0.79	96.44	40
CD-18-09_BTE_2-9	35.68	2.42	15.68	22.49	0.64	8.54	0.02	0.04	10.37	0.16	96.04	40
CD-18-09_BTE_2-10	35.94	3.55	15.06	22.28	0.65	8.28	0.03	0.03	9.93	0.73	96.49	40
CD-18-09_BTE_2-11	35.92	3.21	15.40	22.84	0.62	8.38	0.04	0.04	9.95	0.82	97.23	40
CD-18-09_BTE_2-12	35.46	3.65	15.26	22.72	0.66	8.11	0.01	0.04	9.99	0.91	96.82	39
CD-18-09_BTE_2-13	36.07	3.22	15.28	21.47	0.60	8.60	0.04	0.03	9.78	0.71	95.79	42
CD-18-09_BTE_2-14	35.53	3.67	14.97	22.43	0.68	8.27	0.02	0.04	9.92	0.75	96.28	40
CD-18-09_BTE_2-15	35.94	2.89	15.75	21.66	0.63	8.71	0.01	0.01	9.91	0.29	95.80	42
CD-18-09_BTE_2-16	39.62	2.42	15.71	19.44	0.53	7.76	0.04	0.03	9.25	0.30	95.10	42
CD-18-09_BTE_2-17	35.93	2.81	15.63	21.53	0.62	8.81	0.01	0.03	10.18	0.52	96.07	42
CD-18-09_BTE_2-18	36.32	2.90	16.81	20.41	0.53	8.62	0.02	0.03	10.10	0.74	96.47	43
CD-18-09_BTE_2-19	35.81	3.93	14.77	22.63	0.69	8.47	0.00	0.05	10.10	0.44	96.88	40
CD-18-09_BTE_2-20	38.02	2.75	16.22	20.65	0.57	7.53	0.00	0.04	9.37	0.36	95.50	39
CD-18-09_BTE_2-21	35.96	3.15	15.56	22.78	0.55	7.77	0.04	0.03	9.37	0.26	95.47	38
CD-18-09_BTE_2-22	35.99	3.45	15.06	22.89	0.66	8.49	0.02	0.03	9.74	0.40	96.73	40
CD-18-09_BTE_2-23	32.92	2.51	17.03	25.92	0.74	7.52	0.01	0.02	8.95	0.05	95.67	34
CD-18-09_BTE_2-24	35.37	3.08	15.62	22.65	0.62	8.44	0.01	0.02	9.92	0.84	96.57	40
CD-18-09_BTE_2-25	35.75	3.03	15.73	22.52	0.64	8.17	0.01	0.02	10.13	0.81	96.81	39
CD-18-09_BTE_2-26	35.87	2.71	15.81	22.33	0.63	8.63	0.03	0.03	10.11	0.77	96.93	41
CD-18-09_BTE_2-27	35.61	2.77	15.58	22.49	0.62	8.81	0.00	0.06	9.99	0.73	96.66	41

CD-18-09_BTE_2-28	35.52	3.24	15.43	23.03	0.65	8.26	0.02	0.04	9.89	0.83	96.91	39
CD-18-09_BTE_2-29	36.23	1.99	16.25	21.62	0.56	8.87	0.04	0.04	9.63	0.64	95.87	42
CD-18-09_BTE_2-30	35.57	3.36	15.16	22.85	0.63	8.08	0.01	0.02	10.15	0.70	96.53	39
CD-18-09_BTE_2-31	35.74	2.98	15.86	22.58	0.63	8.09	0.03	0.04	9.79	0.77	96.50	39
CD-18-09_BTE_2-32	35.58	2.76	15.92	22.19	0.59	8.46	0.01	0.04	10.17	0.74	96.45	40
CD-18-09_BTE_2-33	35.82	2.74	15.92	22.12	0.58	8.08	0.04	0.02	9.55	0.75	95.62	39
CD-18-09_BTE_2-35	35.99	3.18	15.69	22.48	0.61	8.03	0.02	0.04	9.82	0.84	96.70	39
CD-18-09_BTE_2-36	35.85	3.10	16.12	22.71	0.61	7.62	0.02	0.03	9.89	0.57	96.53	37
CD-18-09_BTE_2-37	36.13	3.16	15.56	22.47	0.61	8.25	0.04	0.03	10.04	0.49	96.79	40
CD-18-09_BTE_2-38	35.93	2.80	15.83	22.90	0.63	8.08	0.02	0.03	9.68	0.62	96.53	39
CD-18-09_BTE_2-39	35.39	3.17	15.60	22.63	0.62	7.82	0.04	0.02	9.61	0.76	95.67	38
CD-18-09_BTE_3-1	35.04	2.60	16.21	26.59	0.52	4.92	0.00	0.02	10.02	0.64	96.55	25
CD-18-09_BTE_3-3	35.33	2.48	16.27	26.33	0.56	5.14	0.02	0.03	10.03	0.66	96.85	26
CD-18-09_BTE_3-4	35.55	2.03	16.91	26.34	0.54	5.01	0.03	0.04	10.07	0.46	96.97	25
CD-18-09_BTE_3-5	34.89	2.39	16.34	26.02	0.52	5.21	0.04	0.03	10.04	0.66	96.14	26
CD-18-09_BTE_3-6	34.75	2.68	16.20	26.67	0.54	4.88	0.00	0.03	10.15	0.62	96.51	25
CD-18-09_BTE_3-7	34.73	2.30	16.61	26.28	0.49	4.89	0.03	0.02	9.92	0.57	95.85	25
CD-18-09_BTE_3-8	34.65	2.58	16.15	26.65	0.55	4.88	0.01	0.02	9.94	0.59	96.03	25
CD-18-09_BTE_3-9	33.87	3.82	15.73	26.68	0.79	4.76	0.05	0.04	9.57	0.56	95.86	24
CD-18-09_BTE_3-10	34.64	2.82	16.03	26.34	0.58	4.91	0.04	0.04	9.91	0.57	95.87	25
CD-18-09_BTE_3-13	34.99	2.87	15.43	26.90	0.59	4.79	0.00	0.05	9.82	0.45	95.90	24
CD-18-09_BTE_3-14	35.25	2.59	16.10	26.31	0.53	5.01	0.01	0.03	9.73	0.40	95.97	25
CD-18-09_BTE_3-15	35.07	2.66	15.83	26.27	0.54	5.06	0.02	0.03	9.89	0.38	95.75	26

CD-18-09_BTE_3-18	35.31	2.29	16.92	25.42	0.49	4.81	0.04	0.06	9.75	0.59	95.67	25
CD-18-09_BTE_3-20	35.26	2.50	16.29	25.86	0.54	4.95	0.01	0.03	9.99	0.41	95.85	25
CD-18-09_BTE_3-21	35.31	2.58	16.25	26.92	0.55	4.89	0.02	0.01	9.79	0.70	97.02	24
CD-18-09_BTE_3-22	35.29	2.59	16.36	26.68	0.55	4.86	0.00	0.04	9.88	0.73	96.98	25
CD-18-09_BTE_3-23	34.74	2.54	16.16	26.58	0.52	5.16	0.03	0.04	9.78	0.59	96.14	26
CD-18-09_BTE_4-1	35.35	3.73	15.14	22.75	0.57	7.94	0.02	0.05	10.00	0.81	96.35	38
CD-18-09_BTE_4-2	35.83	3.63	15.42	22.45	0.55	8.09	0.02	0.05	10.08	0.83	96.95	39
CD-18-09_BTE_4-3	35.94	3.36	15.45	22.17	0.50	8.20	0.00	0.04	10.02	0.81	96.49	40
CD-18-09_BTE_4-4	36.11	2.83	15.88	22.16	0.52	8.64	0.02	0.03	10.20	0.83	97.21	41
CD-18-09_BTE_4-5	35.69	2.90	15.67	22.18	0.54	8.57	0.01	0.03	10.07	0.72	96.38	41
CD-18-09_BTE_4-6	35.69	3.02	15.72	21.71	0.55	8.33	0.06	0.05	10.15	0.79	96.07	41
CD-18-09_BTE_4-7	35.31	3.30	15.56	22.37	0.55	8.09	0.02	0.04	9.91	0.76	95.90	39
CD-18-09_BTE_4-8	35.83	2.89	15.96	22.07	0.54	8.37	0.02	0.05	10.16	0.76	96.64	40
CD-18-09_BTE_4-9	35.64	3.43	15.63	22.41	0.53	8.07	0.00	0.04	10.12	0.76	96.63	39
CD-18-09_BTE_4-10	35.46	3.53	15.51	22.54	0.54	8.08	0.02	0.04	9.95	0.80	96.46	39
CD-18-09_BTE_4-11	35.20	4.24	15.08	22.66	0.56	7.93	0.00	0.05	10.00	0.78	96.49	38
CD-18-09_BTE_4-12	34.78	4.86	15.04	22.33	0.56	7.90	0.01	0.06	9.87	0.85	96.25	39
CD-18-09_BTE_4-13	35.71	3.39	15.65	22.28	0.55	8.04	0.01	0.05	10.01	0.78	96.48	39
CD-18-09_BTE_4-14	35.40	3.58	15.10	22.83	0.56	8.05	0.01	0.05	10.04	0.85	96.46	39
CD-18-09_BTE_4-15	35.56	3.80	15.02	22.60	0.59	7.96	0.01	0.08	9.96	0.84	96.43	39
CD-18-09_BTE_4-16	35.28	3.46	15.41	22.25	0.56	8.05	0.02	0.06	9.94	0.85	95.87	39
CD-18-09_BTE_4-17	35.66	3.35	14.97	22.26	0.56	8.33	0.01	0.03	9.87	0.93	95.95	40
CD-18-09_BTE_4-18	35.96	3.26	16.17	21.72	0.50	8.28	0.03	0.04	9.86	0.75	96.55	40

CD-18-09_BTE_4-19	35.79	2.88	15.72	22.05	0.53	8.43	0.01	0.04	9.99	0.82	96.25	41
CD-18-09_BTE_4-20	35.44	3.05	15.50	22.07	0.52	8.23	0.07	0.04	9.83	0.68	95.43	40
CD-18-09_BTE_4-21	35.48	3.34	15.24	23.00	0.56	8.05	0.02	0.05	9.83	0.86	96.43	38
CD-18-09_BTE_4-22	35.27	3.35	15.26	22.54	0.55	8.13	0.00	0.04	9.94	0.86	95.94	39
CD-18-09_BTE_4-23	35.24	3.22	15.40	22.37	0.52	8.23	0.03	0.06	10.09	0.79	95.95	40
CD-18-09_BTE_4-24	35.37	3.48	15.31	22.70	0.57	7.91	0.00	0.05	9.97	0.82	96.19	38
CD-18-09_BTE_4-25	35.41	3.10	15.61	22.49	0.53	8.37	0.01	0.06	10.11	0.71	96.40	40
CD-18-09_BTE_5-1	35.94	3.42	15.35	23.22	0.63	8.33	0.01	0.06	9.67	0.66	97.30	39
CD-18-09_BTE_5-2	35.92	3.52	15.26	23.19	0.63	8.18	0.00	0.06	9.76	0.66	97.18	39
CD-18-09_BTE_5-5	36.09	3.28	16.01	22.67	0.62	8.19	0.00	0.02	9.84	0.69	97.39	39
CD-18-09_BTE_5-6	35.03	3.81	15.01	23.08	0.63	7.62	0.01	0.06	9.93	0.62	95.79	37
CD-18-09_BTE_5-7	35.37	3.71	15.08	23.49	0.64	7.67	0.03	0.06	9.88	0.69	96.63	37
CD-18-09_BTE_5-8	35.36	3.05	15.48	22.83	0.61	8.10	0.03	0.06	9.83	0.65	96.01	39
CD-18-09_BTE_5-9	35.35	3.34	15.17	23.38	0.62	8.14	0.01	0.07	9.96	0.65	96.70	38
CD-18-09_BTE_5-11	35.76	3.00	15.00	22.70	0.57	8.32	0.05	0.07	9.87	0.40	95.74	40
CD-18-09_BTE_5-12	35.53	3.55	14.77	23.37	0.63	8.06	0.02	0.05	9.97	0.57	96.52	38
CD-18-09_BTE_5-13	35.61	3.72	14.65	23.21	0.66	7.96	0.02	0.07	9.99	0.56	96.43	38
CD-18-09_BTE_5-14	35.74	3.47	15.10	23.02	0.60	8.07	0.01	0.05	10.05	0.57	96.66	38
CD-18-09_BTE_5-15	35.55	3.53	15.24	23.12	0.65	7.85	0.00	0.05	10.07	0.65	96.70	38
CD-18-09_BTE_6-1	35.18	3.54	14.78	21.61	0.54	9.05	0.02	0.07	10.08	0.83	95.70	43
CD-18-09_BTE_6-2	35.98	3.47	15.06	21.32	0.54	9.20	0.01	0.07	10.08	0.23	95.96	43
CD-18-09_BTE_6-3	35.76	3.31	14.99	21.15	0.55	9.30	0.06	0.06	10.09	0.10	95.38	44
CD-18-09_BTE_6-5	35.48	3.37	15.22	21.39	0.57	9.17	0.00	0.07	10.24	0.91	96.41	43

CD-18-09_BTE_6-6	35.29	2.87	15.34	21.09	0.54	9.52	0.03	0.04	9.82	0.87	95.41	45
CD-18-09_BTE_6-7	35.68	3.17	15.40	21.12	0.54	9.38	0.02	0.05	10.16	0.78	96.30	44
CD-18-09_BTE_6-8	35.49	3.38	15.38	21.12	0.55	9.35	0.02	0.05	9.99	0.83	96.15	44
CD-18-09_BTE_6-9	35.58	3.21	15.13	21.20	0.57	9.39	0.05	0.04	9.92	0.86	95.95	44
CD-18-09_BTE_6-10	35.60	3.21	15.11	21.44	0.54	9.58	0.00	0.05	9.99	0.89	96.41	44
CD-18-09_BTE_6-11	36.13	3.55	15.29	21.49	0.54	9.35	0.00	0.06	10.04	0.85	97.29	44
CD-18-09_BTE_6-12	35.82	2.73	15.27	21.23	0.53	9.80	0.03	0.04	10.06	0.67	96.18	45
CD-18-09_BTE_6-13	35.61	3.35	14.99	21.49	0.57	9.34	0.03	0.06	9.90	0.82	96.15	44
CD-18-09_BTE_6-14	35.55	3.69	14.74	21.40	0.54	9.30	0.02	0.06	9.80	0.85	95.94	44
CD-18-09_BTE_6-15	35.31	3.69	14.74	21.39	0.56	9.20	0.03	0.04	9.97	0.84	95.75	43
CD-18-09_BTE_6-16	35.35	3.83	14.65	21.32	0.55	9.27	0.01	0.07	10.00	0.90	95.96	44
CD-18-09_BTE_6-17	35.77	3.33	14.93	21.14	0.56	9.49	0.02	0.04	10.01	0.86	96.14	44
CD-18-09_BTE_6-18	35.46	3.83	14.70	21.50	0.56	9.25	0.02	0.06	9.82	0.84	96.04	43
CD-18-09_BTE_6-19	35.75	3.80	14.80	21.33	0.55	9.39	0.00	0.08	10.00	0.87	96.54	44
CD-18-09_BTE_6-20	35.58	3.90	14.53	21.22	0.54	9.49	0.01	0.07	9.71	0.90	95.95	44
CD-18-09_BTE_6-21	35.38	3.99	14.69	21.32	0.55	9.25	0.00	0.08	9.83	0.98	96.07	44
CD-18-09_BTE_6-22	35.63	3.87	14.74	21.62	0.55	9.37	0.03	0.09	10.06	0.87	96.82	44
CD-18-09_BTE_6-23	35.65	3.92	14.51	20.88	0.55	9.33	0.01	0.09	9.82	0.89	95.65	44
CD-18-09_BTE_6-24	35.65	3.92	14.59	21.97	0.56	9.24	0.00	0.08	9.91	0.94	96.86	43
CD-18-09_BTE_6-25	35.53	3.85	14.70	21.65	0.57	9.05	0.01	0.07	10.00	0.78	96.20	43
CD-18-09_BTE_6-26	35.93	3.41	15.17	21.62	0.56	9.13	0.01	0.05	9.98	0.83	96.70	43
CD-18-09_BTE_6-27	35.75	3.13	15.27	21.40	0.53	9.34	0.00	0.04	10.22	0.81	96.48	44
CD-18-09_BTE_7-1	35.55	3.93	14.53	21.74	0.57	9.02	0.02	0.08	9.85	0.84	96.13	43

CD-18-09_BTE_7-2	35.86	3.84	14.65	21.75	0.54	9.09	0.01	0.09	9.96	0.89	96.68	43
CD-18-09_BTE_7-3	35.70	3.71	14.88	21.67	0.56	9.08	0.02	0.09	9.73	0.95	96.38	43
CD-18-09_BTE_7-4	35.56	3.00	15.21	21.45	0.57	9.47	0.00	0.07	10.15	0.75	96.22	44
CD-18-09_BTE_7-5	35.62	2.78	15.38	20.95	0.55	9.67	0.02	0.04	10.01	0.69	95.70	45
CD-18-09_BTE_7-6	36.06	3.44	15.09	21.41	0.54	9.36	0.01	0.05	9.85	0.88	96.69	44
CD-18-09_BTE_7-7	35.85	3.68	14.88	21.40	0.56	9.29	0.00	0.06	9.79	0.90	96.40	44
CD-18-09_BTE_7-8	35.66	3.86	14.61	21.46	0.56	9.29	0.01	0.06	10.09	0.76	96.35	44
CD-18-09_BTE_7-9	35.98	3.47	14.63	21.26	0.53	9.59	0.00	0.09	9.98	0.77	96.31	45
CD-18-09_BTE_7-10	35.56	3.62	14.98	21.26	0.55	9.02	0.01	0.04	10.09	0.81	95.94	43
CD-18-09_BTE_7-11	35.37	3.80	14.98	21.38	0.55	8.91	0.02	0.06	9.96	0.76	95.78	43
CD-18-09_BTE_7-12	36.06	3.57	14.73	21.33	0.56	9.56	0.05	0.06	9.97	0.49	96.38	44
CD-18-09_BTE_7-13	35.53	2.94	15.34	21.07	0.53	9.76	0.00	0.07	10.14	0.56	95.95	45
CD-18-09_BTE_7-14	35.82	2.82	15.86	20.94	0.53	9.44	0.00	0.05	9.96	0.81	96.23	45
CD-18-09_BTE_7-15	35.50	3.85	14.71	21.78	0.57	9.01	0.02	0.07	10.03	0.80	96.32	42
CD-18-09_BTE_7-16	35.33	3.79	15.15	21.76	0.59	8.87	0.01	0.06	10.00	0.85	96.41	42
CD-18-09_BTE_7-17	35.72	3.86	14.88	21.71	0.55	9.29	0.00	0.07	10.04	0.87	97.00	43
CD-18-09_BTE_7-18	35.61	3.06	14.87	20.78	0.57	10.05	0.00	0.04	10.29	0.69	95.96	46
CD-18-09_BTE_7-19	35.81	3.59	15.34	21.58	0.54	9.29	0.02	0.06	10.09	0.56	96.88	43
CD-18-09_BTE_7-20	36.12	3.81	14.33	21.08	0.56	9.67	0.02	0.07	10.28	0.25	96.20	45
CD-18-09_BTE_7-21	36.18	3.46	14.80	21.19	0.55	9.81	0.01	0.05	10.28	0.29	96.62	45
CD-18-09_BTE_7-22	36.79	3.49	14.85	20.41	0.53	9.43	0.02	0.03	10.06	0.67	96.28	45
CD-18-09_BTE_7-23	35.78	3.07	15.28	20.97	0.52	9.71	0.01	0.06	10.03	0.68	96.12	45
CD-18-09_BTE_7-24	35.42	3.46	14.86	21.49	0.54	9.41	0.02	0.04	10.15	0.40	95.79	44

CD-18-09_BTE_7-25	36.10	2.55	15.31	21.03	0.54	10.14	0.00	0.04	10.31	0.35	96.37	46
CD-18-09_BTE_7-26	35.89	2.57	15.48	21.02	0.53	10.13	0.02	0.02	10.17	0.32	96.14	46
CD-18-09_BTE_7-27	35.96	3.30	14.77	21.09	0.58	9.94	0.01	0.05	10.04	0.54	96.28	46
CD-18-09_BTE_7-28	35.60	3.63	14.64	21.09	0.56	9.50	0.04	0.05	10.15	0.39	95.64	45
CD-18-09_BTE_7-29	35.47	3.62	14.61	21.32	0.55	9.71	0.01	0.04	10.11	0.57	96.00	45
CD-18-09_BTE_7-30	35.78	3.81	14.92	21.32	0.55	9.00	0.00	0.05	9.99	0.78	96.19	43
CD-18-09_BTE_7-31	35.99	2.88	15.55	20.75	0.55	9.53	0.02	0.04	10.18	0.62	96.11	45
CD-18-09_BTE_7-32	35.65	3.12	14.97	21.11	0.53	9.69	0.02	0.03	10.00	0.79	95.90	45
CD-18-09_BTE_7-33	35.22	3.52	14.63	21.35	0.55	9.34	0.01	0.04	9.88	0.71	95.25	44
CD-18-09_BTE_7-34	34.70	5.21	14.59	20.54	0.53	9.41	0.04	0.05	9.63	0.85	95.55	45
CD-18-09_BTE_7-36	35.36	4.00	14.84	21.46	0.58	8.93	0.01	0.06	9.81	0.90	95.96	43
CD-18-09_BTE_7-37	35.23	3.62	15.11	21.27	0.59	8.93	0.00	0.07	10.05	0.92	95.79	43
CD-18-09_BTE_7-38	35.54	3.85	14.68	21.66	0.58	9.06	0.03	0.08	9.80	0.84	96.11	43
CD-18-09_BTE_7-39	35.69	2.89	15.23	21.21	0.58	9.46	0.07	0.04	10.22	0.18	95.56	44
CD-18-09_BTE_7-40	35.87	3.71	14.55	21.71	0.56	9.07	0.02	0.07	9.89	0.36	95.80	43
CD-18-09_BTE_7-41	34.49	2.15	16.94	22.37	0.57	8.79	0.03	0.07	10.03	0.11	95.55	41
CD-18-09_BTE_7-42	35.71	3.70	14.87	21.58	0.58	9.01	0.01	0.07	10.11	0.27	95.90	43
CD-18-09_BTE_7-43	36.55	3.45	15.53	20.99	0.51	8.65	0.06	0.08	9.46	0.40	95.68	42
CD-18-09_BTE_7-44	35.61	3.63	14.85	21.69	0.59	9.12	0.02	0.09	10.16	0.10	95.86	43
CD-18-09_BTE_7-45	35.62	3.85	14.75	21.87	0.59	9.10	0.03	0.09	9.86	0.82	96.56	43
CD-18-09_BTE_7-46	35.23	3.57	14.96	21.76	0.56	8.97	0.02	0.04	10.31	0.29	95.71	42
CD-18-09_BTE_7-47	35.49	3.80	14.76	21.71	0.58	8.84	0.04	0.05	10.03	0.36	95.67	42
CD-18-09_BTE_7-48	35.45	3.77	14.97	21.96	0.60	8.90	0.03	0.06	10.19	0.39	96.34	42

CD-18-09_BTE_7-49	35.89	3.69	15.09	21.45	0.57	9.17	0.01	0.05	10.19	0.03	96.13	43
CD-18-09_BTE_7-50	35.51	3.60	15.17	21.35	0.55	9.26	0.00	0.05	10.22	0.76	96.44	44
CD-18-09_BTE_7-51	35.34	3.05	15.26	21.23	0.54	9.61	0.00	0.06	10.18	0.86	96.12	45
CD-18-09_BTE_7-52	35.68	3.16	15.34	21.31	0.57	9.39	0.01	0.05	10.02	0.82	96.36	44
CD-18-09_BTE_7-56	35.63	2.45	16.05	20.22	0.52	9.91	0.02	0.05	10.31	0.68	95.82	47
CD-18-09_BTE_7-57	36.02	3.32	15.67	21.40	0.54	9.03	0.02	0.04	10.04	0.85	96.92	43
CD-18-09_BTE_7-58	35.93	3.40	14.93	21.67	0.54	9.26	0.02	0.07	10.16	0.47	96.45	43
CD-18-09_BTE_7-59	35.64	3.66	14.89	21.80	0.59	8.96	0.01	0.07	10.11	0.62	96.35	42
CD-18-09_BTE_7-60	35.48	3.41	15.13	21.51	0.57	9.24	0.02	0.07	10.07	0.62	96.12	43
CD-18-09_BTE_7-61	35.77	3.38	15.22	21.20	0.54	9.14	0.01	0.04	10.37	0.32	95.98	43
CD-18-09_BTE_7-62	35.68	3.17	15.06	21.63	0.56	9.32	0.00	0.05	10.05	0.57	96.10	43
CD-18-09_BTE_7-63	35.59	3.32	15.39	21.85	0.58	8.74	0.02	0.06	10.03	0.69	96.26	42
CD-18-09_BTE_7-64	35.99	2.94	15.63	21.40	0.57	9.13	0.01	0.03	10.21	0.36	96.26	43
CD-18-09_BTE_7-65	35.66	2.72	15.35	21.65	0.55	9.36	0.04	0.05	10.06	0.61	96.05	44
CD-18-09_BTE_7-66	35.81	2.80	15.46	21.25	0.55	9.46	0.01	0.04	10.10	0.15	95.63	44
CD-18-09_BTE_7-67	35.66	3.62	15.22	21.22	0.57	9.06	0.01	0.03	10.29	0.08	95.76	43
CD-18-09_BTE_7-68	35.88	2.42	15.32	21.06	0.54	10.22	0.01	0.03	10.32	0.08	95.89	46
CD-18-09_BTE_7-69	35.68	3.69	14.89	21.75	0.58	8.82	0.01	0.05	10.15	0.10	95.72	42
CD-18-09_BTE_7-70	35.41	3.21	15.14	21.41	0.54	9.45	0.03	0.05	10.03	1.02	96.30	44
CD-18-09_BTE_7-71	35.51	3.33	15.14	22.09	0.57	9.09	0.00	0.06	10.37	0.08	96.24	42
CD-18-09_BTE_7-72	35.66	3.21	15.50	21.38	0.55	8.91	0.04	0.03	10.34	0.09	95.70	43
CD-18-09_BTE_7-73	35.83	2.38	15.36	21.51	0.55	9.68	0.00	0.04	10.26	0.21	95.81	45
CD-18-09_BTE_7-74	35.71	3.38	15.05	21.91	0.57	8.98	0.01	0.03	10.03	0.29	95.98	42

	Average	**35.62**	**3.25**	**15.36**	22.26	**0.57**	**8.47**	**0.02**	**0.05**	9.99	**0.64**	**96.22**	40
	Standard Deviation	**0.54**	**0.51**	**0.55**	1.50	**0.04**	**1.27**	**0.02**	**0.02**	0.20	**0.23**	**0.44**	5
CD-18-12	CD-18-12_BTE_1-1	35.91	3.69	14.76	22.93	0.48	7.52	0.03	0.06	10.08	0.19	95.66	37
	CD-18-12_BTE_1-4	35.99	3.54	15.01	22.87	0.46	7.70	0.00	0.05	10.19	0.28	96.09	37
	CD-18-12_BTE_1-5	35.85	3.48	14.98	23.33	0.47	7.69	0.02	0.06	9.93	0.25	96.06	37
	CD-18-12_BTE_1-6	35.85	3.10	15.18	22.62	0.45	7.87	0.03	0.06	10.20	0.10	95.45	38
	CD-18-12_BTE_2-1	34.87	3.42	16.07	23.86	0.45	6.52	0.00	0.07	9.95	1.32	96.53	33
	CD-18-12_BTE_2-2	34.90	3.79	15.79	23.31	0.41	6.72	0.01	0.03	9.89	1.09	95.94	34
	CD-18-12_BTE_2-3	35.35	2.60	16.02	23.13	0.37	7.26	0.04	0.02	9.59	0.95	95.34	36
	CD-18-12_BTE_2-4	35.14	3.32	16.05	23.38	0.43	6.96	0.01	0.04	10.06	1.07	96.45	35
	CD-18-12_BTE_2-5	35.31	3.85	16.15	23.58	0.44	6.78	0.02	0.06	10.01	0.97	97.16	34
	CD-18-12_BTE_2-6	35.93	3.03	15.77	23.27	0.42	7.30	0.00	0.06	10.37	0.27	96.41	36
	CD-18-12_BTE_2-7	35.33	2.63	16.52	23.45	0.43	7.13	0.00	0.02	10.12	1.05	96.67	35
	CD-18-12_BTE_2-8	36.55	2.46	15.57	22.12	0.37	7.85	0.04	0.04	10.15	0.41	95.56	39
	CD-18-12_BTE_2-9	36.07	2.49	16.11	23.18	0.38	7.59	0.00	0.03	10.43	0.26	96.55	37
	CD-18-12_BTE_2-10	36.41	2.61	15.79	22.66	0.37	7.71	0.02	0.03	10.12	0.47	96.20	38
	CD-18-12_BTE_2-11	34.93	2.89	16.55	24.20	0.42	6.66	0.00	0.04	9.80	1.22	96.72	33
	CD-18-12_BTE_2-12	35.80	2.47	16.06	23.52	0.37	7.01	0.05	0.03	9.68	1.00	95.98	35
	CD-18-12_BTE_3-1	39.35	2.04	17.91	20.22	0.38	6.56	0.03	0.04	8.60	0.26	95.38	37
	CD-18-12_BTE_3-3	35.90	3.05	15.53	23.44	0.50	7.41	0.00	0.06	10.26	0.66	96.80	36
	CD-18-12_BTE_3-4	36.71	2.85	15.78	22.61	0.44	7.52	0.03	0.05	9.92	0.50	96.40	37
	CD-18-12_BTE_3-6	36.41	2.63	16.03	22.79	0.48	7.26	0.01	0.03	9.95	0.51	96.07	36
	CD-18-12_BTE_3-7	36.23	2.00	15.67	23.34	0.44	7.87	0.02	0.04	9.64	0.42	95.67	38

CD-18-12_BTE_3-8	36.41	2.54	16.51	22.06	0.42	7.07	0.02	0.02	9.99	0.35	95.39	36
CD-18-12_BTE_3-9	36.19	3.07	15.43	23.20	0.52	7.40	0.01	0.03	10.15	0.54	96.53	36
CD-18-12_BTE_3-10	36.33	2.81	15.46	23.29	0.50	7.68	0.01	0.03	10.31	0.50	96.92	37
CD-18-12_BTE_3-11	36.23	2.86	15.92	22.65	0.49	7.49	0.01	0.05	10.21	0.48	96.39	37
CD-18-12_BTE_3-12	36.46	2.52	15.58	22.52	0.46	7.84	0.01	0.02	10.34	0.47	96.23	38
CD-18-12_BTE_4-2	36.18	3.49	14.44	23.55	0.55	8.05	0.02	0.13	9.88	0.14	96.41	38
CD-18-12_BTE_4-3	36.22	3.12	14.90	23.10	0.52	8.46	0.02	0.10	9.98	0.10	96.51	39
CD-18-12_BTE_4-4	36.30	3.14	14.94	23.09	0.53	8.42	0.01	0.12	10.02	0.11	96.68	39
CD-18-12_BTE_4-5	35.10	3.58	14.40	23.65	0.58	7.69	0.01	0.10	9.89	0.56	95.55	37
CD-18-12_BTE_4-10	36.38	2.43	15.77	22.87	0.52	8.19	0.00	0.05	10.28	0.06	96.53	39
CD-18-12_BTE_4-12	36.38	2.69	15.53	23.27	0.57	8.13	0.01	0.06	10.03	0.15	96.82	38
CD-18-12_BTE_5-1	35.64	2.74	16.06	23.59	0.55	7.22	0.00	0.03	10.04	0.74	96.60	35
CD-18-12_BTE_5-2	35.41	2.74	15.88	23.84	0.55	7.28	0.00	0.04	10.10	0.80	96.66	35
CD-18-12_BTE_5-3	34.43	4.92	15.18	23.75	0.80	7.44	0.02	0.03	9.58	0.61	96.77	36
CD-18-12_BTE_5-4	35.54	2.81	15.69	23.94	0.55	7.37	0.01	0.04	10.09	0.80	96.84	35
CD-18-12_BTE_5-5	36.41	2.75	15.57	23.38	0.52	7.44	0.01	0.03	10.29	0.40	96.79	36
CD-18-12_BTE_5-6	35.77	2.99	15.59	23.67	0.54	7.31	0.01	0.04	10.23	0.44	96.58	36
CD-18-12_BTE_5-7	36.10	2.39	16.01	22.73	0.54	7.74	0.01	0.05	10.44	0.15	96.16	38
CD-18-12_BTE_5-8	36.07	2.82	15.17	23.43	0.54	7.75	0.00	0.05	10.30	0.41	96.53	37
CD-18-12_BTE_5-9	35.99	2.70	15.68	23.41	0.52	7.57	0.00	0.04	10.02	0.79	96.72	37
CD-18-12_BTE_5-10	35.64	2.94	15.09	23.75	0.55	7.68	0.01	0.05	10.05	0.46	96.24	37
CD-18-12_BTE_5-11	35.62	2.55	15.76	23.25	0.56	7.72	0.01	0.03	10.03	0.47	96.00	37
CD-18-12_BTE_5-12	35.71	2.23	15.69	22.89	0.49	7.97	0.00	0.02	10.22	0.49	95.73	38

CD-18-12_BTE_5-13	36.66	1.98	15.90	22.51	0.52	8.39	0.00	0.04	10.24	0.09	96.31	40
CD-18-12_BTE_6-1	36.35	3.24	15.00	22.66	0.55	8.38	0.00	0.07	10.47	0.14	96.87	40
CD-18-12_BTE_6-2	36.16	3.11	14.96	22.69	0.55	8.31	0.02	0.06	10.17	0.46	96.51	40
CD-18-12_BTE_6-3	35.25	3.60	14.96	23.45	0.57	8.04	0.00	0.09	9.95	0.99	96.89	38
CD-18-12_BTE_6-4	35.94	3.07	15.23	22.80	0.55	8.33	0.04	0.06	10.18	0.69	96.87	39
CD-18-12_BTE_6-5	36.36	2.96	15.10	22.46	0.54	8.51	0.02	0.05	10.34	0.37	96.70	40
CD-18-12_BTE_6-6	36.01	2.91	15.02	22.92	0.55	8.33	0.02	0.05	10.13	0.41	96.34	39
CD-18-12_BTE_6-7	36.04	3.57	14.83	23.25	0.59	7.93	0.01	0.08	10.07	0.69	97.05	38
CD-18-12_BTE_6-8	35.63	3.65	14.59	23.35	0.59	7.92	0.00	0.06	10.00	0.80	96.61	38
CD-18-12_BTE_6-9	36.07	3.50	14.83	23.26	0.58	8.16	0.00	0.07	10.11	0.68	97.26	38
CD-18-12_BTE_6-10	35.96	2.51	15.26	22.84	0.58	8.42	0.01	0.03	10.25	0.46	96.31	40
CD-18-12_BTE_6-12	36.27	3.49	14.84	23.04	0.59	8.31	0.02	0.07	10.14	0.52	97.28	39
CD-18-12_BTE_6-13	36.10	3.24	14.93	22.52	0.55	8.45	0.01	0.05	10.14	0.46	96.46	40
CD-18-12_BTE_6-14	35.59	3.63	14.39	23.29	0.60	8.23	0.00	0.07	10.03	0.58	96.41	39
CD-18-12_BTE_6-15	36.45	2.94	15.12	22.56	0.53	8.48	0.00	0.06	10.18	0.17	96.49	40
CD-18-12_BTE_6-16	36.30	2.86	15.25	22.67	0.56	8.47	0.01	0.06	10.16	0.36	96.71	40
CD-18-12_BTE_6-17	36.36	2.92	15.16	23.05	0.56	8.44	0.00	0.06	10.24	0.36	97.12	39
CD-18-12_BTE_6-18	35.78	3.55	14.38	22.82	0.57	8.41	0.00	0.06	10.08	0.61	96.25	40
CD-18-12_BTE_6-19	36.10	3.19	14.86	22.95	0.55	8.43	0.00	0.09	10.29	0.15	96.60	40
CD-18-12_BTE_6-20	35.29	3.86	14.08	23.02	0.60	8.40	0.00	0.08	9.87	1.28	96.47	39
CD-18-12_BTE_6-21	35.84	3.71	13.55	22.81	0.63	9.13	0.00	0.07	9.95	0.62	96.29	42
CD-18-12_BTE_6-22	35.98	3.79	13.72	23.41	0.65	8.77	0.00	0.10	10.11	0.21	96.74	40
CD-18-12_BTE_6-23	35.97	3.08	14.65	22.31	0.60	9.33	0.00	0.03	10.33	0.72	97.02	43

	CD-18-12_BTE_6-24	35.12	3.53	14.50	23.20	0.66	8.58	0.00	0.06	9.91	1.21	96.75	40
	CD-18-12_BTE_6-25	35.96	3.73	14.35	23.31	0.58	8.07	0.00	0.06	10.11	0.38	96.56	38
	CD-18-12_BTE_6-26	35.65	3.19	14.57	23.44	0.58	8.46	0.01	0.06	10.17	0.63	96.76	39
	CD-18-12_BTE_6-27	35.18	3.93	14.20	23.08	0.62	8.27	0.04	0.09	10.03	0.99	96.44	39
	CD-18-12_BTE_6-28	35.86	3.71	14.24	23.40	0.58	8.36	0.01	0.06	10.20	0.45	96.87	39
	Average	**35.94**	**3.07**	**15.31**	23.08	**0.52**	**7.85**	**0.01**	**0.05**	10.07	**0.54**	**96.44**	38
	Standard Deviation	**0.63**	**0.53**	**0.73**	0.55	**0.08**	**0.60**	**0.01**	**0.02**	0.26	**0.32**	**0.46**	2
CD-18-14-2	CD-18-14-2_BTE_6-1	34.99	2.88	15.46	23.37	0.24	7.91	0.00	0.06	10.13	0.33	95.37	38
	CD-18-14-2_BTE_6-2	35.27	2.87	15.66	23.27	0.25	7.94	0.00	0.08	10.23	0.36	95.91	38
	CD-18-14-2_BTE_6-3	35.07	2.88	15.62	23.12	0.27	7.87	0.02	0.07	9.97	0.35	95.24	38
	CD-18-14-2_BTE_6-6	35.31	2.98	15.76	22.93	0.25	8.07	0.02	0.06	10.19	0.31	95.89	39
	CD-18-14-2_BTE_6-8	35.20	2.82	15.62	22.89	0.26	8.14	0.09	0.05	9.69	0.29	95.05	39
	CD-18-14-2_BTE_6-10	35.07	2.87	15.52	23.07	0.26	8.18	0.00	0.07	10.02	0.44	95.50	39
	CD-18-14-2_BTE_6-11	35.52	2.71	15.91	22.42	0.23	8.36	0.03	0.06	9.82	0.31	95.35	40
	CD-18-14-2_BTE_6-12	35.70	2.82	16.06	22.68	0.24	8.31	0.02	0.08	9.97	0.33	96.21	40
	CD-18-14-2_BTE_7-1	36.03	3.52	14.19	23.55	0.60	8.66	0.02	0.05	10.14	0.10	96.85	40
	CD-18-14-2_BTE_7-2	36.00	3.61	14.11	23.76	0.60	8.65	0.00	0.05	10.22	0.13	97.13	39
	CD-18-14-2_BTE_7-3	36.44	2.83	14.69	23.05	0.57	9.02	0.00	0.02	10.25	0.20	97.07	41
	CD-18-14-2_BTE_7-4	36.07	2.95	14.52	23.27	0.58	9.10	0.01	0.02	10.09	0.05	96.66	41
	CD-18-14-	36.02	3.21	14.32	22.86	0.58	8.79	0.00	0.03	10.08	0.15	96.02	41

2_BTE_7-5 CD-18-14-												
2_BTE_7-6 CD-18-14-	35.76	3.22	14.32	23.17	0.57	8.69	0.02	0.04	10.11	0.06	95.95	40
2_BTE_7-7 CD-18-14-	35.98	3.33	14.62	23.23	0.58	8.59	0.03	0.03	10.14	0.08	96.62	40
2_BTE_7-8 CD-18-14-	35.93	2.87	14.46	23.08	0.56	8.94	0.00	0.02	10.19	0.11	96.15	41
2_BTE_7-9 CD-18-14-	36.09	2.53	14.56	23.10	0.56	9.38	0.02	0.02	10.17	0.09	96.53	42
2_BTE_7-10 CD-18-14-	36.25	3.54	14.18	23.79	0.58	8.64	0.00	0.04	10.02	0.06	97.11	39
2_BTE_8-1 CD-18-14-	35.88	3.29	14.10	23.48	0.49	8.62	0.00	0.04	9.95	0.16	96.02	40
2_BTE_8-2 CD-18-14-	35.76	3.30	14.07	23.60	0.52	8.62	0.00	0.04	10.05	0.32	96.28	39
2_BTE_8-3 CD-18-14-	36.23	3.31	13.92	23.22	0.49	8.97	0.00	0.03	10.03	0.45	96.65	41
2_BTE_8-4 CD-18-14-	35.59	3.23	14.71	23.95	0.51	8.17	0.01	0.04	9.93	0.70	96.86	38
2_BTE_8-5 CD-18-14-	36.25	2.92	14.44	23.33	0.51	8.69	0.03	0.03	9.89	0.52	96.61	40
2_BTE_8-6 CD-18-14-	35.87	3.25	14.14	23.46	0.51	8.58	0.01	0.04	10.04	0.20	96.09	39
2_BTE_8-7 CD-18-14-	36.05	3.07	14.23	23.75	0.51	8.53	0.01	0.03	10.07	0.15	96.40	39
2_BTE_8-8 CD-18-14-	35.89	3.30	14.34	23.59	0.48	8.52	0.00	0.04	9.89	0.18	96.23	39
2_BTE_8-9 CD-18-14-	36.01	2.89	14.59	23.38	0.48	8.63	0.00	0.04	10.19	0.11	96.32	40
2_BTE_9-1 CD-18-14-	36.44	3.06	15.25	21.47	0.53	9.11	0.00	0.05	9.42	0.40	95.74	43
2_BTE_9-2 CD-18-14-	36.07	2.98	14.08	22.66	0.54	9.88	0.00	0.03	10.07	0.29	96.58	44
2_BTE_9-3	35.37	3.34	13.87	22.67	0.54	9.40	0.02	0.04	9.87	0.69	95.79	42

CD-18-14-2_BTE_9-4	35.80	3.24	14.21	22.98	0.55	9.33	0.02	0.04	9.92	0.67	96.75	42
CD-18-14-2_BTE_9-5	35.66	2.52	14.20	22.35	0.51	10.04	0.01	0.04	10.14	0.46	95.92	44
CD-18-14-2_BTE_9-6	36.43	2.28	15.02	21.85	0.52	9.90	0.01	0.02	10.16	0.36	96.55	45
CD-18-14-2_BTE_9-7	36.14	2.59	14.88	22.29	0.51	9.39	0.03	0.01	10.04	0.57	96.44	43
CD-18-14-2_BTE_9-8	35.71	2.93	14.53	22.51	0.53	9.15	0.00	0.04	10.18	0.30	95.87	42
CD-18-14-2_BTE_9-9	35.85	2.90	14.63	22.85	0.55	9.10	0.02	0.03	9.92	0.40	96.25	42
CD-18-14-2_BTE_9-10	35.94	3.09	14.22	22.62	0.54	9.31	0.03	0.03	9.90	0.51	96.18	42
CD-18-14-2_BTE_9-11	36.03	3.22	14.33	22.42	0.54	9.38	0.06	0.04	10.08	0.60	96.71	43
CD-18-14-2_BTE_10-1	35.93	3.57	14.11	22.53	0.50	9.51	0.00	0.06	10.07	0.18	96.44	43
CD-18-14-2_BTE_10-2	35.39	3.40	14.01	22.55	0.48	9.54	0.03	0.08	9.82	0.15	95.45	43
CD-18-14-2_BTE_10-3	36.09	3.20	14.50	21.87	0.51	9.70	0.00	0.04	10.15	0.20	96.27	44
CD-18-14-2_BTE_10-4	36.13	3.06	14.49	21.93	0.48	9.54	0.00	0.02	10.22	0.16	96.00	44
CD-18-14-2_BTE_10-5	35.80	3.25	14.18	21.88	0.50	9.51	0.00	0.03	10.09	0.12	95.37	44
CD-18-14-2_BTE_10-6	36.08	2.83	14.60	21.89	0.46	10.10	0.00	0.04	9.95	0.35	96.30	45
CD-18-14-2_BTE_10-7	36.01	2.99	14.45	22.04	0.50	10.04	0.02	0.05	10.04	0.23	96.37	45
CD-18-14-2_BTE_10-8	35.82	2.56	14.54	21.44	0.49	10.13	0.00	0.02	10.05	0.70	95.76	46
CD-18-14-2_BTE_10-9	36.08	2.97	14.32	21.72	0.50	9.88	0.01	0.04	10.02	0.56	96.10	45
CD-18-14-	35.77	3.12	14.48	22.00	0.47	9.73	0.00	0.04	10.04	0.66	96.31	44

	CD-18-14-2_BTE_10-10												
	CD-18-14-2_BTE_10-11	35.87	3.37	14.29	22.35	0.48	9.48	0.00	0.04	10.24	0.10	96.22	43
	CD-18-14-2_BTE_10-12	36.15	3.17	14.36	21.54	0.50	9.69	0.01	0.06	10.07	0.07	95.61	44
	CD-18-14-2_BTE_11-1	35.18	3.34	13.89	23.95	0.44	8.16	0.01	0.07	9.92	0.25	95.21	38
	CD-18-14-2_BTE_11-2	35.25	3.35	14.05	24.73	0.46	8.24	0.02	0.05	9.38	0.36	95.89	37
	CD-18-14-2_BTE_11-3	34.71	3.65	13.83	24.63	0.47	7.67	0.00	0.06	10.00	0.23	95.24	36
	CD-18-14-2_BTE_11-4	35.67	3.48	14.22	24.75	0.47	7.95	0.01	0.08	9.79	0.23	96.65	36
	CD-18-14-2_BTE_11-5	34.87	3.26	13.87	24.41	0.45	8.08	0.00	0.06	9.87	0.31	95.18	37
	CD-18-14-2_BTE_11-6	35.35	3.58	13.68	24.75	0.44	8.35	0.02	0.10	9.91	0.32	96.49	38
	CD-18-14-2_BTE_11-7	35.42	3.68	13.88	24.68	0.48	8.04	0.00	0.07	9.92	0.25	96.42	37
	CD-18-14-2_BTE_11-8	35.84	3.63	13.69	24.48	0.46	8.38	0.01	0.08	9.78	0.28	96.62	38
	Average	**35.78**	**3.11**	**14.50**	23.02	**0.48**	**8.90**	**0.01**	**0.05**	10.01	**0.30**	**96.15**	41
	Standard Deviation	**0.40**	**0.32**	**0.58**	0.88	**0.10**	**0.68**	**0.02**	**0.02**	0.17	**0.18**	**0.52**	3
CD-18-16	CD-18-16_BTE_4-1	35.47	2.87	15.08	23.43	0.58	8.82	0.02	0.04	10.13	-0.02	96.42	40
	CD-18-16_BTE_4-2	35.95	2.88	14.79	23.28	0.60	9.01	0.03	0.04	10.27	0.02	96.86	41
	CD-18-16_BTE_4-3	35.82	2.69	15.07	23.62	0.58	8.75	0.01	0.04	10.22	-0.01	96.79	40
	CD-18-16_BTE_4-4	35.64	2.72	15.10	23.02	0.55	8.83	0.00	0.02	10.20	-0.01	96.07	41
	CD-18-16_BTE_4-5	35.84	2.87	14.57	22.72	0.58	9.29	0.00	0.06	10.07	0.00	95.99	42
	CD-18-16_BTE_4-6	35.32	2.77	14.87	22.85	0.57	8.96	0.05	0.04	10.02	0.05	95.49	41
	CD-18-16_BTE_4-7	35.60	2.68	14.88	23.72	0.59	8.82	0.02	0.03	10.04	0.03	96.41	40

CD-18-16_BTE_4-8	35.52	2.94	14.90	23.16	0.55	9.02	0.04	0.04	10.10	0.03	96.31	41
CD-18-16_BTE_4-9	35.71	2.66	15.27	23.09	0.57	8.69	0.01	0.01	10.21	0.04	96.27	40
CD-18-16_BTE_4-10	35.75	2.84	14.91	23.05	0.60	8.86	0.00	0.04	10.19	-0.03	96.19	41
CD-18-16_BTE_4-11	35.40	3.00	14.64	23.37	0.59	9.11	0.01	0.04	10.07	-0.01	96.23	41
CD-18-16_BTE_4-12	35.94	3.02	14.54	23.15	0.55	9.13	0.01	0.05	10.10	0.05	96.54	41
CD-18-16_BTE_4-13	35.38	3.05	14.79	23.52	0.60	8.97	0.01	0.04	10.04	0.01	96.41	40
CD-18-16_BTE_4-14	35.52	3.03	14.73	23.15	0.56	8.95	0.02	0.05	9.99	0.02	96.00	41
CD-18-16_BTE_4-15	35.73	2.78	15.20	23.48	0.58	8.91	0.00	0.03	10.24	0.06	97.02	40
CD-18-16_BTE_4-16	35.48	2.77	15.10	23.60	0.59	8.74	0.00	0.02	10.17	0.02	96.48	40
CD-18-16_BTE_4-17	36.09	2.68	15.30	23.15	0.58	8.60	0.01	0.03	10.30	0.02	96.75	40
CD-18-16_BTE_4-18	35.89	2.77	14.97	23.06	0.57	8.85	0.01	0.02	10.08	-0.01	96.21	41
CD-18-16_BTE_4-19	35.67	2.93	14.65	23.18	0.59	8.95	0.01	0.03	10.10	0.00	96.10	41
CD-18-16_BTE_4-20	35.71	2.87	14.96	23.22	0.58	9.03	0.00	0.04	10.06	-0.01	96.47	41
CD-18-16_BTE_4-21	35.64	2.66	15.23	22.93	0.56	8.72	0.01	0.02	10.14	0.02	95.93	40
CD-18-16_BTE_4-22	35.69	2.75	15.06	23.14	0.58	8.72	0.00	0.03	10.15	0.05	96.17	40
CD-18-16_BTE_4-23	35.59	2.85	15.24	23.28	0.60	8.88	0.00	0.03	10.04	0.05	96.55	40
CD-18-16_BTE_4-24	35.74	3.04	14.46	23.10	0.56	9.17	0.02	0.05	10.03	0.00	96.16	41
CD-18-16_BTE_5-1	35.30	2.94	14.28	23.23	0.25	9.64	0.01	0.04	10.04	0.51	96.25	43
CD-18-16_BTE_5-2	35.66	3.05	14.16	23.71	0.27	9.66	0.01	0.04	10.13	0.13	96.81	42
CD-18-16_BTE_5-3	35.86	2.50	15.06	23.33	0.25	9.26	0.00	0.02	9.98	0.00	96.28	41
CD-18-16_BTE_5-6	35.66	3.05	14.30	23.54	0.27	9.61	0.00	0.03	10.01	0.54	97.03	42
CD-18-16_BTE_5-7	35.95	2.90	14.57	23.36	0.27	9.61	0.00	0.02	10.25	0.06	96.98	42
CD-18-16_BTE_5-8	35.69	3.45	14.06	23.83	0.29	9.41	0.00	0.06	9.95	0.22	96.94	41

	CD-18-16_BTE_5-9	35.60	3.34	14.18	23.86	0.27	9.40	0.02	0.06	10.07	0.18	96.99	41
	CD-18-16_BTE_5-11	35.61	3.22	14.31	23.76	0.26	9.61	0.01	0.06	10.09	0.08	97.01	42
	CD-18-16_BTE_5-12	35.45	3.42	14.07	23.75	0.25	9.33	0.00	0.05	9.91	0.51	96.71	41
	CD-18-16_BTE_5-13	35.72	3.26	14.09	23.75	0.26	9.66	0.02	0.06	10.10	0.23	97.14	42
	CD-18-16_BTE_5-14	35.64	3.30	14.06	23.87	0.26	9.64	0.01	0.07	10.13	0.26	97.23	42
	CD-18-16_BTE_6-1	35.27	3.68	14.11	23.60	0.20	8.70	0.02	0.04	9.72	0.39	95.73	40
	CD-18-16_BTE_6-2	35.84	3.67	14.55	23.38	0.23	9.40	0.00	0.05	10.18	0.07	97.35	42
	CD-18-16_BTE_6-3	36.15	3.51	14.37	23.13	0.22	9.66	0.01	0.02	10.26	0.00	97.33	43
	CD-18-16_BTE_6-4	35.80	3.33	14.63	24.04	0.21	8.73	0.01	0.02	10.26	0.03	97.05	39
	CD-18-16_BTE_6-5	35.73	2.80	14.27	24.13	0.22	9.30	0.02	0.02	10.01	0.00	96.50	41
	CD-18-16_BTE_6-6	35.32	3.70	14.10	23.58	0.27	9.45	0.03	0.03	10.18	0.06	96.72	42
	CD-18-16_BTE_6-7	35.98	3.16	14.23	23.04	0.21	10.09	0.02	0.02	10.18	0.24	97.17	44
	CD-18-16_BTE_6-11	35.60	3.48	14.84	24.31	0.19	8.52	0.01	0.02	10.11	0.03	97.10	38
	CD-18-16_BTE_6-13	36.13	2.88	14.46	23.66	0.18	9.12	0.00	0.01	9.99	0.03	96.48	41
	CD-18-16_BTE_6-14	35.86	3.49	14.35	22.26	0.25	9.86	0.01	0.05	10.01	0.05	96.18	44
	CD-18-16_BTE_6-15	35.72	3.37	13.57	23.48	0.22	9.93	0.00	0.03	10.09	0.07	96.47	43
	CD-18-16_BTE_6-16	35.60	3.28	13.84	24.41	0.17	9.08	0.00	0.03	10.13	0.18	96.70	40
	CD-18-16_BTE_6-17	35.80	2.68	14.57	23.58	0.19	9.83	0.00	0.05	10.18	0.18	97.06	43
	CD-18-16_BTE_6-18	35.56	2.98	14.16	22.88	0.22	10.33	0.01	0.06	10.12	0.11	96.42	45
	Average	**35.69**	**3.03**	**14.60**	23.40	**0.40**	**9.20**	**0.01**	**0.04**	10.10	**0.09**	**96.56**	41
	Standard Deviation	**0.21**	**0.31**	**0.43**	0.41	**0.17**	**0.43**	**0.01**	**0.01**	0.11	**0.14**	**0.44**	1
Excluded Points	**Chloritized biotite**												
	CD-18-14-	24.60	0.14	19.86	32.43	1.18	10.41	0.07	0.00	0.07	0.02	88.79	

2_BTE_5-1 CD-18-14-											
2_BTE_5-2 CD-18-14-	24.47	0.10	19.75	32.09	1.17	10.33	0.03	0.00	0.00	0.01	87.95
2_BTE_5-3 CD-18-14-	24.77	0.05	19.50	31.92	1.14	11.03	0.01	0.00	0.03	-0.03	88.43
2_BTE_5-4 CD-18-14-	24.68	0.14	19.64	31.68	1.14	11.00	0.06	0.01	0.01	0.01	88.35
2_BTE_5-5 CD-18-14-	24.75	0.17	19.82	31.77	1.14	10.87	0.06	0.00	0.01	-0.05	88.53
2_BTE_5-6	24.49	0.12	19.96	32.64	1.16	10.43	0.01	-0.01	0.01	0.02	88.85

Table A-0-3 Whole-rock major and minor element concentrations (wt%) for previously published samples from Glass Mountain (Gordon et al., 2026), Bishop Tuff (Jolles and Lange, 2019), and the Benton Range (Mesa, 2021)

Sample	SiO_2	TiO_2	Al_2O_3	FeO^T	MnO	MgO	CaO	Na_2O	K_2O	Total	Ba (ppm)
GM-18	77.87	0.06	12.37	0.86	0.06	0.03	0.37	4.00	4.28	99.20	3
GM-01	77.44	0.06	12.55	0.68	0.09	0.04	0.34	4.28	4.44	99.90	4
GM-07	76.94	0.06	13.04	0.76	0.07	0.03	0.36	4.27	4.38	98.71	3
GM-20	77.75	0.07	12.48	0.87	0.04	0.04	0.40	3.85	4.41	100.60	<2
GM-10	77.43	0.07	12.50	0.78	0.04	0.06	0.49	3.92	4.60	99.91	4
BT.22B	77.95	0.07	12.25	0.69	0.04	0.07	0.51	3.52	4.92	100.80	16
BT.22A	77.06	0.07	12.83	0.73	0.03	0.05	0.48	3.86	4.88	99.80	16
BT.8B	78.06	0.10	11.94	0.83	0.03	0.10	0.56	3.38	4.99	100.30	29
BT-16B	77.44	0.07	12.42	0.78	0.04	0.07	0.51	3.80	4.89	100.00	8
BT-13A	77.19	0.09	12.41	0.80	0.03	0.12	0.62	3.29	5.43	99.00	35
BT-19D	77.54	0.12	12.43	0.79	0.03	0.10	0.63	3.00	5.32	99.20	118
BT-21F	76.15	0.19	13.48	1.08	0.03	0.17	0.71	2.69	5.39	99.00	258
BT-19F	75.04	0.20	13.14	1.00	0.02	0.35	1.40	3.05	5.68	98.40	592
BT-19H	75.27	0.18	13.33	0.91	0.04	0.28	1.10	2.92	5.71	98.80	528
BT-19I	75.04	0.20	13.25	1.00	0.03	0.28	1.08	3.09	5.85	98.10	613
BT-3A	75.85	0.18	13.34	0.92	0.02	0.17	0.83	3.29	5.27	100.50	576
CD-18-09	75.80	0.11	13.30	1.20	0.04	0.12	0.88	3.34	5.14	98.50	1237
CD-18-12	76.60	0.11	12.60	1.34	0.02	0.14	0.91	3.42	4.80	98.60	455
CD-18-14	76.30	0.12	13.10	1.02	0.02	0.17	1.04	3.42	4.70	98.60	484
CD-18-16	76.60	0.08	13.20	1.02	0.02	0.07	1.08	3.71	4.26	98.70	221
MC-24	77.14	0.07	12.46	1.18	0.04	0.04	0.63	3.55	4.88	99.06	71
BT-3B	76.61	0.20	12.69	1.01	0.02	0.18	0.74	3.33	5.07	100.70	442

Table A-0-4 Experimental individual biotite analyses (wt%)

EXP	Point	SiO_2	TiO_2	Al_2O_3	FeO	MnO	MgO	CaO	Na_2O	K_2O	BaO	Total	Mg#
BT: 1	25BT3B_OX_1_BT E_1-1	38.59	4.87	14.50	15.76	0.18	13.33	0.00	0.36	9.32	0.13	97.03	60
	25BT3B_OX_1_BT E_1-16	37.31	4.91	13.60	17.24	0.15	14.30	0.01	0.49	9.14	0.13	97.27	60
800 °C	25BT3B_OX_1_BT E_2-2	36.86	4.84	12.76	17.62	0.16	11.77	0.00	0.37	9.34	0.16	93.88	54
200 MPa	25BT3B_OX_1_BT E_2-3	36.78	4.94	12.73	18.10	0.15	11.73	0.01	0.39	9.41	0.12	94.35	54
	25BT3B_OX_1_BT E_2-4	35.55	4.70	15.11	17.31	0.16	11.13	0.00	0.40	9.07	0.13	93.54	53
	25BT3B_OX_1_BT E_2-5	36.12	4.75	13.24	18.01	0.16	11.38	0.00	0.39	9.16	0.11	93.30	53
	25BT3B_OX_1_BT E_2-6	36.14	4.84	12.78	18.19	0.15	11.32	0.00	0.39	9.20	0.18	93.19	53
	25BT3B_OX_1_BT E_2-7	35.70	4.86	12.46	17.56	0.14	12.69	0.02	0.50	9.17	0.13	93.22	56
	25BT3B_OX_1_BT E_2-21	36.80	4.77	13.54	16.70	0.15	11.91	0.00	0.36	9.23	0.10	93.57	56
	25BT3B_OX_1_BT E_2-22	38.26	4.81	14.18	16.47	0.16	12.24	0.00	0.34	9.47	0.10	96.01	57
	25BT3B_OX_1_BT E_2-24	37.76	4.75	13.25	16.73	0.14	14.67	0.04	0.49	9.32	0.12	97.29	61
	25BT3B_OX_1_BT E_2-25	39.50	4.41	12.83	15.08	0.15	13.28	0.06	0.45	8.61	0.13	94.50	61
	25BT3B_OX_1_BT E_2-26	38.37	4.72	13.17	16.15	0.13	14.06	0.01	0.45	9.16	0.15	96.37	61
	25BT3B_OX_1_BT E_2-28	38.33	4.59	12.84	15.33	0.14	14.23	0.02	0.46	8.99	0.13	95.06	62
	25BT3B_OX_1_BT E_2-29	39.06	4.75	13.12	15.89	0.15	14.23	0.04	0.38	7.76	0.11	95.50	61
	25BT3B_OX_1_BT E_3-1	36.03	4.81	12.63	17.68	0.15	12.40	0.00	0.39	9.11	0.11	93.30	56
	25BT3B_OX_1_BT E_3-5	37.17	4.91	12.89	16.67	0.15	13.29	0.00	0.40	9.36	0.13	94.97	59
	25BT3B_OX_1_BT E_3-6	36.35	4.94	12.57	16.54	0.17	13.36	0.01	0.39	9.23	0.13	93.69	59
	25BT3B_OX_1_BT E_4-10	36.90	4.82	12.75	17.60	0.16	12.47	0.00	0.40	9.16	0.20	94.47	56
	25BT3B_OX_1_BT E_4-12	36.57	4.81	12.84	18.90	0.14	12.14	0.00	0.42	9.13	0.16	95.11	53
	25BT3B_OX_1_BT E_4-13	36.39	4.79	12.75	18.59	0.15	12.19	0.00	0.43	9.04	0.15	94.48	54
	25BT3B_OX_1_BT E_4-14	36.57	4.67	13.12	18.50	0.15	11.23	0.00	0.43	9.05	0.14	93.85	52

	25BT3B_OX_1_BTE_4-16	36.29	4.92	12.86	17.26	0.18	13.17	0.00	0.40	9.43	0.18	94.68	58
	25BT3B_OX_1_BTE_4-17	36.61	4.86	12.77	18.33	0.14	12.23	0.00	0.39	9.22	0.16	94.69	54
	25BT3B_OX_1_BTE_4-18	36.34	4.82	12.60	18.83	0.17	12.00	0.01	0.43	9.25	0.19	94.62	53
	25BT3B_OX_1_BTE_4-19	36.09	4.86	12.69	18.62	0.14	11.96	0.01	0.44	9.21	0.11	94.13	53
	25BT3B_OX_1_BTE_4-21	36.40	4.90	12.73	17.90	0.17	12.64	0.03	0.43	9.24	0.18	94.61	56
	25BT3B_OX_1_BTE_4-27	35.62	4.77	13.04	18.58	0.13	11.62	0.01	0.41	9.07	0.15	93.41	53
	25BT3B_OX_1_BTE_4-28	35.96	4.71	12.80	18.29	0.16	11.67	0.01	0.40	8.97	0.13	93.10	53
	25BT3B_OX_1_BTE_4-31	36.17	4.90	12.54	17.80	0.15	12.99	0.00	0.43	9.15	0.12	94.24	57
	25BT3B_OX_1_BTE_4-32	36.33	4.91	12.69	18.17	0.14	12.25	0.00	0.39	9.25	0.13	94.28	55
	25BT3B_OX_1_BTE_4-33	35.87	4.94	12.40	18.02	0.15	12.75	0.00	0.45	9.38	0.16	94.13	56
	25BT3B_OX_1_BTE_5-7	36.07	4.75	12.69	17.76	0.16	12.15	0.00	0.38	9.09	0.12	93.15	55
	25BT3B_OX_1_BTE_5-16	36.40	4.72	12.52	17.25	0.14	12.46	0.02	0.35	9.11	0.13	93.10	56
	Average	**36.80**	**4.80**	**13.00**	**17.45**	**0.15**	**12.57**	**0.01**	**0.41**	**9.14**	**0.14**	**94.47**	56
	Standard Deviation	**1.02**	**0.11**	**0.59**	**0.95**	**0.01**	**0.01**	**0.01**	**0.04**	**0.29**	**0.03**	**1.19**	3
BT: 2 750 °C 200 MPa	25_BT3B_OX_6_BTE_1-1	36.92	4.68	12.92	18.66	0.22	11.92	0.09	0.38	9.56	0.05	95.38	53
	25_BT3B_OX_6_BTE_1-2	36.86	4.70	13.06	18.63	0.21	11.73	0.03	0.40	9.47	0.00	95.08	53
	25_BT3B_OX_6_BTE_1-3	37.41	4.69	13.36	18.86	0.23	12.12	0.02	0.49	9.57	0.07	96.80	53
	25_BT3B_OX_6_BTE_1-4	37.01	4.76	13.09	18.65	0.24	11.88	0.02	0.47	9.72	0.05	95.89	53
	25_BT3B_OX_6_BTE_1-5	36.36	4.69	13.07	18.05	0.23	12.49	0.18	0.42	9.57	0.05	95.10	55
	25_BT3B_OX_6_BTE_1-6	36.96	4.73	13.24	18.66	0.22	12.00	0.07	0.43	9.42	0.01	95.75	53
	25_BT3B_OX_6_BTE_1-7	36.93	4.65	13.35	16.94	0.21	12.77	0.52	0.39	9.43	0.02	95.21	57
	25_BT3B_OX_6_BTE_1-8	38.17	4.52	13.67	16.04	0.23	13.20	0.02	0.39	9.28	0.03	95.55	59
	25_BT3B_OX_6_BTE_1-9	36.87	4.66	13.77	16.77	0.22	12.93	0.01	0.41	9.37	0.10	95.11	58

	25_BT3B_OX_6_BTE_1-10	36.75	4.62	13.57	16.92	0.21	12.55	0.06	0.42	9.46	0.03	94.60	57
	25_BT3B_OX_6_BTE_1-11	36.91	4.63	12.99	18.76	0.21	12.21	0.13	0.48	9.29	0.03	95.64	54
	25_BT3B_OX_6_BTE_1-12	36.95	4.56	13.16	18.91	0.21	12.05	0.07	0.42	9.48	0.04	95.85	53
	25_BT3B_OX_6_BTE_1-13	37.44	4.50	13.37	18.38	0.21	12.02	0.04	0.41	9.38	0.03	95.79	54
	25_BT3B_OX_6_BTE_1-14	37.31	4.61	13.60	18.41	0.21	12.16	0.04	0.43	9.31	0.06	96.14	54
	25_BT3B_OX_6_BTE_1-15	37.62	4.48	14.53	17.24	0.21	12.02	0.02	0.42	9.35	0.05	95.93	55
	25_BT3B_OX_6_BTE_1-16	37.04	4.84	13.16	18.62	0.21	11.79	0.02	0.48	9.68	0.07	95.90	53
	25_BT3B_OX_6_BTE_1-17	36.99	4.75	13.12	18.99	0.20	11.76	0.03	0.48	9.66	0.04	96.04	52
	25_BT3B_OX_6_BTE_1-18	36.87	4.81	13.18	18.71	0.22	11.90	0.02	0.45	9.61	0.03	95.79	53
	25_BT3B_OX_6_BTE_2-4	37.16	4.90	13.34	18.85	0.12	12.52	0.01	0.49	9.36	0.19	96.93	54
	25_BT3B_OX_6_BTE_2-5	36.22	4.82	12.94	16.48	0.16	13.24	0.01	0.44	9.07	0.25	93.64	59
	25_BT3B_OX_6_BTE_2-7	36.87	4.98	13.36	18.57	0.14	12.11	0.00	0.45	9.48	0.20	96.13	54
	25_BT3B_OX_6_BTE_2-8	37.16	4.94	13.50	19.27	0.16	12.39	0.01	0.48	9.48	0.16	97.53	53
	25_BT3B_OX_6_BTE_2-9	36.05	4.97	12.99	19.22	0.15	11.86	0.02	0.47	9.41	0.21	95.35	52
	25_BT3B_OX_6_BTE_2-10	36.18	5.08	12.95	19.77	0.13	11.98	0.00	0.47	9.50	0.20	96.25	52
	25_BT3B_OX_6_BTE_2-17	35.43	4.94	12.83	19.10	0.15	11.61	0.00	0.45	9.27	0.30	94.06	52
	25_BT3B_OX_6_BTE_2-26	36.88	4.82	14.53	18.65	0.14	9.89	0.01	0.36	9.20	0.29	94.77	49
	25_BT3B_OX_6_BTE_2-38	36.71	5.01	13.41	19.41	0.16	12.30	0.01	0.49	9.47	0.37	97.35	53
	25_BT3B_OX_6_BTE_2-39	36.04	4.99	12.94	19.69	0.15	11.94	0.00	0.50	9.34	0.29	95.87	52
	AVG	**36.86**	**4.76**	**13.32**	**18.40**	**0.19**	**12.12**	**0.05**	**0.44**	**9.43**	**0.11**	**95.69**	54
	SD	**0.54**	**0.17**	**0.42**	**0.98**	**0.04**	**0.61**	**0.10**	**0.04**	**0.15**	**0.11**	**0.87**	2
BT: 3	25_BT3B_OX_4_BTE_1-1	37.41	4.79	13.34	19.38	0.14	11.91	0.01	0.49	9.35	0.14	96.96	52
	25_BT3B_OX_4_BTE_1-2	37.46	4.77	13.50	19.21	0.13	11.95	0.00	0.51	9.38	0.14	97.04	53

700 °C 200 MPa	25_BT3B_OX_4_BTE_1-3	37.49	4.75	13.45	19.30	0.16	12.03	-0.03	0.47	9.36	0.14	97.11	53
	25_BT3B_OX_4_BTE_1-4	37.27	4.86	13.25	19.43	0.15	12.04	-0.01	0.48	9.36	0.16	96.98	52
	25_BT3B_OX_4_BTE_1-5	37.44	4.79	13.22	19.34	0.16	12.12	0.00	0.49	9.35	0.09	96.99	53
	25_BT3B_OX_4_BTE_1-6	37.54	4.83	13.52	19.46	0.15	12.08	0.01	0.49	9.32	0.15	97.55	53
	25_BT3B_OX_4_BTE_1-7	37.62	4.83	13.33	19.54	0.13	11.88	0.00	0.46	9.44	0.12	97.35	52
	25_BT3B_OX_4_BTE_1-8	37.63	4.79	13.46	19.36	0.17	12.13	0.00	0.49	9.33	0.13	97.48	53
	25_BT3B_OX_4_BTE_1-9	37.73	4.85	13.58	19.41	0.16	12.08	-0.01	0.47	9.29	0.16	97.71	53
	25_BT3B_OX_4_BTE_1-10	37.12	4.90	13.25	19.88	0.16	11.92	-0.01	0.49	9.35	0.16	97.20	52
	25_BT3B_OX_4_BTE_1-11	37.32	4.70	13.30	19.72	0.17	11.28	-0.01	0.44	9.11	0.15	96.19	50
	25_BT3B_OX_4_BTE_1-12	37.29	4.83	13.19	19.43	0.18	11.44	-0.02	0.45	9.26	0.19	96.25	51
	25_BT3B_OX_4_BTE_1-13	37.64	4.86	13.41	19.62	0.14	11.41	0.02	0.46	9.36	0.21	97.13	51
	25_BT3B_OX_4_BTE_1-14	37.36	4.83	13.20	19.92	0.15	11.83	-0.02	0.51	9.31	0.17	97.28	51
	25_BT3B_OX_4_BTE_1-15	37.65	4.84	13.30	19.60	0.16	12.00	-0.01	0.50	9.35	0.16	97.56	52
	25_BT3B_OX_4_BTE_1-17	37.68	4.83	13.52	19.05	0.14	11.70	0.01	0.46	9.42	0.17	96.99	52
	25_BT3B_OX_4_BTE_1-18	37.63	4.80	13.50	19.24	0.15	11.68	0.01	0.47	9.30	0.13	96.90	52
	25_BT3B_OX_4_BTE_1-19	37.25	4.84	13.26	19.25	0.18	11.47	0.00	0.46	9.43	0.13	96.26	52
	25_BT3B_OX_4_BTE_1-20	37.21	4.79	13.36	19.26	0.16	11.50	-0.02	0.49	9.29	0.10	96.13	52
	25_BT3B_OX_4_BTE_1-21	37.55	4.82	13.41	19.40	0.14	11.52	0.00	0.47	9.40	0.16	96.86	51
	25_BT3B_OX_4_BTE_1-22	37.57	4.81	13.37	19.43	0.12	11.64	-0.02	0.47	9.41	0.20	97.00	52
	25_BT3B_OX_4_BTE_1-24	37.80	4.90	13.47	19.50	0.15	11.79	0.00	0.48	9.40	0.15	97.63	52
	25_BT3B_OX_4_BTE_1-27	37.89	4.87	13.33	19.28	0.17	12.00	0.02	0.48	9.42	0.17	97.63	53
	25_BT3B_OX_4_BTE_1-28	37.31	4.85	13.33	19.40	0.14	11.60	-0.02	0.45	9.42	0.13	96.61	52
	25_BT3B_OX_4_BTE_1-29	37.61	4.88	13.47	19.24	0.15	11.65	-0.01	0.44	9.38	0.14	96.94	52

25_BT3B_OX_4_BTE_1-30	37.35	4.75	13.38	20.04	0.17	11.63	-0.02	0.47	9.20	0.14	97.10	51
25_BT3B_OX_4_BTE_1-31	37.14	4.92	13.14	19.70	0.16	11.59	0.00	0.49	9.33	0.11	96.58	51
25_BT3B_OX_4_BTE_1-32	36.72	4.80	13.09	19.55	0.16	11.41	-0.01	0.46	9.37	0.09	95.65	51
25_BT3B_OX_4_BTE_1-33	37.24	4.86	13.20	19.73	0.15	11.39	0.00	0.49	9.34	0.12	96.52	51
25_BT3B_OX_4_BTE_1-34	36.82	4.82	13.20	19.96	0.15	11.20	-0.01	0.43	9.31	0.13	96.01	50
25_BT3B_OX_4_BTE_1-44	36.78	4.79	13.03	19.46	0.15	11.88	-0.01	0.42	9.19	0.13	95.82	52
25_BT3B_OX_4_BTE_1-45	35.47	4.71	12.59	19.50	0.16	11.89	0.01	0.45	8.97	0.16	93.92	52
25_BT3B_OX_4_BTE_1-50	36.16	4.74	13.05	19.45	0.14	12.38	0.01	0.49	9.08	0.15	95.65	53
25_BT3B_OX_4_BTE_1-51	35.60	4.59	12.63	19.33	0.13	11.63	0.01	0.44	9.00	0.16	93.50	52
25_BT3B_OX_4_BTE_1-52	36.41	4.68	12.91	19.43	0.17	11.74	0.02	0.44	8.90	0.16	94.86	52
25_BT3B_OX_4_BTE_2-1	36.38	4.93	12.72	19.47	0.15	12.21	0.00	0.49	9.40	0.11	95.86	53
25_BT3B_OX_4_BTE_2-2	35.80	4.92	12.75	19.40	0.15	11.87	0.00	0.50	9.36	0.13	94.87	52
25_BT3B_OX_4_BTE_2-3	36.09	4.91	12.74	19.57	0.16	12.36	0.00	0.51	9.27	0.13	95.72	53
25_BT3B_OX_4_BTE_2-4	35.95	4.97	12.98	19.65	0.15	11.68	0.00	0.53	9.40	0.18	95.49	51
25_BT3B_OX_4_BTE_2-5	36.26	4.94	13.09	19.58	0.14	12.19	-0.01	0.53	9.37	0.15	96.25	53
25_BT3B_OX_4_BTE_2-6	35.68	4.87	12.90	19.91	0.16	11.33	0.01	0.45	9.22	0.11	94.65	50
25_BT3B_OX_4_BTE_2-7	36.47	4.97	13.19	19.95	0.17	11.97	0.40	0.49	9.58	0.14	97.35	52
25_BT3B_OX_4_BTE_2-8	34.16	4.89	13.69	19.57	0.16	10.88	0.02	0.45	9.14	0.09	93.05	50
25_BT3B_OX_4_BTE_2-9	36.37	4.90	13.31	19.88	0.13	11.27	0.00	0.46	9.29	0.12	95.72	50
25_BT3B_OX_4_BTE_2-10	35.33	4.97	14.13	19.35	0.15	10.71	0.00	0.42	9.33	0.10	94.48	50
25_BT3B_OX_4_BTE_2-11	36.27	4.89	12.83	19.46	0.13	11.92	0.00	0.51	9.35	0.15	95.51	52
25_BT3B_OX_4_BTE_2-12	36.51	4.87	12.93	19.73	0.14	12.39	0.00	0.50	9.35	0.14	96.55	53
25_BT3B_OX_4_BTE_2-13	36.34	4.94	12.89	19.43	0.17	12.53	0.00	0.56	9.23	0.16	96.24	53

	25_BT3B_OX_4_BTE_2-14	36.01	4.90	12.70	19.70	0.15	12.27	0.01	0.51	9.38	0.13	95.76	53
	25_BT3B_OX_4_BTE_2-15	35.96	4.89	12.60	19.55	0.15	12.34	0.00	0.56	9.34	0.15	95.54	53
	25_BT3B_OX_4_BTE_2-16	35.96	4.97	12.69	19.96	0.14	11.77	0.00	0.49	9.49	0.12	95.59	51
	25_BT3B_OX_4_BTE_2-17	35.38	4.99	12.55	19.35	0.14	11.73	-0.02	0.50	9.38	0.14	94.13	52
	25_BT3B_OX_4_BTE_2-18	36.99	4.86	13.02	19.44	0.14	12.39	-0.01	0.54	9.30	0.13	96.82	53
	25_BT3B_OX_4_BTE_2-20	35.99	4.98	13.32	19.97	0.14	12.14	-0.01	0.53	9.45	0.12	96.64	52
	25_BT3B_OX_4_BTE_3-11	35.17	4.81	13.04	19.78	0.17	10.89	0.01	0.45	9.09	0.10	93.51	50
	Average	**36.77**	**4.85**	**13.17**	**19.54**	**11.79**	**0.15**	**0.01**	**0.48**	**9.31**	**0.14**	**96.20**	52
	Standard Deviation	**0.85**	**0.08**	**0.32**	**0.23**	**0.40**	**0.01**	**0.06**	**0.03**	**0.13**	**0.03**	**1.15**	1
BT: 7	25BT3B_ox_09_BTE_1-2	36.51	4.73	13.74	17.00	0.14	12.54	0.00	0.42	9.40	0.08	94.53	57
	25BT3B_ox_09_BTE_1-3	36.98	4.69	13.51	15.97	0.15	13.13	0.00	0.43	9.44	0.20	94.50	59
750 °C	25BT3B_ox_09_BTE_1-4	37.51	4.70	13.30	17.42	0.13	12.81	0.01	0.38	9.51	0.13	95.90	57
125 MPa	25BT3B_ox_09_BTE_1-5	37.43	4.67	13.56	16.63	0.14	12.89	0.00	0.41	9.45	0.15	95.33	58
	25BT3B_ox_09_BTE_1-6	36.78	4.70	13.99	16.05	0.13	13.10	0.00	0.40	9.21	0.11	94.46	59
	25BT3B_ox_09_BTE_1-7	37.54	4.79	13.31	17.47	0.13	12.85	0.00	0.43	9.36	0.14	96.02	57
	25BT3B_ox_09_BTE_1-8	37.50	4.79	13.28	18.54	0.11	12.47	0.00	0.44	9.53	0.17	96.83	55
	25BT3B_ox_09_BTE_1-9	37.35	4.76	13.14	17.95	0.14	12.54	0.00	0.41	9.50	0.14	95.93	55
	25BT3B_ox_09_BTE_1-12	37.83	4.81	13.48	16.94	0.13	13.31	0.01	0.42	9.44	0.11	96.49	58
	25BT3B_ox_09_BTE_1-13	37.69	4.76	13.32	17.76	0.14	12.90	0.00	0.43	9.47	0.12	96.58	56
	25BT3B_ox_09_BTE_1-16	37.14	4.74	13.17	18.15	0.15	12.40	0.01	0.41	9.53	0.12	95.83	55
	25BT3B_ox_09_BTE_1-17	36.45	4.59	14.71	16.92	0.15	12.99	0.00	0.44	9.25	0.13	95.62	58
	25BT3B_ox_09_BTE_1-29	37.92	4.79	13.82	16.55	0.13	14.15	0.00	0.46	9.50	0.15	97.47	60
	25BT3B_ox_09_BTE_1-30	37.35	4.70	14.83	15.92	0.14	13.85	0.00	0.45	9.28	0.14	96.65	61

25BT3B_ox_09_BTE_1-33	36.18	4.68	13.58	15.72	0.12	13.06	0.00	0.40	9.29	0.14	93.17	60
25BT3B_ox_09_BTE_1-34	37.31	4.71	13.25	18.28	0.13	12.55	0.00	0.43	9.54	0.12	96.32	55
25BT3B_ox_09_BTE_1-35	37.39	4.73	13.17	17.31	0.14	12.97	0.00	0.42	9.52	0.08	95.73	57
25BT3B_ox_09_BTE_3-7	37.54	4.68	13.51	18.11	0.16	12.76	0.00	0.45	9.26	0.15	96.62	56
25BT3B_ox_09_BTE_3-8	36.18	4.86	12.86	18.72	0.16	12.14	0.00	0.43	9.47	0.11	94.92	54
25BT3B_ox_09_BTE_3-9	35.40	4.95	12.43	18.73	0.15	11.94	0.01	0.43	9.52	0.14	93.71	53
25BT3B_ox_09_BTE_3-10	37.04	4.97	12.95	16.48	0.16	13.33	0.00	0.44	9.62	0.11	95.10	59
25BT3B_ox_09_BTE_3-11	36.28	5.06	12.78	17.08	0.15	13.32	0.02	0.46	9.70	0.13	94.98	58
25BT3B_ox_09_BTE_3-16	35.28	4.86	12.59	19.52	0.15	11.84	0.00	0.43	9.39	0.10	94.16	52
25BT3B_ox_09_BTE_3-17	35.65	4.86	12.72	19.09	0.17	11.79	0.01	0.42	9.47	0.11	94.30	52
25BT3B_ox_09_BTE_3-18	35.61	4.84	12.70	19.43	0.16	11.77	0.00	0.43	9.43	0.11	94.46	52
25BT3B_ox_09_BTE_3-19	36.65	4.73	12.97	19.26	0.17	12.06	0.02	0.42	9.19	0.10	95.58	53
25BT3B_ox_09_BTE_3-20	34.86	4.92	12.49	19.31	0.16	11.50	0.00	0.46	9.39	0.12	93.20	51
25BT3B_ox_09_BTE_3-21	35.56	4.80	12.64	19.34	0.15	11.67	0.00	0.43	9.34	0.12	94.04	52
25BT3B_ox_09_BTE_3-22	34.85	4.82	12.33	19.54	0.14	11.49	0.01	0.45	9.32	0.17	93.11	51
25BT3B_ox_09_BTE_3-23	35.69	4.78	12.57	19.26	0.14	11.53	0.01	0.46	9.38	0.13	93.95	52
25BT3B_ox_09_BTE_3-24	35.99	4.70	12.72	18.65	0.15	11.79	0.00	0.44	9.09	0.08	93.62	53
25BT3B_ox_09_BTE_3-25	35.68	4.63	12.77	18.36	0.16	11.80	0.00	0.42	9.15	0.17	93.14	53
25BT3B_ox_09_BTE_3-27	35.71	4.82	12.90	19.12	0.14	11.90	0.00	0.45	9.56	0.12	94.73	53
25BT3B_ox_09_BTE_3-29	34.74	4.89	12.51	18.48	0.16	12.36	0.00	0.41	9.48	0.13	93.16	54
25BT3B_ox_09_BTE_3-35	36.23	4.87	12.94	18.53	0.17	12.47	0.02	0.44	9.40	0.12	95.19	55
25BT3B_ox_09_BTE_3-36	36.22	4.87	12.90	18.35	0.16	12.61	0.00	0.45	9.56	0.14	95.25	55
25BT3B_ox_09_BTE_3-41	36.66	4.84	12.72	15.65	0.13	13.31	0.01	0.45	9.41	0.12	93.32	60

25BT3B_ox_09_BTE_3-45	36.06	4.84	12.69	18.75	0.15	12.00	0.03	0.42	9.31	0.14	94.40	53
25BT3B_ox_09_BTE_3-46	36.21	4.77	12.92	19.06	0.15	12.07	0.00	0.46	9.37	0.10	95.10	53
25BT3B_ox_09_BTE_3-47	36.60	4.81	12.84	18.57	0.13	12.19	0.00	0.46	9.43	0.13	95.16	54
25BT3B_ox_09_BTE_3-48	36.28	4.80	12.81	18.71	0.15	12.23	0.01	0.41	9.49	0.13	95.00	54
25BT3B_ox_09_BTE_3-51	39.46	4.64	12.97	14.61	0.12	14.22	0.05	0.57	8.95	0.11	95.69	63
25BT3B_ox_09_BTE_3-52	36.22	4.90	12.71	17.73	0.14	12.58	0.02	0.42	9.43	0.11	94.27	56
25BT3B_ox_09_BTE_3-53	35.56	4.77	12.38	18.97	0.14	12.06	0.01	0.43	9.27	0.11	93.69	53
25BT3B_ox_09_BTE_3-54	35.23	4.78	12.26	19.00	0.15	11.85	0.00	0.42	9.42	0.12	93.22	53
25BT3B_ox_09_BTE_3-55	36.88	4.73	12.86	17.89	0.16	12.80	0.00	0.44	9.26	0.12	95.11	56
25BT3B_ox_09_BTE_3-56	36.19	4.82	12.84	17.87	0.16	12.36	0.01	0.40	9.51	0.14	94.29	55
25BT3B_ox_09_BTE_3-57	36.61	4.67	12.76	18.86	0.16	12.66	0.02	0.45	9.13	0.15	95.47	54
25BT3B_ox_09_BTE_3-59	36.32	4.78	12.90	18.92	0.16	12.83	0.00	0.45	9.20	0.11	95.68	55
25BT3B_ox_09_BTE_3-63	37.66	4.79	14.17	17.12	0.17	12.53	0.01	0.42	8.97	0.14	95.97	57
25BT3B_ox_09_BTE_3-67	38.75	4.66	14.02	16.72	0.14	13.37	0.00	0.45	9.32	0.10	97.53	59
25BT3B_ox_09_BTE_3-68	35.45	4.43	16.13	14.60	0.16	13.48	0.02	0.46	8.73	0.13	93.60	62
25BT3B_ox_09_BTE_3-70	38.30	4.73	13.96	18.41	0.15	12.12	0.01	0.44	9.47	0.12	97.71	54
25BT3B_ox_09_BTE_3-72	37.33	4.72	13.48	19.31	0.16	12.13	0.00	0.46	9.32	0.12	97.01	53
25BT3B_ox_09_BTE_3-73	36.47	4.81	13.41	19.59	0.15	12.04	0.00	0.45	9.34	0.15	96.38	52
25BT3B_ox_09_BTE_3-74	36.49	4.87	12.90	19.12	0.14	12.14	0.00	0.43	9.36	0.17	95.62	53
25BT3B_ox_09_BTE_3-79	39.04	4.64	15.56	16.95	0.14	10.95	0.02	0.37	9.07	0.13	96.88	54
25BT3B_ox_09_BTE_3-81	36.27	4.81	12.79	18.37	0.15	12.80	0.00	0.43	9.20	0.13	94.96	55
25BT3B_ox_09_BTE_3-85	36.09	4.77	12.68	19.10	0.14	12.21	0.01	0.43	9.35	0.14	94.92	53
25BT3B_ox_09_BTE_3-88	35.50	4.90	12.51	19.20	0.16	11.66	0.00	0.41	9.47	0.13	93.94	52

	25BT3B_ox_09_BTE_4-11	36.14	4.45	14.81	14.72	0.16	13.58	0.04	0.43	8.91	0.07	93.31	62
	25BT3B_ox_09_BTE_4-12	38.04	4.40	14.41	14.87	0.15	13.65	0.07	0.45	8.90	0.10	95.05	62
	Average	**36.61**	**4.76**	**13.23**	**17.88**	**0.15**	**12.52**	**0.01**	**0.43**	**9.35**	**0.13**	**95.06**	56
	Standard Deviation	**1.02**	**0.12**	**0.77**	**1.37**	**0.01**	**0.69**	**0.01**	**0.03**	**0.19**	**0.02**	**1.23**	3
MC: 2	25MC24_OX_3_BTE_1-1	37.17	4.97	13.11	19.09	0.16	12.25	0.01	0.55	9.48	0.19	96.98	53
	25MC24_OX_3_BTE_1-2	37.01	4.97	13.02	19.33	0.17	12.30	0.00	0.54	9.44	0.17	96.95	53
750 °C	25MC24_OX_3_BTE_1-3	36.99	4.91	13.00	19.14	0.15	12.16	0.00	0.51	9.36	0.15	96.37	53
200 MPa	25MC24_OX_3_BTE_1-4	36.30	4.92	13.24	18.72	0.14	11.87	0.00	0.51	9.34	0.17	95.21	53
	25MC24_OX_3_BTE_1-5	36.96	4.89	13.76	18.62	0.13	11.78	0.00	0.50	9.54	0.13	96.31	53
	25MC24_OX_3_BTE_1-6	36.49	4.99	12.68	19.07	0.15	11.86	0.00	0.47	9.57	0.13	95.40	53
	25MC24_OX_3_BTE_1-7	37.07	4.94	13.21	19.18	0.16	12.12	0.00	0.52	9.38	0.17	96.74	53
	25MC24_OX_3_BTE_1-8	36.64	4.86	14.44	18.54	0.14	11.82	0.00	0.48	9.17	0.17	96.26	53
	25MC24_OX_3_BTE_1-9	37.13	4.89	13.39	18.73	0.16	11.94	0.01	0.46	9.49	0.15	96.34	53
	25MC24_OX_3_BTE_1-10	37.41	4.85	13.32	18.85	0.14	12.25	0.03	0.48	9.43	0.18	96.94	54
	25MC24_OX_3_BTE_1-11	37.18	4.92	13.26	18.66	0.14	12.18	0.00	0.48	9.51	0.16	96.49	54
	25MC24_OX_3_BTE_1-12	36.80	4.82	14.96	18.60	0.13	12.12	0.01	0.50	9.31	0.17	97.41	54
	25MC24_OX_3_BTE_1-13	36.97	4.93	13.34	18.83	0.15	11.98	0.01	0.51	9.43	0.15	96.30	53
	25MC24_OX_3_BTE_1-14	37.22	4.88	13.12	18.85	0.16	12.02	0.00	0.52	9.50	0.16	96.43	53
	25MC24_OX_3_BTE_1-15	36.83	4.96	12.88	19.02	0.14	11.86	0.02	0.47	9.54	0.20	95.93	53
	25MC24_OX_3_BTE_1-16	36.82	4.95	12.91	18.75	0.17	12.03	0.00	0.51	9.48	0.21	95.83	53
	25MC24_OX_3_BTE_1-17	37.00	4.96	12.95	18.98	0.17	11.99	0.00	0.52	9.48	0.17	96.21	53
	25MC24_OX_3_BTE_1-18	35.86	4.89	13.63	18.58	0.14	11.79	0.00	0.51	9.27	0.16	94.83	53
	25MC24_OX_3_BTE_1-19	36.70	4.95	13.01	19.25	0.15	12.04	0.00	0.53	9.45	0.18	96.26	53

25MC24_OX_3_BTE_1-20	37.11	4.88	13.25	19.37	0.16	12.21	0.00	0.51	9.43	0.15	97.07	53
25MC24_OX_3_BTE_1-21	37.11	4.88	13.20	19.07	0.14	12.10	0.01	0.50	9.47	0.18	96.67	53
25MC24_OX_3_BTE_1-22	37.10	4.89	13.50	18.90	0.14	11.98	0.00	0.48	9.51	0.15	96.65	53
25MC24_OX_3_BTE_1-23	37.13	4.88	13.29	18.87	0.17	12.09	0.00	0.48	9.36	0.17	96.44	53
25MC24_OX_3_BTE_1-24	37.09	4.91	13.46	18.90	0.15	12.08	0.02	0.46	9.39	0.18	96.63	53
25MC24_OX_3_BTE_1-25	35.92	4.83	14.98	18.11	0.17	11.51	0.01	0.46	9.28	0.10	95.36	53
25MC24_OX_3_BTE_1-26	36.64	4.88	13.51	18.24	0.16	12.07	0.00	0.45	9.28	0.13	95.35	54
25MC24_OX_3_BTE_1-27	32.46	4.62	17.82	16.36	0.19	12.57	0.01	0.45	8.79	0.11	93.39	58
25MC24_OX_3_BTE_1-28	34.22	4.62	16.91	18.11	0.17	11.47	0.02	0.46	9.09	0.13	95.20	53
25MC24_OX_3_BTE_1-29	37.35	4.89	13.43	19.10	0.18	12.02	0.00	0.43	9.47	0.15	97.02	53
25MC24_OX_3_BTE_1-30	37.10	4.97	13.26	18.90	0.15	12.03	0.00	0.50	9.44	0.18	96.52	53
25MC24_OX_3_BTE_1-31	36.97	4.94	13.11	19.21	0.14	11.97	0.01	0.50	9.49	0.23	96.58	53
25MC24_OX_3_BTE_1-32	37.01	4.88	13.19	18.57	0.13	11.99	0.00	0.50	9.34	0.18	95.80	54
25MC24_OX_3_BTE_1-33	37.18	4.93	13.15	18.78	0.15	12.05	0.01	0.53	9.58	0.18	96.55	53
25MC24_OX_3_BTE_1-34	36.95	4.91	13.20	18.78	0.14	12.08	0.00	0.49	9.56	0.14	96.26	53
25MC24_OX_3_BTE_1-36	36.55	4.92	13.09	18.76	0.15	11.83	0.02	0.50	9.43	0.16	95.41	53
25MC24_OX_3_BTE_1-37	36.55	4.86	12.88	19.68	0.15	11.45	0.00	0.48	9.64	0.09	95.76	51
25MC24_OX_3_BTE_1-39	36.67	4.96	12.92	19.12	0.15	12.04	0.00	0.52	9.42	0.20	95.99	53
25MC24_OX_3_BTE_1-40	36.64	5.00	12.77	19.18	0.17	12.13	0.00	0.50	9.51	0.21	96.10	53
25MC24_OX_3_BTE_1-41	37.03	4.95	13.31	18.96	0.15	12.17	0.01	0.53	9.52	0.18	96.81	53
25MC24_OX_3_BTE_1-42	37.00	4.95	12.77	19.28	0.14	12.17	0.01	0.54	9.47	0.16	96.47	53
25MC24_OX_3_BTE_1-43	37.00	4.90	12.97	19.09	0.16	12.14	0.00	0.52	9.41	0.17	96.35	53
25MC24_OX_3_BTE_1-44	36.97	4.89	13.05	18.72	0.14	12.09	0.00	0.51	9.35	0.16	95.87	54

25MC24_OX_3_BTE_1-45	37.02	4.94	13.21	19.16	0.15	12.08	0.00	0.52	9.44	0.13	96.63	53
25MC24_OX_3_BTE_1-46	37.04	4.87	12.92	18.86	0.13	12.22	0.00	0.51	9.47	0.19	96.22	54
25MC24_OX_3_BTE_1-47	36.90	4.92	12.97	19.24	0.13	12.11	0.00	0.52	9.46	0.21	96.46	53
25MC24_OX_3_BTE_1-48	36.83	4.94	12.76	18.86	0.14	12.18	0.00	0.52	9.54	0.18	95.96	54
25MC24_OX_3_BTE_1-49	36.83	4.94	12.80	19.58	0.15	12.19	0.00	0.53	9.48	0.17	96.67	53
25MC24_OX_3_BTE_1-50	37.09	4.94	12.84	19.36	0.15	12.25	0.00	0.53	9.45	0.15	96.76	53
25MC24_OX_3_BTE_2-1	36.77	4.93	12.91	19.09	0.16	11.70	0.00	0.43	9.42	0.10	95.49	52
25MC24_OX_3_BTE_2-2	36.68	4.92	12.85	18.90	0.15	11.69	0.00	0.44	9.62	0.14	95.38	52
25MC24_OX_3_BTE_2-3	36.83	4.89	12.97	19.02	0.15	11.76	0.01	0.45	9.61	0.10	95.78	52
25MC24_OX_3_BTE_2-4	36.62	4.93	12.96	18.68	0.15	11.80	0.02	0.44	9.53	0.08	95.21	53
25MC24_OX_3_BTE_2-5	36.71	4.93	12.81	18.71	0.15	11.65	0.01	0.43	9.57	0.14	95.11	53
25MC24_OX_3_BTE_2-6	34.46	4.60	16.52	17.17	0.14	10.46	0.27	0.50	8.89	0.08	93.11	52
25MC24_OX_3_BTE_2-7	37.04	4.92	13.06	18.86	0.14	11.81	0.00	0.46	9.56	0.16	96.02	53
25MC24_OX_3_BTE_2-8	35.67	4.67	13.84	17.90	0.15	11.53	0.02	0.39	8.90	0.17	93.24	53
25MC24_OX_3_BTE_2-9	36.23	4.88	13.47	18.71	0.14	11.67	0.01	0.41	9.24	0.09	94.85	53
25MC24_OX_3_BTE_2-19	36.56	4.97	12.70	18.67	0.15	11.72	0.00	0.44	9.35	0.33	94.89	53
25MC24_OX_3_BTE_2-20	36.94	4.95	12.84	18.95	0.16	11.92	0.00	0.46	9.46	0.33	96.01	53
25MC24_OX_3_BTE_2-23	36.64	4.89	12.84	18.82	0.15	11.67	0.00	0.43	9.49	0.38	95.31	53
25MC24_OX_3_BTE_2-24	37.57	4.84	12.82	17.68	0.14	12.49	0.00	0.45	9.26	0.27	95.51	56
25MC24_OX_3_BTE_2-26	36.42	4.88	12.78	18.46	0.15	11.77	0.00	0.45	9.38	0.17	94.46	53
25MC24_OX_3_BTE_2-27	36.62	4.86	13.00	18.51	0.14	11.81	0.00	0.39	9.56	0.15	95.04	53
25MC24_OX_3_BTE_2-31	37.15	4.75	12.85	17.07	0.18	12.50	0.08	0.42	9.26	0.12	94.38	57
25MC24_OX_3_BTE_2-35	36.68	4.79	13.40	17.31	0.15	12.44	0.01	0.40	9.40	0.11	94.69	56

25MC24_OX_3_BTE_2-36	36.10	4.83	14.07	18.34	0.15	11.85	0.00	0.42	9.33	0.11	95.19	54
25MC24_OX_3_BTE_2-37	36.99	4.87	12.93	19.00	0.17	11.90	0.01	0.46	9.49	0.12	95.94	53
25MC24_OX_3_BTE_2-38	36.51	4.89	13.02	18.86	0.17	11.84	0.02	0.47	9.37	0.12	95.27	53
25MC24_OX_3_BTE_2-39	36.52	4.95	12.90	18.42	0.15	11.93	0.02	0.43	9.46	0.09	94.88	54
25MC24_OX_3_BTE_2-40	36.56	4.88	12.81	19.06	0.16	11.74	0.00	0.43	9.61	0.13	95.36	52
25MC24_OX_3_BTE_2-41	36.61	4.93	12.90	18.82	0.16	11.77	0.00	0.46	9.38	0.09	95.12	53
25MC24_OX_3_BTE_2-42	36.93	4.92	12.98	18.71	0.13	11.73	0.01	0.45	9.44	0.13	95.42	53
25MC24_OX_3_BTE_2-43	36.95	4.93	13.03	18.57	0.14	11.74	0.01	0.44	9.40	0.15	95.36	53
25MC24_OX_3_BTE_2-44	36.82	4.92	13.12	18.83	0.15	11.97	0.07	0.46	9.36	0.09	95.78	53
25MC24_OX_3_BTE_2-45	36.04	4.69	14.41	17.64	0.15	11.82	0.00	0.41	9.25	0.07	94.48	54
25MC24_OX_3_BTE_2-46	35.81	4.67	14.44	17.51	0.17	11.74	0.02	0.42	9.02	0.13	93.93	54
25MC24_OX_3_BTE_2-47	37.01	4.92	13.22	18.74	0.16	11.83	0.00	0.43	9.50	0.09	95.90	53
25MC24_OX_3_BTE_2-48	36.97	4.89	12.96	18.52	0.16	12.13	0.02	0.42	9.43	0.10	95.61	54
25MC24_OX_3_BTE_2-49	36.66	4.92	12.95	18.26	0.16	12.20	0.03	0.42	9.28	0.13	95.03	54
25MC24_OX_3_BTE_3-1	37.10	4.98	12.33	17.18	0.23	14.11	0.00	0.66	9.45	0.21	96.25	59
25MC24_OX_3_BTE_3-2	37.21	4.94	12.32	17.00	0.24	14.25	0.00	0.65	9.37	0.25	96.22	60
25MC24_OX_3_BTE_3-3	37.30	4.96	12.38	17.14	0.23	14.02	0.00	0.67	9.34	0.25	96.30	59
25MC24_OX_3_BTE_3-4	37.23	5.00	12.44	17.26	0.25	13.93	0.00	0.67	9.55	0.30	96.63	59
25MC24_OX_3_BTE_3-5	37.21	4.95	12.65	16.94	0.23	14.33	0.00	0.67	9.40	0.23	96.61	60
25MC24_OX_3_BTE_3-6	37.02	4.85	12.95	16.64	0.23	13.15	0.00	0.60	9.22	0.25	94.90	58
25MC24_OX_3_BTE_3-7	37.03	4.99	12.34	16.75	0.24	14.47	0.00	0.67	9.38	0.23	96.10	61
25MC24_OX_3_BTE_3-8	36.63	4.87	12.44	17.39	0.24	13.58	0.00	0.71	9.12	0.33	95.29	58
25MC24_OX_3_BTE_3-9	37.07	4.87	12.57	17.13	0.25	13.84	0.00	0.69	9.30	0.28	96.01	59

25MC24_OX_3_BTE_3-10	37.36	4.88	12.39	17.07	0.23	14.83	0.01	0.68	9.36	0.22	97.04	61
25MC24_OX_3_BTE_3-11	37.15	4.89	12.29	16.66	0.23	15.00	0.02	0.65	9.29	0.25	96.43	62
25MC24_OX_3_BTE_3-12	37.83	4.84	12.85	16.26	0.22	14.77	0.02	0.69	9.40	0.18	97.07	62
25MC24_OX_3_BTE_3-13	37.21	4.90	12.92	17.35	0.22	14.18	0.00	0.69	9.28	0.26	97.02	59
25MC24_OX_3_BTE_3-14	37.06	4.83	12.90	16.42	0.25	14.40	0.03	0.66	9.20	0.25	96.01	61
25MC24_OX_3_BTE_3-15	37.07	4.84	12.65	16.55	0.22	14.37	0.00	0.69	9.39	0.24	96.02	61
25MC24_OX_3_BTE_3-16	36.77	4.91	12.72	17.21	0.24	13.66	0.01	0.66	9.40	0.20	95.78	59
25MC24_OX_3_BTE_3-17	37.37	4.89	12.59	17.37	0.24	14.27	0.00	0.67	9.44	0.23	97.09	59
25MC24_OX_3_BTE_3-18	36.36	4.88	13.94	16.92	0.22	12.72	0.00	0.58	9.24	0.24	95.09	57
25MC24_OX_3_BTE_3-19	37.13	4.98	12.22	17.41	0.23	14.33	0.00	0.65	9.31	0.21	96.47	59
25MC24_OX_3_BTE_3-20	37.08	4.98	12.24	17.82	0.22	14.27	0.00	0.66	9.47	0.21	96.94	59
25MC24_OX_3_BTE_3-21	37.22	4.94	12.55	18.13	0.23	14.27	0.00	0.67	9.24	0.27	97.52	58
25MC24_OX_3_BTE_3-22	36.57	4.77	12.42	16.91	0.22	13.92	0.00	0.66	8.95	0.23	94.64	59
25MC24_OX_3_BTE_3-23	37.18	4.83	12.60	16.84	0.21	14.15	0.00	0.67	9.34	0.19	95.98	60
25MC24_OX_3_BTE_3-24	37.35	4.89	12.31	17.68	0.21	14.38	0.01	0.66	9.23	0.25	96.98	59
25MC24_OX_3_BTE_3-25	37.03	4.97	12.41	16.86	0.22	14.30	0.01	0.66	9.35	0.24	96.06	60
25MC24_OX_3_BTE_3-26	36.94	4.90	12.43	17.07	0.22	14.12	0.00	0.64	9.27	0.22	95.78	60
25MC24_OX_3_BTE_3-27	36.89	4.93	12.42	16.93	0.23	14.14	0.01	0.67	9.37	0.19	95.77	60
25MC24_OX_3_BTE_3-28	36.97	4.89	12.71	17.21	0.22	14.37	0.00	0.68	9.35	0.22	96.59	60
25MC24_OX_3_BTE_3-29	37.76	4.86	12.98	17.24	0.22	13.46	0.00	0.62	9.36	0.18	96.66	58
25MC24_OX_3_BTE_3-31	37.10	4.82	12.59	17.10	0.22	14.33	0.00	0.72	9.48	0.28	96.61	60
25MC24_OX_3_BTE_3-33	37.62	4.95	12.68	17.10	0.21	14.46	0.00	0.68	9.46	0.25	97.40	60
25MC24_OX_3_BTE_3-34	36.89	4.92	12.16	17.21	0.22	14.05	0.00	0.67	9.29	0.16	95.55	59

	25MC24_OX_3_BTE_3-35	37.86	4.95	12.53	16.97	0.22	14.34	0.00	0.68	9.30	0.22	97.06	60
	25MC24_OX_3_BTE_3-41	37.62	4.89	12.96	17.05	0.22	14.51	0.01	0.69	9.26	0.27	97.49	60
	25MC24_OX_3_BTE_3-42	37.01	4.97	12.52	18.14	0.25	14.09	0.00	0.69	9.47	0.23	97.36	58
	25MC24_OX_3_BTE_3-43	37.59	4.92	12.56	17.10	0.25	14.38	0.00	0.67	9.35	0.20	97.03	60
	25MC24_OX_3_BTE_3-44	36.89	4.96	12.39	16.90	0.20	14.01	0.01	0.65	9.43	0.25	95.69	60
	25MC24_OX_3_BTE_3-45	37.14	4.99	12.43	16.91	0.23	14.09	0.00	0.66	9.42	0.28	96.13	60
	25MC24_OX_3_BTE_3-46	36.99	4.95	12.43	17.02	0.21	13.90	0.00	0.64	9.28	0.25	95.67	59
	25MC24_OX_3_BTE_3-47	37.33	4.98	12.53	17.01	0.22	14.09	0.00	0.67	9.31	0.22	96.35	60
	25MC24_OX_3_BTE_3-48	37.52	4.94	12.47	17.06	0.21	13.85	0.00	0.65	9.42	0.24	96.36	59
	25MC24_OX_3_BTE_3-49	37.35	5.01	12.48	17.07	0.23	13.85	0.00	0.64	9.48	0.20	96.31	59
	25MC24_OX_3_BTE_3-50	37.57	5.01	12.90	16.97	0.23	14.10	0.00	0.67	9.40	0.33	97.16	60
	Average	**36.86**	**4.90**	**13.07**	**18.14**	**0.18**	**12.72**	**0.01**	**0.54**	**9.38**	**0.19**	**95.98**	55
	Standard Deviation	**0.65**	**0.08**	**0.82**	**0.93**	**0.04**	**1.10**	**0.03**	**0.10**	**0.15**	**0.06**	**0.87**	3
MC: 4	25MC24_OX_01_BTE 1-5	37.02	5.14	13.43	18.64	0.13	11.26	0.24	0.44	9.33	0.13	95.76	52
	25MC24_OX_01_BTE 1-6	37.54	4.96	13.43	19.49	0.16	11.87	0.02	0.46	9.58	0.09	97.58	52
675 °C	25MC24_OX_01_BTE 1-7	36.68	5.07	13.01	19.45	0.14	11.84	0.00	0.46	9.53	0.05	96.22	52
200 Mpa	25MC24_OX_01_BTE 1-8	36.89	5.03	13.04	19.44	0.12	11.95	0.00	0.47	9.62	0.06	96.61	52
	25MC24_OX_01_BTE 1-11	36.05	4.96	12.84	19.64	0.16	12.06	0.01	0.44	9.56	0.09	95.81	52
	25MC24_OX_01_BTE 1-12	37.21	4.91	13.22	19.23	0.12	11.93	0.02	0.47	9.52	0.09	96.70	53
	25MC24_OX_01_BTE 1-13	36.28	4.77	13.04	18.46	0.15	11.50	0.01	0.41	9.32	0.07	94.01	53
	25MC24_OX_01_BTE 1-14	36.12	5.04	12.82	19.23	0.12	11.93	0.01	0.44	9.41	0.07	95.21	53
	25MC24_OX_01_BTE 1-15	36.32	5.08	12.78	19.14	0.14	11.89	0.01	0.44	9.44	0.06	95.30	53
	25MC24_OX_01_BTE 1-16	36.62	5.06	12.94	19.25	0.16	12.05	0.02	0.45	9.61	0.07	96.24	53

25MC24_OX_01_BTE 1-17	39.50	4.52	13.01	18.16	0.17	11.14	0.04	0.51	9.17	0.11	96.34	52
25MC24_OX_01_BTE 1-18	37.59	4.89	13.33	19.09	0.15	11.85	0.01	0.46	9.60	0.08	97.04	53
25MC24_OX_01_BTE 1-19	36.68	4.99	12.98	19.19	0.17	12.06	0.11	0.42	9.54	0.20	96.36	53
25MC24_OX_01_BTE 1-21	35.87	4.12	12.44	27.55	0.25	6.36	0.55	0.40	6.61	0.05	94.19	29
25MC24_OX_01_BTE 1-24	36.96	5.12	13.07	19.41	0.16	11.93	0.03	0.47	9.55	0.11	96.80	52
25MC24_OX_01_BTE 1-25	36.75	5.04	13.00	19.29	0.15	11.96	0.04	0.46	9.64	0.12	96.46	53
25MC24_OX_01_BTE 1-26	37.05	4.89	12.93	18.26	0.14	11.44	0.04	0.41	9.27	0.10	94.53	53
25MC24_OX_01_BTE 1-29	36.91	4.93	13.11	19.00	0.20	12.19	0.14	0.42	9.60	0.07	96.57	53
25MC24_OX_01_BTE 1-31	37.06	4.98	13.28	19.46	0.16	12.06	0.05	0.49	9.43	0.06	97.05	52
25MC24_OX_01_BTE 1-32	36.56	4.99	13.12	19.59	0.17	12.03	0.05	0.51	9.55	0.10	96.65	52
25MC24_OX_01_BTE 1-33	36.52	4.96	13.03	19.54	0.16	11.97	0.04	0.50	9.42	0.08	96.22	52
25MC24_OX_01_BTE 1-34	36.88	5.01	13.11	19.45	0.15	12.10	0.01	0.50	9.41	0.09	96.72	53
25MC24_OX_01_BTE 1-35	36.78	5.07	13.07	19.82	0.16	12.18	0.00	0.52	9.59	0.08	97.27	52
25MC24_OX_01_BTE 1-36	36.60	4.98	13.03	19.33	0.15	11.93	0.00	0.50	9.51	0.08	96.11	52
25MC24_OX_01_BTE 1-37	36.65	4.99	13.02	19.58	0.15	12.04	0.01	0.49	9.51	0.09	96.55	52
25MC24_OX_01_BTE 1-38	36.63	5.03	12.97	19.51	0.16	11.94	0.00	0.46	9.55	0.07	96.32	52
25MC24_OX_01_BTE 1-39	36.25	4.94	13.34	19.34	0.14	11.84	0.01	0.43	9.50	0.14	95.92	52
25MC24_OX_01_BTE 1-41	36.20	4.90	13.13	19.40	0.16	11.66	0.03	0.48	9.51	0.07	95.56	52
25MC24_OX_01_BTE 1-42	36.62	5.02	13.02	19.70	0.16	12.08	0.00	0.49	9.50	0.06	96.63	52
25MC24_OX_01_BTE 1-43	36.79	5.01	13.28	19.48	0.15	12.09	0.01	0.52	9.69	0.11	97.12	53
25MC24_OX_01_BTE 1-44	37.03	4.96	13.13	19.50	0.15	12.07	0.02	0.48	9.46	0.09	96.90	52
25MC24_OX_01_BTE 1-45	37.36	5.02	13.41	19.33	0.18	12.13	0.06	0.46	9.53	0.18	97.67	53
25MC24_OX_01_BTE 1-46	39.10	4.82	13.22	18.77	0.19	11.67	0.05	0.44	9.35	0.15	97.76	53

25MC24_OX_01_BTE 1-47	36.76	4.97	13.12	19.81	0.16	12.12	0.01	0.49	9.63	0.08	97.15	52
25MC24_OX_01_BTE 1-48	37.03	5.05	13.11	18.93	0.16	12.15	0.08	0.41	9.59	0.08	96.58	53
25MC24_OX_01_BTE 1-50	36.55	5.04	13.02	19.67	0.14	12.00	0.00	0.48	9.49	0.06	96.46	52
25MC24_OX_01_BTE 2-1	38.05	4.30	12.29	19.31	0.29	12.18	0.13	0.27	9.89	0.05	96.77	53
25MC24_OX_01_BTE 2-2	38.39	4.34	12.33	19.13	0.28	12.17	0.02	0.27	9.79	0.06	96.77	53
25MC24_OX_01_BTE 2-3	38.37	4.31	12.41	19.12	0.29	12.19	0.05	0.30	9.86	0.01	96.90	53
25MC24_OX_01_BTE 2-4	38.01	4.36	12.40	18.69	0.28	11.94	0.01	0.27	9.76	0.08	95.79	53
25MC24_OX_01_BTE 2-5	35.35	4.09	11.71	24.79	0.31	11.56	0.01	0.24	8.81	0.05	96.93	45
25MC24_OX_01_BTE 2-7	38.03	4.31	12.43	19.21	0.28	12.21	0.01	0.29	9.72	0.01	96.50	53
25MC24_OX_01_BTE 2-8	38.16	4.33	12.43	19.25	0.27	12.27	0.00	0.30	9.75	0.07	96.83	53
25MC24_OX_01_BTE 2-9	38.24	4.31	12.24	19.24	0.29	12.34	0.00	0.27	9.77	0.03	96.72	53
25MC24_OX_01_BTE 2-10	37.57	4.29	12.30	19.04	0.31	11.96	0.00	0.26	9.60	0.03	95.36	53
25MC24_OX_01_BTE 2-11	37.88	4.20	12.94	18.86	0.30	12.65	0.00	0.28	9.60	0.04	96.74	54
25MC24_OX_01_BTE 2-12	38.09	4.29	12.41	19.18	0.28	12.35	0.00	0.27	9.72	0.03	96.62	53
25MC24_OX_01_BTE 2-13	37.93	4.35	12.37	19.25	0.31	12.23	0.00	0.28	9.67	0.04	96.43	53
25MC24_OX_01_BTE 2-14	37.91	4.28	12.20	18.97	0.31	12.34	0.00	0.27	9.78	0.08	96.13	54
25MC24_OX_01_BTE 2-15	37.10	4.23	13.53	18.73	0.28	11.68	0.00	0.25	9.46	0.06	95.32	53
25MC24_OX_01_BTE 2-18	37.88	4.53	12.79	19.34	0.28	11.85	0.01	0.33	9.74	0.10	96.86	52
25MC24_OX_01_BTE 2-19	37.62	4.13	12.82	19.23	0.28	12.24	0.02	0.29	9.57	0.04	96.24	53
25MC24_OX_01_BTE 2-21	38.28	4.17	12.69	19.55	0.30	12.34	0.01	0.29	9.78	0.03	97.44	53
25MC24_OX_01_BTE 2-22	38.07	4.26	12.56	19.52	0.30	12.27	0.01	0.29	9.64	0.07	96.99	53
25MC24_OX_01_BTE 2-23	37.73	4.16	12.73	18.97	0.27	12.21	0.26	0.30	9.52	0.08	96.23	53
25MC24_OX_01_BTE 2-24	36.14	4.22	12.04	19.01	0.30	11.27	0.11	0.25	9.69	0.03	93.07	51

25MC24_OX_01_BTE 2-25	37.73	4.13	12.78	18.92	0.27	12.27	0.03	0.30	9.59	0.06	96.07	54
25MC24_OX_01_BTE 2-26	37.35	4.09	13.22	19.03	0.28	11.65	0.17	0.27	9.59	0.00	95.66	52
25MC24_OX_01_BTE 2-28	38.13	4.27	12.50	18.76	0.28	11.95	0.01	0.29	9.78	0.07	96.03	53
25MC24_OX_01_BTE 2-29	38.55	4.32	12.36	19.10	0.28	12.20	0.01	0.27	9.75	0.08	96.91	53
25MC24_OX_01_BTE 3-1	36.15	5.08	13.20	19.79	0.15	12.07	0.02	0.50	9.60	0.28	96.85	52
25MC24_OX_01_BTE 3-2	36.29	5.05	13.31	19.94	0.14	12.07	0.01	0.50	9.46	0.29	97.08	52
25MC24_OX_01_BTE 3-3	36.08	5.04	13.16	20.07	0.17	11.82	0.00	0.51	9.62	0.37	96.84	51
25MC24_OX_01_BTE 3-4	36.21	5.10	13.24	20.21	0.17	11.93	0.00	0.51	9.37	0.35	97.10	51
25MC24_OX_01_BTE 3-5	36.46	5.03	13.36	20.11	0.14	12.02	0.00	0.52	9.48	0.31	97.42	52
25MC24_OX_01_BTE 3-6	36.51	4.95	13.05	19.89	0.15	12.02	0.00	0.50	9.43	0.14	96.61	52
25MC24_OX_01_BTE 3-7	36.69	5.01	13.04	19.66	0.16	12.11	0.01	0.50	9.51	0.18	96.87	52
25MC24_OX_01_BTE 3-8	36.32	4.94	13.00	19.74	0.15	12.09	0.00	0.50	9.43	0.13	96.30	52
25MC24_OX_01_BTE 3-9	36.66	4.94	12.94	19.67	0.16	12.00	0.00	0.47	9.71	0.09	96.62	52
25MC24_OX_01_BTE 3-10	36.85	4.98	12.92	19.84	0.18	12.15	0.02	0.50	9.67	0.06	97.16	52
25MC24_OX_01_BTE 3-11	36.63	4.91	12.96	19.83	0.14	12.08	0.00	0.51	9.60	0.05	96.71	52
25MC24_OX_01_BTE 3-12	36.77	4.92	13.00	19.92	0.15	12.04	0.02	0.53	9.55	0.06	96.95	52
25MC24_OX_01_BTE 3-13	36.46	4.95	13.05	19.64	0.16	12.13	0.01	0.53	9.59	0.04	96.55	52
25MC24_OX_01_BTE 3-14	36.59	4.94	12.87	19.87	0.15	11.91	0.01	0.52	9.52	0.10	96.48	52
25MC24_OX_01_BTE 3-15	36.78	4.86	13.01	19.63	0.13	12.07	0.00	0.50	9.61	0.06	96.66	52
25MC24_OX_01_BTE 3-16	36.78	4.95	13.05	19.55	0.16	12.09	0.01	0.48	9.59	0.05	96.69	52
25MC24_OX_01_BTE 3-17	36.78	4.97	13.06	19.79	0.15	11.94	0.00	0.46	9.49	0.09	96.73	52
25MC24_OX_01_BTE 3-18	36.80	4.96	13.04	19.72	0.15	11.96	0.00	0.49	9.60	0.09	96.79	52
25MC24_OX_01_BTE 3-19	36.59	4.85	13.01	20.83	0.14	11.93	0.00	0.47	9.43	0.06	97.31	51

25MC24_OX_01_BTE 3-20	36.89	4.95	13.05	19.71	0.14	12.08	0.00	0.43	9.61	0.10	96.96	52
25MC24_OX_01_BTE 3-21	37.34	4.85	13.49	19.52	0.15	12.19	0.00	0.44	9.53	0.09	97.59	53
25MC24_OX_01_BTE 3-22	36.40	4.99	13.11	19.57	0.17	11.94	0.00	0.43	9.58	0.05	96.25	52
25MC24_OX_01_BTE 3-23	36.84	4.97	13.07	19.83	0.16	11.97	0.00	0.46	9.50	0.06	96.83	52
25MC24_OX_01_BTE 3-24	36.50	4.96	13.03	19.70	0.16	12.05	0.00	0.47	9.42	0.07	96.36	52
25MC24_OX_01_BTE 3-25	36.92	4.95	13.16	19.93	0.15	12.15	0.01	0.48	9.41	0.06	97.21	52
25MC24_OX_01_BTE 3-26	36.49	4.97	12.99	19.97	0.17	12.07	0.01	0.51	9.63	0.05	96.86	52
25MC24_OX_01_BTE 3-27	37.07	4.97	13.18	20.08	0.15	12.03	0.00	0.49	9.68	0.03	97.67	52
25MC24_OX_01_BTE 3-28	36.72	4.98	12.97	19.89	0.15	12.16	0.00	0.53	9.63	0.09	97.09	52
25MC24_OX_01_BTE 3-29	36.84	4.91	13.10	19.95	0.16	12.19	0.00	0.54	9.56	0.05	97.31	52
25MC24_OX_01_BTE 3-30	36.64	4.91	13.09	19.86	0.15	12.23	0.00	0.52	9.55	0.06	96.99	52
25MC24_OX_01_BTE 3-31	36.78	4.93	13.07	19.71	0.16	12.17	0.00	0.52	9.45	0.06	96.83	52
25MC24_OX_01_BTE 3-32	34.83	4.90	12.38	23.16	0.17	11.89	0.01	0.41	9.07	0.08	96.90	48
25MC24_OX_01_BTE 3-33	37.00	4.95	12.98	19.94	0.15	12.12	0.01	0.49	9.57	0.07	97.29	52
25MC24_OX_01_BTE 3-34	36.78	4.93	13.06	19.57	0.16	12.09	0.02	0.47	9.52	0.09	96.69	52
25MC24_OX_01_BTE 3-35	36.93	4.95	13.24	19.57	0.16	12.25	0.02	0.50	9.46	0.07	97.15	53
25MC24_OX_01_BTE 3-36	36.90	5.01	13.31	19.70	0.17	12.27	0.00	0.50	9.54	0.27	97.64	53
25MC24_OX_01_BTE 3-37	36.60	4.96	12.93	19.69	0.16	12.08	0.02	0.51	9.51	0.22	96.68	52
25MC24_OX_01_BTE 3-38	36.52	5.06	13.32	20.15	0.16	11.89	0.00	0.48	9.37	0.43	97.38	51
25MC24_OX_01_BTE 3-39	36.75	4.91	13.02	19.60	0.15	12.21	0.01	0.52	9.58	0.06	96.81	53
25MC24_OX_01_BTE 3-40	36.55	4.90	13.17	19.84	0.15	12.29	0.00	0.55	9.42	0.06	96.93	52
25MC24_OX_01_BTE 3-41	36.78	4.94	13.19	19.77	0.15	12.27	0.02	0.47	9.55	0.08	97.21	53
25MC24_OX_01_BTE 3-42	36.87	4.88	13.04	19.70	0.15	12.21	0.02	0.51	9.60	0.07	97.04	52

25MC24_OX_01_BTE 3-43	36.85	4.88	12.99	19.55	0.16	12.05	0.00	0.50	9.40	0.10	96.48	52
25MC24_OX_01_BTE 3-44	36.99	4.88	13.17	19.61	0.16	11.99	0.01	0.43	9.60	0.11	96.95	52
25MC24_OX_01_BTE 3-45	36.93	4.86	13.13	19.31	0.15	12.03	0.00	0.44	9.57	0.09	96.51	53
25MC24_OX_01_BTE 3-46	36.72	4.89	13.10	19.58	0.14	12.05	0.00	0.48	9.51	0.08	96.57	52
25MC24_OX_01_BTE 3-47	37.25	4.87	13.19	19.65	0.16	12.08	0.01	0.48	9.49	0.06	97.23	52
25MC24_OX_01_BTE 3-49	36.88	4.95	12.97	19.69	0.17	12.13	0.00	0.52	9.61	0.15	97.06	52
25MC24_OX_01_BTE 3-50	36.80	4.94	13.00	19.68	0.15	12.10	0.00	0.54	9.48	0.08	96.74	52
25MC24_OX_01_BTE 3-51	36.79	4.84	13.02	19.67	0.17	12.34	0.01	0.55	9.46	0.07	96.92	53
25MC24_OX_01_BTE 3-52	36.79	4.94	12.98	19.72	0.16	12.17	0.02	0.55	9.47	0.07	96.87	52
25MC24_OX_01_BTE 3-53	36.70	4.89	12.89	19.62	0.13	12.15	0.02	0.52	9.46	0.07	96.46	52
25MC24_OX_01_BTE 3-54	36.83	4.97	12.97	19.65	0.15	12.21	0.00	0.48	9.57	0.10	96.91	53
25MC24_OX_01_BTE 3-55	35.78	4.76	12.79	18.93	0.17	11.87	0.00	0.46	9.35	0.11	94.22	53
25MC24_OX_01_BTE 3-56	36.77	4.98	13.13	19.44	0.16	12.00	0.01	0.47	9.52	0.08	96.56	52
25MC24_OX_01_BTE 3-57	36.87	4.93	13.16	19.15	0.16	12.15	0.00	0.50	9.43	0.04	96.39	53
25MC24_OX_01_BTE 3-58	36.96	4.86	13.13	19.24	0.17	12.19	0.01	0.50	9.46	0.07	96.60	53
25MC24_OX_01_BTE 3-59	36.70	4.94	13.15	19.49	0.16	12.16	0.00	0.52	9.47	0.06	96.65	53
25MC24_OX_01_BTE 3-60	36.61	4.92	13.00	19.39	0.14	12.08	0.00	0.51	9.42	0.10	96.17	53
25MC24_OX_01_BTE 3-63	36.91	4.96	13.10	19.54	0.16	12.14	0.00	0.51	9.55	0.07	96.93	53
25MC24_OX_01_BTE 3-64	37.28	4.82	13.20	19.45	0.14	12.48	0.00	0.51	9.44	0.11	97.43	53
25MC24_OX_01_BTE 3-65	36.82	4.88	13.05	20.01	0.14	12.26	0.01	0.53	9.45	0.08	97.22	52
25MC24_OX_01_BTE 3-66	36.76	4.92	13.05	19.70	0.14	12.23	0.00	0.56	9.57	0.14	97.04	53
25MC24_OX_01_BTE 3-67	36.69	4.95	13.15	19.65	0.16	12.21	0.00	0.52	9.65	0.04	97.03	53
25MC24_OX_01_BTE 3-68	36.93	4.93	13.09	19.91	0.16	12.25	0.00	0.52	9.62	0.06	97.47	52

	25MC24_OX_01_BTE_Tail 3-71	36.30	4.76	13.73	21.17	0.20	11.04	0.01	0.40	9.09	0.10	96.78	48
	25MC24_OX_01_BTE_Tail 3-78	35.69	4.61	15.54	20.18	0.20	10.57	0.05	0.41	8.51	0.11	95.86	48
	25MC24_OX_01_BTE_Tail 3-85	38.67	4.24	13.24	18.89	0.18	9.75	0.01	0.40	8.26	0.11	93.75	48
	25MC24_OX_01_BTE_Tail 3-87	36.29	4.56	14.03	19.31	0.21	10.91	0.39	0.40	9.05	0.07	95.23	50
	25MC24_OX_01_BTE_Tail 3-88	34.89	4.43	16.59	18.65	0.23	10.44	0.01	0.33	8.56	0.09	94.24	50
	Average	**36.93**	**4.80**	**13.03**	**19.62**	**0.18**	**11.95**	**0.03**	**0.44**	**9.48**	**0.09**	**96.55**	52
	Standard Deviation	**0.73**	**0.29**	**0.51**	**1.00**	**0.05**	**0.62**	**0.07**	**0.09**	**0.34**	**0.07**	**0.81**	2
MC: 5	25MC24_OX_04_BTE_2-1	36.94	4.84	13.20	17.55	0.15	12.74	0.00	0.41	9.28	0.09	95.20	56
	25MC24_OX_04_BTE_2-2	37.44	4.85	13.21	17.76	0.12	12.59	0.01	0.44	9.19	0.13	95.74	56
750 °C	25MC24_OX_04_BTE_2-3	37.25	4.86	13.30	17.83	0.13	12.63	0.00	0.44	9.28	0.12	95.86	56
225 MPa	25MC24_OX_04_BTE_2-4	37.35	4.88	13.31	17.82	0.12	12.63	0.00	0.43	9.36	0.07	95.96	56
	25MC24_OX_04_BTE_2-5	37.45	4.85	13.26	18.01	0.14	12.48	0.01	0.47	9.28	0.09	96.04	55
	25MC24_OX_04_BTE_2-6	35.68	4.56	17.73	16.19	0.15	12.13	0.01	0.43	8.94	0.07	95.87	57
	25MC24_OX_04_BTE_2-7	36.94	4.81	12.99	18.01	0.13	12.67	0.00	0.44	9.25	0.15	95.39	56
	25MC24_OX_04_BTE_2-8	37.31	4.87	13.17	17.75	0.12	12.62	0.02	0.45	9.31	0.11	95.74	56
	25MC24_OX_04_BTE_2-9	37.22	4.82	13.14	17.83	0.12	12.66	0.01	0.44	9.30	0.10	95.64	56
	25MC24_OX_04_BTE_2-10	37.19	4.79	13.39	17.82	0.12	12.60	0.00	0.42	9.27	0.14	95.72	56
	25MC24_OX_04_BTE_2-11	36.98	4.82	13.14	17.55	0.16	12.68	0.00	0.43	9.26	0.12	95.12	56
	25MC24_OX_04_BTE_2-12	37.26	4.87	13.19	17.32	0.14	12.87	0.00	0.42	9.15	0.08	95.29	57
	25MC24_OX_04_BTE_2-13	37.51	4.84	13.43	17.81	0.15	12.67	0.00	0.43	9.28	0.09	96.20	56
	25MC24_OX_04_BTE_2-14	37.22	4.84	13.26	17.98	0.15	12.42	0.00	0.43	9.38	0.11	95.79	55
	25MC24_OX_04_BTE_2-15	37.14	4.87	13.19	17.98	0.12	12.56	0.00	0.44	9.17	0.13	95.61	55

25MC24_OX_04_BTE_2-16	37.21	4.85	13.23	17.48	0.16	12.79	0.00	0.44	9.39	0.09	95.63	57
25MC24_OX_04_BTE_2-17	37.45	4.85	13.52	17.53	0.16	13.02	0.00	0.45	9.19	0.10	96.25	57
25MC24_OX_04_BTE_2-18	37.23	4.84	13.20	17.89	0.14	12.56	0.00	0.44	9.15	0.11	95.55	56
25MC24_OX_04_BTE_2-19	37.49	4.82	13.32	17.96	0.11	12.70	0.00	0.45	9.29	0.10	96.24	56
25MC24_OX_04_BTE_2-21	37.47	4.81	13.33	17.81	0.13	12.69	0.00	0.45	9.42	0.13	96.24	56
25MC24_OX_04_BTE_2-22	37.25	4.89	13.32	17.94	0.14	12.58	0.00	0.42	9.28	0.16	95.96	56
25MC24_OX_04_BTE_2-23	37.31	4.81	13.26	17.97	0.11	12.58	0.00	0.45	9.11	0.12	95.70	55
25MC24_OX_04_BTE_2-24	37.33	4.85	13.31	17.85	0.12	12.52	0.00	0.45	9.24	0.11	95.75	56
25MC24_OX_04_BTE_2-25	37.17	4.79	14.46	16.58	0.18	13.14	0.00	0.45	9.14	0.11	96.01	59
25MC24_OX_04_BTE_3-2	36.61	4.94	12.99	17.80	0.12	12.92	0.00	0.47	9.33	0.15	95.33	56
25MC24_OX_04_BTE_3-7	36.54	5.01	13.13	17.85	0.12	12.43	0.00	0.44	9.37	0.12	95.00	55
25MC24_OX_04_BTE_3-8	36.76	5.03	13.03	17.91	0.13	12.67	0.01	0.47	9.39	0.09	95.48	56
25MC24_OX_04_BTE_3-9	36.27	4.93	12.94	18.07	0.12	12.87	0.00	0.43	9.18	0.07	94.87	56
25MC24_OX_04_BTE_4-1	36.80	4.97	12.92	18.04	0.12	12.72	0.00	0.46	9.49	0.16	95.68	56
25MC24_OX_04_BTE_4-2	36.53	4.94	12.96	18.06	0.13	12.81	0.00	0.46	9.18	0.18	95.24	56
25MC24_OX_04_BTE_4-3	36.16	4.93	12.77	17.73	0.12	12.87	0.00	0.43	9.39	0.13	94.52	56
25MC24_OX_04_BTE_4-4	35.74	4.95	12.61	17.64	0.12	12.95	0.00	0.44	9.36	0.16	93.95	57
25MC24_OX_04_BTE_4-6	36.09	4.97	12.69	17.94	0.12	12.87	0.00	0.45	9.34	0.13	94.59	56
25MC24_OX_04_BTE_4-7	36.96	4.97	13.05	18.12	0.12	12.68	0.00	0.43	9.47	0.16	95.96	56
25MC24_OX_04_BTE_4-8	36.40	4.87	13.11	17.85	0.10	12.37	0.00	0.47	9.29	0.19	94.63	55
25MC24_OX_04_BTE_4-9	36.39	4.90	12.95	18.06	0.13	12.69	0.00	0.46	9.30	0.19	95.08	56
25MC24_OX_04_BTE_4-10	36.22	4.92	12.94	17.92	0.14	13.01	0.00	0.45	9.20	0.20	94.97	56
25MC24_OX_04_BTE_4-12	36.36	4.99	12.90	18.20	0.13	12.92	0.00	0.47	9.37	0.15	95.49	56

	Average	**36.91**	**4.87**	**13.29**	**17.77**	**0.13**	**12.69**	**0.00**	**0.44**	**9.28**	**0.12**	**95.51**	56
	Standard Deviation	**0.51**	**0.08**	**0.80**	**0.38**	**0.02**	**0.20**	**0.00**	**0.02**	**0.11**	**0.03**	**0.53**	1
MC: 6	25MC24_OX_5_BTE_1-1	35.78	4.88	12.77	18.51	0.16	11.91	0.06	0.46	9.40	0.23	94.17	53
	25MC24_OX_5_BTE_1-2	36.24	5.03	12.78	18.67	0.17	11.49	0.03	0.47	9.21	0.20	94.30	52
750 °C	25MC24_OX_5_BTE_1-3	36.26	5.04	12.76	18.42	0.17	11.43	0.04	0.42	9.37	0.18	94.09	53
150 MPa	25MC24_OX_5_BTE_1-4	36.33	4.82	14.54	18.04	0.13	11.95	0.04	0.46	9.11	0.22	95.66	54
	25MC24_OX_5_BTE_1-5	36.66	4.92	12.81	18.11	0.16	11.89	0.05	0.48	9.37	0.22	94.67	54
	25MC24_OX_5_BTE_1-6	36.68	5.01	13.50	17.14	0.15	13.12	0.00	0.44	9.44	0.19	95.67	58
	25MC24_OX_5_BTE_1-8	36.81	5.00	13.36	17.92	0.17	11.73	0.02	0.42	9.36	0.18	94.97	54
	25MC24_OX_5_BTE_1-9	36.15	4.98	12.75	17.85	0.13	11.16	0.05	0.42	9.43	0.25	93.18	53
	25MC24_OX_5_BTE_1-10	36.56	4.99	12.79	18.27	0.16	11.75	0.02	0.46	9.34	0.24	94.59	53
	25MC24_OX_5_BTE_1-11	36.13	4.99	12.63	18.44	0.15	11.44	0.01	0.43	9.36	0.23	93.84	53
	25MC24_OX_5_BTE_1-12	36.48	4.97	12.74	18.10	0.15	11.63	0.03	0.43	9.40	0.22	94.15	53
	25MC24_OX_5_BTE_1-14	37.15	4.95	13.07	18.83	0.12	11.56	0.04	0.45	9.39	0.21	95.78	52
	25MC24_OX_5_BTE_1-15	36.81	4.98	12.95	18.50	0.14	11.69	0.00	0.42	9.53	0.20	95.23	53
	25MC24_OX_5_BTE_1-16	35.27	4.94	12.36	19.40	0.14	11.74	0.02	0.42	9.21	0.22	93.71	52
	25MC24_OX_5_BTE_1-17	36.34	5.04	12.79	18.32	0.17	11.55	0.00	0.43	9.50	0.19	94.32	53
	25MC24_OX_5_BTE_1-18	36.30	4.75	13.82	18.85	0.15	11.64	0.02	0.42	9.36	0.20	95.50	52
	25MC24_OX_5_BTE_1-20	36.08	4.98	12.69	18.31	0.14	11.57	0.02	0.42	9.40	0.22	93.81	53
	25MC24_OX_5_BTE_1-21	36.41	4.96	12.88	18.36	0.14	11.57	0.02	0.42	9.42	0.19	94.36	53
	25MC24_OX_5_BTE_1-22	35.37	5.00	12.31	22.48	0.17	11.15	0.11	0.51	8.67	0.23	95.98	47
	25MC24_OX_5_BTE_1-23	36.41	5.05	12.80	18.65	0.14	11.87	0.04	0.43	9.34	0.27	95.01	53
	25MC24_OX_5_BTE_1-24	36.03	4.95	12.67	19.44	0.12	11.63	0.07	0.46	9.37	0.21	94.97	52

25MC24_OX_5_BTE_1-25	36.95	5.00	13.03	18.51	0.15	12.00	0.02	0.42	9.37	0.22	95.68	54
25MC24_OX_5_BTE_1-26	36.13	5.01	12.80	18.58	0.14	11.70	0.02	0.43	9.36	0.16	94.32	53
25MC24_OX_5_BTE_1-27	36.31	5.01	12.81	18.71	0.17	11.40	0.00	0.40	9.34	0.27	94.43	52
25MC24_OX_5_BTE_1-28	36.31	4.97	12.51	19.61	0.16	11.47	0.04	0.40	9.07	0.25	94.79	51
25MC24_OX_5_BTE_1-29	35.91	4.99	12.64	19.06	0.16	11.90	0.05	0.47	9.22	0.20	94.60	53
25MC24_OX_5_BTE_1-30	35.62	4.98	12.44	18.64	0.16	11.94	0.02	0.42	9.55	0.19	93.95	53
25MC24_OX_5_BTE_1-31	36.46	4.92	13.07	19.15	0.14	12.14	0.04	0.43	9.25	0.23	95.82	53
25MC24_OX_5_BTE_1-32	36.50	4.86	12.80	18.66	0.17	11.92	0.02	0.42	8.98	0.20	94.54	53
25MC24_OX_5_BTE_1-33	36.17	5.03	12.73	18.25	0.14	11.33	0.01	0.40	9.53	0.20	93.77	53
25MC24_OX_5_BTE_1-34	35.87	5.05	12.53	19.35	0.15	11.30	0.03	0.44	9.27	0.22	94.20	51
25MC24_OX_5_BTE_1-35	36.50	5.02	12.80	18.54	0.15	11.60	0.04	0.41	9.36	0.19	94.62	53
25MC24_OX_5_BTE_1-36	35.93	4.95	12.50	19.08	0.17	11.39	0.02	0.43	9.44	0.21	94.12	52
25MC24_OX_5_BTE_1-37	34.44	4.73	12.06	23.01	0.16	11.06	0.12	0.48	8.74	0.21	95.01	46
25MC24_OX_5_BTE_1-38	36.50	5.00	12.86	18.24	0.14	11.71	0.04	0.46	9.38	0.22	94.54	53
25MC24_OX_5_BTE_1-39	36.55	5.00	12.88	18.94	0.15	11.77	0.03	0.45	9.39	0.23	95.39	53
25MC24_OX_5_BTE_1-40	36.81	4.97	12.95	18.35	0.15	12.03	0.03	0.47	9.35	0.23	95.34	54
25MC24_OX_5_BTE_1-41	36.78	5.04	12.99	18.32	0.15	11.54	0.03	0.41	9.47	0.21	94.94	53
25MC24_OX_5_BTE_1-42	36.22	4.98	13.38	18.06	0.14	10.95	0.03	0.42	9.45	0.19	93.83	52
25MC24_OX_5_BTE_1-43	36.35	4.99	12.56	17.90	0.14	11.83	0.04	0.44	9.26	0.25	93.76	54
25MC24_OX_5_BTE_1-44	35.94	4.91	12.70	19.89	0.16	11.55	0.07	0.46	9.18	0.22	95.08	51
25MC24_OX_5_BTE_1-45	35.84	4.90	12.41	19.04	0.15	11.28	0.06	0.41	9.19	0.14	93.41	51
25MC24_OX_5_BTE_2-1	36.89	4.91	12.88	19.01	0.14	12.52	0.01	0.50	9.27	0.17	96.30	54
25MC24_OX_5_BTE_2-2	36.68	4.97	12.79	18.76	0.16	12.57	0.01	0.49	9.41	0.12	95.96	54

25MC24_OX_5_BTE_2-3	36.32	4.97	12.82	18.73	0.16	12.63	0.00	0.49	9.30	0.14	95.55	55
25MC24_OX_5_BTE_2-4	36.04	4.91	12.66	19.16	0.15	12.62	0.00	0.50	9.31	0.17	95.48	54
25MC24_OX_5_BTE_2-5	36.03	4.98	12.60	18.87	0.15	12.72	0.00	0.52	9.37	0.19	95.43	55
25MC24_OX_5_BTE_2-6	36.80	4.95	13.03	18.83	0.14	12.59	0.00	0.48	9.27	0.17	96.25	54
25MC24_OX_5_BTE_2-7	36.69	4.92	12.92	19.05	0.13	12.54	0.00	0.45	9.45	0.17	96.32	54
25MC24_OX_5_BTE_2-8	35.48	4.88	12.29	18.06	0.15	12.53	0.00	0.46	9.28	0.14	93.28	55
25MC24_OX_5_BTE_2-9	36.40	4.99	12.92	18.21	0.17	12.83	0.00	0.46	9.44	0.21	95.62	56
25MC24_OX_5_BTE_2-10	36.02	4.96	12.66	18.45	0.15	12.53	0.00	0.48	9.29	0.14	94.66	55
25MC24_OX_5_BTE_2-11	36.28	4.94	12.70	18.71	0.14	12.54	0.01	0.46	9.33	0.14	95.26	54
25MC24_OX_5_BTE_2-12	36.66	4.92	13.02	18.93	0.17	12.61	0.00	0.49	9.29	0.15	96.21	54
25MC24_OX_5_BTE_2-13	36.60	4.97	12.79	18.54	0.14	12.61	0.00	0.46	9.54	0.15	95.80	55
25MC24_OX_5_BTE_2-14	36.53	4.96	12.94	18.54	0.13	12.66	0.00	0.49	9.26	0.23	95.74	55
25MC24_OX_5_BTE_2-15	36.49	4.98	12.86	18.68	0.14	12.53	0.00	0.50	9.17	0.17	95.51	54
25MC24_OX_5_BTE_2-16	36.19	4.94	12.72	18.65	0.14	12.57	0.01	0.53	9.30	0.19	95.22	55
25MC24_OX_5_BTE_2-17	35.98	4.96	12.80	19.10	0.14	12.68	0.00	0.51	9.32	0.19	95.68	54
25MC24_OX_5_BTE_2-18	36.05	4.99	12.67	18.60	0.15	12.62	0.01	0.52	9.35	0.21	95.17	55
25MC24_OX_5_BTE_2-19	36.24	4.91	13.07	19.08	0.13	12.61	0.01	0.49	9.30	0.14	95.98	54
25MC24_OX_5_BTE_2-20	36.34	4.94	12.80	18.87	0.14	12.47	0.01	0.47	9.32	0.17	95.53	54
25MC24_OX_5_BTE_2-21	36.39	4.97	12.91	18.95	0.13	12.73	0.01	0.49	9.30	0.20	96.08	54
25MC24_OX_5_BTE_2-22	36.74	4.93	13.28	18.76	0.14	12.49	0.00	0.49	9.40	0.16	96.38	54
25MC24_OX_5_BTE_2-23	36.60	4.93	13.04	18.84	0.14	12.57	0.00	0.50	9.41	0.21	96.22	54
25MC24_OX_5_BTE_2-24	36.17	4.94	13.09	18.80	0.12	12.50	0.01	0.49	9.47	0.18	95.77	54
25MC24_OX_5_BTE_2-25	36.65	4.96	13.11	18.80	0.13	12.69	0.00	0.51	9.45	0.20	96.50	55

25MC24_OX_5_BTE_2-26	36.64	4.95	12.85	18.74	0.13	12.50	0.00	0.52	9.47	0.16	95.95	54
25MC24_OX_5_BTE_2-27	36.36	4.95	12.82	18.76	0.14	12.63	0.02	0.46	9.31	0.20	95.66	55
25MC24_OX_5_BTE_2-28	36.49	4.96	12.93	18.78	0.14	12.57	0.01	0.49	9.37	0.15	95.90	54
25MC24_OX_5_BTE_2-29	36.52	5.00	12.79	18.78	0.15	12.57	0.00	0.49	9.42	0.16	95.88	54
25MC24_OX_5_BTE_2-30	36.36	4.94	12.76	18.69	0.14	12.59	0.00	0.52	9.38	0.19	95.58	55
25MC24_OX_5_BTE_2-31	35.86	4.97	12.95	18.58	0.13	12.54	0.00	0.49	9.27	0.19	94.97	55
25MC24_OX_5_BTE_2-32	35.76	4.99	12.78	19.22	0.12	12.27	0.00	0.47	9.38	0.20	95.20	53
25MC24_OX_5_BTE_2-33	35.98	5.02	12.52	18.81	0.16	12.35	0.01	0.46	9.30	0.19	94.81	54
25MC24_OX_5_BTE_2-34	35.93	4.99	12.56	18.93	0.14	12.48	0.00	0.44	9.42	0.13	95.02	54
25MC24_OX_5_BTE_2-35	36.53	4.98	12.96	18.76	0.14	12.71	0.00	0.49	9.40	0.17	96.14	55
25MC24_OX_5_BTE_2-36	36.55	4.96	13.02	18.73	0.14	12.55	0.01	0.47	9.41	0.21	96.06	54
25MC24_OX_5_BTE_2-37	35.57	4.99	12.38	18.57	0.15	12.42	0.01	0.48	9.28	0.19	94.02	54
25MC24_OX_5_BTE_2-38	35.98	4.99	12.54	18.68	0.12	12.47	0.00	0.47	9.25	0.13	94.62	54
25MC24_OX_5_BTE_2-39	35.74	4.93	12.57	18.67	0.14	12.44	0.00	0.47	9.25	0.16	94.38	54
25MC24_OX_5_BTE_2-40	35.76	5.02	12.66	18.51	0.16	12.76	0.00	0.48	9.40	0.13	94.88	55
25MC24_OX_5_BTE_2-41	35.64	4.93	12.43	18.37	0.15	12.63	0.00	0.45	9.15	0.13	93.85	55
25MC24_OX_5_BTE_2-42	36.01	4.97	12.55	18.33	0.16	12.80	0.01	0.47	9.36	0.15	94.81	55
25MC24_OX_5_BTE_2-43	36.41	5.01	12.72	18.01	0.15	13.19	0.01	0.44	9.31	0.15	95.41	57
25MC24_OX_5_BTE_2-44	36.17	4.99	12.70	18.57	0.14	12.59	0.02	0.46	9.28	0.19	95.12	55
25MC24_OX_5_BTE_2-45	36.00	4.95	12.54	18.27	0.15	12.47	0.00	0.46	9.31	0.14	94.29	55
25MC24_OX_5_BTE_2-46	35.59	4.97	12.57	18.50	0.16	12.52	0.00	0.48	9.09	0.13	94.01	55
25MC24_OX_5_BTE_2-47	36.45	4.99	12.83	17.11	0.17	13.69	0.00	0.44	9.37	0.17	95.21	59
25MC24_OX_5_BTE_2-48	36.55	4.99	12.85	18.00	0.15	13.34	0.00	0.46	9.33	0.19	95.84	57

	25MC24_OX_5_BTE_2-49	36.39	4.98	12.83	17.67	0.15	13.38	0.00	0.44	9.47	0.15	95.45	57
	25MC24_OX_5_BTE_2-50	36.50	4.93	12.64	18.10	0.14	12.88	0.00	0.42	9.24	0.13	94.97	56
	Average	**36.25**	**4.96**	**12.81**	**18.69**	**0.15**	**12.19**	**0.02**	**0.46**	**9.33**	**0.19**	**95.04**	54
	Standard Deviation	**0.42**	**0.05**	**0.32**	**0.76**	**0.01**	**0.59**	**0.02**	**0.03**	**0.14**	**0.04**	**0.81**	2
MC: 7	25MC24_OX_6_BTE_1-3	36.60	4.98	12.85	18.30	0.12	12.28	0.00	0.44	9.47	0.01	95.06	54
	25MC24_OX_6_BTE_1-6	35.59	4.78	12.66	18.10	0.12	11.97	0.00	0.44	9.38	0.01	93.06	54
750 °C	25MC24_OX_6_BTE_1-12	36.44	4.86	12.74	18.63	0.13	12.17	0.00	0.43	9.53	0.00	94.91	54
125 MPa	25MC24_OX_6_BTE_1-14	36.33	4.88	12.82	18.23	0.13	12.23	0.00	0.44	9.46	0.03	94.53	54
	25MC24_OX_6_BTE_1-15	36.02	4.84	13.37	17.95	0.12	12.01	0.01	0.42	9.33	0.01	94.07	54
	25MC24_OX_6_BTE_1-17	35.36	4.89	12.46	18.53	0.13	11.95	0.00	0.43	9.51	0.04	93.31	53
	25MC24_OX_6_BTE_1-20	36.42	4.89	12.68	18.07	0.13	12.25	0.00	0.45	9.37	0.02	94.27	55
	25MC24_OX_6_BTE_1-23	36.66	4.80	12.84	17.22	0.15	12.39	0.00	0.42	9.14	0.00	93.62	56
	25MC24_OX_6_BTE_1-24	36.84	4.86	12.89	18.24	0.12	12.19	0.01	0.44	9.38	0.00	94.97	54
	25MC24_OX_6_BTE_1-25	36.94	4.95	12.93	18.04	0.12	12.28	0.00	0.44	9.57	0.02	95.29	55
	25MC24_OX_6_BTE_1-26	36.97	4.91	12.96	17.22	0.16	12.86	0.00	0.45	9.48	0.03	95.03	57
	25MC24_OX_6_BTE_1-27	37.08	4.92	13.11	16.68	0.18	13.20	0.00	0.41	9.46	0.04	95.08	59
	25MC24_OX_6_BTE_1-28	36.39	4.87	12.74	18.12	0.12	12.16	0.00	0.42	9.24	0.02	94.06	54
	25MC24_OX_6_BTE_1-29	36.02	4.84	12.62	18.12	0.11	11.99	0.00	0.41	9.07	0.00	93.18	54
	25MC24_OX_6_BTE_1-30	36.57	4.94	12.68	17.73	0.13	12.43	0.00	0.42	9.31	0.03	94.24	56
	25MC24_OX_6_BTE_1-31	36.83	4.88	12.87	18.36	0.13	12.26	0.02	0.45	9.46	0.01	95.28	54
	25MC24_OX_6_BTE_1-32	37.14	4.76	12.73	16.91	0.15	12.51	0.00	0.44	9.13	0.01	93.78	57
	25MC24_OX_6_BTE_1-33	36.22	4.89	12.63	18.23	0.14	12.09	0.01	0.45	9.35	0.04	94.03	54
	25MC24_OX_6_BTE_1-34	36.35	4.96	12.66	18.05	0.14	12.12	0.01	0.47	9.61	0.01	94.38	54

25MC24_OX_6_BTE_1-35	36.70	5.02	12.67	18.06	0.13	12.35	0.01	0.44	9.44	0.06	94.88	55
25MC24_OX_6_BTE_1-36	36.77	5.04	12.71	18.18	0.11	12.27	0.00	0.44	9.56	0.06	95.14	55
25MC24_OX_6_BTE_1-37	36.97	4.95	13.38	18.22	0.12	12.30	0.00	0.42	9.56	0.08	95.98	55
25MC24_OX_6_BTE_1-40	36.22	5.02	12.75	18.36	0.12	12.30	0.00	0.47	9.53	0.05	94.82	54
25MC24_OX_6_BTE_1-41	36.32	4.83	13.12	18.50	0.11	11.34	0.00	0.40	9.45	0.05	94.12	52
25MC24_OX_6_BTE_1-42	37.29	5.09	13.27	18.27	0.12	12.55	0.02	0.46	9.47	0.06	96.59	55
25MC24_OX_6_BTE_1-45	36.72	4.94	12.82	18.15	0.12	12.33	0.00	0.43	9.45	0.05	95.00	55
25MC24_OX_6_BTE_1-46	37.08	4.97	12.93	17.09	0.17	12.62	0.01	0.43	9.53	0.04	94.86	57
25MC24_OX_6_BTE_1-47	36.75	4.95	13.05	17.26	0.16	12.69	0.00	0.43	9.52	0.05	94.86	57
25MC24_OX_6_BTE_1-48	36.37	4.96	12.63	18.13	0.15	12.39	0.00	0.39	9.45	0.00	94.47	55
25MC24_OX_6_BTE_1-49	36.77	4.90	12.81	18.11	0.13	12.41	0.00	0.43	9.41	0.05	95.01	55
25MC24_OX_6_BTE_1-50	36.39	4.98	12.70	17.80	0.13	11.90	0.00	0.44	9.41	0.02	93.75	54
25MC24_OX_6_BTE_2-1	37.07	4.84	13.74	17.98	0.12	13.80	0.00	0.53	9.13	0.03	97.24	58
25MC24_OX_6_BTE_2-2	37.01	4.86	13.53	18.48	0.12	13.68	0.02	0.52	9.25	0.03	97.50	57
25MC24_OX_6_BTE_2-3	36.85	4.91	13.12	17.86	0.14	13.79	0.00	0.50	9.12	0.05	96.33	58
25MC24_OX_6_BTE_2-5	36.64	4.89	13.59	17.94	0.12	13.70	0.01	0.50	9.21	0.02	96.62	58
25MC24_OX_6_BTE_2-6	36.14	4.80	13.05	17.75	0.13	13.87	0.00	0.51	9.09	0.05	95.36	58
25MC24_OX_6_BTE_2-9	35.66	4.97	12.62	18.13	0.14	12.13	0.00	0.45	9.46	0.06	93.61	54
25MC24_OX_6_BTE_2-10	36.22	4.98	13.35	18.11	0.11	12.52	0.00	0.44	9.47	0.04	95.22	55
25MC24_OX_6_BTE_2-11	35.83	4.86	13.55	18.60	0.12	12.41	0.02	0.47	9.35	0.03	95.24	54
25MC24_OX_6_BTE_2-12	35.72	4.92	13.13	18.79	0.12	12.39	0.00	0.47	9.24	0.03	94.80	54
25MC24_OX_6_BTE_2-13	36.24	4.94	12.85	18.46	0.12	12.80	0.01	0.45	9.44	0.04	95.36	55
25MC24_OX_6_BTE_2-14	35.54	4.97	12.69	18.41	0.13	12.47	0.00	0.45	9.48	0.04	94.19	55

25MC24_OX_6_BTE_2-15	35.90	4.92	13.08	18.49	0.11	12.80	0.02	0.48	9.30	0.02	95.12	55
25MC24_OX_6_BTE_2-16	36.31	4.94	13.37	18.15	0.12	12.67	0.00	0.48	9.37	0.00	95.41	55
25MC24_OX_6_BTE_2-17	36.35	4.94	13.24	18.02	0.12	12.89	0.01	0.50	9.33	0.01	95.40	56
25MC24_OX_6_BTE_2-18	37.17	4.94	13.33	17.98	0.10	13.03	0.00	0.48	9.33	0.05	96.41	56
25MC24_OX_6_BTE_2-19	36.59	4.89	13.20	18.04	0.13	12.93	0.00	0.46	9.26	0.02	95.50	56
25MC24_OX_6_BTE_2-21	37.77	4.88	13.68	18.07	0.13	13.29	0.00	0.50	9.31	0.04	97.65	57
25MC24_OX_6_BTE_2-22	37.06	4.93	13.55	17.97	0.12	13.59	0.00	0.49	9.32	0.05	97.05	57
25MC24_OX_6_BTE_2-23	37.18	4.97	13.41	18.20	0.12	12.99	0.00	0.50	9.24	0.01	96.62	56
25MC24_OX_6_BTE_2-24	36.27	4.88	13.47	18.20	0.12	12.57	0.01	0.46	9.33	0.01	95.30	55
25MC24_OX_6_BTE_2-25	36.20	4.76	13.89	18.29	0.14	12.35	0.00	0.46	9.40	0.05	95.52	55
25MC24_OX_6_BTE_2-26	35.67	4.86	13.95	17.82	0.12	12.18	0.01	0.42	9.14	0.02	94.19	55
25MC24_OX_6_BTE_2-27	36.09	4.75	14.09	18.15	0.11	12.53	0.01	0.47	9.26	0.04	95.50	55
25MC24_OX_6_BTE_2-28	36.56	4.81	13.69	18.52	0.13	12.63	0.01	0.50	9.32	0.03	96.19	55
25MC24_OX_6_BTE_2-29	36.91	4.84	13.57	17.57	0.14	12.89	0.00	0.48	9.44	0.01	95.85	57
25MC24_OX_6_BTE_2-30	36.38	4.94	13.04	17.61	0.15	13.16	0.01	0.46	9.23	0.01	94.98	57
25MC24_OX_6_BTE_2-31	35.99	4.63	15.63	17.21	0.14	13.07	0.00	0.48	8.89	0.03	96.07	58
25MC24_OX_6_BTE_2-32	36.31	4.91	13.15	17.89	0.16	13.57	0.04	0.53	9.13	0.02	95.69	57
25MC24_OX_6_BTE_2-33	36.13	4.87	13.56	17.64	0.14	13.41	0.01	0.49	9.10	0.03	95.37	58
25MC24_OX_6_BTE_2-34	34.11	4.67	16.10	17.84	0.13	12.79	0.01	0.46	8.85	0.05	95.00	56
25MC24_OX_6_BTE_2-35	36.42	4.78	13.67	18.24	0.12	13.27	0.02	0.50	9.02	0.06	96.11	56
25MC24_OX_6_BTE_2-36	35.94	4.60	14.17	17.84	0.09	13.05	0.01	0.49	9.11	0.03	95.33	57
25MC24_OX_6_BTE_2-37	37.25	4.70	14.94	17.61	0.11	13.26	0.00	0.49	9.19	0.00	97.53	57
25MC24_OX_6_BTE_2-38	37.22	4.95	13.69	18.26	0.12	13.18	0.00	0.49	9.28	0.03	97.22	56

25MC24_OX_6_BTE_2-39	36.60	4.88	13.11	18.21	0.12	13.03	0.02	0.50	9.43	0.01	95.91	56
25MC24_OX_6_BTE_2-40	37.60	4.94	13.65	18.15	0.13	13.43	0.00	0.50	9.32	0.04	97.76	57
Average	**36.48**	**4.89**	**13.25**	**18.02**	**0.13**	**12.67**	**0.00**	**0.46**	**9.33**	**0.03**	**95.25**	56
Standard Deviation	**0.59**	**0.09**	**0.66**	**0.41**	**0.02**	**0.55**	**0.01**	**0.03**	**0.16**	**0.02**	**1.11**	1

Table A-0-5 Experimental individual glass analyses (wt%)

EXP	Point	SiO_2	TiO_2	Al_2O_3	FeO	MnO	MgO	CaO	Na_2O	K_2O	Total	Total $+H_2O$
BT:1	25BT_3B_OX_1_Glass_5-4	75.86	0.16	14.20	0.60	0.03	0.07	1.04	3.18	4.86	95.02	100.89
	25BT_3B_OX_1_Glass_6-1	75.07	0.13	14.15	0.82	0.02	0.06	1.03	3.84	4.88	94.18	100.05
800 °C	25BT_3B_OX_1_Glass_6-2	75.56	0.16	13.93	0.70	0.00	0.08	1.08	3.58	4.87	93.46	99.32
200 MPa	25BT_3B_OX_1_Glass_6-3	75.42	0.10	14.16	0.69	0.04	0.07	1.01	3.57	4.98	93.96	99.83
*H_2O: 5.86	25BT_3B_OX_1_Glass_6-4	75.98	0.13	14.00	0.76	0.03	0.07	1.01	2.98	5.02	92.94	98.81
	25BT_3B_OX_1_Glass_6-5	75.27	0.12	13.87	0.77	0.05	0.08	1.06	3.61	5.15	94.47	100.33
	25BT_3B_OX_1_Glass_6-6	75.82	0.11	14.20	0.66	0.03	0.07	1.02	3.17	4.91	93.00	98.87
	25BT_3B_OX_1_Glass_6-7	75.93	0.18	13.78	0.67	0.00	0.07	1.04	3.60	4.75	94.26	100.13
	25BT_3B_OX_1_Glass_6-8	75.45	0.17	13.75	0.73	0.03	0.07	1.07	3.87	4.84	94.31	100.17
	25BT_3B_OX_1_Glass_6-9	75.60	0.14	14.16	0.72	0.04	0.07	1.05	3.22	5.00	92.94	98.81
	25BT_3B_OX_1_Glass_6-10	75.63	0.18	14.12	0.80	0.00	0.08	1.05	3.21	4.97	94.06	99.92
	25BT_3B_OX_1_Glass_6-11	75.39	0.16	14.32	0.76	0.03	0.07	0.95	3.45	4.85	94.23	100.10
	25BT_3B_OX_1_Glass_6-12	75.51	0.16	13.85	1.00	0.02	0.08	1.08	3.30	4.95	94.00	99.87
	25BT_3B_OX_1_Glass_7-1	76.88	0.13	13.59	0.70	-0.01	0.09	1.02	2.82	4.82	93.05	98.91
	25BT_3B_OX_1_Glass_7-2	76.30	0.19	13.80	0.71	0.02	0.08	0.93	3.28	4.67	93.27	99.13
	25BT_3B_OX_1_Glass_7-3	76.41	0.14	13.64	0.66	0.02	0.08	1.03	3.24	4.77	92.01	97.87
	25BT_3B_OX_1_Glass_7-4	76.94	0.13	13.63	0.66	0.04	0.09	0.98	2.74	4.77	92.33	98.19
	25BT_3B_OX_1_Glass_7-5	76.28	0.15	13.82	0.69	0.00	0.09	1.00	2.99	4.95	92.93	98.80
	25BT_3B_OX_1_Glass_7-6	76.34	0.19	13.86	0.72	0.02	0.08	0.97	2.87	4.96	93.28	99.14
	25BT_3B_OX_1_Glass_7-7	76.12	0.10	13.79	0.66	0.02	0.08	1.06	3.21	4.89	92.95	98.82
	25BT_3B_OX_1_Glass_7-8	76.61	0.15	13.51	0.67	0.03	0.09	1.00	3.04	4.91	93.09	98.95
	25BT_3B_OX 1 Glass_7-9	76.84	0.13	13.78	0.68	0.03	0.09	1.04	2.44	4.95	93.11	98.98
	25BT_3B_OX_1_Glass_7-10	76.36	0.14	13.40	0.76	0.02	0.08	1.23	2.87	4.84	93.03	98.89
	25BT_3B_OX_1_Glass_9-1	76.30	0.12	13.54	1.19	0.01	0.08	1.02	3.14	4.62	94.30	100.17
	25BT_3B_OX_1_Glass_9-2	76.00	0.12	13.50	1.10	0.04	0.07	0.96	3.44	4.76	94.07	99.93
	25BT_3B_OX_1_Glass_9-3	76.40	0.16	13.56	0.92	0.04	0.08	0.94	3.20	4.72	93.92	99.78
	25BT_3B_OX_1_Glass_9-4	75.82	0.19	13.60	1.16	0.05	0.09	0.89	3.43	4.75	93.78	99.65
	25BT_3B_OX_1_Glass_9-5	76.33	0.21	13.79	1.34	0.06	0.08	0.99	2.44	4.75	92.72	98.58
	25BT_3B_OX_1_Glass_9-7	75.90	0.17	13.53	1.33	0.06	0.08	0.97	3.13	4.84	94.08	99.94
	25BT_3B_OX_1_Glass_9-8	76.26	0.19	13.69	1.11	0.02	0.07	0.95	2.76	4.90	93.28	99.14

	25BT_3B_OX_1_Glass_9-9	76.52	0.18	13.31	1.12	0.01	0.07	1.01	2.97	4.80	93.45	99.32
	25BT_3B_OX_1_Glass_10-2	74.87	0.20	14.12	1.36	0.04	0.07	1.14	3.35	4.80	93.60	99.46
	25BT_3B_OX_1_Glass_10-5	77.78	0.26	14.39	1.39	0.05	0.07	1.06	1.16	3.84	91.91	97.78
	25BT_3B_OX_1_Glass_10-6	75.71	0.16	13.89	1.34	0.02	0.08	1.05	2.66	5.13	91.81	97.67
	25BT_3B_OX_1_Glass_10-10	75.34	0.14	13.83	1.26	0.04	0.06	1.06	3.13	5.15	91.95	97.82
	25BT_3B_OX_1_Glass_11-1	76.03	0.09	13.86	0.85	0.03	0.06	1.01	3.14	4.90	92.68	98.54
	25BT_3B_OX_1_Glass_11-2	75.97	0.16	13.71	0.85	0.02	0.08	1.08	3.13	5.01	92.03	97.90
	25BT_3B_OX_1_Glass_11-3	76.02	0.18	14.01	0.80	0.01	0.07	1.08	2.80	5.01	92.78	98.64
	25BT_3B_OX_1_Glass_11-4	75.95	0.12	13.96	0.83	0.02	0.08	1.05	3.12	4.90	93.40	99.27
	25BT_3B_OX_1_Glass_11-5	75.67	0.14	14.11	0.89	0.04	0.07	1.00	3.08	4.98	93.64	99.50
	25BT_3B_OX_1_Glass_11-6	76.88	0.15	13.74	0.89	0.03	0.08	1.06	2.23	4.94	92.73	98.59
	25BT_3B_OX_1_Glass_11-7	75.89	0.18	13.93	0.91	0.02	0.07	1.08	3.01	4.90	93.64	99.50
	25BT_3B_OX_1_Glass_11-8	76.08	0.18	14.01	0.85	0.04	0.08	1.09	2.85	4.78	94.47	100.33
	25BT_3B_OX_1_Glass_11-9	75.86	0.18	13.92	0.84	0.02	0.07	0.98	3.33	4.82	94.07	99.94
	25BT_3B_OX_1_Glass_11-11	76.08	0.15	14.19	0.89	0.04	0.07	1.03	2.73	4.79	93.75	99.62
	25BT_3B_OX_1_Glass_11-12	78.06	0.19	14.08	0.97	-0.01	0.06	1.10	1.33	4.20	91.76	97.63
	25BT_3B_OX_1_Glass_11-13	79.06	0.14	14.12	0.93	0.02	0.09	1.13	0.85	3.65	91.89	97.75
	25BT_3B_OX_1_Glass_11-14	76.25	0.16	13.80	0.85	0.02	0.08	1.08	2.82	4.92	92.96	98.82
	Average	**76.14**	**0.16**	**13.87**	**0.89**	**0.03**	**0.08**	**1.03**	**2.99**	**4.82**	**93.30**	**99.17**
	Standard Deviation	**0.74**	**0.03**	**0.25**	**0.22**	**0.02**	**0.01**	**0.06**	**0.60**	**0.27**	**0.82**	**0.82**
BT: 2 750 °C 200 MPa *H_2O: 6.06	25BT_3B_OX_6_Glass_1-1	77.75	0.11	12.43	0.78	0.02	0.06	0.70	3.35	4.81	94.77	100.83
	25BT_3B_OX_6_Glass_1-3	77.55	0.14	12.53	1.05	0.04	0.06	0.72	3.13	4.76	94.18	100.24
	25BT_3B_OX_6_Glass_1-5	78.08	0.08	12.54	0.69	0.06	0.04	0.72	3.30	4.49	94.13	100.19
	25BT_3B_OX_6_Glass_1-6	78.08	0.11	12.51	0.83	0.00	0.05	0.71	3.23	4.49	94.31	100.37
	25BT_3B_OX_6_Glass_1-8	77.66	0.09	12.63	0.78	0.04	0.05	0.67	3.19	4.88	94.04	100.10

25BT_3B_OX_6_Glass_1-9	77.76	0.09	12.82	0.72	0.03	0.05	0.76	2.94	4.83	94.87	100.92
25BT_3B_OX_6_Glass_1-10	77.72	0.11	12.64	0.84	0.05	0.06	0.66	3.14	4.79	94.35	100.41
25BT_3B_OX_6_Glass_1-11	78.01	0.12	12.51	0.68	0.04	0.06	0.72	3.12	4.75	94.68	100.74
25BT_3B_OX_6_Glass_1-12	77.58	0.10	12.75	0.71	0.02	0.04	0.67	3.34	4.81	94.59	100.65
25BT_3B_OX_6_Glass_1-13	77.40	0.06	12.89	0.87	0.03	0.05	0.74	3.19	4.75	94.69	100.75
25BT_3B_OX_6_Glass_1-15	77.85	0.10	12.31	1.04	0.03	0.06	0.60	3.29	4.71	94.83	100.89
25BT_3B_OX_6_Glass_1-16	78.00	0.09	12.42	0.98	0.04	0.05	0.64	3.07	4.68	94.69	100.75
25BT_3B_OX_6_Glass_1-17	78.53	0.05	12.32	0.81	0.07	0.06	0.72	2.75	4.70	94.80	100.85
25BT_3B_OX_6_Glass_1-18	77.87	0.09	12.69	0.64	0.01	0.05	0.71	3.19	4.77	93.74	99.79
25BT_3B_OX_6_Glass_1-19	77.99	0.10	12.68	0.58	0.03	0.05	0.67	3.10	4.80	93.76	99.81
25BT_3B_OX_6_Glass_1-20	77.78	0.08	12.81	0.64	0.03	0.06	0.72	3.13	4.75	94.35	100.41
25BT_3B_OX_6_Glass_1-21	78.05	0.12	12.47	0.57	0.02	0.06	0.72	3.38	4.61	93.90	99.95
25BT_3B_OX_6_Glass_1-22	78.54	0.13	12.38	0.65	0.01	0.04	0.68	3.08	4.46	93.26	99.32
25BT_3B_OX_6_Glass_1-23	78.51	0.08	12.62	0.63	0.03	0.05	0.70	2.85	4.56	93.29	99.34
25BT_3B_OX_6_Glass_1-24	77.95	0.10	12.76	0.72	0.03	0.06	0.69	3.27	4.43	93.74	99.80
25BT_3B_OX_6_Glass_1-25	77.67	0.09	12.68	0.66	0.04	0.07	0.66	3.36	4.76	94.63	100.68
25BT_3B_OX_6_Glass_1-28	77.68	0.14	12.57	0.60	0.03	0.06	0.78	3.40	4.74	94.85	100.90
25BT_3B_OX_6_Glass_1-29	77.29	0.08	12.90	0.62	0.03	0.05	0.75	3.51	4.77	94.22	100.27
25BT_3B_OX_6_Glass_1-30	77.39	0.07	12.95	0.71	0.01	0.05	0.76	3.30	4.75	94.60	100.66
25BT_3B_OX_6_Glass_1-32	77.45	0.11	12.78	0.64	0.07	0.06	0.77	3.30	4.79	94.84	100.90
25BT_3B_OX_6_Glass_2-1	76.13	0.22	13.32	0.69	0.02	0.30	0.85	3.59	4.87	94.21	100.26
25BT_3B_OX_6_Glass_2-2	77.30	0.14	13.13	0.48	0.01	0.08	0.76	3.34	4.79	94.12	100.17
25BT_3B_OX_6_Glass_4-34	75.11	0.38	13.36	1.27	0.04	1.00	0.73	3.03	5.06	94.57	100.63
25BT_3B_OX_6_Glass_2-3	77.43	0.17	12.98	0.58	0.00	0.06	0.73	3.32	4.72	93.81	99.87
25BT_3B_OX_6_Glass_2-5	77.72	0.15	13.01	0.53	-0.01	0.06	0.86	3.04	4.64	93.38	99.43

25BT_3B_OX_6_Glass_2-6	77.53	0.17	12.92	0.52	0.01	0.07	0.73	3.15	4.90	93.61	99.67
25BT_3B_OX_6_Glass_2-7	77.39	0.15	13.07	0.51	0.03	0.07	0.83	3.21	4.73	93.87	99.93
25BT_3B_OX_6_Glass_2-8	77.31	0.12	13.03	0.53	0.03	0.08	0.76	3.29	4.83	94.38	100.44
25BT_3B_OX_6_Glass_2-9	77.18	0.15	13.27	0.58	0.00	0.07	0.79	3.18	4.77	94.26	100.31
25BT_3B_OX_6_Glass_2-10	77.42	0.16	13.06	0.52	0.01	0.07	0.78	3.22	4.74	94.65	100.70
25BT_3B_OX_6_Glass_2-11	76.86	0.15	13.01	0.53	0.03	0.07	0.82	3.66	4.86	94.56	100.62
25BT_3B_OX_6_Glass_2-12	77.56	0.11	12.95	0.56	0.00	0.08	0.84	3.05	4.82	94.16	100.22
25BT_3B_OX_6_Glass_2-13	77.23	0.11	13.14	0.54	0.00	0.09	0.75	3.30	4.86	93.72	99.77
25BT_3B_OX_6_Glass_2-14	76.93	0.16	13.14	0.62	0.01	0.24	0.90	3.18	4.77	94.78	100.84
25BT_3B_OX_6_Glass_2-15	77.18	0.16	12.88	0.56	0.02	0.06	0.80	3.54	4.79	94.72	100.78
25BT_3B_OX_6_Glass_2-16	77.12	0.15	13.07	0.56	0.03	0.05	0.88	3.15	4.87	94.66	100.72
25BT_3B_OX_6_Glass_2-17	76.91	0.11	13.07	0.59	0.03	0.07	0.82	3.50	4.89	94.01	100.07
25BT_3B_OX_6_Glass_2-18	77.13	0.10	13.22	0.56	0.04	0.07	0.77	3.21	4.91	94.36	100.41
25BT_3B_OX_6_Glass_2-19	76.00	0.29	13.02	0.99	0.02	0.54	0.75	3.34	5.04	94.21	100.26
25BT_3B_OX_6_Glass_2-20	76.79	0.24	12.97	0.72	0.04	0.32	0.74	3.26	4.93	93.68	99.74
25BT_3B_OX_6_Glass_2-21	77.32	0.13	13.04	0.55	0.03	0.07	0.85	3.05	4.93	93.75	99.80
25BT_3B_OX_6_Glass_2-22	76.80	0.14	13.19	0.57	0.02	0.06	0.77	3.64	4.80	94.11	100.16
25BT_3B_OX_6_Glass_2-23	77.36	0.15	13.08	0.50	0.00	0.06	0.81	3.24	4.78	93.93	99.99
25BT_3B_OX_6_Glass_2-24	77.23	0.12	13.11	0.62	-0.02	0.07	0.79	3.29	4.78	94.33	100.39
25BT_3B_OX_6_Glass_2-25	77.42	0.17	13.01	0.56	0.02	0.11	0.81	3.11	4.77	94.21	100.27
25BT_3B_OX_6_Glass_2-26	77.18	0.12	13.24	0.52	0.04	0.06	0.82	3.31	4.70	94.02	100.08
25BT_3B_OX_6_Glass_2-28	77.41	0.15	13.07	0.52	0.03	0.13	0.79	3.15	4.70	94.08	100.13
25BT_3B_OX_6_Glass_2-29	76.82	0.22	13.25	0.65	0.04	0.13	0.78	3.28	4.79	93.97	100.03
25BT_3B_OX_6_Glass_3-8	77.36	0.13	12.71	0.92	0.04	0.03	0.35	4.04	4.40	94.79	100.85
25BT_3B_OX_6_Glass_3-9	77.58	0.06	12.56	0.79	0.01	0.03	0.35	4.07	4.59	94.75	100.81

25BT_3B_OX_6_Glass_3-12	77.18	0.10	12.60	1.09	0.04	0.04	0.39	4.26	4.27	94.53	100.59
25BT_3B_OX_6_Glass_4-1	77.33	0.09	13.13	0.55	0.02	0.06	0.71	3.38	4.71	94.66	100.71
25BT_3B_OX_6_Glass_4-3	77.42	0.10	12.85	0.56	0.05	0.06	0.80	3.38	4.79	94.16	100.22
25BT_3B_OX_6_Glass_4-4	77.01	0.10	13.58	0.49	-0.02	0.06	0.87	3.20	4.71	94.31	100.36
25BT_3B_OX_6_Glass_4-5	77.20	0.15	13.33	0.49	0.00	0.06	0.76	3.20	4.80	93.90	99.96
25BT_3B_OX_6_Glass_4-6	76.46	0.23	13.20	0.87	0.02	0.48	0.77	3.04	4.94	93.46	99.52
25BT_3B_OX_6_Glass_4-8	77.14	0.19	13.11	0.59	0.02	0.27	0.74	3.05	4.88	93.57	99.63
25BT_3B_OX_6_Glass_4-9	77.36	0.13	13.42	0.55	0.02	0.11	0.74	2.86	4.82	93.89	99.95
25BT_3B_OX_6_Glass_4-10	77.28	0.17	13.09	0.55	0.02	0.07	0.81	3.22	4.80	93.47	99.53
25BT_3B_OX_6_Glass_4-11	77.52	0.14	12.97	0.53	0.02	0.05	0.77	3.15	4.83	94.09	100.14
25BT_3B_OX_6_Glass_4-12	76.90	0.23	12.95	0.74	0.02	0.34	0.81	3.11	4.89	94.44	100.50
25BT_3B_OX_6_Glass_4-14	77.46	0.13	13.00	0.53	0.02	0.07	0.81	3.11	4.86	93.94	100.00
25BT_3B_OX_6_Glass_4-16	76.67	0.22	13.03	0.74	0.04	0.33	0.74	3.37	4.85	94.32	100.38
25BT_3B_OX_6_Glass_4-17	77.44	0.19	13.00	0.52	0.05	0.07	0.81	3.08	4.84	94.05	100.11
25BT_3B_OX_6_Glass_4-18	77.52	0.12	13.07	0.55	0.03	0.07	0.78	3.14	4.70	94.02	100.08
25BT_3B_OX_6_Glass_4-19	77.53	0.19	13.28	0.50	-0.01	0.06	0.79	2.90	4.76	93.78	99.83
25BT_3B_OX_6_Glass_4-20	77.61	0.13	13.18	0.59	-0.01	0.07	0.77	2.86	4.79	93.15	99.21
25BT_3B_OX_6_Glass_4-21	77.34	0.15	12.97	0.55	0.02	0.07	0.88	3.11	4.85	94.15	100.21
25BT_3B_OX_6_Glass_4-22	79.20	0.14	13.35	0.58	0.03	0.08	1.17	1.46	3.67	93.22	99.27
25BT_3B_OX_6_Glass_4-23	77.67	0.12	12.97	0.48	-0.01	0.08	0.79	3.07	4.80	94.12	100.18
25BT_3B_OX_6_Glass_4-24	77.88	0.13	13.00	0.47	-0.02	0.09	0.75	2.92	4.77	93.88	99.94
25BT_3B_OX_6_Glass_4-25	77.39	0.15	13.03	0.54	0.02	0.07	0.78	3.39	4.63	94.54	100.60
25BT_3B_OX_6_Glass_4-26	76.27	0.23	13.45	0.74	0.02	0.34	0.82	3.31	4.73	94.53	100.58
25BT_3B_OX_6_Glass_4-27	77.41	0.12	13.20	0.54	0.00	0.06	0.73	3.01	4.91	94.17	100.23
25BT_3B_OX_6_Glass_4-28	77.23	0.15	12.67	0.93	0.01	0.07	0.75	3.43	4.75	93.43	99.49

	25BT_3B_OX_6_Glass_4-29	77.13	0.13	12.92	0.53	0.02	0.07	0.78	3.60	4.81	94.03	100.09
	25BT_3B_OX_6_Glass_4-30	79.69	0.15	13.09	0.60	0.01	0.07	0.82	1.43	4.14	92.71	98.76
	25BT_3B_OX_6_Glass_4-31	77.33	0.16	13.12	0.51	0.00	0.05	0.78	3.22	4.81	94.32	100.38
	25BT_3B_OX_6_Glass_4-32	77.45	0.11	12.94	0.53	0.03	0.07	0.86	3.14	4.83	93.86	99.91
	25BT_3B_OX_6_Glass_4-33	77.33	0.13	13.04	0.54	0.04	0.06	0.79	3.29	4.79	94.56	100.62
	25BT_3B_OX_6_Glass_4-35	77.31	0.14	12.94	0.59	0.04	0.06	0.78	3.33	4.83	94.85	100.90
	Average	**77.42**	**0.14**	**12.94**	**0.65**	**0.02**	**0.11**	**0.76**	**3.21**	**4.75**	**94.16**	**100.22**
	Standard Deviation	**0.61**	**0.05**	**0.28**	**0.16**	**0.02**	**0.14**	**0.10**	**0.37**	**0.19**	**0.47**	**0.47**
BT:3 700 °C 200 MPa *H_2O: 6.21	25BT3B_OX_4_Glass_1_1	78.53	0.01	11.91	0.67	0.03	0.01	0.59	3.48	4.75	93.36	99.57
	25BT3B_OX_4_Glass_1_2	78.84	0.09	11.90	0.67	0.02	0.02	0.63	3.04	4.79	93.63	99.84
	25BT3B_OX_4_Glass_1_3	78.54	0.06	11.94	0.73	0.01	0.01	0.58	3.31	4.81	92.57	98.78
	25BT3B_OX_4_Glass_1_4	79.43	0.00	11.76	0.63	0.03	0.02	0.62	2.66	4.90	92.93	99.14
	25BT3B_OX_4_Glass_1_5	79.00	0.08	12.12	0.69	0.02	0.01	0.60	2.62	4.87	92.86	99.07
	25BT3B_OX_4_Glass_1_6	78.90	0.08	11.99	0.71	0.05	0.02	0.65	2.84	4.77	93.76	99.96
	25BT3B_OX_4_Glass_1_7	78.97	0.05	12.06	0.65	0.03	0.02	0.63	2.68	4.91	93.81	100.02
	25BT3B_OX_4_Glass_1_8	79.19	0.09	12.20	0.68	-0.01	0.02	0.61	2.36	4.86	92.15	98.36
	25BT3B_OX_4_Glass_1_11	79.41	0.08	12.03	0.73	-0.01	0.01	0.62	2.22	4.91	93.11	99.32
	25BT3B_OX_4_Glass_1_12	79.33	0.04	12.12	0.67	-0.01	0.03	0.66	2.34	4.81	93.25	99.46
	25BT3B_OX_4_Glass_1_14	79.69	0.06	12.20	0.66	0.03	0.02	0.62	1.93	4.79	93.04	99.25
	25BT3B_OX_4_Glass_3_1	78.95	0.03	11.84	0.39	-0.02	0.00	0.57	3.53	4.70	92.79	99.00
	25BT3B_OX_4_Glass_3_2	79.35	0.02	11.73	0.38	0.02	0.01	0.59	3.19	4.70	92.71	98.92
	25BT3B_OX_4_Glass_3_4	79.83	0.06	12.04	0.40	0.02	0.02	0.62	2.26	4.74	91.91	98.11
	25BT3B_OX_4_Glass_3_5	79.64	0.05	11.76	0.39	-0.01	-0.01	0.65	2.80	4.72	91.97	98.18
	25BT3B_OX_4_Glass_3_6	79.34	0.04	11.94	0.37	0.00	0.02	0.61	2.85	4.83	92.38	98.59
	25BT3B_OX_4_Glass_3_7	78.89	0.05	12.25	0.43	0.03	0.00	0.64	2.96	4.74	92.99	99.20
	25BT3B_OX_4_Glass_3_8	78.79	0.04	12.07	0.39	0.00	0.02	0.63	3.27	4.79	93.58	99.78
	25BT3B_OX_4_Glass_3_9	79.15	0.05	12.38	0.38	-0.01	0.00	0.65	2.57	4.82	93.32	99.53
	25BT3B_OX_4_Glass_3_10	79.11	0.03	12.00	0.36	0.03	0.01	0.63	3.00	4.83	92.92	99.13
	25BT3B_OX_4_Glass_3_11	79.23	0.08	12.28	0.39	0.00	0.01	0.65	2.60	4.76	92.22	98.43
	25BT3B_OX_4_Glass_3_13	79.35	0.00	11.83	0.41	0.05	0.01	0.58	3.08	4.68	94.17	100.38
	25BT3B_OX_4_Glass_3_14	79.21	0.02	11.99	0.35	0.04	0.02	0.61	3.13	4.64	93.10	99.31

25BT3B_OX_4_Glass_3_15	79.24	0.01	11.79	0.41	0.00	0.03	0.55	3.10	4.86	93.08	99.29
25BT3B_OX_4_Glass_3_16	79.29	0.04	11.91	0.41	0.02	0.01	0.57	3.03	4.72	93.38	99.59
25BT3B_OX_4_Glass_3_17	79.57	0.05	11.95	0.37	0.01	0.01	0.63	2.64	4.76	92.97	99.18
25BT3B_OX_4_Glass_3_18	78.78	0.04	12.40	0.38	0.01	0.02	0.61	2.94	4.81	93.20	99.41
25BT3B_OX_4_Glass_3_20	79.78	0.03	11.98	0.42	0.03	0.00	0.61	2.45	4.70	92.46	98.67
25BT3B_OX_4_Glass_3_21	79.16	0.04	11.84	0.40	0.00	0.01	0.62	3.05	4.86	93.65	99.86
25BT3B_OX_4_Glass_3_22	79.69	0.09	12.01	0.38	0.01	0.02	0.66	2.42	4.72	92.58	98.79
25BT3B_OX_4_Glass_3_23	79.37	0.01	11.86	0.40	0.03	0.02	0.60	2.88	4.82	92.97	99.18
25BT3B_OX_4_Glass_3_25	79.69	0.09	12.04	0.43	0.01	0.01	0.58	2.46	4.68	92.77	98.97
25BT3B_OX_4_Glass_3_27	79.84	0.05	12.28	0.39	0.01	0.01	0.65	2.05	4.73	92.73	98.94
25BT3B_OX_4_Glass_5_1	76.34	0.26	12.62	1.17	0.05	0.24	0.83	3.46	5.05	93.35	99.56
25BT3B_OX_4_Glass_5_2	76.55	0.15	12.78	1.10	0.03	0.21	0.76	3.50	4.92	93.44	99.65
25BT3B_OX_4_Glass_5_3	77.53	0.00	12.85	0.44	0.00	0.01	0.78	3.44	4.96	92.72	98.93
25BT3B_OX_4_Glass_5_4	77.02	0.23	12.45	0.99	0.05	0.18	0.74	3.40	4.92	93.42	99.63
25BT3B_OX_4_Glass_5_6	77.99	0.01	12.51	0.43	0.03	0.01	0.74	3.36	4.91	92.78	98.99
25BT3B_OX_4_Glass_5_7	77.35	0.10	12.67	0.82	0.01	0.14	0.77	3.13	5.00	92.98	99.19
25BT3B_OX_4_Glass_5_8	76.73	0.14	12.76	0.82	0.03	0.16	0.83	3.47	5.05	92.45	98.66
25BT3B_OX_4_Glass_5_9	77.71	0.10	12.44	0.46	0.00	0.03	0.78	3.53	4.95	92.25	98.46
25BT3B_OX_4_Glass_5_10	77.59	0.14	12.67	0.57	0.02	0.05	0.80	3.13	5.03	91.87	98.07
25BT3B_OX_4_Glass_5_11	77.50	0.07	12.65	0.64	0.00	0.07	0.78	3.40	4.89	92.64	98.85
25BT3B_OX_4_Glass_5_12	78.00	0.06	12.69	0.51	0.00	0.02	0.82	2.89	5.00	91.54	97.75
25BT3B_OX_4_Glass_5_13	77.45	0.10	12.88	0.72	0.02	0.09	0.84	2.97	4.93	92.45	98.66
25BT3B_OX_4_Glass_5_15	77.83	0.03	12.44	0.42	0.01	0.00	0.78	3.62	4.86	92.46	98.66
25BT3B_OX_4_Glass_5_16	77.35	0.10	12.59	0.64	0.02	0.07	0.85	3.31	5.07	92.92	99.13
25BT3B_OX_4_Glass_5_17	76.94	0.20	12.68	1.09	0.03	0.23	0.72	3.13	4.97	93.11	99.32
25BT3B_OX_4_Glass_5_18	76.90	0.09	13.06	0.56	0.04	0.06	0.84	3.53	4.92	94.31	100.51
25BT3B_OX_4_Glass_5_19	77.14	0.12	12.57	0.89	0.01	0.16	0.80	3.37	4.94	92.48	98.69
25BT3B_OX_4_Glass_5_20	76.65	0.23	12.78	1.04	0.02	0.17	0.79	3.36	4.98	93.23	99.44
25BT3B_OX_4_Glass_5_21	76.65	0.23	12.80	1.17	0.01	0.23	0.70	3.28	4.92	93.17	99.37
25BT3B_OX_4_Glass_5_23	77.59	0.21	12.70	1.21	0.01	0.21	0.78	2.25	5.05	92.70	98.91
25BT3B_OX_4_Glass_5_26	77.29	0.16	12.70	0.69	0.04	0.08	0.79	3.33	4.93	92.58	98.79
25BT3B_OX_4_Glass_5_27	77.41	0.11	12.52	0.54	0.02	0.07	0.81	3.61	4.90	92.64	98.85
25BT3B_OX_4_Glass_5_28	78.34	0.04	12.97	0.49	0.01	0.04	0.77	2.47	4.85	92.54	98.75
25BT3B_OX_4_Glass_5_29	78.83	0.15	12.74	0.88	0.05	0.18	0.84	1.53	4.81	91.72	97.93
25BT3B_OX_4_Glass_5_30	76.99	0.20	12.61	0.85	0.05	0.15	0.75	3.47	4.92	93.89	100.10

	25BT3B_OX_4_Glass_5_31	77.10	0.17	12.63	0.87	0.04	0.16	0.71	3.26	5.06	93.05	99.26
	25BT3B_OX_4_Glass_5_32	77.28	0.16	12.74	0.72	0.00	0.11	0.78	3.35	4.89	93.03	99.24
	25BT3B_OX_4_Glass_5_33	77.28	0.10	12.57	0.73	0.03	0.12	0.80	3.47	4.90	92.55	98.76
	25BT3B_OX_4_Glass_5_34	76.80	0.27	12.47	1.31	0.01	0.25	0.84	3.09	4.96	93.50	99.71
	25BT3B_OX_4_Glass_5_35	76.64	0.24	12.68	1.20	0.01	0.26	0.80	3.25	4.91	93.38	99.59
	25BT3B_OX_4_Glass_5_36	76.24	0.25	12.67	1.38	0.00	0.32	0.76	3.21	5.17	93.13	99.33
	25BT3B_OX_4_Glass_5_37	77.64	0.10	12.28	0.67	-0.01	0.12	0.72	3.58	4.90	93.23	99.44
	25BT3B_OX_4_Glass_5_38	77.36	0.14	12.74	0.78	0.06	0.16	0.79	2.84	5.13	92.22	98.43
	25BT3B_OX_4_Glass_5_39	76.63	0.17	12.88	0.92	0.00	0.19	0.76	3.37	5.09	93.56	99.77
	25BT3B_OX_4_Glass_5_40	76.68	0.17	12.67	0.94	0.01	0.16	0.84	3.55	4.96	94.11	100.32
	25BT3B_OX_4_Glass_5_41	77.13	0.09	12.58	0.87	0.03	0.18	0.82	3.36	4.93	93.13	99.34
	25BT3B_OX_4_Glass_5_42	76.84	0.15	12.63	0.95	0.02	0.21	0.81	3.37	5.02	92.74	98.95
	25BT3B_OX_4_Glass_5_43	77.12	0.21	12.35	0.99	0.03	0.16	0.81	3.35	4.97	93.57	99.78
	25BT3B_OX_4_Glass_5_44	77.42	0.09	12.63	0.94	0.02	0.15	0.76	3.11	4.89	93.28	99.48
	25BT3B_OX_4_Glass_5_45	76.90	0.13	12.61	0.98	0.02	0.19	0.79	3.45	4.92	93.33	99.54
	25BT3B_OX_4_Glass_5_46	77.76	0.12	12.52	0.73	0.05	0.10	0.71	3.02	4.99	93.50	99.71
	25BT3B_OX_4_Glass_5_47	76.46	0.18	12.56	1.23	0.03	0.23	0.80	3.52	5.00	93.08	99.29
	25BT3B_OX_4_Glass_5_48	77.38	0.15	12.54	0.78	0.04	0.13	0.76	3.33	4.88	92.83	99.04
	25BT3B_OX_4_Glass_5_49	77.80	0.07	12.31	0.55	0.02	0.06	0.75	3.56	4.89	93.71	99.92
	Average	**78.09**	**0.10**	**12.37**	**0.69**	**0.02**	**0.09**	**0.71**	**3.05**	**4.88**	**92.97**	99.18
	Standard Deviation	**1.11**	**0.07**	**0.36**	**0.27**	**0.02**	**0.09**	**0.09**	**0.45**	**0.11**	**0.56**	0.56
BT: 7 750 °C 125 MPa *H_2O: 4.74	25BT3B_OX_9_Glass_1_6	77.09	0.18	12.61	1.05	0.03	0.06	0.69	3.55	4.74	93.08	97.83
	25BT3B_OX_9_Glass_1_8	76.94	0.17	12.74	1.34	0.07	0.04	0.77	3.00	4.92	93.21	97.96
	25BT3B_OX_9_Glass_1_11	77.67	0.20	12.98	1.16	0.00	0.05	0.70	2.46	4.77	92.64	97.38
	25BT3B_OX_9_Glass_2_1	77.11	0.16	12.81	0.64	0.02	0.07	0.77	3.17	5.26	94.17	98.91
	25BT3B_OX_9_Glass_2_2	76.91	0.20	12.51	0.77	0.03	0.10	0.74	3.48	5.26	94.22	98.97
	25BT3B_OX_9_Glass_2_4	79.20	0.14	13.07	0.59	0.02	0.07	0.76	1.30	4.87	94.86	99.60
	25BT3B_OX_9_Glass_2_5	76.86	0.18	12.40	0.60	0.02	0.08	0.77	3.76	5.30	93.50	98.25
	25BT3B_OX_9_Glass_2_6	77.21	0.20	12.60	0.68	0.02	0.09	0.73	3.40	5.06	94.72	99.46
	25BT3B_OX_9_Glass_2_7	77.33	0.14	12.60	0.57	0.01	0.06	0.71	3.47	5.09	94.41	99.16
	25BT3B_OX_9_Glass_2_8	77.11	0.12	12.55	0.62	0.02	0.08	0.84	3.45	5.22	94.01	98.76
	25BT3B_OX_9_Glass_2_9	77.57	0.15	12.69	0.65	-0.01	0.07	0.74	2.95	5.19	92.79	97.54
	25BT3B_OX_9_Glass_2_10	77.11	0.15	12.49	0.60	0.04	0.09	0.75	3.64	5.12	94.59	99.33
	25BT3B_OX_9_Glass_2_11	77.09	0.22	12.55	0.91	0.03	0.08	0.75	3.37	4.99	95.47	100.21

25BT3B_OX_9_Glass_2_13	76.86	0.16	12.71	0.74	0.02	0.09	0.72	3.52	5.17	94.87	99.61
25BT3B_OX_9_Glass_2_14	76.88	0.14	12.79	0.65	0.01	0.08	0.78	3.45	5.22	93.34	98.09
25BT3B_OX_9_Glass_2_16	77.73	0.21	12.41	0.64	0.02	0.08	0.67	3.14	5.10	93.74	98.48
25BT3B_OX_9_Glass_2_17	77.58	0.16	12.62	0.70	0.04	0.08	0.78	2.88	5.16	93.52	98.26
25BT3B_OX_9_Glass_2_18	77.16	0.16	12.48	0.65	0.02	0.10	0.73	3.56	5.15	94.16	98.91
25BT3B_OX_9_Glass_4_1	76.80	0.22	12.75	0.80	0.03	0.24	0.68	3.31	5.16	93.90	98.64
25BT3B_OX_9_Glass_4_2	77.41	0.13	13.00	0.68	0.02	0.10	0.74	3.00	4.90	96.11	100.85
25BT3B_OX_9_Glass_4_3	76.93	0.16	12.62	0.70	0.01	0.10	0.75	3.49	5.24	93.11	97.85
25BT3B_OX_9_Glass_4_5	77.61	0.16	12.77	0.77	0.00	0.23	0.70	2.73	5.03	95.21	99.96
25BT3B_OX_9_Glass_5_1	76.84	0.19	12.71	0.82	0.01	0.22	0.68	3.47	5.05	95.26	100.01
25BT3B_OX_9_Glass_5_2	76.71	0.18	12.35	1.19	0.03	0.09	0.88	3.45	5.12	94.00	98.75
25BT3B_OX_9_Glass_5_3	76.90	0.21	12.58	0.85	0.02	0.08	0.71	3.43	5.21	94.53	99.28
25BT3B_OX_9_Glass_5_4	78.49	0.20	12.74	0.88	0.03	0.21	0.88	1.49	5.09	92.77	97.51
25BT3B_OX_9_Glass_5_5	78.68	0.16	12.64	1.29	-0.01	0.10	0.85	1.26	5.03	92.98	97.73
25BT3B_OX_9_Glass_5_6	77.11	0.22	12.53	0.70	0.03	0.20	0.72	3.29	5.19	94.67	99.42
25BT3B_OX_9_Glass_5_7	76.89	0.19	12.75	0.82	0.02	0.12	0.74	3.46	5.01	95.02	99.77
25BT3B_OX_9_Glass_5_9	76.98	0.14	12.64	0.80	0.03	0.10	0.76	3.39	5.17	93.00	97.75
25BT3B_OX_9_Glass_5_10	77.54	0.14	12.46	0.79	0.01	0.13	0.69	3.17	5.06	92.88	97.62
25BT3B_OX_9_Glass_5_11	76.63	0.19	12.69	0.78	0.04	0.10	0.76	3.64	5.16	92.63	97.37
25BT3B_OX_9_Glass_5_13	76.15	0.20	12.68	1.17	0.03	0.26	0.75	3.57	5.19	93.98	98.72
25BT3B_OX_9_Glass_5_14	77.12	0.17	12.54	0.76	0.01	0.10	0.76	3.40	5.14	93.40	98.14
25BT3B_OX_9_Glass_5_15	76.73	0.16	12.55	0.72	0.02	0.12	0.76	3.64	5.30	93.36	98.11
25BT3B_OX_9_Glass_5_16	76.37	0.22	12.59	0.89	0.02	0.25	0.70	3.71	5.25	94.02	98.76
25BT3B_OX_9_Glass_5_17	76.66	0.21	12.67	0.72	0.06	0.20	0.77	3.46	5.26	92.66	97.41
25BT3B_OX_9_Glass_5_18	76.80	0.15	12.75	0.72	0.05	0.12	0.74	3.40	5.27	93.10	97.84
25BT3B_OX_9_Glass_5_20	76.83	0.16	12.60	0.99	0.03	0.21	0.75	3.28	5.15	94.83	99.57
25BT3B_OX_9_Glass_5_21	76.44	0.14	12.65	1.23	0.04	0.13	0.68	3.47	5.24	94.15	98.90
25BT3B_OX_9_Glass_5_22	76.54	0.15	12.79	0.87	0.04	0.17	0.67	3.63	5.12	93.89	98.63
25BT3B_OX_9_Glass_5_23	77.67	0.20	12.85	0.85	0.07	0.13	0.77	2.37	5.08	94.40	99.14
25BT3B_OX_9_Glass_5_24	76.70	0.18	12.71	0.81	0.02	0.09	0.69	3.66	5.13	94.24	98.99
25BT3B_OX_9_Glass_5_25	78.18	0.19	12.81	0.86	0.02	0.16	0.75	1.93	5.10	93.86	98.60
25BT3B_OX_9_Glass_5_26	76.48	0.21	12.92	0.91	-0.01	0.09	0.77	3.56	5.08	94.49	99.24
25BT3B_OX_9_Glass_5_27	76.48	0.16	13.09	0.93	0.03	0.13	0.78	3.18	5.21	92.82	97.56
25BT3B_OX_9_Glass_5_28	78.37	0.15	13.33	0.75	0.01	0.13	0.77	1.58	4.92	92.78	97.53
25BT3B_OX_9_Glass_5_29	76.68	0.16	12.73	0.79	0.02	0.08	0.77	3.60	5.16	94.82	99.56

25BT3B_OX_9_Glass_5_32	76.28	0.25	12.90	0.96	0.06	0.39	0.74	3.20	5.23	93.25	97.99
25BT3B_OX_9_Glass_5_33	76.12	0.30	12.73	0.97	0.02	0.31	0.82	3.44	5.28	93.29	98.03
25BT3B_OX_9_Glass_5_36	76.60	0.11	12.87	0.69	0.03	0.09	0.77	3.64	5.20	93.24	97.98
25BT3B_OX_9_Glass_5_37	76.00	0.24	12.68	0.91	0.04	0.26	0.77	3.72	5.37	93.43	98.17
25BT3B_OX_9_Glass_5_38	76.45	0.34	12.87	1.28	0.02	0.67	0.75	2.35	5.27	92.72	97.46
25BT3B_OX_9_Glass_5_39	76.93	0.18	12.58	0.74	0.05	0.10	0.72	3.47	5.22	94.59	99.33
25BT3B_OX_9_Glass_5_42	76.72	0.22	12.83	0.83	0.01	0.22	0.72	3.30	5.16	93.44	98.18
25BT3B_OX_9_Glass_5_43	77.30	0.13	12.66	0.72	0.02	0.10	0.76	3.22	5.09	93.68	98.42
25BT3B_OX_9_Glass_5_44	78.86	0.18	13.17	0.71	0.03	0.10	0.74	1.25	4.97	93.29	98.03
25BT3B_OX_9_Glass_5_45	77.71	0.17	12.73	0.78	0.00	0.15	0.72	2.74	5.00	94.94	99.68
25BT3B_OX_9_Glass_5_46	75.78	0.28	12.49	1.25	0.02	0.70	0.71	3.37	5.42	93.54	98.28
25BT3B_OX_9_Glass_5_48	77.09	0.11	12.82	0.78	0.03	0.09	0.76	3.27	5.03	93.87	98.61
25BT3B_OX_9_Glass_5_49	76.61	0.23	12.72	1.05	0.01	0.06	0.75	3.47	5.09	94.60	99.34
25BT3B_OX_9_Glass_5_50	76.89	0.21	12.67	0.96	0.03	0.06	0.69	3.46	5.02	95.18	99.93
25BT3B_OX_9_Glass_6_1	77.02	0.16	12.69	0.66	0.03	0.09	0.74	3.55	5.05	94.79	99.53
25BT3B_OX_9_Glass_6_2	77.00	0.14	12.59	0.66	0.02	0.10	0.72	3.65	5.11	94.71	99.46
25BT3B_OX_9_Glass_6_3	79.27	0.20	13.08	0.68	0.03	0.09	0.79	1.10	4.75	93.97	98.72
25BT3B_OX_9_Glass_6_5	77.59	0.12	12.55	0.66	-0.01	0.11	0.73	3.16	5.08	94.36	99.10
25BT3B_OX_9_Glass_6_6	77.41	0.16	12.67	0.67	0.03	0.11	0.72	3.12	5.12	94.99	99.74
25BT3B_OX_9_Glass_6_7	79.69	0.10	12.97	0.67	0.04	0.09	0.74	1.00	4.68	93.76	98.50
25BT3B_OX_9_Glass_6_8	77.47	0.16	12.54	0.63	0.02	0.08	0.75	3.38	4.96	95.11	99.85
25BT3B_OX_9_Glass_6_9	76.79	0.20	13.25	0.65	0.01	0.08	0.73	3.24	5.05	93.36	98.11
25BT3B_OX_9_Glass_6_10	77.20	0.16	12.62	0.66	0.04	0.09	0.74	3.36	5.12	94.49	99.23
25BT3B_OX_9_Glass_6_11	79.17	0.13	12.66	0.73	0.00	0.08	0.79	1.32	5.11	93.25	97.99
25BT3B_OX_9_Glass_6_12	79.06	0.17	12.78	0.63	0.00	0.10	0.75	1.72	4.80	93.09	97.84
25BT3B_OX_9_Glass_6_13	77.18	0.17	12.50	0.70	0.02	0.10	0.78	3.46	5.09	94.94	99.68
25BT3B_OX_9_Glass_6_14	77.07	0.18	12.66	0.62	0.05	0.09	0.71	3.47	5.15	93.73	98.47
25BT3B_OX_9_Glass_6_15	78.96	0.21	12.82	0.63	0.02	0.08	0.78	1.57	4.93	93.09	97.83
25BT3B_OX_9_Glass_6_16	76.86	0.12	12.66	0.83	0.03	0.09	0.74	3.51	5.15	94.97	99.72
25BT3B_OX_9_Glass_6_17	78.54	0.22	13.00	0.68	0.00	0.09	0.75	1.71	5.00	93.08	97.83
25BT3B_OX_9_Glass_6_18	76.55	0.19	12.56	1.35	0.04	0.10	0.72	3.35	5.13	93.93	98.67
25BT3B_OX_9_Glass_6_19	77.25	0.19	12.62	0.71	0.03	0.10	0.78	3.19	5.13	94.63	99.38
25BT3B_OX_9_Glass_6_20	77.14	0.12	12.68	0.67	0.05	0.14	0.75	3.34	5.11	94.56	99.31
25BT3B_OX_9_Glass_6_21	76.53	0.24	12.91	0.85	0.00	0.34	0.73	3.28	5.11	95.85	100.59
25BT3B_OX_9_Glass_6_22	76.04	0.34	12.50	1.16	0.03	0.66	0.66	3.31	5.31	95.05	99.80

	25BT3B_OX_9_Glass_6_23	76.53	0.24	12.66	0.84	0.04	0.36	0.75	3.39	5.19	94.98	99.72
	25BT3B_OX_9_Glass_6_24	77.35	0.29	12.71	1.08	0.02	0.63	0.72	1.89	5.29	94.97	99.71
	25BT3B_OX_9_Glass_6_25	77.01	0.28	12.84	0.87	0.02	0.40	0.69	2.68	5.21	94.98	99.72
	25BT3B_OX_9_Glass_6_26	75.43	0.26	13.19	1.17	0.00	0.52	0.70	3.67	5.05	95.36	100.10
	25BT3B_OX_9_Glass_6_27	76.66	0.20	13.12	0.66	0.02	0.10	0.74	3.60	4.89	93.98	98.73
	25BT3B_OX_9_Glass_6_28	77.48	0.36	12.83	1.15	0.02	0.65	0.67	1.65	5.18	93.58	98.32
	25BT3B_OX_9_Glass_6_29	77.35	0.23	12.62	0.69	0.01	0.14	0.65	3.22	5.09	94.94	99.68
	25BT3B_OX_9_Glass_6_30	76.99	0.15	12.49	0.73	0.05	0.21	0.77	3.48	5.11	95.05	99.79
	25BT3B_OX_9_Glass_6_31	75.78	0.19	14.28	0.60	0.03	0.08	0.71	3.30	5.02	93.40	98.14
	25BT3B_OX_9_Glass_6_32	78.19	0.15	13.02	0.75	0.03	0.17	0.74	1.89	5.06	93.49	98.24
	25BT3B_OX_9_Glass_6_33	76.95	0.18	13.20	0.76	-0.02	0.20	0.72	2.92	5.06	92.78	97.53
	25BT3B_OX_9_Glass_6_34	77.11	0.17	12.62	0.80	0.04	0.28	0.72	3.11	5.13	94.36	99.10
	25BT3B_OX_9_Glass_6_35	76.64	0.17	12.87	0.86	0.04	0.16	0.75	3.39	5.11	94.20	98.94
	25BT3B_OX_9_Glass_6_36	78.63	0.16	12.82	0.77	0.02	0.11	0.83	1.69	4.95	93.82	98.56
	25BT3B_OX_9_Glass_6_37	77.28	0.18	12.55	1.07	0.03	0.09	0.81	2.87	5.12	94.62	99.36
	25BT3B_OX_9_Glass_6_38	77.29	0.15	12.97	0.71	0.04	0.10	0.74	2.90	5.11	94.46	99.20
	25BT3B_OX_9_Glass_6_39	76.81	0.17	13.21	0.67	0.03	0.11	0.80	3.20	4.98	93.63	98.37
	Average	**77.18**	**0.19**	**12.75**	**0.82**	**0.02**	**0.16**	**0.74**	**3.03**	**5.10**	**94.04**	**98.78**
	Standard Deviation	**0.80**	**0.05**	**0.26**	**0.19**	**0.02**	**0.14**	**0.04**	**0.72**	**0.13**	**0.82**	**0.82**
MC: 2 750 °C 200 MPa *H_2O: 6.01	25MC24_OX_3_Glass 1-1	77.42	0.07	12.53	1.27	0.01	0.05	0.67	3.36	4.61	94.74	100.75
	25MC24_OX_3_Glass 1-2	77.89	0.11	12.32	1.14	0.04	0.06	0.66	3.15	4.63	94.08	100.08
	25MC24_OX_3_Glass 1-5	77.31	0.13	12.39	1.18	0.03	0.04	0.66	3.67	4.59	94.95	100.96
	25MC24_OX_3_Glass 1-6	77.01	0.14	12.36	1.29	0.06	0.07	0.92	3.60	4.56	94.32	100.33
	25MC24_OX_3_Glass 1-39	77.80	0.03	12.56	0.56	0.04	0.07	0.65	3.67	4.62	94.53	100.54
	25MC24_OX_3_Glass 3-15	79.37	0.04	12.99	0.44	-0.02	0.06	0.75	1.99	4.38	92.69	98.70
	25MC24_OX_3_Glass 1-10	77.53	0.13	12.24	0.95	0.01	0.06	0.68	3.50	4.91	92.12	98.13
	25MC24_OX_3_Glass 1-11	77.60	0.12	12.31	0.89	0.06	0.04	0.71	3.45	4.82	92.97	98.98
	25MC24_OX_3_Glass 1-12	77.49	0.10	12.56	1.07	0.01	0.06	0.64	3.28	4.80	93.29	99.30
	25MC24_OX_3_Glass 1-13	77.69	0.16	12.34	1.08	0.02	0.06	0.70	3.29	4.66	92.37	98.38
	25MC24_OX_3_Glass 1-14	77.63	0.09	12.42	0.88	0.01	0.03	0.70	3.49	4.73	92.67	98.68
	25MC24_OX_3_Glass 1-15	77.92	0.17	12.30	0.83	0.05	0.07	0.68	3.27	4.72	92.94	98.95
	25MC24_OX_3_Glass 1-16	77.53	0.10	12.41	0.96	0.04	0.04	0.71	3.60	4.62	94.22	100.23
	25MC24_OX_3_Glass 1-17	78.09	0.08	12.79	0.80	0.04	0.06	0.67	2.90	4.56	94.24	100.25
	25MC24_OX_3_Glass 1-18	78.57	0.11	12.33	0.81	0.04	0.05	0.69	2.69	4.71	92.81	98.82

25MC24_OX_3_Glass 1-19	78.95	0.08	12.71	0.85	0.02	0.05	0.74	1.92	4.67	91.79	97.80
25MC24_OX_3_Glass 1-20	78.16	0.13	12.45	0.98	0.03	0.03	0.67	2.90	4.64	93.88	99.89
25MC24_OX_3_Glass 1-21	77.86	0.12	12.21	1.14	0.05	0.04	0.65	3.11	4.81	93.37	99.38
25MC24_OX_3_Glass 1-22	77.98	0.11	12.33	1.05	0.05	0.04	0.65	3.14	4.65	93.70	99.71
25MC24_OX_3_Glass 1-23	79.01	0.14	12.43	1.29	0.03	0.07	0.64	1.85	4.53	93.16	99.17
25MC24_OX_3_Glass 1-24	77.99	0.13	12.30	0.82	0.00	0.04	0.59	3.45	4.67	94.40	100.41
25MC24_OX_3_Glass 1-25	79.92	0.13	12.74	1.15	0.00	0.05	0.66	1.10	4.25	93.33	99.34
25MC24_OX_3_Glass 1-26	77.54	0.12	12.43	1.05	0.04	0.06	0.68	3.41	4.68	94.39	100.40
25MC24_OX_3_Glass 1-27	79.26	0.12	12.75	0.81	0.04	0.05	0.69	1.94	4.35	93.31	99.32
25MC24_OX_3_Glass 1-29	79.41	0.09	12.77	0.86	0.04	0.04	0.68	1.78	4.32	93.34	99.35
25MC24_OX_3_Glass 1-31	77.61	0.15	12.54	0.64	0.01	0.05	0.67	3.64	4.69	94.25	100.25
25MC24_OX_3_Glass 1-32	77.88	0.09	12.40	0.64	0.00	0.04	0.64	3.55	4.76	94.59	100.60
25MC24_OX_3_Glass 1-33	77.95	0.12	12.59	0.66	0.01	0.04	0.68	3.29	4.66	94.31	100.32
25MC24_OX_3_Glass 1-34	77.42	0.10	12.29	1.21	0.04	0.06	0.68	3.63	4.57	93.68	99.69
25MC24_OX_3_Glass 1-36	77.93	0.08	12.38	0.73	0.02	0.05	0.62	3.58	4.62	94.41	100.42
25MC24_OX_3_Glass 1-37	78.44	0.11	12.61	0.74	0.05	0.05	0.73	2.75	4.51	93.38	99.39
25MC24_OX_3_Glass 1-38	77.54	0.11	12.37	1.03	0.03	0.05	0.67	3.46	4.74	94.14	100.15
25MC24_OX_3_Glass 2-1	77.29	0.09	12.27	1.32	0.04	0.06	0.65	3.68	4.59	94.69	100.70
25MC24_OX_3_Glass 2-2	77.25	0.11	12.44	1.27	0.02	0.04	0.69	3.55	4.62	93.80	99.80
25MC24_OX_3_Glass 2-3	77.96	0.12	12.14	1.24	0.06	0.05	0.65	3.02	4.75	93.54	99.55
25MC24_OX_3_Glass 2-4	77.35	0.16	12.20	1.34	0.03	0.06	0.60	3.63	4.63	94.21	100.22
25MC24_OX_3_Glass 2-5	75.67	0.16	14.09	1.23	0.06	0.04	0.69	3.43	4.61	94.21	100.22
25MC24_OX_3_Glass 2-6	77.20	0.13	12.41	1.28	0.05	0.04	0.66	3.63	4.61	94.68	100.69
25MC24_OX_3_Glass 2-7	77.00	0.12	12.90	1.19	0.03	0.03	0.81	3.32	4.59	94.55	100.56
25MC24_OX_3_Glass 2-8	77.45	0.10	13.28	1.19	0.03	0.06	0.62	2.73	4.53	94.68	100.69
25MC24_OX_3_Glass 2-9	76.99	0.16	13.93	1.35	0.04	0.06	0.63	2.26	4.57	92.00	98.01
25MC24_OX_3_Glass 2-10	79.63	0.13	12.72	1.39	0.00	0.05	0.64	1.26	4.17	92.73	98.74
25MC24_OX_3_Glass 2-11	79.24	0.15	12.62	1.37	0.03	0.05	0.66	1.70	4.18	93.54	99.55
25MC24_OX_3_Glass 2-12	79.73	0.17	12.61	1.35	0.02	0.06	0.65	1.37	4.06	92.49	98.50
25MC24_OX_3_Glass 2-13	77.74	0.14	12.01	1.38	0.05	0.06	0.65	3.28	4.68	94.18	100.19
25MC24_OX_3_Glass 2-14	78.08	0.11	12.94	1.33	0.04	0.05	0.61	2.32	4.52	94.38	100.39
25MC24_OX_3_Glass 2-15	79.51	0.17	12.62	1.28	-0.02	0.07	0.68	1.48	4.21	93.14	99.15
25MC24_OX_3_Glass 2-16	79.32	0.09	12.80	1.29	0.02	0.06	0.70	1.47	4.24	92.32	98.33
25MC24_OX_3_Glass 2-17	79.68	0.14	12.42	1.21	0.03	0.05	0.69	1.54	4.23	92.98	98.99
25MC24_OX_3_Glass 2-19	78.95	0.15	12.91	1.30	0.03	0.07	0.65	1.87	4.06	93.48	99.49

	25MC24_OX_3_Glass 2-21	79.95	0.11	12.68	1.26	-0.01	0.06	0.68	1.18	4.07	93.38	99.38
	25MC24_OX_3_Glass 2-23	76.22	0.13	14.04	1.37	0.05	0.05	0.70	2.94	4.50	93.46	99.47
	25MC24_OX_3_Glass 2-25	78.63	0.16	14.01	1.31	0.04	0.05	0.62	0.98	4.21	92.59	98.60
	25MC24_OX_3_Glass 2-26	77.24	0.09	12.96	1.36	0.00	0.07	0.74	2.93	4.60	92.97	98.98
	25MC24_OX_3_Glass 2-27	77.46	0.11	12.38	1.16	0.04	0.06	0.66	3.53	4.60	94.40	100.41
	25MC24_OX_3_Glass 2-30	78.80	0.14	12.48	1.19	0.00	0.06	0.61	2.26	4.46	93.83	99.84
	25MC24_OX_3_Glass 2-32	79.22	0.11	12.46	1.30	0.03	0.05	0.62	1.75	4.46	92.58	98.59
	25MC24_OX_3_Glass 2-33	76.80	0.12	13.34	1.19	0.03	0.04	0.69	3.21	4.55	94.62	100.63
	25MC24_OX_3_Glass 2-34	77.51	0.11	12.56	1.22	0.05	0.04	0.70	3.11	4.69	94.62	100.63
	25MC24_OX_3_Glass 2-35	77.11	0.10	12.99	1.19	0.03	0.04	0.69	3.25	4.60	93.92	99.93
	25MC24_OX_3_Glass 2-37	77.42	0.15	12.75	1.16	0.03	0.04	0.61	3.21	4.61	94.32	100.33
	25MC24_OX_3_Glass 2-38	79.06	0.14	12.68	1.15	0.00	0.05	0.69	1.86	4.37	92.86	98.87
	25MC24_OX_3_Glass 2-39	79.76	0.11	13.50	1.22	0.03	0.06	0.72	0.69	3.90	92.83	98.83
	25MC24_OX_3_Glass 3-1	77.83	0.07	12.57	0.53	-0.01	0.06	0.87	3.50	4.56	92.38	98.39
	25MC24_OX_3_Glass 3-7	77.51	0.11	13.35	0.55	0.01	0.05	0.73	3.22	4.45	92.88	98.89
	25MC24_OX_3_Glass 3-10	78.06	0.12	12.73	0.54	0.03	0.08	0.80	2.91	4.73	93.10	99.11
	25MC24_OX_3_Glass 3-11	79.02	0.08	12.75	0.53	0.00	0.07	0.76	2.23	4.55	92.26	98.27
	25MC24_OX_3_Glass 3-12	79.65	0.08	12.94	0.55	0.03	0.06	0.73	1.63	4.32	91.74	97.75
	25MC24_OX_3_Glass 3-13	77.99	0.07	12.92	0.54	0.02	0.05	0.75	3.00	4.67	92.63	98.64
	25MC24_OX_3_Glass 3-14	79.30	0.06	13.17	0.53	0.02	0.07	0.78	1.80	4.28	92.49	98.50
	Average	**78.12**	**0.12**	**12.68**	**1.04**	**0.03**	**0.05**	**0.68**	**2.74**	**4.53**	**93.51**	**99.52**
	Standard Deviation	**0.95**	**0.03**	**0.45**	**0.28**	**0.02**	**0.01**	**0.06**	**0.85**	**0.21**	**0.85**	**0.85**
MC:4 675 °C 200 Mpa *H_2O: 6.30	25MC24_ox_1_Glass-1-1	77.44	0.06	12.80	0.42	0.04	0.07	0.70	3.57	4.89	93.84	100.14
	25MC24_ox_1_Glass-1-2	77.13	0.09	12.70	0.62	0.00	0.16	0.77	3.51	5.02	93.73	100.04
	25MC24_ox_1_Glass-1-3	77.57	0.08	12.65	0.45	0.03	0.07	0.69	3.62	4.83	93.42	99.73
	25MC24_ox_1_Glass-1-4	77.55	0.02	12.81	0.40	0.01	0.03	0.71	3.61	4.86	93.26	99.57
	25MC24_ox_1_Glass-1-5	77.92	0.07	12.50	0.43	0.02	0.05	0.67	3.44	4.89	92.15	98.45
	25MC24_ox_1_Glass-1-6	77.93	0.05	12.84	0.46	0.00	0.07	0.67	3.05	4.93	93.06	99.37
	25MC24_ox_1_Glass-1-7	77.60	0.01	12.64	0.55	0.01	0.13	0.70	3.52	4.83	93.46	99.77
	25MC24_ox_1_Glass-1-8	77.15	0.09	12.92	0.55	0.00	0.09	0.68	3.67	4.85	94.32	100.63
	25MC24_ox_1_Glass-1-9	76.99	0.11	12.73	0.58	0.03	0.16	0.64	3.82	4.92	92.88	99.19
	25MC24_ox_1_Glass-1-10	77.61	0.09	12.49	0.52	0.02	0.06	0.72	3.64	4.83	93.96	100.27
	25MC24_ox_1_Glass-1-11	77.25	0.11	12.78	0.64	0.04	0.19	0.64	3.47	4.88	93.49	99.79
	25MC24_ox_1_Glass-1-12	77.55	0.05	12.80	0.33	0.04	0.01	0.70	3.56	4.94	93.74	100.04

25MC24_ox_1_Glass-1-13	77.75	0.03	12.66	0.50	0.02	0.09	0.70	3.38	4.88	93.42	99.72
25MC24_ox_1_Glass-1-14	77.86	0.09	12.61	0.41	0.02	0.02	0.72	3.33	4.94	93.40	99.71
25MC24_ox_1_Glass-1-15	77.44	0.08	12.79	0.42	0.03	0.06	0.69	3.59	4.90	93.68	99.99
25MC24_ox_1_Glass-1-16	77.68	0.08	12.64	0.42	0.08	0.02	0.71	3.58	4.79	93.84	100.15
25MC24_ox_1_Glass-1-17	77.73	0.11	12.69	0.43	0.04	0.07	0.66	3.49	4.79	93.40	99.71
25MC24_ox_1_Glass-1-18	76.92	0.04	12.58	1.05	0.02	0.09	0.68	3.88	4.74	94.18	100.48
25MC24_ox_1_Glass-1-19	78.13	0.06	12.47	0.53	0.03	0.13	0.66	3.07	4.91	93.04	99.35
25MC24_ox_1_Glass-1-20	77.60	0.03	12.73	0.49	0.00	0.06	0.69	3.59	4.82	92.98	99.29
25MC24_ox_1_Glass-1-21	77.06	0.10	12.72	0.77	0.01	0.13	0.69	3.63	4.88	93.66	99.96
25MC24_ox_1_Glass-1-22	77.52	0.00	12.70	0.53	0.01	0.09	0.69	3.63	4.83	93.85	100.15
25MC24_ox_1_Glass-1-23	78.07	0.08	12.59	0.39	0.04	0.02	0.70	3.31	4.81	93.52	99.82
25MC24_ox_1_Glass-1-24	77.76	0.02	12.69	0.33	-0.01	0.01	0.70	3.62	4.88	93.99	100.30
25MC24_ox_1_Glass-1-25	77.70	0.08	12.63	0.47	0.03	0.09	0.69	3.56	4.75	93.88	100.19
25MC24_ox_1_Glass-1-26	77.51	0.07	12.84	0.44	0.04	0.08	0.65	3.45	4.92	93.93	100.24
25MC24_ox_1_Glass-1-27	77.68	0.04	12.76	0.38	0.02	0.03	0.68	3.67	4.75	94.00	100.30
25MC24_ox_1_Glass-1-28	77.63	0.08	12.69	0.48	0.01	0.05	0.74	3.41	4.91	92.74	99.04
25MC24_ox_1_Glass-1-29	77.28	0.08	12.74	0.58	0.01	0.10	0.70	3.66	4.86	93.76	100.06
25MC24_ox_1_Glass-1-30	77.03	0.07	12.73	0.80	0.01	0.09	0.69	3.66	4.91	92.96	99.27
25MC24_ox_1_Glass-1-31	77.08	0.10	12.90	0.51	0.04	0.11	0.69	3.62	4.94	93.26	99.56
25MC24_ox_1_Glass-1-32	77.39	0.12	12.63	0.44	0.04	0.07	0.71	3.79	4.79	93.78	100.08
25MC24_ox_1_Glass-1-33	77.76	0.04	12.71	0.36	0.03	0.03	0.76	3.52	4.80	93.34	99.65
25MC24_ox_1_Glass-1-34	77.22	0.12	12.76	0.87	0.00	0.16	0.71	3.23	4.93	92.77	99.08
25MC24_ox_1_Glass-1-36	79.10	0.11	11.63	0.44	0.01	0.02	0.50	3.01	5.18	94.02	100.33
25MC24_ox_1_Glass-1-37	78.27	0.12	12.30	0.53	0.00	0.12	0.64	3.37	4.64	94.43	100.74
25MC24_ox_1_Glass-1-39	77.11	0.10	12.79	1.13	0.05	0.11	0.71	3.23	4.77	94.14	100.45
25MC24_ox_1_Glass-1-40	77.31	0.03	13.00	0.42	0.01	0.03	0.65	3.66	4.86	93.94	100.25
25MC24_ox_1_Glass-1-41	77.68	0.10	12.69	0.41	0.03	0.05	0.71	3.43	4.89	93.67	99.97
25MC24_ox_1_Glass-1-42	77.52	0.06	12.77	0.38	0.02	0.02	0.72	3.73	4.80	94.10	100.40
25MC24_ox_1_Glass-1-43	77.28	0.06	12.80	0.43	0.04	0.05	0.74	3.72	4.88	93.35	99.65
25MC24_ox_1_Glass-1-44	77.24	0.08	12.72	0.58	0.01	0.11	0.73	3.63	4.91	93.23	99.53
25MC24_ox_1_Glass-1-45	77.26	0.10	12.73	0.38	0.05	0.05	0.72	3.78	4.93	94.63	100.93
25MC24_ox_1_Glass-1-46	77.55	0.10	12.63	0.49	0.01	0.06	0.74	3.66	4.76	93.52	99.83
25MC24_ox_1_Glass-1-47	77.72	0.03	12.67	0.37	0.02	0.02	0.69	3.74	4.75	93.50	99.80
25MC24_ox_1_Glass-1-48	77.74	0.04	12.79	0.47	0.02	0.05	0.70	3.46	4.72	93.67	99.97
25MC24_ox_1_Glass-1-49	77.28	0.05	12.67	0.91	0.04	0.05	0.74	3.52	4.73	94.21	100.51

25MC24_ox_1_Glass-1-50	77.67	0.04	12.62	0.32	0.03	0.01	0.73	3.76	4.82	93.89	100.19
25MC24_ox_1_Glass-2-1	77.77	0.07	12.63	0.41	0.02	0.02	0.70	3.58	4.79	92.84	99.15
25MC24_ox_1_Glass-2-2	78.37	0.03	12.38	0.36	0.02	0.02	0.63	3.39	4.79	93.47	99.77
25MC24_ox_1_Glass-2-3	77.66	0.05	12.64	0.50	0.01	0.04	0.65	3.56	4.88	92.62	98.93
25MC24_ox_1_Glass-2-4	77.72	0.07	12.60	0.74	0.02	0.03	0.66	3.32	4.84	93.07	99.38
25MC24_ox_1_Glass-2-5	78.00	0.06	12.38	0.34	0.02	0.02	0.70	3.77	4.72	93.72	100.02
25MC24_ox_1_Glass-2-6	77.68	0.02	12.42	0.75	0.03	0.05	0.67	3.52	4.85	93.88	100.18
25MC24_ox_1_Glass-2-7	77.42	0.08	12.64	0.61	0.04	0.04	0.78	3.58	4.80	93.34	99.65
25MC24_ox_1_Glass-2-8	78.39	0.06	12.72	0.48	0.04	0.04	0.70	2.75	4.81	92.74	99.04
25MC24_ox_1_Glass-2-9	77.55	0.04	12.49	0.75	0.03	0.05	0.66	3.60	4.82	92.89	99.20
25MC24_ox_1_Glass-2-10	77.73	0.07	12.50	0.41	0.04	0.02	0.69	3.73	4.79	93.50	99.80
25MC24_ox_1_Glass-2-11	76.89	0.08	12.59	1.07	0.06	0.02	0.70	3.75	4.84	92.17	98.47
25MC24_ox_1_Glass-2-13	77.74	0.07	12.50	0.57	0.06	0.04	0.65	3.51	4.86	93.54	99.84
25MC24_ox_1_Glass-2-14	77.78	0.04	12.34	0.67	0.03	0.03	0.69	3.60	4.82	92.74	99.05
25MC24_ox_1_Glass-2-15	76.97	0.05	12.54	1.31	0.01	0.01	0.63	3.72	4.75	93.50	99.81
25MC24_ox_1_Glass-2-16	77.98	0.05	12.58	0.36	0.05	0.02	0.68	3.44	4.84	92.75	99.05
25MC24_ox_1_Glass-2-17	77.31	0.07	12.57	0.78	0.06	0.14	0.69	3.56	4.83	93.70	100.00
25MC24_ox_1_Glass-2-18	76.70	0.11	12.64	0.83	0.06	0.15	0.67	3.88	4.95	93.81	100.11
25MC24_ox_1_Glass-2-19	78.01	0.00	12.48	0.45	0.02	0.03	0.69	3.63	4.69	93.74	100.05
25MC24_ox_1_Glass-2-20	77.87	0.08	12.46	0.44	0.02	0.02	0.68	3.62	4.81	93.80	100.10
25MC24_ox_1_Glass-2-21	77.39	0.09	12.62	0.70	0.01	0.06	0.72	3.52	4.87	93.63	99.94
25MC24_ox_1_Glass-2-22	77.51	0.02	12.69	0.52	0.02	0.04	0.72	3.64	4.82	92.87	99.18
25MC24_ox_1_Glass-2-24	77.85	0.04	12.61	0.45	0.02	0.04	0.66	3.53	4.78	92.65	98.95
25MC24_ox_1_Glass-2-27	77.62	0.02	12.55	0.61	0.06	0.03	0.67	3.71	4.73	93.90	100.21
25MC24_ox_1_Glass-2-28	77.71	0.06	12.76	0.63	0.07	0.01	0.69	3.36	4.70	93.25	99.56
25MC24_ox_1_Glass-2-30	77.19	0.05	12.32	1.14	0.05	0.04	0.65	3.82	4.74	94.40	100.71
25MC24_ox_1_Glass-2-33	77.94	0.07	12.51	0.39	0.03	0.04	0.66	3.54	4.83	93.86	100.17
25MC24_ox_1_Glass-2-34	77.55	0.04	12.56	0.72	0.05	0.02	0.70	3.57	4.79	92.16	98.47
25MC24_ox_1_Glass-2-35	77.27	0.07	12.82	0.41	0.04	0.04	0.71	3.78	4.87	93.71	100.01
25MC24_ox_1_Glass-2-37	77.19	0.06	12.49	0.94	0.04	0.02	0.95	3.60	4.72	93.58	99.89
25MC24_ox_1_Glass-2-38	77.64	0.06	12.68	0.79	0.06	0.04	0.67	3.19	4.86	94.20	100.50
25MC24_ox_1_Glass-2-39	77.38	0.05	12.77	0.78	0.03	0.06	0.70	3.46	4.79	93.38	99.68
25MC24_ox_1_Glass-2-40	77.89	0.04	12.62	0.42	0.01	0.03	0.64	3.58	4.77	93.85	100.16
25MC24_ox_1_Glass-2-41	77.64	0.06	12.51	0.44	0.06	0.06	0.72	3.75	4.75	93.42	99.72
25MC24_ox_1_Glass-2-42	77.38	0.09	12.54	0.79	-0.01	0.05	0.67	3.63	4.84	93.91	100.22

25MC24_ox_1_Glass-2-44	78.51	0.12	12.71	0.63	0.05	0.09	0.64	2.43	4.82	92.49	98.79
25MC24_ox_1_Glass-2-45	77.77	0.07	12.76	0.62	0.04	0.06	0.60	3.21	4.86	92.91	99.21
25MC24_ox_1_Glass-2-46	77.91	0.04	12.47	0.36	0.00	0.02	0.73	3.60	4.85	93.33	99.63
25MC24_ox_1_Glass-2-48	77.68	0.08	12.51	0.75	0.06	0.06	0.71	3.38	4.78	93.22	99.52
25MC24_ox_1_Glass-2-49	77.53	0.08	12.83	0.44	0.03	0.05	0.65	3.47	4.93	94.41	100.72
25MC24_ox_1_Glass-2-50	78.02	0.01	12.55	0.34	0.00	0.02	0.72	3.62	4.72	94.03	100.34
25MC24_ox_1_Glass-3-1	77.99	0.00	12.58	0.38	0.02	0.02	0.67	3.64	4.71	93.04	99.34
25MC24_ox_1_Glass-3-2	77.76	0.08	12.43	0.70	0.05	0.04	0.72	3.42	4.81	93.49	99.79
25MC24_ox_1_Glass-3-3	77.60	0.08	12.72	0.66	0.07	0.06	0.69	3.37	4.75	94.58	100.88
25MC24_ox_1_Glass-3-6	77.98	0.03	12.62	0.90	0.08	0.01	0.64	2.96	4.77	93.97	100.28
25MC24_ox_1_Glass-3-7	79.35	0.02	12.78	0.36	0.01	0.02	0.76	1.98	4.70	93.67	99.98
25MC24_ox_1_Glass-3-8	78.13	0.09	12.70	0.45	0.05	0.05	0.69	3.04	4.79	92.75	99.05
25MC24_ox_1_Glass-3-9	78.54	0.06	12.60	0.40	0.05	0.04	0.62	2.89	4.78	93.51	99.81
25MC24_ox_1_Glass-3-12	77.49	0.04	12.71	0.57	0.05	0.14	0.66	3.37	4.96	93.63	99.94
25MC24_ox_1_Glass-3-13	77.88	0.04	12.59	0.38	0.02	0.02	0.66	3.49	4.92	92.46	98.76
25MC24_ox_1_Glass-3-14	77.95	0.06	12.75	0.43	0.07	0.02	0.69	3.22	4.81	94.00	100.30
25MC24_ox_1_Glass-3-15	78.17	0.05	12.49	0.52	0.03	0.03	0.66	3.17	4.88	92.76	99.07
25MC24_ox_1_Glass-3-16	78.04	0.08	12.86	0.46	0.04	0.02	0.72	3.10	4.70	93.34	99.65
25MC24_ox_1_Glass-3-17	77.73	0.04	12.70	0.36	0.08	0.03	0.66	3.70	4.70	93.85	100.15
25MC24_ox_1_Glass-3-19	78.19	0.07	12.81	0.53	0.05	0.01	0.70	3.09	4.55	94.03	100.33
25MC24_ox_1_Glass-3-21	78.53	0.08	12.66	0.47	0.04	0.04	0.74	2.75	4.69	93.06	99.36
25MC24_ox_1_Glass-3-22	78.25	0.05	12.70	0.38	0.05	0.02	0.74	2.94	4.88	92.76	99.07
25MC24_ox_1_Glass-3-24	78.38	0.03	12.86	0.40	0.04	0.03	0.66	2.87	4.75	92.86	99.17
25MC24_ox_1_Glass-3-25	77.97	0.05	12.58	0.41	0.05	0.02	0.75	3.29	4.89	93.21	99.51
25MC24_ox_1_Glass-3-26	79.40	-0.01	12.68	0.36	0.04	0.02	0.70	2.04	4.77	92.45	98.75
25MC24_ox_1_Glass-3-27	78.30	0.07	12.72	1.08	0.02	0.02	0.72	2.47	4.61	93.43	99.74
25MC24_ox_1_Glass-3-28	78.14	0.07	12.67	0.45	0.03	0.03	0.67	3.16	4.77	93.43	99.73
25MC24_ox_1_Glass-3-29	78.51	0.06	12.78	0.35	0.00	0.02	0.70	2.73	4.85	93.14	99.45
25MC24_ox_1_Glass-3-30	78.38	0.02	12.69	0.33	0.01	0.03	0.64	3.11	4.80	93.37	99.68
25MC24_ox_1_Glass-3-31	76.07	0.08	14.14	0.67	0.04	0.12	0.71	3.32	4.85	93.57	99.88
25MC24_ox_1_Glass-3-32	78.22	0.07	12.65	0.52	0.03	0.05	0.73	2.87	4.85	94.26	100.56
25MC24_ox_1_Glass-3-33	78.05	0.06	12.89	0.48	0.01	0.08	0.65	2.87	4.91	93.26	99.56
25MC24_ox_1_Glass-3-34	79.77	0.04	12.78	0.49	0.06	0.04	0.71	1.36	4.74	93.00	99.31
25MC24_ox_1_Glass-3-35	78.67	0.08	12.74	0.85	0.03	0.02	0.73	1.98	4.89	92.57	98.88
25MC24_ox_1_Glass-3-36	78.60	0.07	12.70	0.36	0.03	0.03	0.73	2.52	4.98	92.51	98.82

	25MC24_ox_1_Glass-3-39	79.96	0.10	12.82	0.35	0.05	0.01	0.69	1.50	4.53	92.21	98.51
	Average	**77.77**	**0.06**	**12.66**	**0.55**	**0.03**	**0.05**	**0.69**	**3.36**	**4.82**	**93.44**	**99.75**
	Standard Deviation	**0.57**	**0.03**	**0.21**	**0.20**	**0.02**	**0.04**	**0.04**	**0.46**	**0.09**	**0.55**	**0.55**
MC: 5 25MC24_OX_4 750 °C 225 MPa *H_2O: 6.43	25MC24_ox_4_Glass-1-1	78.15	0.06	12.05	0.65	0.02	0.06	0.65	3.49	4.88	93.42	99.85
	25MC24_ox_4_Glass-1-2	78.12	0.08	12.22	0.65	0.02	0.06	0.59	3.45	4.81	93.25	99.68
	25MC24_ox_4_Glass-1-4	78.17	0.04	12.08	0.83	0.03	0.04	0.61	3.40	4.78	93.75	100.18
	25MC24_ox_4_Glass-1-5	78.05	0.06	12.10	0.69	0.01	0.05	0.65	3.59	4.80	93.89	100.32
	25MC24_ox_4_Glass-1-7	78.87	0.08	12.23	0.69	0.03	0.06	0.59	2.64	4.80	92.49	98.92
	25MC24_ox_4_Glass-1-8	78.72	0.03	12.18	0.83	0.02	0.06	0.61	2.77	4.78	92.38	98.81
	25MC24_ox_4_Glass-1-9	77.91	0.04	12.16	0.64	0.03	0.06	1.05	3.28	4.82	92.23	98.66
	25MC24_ox_4_Glass-1-10	77.89	0.07	12.53	0.62	0.04	0.05	0.62	3.33	4.85	93.43	99.86
	25MC24_ox_4_Glass-1-11	77.74	0.06	12.54	0.67	0.03	0.06	0.69	3.21	5.00	92.59	99.02
	25MC24_ox_4_Glass-1-13	77.90	0.07	12.45	0.71	0.02	0.06	0.65	3.35	4.80	92.68	99.11
	25MC24_ox_4_Glass-1-14	78.10	0.07	12.46	0.70	0.01	0.06	0.67	3.11	4.82	93.57	100.00
	25MC24_ox_4_Glass-1-15	79.66	0.08	12.75	0.66	0.04	0.04	0.69	1.40	4.67	92.69	99.12
	25MC24_ox_4_Glass-1-16	79.29	0.04	12.62	0.71	0.04	0.05	0.62	2.07	4.54	93.44	99.87
	25MC24_ox_4_Glass-1-18	78.59	0.07	12.65	0.64	0.02	0.06	0.65	2.45	4.87	93.34	99.77
	25MC24_ox_4_Glass-1-19	78.63	0.09	12.62	0.66	0.02	0.05	0.61	2.60	4.72	92.63	99.06
	25MC24_ox_4_Glass-1-20	79.30	0.05	12.60	0.67	0.01	0.06	0.70	1.89	4.71	91.84	98.27
	25MC24_ox_4_Glass-1-22	78.34	0.08	12.75	0.66	0.03	0.06	0.67	2.60	4.80	92.87	99.30
	25MC24_ox_4_Glass-1-23	78.44	0.06	12.79	0.66	0.03	0.05	0.63	2.55	4.77	92.62	99.05
	25MC24_ox_4_Glass-1-24	78.53	0.08	12.61	0.72	0.02	0.05	0.67	2.48	4.85	93.26	99.69
	25MC24_ox_4_Glass-1-26	79.48	0.07	12.62	0.69	0.05	0.06	0.68	1.62	4.72	92.52	98.95
	25MC24_ox_4_Glass-1-28	77.95	0.04	12.82	0.78	0.05	0.06	0.73	2.79	4.79	93.54	99.97
	25MC24_ox_4_Glass-1-29	77.98	0.12	12.63	0.61	0.01	0.06	0.73	3.04	4.81	92.43	98.86
	25MC24_ox_4_Glass-1-30	77.24	0.08	12.68	1.01	0.04	0.06	0.76	3.26	4.85	93.52	99.95
	25MC24_ox_4_Glass-1-31	77.79	0.13	12.69	0.84	0.02	0.05	0.70	3.01	4.77	93.08	99.51
	25MC24_ox_4_Glass-1-32	78.34	0.08	12.66	0.68	0.00	0.05	0.64	2.71	4.84	92.30	98.73
	25MC24_ox_4_Glass-1-33	78.41	0.05	12.77	0.67	0.00	0.04	0.69	2.62	4.73	93.13	99.56
	25MC24_ox_4_Glass-1-34	79.35	0.10	12.81	0.65	0.04	0.07	0.69	1.59	4.70	92.62	99.05
	25MC24_ox_4_Glass-1-35	77.83	0.08	12.81	0.67	0.02	0.07	0.67	2.99	4.86	93.40	99.83
	25MC24_ox_4_Glass-1-36	78.14	0.09	12.70	0.67	0.01	0.05	0.74	2.72	4.88	92.67	99.10
	25MC24_ox_4_Glass-1-37	78.61	0.13	12.87	0.67	0.00	0.05	0.68	2.26	4.71	91.97	98.40
	25MC24_ox_4_Glass-1-38	78.11	0.11	12.66	0.66	0.03	0.06	0.73	2.83	4.81	94.34	100.77

25MC24_ox_4_Glass-1-39	78.17	0.11	12.83	0.59	0.05	0.07	0.73	2.72	4.73	93.24	99.67
25MC24_ox_4_Glass-1-40	77.82	0.13	12.57	0.68	0.04	0.05	0.69	3.25	4.76	93.78	100.21
25MC24_ox_4_Glass-1-41	77.98	0.08	12.67	0.61	0.04	0.03	0.68	3.09	4.81	93.34	99.77
25MC24_ox_4_Glass-1-42	77.67	0.09	12.83	0.85	0.02	0.06	0.63	3.16	4.71	93.57	100.00
25MC24_ox_4_Glass-1-44	78.38	0.09	12.74	0.66	0.04	0.06	0.71	2.56	4.77	92.58	99.01
25MC24_ox_4_Glass-1-45	78.08	0.09	12.67	0.65	0.04	0.05	0.70	2.88	4.85	92.60	99.03
25MC24_ox_4_Glass-1-46	79.17	0.14	12.78	0.69	0.04	0.06	0.72	1.78	4.63	92.22	98.65
25MC24_ox_4_Glass-1-47	78.48	0.07	12.65	0.61	0.02	0.07	0.70	2.58	4.81	92.70	99.13
25MC24_ox_4_Glass-1-48	77.97	0.11	12.78	0.64	0.02	0.06	0.66	2.90	4.86	92.77	99.20
25MC24_ox_4_Glass-1-49	77.89	0.10	12.50	0.74	0.04	0.05	0.71	3.19	4.79	93.03	99.46
25MC24_ox_4_Glass-1-50	78.40	0.10	12.67	0.64	0.03	0.06	0.58	2.69	4.83	92.60	99.03
25MC24_ox_4_Glass-1-51	78.24	0.09	12.88	0.60	0.00	0.05	0.68	2.72	4.73	92.55	98.98
25MC24_ox_4_Glass-1-52	77.82	0.13	12.91	0.79	0.01	0.04	0.73	2.89	4.67	93.63	100.06
25MC24_ox_4_Glass-1-53	78.33	0.14	12.63	0.83	0.01	0.06	0.66	2.51	4.82	93.03	99.46
25MC24_ox_4_Glass-1-54	79.19	0.12	12.65	0.67	-0.01	0.06	0.74	1.96	4.61	92.98	99.41
25MC24_ox_4_Glass-1-55	78.59	0.10	12.99	0.63	0.02	0.05	0.63	2.13	4.85	92.90	99.33
25MC24_ox_4_Glass-1-56	78.97	0.16	12.99	0.73	0.02	0.05	0.77	1.74	4.57	93.45	99.88
25MC24_ox_4_Glass-2-3	77.28	0.12	12.47	1.07	-0.02	0.06	0.73	3.35	4.93	94.00	100.43
25MC24_ox_4_Glass-2-5	77.13	0.14	12.90	1.30	0.03	0.04	0.65	3.00	4.80	94.26	100.69
25MC24_ox_4_Glass-2-6	76.93	0.15	12.49	1.22	0.02	0.07	0.78	3.54	4.81	93.02	99.45
25MC24_ox_4_Glass-2-7	76.52	0.16	12.38	1.38	0.03	0.06	0.71	3.96	4.78	93.56	99.99
25MC24_ox_4_Glass-2-8	77.36	0.13	12.48	1.39	0.04	0.06	0.70	3.02	4.81	92.99	99.42
25MC24_ox_4_Glass-2-9	76.68	0.16	12.77	1.25	0.02	0.06	0.68	3.56	4.82	93.93	100.36
25MC24_ox_4_Glass-2-12	77.15	0.14	12.59	1.07	0.00	0.05	0.68	3.51	4.82	93.50	99.93
25MC24_ox_4_Glass-2-13	77.46	0.14	12.54	1.28	0.01	0.06	0.67	3.07	4.77	93.00	99.43
25MC24_ox_4_Glass-2-14	77.23	0.17	12.52	1.15	0.04	0.07	0.67	3.36	4.80	93.75	100.18
25MC24_ox_4_Glass-2-15	78.08	0.17	12.40	1.24	0.02	0.06	0.71	2.52	4.81	92.98	99.41
25MC24_ox_4_Glass-2-16	76.89	0.12	12.71	1.35	0.05	0.08	0.71	3.32	4.76	93.16	99.59
25MC24_ox_4_Glass-2-19	76.84	0.16	12.53	1.21	0.04	0.07	0.72	3.60	4.85	93.92	100.34
25MC24_ox_4_Glass-2-20	76.96	0.18	12.55	1.19	0.01	0.05	0.76	3.51	4.78	93.46	99.89
25MC24_ox_4_Glass-2-21	77.28	0.15	12.37	1.14	0.06	0.05	0.72	3.43	4.81	93.72	100.15
25MC24_ox_4_Glass-2-22	77.48	0.18	12.68	1.19	0.02	0.06	0.74	2.86	4.80	93.69	100.12
25MC24_ox_4_Glass-2-23	77.04	0.13	12.71	0.89	0.03	0.07	0.67	3.57	4.86	93.46	99.89
25MC24_ox_4_Glass-2-24	77.44	0.14	12.64	0.80	0.03	0.06	0.71	3.45	4.74	93.74	100.17
25MC24_ox_4_Glass-2-25	77.20	0.13	12.66	0.86	0.01	0.06	0.68	3.73	4.66	94.07	100.50

25MC24_ox_4_Glass-2-26	77.94	0.11	12.51	0.87	0.02	0.05	0.68	2.98	4.83	93.63	100.06
25MC24_ox_4_Glass-2-27	77.25	0.10	12.79	0.84	0.01	0.06	0.63	3.60	4.70	94.28	100.71
25MC24_ox_4_Glass-2-28	77.40	0.12	12.78	0.92	0.03	0.07	0.73	3.17	4.78	93.47	99.90
25MC24_ox_4_Glass-2-29	77.44	0.17	12.67	0.90	0.00	0.07	0.70	3.25	4.81	93.21	99.64
25MC24_ox_4_Glass-2-30	77.54	0.10	12.69	0.88	0.02	0.04	0.71	3.27	4.74	93.39	99.82
25MC24_ox_4_Glass-2-31	77.24	0.10	12.94	0.77	0.04	0.06	0.66	3.41	4.78	93.59	100.02
25MC24_ox_4_Glass-2-32	77.41	0.12	12.73	0.87	0.04	0.06	0.69	3.33	4.75	93.50	99.93
25MC24_ox_4_Glass-2-33	77.29	0.11	12.85	0.85	0.04	0.07	0.70	3.32	4.78	92.98	99.41
25MC24_ox_4_Glass-2-34	77.40	0.12	12.70	0.93	0.02	0.05	0.66	3.42	4.70	93.99	100.42
25MC24_ox_4_Glass-2-35	77.73	0.14	12.77	0.75	0.04	0.06	0.71	3.04	4.75	93.25	99.68
25MC24_ox_4_Glass-2-36	77.57	0.14	12.41	0.74	0.04	0.05	0.72	3.48	4.87	93.40	99.83
25MC24_ox_4_Glass-2-37	77.38	0.10	12.72	0.73	0.02	0.04	0.72	3.46	4.83	92.83	99.26
25MC24_ox_4_Glass-2-38	77.85	0.08	12.64	0.72	-0.01	0.06	0.75	3.25	4.66	93.40	99.83
25MC24_ox_4_Glass-2-39	77.08	0.13	12.61	1.31	0.05	0.06	0.67	3.32	4.75	93.90	100.33
25MC24_ox_4_Glass-2-40	77.26	0.12	12.70	0.78	0.02	0.06	0.67	3.61	4.78	94.08	100.51
25MC24_ox_4_Glass-2-41	77.52	0.11	12.82	0.75	0.00	0.05	0.68	3.27	4.79	94.05	100.48
25MC24_ox_4_Glass-2-42	77.57	0.13	12.89	0.76	-0.01	0.06	0.66	3.21	4.71	93.39	99.82
25MC24_ox_4_Glass-2-43	77.53	0.13	12.56	0.79	0.04	0.06	0.73	3.48	4.69	92.94	99.37
25MC24_ox_4_Glass-2-44	77.57	0.14	12.66	0.71	0.05	0.07	0.71	3.31	4.78	93.17	99.60
25MC24_ox_4_Glass-2-45	77.58	0.18	12.45	0.77	0.01	0.05	0.72	3.43	4.83	93.19	99.61
25MC24_ox_4_Glass-2-47	77.36	0.12	12.78	0.73	0.03	0.06	0.67	3.51	4.72	94.09	100.52
25MC24_ox_4_Glass-2-48	77.63	0.14	12.65	0.78	0.00	0.06	0.71	3.16	4.87	93.28	99.71
25MC24_ox_4_Glass-2-50	77.15	0.13	12.75	0.83	0.03	0.06	0.73	3.48	4.85	93.61	100.04
25MC24_ox_4_Glass-2-51	78.14	0.13	12.66	0.92	0.03	0.05	0.73	2.58	4.76	93.75	100.17
25MC24_ox_4_Glass-2-52	77.65	0.08	12.72	0.82	0.02	0.06	0.72	3.19	4.73	94.25	100.68
25MC24_ox_4_Glass-3-1	76.73	0.17	12.48	1.19	0.02	0.07	0.74	3.72	4.88	94.13	100.56
25MC24_ox_4_Glass-3-2	76.92	0.15	12.81	1.05	0.03	0.05	0.67	3.36	4.94	93.93	100.36
25MC24_ox_4_Glass-3-3	79.30	0.15	12.85	1.11	0.03	0.06	0.69	1.18	4.63	92.04	98.47
25MC24_ox_4_Glass-3-4	77.72	0.12	12.69	1.00	0.02	0.06	0.72	2.81	4.87	93.30	99.73
25MC24_ox_4_Glass-3-5	77.02	0.16	12.67	0.83	0.06	0.07	0.71	3.49	4.99	93.35	99.78
25MC24_ox_4_Glass-3-6	77.10	0.10	12.83	0.76	0.05	0.05	0.68	3.62	4.82	93.77	100.20
25MC24_ox_4_Glass-3-7	77.19	0.13	12.99	0.78	0.06	0.05	0.69	3.16	4.95	93.37	99.80
25MC24_ox_4_Glass-3-8	78.80	0.13	12.67	0.80	0.04	0.05	0.76	1.98	4.78	91.72	98.15
25MC24_ox_4_Glass-3-9	77.72	0.13	12.78	0.73	0.01	0.07	0.66	2.95	4.94	93.08	99.51
25MC24_ox_4_Glass-3-10	77.44	0.10	12.93	0.76	0.03	0.05	0.69	3.03	4.96	93.27	99.70

25MC24_ox_4_Glass-3-11	77.42	0.15	12.77	0.92	0.01	0.05	0.70	2.96	5.02	92.98	99.41
25MC24_ox_4_Glass-3-13	77.97	0.15	13.03	0.85	0.04	0.06	0.64	2.30	4.96	92.22	98.65
25MC24_ox_4_Glass-3-14	77.90	0.19	12.82	0.96	0.04	0.06	0.66	2.32	5.04	92.64	99.07
25MC24_ox_4_Glass-3-15	79.52	0.16	13.01	0.88	0.05	0.06	0.69	1.06	4.57	92.38	98.81
25MC24_ox_4_Glass-3-16	78.75	0.09	13.02	0.79	0.04	0.06	0.61	1.90	4.73	92.51	98.94
25MC24_ox_4_Glass-3-17	79.10	0.12	12.78	0.83	0.02	0.06	0.72	1.68	4.70	91.83	98.26
25MC24_ox_4_Glass-3-19	77.67	0.15	12.97	1.00	0.02	0.05	0.73	2.54	4.85	93.82	100.25
25MC24_ox_4_Glass-3-20	78.33	0.17	13.01	1.15	0.03	0.05	0.66	1.87	4.73	94.10	100.53
25MC24_ox_4_Glass-3-21	76.82	0.18	13.04	0.86	0.02	0.05	0.70	3.43	4.89	93.27	99.70
25MC24_ox_4_Glass-3-22	77.40	0.12	12.51	0.87	0.01	0.06	0.76	3.38	4.90	93.67	100.10
25MC24_ox_4_Glass-3-23	77.20	0.14	12.78	0.92	0.03	0.13	0.68	3.15	4.98	93.23	99.66
25MC24_ox_4_Glass-3-24	77.85	0.12	12.78	0.99	0.03	0.06	0.74	2.49	4.94	93.10	99.53
25MC24_ox_4_Glass-3-25	77.54	0.14	13.01	1.03	0.04	0.05	0.75	2.49	4.94	93.63	100.06
25MC24_ox_4_Glass-3-26	77.69	0.14	12.80	0.94	0.01	0.06	0.69	2.64	5.02	92.29	98.72
25MC24_ox_4_Glass-3-27	78.81	0.18	12.90	0.94	0.03	0.07	0.73	1.66	4.67	92.50	98.93
25MC24_ox_4_Glass-3-28	77.33	0.09	12.87	0.81	0.00	0.06	0.75	3.21	4.89	93.15	99.58
25MC24_ox_4_Glass-3-29	78.28	0.15	12.96	0.82	0.00	0.07	0.71	2.19	4.82	92.05	98.47
25MC24_ox_4_Glass-3-30	77.71	0.14	12.79	0.84	0.03	0.06	0.75	2.66	5.02	92.54	98.97
25MC24_ox_4_Glass-3-31	76.96	0.16	12.81	0.96	0.01	0.06	0.72	3.25	5.07	93.29	99.72
25MC24_ox_4_Glass-3-32	77.18	0.15	12.92	0.87	0.04	0.07	0.68	3.15	4.94	92.56	98.99
25MC24_ox_4_Glass-3-33	77.58	0.17	12.68	0.89	0.02	0.06	0.71	2.93	4.95	93.85	100.28
25MC24_ox_4_Glass-3-34	77.91	0.15	13.04	0.94	0.03	0.06	0.70	2.23	4.94	94.44	100.87
25MC24_ox_4_Glass-3-35	77.09	0.14	12.77	0.96	0.03	0.04	0.74	3.22	5.01	92.63	99.06
25MC24_ox_4_Glass-3-36	77.37	0.14	12.66	0.82	0.03	0.06	0.69	3.26	4.97	93.95	100.38
25MC24_ox_4_Glass-3-37	76.85	0.13	12.98	0.89	0.00	0.06	0.70	3.41	4.99	93.44	99.87
25MC24_ox_4_Glass-3-38	77.55	0.16	13.01	0.86	0.01	0.05	0.71	2.75	4.91	93.01	99.44
25MC24_ox_4_Glass-3-39	77.28	0.15	12.45	1.03	0.05	0.07	0.74	3.19	5.04	91.60	98.03
25MC24_ox_4_Glass-3-40	77.08	0.17	12.71	0.95	0.01	0.07	0.72	3.39	4.90	93.89	100.32
25MC24_ox_4_Glass-3-41	77.28	0.13	12.63	1.04	0.03	0.06	0.68	3.14	5.01	93.43	99.86
25MC24_ox_4_Glass-3-42	78.53	0.12	12.73	0.89	0.01	0.06	0.73	2.01	4.92	92.47	98.90
25MC24_ox_4_Glass-3-43	77.62	0.20	12.63	0.85	0.03	0.05	0.70	3.04	4.88	92.95	99.38
25MC24_ox_4_Glass-3-44	77.21	0.13	12.74	1.04	0.03	0.07	0.67	3.15	4.95	92.65	99.08
25MC24_ox_4_Glass-3-45	77.13	0.16	12.77	1.02	0.04	0.04	0.74	3.22	4.86	93.69	100.12
25MC24_ox_4_Glass-3-46	77.27	0.17	12.80	1.28	0.02	0.05	0.69	2.80	4.92	94.27	100.70
25MC24_ox_4_Glass-3-47	76.53	0.17	12.91	1.39	0.02	0.06	0.66	3.33	4.90	93.83	100.26

	25MC24_ox_4_Glass-3-48	77.04	0.16	13.04	1.20	0.04	0.06	0.73	3.21	4.53	93.69	100.12
	25MC24_ox_4_Glass-3-49	77.22	0.13	12.94	1.00	0.03	0.04	0.69	3.18	4.74	94.44	100.87
	25MC24_ox_4_Glass-3-51	76.77	0.19	12.90	0.94	0.01	0.06	0.68	3.61	4.84	93.64	100.07
	25MC24_ox_4_Glass-3-52	77.57	0.14	12.73	0.88	0.03	0.07	0.69	3.04	4.85	93.02	99.45
	25MC24_ox_4_Glass-3-53	78.25	0.15	13.06	0.93	0.03	0.06	0.68	2.18	4.65	92.51	98.94
	25MC24_ox_4_Glass-3-54	79.33	0.16	13.08	0.88	0.02	0.06	0.73	1.16	4.58	91.87	98.30
	25MC24_ox_4_Glass-3-55	78.29	0.10	12.79	0.79	0.02	0.05	0.74	2.22	4.99	92.14	98.57
	25MC24_ox_4_Glass-3-56	77.14	0.18	12.82	1.03	0.03	0.06	0.71	3.22	4.81	94.09	100.52
	25MC24_ox_4_Glass-3-57	78.58	0.16	12.84	1.09	0.03	0.05	0.74	1.87	4.64	92.20	98.63
	25MC24_ox_4_Glass-3-58	77.92	0.17	12.82	1.02	0.05	0.04	0.68	2.50	4.78	92.23	98.66
	25MC24_ox_4_Glass-3-12	79.55	0.22	13.34	0.91	0.02	0.05	0.78	0.64	4.49	93.00	99.43
	25MC24_ox_4_Glass-3-60	79.53	0.14	12.88	0.94	0.01	0.05	0.73	1.12	4.60	92.52	98.95
	Average	**77.82**	**0.12**	**12.71**	**0.87**	**0.02**	**0.06**	**0.70**	**2.87**	**4.81**	**93.18**	**99.61**
	Standard Deviation	**0.72**	**0.04**	**0.21**	**0.19**	**0.02**	**0.01**	**0.05**	**0.64**	**0.11**	**0.64**	**0.64**
MC: 6 25MC24_OX_5 750 °C 150 MPa *H_2O: 5.10	25MC24_OX_5_Glass 3-1	77.00	0.22	12.60	1.01	0.06	0.09	0.80	3.43	4.79	93.79	98.89
	25MC24_OX_5_Glass 3-7	79.42	0.22	13.20	1.12	0.02	0.11	0.87	1.03	4.02	92.45	97.55
	25MC24_OX_5_Glass 3-19	77.77	0.16	14.51	1.31	0.03	0.09	0.83	1.08	4.21	92.90	98.01
	25MC24_OX_5_Glass 3-20	79.08	0.19	13.01	1.31	0.03	0.10	0.76	1.23	4.28	92.34	97.44
	25MC24_OX_5_Glass 4-1	77.52	0.13	12.37	1.10	0.00	0.06	0.74	3.37	4.71	94.69	99.79
	25MC24_OX_5_Glass 4-2	77.29	0.13	12.56	0.95	0.02	0.06	0.76	3.56	4.67	94.89	99.99
	25MC24_OX_5_Glass 4-4	77.44	0.11	12.72	1.01	0.03	0.08	0.74	3.24	4.62	95.11	100.22
	25MC24_OX_5_Glass 4-5	76.75	0.17	12.56	1.35	0.04	0.06	0.76	3.53	4.79	95.25	100.35
	25MC24_OX_5_Glass 4-6	77.58	0.16	12.83	1.19	0.01	0.05	0.75	2.85	4.58	95.41	100.51
	25MC24_OX_5_Glass 4-7	79.08	0.14	13.00	1.16	0.01	0.05	0.74	1.56	4.27	94.30	99.41
	25MC24_OX_5_Glass 4-8	76.55	0.14	12.59	1.27	0.04	0.07	0.72	3.80	4.83	94.81	99.92
	25MC24_OX_5_Glass 4-9	77.72	0.16	12.90	1.25	0.02	0.07	0.76	2.39	4.72	94.25	99.35
	25MC24_OX_5_Glass 4-10	77.30	0.13	12.68	1.24	0.03	0.06	0.73	3.14	4.69	94.96	100.06
	25MC24_OX_5_Glass 4-11	76.94	0.15	12.74	1.08	0.01	0.05	0.78	3.70	4.54	95.23	100.33
	25MC24_OX_5_Glass 4-13	77.95	0.15	12.82	1.03	0.01	0.04	0.70	2.77	4.51	93.59	98.69
	25MC24_OX_5_Glass 4-14	77.66	0.14	13.00	0.96	0.04	0.07	0.68	2.92	4.53	94.28	99.39
	25MC24_OX_5_Glass 4-15	79.52	0.16	12.99	1.00	0.04	0.07	0.77	1.22	4.22	94.12	99.22
	25MC24_OX_5_Glass 4-16	77.88	0.10	12.65	1.05	0.01	0.07	0.73	2.77	4.75	94.32	99.42
	25MC24_OX_5_Glass 4-17	78.15	0.13	12.85	1.07	0.00	0.06	0.70	2.41	4.62	94.44	99.54
	25MC24_OX_5_Glass 4-18	78.57	0.16	12.70	1.14	0.05	0.06	0.73	2.08	4.51	94.30	99.40

	25MC24_OX_5_Glass 4-19	77.20	0.15	12.57	1.29	0.07	0.06	0.69	3.33	4.64	95.26	100.36
	25MC24_OX_5_Glass 4-20	78.29	0.12	12.95	1.16	0.02	0.05	1.00	1.93	4.49	94.24	99.34
	25MC24_OX_5_Glass 4-21	79.63	0.13	13.01	1.34	0.02	0.06	0.76	1.04	4.01	94.49	99.59
	25MC24_OX_5_Glass 4-22	78.68	0.11	12.81	1.14	0.01	0.06	0.75	1.95	4.50	94.02	99.13
	25MC24_OX_5_Glass 4-23	79.67	0.13	13.13	1.03	0.04	0.08	0.75	0.97	4.20	93.61	98.72
	25MC24_OX_5_Glass 4-3	77.79	0.07	12.58	0.97	0.07	0.06	0.69	3.04	4.74	94.51	99.62
	25MC24_OX_5_Glass 4-24	77.98	0.15	13.08	0.94	0.05	0.06	0.73	2.47	4.53	95.03	100.13
	25MC24_OX_5_Glass 4-25	78.65	0.12	12.91	1.27	0.02	0.06	0.83	1.81	4.33	94.22	99.32
	25MC24_OX_5_Glass 4-26	78.90	0.10	14.08	0.99	0.04	0.06	0.74	1.09	3.98	92.83	97.93
	25MC24_OX_5_Glass 4-27	79.16	0.16	13.53	1.01	0.03	0.06	0.74	1.09	4.22	92.91	98.01
	25MC24_OX_5_Glass 4-28	77.94	0.18	12.91	1.20	0.03	0.07	0.81	2.23	4.63	93.58	98.68
	25MC24_OX_5_Glass 4-30	78.11	0.17	12.86	1.14	0.04	0.05	0.80	2.23	4.60	94.59	99.70
	Average	**78.10**	**0.14**	**12.93**	**1.13**	**0.03**	**0.06**	**0.76**	**2.35**	**4.49**	**94.21**	**99.31**
	Standard Deviation	**0.88**	**0.03**	**0.43**	**0.13**	**0.02**	**0.01**	**0.06**	**0.93**	**0.24**	**0.83**	**0.83**
MC: 7 25MC24_OX_6 750 °C 125 MPa *H_2O: 4.71	25MC24_OX_6_Glass 1-1	78.09	0.04	12.26	0.65	0.00	0.05	0.62	3.62	4.67	93.89	98.60
	25MC24_OX_6_Glass 1-4	78.41	0.07	12.45	0.84	0.04	0.04	0.60	2.78	4.74	92.99	97.70
	25MC24_OX_6_Glass 1-5	77.77	0.05	12.39	0.57	0.04	0.04	0.66	3.70	4.77	94.89	99.60
	25MC24_OX_6_Glass 1-6	78.24	0.02	12.67	0.63	0.04	0.06	0.73	2.91	4.68	94.18	98.89
	25MC24_OX_6_Glass 1-7	79.50	0.09	12.66	0.74	0.03	0.04	0.75	1.62	4.56	93.31	98.02
	25MC24_OX_6_Glass 1-9	77.60	0.09	12.26	0.65	0.06	0.03	0.69	3.86	4.76	94.74	99.45
	25MC24_OX_6_Glass 1-10	77.75	0.05	12.49	0.67	0.03	0.04	0.70	3.50	4.76	92.81	97.52
	25MC24_OX_6_Glass 1-12	77.76	0.07	12.46	0.60	0.00	0.05	0.71	3.67	4.69	94.19	98.90
	25MC24_OX_6_Glass 1-13	79.54	0.04	12.41	0.76	0.02	0.04	0.63	1.95	4.61	93.16	97.87
	25MC24_OX_6_Glass 1-14	78.08	0.02	12.24	0.68	0.03	0.06	0.67	3.48	4.73	94.62	99.33
	25MC24_OX_6_Glass 1-16	77.82	0.08	12.60	0.63	0.01	0.03	0.64	3.58	4.61	93.72	98.43
	25MC24_OX_6_Glass 1-17	78.13	0.03	12.68	0.64	0.04	0.04	0.68	3.12	4.63	93.60	98.31
	25MC24_OX_6_Glass 1-18	77.98	0.09	13.39	0.62	0.03	0.06	0.69	2.49	4.65	93.12	97.83
	25MC24_OX_6_Glass 1-22	77.62	0.05	12.51	1.32	0.06	0.04	0.71	3.14	4.54	94.99	99.70
	25MC24_OX_6_Glass 1-23	78.48	0.05	12.72	0.59	0.01	0.05	0.67	2.79	4.62	94.35	99.06
	25MC24_OX_6_Glass 1-24	77.70	0.05	12.53	0.88	0.04	0.05	0.66	3.32	4.75	94.80	99.51
	25MC24_OX_6_Glass 1-27	77.65	0.07	12.49	0.68	0.05	0.06	0.71	3.48	4.81	94.98	99.69
	25MC24_OX_6_Glass 1-29	79.31	0.04	12.85	0.72	0.03	0.04	0.67	1.83	4.50	94.32	99.03
	25MC24_OX_6_Glass 1-30	77.15	0.06	15.25	1.40	0.03	0.05	0.67	1.27	4.07	92.51	97.22
	25MC24_OX_6_Glass 1-35	79.62	0.04	12.81	0.61	0.04	0.06	0.66	1.66	4.51	93.05	97.76

25MC24_OX_6_Glass 1-40	79.61	0.09	12.71	0.62	0.05	0.06	0.70	1.68	4.48	94.30	99.01
25MC24_OX_6_Glass 2-7	77.66	0.10	12.34	0.91	0.03	0.06	0.60	3.59	4.71	95.83	100.54
25MC24_OX_6_Glass 2-8	77.26	0.10	12.54	0.91	0.05	0.04	1.02	3.48	4.59	94.74	99.45
25MC24_OX_6_Glass 2-11	77.22	0.12	12.16	1.35	0.05	0.05	0.64	3.62	4.79	94.47	99.18
25MC24_OX_6_Glass 2-13	78.97	0.06	12.54	0.92	0.03	0.05	0.64	2.17	4.60	93.58	98.29
25MC24_OX_6_Glass 2-14	79.22	0.09	12.49	1.07	0.05	0.06	0.72	1.67	4.63	93.51	98.21
25MC24_OX_6_Glass 2-15	78.87	0.06	12.84	0.63	0.03	0.05	0.67	2.09	4.76	93.42	98.13
25MC24_OX_6_Glass 2-17	76.71	0.06	13.70	0.68	0.00	0.03	0.59	3.52	4.69	93.00	97.71
25MC24_OX_6_Glass 2-19	77.88	0.02	12.28	1.00	0.04	0.05	0.67	3.43	4.62	93.11	97.82
25MC24_OX_6_Glass 2-21	79.01	0.05	12.77	0.83	0.01	0.06	0.69	2.06	4.52	94.60	99.31
25MC24_OX_6_Glass 2-23	77.91	0.09	12.51	0.74	0.03	0.04	0.65	3.30	4.73	95.51	100.22
25MC24_OX_6_Glass 3-1	77.74	0.09	12.39	0.73	0.04	0.05	0.69	3.49	4.76	94.54	99.25
25MC24_OX_6_Glass 3-3	77.45	0.11	12.44	0.74	0.05	0.05	0.63	3.72	4.80	95.17	99.88
25MC24_OX_6_Glass 3-4	78.88	0.09	12.74	0.76	0.03	0.06	0.69	2.01	4.74	93.53	98.24
25MC24_OX_6_Glass 3-5	78.10	0.15	12.71	0.68	0.01	0.06	0.77	2.68	4.83	93.58	98.29
25MC24_OX_6_Glass 3-6	78.24	0.09	12.77	0.68	0.02	0.04	0.83	2.46	4.86	93.48	98.19
25MC24_OX_6_Glass 3-8	76.04	0.09	14.38	0.74	0.03	0.04	0.57	3.24	4.84	92.96	97.67
25MC24_OX_6_Glass 3-9	77.08	0.10	12.70	0.94	0.02	0.07	0.65	3.62	4.81	94.66	99.36
25MC24_OX_6_Glass 3-10	77.32	0.12	13.01	0.84	0.02	0.06	0.64	3.18	4.81	93.25	97.96
25MC24_OX_6_Glass 3-13	77.18	0.23	12.76	0.76	0.02	0.07	0.75	3.49	4.74	95.39	100.10
25MC24_OX_6_Glass 3-14	78.35	0.16	12.97	0.86	0.03	0.06	0.71	2.09	4.75	94.29	99.00
25MC24_OX_6_Glass 3-16	77.62	0.19	12.70	1.08	0.02	0.07	0.67	2.87	4.77	94.11	98.82
25MC24_OX_6_Glass 3-18	78.01	0.19	13.00	0.81	0.05	0.06	0.70	2.37	4.80	94.63	99.34
25MC24_OX_6_Glass 3-19	77.13	0.19	12.94	0.71	0.04	0.05	0.75	3.41	4.79	95.82	100.53
25MC24_OX_6_Glass 3-20	78.14	0.17	13.15	0.73	0.00	0.06	0.75	2.36	4.63	95.83	100.54
25MC24_OX_6_Glass 3-24	76.10	0.14	14.17	0.75	0.04	0.05	1.29	3.08	4.37	94.90	99.61
25MC24_OX_6_Glass 3-26	75.81	0.12	14.14	0.64	0.00	0.05	1.25	3.70	4.29	94.79	99.50
25MC24_OX_6_Glass 3-27	77.66	0.13	12.51	0.68	0.03	0.05	0.74	3.38	4.81	94.80	99.51
25MC24_OX_6_Glass 3-29	74.84	0.18	16.34	0.65	0.02	0.06	0.64	2.68	4.57	93.26	97.97
25MC24_OX_6_Glass 3-31	77.06	0.10	14.28	0.73	0.03	0.04	1.30	2.27	4.19	94.88	99.59
25MC24_OX_6_Glass 3-33	77.68	0.14	12.60	0.67	0.05	0.04	0.70	3.44	4.68	95.10	99.81
25MC24_OX_6_Glass 3-34	78.65	0.13	13.15	0.69	0.02	0.04	0.65	2.03	4.62	93.46	98.17
25MC24_OX_6_Glass 3-35	77.53	0.12	12.58	0.65	0.00	0.05	0.63	3.67	4.77	94.94	99.65
25MC24_OX_6_Glass 3-37	78.73	0.12	12.40	0.66	0.02	0.06	0.69	2.43	4.87	93.62	98.33
25MC24_OX_6_Glass 3-38	78.67	0.14	12.63	1.28	0.02	0.07	0.68	1.91	4.59	93.40	98.11

25MC24_OX_6_Glass 3-39	79.98	0.11	12.37	0.76	0.03	0.07	0.65	1.36	4.67	92.89	97.60
25MC24_OX_6_Glass 3-40	79.26	0.13	12.89	1.26	0.04	0.05	0.71	1.17	4.49	93.37	98.08
25MC24_OX_6_Glass 4-4	77.26	0.17	12.43	1.26	0.03	0.05	0.68	3.25	4.87	94.51	99.22
25MC24_OX_6_Glass 4-6	77.77	0.21	12.37	1.31	0.02	0.05	0.68	2.78	4.81	94.67	99.38
25MC24_OX_6_Glass 4-8	77.16	0.13	12.66	0.92	0.01	0.05	0.65	3.63	4.78	95.83	100.54
25MC24_OX_6_Glass 4-10	77.87	0.12	12.03	0.74	0.01	0.06	0.63	3.66	4.88	94.01	98.72
25MC24_OX_6_Glass 4-11	77.24	0.16	12.13	1.11	0.00	0.05	0.65	3.80	4.85	93.76	98.47
25MC24_OX_6_Glass 4-12	77.66	0.13	12.34	0.75	0.04	0.04	0.66	3.55	4.81	94.24	98.95
25MC24_OX_6_Glass 4-13	77.50	0.15	12.34	0.87	0.01	0.05	0.65	3.70	4.73	94.08	98.79
25MC24_OX_6_Glass 4-14	77.74	0.14	12.21	0.77	0.02	0.06	0.67	3.59	4.80	94.67	99.38
25MC24_OX_6_Glass 4-15	77.06	0.14	12.48	1.17	0.01	0.05	0.72	3.55	4.81	95.31	100.02
25MC24_OX_6_Glass 4-16	77.51	0.13	12.45	0.73	0.01	0.05	0.70	3.62	4.80	95.90	100.61
25MC24_OX_6_Glass 4-17	77.63	0.13	12.41	0.71	0.01	0.06	0.64	3.59	4.83	95.28	99.99
25MC24_OX_6_Glass 4-18	77.78	0.13	12.22	0.72	0.00	0.05	0.70	3.72	4.70	94.94	99.65
25MC24_OX_6_Glass 4-19	77.57	0.10	12.61	0.80	0.02	0.04	0.69	3.42	4.74	95.13	99.84
25MC24_OX_6_Glass 4-20	76.97	0.21	12.35	1.29	0.03	0.05	0.76	3.63	4.73	95.82	100.53
25MC24_OX_6_Glass 4-21	77.57	0.18	12.55	0.83	0.01	0.04	0.64	3.44	4.72	95.18	99.89
25MC24_OX_6_Glass 4-23	77.21	0.14	12.74	0.83	-0.02	0.05	0.63	3.71	4.72	95.29	100.00
25MC24_OX_6_Glass 4-25	78.38	0.12	12.64	0.74	0.01	0.05	0.62	2.63	4.81	94.13	98.84
25MC24_OX_6_Glass 4-26	77.87	0.18	12.53	0.78	0.00	0.04	0.64	3.16	4.79	94.58	99.29
25MC24_OX_6_Glass 4-27	77.48	0.17	12.40	0.85	0.02	0.06	0.65	3.63	4.73	94.90	99.61
25MC24_OX_6_Glass 4-28	77.20	0.14	12.53	0.67	0.00	0.05	0.72	3.92	4.77	96.11	100.82
25MC24_OX_6_Glass 4-29	77.62	0.09	12.36	0.72	0.00	0.04	0.68	3.54	4.94	95.16	99.87
25MC24_OX_6_Glass 4-30	77.73	0.10	12.39	0.63	0.02	0.04	0.65	3.62	4.81	94.45	99.16
25MC24_OX_6_Glass 4-31	78.33	0.14	12.20	0.68	0.02	0.04	0.69	3.02	4.88	93.66	98.37
Average	**77.85**	**0.11**	**12.74**	**0.81**	**0.02**	**0.05**	**0.70**	**3.01**	**4.70**	**94.33**	**99.04**
Standard Deviation	**0.88**	**0.05**	**0.68**	**0.21**	**0.02**	**0.01**	**0.13**	**0.74**	**0.15**	**0.88**	**0.88**

Table A-0-6 Natural individual biotite analyses (wt%) for previously published samples from the Bishop Tuff (Jolles and Lange, 2019)

Sample	Point	SiO_2	TiO_2	Al_2O_3	FeO	MnO	MgO	CaO	Na_2O	K_2O	BaO	Total	Mg#
BT-22A	BTE 5-1	36.01	3.99	12.19	23.79	0.31	9.26	0.03	0.45	9.32	0.02	95.37	41
BT-22A	BTE 5-2	36.47	4.18	12.61	23.63	0.32	9.62	0.04	0.48	9.35	0.00	96.69	42
BT-22A	BTE 5-3	36.85	4.21	12.70	23.68	0.31	9.64	0.05	0.47	9.29	0.04	97.23	42
BT-22A	BTE 5-5	37.55	4.16	12.09	23.14	0.30	9.33	0.11	0.39	9.03	0.07	96.18	42
	Average	**36.72**	**4.13**	**12.40**	**23.56**	**0.31**	**9.46**	**0.06**	**0.45**	**9.25**	**0.03**	**96.37**	**42**
	Standard Deviation	**0.65**	**0.10**	**0.30**	**0.29**	**0.01**	**0.19**	**0.04**	**0.04**	**0.14**	**0.03**	**0.79**	**1**
BT-22B	BTE 1-1	36.01	4.19	12.18	24.62	0.33	8.62	0.10	0.44	8.94	0.04	95.46	38
BT-22B	BTE 4-1	35.67	4.25	12.52	24.67	0.34	8.98	0.02	0.40	9.47	0.04	96.35	39
BT-22B	BTE 4-2	36.01	4.26	12.25	24.85	0.52	9.04	0.02	0.43	9.44	0.05	96.87	39
BT-22B	BTE 4-3	35.50	4.25	12.66	24.79	0.34	8.86	0.02	0.40	9.54	0.02	96.37	39
BT-22B	BTE 5-1	36.39	4.25	12.53	24.60	0.36	8.96	0.12	0.43	9.11	0.03	96.77	39
BT-22B	BTE 5-2	35.97	4.26	12.06	24.46	0.31	8.71	0.23	0.46	9.17	0.03	95.65	39
BT-22B	BTE 5-4	35.63	4.27	12.50	25.02	0.33	8.68	0.07	0.42	9.45	0.00	96.38	38
BT-22B	BTE 9-2	36.08	4.14	12.45	24.10	0.33	8.75	0.14	0.44	8.86	0.06	95.35	39
BT-22B	BTE 11-2	37.02	4.13	12.72	23.39	0.30	8.99	0.58	0.37	8.80	0.05	96.33	41
BT-22B	BTE 15-1	35.36	4.21	12.51	24.91	0.33	8.78	0.02	0.39	9.38	0.06	95.94	39
BT-22B	BTE 15-2	35.78	4.25	12.75	24.97	0.34	9.05	0.03	0.39	9.37	0.03	96.96	39
BT-22B	BTE 15-3	36.12	4.25	12.89	25.10	0.35	9.20	0.16	0.41	9.23	0.02	97.73	40
BT-22B	BTE 15-4	35.33	4.15	12.28	24.45	0.35	8.85	0.80	0.42	9.03	0.00	95.66	39
BT-22B	BTE 15-5	35.67	4.22	12.26	24.76	0.41	8.88	0.01	0.41	9.26	0.06	95.95	39
BT-22B	BTE 15-6	35.20	4.24	12.18	24.82	0.35	8.55	0.07	0.38	9.17	0.03	94.99	38
BT-22B	BTE 15-7	36.32	4.25	12.19	24.73	0.67	9.01	0.10	0.38	9.06	0.07	96.78	39
	Average	**35.88**	**4.22**	**12.43**	**24.64**	**0.37**	**8.87**	**0.16**	**0.41**	**9.21**	**0.04**	**96.22**	**39**
	Standard Deviation	**0.46**	**0.05**	**0.24**	**0.42**	**0.09**	**0.18**	**0.22**	**0.02**	**0.23**	**0.02**	**0.71**	**1**
BT-16B	BTE 19-1	36.25	4.15	12.72	24.39	0.33	9.22	0.04	0.43	9.32	0.00	96.84	40
BT-16B	BTE 19-2	35.69	4.16	12.80	24.69	0.34	9.14	0.06	0.43	9.35	0.06	96.71	40
BT-16B	BTE 19-3	35.32	4.19	12.58	24.28	0.34	9.09	0.07	0.39	9.16	0.00	95.42	40
	Average	**35.75**	**4.17**	**12.70**	**24.45**	**0.34**	**9.15**	**0.06**	**0.42**	**9.28**	**0.02**	**96.32**	**40**
	Standard Deviation	**0.47**	**0.02**	**0.12**	**0.21**	**0.01**	**0.06**	**0.02**	**0.02**	**0.10**	**0.03**	**0.78**	**0**
BT-13A	BTE 8-1	35.49	4.47	12.52	22.58	0.32	10.55	0.11	0.42	8.92	0.24	95.62	45
BT-13A	BTE 8-2	35.01	4.51	12.62	22.35	0.25	10.51	0.12	0.48	9.02	0.13	94.99	46
	Average	**35.25**	**4.49**	**12.57**	**22.46**	**0.28**	**10.53**	**0.11**	**0.45**	**8.97**	**0.19**	**95.31**	**46**
	Standard Deviation	**0.34**	**0.03**	**0.07**	**0.16**	**0.05**	**0.03**	**0.01**	**0.04**	**0.07**	**0.08**	**0.45**	**0**
BT-8B	BTE 5-2	36.69	4.47	12.28	22.02	0.26	10.24	0.04	0.43	9.34	0.04	95.81	45
BT-8B	BTE 5-3	37.10	4.40	12.32	21.83	0.25	10.08	0.14	0.45	8.57	0.05	95.19	45
BT-8B	BTE 15-1	36.49	4.46	12.30	22.12	0.27	10.28	0.08	0.45	9.03	0.05	95.53	45
BT-8B	BTE 15-3	36.20	4.48	12.17	22.12	0.25	10.20	0.07	0.47	8.93	0.04	94.95	45

BT-8B	BTE 15-6	36.59	4.42	12.23	22.03	0.27	10.30	0.05	0.43	8.89	0.04	95.25	45
BT-8B	BTE 16-1	36.42	4.37	12.34	22.01	0.26	9.99	0.04	0.44	9.06	0.06	94.99	45
BT-8B	BTE 16-3	36.39	4.40	12.37	22.29	0.26	10.18	0.04	0.42	9.12	0.04	95.49	45
BT-8B	BTE 16-8	36.86	4.39	12.12	22.25	0.26	10.35	0.06	0.41	9.21	0.03	95.95	45
BT-8B	BTE 16-9	36.47	4.37	12.25	22.09	0.25	10.19	0.02	0.40	9.27	0.04	95.35	45
	Average	**36.58**	**4.42**	**12.27**	**22.08**	**0.26**	**10.20**	**0.06**	**0.43**	**9.05**	**0.04**	**95.39**	**45**
	Standard Deviation	**0.27**	**0.04**	**0.08**	**0.14**	**0.01**	**0.11**	**0.03**	**0.02**	**0.23**	**0.01**	**0.34**	**0**
BT-19D	BTE 1-3	36.22	4.79	12.82	21.02		10.76	0.02	0.55	9.47	0.00	95.66	48
BT-19D	BTE 1-5	36.01	4.81	12.48	21.07		10.99	0.02	0.53	9.52	0.05	95.50	48
BT-19D	BTE 1-6	36.38	4.72	12.74	20.83		10.97	0.04	0.51	9.45	0.01	95.64	48
BT-19D	BTE 1-9	35.75	4.89	12.23	21.14		11.34	0.01	0.57	9.72	0.10	95.76	49
BT-19D	BTE 1-10	35.57	4.78	12.16	20.80		11.29	0.34	0.59	9.56	0.07	95.17	49
BT-19D	BTE 1-11	35.57	4.84	12.26	21.08		11.28	0.00	0.62	9.57	0.08	95.31	49
BT-19D	BTE 1-14	35.84	4.79	12.48	21.10		10.88	0.06	0.57	9.50	0.05	95.26	48
BT-19D	BTE 1-15	35.61	4.77	12.40	20.88		11.08	0.02	0.53	9.56	0.09	94.96	49
BT-19D	BTE 1-17	35.56	4.84	12.34	21.06		11.41	0.03	0.57	9.62	0.02	95.45	49
BT-19D	BTE 1-18	35.82	4.84	12.36	20.90		11.28	0.02	0.58	9.60	0.10	95.50	49
BT-19D	BTE 1-19	35.65	4.85	12.32	21.09		11.41	0.00	0.58	9.58	0.06	95.54	49
BT-19D	BTE 3-5	35.98	4.79	12.25	21.00		11.02	0.02	0.50	9.54	0.17	95.27	48
BT-19D	BTE 3-14	36.19	4.84	12.39	20.82		10.98	0.05	0.53	9.47	0.08	95.36	48
BT-19D	BTE 4-1	35.61	4.80	12.13	20.75		11.41	0.01	0.60	9.66	0.04	95.02	50
BT-19D	BTE 4-3	35.56	4.77	12.18	21.30		11.42	0.03	0.59	9.74	0.02	95.61	49
BT-19D	BTE 4-7	35.14	4.97	12.47	21.15		10.80	0.05	0.54	9.39	0.49	95.01	48
BT-19D	BTE 4-10	36.27	4.71	12.61	20.92		11.16	0.02	0.56	9.42	0.10	95.76	49
BT-19D	BTE 4-11	35.96	4.80	12.30	20.73		11.26	0.01	0.52	9.57	0.11	95.24	49
BT-19D	BTE 4-12	35.84	4.81	12.42	20.98		11.42	0.00	0.56	9.72	0.06	95.81	49
BT-19D	BTE 4-13	35.47	4.76	12.24	21.11		11.43	0.00	0.59	9.72	0.05	95.38	49
BT-19D	BTE 4-14	36.17	4.61	12.78	20.38		10.82	0.18	0.57	9.30	0.16	94.96	49
BT-19D	BTE 5-2	36.29	4.74	12.40	20.76		11.23	0.04	0.61	9.59	0.21	95.87	49
BT-19D	BTE 5-3	36.45	4.82	12.61	20.93		11.34	0.04	0.56	9.65	0.24	96.64	49
BT-19D	BTE 5-4	35.99	4.76	12.27	21.03		11.47	0.03	0.58	9.69	0.22	96.04	49
BT-19D	BTE 6-1	36.08	4.89	12.42	21.10		11.30	0.00	0.59	9.66	0.08	96.10	49
BT-19D	BTE 6-2	35.86	4.79	12.21	20.95		11.20	0.00	0.57	9.47	0.11	95.16	49
BT-19D	BTE 7-1	36.04	4.81	12.25	20.70		11.30	0.02	0.57	9.64	0.12	95.45	49
BT-19D	BTE 7-2	35.70	4.78	12.31	20.95		11.24	0.10	0.55	9.55	0.15	95.33	49
BT-19D	BTE 7-3	36.02	4.88	12.35	20.94		11.15	0.00	0.58	9.55	0.13	95.61	49
BT-19D	BTE 7-4	35.85	4.75	12.31	20.81		11.11	0.01	0.55	9.62	0.11	95.11	49
BT-19D	BTE 7-5	35.77	4.81	12.31	21.01		11.16	0.01	0.58	9.61	0.09	95.35	49
BT-19D	BTE 7-6	36.08	4.87	12.47	20.89		11.29	0.01	0.53	9.61	0.18	95.92	49
BT-19D	BTE 7-7	35.93	4.78	12.46	20.86		11.29	0.06	0.54	9.54	0.10	95.57	49
BT-19D	BTE 7-8	35.78	4.86	12.26	20.96		11.32	0.00	0.54	9.52	0.12	95.34	49
BT-19D	BTE 7-9	35.64	4.85	12.27	20.97		11.30	0.00	0.57	9.48	0.11	95.20	49
BT-19D	BTE 7-10	35.86	4.81	12.40	20.98		11.42	0.01	0.57	9.41	0.18	95.65	49

BT-19D	BTE 7-11	35.52	4.95	12.27	20.76	11.25	0.02	0.55	9.46	0.51	95.30	49
BT-19D	BTE 7-12	35.49	5.04	12.63	21.23	11.18	0.00	0.54	9.53	0.51	96.16	48
BT-19D	BTE 7-13	35.63	4.97	12.59	21.04	10.99	0.02	0.54	9.35	0.59	95.73	48
BT-19D	BTE 7-14	35.35	4.97	12.57	21.19	10.95	0.03	0.56	9.27	0.61	95.50	48
BT-19D	BTE 7-15	35.50	4.86	12.61	20.85	10.99	0.03	0.54	9.37	0.37	95.13	48
BT-19D	BTE 7-16	36.07	4.86	12.52	20.96	11.20	0.00	0.54	9.57	0.09	95.83	49
BT-19D	BTE 8-2	35.53	4.80	12.44	20.95	11.32	0.12	0.61	9.50	0.10	95.35	49
BT-19D	BTE 8-3	35.74	4.80	12.36	21.20	11.37	0.00	0.57	9.66	0.05	95.76	49
BT-19D	BTE 8-4	35.72	4.80	12.46	20.89	11.30	0.05	0.48	9.63	0.10	95.43	49
BT-19D	BTE 8-7	35.28	4.89	12.28	21.29	11.09	0.03	0.56	9.56	0.26	95.23	48
BT-19D	BTE 8-8	35.80	4.84	12.22	21.31	11.23	0.00	0.54	9.68	0.13	95.77	48
BT-19D	BTE 8-10	35.77	4.78	12.76	20.48	11.08	0.11	0.54	9.42	0.08	95.01	49
BT-19D	BTE 8-11	35.27	4.82	12.29	20.98	11.28	0.01	0.55	9.67	0.09	94.97	49
BT-19D	BTE 8-12	35.77	4.81	12.26	20.87	11.36	0.01	0.57	9.58	0.07	95.29	49
BT-19D	BTE 8-13	35.55	4.82	12.42	20.93	11.27	0.13	0.55	9.62	0.13	95.42	49
BT-19D	BTE 8-14	35.84	4.87	12.36	21.11	11.27	0.01	0.61	9.57	0.13	95.78	49
BT-19D	BTE 9-1	35.38	4.80	12.38	21.03	10.92	0.25	0.53	9.37	0.37	95.03	48
BT-19D	BTE 9-3	35.70	4.90	12.82	21.03	11.02	0.00	0.53	9.46	0.31	95.77	48
BT-19D	BTE 9-4	35.82	4.88	12.26	21.11	11.32	0.00	0.55	9.60	0.21	95.76	49
BT-19D	BTE 9-5	36.18	4.84	12.49	21.07	11.24	0.00	0.54	9.64	0.19	96.20	49
BT-19D	BTE 9-6	36.12	4.84	12.28	20.86	11.19	0.00	0.50	9.64	0.07	95.49	49
BT-19D	BTE 9-7	36.27	4.85	12.50	20.94	11.25	0.00	0.59	9.64	0.14	96.18	49
BT-19D	BTE 9-8	35.55	4.96	13.48	21.26	10.41	0.09	0.53	9.39	0.70	96.37	47
BT-19D	BTE 9-9	35.99	4.81	12.30	20.98	11.26	0.01	0.59	9.59	0.13	95.65	49
BT-19D	BTE 9-10	35.77	4.76	12.35	20.81	11.16	0.10	0.58	9.54	0.15	95.22	49
BT-19D	BTE 10-1	35.41	4.91	12.70	21.16	10.95	0.04	0.55	9.41	0.41	95.54	48
BT-19D	BTE 10-3	36.05	4.84	12.41	20.87	11.01	0.01	0.56	9.58	0.16	95.49	48
BT-19D	BTE 10-4	36.08	4.80	12.35	20.93	11.23	0.00	0.57	9.56	0.07	95.60	49
BT-19D	BTE 10-7	36.23	4.78	12.54	21.09	11.33	0.08	0.55	9.51	0.20	96.31	49
BT-19D	BTE 10-8	36.07	4.84	12.29	20.90	11.07	0.03	0.56	9.46	0.11	95.33	49
BT-19D	BTE 11-3	36.05	4.70	12.48	20.61	11.24	0.09	0.55	9.39	0.04	95.17	49
BT-19D	BTE 11-5	35.62	4.90	12.65	21.03	11.06	0.02	0.55	9.48	0.28	95.59	48
BT-19D	BTE 11-6	35.67	4.77	12.36	20.80	11.36	0.08	0.58	9.51	0.14	95.28	49
BT-19D	BTE 11-8	35.94	4.74	12.44	20.57	11.33	0.02	0.56	9.54	0.09	95.22	50
BT-19D	BTE 12-1	36.03	4.77	12.35	20.65	11.31	0.02	0.56	9.54	0.10	95.33	49
BT-19D	BTE 13-1	36.29	4.86	12.45	21.16	11.36	0.01	0.61	9.66	0.08	96.48	49
BT-19D	BTE 13-2	36.12	4.82	12.36	21.21	11.27	0.02	0.58	9.73	0.02	96.13	49
BT-19D	BTE 13-3	36.09	4.79	12.40	21.12	11.34	0.02	0.57	9.68	0.03	96.04	49
BT-19D	BTE 13-4	35.85	4.83	12.52	21.04	11.42	0.04	0.58	9.55	0.05	95.88	49
BT-19D	BTE 13-5	35.95	4.83	12.47	21.00	11.29	0.01	0.52	9.68	0.08	95.83	49
BT-19D	BTE 13-6	35.75	4.89	12.27	21.27	11.23	0.00	0.57	9.77	0.05	95.79	48
BT-19D	BTE 13-7	35.92	4.85	12.35	21.14	11.35	0.01	0.56	9.65	0.04	95.85	49
BT-19D	BTE 14-1	36.08	4.82	12.41	21.16	11.32	0.01	0.61	9.63	0.01	96.06	49
BT-19D	BTE 14-2	36.20	4.80	12.42	21.04	11.27	0.02	0.57	9.69	0.03	96.03	49
BT-19D	BTE 14-3	36.08	4.82	12.45	21.05	11.13	0.01	0.56	9.66	0.04	95.80	49

BT-19D	BTE 14-4	35.76	4.79	12.29	20.87		11.11	0.02	0.54	9.56	0.04	94.99	49
BT-19D	BTE 14-6	36.31	4.83	12.54	21.39		11.34	0.00	0.59	9.76	0.05	96.80	49
BT-19D	BTE 14-7	36.01	4.80	12.46	21.36		11.27	0.01	0.57	9.70	0.06	96.24	48
BT-19D	BTE 14-8	35.80	4.79	12.42	21.17		11.14	0.03	0.60	9.64	0.02	95.61	48
BT-19D	BTE 14-9	36.17	4.75	12.57	21.07		11.19	0.03	0.58	9.65	0.01	96.02	49
BT-19D	BTE 14-11	36.01	4.69	12.51	20.68		11.13	0.09	0.56	9.43	0.05	95.14	49
BT-19D	BTE 14-16	36.15	4.73	12.33	21.17		11.28	0.00	0.55	9.72	0.11	96.05	49
BT-19D	BTE 14-17	35.88	4.76	12.32	20.90		11.19	0.11	0.57	9.62	0.05	95.41	49
BT-19D	BTE 14-18	35.68	4.73	12.26	20.56		11.01	0.77	0.53	9.36	0.08	94.98	49
BT-19D	BTE 14-21	35.89	4.84	12.39	21.17		11.29	0.13	0.55	9.59	0.04	95.89	49
BT-19D	BTE 14-22	36.27	4.90	12.38	21.21		11.36	0.00	0.53	9.68	0.00	96.34	49
BT-19D	BTE 14-26	35.93	4.81	12.50	20.89		11.24	0.09	0.58	9.62	0.03	95.68	49
BT-19D	BTE 15-1	35.76	4.81	12.37	20.90		11.15	0.02	0.54	9.44	0.22	95.20	49
BT-19D	BTE 15-2	35.61	4.81	12.31	20.89		11.14	0.00	0.54	9.63	0.22	95.15	49
BT-19D	BTE 15-5	36.38	4.79	12.24	20.93		11.09	0.00	0.53	9.63	0.09	95.68	49
BT-19D	BTE 16-1	35.74	4.89	13.01	21.01		10.79	0.03	0.53	9.43	0.45	95.87	48
BT-19D	BTE 16-4	35.43	4.84	12.57	20.93		11.21	0.01	0.57	9.62	0.37	95.54	49
BT-19D	BTE 16-6	35.92	4.73	12.29	20.45		11.27	0.02	1.11	9.59	0.13	95.51	50
BT-19D	BTE 16-7	35.98	4.73	12.29	20.81		11.38	0.01	0.63	9.51	0.11	95.44	49
BT-19D	BTE 21-1	37.23	4.78	12.79	20.67	0.19	10.87	0.04	0.52	9.41	0.08	96.59	48
BT-19D	BTE 21-2	36.84	4.76	12.63	20.37	0.19	11.04	0.06	0.54	9.35	0.00	95.78	49
BT-19D	BTE 21-3	36.96	4.71	12.93	20.34	0.18	11.00	0.09	0.52	9.22	0.03	95.99	49
BT-19D	BTE 21-4	35.89	4.69	12.48	20.72	0.18	10.92	0.67	0.54	9.19	0.03	95.30	48
BT-19D	BTE 21-7	36.63	4.72	12.58	20.75	0.18	11.26	0.04	0.59	9.52	0.04	96.32	49
BT-19D	BTE 21-8	36.30	4.74	12.52	20.64	0.20	11.08	0.18	0.54	9.43	0.05	95.68	49
BT-19D	BTE 21-9	36.99	4.73	12.62	20.89	0.18	11.04	0.05	0.50	9.43	0.05	96.48	49
BT-19D	BTE 21-10	36.45	4.69	12.82	20.63	0.20	11.21	0.04	0.57	9.29	0.01	95.90	49
BT-19D	BTE 21-11	36.85	4.72	12.69	20.84	0.18	10.90	0.04	0.55	9.22	0.06	96.05	48
BT-19D	BTE 21-12	36.82	4.75	12.54	20.78	0.18	11.14	0.03	0.57	9.47	0.09	96.38	49
BT-19D	BTE 21-13	36.65	4.81	12.49	20.77	0.19	10.96	0.03	0.54	9.45	0.08	95.97	48
BT-19D	BTE 21-15	36.70	4.65	12.94	20.59	0.19	11.07	0.08	0.53	9.28	0.07	96.11	49
BT-19D	BTE 21-16	35.98	4.73	12.42	20.70	0.17	11.13	0.03	0.52	9.28	0.04	95.02	49
BT-19D	BTE 21-18	36.15	4.77	12.33	20.80	0.18	11.41	0.03	0.56	9.38	0.05	95.65	49
BT-19D	BTE 21-19	36.07	4.77	12.13	20.75	0.20	11.33	0.05	0.56	9.51	0.10	95.46	49
BT-19D	BTE 21-21	36.22	4.81	12.39	20.76	0.19	11.26	0.01	0.56	9.49	0.11	95.79	49
BT-19D	BTE 21-22	36.44	4.75	12.41	20.88	0.20	11.22	0.02	0.55	9.42	0.11	96.01	49
BT-19D	BTE 21-23	36.49	4.80	12.36	20.92	0.19	11.35	0.03	0.56	9.48	0.01	96.19	49
BT-19D	BTE 21-24	37.68	4.67	12.68	20.42	0.17	11.02	0.19	0.54	9.19	0.00	96.56	49
BT-19D	BTE 21-25	36.02	4.77	12.36	20.91	0.20	11.28	0.02	0.58	9.45	0.04	95.63	49
BT-19D	BTE 21-26	36.39	4.81	11.67	20.80	0.20	11.24	0.04	0.58	9.47	0.14	95.34	49
BT-19D	BTE 21-27	36.12	4.74	12.08	20.82	0.20	11.31	0.01	0.59	9.51	0.10	95.46	49
BT-19D	BTE 21-29	36.37	4.77	12.37	20.68	0.19	11.08	0.06	0.55	9.46	0.05	95.57	49
BT-19D	BTE 21-32	36.03	4.82	12.31	20.73	0.19	11.24	0.04	0.56	9.42	0.08	95.40	49
BT-19D	BTE 22-6	36.28	4.88	12.78	20.77	0.20	11.16	0.04	0.50	9.26	0.53	96.39	49
BT-19D	BTE 22-8	36.43	4.81	12.18	20.50	0.20	11.22	0.04	0.54	9.31	0.04	95.26	49

BT-19D	BTE 22-11	36.64	4.74	12.44	20.82	0.18	11.26	0.04	0.55	9.44	0.14	96.25	49
BT-19D	BTE 23-2	36.07	4.81	12.05	21.00	0.22	11.48	0.04	0.55	9.26	0.15	95.63	49
BT-19D	BTE 23-4	36.48	4.79	12.15	20.55	0.20	11.17	0.05	0.54	9.34	0.17	95.44	49
BT-19D	BTE 23-5	36.67	4.84	12.38	20.52	0.18	10.79	0.09	0.52	9.26	0.14	95.38	48
BT-19D	BTE 24-2	35.74	4.61	12.35	22.05	0.19	10.76	0.10	0.54	9.01	0.18	95.53	47
BT-19D	BTE 24-3	35.84	4.83	12.75	20.72	0.20	10.82	0.07	0.56	9.07	0.55	95.41	48
BT-19D	BTE 24-5	36.05	4.85	12.71	20.99	0.21	10.88	0.01	0.52	9.24	0.49	95.96	48
BT-19D	BTE 24-6	35.98	4.67	12.45	20.79	0.21	11.44	0.05	0.57	9.30	0.03	95.50	50
BT-19D	BTE 24-11	36.11	4.71	12.39	20.78	0.20	11.33	0.01	0.59	9.36	0.05	95.53	49
BT-19D	BTE 24-14	36.74	4.69	12.94	19.90	0.18	10.46	0.17	0.57	8.94	0.55	95.14	48
BT-19D	BTE 24-15	36.53	4.68	12.57	20.51	0.19	11.28	0.04	0.54	9.40	0.10	95.84	49
BT-19D	BTE 24-16	36.29	4.65	12.49	20.57	0.18	11.12	0.10	0.56	9.34	0.06	95.36	49
BT-19D	BTE 24-17	36.47	4.74	12.38	20.89	0.19	11.11	0.01	0.56	9.44	0.03	95.83	49
BT-19D	BTE 24-18	36.86	4.66	12.43	20.54	0.17	11.03	0.07	0.55	9.36	0.04	95.72	49
BT-19D	BTE 24-19	35.97	4.63	12.36	20.76	0.20	11.18	0.07	0.54	9.40	0.01	95.14	49
BT-19D	BTE 24-20	36.79	4.69	11.91	20.41	0.19	11.16	0.03	0.51	9.54	0.06	95.30	49
BT-19D	BTE 24-21	38.66	4.44	12.44	19.55	0.23	10.57	0.11	0.62	9.13	0.08	95.83	49
BT-19D	BTE 24-22	37.00	4.84	12.30	20.83	0.19	11.18	0.03	0.54	9.42	0.19	96.53	49
BT-19D	BTE 24-24	36.06	4.80	13.06	20.47	0.19	10.66	0.11	0.53	9.07	0.50	95.43	48
BT-19D	BTE 24-25	36.52	4.91	11.63	20.71	0.20	10.97	0.01	0.56	9.42	0.47	95.42	49
	Average	**36.06**	**4.79**	**12.43**	**20.88**	**0.19**	**11.17**	**0.05**	**0.56**	**9.49**	**0.14**	**95.64**	**49**
	Standard Deviation	**0.47**	**0.08**	**0.23**	**0.28**	**0.01**	**0.20**	**0.09**	**0.05**	**0.16**	**0.15**	**0.41**	**0**
BT-21F	BTE 1-8	35.85	4.93	12.76	20.21	0.15	11.65	0.06	0.44	9.03	0.18	95.26	51
BT-21F	BTE 4-1	36.82	4.86	12.65	20.11	0.16	12.07	0.02	0.58	9.13	0.22	96.61	52
BT-21F	BTE 4-2	36.64	4.83	12.50	19.61	0.16	12.02	0.03	0.57	9.19	0.23	95.78	52
BT-21F	BTE 4-3	36.33	4.82	12.74	20.10	0.17	12.11	0.12	0.50	8.51	0.17	95.58	52
BT-21F	BTE 4-4	36.06	4.86	12.55	19.87	0.17	12.08	0.01	0.58	9.25	0.14	95.57	52
BT-21F	BTE 4-5	36.08	4.92	12.54	20.05	0.77	12.03	0.01	0.60	9.38	0.16	96.54	52
BT-21F	BTE 4-6	35.82	4.88	12.52	20.22	0.16	12.03	0.00	0.63	9.39	0.14	95.78	51
BT-21F	BTE 4-10	35.81	4.88	12.37	20.31	0.16	11.91	0.02	0.54	9.24	0.19	95.42	51
BT-21F	BTE 5-1	36.17	4.94	12.53	19.67	0.18	11.99	0.02	0.57	9.28	0.19	95.54	52
BT-21F	BTE 7-5	35.73	4.94	12.89	20.65	0.16	11.87	0.07	0.48	8.89	0.13	95.81	51
BT-21F	BTE 12-2	36.20	4.76	13.44	19.72	0.16	11.51	0.04	0.52	9.05	0.07	95.48	51
BT-21F	BTE 15-3	36.10	4.85	14.45	19.56	0.15	11.26	0.02	0.51	8.52	0.78	96.20	51
	Average	**36.13**	**4.87**	**12.83**	**20.01**	**0.21**	**11.88**	**0.04**	**0.54**	**9.07**	**0.22**	**95.80**	**51**
	Standard Deviation	**0.33**	**0.05**	**0.58**	**0.33**	**0.17**	**0.27**	**0.03**	**0.05**	**0.30**	**0.18**	**0.43**	**1**
BT-19F	BTE 1-2	37.82	5.24	12.90	17.56	0.10	12.12	0.04	0.54	9.05	0.03	95.39	55
BT-19F	BTE 1-4	37.29	5.42	12.47	17.86	0.10	12.89	0.05	0.56	9.48	0.06	96.20	56
BT-19F	BTE 1-6	37.63	5.14	13.27	17.35	0.11	12.19	0.06	0.50	8.86	0.04	95.14	56
BT-19F	BTE 3-1	37.46	4.92	13.80	17.31	0.12	11.34	0.25	0.52	8.73	0.57	95.02	54
BT-19F	BTE 3-2	36.24	5.14	12.92	18.10	0.11	12.18	0.03	0.56	9.38	0.54	95.21	55
BT-19F	BTE 3-3	37.29	5.13	12.40	18.55	0.14	12.78	0.04	0.52	9.68	0.19	96.71	55

BT-19F	BTE 3-4	38.00	4.86	13.75	17.57	0.09	11.75	0.12	0.54	8.88	0.24	95.80	54
BT-19F	BTE 3-5	37.50	5.29	12.87	18.14	0.11	12.37	0.10	0.58	9.35	0.11	96.41	55
BT-19F	BTE 3-6	37.12	5.32	12.43	18.53	0.09	12.67	0.02	0.56	9.50	0.14	96.38	55
BT-19F	BTE 3-7	37.30	5.09	12.55	18.34	0.12	12.64	0.01	0.55	9.39	0.13	96.12	55
BT-19F	BTE 3-8	37.82	4.88	12.26	18.17	0.14	12.10	0.17	0.50	9.27	0.16	95.49	54
BT-19F	BTE 3-9	37.04	5.21	12.32	19.06	0.13	12.26	0.17	0.59	9.50	0.17	96.46	53
BT-19F	BTE 3-10	37.43	5.36	12.41	18.64	0.11	12.60	0.16	0.52	9.62	0.14	96.99	55
BT-19F	BTE 3-11	37.58	4.89	13.24	17.65	0.11	11.85	0.18	0.53	9.13	0.12	95.28	54
BT-19F	BTE 3-12	37.78	4.82	13.39	17.44	0.13	11.76	0.06	0.54	8.93	0.08	94.95	55
BT-19F	BTE 3-13	36.87	5.25	12.97	18.37	0.11	12.19	0.03	0.55	9.38	0.49	96.22	54
BT-19F	BTE 5-1	36.85	5.04	13.24	17.96	0.15	12.08	0.07	0.55	9.20	0.45	95.58	55
BT-19F	BTE 5-2	36.33	5.24	13.35	18.37	0.16	12.14	0.02	0.56	9.23	0.61	96.03	54
BT-19F	BTE 5-4	37.04	4.70	14.45	17.59	0.13	11.60	0.04	0.54	8.79	0.30	95.19	54
BT-19F	BTE 5-5	36.27	5.06	14.02	18.27	0.27	11.73	0.03	0.52	8.85	0.85	95.87	53
BT-19F	BTE 5-6	36.56	5.12	13.15	18.12	0.14	12.29	0.14	0.54	9.35	0.50	95.92	55
BT-19F	BTE 5-7	36.04	5.25	13.41	18.57	0.21	12.08	0.06	0.52	9.31	0.71	96.14	54
BT-19F	BTE 5-9	37.35	4.70	14.09	17.23	0.15	11.68	0.07	0.56	8.87	0.29	94.98	55
BT-19F	BTE 5-10	36.75	5.01	13.06	17.83	0.14	12.22	0.67	0.50	9.14	0.40	95.72	55
BT-19F	BTE 6-1	37.03	5.76	12.35	17.83	0.10	12.39	0.08	0.49	9.21	0.20	95.43	55
BT-19F	BTE 6-2	35.99	5.66	12.63	17.68	0.36	12.63	0.32	0.54	9.46	0.18	95.45	56
BT-19F	BTE 6-3	37.26	5.59	12.70	18.06	0.11	12.39	0.03	0.52	9.25	0.25	96.16	55
BT-19F	BTE 6-4	37.30	5.82	12.22	18.07	0.10	12.63	0.02	0.54	9.46	0.24	96.39	55
BT-19F	BTE 6-5	37.24	5.73	12.30	18.18	0.18	12.63	0.03	0.59	9.42	0.24	96.55	55
BT-19F	BTE 6-6	37.46	5.41	12.96	17.44	0.17	12.07	0.34	0.51	9.05	0.15	95.56	55
BT-19F	BTE 6-7	37.39	5.68	12.51	18.24	0.15	12.51	0.05	0.55	9.50	0.20	96.77	55
BT-19F	BTE 6-8	36.82	5.68	12.32	18.16	0.13	12.65	0.03	0.61	9.36	0.13	95.89	55
BT-19F	BTE 6-9	37.06	5.77	12.50	18.36	0.15	12.85	0.03	0.56	9.49	0.15	96.90	56
BT-19F	BTE 6-10	37.01	5.82	12.26	18.28	0.11	12.86	0.04	0.58	9.52	0.12	96.60	56
BT-19F	BTE 6-11	36.15	5.73	12.38	18.33	0.38	12.86	0.00	0.60	9.63	0.09	96.17	56
BT-19F	BTE 6-12	37.10	5.76	12.48	18.47	0.11	12.82	0.01	0.64	9.74	0.15	97.28	55
BT-19F	BTE 6-13	37.17	5.83	12.30	18.33	0.11	12.75	0.01	0.65	9.69	0.15	96.98	55
BT-19F	BTE 6-14	37.07	5.71	12.62	18.22	0.11	12.46	0.02	0.59	9.48	0.20	96.46	55
BT-19F	BTE 6-15	36.88	5.79	12.37	18.35	0.11	12.41	0.04	0.59	9.61	0.17	96.32	55
BT-19F	BTE 6-16	37.14	5.79	12.43	18.40	0.14	12.90	0.01	0.63	9.60	0.17	97.21	56
BT-19F	BTE 6-17	36.90	5.69	12.28	18.27	0.10	12.76	0.01	0.59	9.64	0.13	96.36	55
BT-19F	BTE 6-18	37.02	5.79	12.34	18.13	0.11	12.94	0.02	0.56	9.64	0.11	96.65	56
BT-19F	BTE 6-19	37.05	5.72	12.42	17.98	0.08	12.65	0.01	0.59	9.38	0.20	96.09	56
BT-19F	BTE 6-20	37.03	5.77	12.34	18.17	0.12	12.74	0.02	0.57	9.52	0.15	96.44	56
BT-19F	BTE 6-21	37.08	5.81	12.44	18.35	0.13	12.89	0.02	0.58	9.61	0.13	97.03	56
BT-19F	BTE 6-22	36.99	5.72	12.42	18.12	0.11	12.95	0.02	0.59	9.61	0.18	96.71	56
BT-19F	BTE 6-23	36.97	5.69	12.16	18.00	0.10	12.81	0.01	0.58	9.59	0.07	95.97	56
BT-19F	BTE 11-1	37.86	5.26	13.77	17.25		12.07	0.12	0.53	8.80	0.02	95.68	56
BT-19F	BTE 11-2	36.85	5.58	12.88	18.02		12.76	0.01	0.60	9.54	0.06	96.31	56
BT-19F	BTE 11-3	37.06	5.47	13.24	17.12		12.02	0.28	0.59	9.25	0.05	95.08	56
BT-19F	BTE 11-4	37.25	5.53	13.30	17.76		12.30	0.07	0.53	9.26	0.11	96.12	55

BT-19F	BTE 11-5	37.37	5.64	13.06	17.71		12.70	0.04	0.57	9.43	0.02	96.55	56
BT-19F	BTE 11-6	37.09	5.68	13.01	18.21		12.91	0.02	0.61	9.53	0.04	97.12	56
BT-19F	BTE 11-7	36.41	5.56	12.61	17.87		12.57	0.07	0.60	9.34	0.03	95.07	56
BT-19F	BTE 11-8	36.40	5.66	12.84	18.20		12.80	0.01	0.62	9.47	0.04	96.04	56
BT-19F	BTE 12-1	36.64	5.51	12.83	17.82		12.82	0.01	0.61	9.43	0.23	95.92	56
BT-19F	BTE 12-2	36.65	5.52	12.77	17.98		12.87	0.02	0.62	9.40	0.15	95.99	56
BT-19F	BTE 12-3	37.25	5.41	13.20	17.69		12.74	0.04	0.59	9.24	0.14	96.32	56
BT-19F	BTE 12-4	36.57	5.32	12.78	17.80		12.84	0.01	0.60	9.61	0.03	95.56	56
BT-19F	BTE 12-6	36.57	5.52	12.80	17.84		12.75	0.01	0.63	9.47	0.15	95.75	56
BT-19F	BTE 12-7	36.67	5.54	12.79	17.62		12.71	0.04	0.58	9.36	0.17	95.49	56
BT-19F	BTE 12-9	36.96	5.28	12.84	17.71		12.88	0.16	0.60	9.40	0.06	95.87	56
BT-19F	BTE 12-12	36.44	5.56	12.78	17.70		12.52	0.02	0.58	9.41	0.14	95.16	56
BT-19F	BTE 13-7	36.18	5.46	12.79	17.69		13.13	0.03	0.60	9.52	0.10	95.49	57
BT-19F	BTE 13-10	36.53	5.27	12.93	17.97		12.85	0.04	0.57	9.38	0.05	95.60	56
BT-19F	BTE 13-11	36.49	5.20	12.89	17.52		12.67	0.18	0.51	9.45	0.05	94.97	56
BT-19F	BTE 13-12	36.48	5.44	12.82	17.88		12.91	0.01	0.59	9.52	0.00	95.66	56
BT-19F	BTE 13-14	36.46	5.23	12.82	17.88		12.90	0.03	0.58	9.45	0.06	95.41	56
BT-19F	BTE 13-15	36.55	5.36	12.98	17.24		12.71	0.49	0.55	9.17	0.00	95.05	57
BT-19F	BTE 13-17	37.32	5.13	13.57	17.07		12.23	0.07	0.56	9.03	0.08	95.06	56
	Average	**36.98**	**5.41**	**12.84**	**17.96**	**0.14**	**12.50**	**0.08**	**0.57**	**9.35**	**0.18**	**95.97**	**55**
	Standard Deviation	**0.46**	**0.31**	**0.50**	**0.40**	**0.06**	**0.40**	**0.12**	**0.04**	**0.24**	**0.17**	**0.63**	**1**
BT-19H	BTE 1-1	36.25	5.17	12.59	18.41		13.03	0.02	0.64	9.49	0.13	95.72	56
BT-19H	BTE 1-3	36.54	5.06	12.73	18.54		12.34	0.09	0.59	9.37	0.14	95.38	54
BT-19H	BTE 1-4	37.12	5.13	12.64	18.81		12.52	0.02	0.54	9.69	0.10	96.56	54
BT-19H	BTE 1-5	37.20	5.08	12.92	18.39		12.36	0.16	0.58	9.44	0.11	96.27	55
BT-19H	BTE 1-11	36.38	5.17	12.55	18.47		12.81	0.05	0.63	9.66	0.16	95.89	55
BT-19H	BTE 1-12	36.08	5.20	12.29	18.84		13.03	0.01	0.66	9.59	0.18	95.87	55
BT-19H	BTE 1-13	35.91	5.24	12.15	18.78		13.03	0.00	0.66	9.56	0.23	95.55	55
BT-19H	BTE 1-15	36.66	5.09	12.46	18.86		12.64	0.01	0.64	9.61	0.07	96.05	54
BT-19H	BTE 1-17	36.26	5.10	12.49	18.72		12.79	0.03	0.63	9.61	0.15	95.77	55
BT-19H	BTE 2-1	36.46	4.98	13.22	18.24		12.07	0.50	0.62	9.26	0.22	95.57	54
BT-19H	BTE 2-1	35.93	4.89	12.89	19.64		12.02	0.25	0.60	9.08	0.10	95.39	52
BT-19H	BTE 2-3	36.66	5.16	12.47	19.26		12.68	0.00	0.54	9.70	0.07	96.55	54
BT-19H	BTE 2-3	36.45	4.86	13.50	18.45		11.77	0.69	0.62	9.06	0.11	95.51	53
BT-19H	BTE 2-4	36.96	5.18	13.23	18.31		12.12	0.03	0.52	9.55	0.09	96.01	54
BT-19H	BTE 2-4	36.79	4.98	13.11	18.87		12.33	0.19	0.58	9.36	0.10	96.31	54
BT-19H	BTE 2-5	36.64	5.22	12.59	19.52		12.61	0.01	0.63	9.63	0.09	96.95	54
BT-19H	BTE 2-5	36.37	5.09	12.45	19.00		12.43	0.09	0.61	9.67	0.08	95.81	54
BT-19H	BTE 2-7	36.38	5.08	12.74	18.78		12.36	0.04	0.61	9.49	0.07	95.56	54
BT-19H	BTE 2-11	36.88	4.95	12.97	18.67		12.35	0.17	0.61	9.44	0.10	96.14	54
BT-19H	BTE 2-12	37.01	5.07	13.24	18.58		12.04	0.03	0.57	9.47	0.28	96.30	54
BT-19H	BTE 3-1	36.98	4.94	12.92	18.50		12.55	0.05	0.66	9.32	0.19	96.10	55
BT-19H	BTE 3-2	36.61	5.21	12.42	18.61		12.78	0.06	0.56	9.52	0.16	95.92	55
BT-19H	BTE 3-3	36.78	5.21	12.57	19.19		12.73	0.01	0.62	9.67	0.23	97.03	54

BT-19H	BTE 3-4	36.75	5.24	12.60	18.81		12.52	0.00	0.58	9.54	0.22	96.25	54
BT-19H	BTE 3-5	36.50	5.15	12.35	18.90		12.79	0.02	0.59	9.66	0.18	96.14	55
BT-19H	BTE 3-6	36.71	5.21	12.58	19.28		12.83	0.00	0.63	9.63	0.14	97.04	54
BT-19H	BTE 4-3	36.82	4.83	13.35	18.18		11.79	0.11	0.58	9.10	0.21	94.96	54
BT-19H	BTE 4-4	36.95	5.17	13.15	18.05		12.05	0.05	0.57	9.36	0.24	95.58	54
	Average	36.61	5.10	12.76	18.74		12.48	0.10	0.60	9.48	0.15	96.01	54
	Standard Deviation	0.34	0.12	0.35	0.39		0.36	0.16	0.04	0.19	0.06	0.51	1
BT-19I	BTE 1-1	37.06	5.70	12.52	18.20	0.10	12.86	0.01	0.60	9.47	0.08	96.60	56
BT-19I	BTE 1-2	37.31	5.70	12.69	18.34	0.10	12.74	0.04	0.58	9.58	0.03	97.10	55
BT-19I	BTE 1-3	37.77	5.27	13.06	17.51	0.11	11.49	0.28	0.53	9.13	0.04	95.21	54
BT-19I	BTE 1-4	37.52	5.58	12.90	18.06	0.10	12.44	0.04	0.56	9.34	0.05	96.58	55
BT-19I	BTE 2-1	37.48	5.58	12.64	18.03	0.10	12.84	0.01	0.59	9.50	0.15	96.91	56
BT-19I	BTE 2-2	37.25	5.52	12.60	17.98	0.10	13.00	0.01	0.57	9.57	0.16	96.76	56
BT-19I	BTE 2-3	37.11	5.62	12.49	17.84	0.10	12.42	0.02	0.54	9.56	0.17	95.88	55
BT-19I	BTE 2-4	37.25	5.42	12.61	18.07	0.10	12.43	0.01	0.55	9.53	0.06	96.02	55
BT-19I	BTE 2-5	37.74	5.30	12.68	18.08	0.10	12.80	0.01	0.58	9.58	0.02	96.88	56
BT-19I	BTE 2-6	37.69	5.25	12.64	17.95	0.09	12.54	0.01	0.56	9.55	0.07	96.35	55
BT-19I	BTE 3-1	38.42	5.28	13.16	17.50	0.10	12.93	0.03	0.48	9.11	0.06	97.07	57
BT-19I	BTE 3-2	37.65	5.32	12.71	17.99	0.10	12.96	0.02	0.51	9.69	0.04	96.99	56
BT-19I	BTE 3-3	37.36	5.28	12.60	18.04	0.11	12.32	0.00	0.55	9.55	0.02	95.85	55
BT-19I	BTE 3-6	36.89	5.17	12.51	17.93	0.10	12.74	0.60	0.49	9.53	0.02	95.98	56
BT-19I	BTE 3-8	37.46	5.38	12.80	17.88	0.10	13.29	0.06	0.57	9.37	0.06	96.96	57
BT-19I	BTE 4-1	37.35	5.74	12.66	17.99	0.10	12.26	0.17	0.46	9.31	0.15	96.18	55
BT-19I	BTE 4-3	36.06	5.38	12.51	17.24	0.09	12.23	2.07	0.52	8.79	0.14	95.02	56
BT-19I	BTE 5-1	37.55	5.56	12.83	18.08	0.09	12.80	0.05	0.56	9.54	0.05	97.11	56
BT-19I	BTE 5-2	37.72	5.46	13.28	18.07	0.10	12.29	0.08	0.51	9.29	0.05	96.84	55
BT-19I	BTE 5-3	37.17	5.72	12.82	18.44	0.10	12.61	0.05	0.59	9.52	0.03	97.05	55
BT-19I	BTE 5-5	36.25	5.49	12.66	18.04	0.10	12.10	1.87	0.58	9.29	0.03	96.40	54
BT-19I	BTE 5-8	37.36	5.67	12.62	18.44	0.10	12.74	0.05	0.57	9.54	0.13	97.23	55
BT-19I	BTE 6-1	37.42	5.12	12.71	17.94	0.09	12.09	0.06	0.55	9.37	0.20	95.57	55
BT-19I	BTE 6-2	37.67	5.02	12.84	18.10	0.09	12.34	0.02	0.53	9.56	8.00	96.35	55
BT-19I	BTE 6-3	37.73	5.08	12.87	18.17	0.10	12.59	0.02	0.55	9.49	0.20	96.80	55
BT-19I	BTE 6-4	37.16	5.08	12.60	18.06	0.09	12.09	0.07	0.57	9.56	0.17	95.45	54
BT-19I	BTE 6-5	37.39	5.19	12.66	17.98	0.10	12.64	0.02	0.56	9.54	0.16	96.25	56
BT-19I	BTE 7-5	36.68	4.44	12.96	18.18	0.10	12.23	0.95	0.50	9.21	0.04	95.27	55
BT-19I	BTE 7-6	36.80	4.59	12.61	18.38	0.09	12.88	0.25	0.56	9.53	0.01	95.70	56
BT-19I	BTE 7-7	37.10	4.65	12.64	18.43	0.10	12.94	0.13	0.50	9.29	0.01	95.78	56
BT-19I	BTE 7-8	37.09	4.61	12.81	18.23	0.10	13.28	0.02	0.57	9.53	0.02	96.25	56
BT-19I	BTE 7-9	37.23	4.46	13.09	18.49	0.10	13.44	0.06	0.56	9.65	0.03	97.11	56
BT-19I	BTE 7-10	37.46	4.66	12.93	18.37	0.10	13.23	0.01	0.52	9.65	0.03	96.96	56
	Average	**37.31**	**5.25**	**12.75**	**18.06**	**0.10**	**12.62**	**0.22**	**0.55**	**9.45**	**0.32**	**96.38**	**55**
	Standard Deviation	**0.45**	**0.38**	**0.20**	**0.27**	**0.00**	**0.42**	**0.49**	**0.03**	**0.19**	**1.38**	**0.64**	**1**
BT-3A	BTE 2-1	36.29	5.11	12.80	18.98		12.20	0.04	0.53	9.36	0.18	95.52	53

BT-3A	BTE 3-3	35.75	5.07	12.87	19.02	12.24	0.02	0.56	9.45	0.04	95.01	53
BT-3A	BTE 3-5	36.41	5.09	12.85	19.18	12.13	0.02	0.54	9.51	0.15	95.87	54
BT-3A	BTE 3-6	36.87	5.07	12.62	18.39	12.16	0.05	0.46	9.36	0.13	95.12	54
BT-3A	BTE 3-7	36.40	5.20	12.98	19.09	12.38	0.01	0.55	9.63	0.21	96.46	54
BT-3A	BTE 3-9	36.88	5.18	12.96	19.23	12.25	0.02	0.59	9.51	0.18	96.81	51
BT-3A	BTE 3-10	36.75	5.21	12.95	19.40	12.38	0.00	0.56	9.56	0.19	96.99	53
BT-3A	BTE 3-11	36.63	5.16	12.95	18.88	12.31	0.03	0.54	9.44	0.19	96.14	53
BT-3A	BTE 3-12	36.64	4.89	12.85	19.68	11.66	0.06	0.60	9.09	0.18	95.67	54
BT-3A	BTE 3-14	36.61	5.13	12.77	18.75	12.20	0.04	0.49	9.36	0.17	95.53	53
BT-3A	BTE 3-15	36.23	5.10	12.76	18.92	12.16	0.01	0.54	9.38	0.19	95.30	53
BT-3A	BTE 3-16	36.56	5.17	12.91	19.30	12.32	0.02	0.55	9.48	0.24	96.54	54
BT-3A	BTE 3-22	36.12	5.17	12.87	19.20	12.37	0.00	0.53	9.62	0.06	95.96	53
BT-3A	BTE 3-24	36.46	5.14	12.83	19.30	12.17	0.01	0.55	9.53	0.09	96.10	54
BT-3A	BTE 3-25	36.64	4.98	12.55	19.02	12.23	0.03	0.56	9.40	0.10	95.50	54
BT-3A	BTE 3-26	36.14	5.12	12.84	19.19	12.48	0.00	0.58	9.44	0.04	95.81	54
BT-3A	BTE 3-29	36.69	5.13	12.88	18.83	12.12	0.02	0.59	9.53	0.11	95.89	54
BT-3A	BTE 3-30	36.40	5.09	12.87	18.99	12.23	0.01	0.54	9.63	0.10	95.84	53
BT-3A	BTE 5-1	36.78	5.16	12.78	19.06	12.34	0.01	0.57	9.54	0.17	96.42	53
BT-3A	BTE 5-2	36.55	5.13	12.88	19.13	12.47	0.00	0.56	9.63	0.09	96.43	53
BT-3A	BTE 5-3	36.79	4.90	12.58	18.28	12.60	0.06	0.57	9.10	0.09	94.98	53
BT-3A	BTE 5-4	36.16	5.08	12.66	18.82	12.17	0.05	0.53	9.39	0.22	95.10	54
BT-3A	BTE 6-1	36.50	5.04	12.77	18.98	12.29	0.03	0.54	9.50	0.04	95.68	53
BT-3A	BTE 6-2	36.95	5.10	12.92	19.10	12.38	0.00	0.60	9.55	0.07	96.68	53
BT-3A	BTE 6-4	36.70	4.94	12.70	18.68	12.47	0.00	0.55	9.35	0.00	95.35	52
BT-3A	BTE 6-7	37.32	5.06	13.01	19.15	12.11	0.02	0.56	9.52	0.06	96.83	51
BT-3A	BTE 6-8	36.81	5.09	12.85	18.98	12.28	0.01	0.56	9.57	0.03	96.19	53
BT-3A	BTE 6-9	36.87	5.13	12.94	18.90	12.32	0.00	0.56	9.64	0.04	96.38	54
BT-3A	BTE 7-1	36.30	5.14	12.76	18.93	12.40	0.01	0.55	9.55	0.05	95.69	53
BT-3A	BTE 7-3	36.80	5.10	12.90	18.96	12.22	0.01	0.58	9.46	0.05	96.08	54
BT-3A	BTE 7-4	36.82	5.12	12.90	19.16	12.50	0.02	0.57	9.45	0.09	96.64	53
BT-3A	BTE 7-9	36.49	5.13	12.76	18.80	12.37	0.02	0.54	9.53	0.07	95.71	54
BT-3A	BTE 7-10	36.41	5.08	12.70	18.98	12.22	0.02	0.55	9.43	0.03	95.43	53
BT-3A	BTE 8-2	36.54	5.11	12.76	18.93	12.39	0.01	0.56	9.54	0.04	95.88	54
BT-3A	BTE 8-3	36.22	5.10	12.73	19.00	12.15	0.02	0.58	9.62	0.03	95.47	52
BT-3A	BTE 9-1	36.72	5.06	13.03	18.76	12.36	0.01	0.55	9.53	0.03	96.07	54
BT-3A	BTE 9-2	36.32	5.06	12.80	18.85	12.39	0.02	0.56	9.44	0.02	95.46	53
BT-3A	BTE 9-3	36.53	5.13	12.95	18.78	12.49	0.01	0.57	9.49	0.04	95.96	55
BT-3A	BTE 9-4	36.07	5.10	12.83	19.49	11.92	0.01	0.60	9.30	0.19	95.50	54
BT-3A	BTE 11-3	36.37	5.06	12.67	19.32	11.83	0.00	0.55	9.07	0.20	95.09	54
BT-3A	BTE 11-4	37.10	5.16	12.80	19.19	12.38	0.10	0.53	9.45	0.15	96.88	54
BT-3A	BTE 11-12	36.29	5.12	12.79	18.98	12.18	0.00	0.54	9.31	0.21	95.40	53
BT-3A	BTE 11-13	36.61	5.12	12.83	19.18	12.25	0.00	0.55	9.39	0.24	96.19	53
BT-3A	BTE 12-1	36.69	5.14	12.78	19.31	12.30	0.01	0.54	9.41	0.15	96.35	51
BT-3A	BTE 12-3	36.64	5.05	12.78	19.27	12.09	0.01	0.52	9.41	0.13	95.89	53
BT-3A	BTE 12-10	36.37	4.96	12.62	18.82	12.18	0.05	0.54	9.27	0.17	94.96	53

BT-3A	BTE 12-11	36.51	5.10	12.81	19.09		12.46	0.01	0.56	9.43	0.10	96.07	54
BT-3A	BTE 12-13	36.34	4.94	12.65	18.70		12.26	0.01	0.54	9.43	0.14	95.02	54
BT-3A	BTE 12-16	36.25	5.14	12.70	19.12		12.23	0.01	0.56	9.40	0.20	95.62	54
BT-3A	BTE 12-18	36.34	5.12	12.85	19.07		12.26	0.01	0.53	9.33	0.11	95.60	52
BT-3A	BTE 12-25	36.82	5.07	12.75	19.10		12.25	0.02	0.55	9.47	0.19	96.20	54
BT-3A	BTE 12-26	36.65	5.09	12.73	18.97		12.39	0.03	0.56	9.47	0.14	96.01	53
BT-3A	BTE 12-27	36.50	5.19	12.80	19.08		12.18	0.02	0.55	9.29	0.22	95.81	53
BT-3A	BTE 12-28	36.21	5.13	12.88	19.00		12.20	0.01	0.52	9.47	0.11	95.55	53
BT-3A	BTE 12-29	36.68	5.11	12.83	19.15		12.26	0.01	0.57	9.39	0.19	96.21	54
BT-3A	BTE 12-30	36.75	5.07	13.01	19.18		12.47	0.03	0.56	9.43	0.18	96.69	54
BT-3A	BTE 31-1	37.40	5.22	13.05	18.58	0.15	12.86	0.00	0.57	9.48	0.22	97.53	55
BT-3A	BTE 31-1	37.48	5.15	12.98	18.47	0.12	12.71	0.00	0.55	9.57	0.15	97.18	55
BT-3A	BTE 31-1	37.43	5.14	13.08	18.52	0.15	12.66	0.00	0.55	9.47	0.24	97.24	55
BT-3A	BTE 31-1	37.66	5.16	13.02	18.77	0.08	12.70	0.01	0.56	9.64	0.18	97.77	55
BT-3A	BTE 31-1	36.45	5.16	12.88	18.48	0.18	12.51	0.00	0.54	9.36	0.15	95.70	55
BT-3A	BTE 32-1	36.60	5.13	12.74	18.71	0.17	12.69	0.01	0.54	9.42	0.18	96.17	55
BT-3A	BTE 32-2	36.84	5.18	12.82	18.66	0.21	12.56	0.00	0.56	9.55	0.15	96.53	55
BT-3A	BTE 32-3	37.18	5.18	13.22	18.92	0.14	12.56	0.01	0.56	9.47	0.24	97.49	54
BT-3A	BTE 33-1	36.37	5.19	12.65	18.72	0.13	12.60	0.03	0.54	9.43	0.10	95.76	55
BT-3A	BTE 33-3	37.58	5.06	13.18	19.10	0.13	12.80	0.03	0.56	9.51	0.09	98.04	54
BT-3A	BTE 33-4	36.73	5.28	12.83	18.70	0.13	12.16	0.03	0.52	9.49	0.10	95.97	54
BT-3A	BTE 33-7	36.07	5.15	12.65	18.93	0.15	12.13	0.00	0.55	9.46	0.13	95.21	53
BT-3A	BTE 33-8	36.06	5.14	12.50	18.79	0.31	12.00	0.04	0.51	9.55	0.10	95.00	53
BT-3A	BTE 33-9	36.99	5.07	12.94	18.70	0.14	12.30	0.03	0.52	9.26	0.10	96.05	54
BT-3A	BTE 33-10	37.11	4.96	13.00	19.17	0.17	12.49	0.01	0.53	9.69	0.16	97.30	54
BT-3A	BTE 33-11	37.34	5.04	12.97	19.27	0.15	12.57	0.00	0.54	9.41	0.19	97.47	54
BT-3A	BTE 33-12	37.53	5.08	13.03	18.76	0.13	12.73	0.01	0.56	9.56	0.18	97.56	55
BT-3A	BTE 33-13	37.17	4.97	12.98	18.75	0.16	12.54	0.03	0.54	9.52	0.19	96.87	54
BT-3A	BTE 33-14	37.14	5.24	12.93	19.06	0.17	12.36	0.00	0.53	9.59	0.13	97.16	54
BT-3A	BTE 33-15	37.01	5.07	12.90	18.98	0.17	12.75	0.01	0.55	9.50	0.13	97.06	55
BT-3A	BTE 34-1	36.17	5.12	12.64	18.69	0.20	12.71	0.00	0.57	9.11	0.21	95.43	55
BT-3A	BTE 34-2	37.31	5.20	13.03	18.64	0.15	12.65	0.01	0.57	9.29	0.20	97.06	55
BT-3A	BTE 34-3	37.36	5.52	13.06	18.72	0.13	12.60	0.02	0.56	9.52	0.20	97.69	55
BT-3A	BTE 34-4	37.42	5.21	13.03	18.76	0.12	12.46	0.02	0.58	9.36	0.24	97.19	54
BT-3A	BTE 34-5	36.98	5.16	12.85	18.57	0.11	12.56	0.02	0.58	9.43	0.12	96.40	55
BT-3A	BTE 34-6	37.17	5.09	12.91	18.81	0.14	12.56	0.01	0.56	9.34	0.14	96.73	54
BT-3A	BTE 34-7	37.30	5.25	13.00	18.90	0.15	12.69	0.00	0.55	9.45	0.15	97.45	54
BT-3A	BTE 35-1	36.70	5.13	12.68	18.79	0.13	12.61	0.01	0.53	9.43	0.25	96.27	54
BT-3A	BTE 35-2	37.16	5.20	12.83	18.76	0.10	12.76	0.02	0.54	9.51	0.26	97.15	55
BT-3A	BTE 35-3	37.44	5.18	13.24	18.70	0.15	12.67	0.01	0.54	9.44	0.21	97.58	55
BT-3A	BTE 35-4	37.77	5.11	13.23	18.83	0.14	12.80	0.00	0.53	9.41	0.19	98.01	55
BT-3A	BTE 35-5	37.76	5.28	13.18	18.89	0.18	12.57	0.00	0.55	9.36	0.19	97.95	54
BT-3A	BTE 35-6	38.27	5.18	13.35	18.51	0.12	12.31	0.01	0.55	9.63	0.11	98.05	54
BT-3A	BTE 35-7	37.60	5.21	13.12	18.69	0.16	12.42	0.00	0.52	9.53	0.13	97.37	54
BT-3A	BTE 35-8	36.98	5.13	12.84	18.76	0.20	12.69	0.00	0.57	9.45	0.14	96.76	55

BT-3A	BTE 35-9	37.23	5.04	12.89	18.87	0.18	12.57	0.01	0.56	9.52	0.14	97.00	54
BT-3A	BTE 35-10	37.43	5.11	12.97	18.59	0.13	12.61	0.01	0.58	9.51	0.07	97.02	55
BT-3A	BTE 35-11	37.52	5.39	13.03	18.72	0.20	12.76	0.01	0.56	9.48	0.16	97.83	55
BT-3A	BTE 35-12	37.03	5.24	12.89	18.97	0.12	12.65	0.01	0.55	9.53	0.19	97.18	54
	Average	**36.79**	**5.12**	**12.87**	**18.92**	**0.15**	**12.39**	**0.02**	**0.55**	**9.45**	**0.14**	**96.32**	**54**
	Standard Deviation	**0.48**	**0.09**	**0.16**	**0.25**	**0.04**	**0.23**	**0.02**	**0.02**	**0.12**	**0.06**	**0.84**	**1**
BT-3B	BTE 1-1	37.69	5.19	12.49	19.16	0.13	12.70	0.02	0.56	9.58	0.31	97.83	54
BT-3B	BTE 1-3	37.03	5.09	12.48	19.40	0.12	12.52	0.03	0.60	9.63	0.06	96.95	53
BT-3B	BTE 1-4	37.17	5.19	12.30	19.04	0.12	12.65	0.02	0.57	9.60	0.21	96.89	54
BT-3B	BTE 1-5	36.87	5.13	12.54	19.16	0.10	12.77	0.03	0.58	9.48	0.22	96.88	54
BT-3B	BTE 1-7	37.35	5.19	12.28	19.14	0.12	12.49	0.02	0.53	9.51	0.21	96.85	54
BT-3B	BTE 1-8	37.06	5.16	12.45	19.10	0.13	12.59	0.02	0.55	9.52	0.24	96.81	54
BT-3B	BTE 1-9	36.94	5.18	12.42	19.32	0.13	12.50	0.01	0.56	9.49	0.23	96.79	54
BT-3B	BTE 1-10	37.24	5.18	12.45	19.21	0.14	12.69	0.00	0.59	9.64	0.21	97.33	54
BT-3B	BTE 1-11	37.08	5.21	12.44	19.33	0.12	12.75	0.00	0.57	9.57	0.22	97.28	54
BT-3B	BTE 1-12	37.16	5.17	12.57	19.18	0.13	12.51	0.01	0.53	9.74	0.26	97.26	54
BT-3B	BTE 1-14	37.03	5.18	12.45	19.18	0.12	12.68	0.01	0.60	9.69	0.21	97.14	54
BT-3B	BTE 1-16	36.89	5.19	12.46	19.28	0.13	12.72	0.00	0.58	9.64	0.23	97.11	54
BT-3B	BTE 1-17	37.06	5.18	12.43	19.32	0.12	12.57	0.02	0.60	9.54	0.24	97.10	54
BT-3B	BTE 1-18	37.04	5.20	12.36	19.18	0.12	12.63	0.00	0.59	9.78	0.18	97.09	54
BT-3B	BTE 1-19	36.99	5.18	12.49	18.97	0.13	12.80	0.01	0.57	9.62	0.25	97.01	55
BT-3B	BTE 1-21	36.98	5.16	12.47	19.35	0.13	12.52	0.00	0.55	9.66	0.15	96.98	54
BT-3B	BTE 1-23	37.00	5.23	12.39	19.08	0.15	12.60	0.02	0.57	9.49	0.26	96.79	54
BT-3B	BTE 1-25	36.94	5.14	12.48	19.11	0.15	12.64	0.01	0.54	9.50	0.27	96.77	54
BT-3B	BTE 1-26	36.87	5.25	12.47	19.19	0.14	12.43	0.01	0.56	9.62	0.22	96.77	54
BT-3B	BTE 1-27	36.87	5.20	12.38	19.31	0.11	12.60	0.02	0.57	9.61	0.08	96.76	54
BT-3B	BTE 3-1	36.69	5.05	12.37	19.03	0.12	12.56	0.02	0.52	9.31	0.04	95.72	54
BT-3B	BTE 3-2	36.76	4.89	12.33	18.98	0.13	12.52	0.00	0.57	9.41	0.10	95.71	54
BT-3B	BTE 4-1	36.66	5.15	12.30	18.85	0.11	12.42	0.01	0.55	9.31	0.34	95.69	54
BT-3B	BTE 4-2	36.82	5.12	12.09	18.70	0.11	12.53	0.09	0.54	9.29	0.16	95.44	54
BT-3B	BTE 4-3	36.49	4.80	12.34	19.02	0.12	12.53	0.01	0.57	9.43	0.12	95.44	54
BT-3B	BTE 4-4	36.45	5.09	12.22	19.11	0.14	12.32	0.01	0.56	9.34	0.19	95.42	53
BT-3B	BTE 4-5	37.32	5.07	12.01	19.06	0.10	12.12	0.06	0.53	9.03	0.09	95.39	53
BT-3B	BTE 4-6	36.33	5.22	12.16	19.16	0.10	12.31	0.00	0.55	9.39	0.15	95.38	53
BT-3B	BTE 4-7	36.46	5.11	12.19	18.78	0.14	12.45	0.02	0.54	9.42	0.27	95.37	54
BT-3B	BTE 4-8	36.35	5.14	12.53	18.65	0.11	12.36	0.01	0.53	9.45	0.23	95.35	54
BT-3B	BTE 4-9	36.52	5.25	12.14	18.79	0.12	12.30	0.01	0.52	9.40	0.28	95.35	54
BT-3B	BTE 4-10	36.40	5.21	12.05	18.91	0.12	12.61	0.00	0.59	9.56	0.21	95.66	54
BT-3B	BTE 4-11	36.87	5.14	12.43	18.69	0.12	12.31	0.06	0.56	9.34	0.12	95.65	54
BT-3B	BTE 4-13	36.75	5.19	12.26	18.82	0.11	12.30	0.02	0.52	9.46	0.22	95.64	54
BT-3B	BTE 4-15	36.86	4.92	12.30	18.98	0.11	12.43	0.03	0.53	9.41	0.07	95.63	54
BT-3B	BTE 4-16	36.99	5.22	12.23	18.60	0.14	12.44	0.05	0.49	9.21	0.19	95.56	54
BT-3B	BTE 4-17	36.46	5.14	12.30	18.87	0.10	12.55	0.04	0.57	9.40	0.08	95.52	54
BT-3B	BTE 4-18	36.38	5.20	12.09	19.02	0.13	12.50	0.02	0.53	9.40	0.19	95.45	54

BT-3B	BTE 6-2	36.69	5.13	12.53	18.52	0.12	12.38	0.02	0.50	9.33	0.12	95.34	54
BT-3B	BTE 6-3	36.62	4.89	12.17	19.01	0.13	12.56	0.04	0.54	9.27	0.10	95.32	54
BT-3B	BTE 8-1	36.96	4.94	12.55	18.68	0.13	12.20	0.09	0.53	9.22	0.02	95.31	54
BT-3B	BTE 8-2	36.36	5.18	12.05	19.02	0.12	12.50	0.02	0.53	9.25	0.22	95.25	54
BT-3B	BTE 8-3	36.31	5.20	12.37	18.86	0.11	12.28	0.03	0.57	9.53	0.00	95.25	54
BT-3B	BTE 8-4	36.68	5.13	12.21	18.64	0.11	12.44	0.02	0.53	9.26	0.22	95.25	54
BT-3B	BTE 9-1	37.42	4.88	12.18	19.05	0.12	11.89	0.07	0.46	9.05	0.09	95.22	53
BT-3B	BTE 9-2	36.71	5.06	12.20	18.73	0.12	12.41	0.00	0.51	9.34	0.12	95.19	54
BT-3B	BTE 9-3	36.83	5.11	11.99	18.93	0.11	12.25	0.05	0.49	9.19	0.17	95.12	54
BT-3B	BTE 9-4	36.67	4.97	12.40	18.99	0.15	11.96	0.03	0.55	9.18	0.14	95.05	53
BT-3B	BTE 9-5	36.23	5.18	12.31	18.96	0.11	12.18	0.00	0.54	9.19	0.29	94.99	53
BT-3B	BTE 11-1	37.00	5.23	12.34	19.36	0.11	12.44	0.00	0.56	9.51	0.21	96.76	53
BT-3B	BTE 11-2	36.32	5.38	12.78	19.25	0.15	12.12	0.01	0.55	9.34	0.81	96.71	53
BT-3B	BTE 11-4	36.93	5.14	12.46	19.17	0.11	12.61	0.02	0.56	9.46	0.21	96.65	54
BT-3B	BTE 11-5	36.89	5.15	12.44	19.10	0.12	12.64	0.01	0.56	9.62	0.11	96.64	54
BT-3B	BTE 11-6	36.85	5.22	12.54	19.23	0.13	12.48	0.00	0.57	9.40	0.22	96.63	54
BT-3B	BTE 11-7	36.87	4.99	12.58	19.39	0.13	12.58	0.00	0.54	9.54	0.01	96.63	54
BT-3B	BTE 11-8	36.80	4.90	12.63	19.21	0.12	12.64	0.01	0.53	9.62	0.15	96.62	54
BT-3B	BTE 11-10	37.00	5.24	12.22	19.26	0.14	12.61	0.00	0.57	9.61	0.13	96.75	54
BT-3B	BTE 11-11	37.20	5.13	12.46	18.99	0.13	12.63	0.00	0.54	9.55	0.10	96.74	54
BT-3B	BTE 11-12	36.99	5.26	12.36	18.99	0.11	12.66	0.00	0.58	9.62	0.17	96.73	54
BT-3B	BTE 13-2	36.42	5.27	12.73	19.20	0.13	12.23	0.01	0.54	9.38	0.69	96.61	53
BT-3B	BTE 13-7	36.84	5.23	12.49	19.30	0.10	12.53	0.00	0.57	9.50	0.04	96.60	54
BT-3B	BTE 13-8	37.16	4.94	12.48	19.43	0.11	12.42	0.07	0.48	9.26	0.23	96.57	53
BT-3B	BTE 13-9	36.98	5.23	12.25	19.30	0.12	12.40	0.00	0.60	9.50	0.20	96.56	53
BT-3B	BTE 13-11	37.01	5.09	12.41	19.25	0.14	12.53	0.00	0.58	9.59	0.01	96.62	54
BT-3B	BTE 13-12	37.00	5.08	12.31	19.15	0.11	12.72	0.02	0.56	9.50	0.16	96.62	54
BT-3B	BTE 13-13	36.75	5.22	12.36	19.07	0.13	12.65	0.03	0.56	9.68	0.15	96.61	54
BT-3B	BTE 14-1	37.16	5.03	12.40	19.14	0.13	12.42	0.00	0.59	9.65	0.03	96.55	54
BT-3B	BTE 14-2	36.81	5.14	12.31	19.11	0.13	12.61	0.00	0.59	9.65	0.19	96.52	54
BT-3B	BTE 14-3	36.97	5.19	12.26	19.10	0.10	12.70	0.02	0.55	9.45	0.17	96.50	54
BT-3B	BTE 14-4	36.75	5.11	12.47	19.21	0.12	12.73	0.02	0.56	9.50	0.03	96.50	54
BT-3B	BTE 14-5	37.22	5.08	12.52	19.00	0.15	12.32	0.02	0.52	9.43	0.23	96.48	54
BT-3B	BTE 14-6	36.88	5.14	12.29	19.18	0.12	12.68	0.00	0.57	9.45	0.16	96.47	54
BT-3B	BTE 14-7	37.19	5.06	12.43	19.18	0.13	12.32	0.02	0.61	9.46	0.05	96.46	53
BT-3B	BTE 14-8	36.86	4.89	12.44	19.27	0.13	12.58	0.03	0.57	9.50	0.18	96.45	54
BT-3B	BTE 14-9	36.71	5.27	12.40	19.29	0.13	12.38	0.03	0.53	9.54	0.17	96.44	53
BT-3B	BTE 14-10	36.81	5.24	12.40	19.02	0.06	12.61	0.02	0.55	9.68	0.15	96.54	54
BT-3B	BTE 14-11	36.71	5.17	12.50	19.21	0.11	12.54	0.02	0.58	9.60	0.11	96.54	54
BT-3B	BTE 14-12	36.85	5.13	12.54	19.19	0.13	12.54	0.02	0.56	9.56	0.01	96.54	54
BT-3B	BTE 15-1	36.84	5.24	12.28	19.10	0.12	12.53	0.04	0.54	9.53	0.21	96.44	54
BT-3B	BTE 15-2	36.61	5.19	12.38	19.63	0.12	12.13	0.01	0.58	9.56	0.21	96.44	52
BT-3B	BTE 15-5	36.80	5.20	12.24	19.42	0.10	12.49	0.01	0.58	9.52	0.05	96.42	53
BT-3B	BTE 15-6	36.61	5.19	12.40	19.13	0.14	12.65	0.00	0.55	9.69	0.06	96.40	54
BT-3B	BTE 16-1	36.97	5.19	12.33	19.06	0.13	12.48	0.03	0.60	9.45	0.15	96.40	54

BT-3B	BTE 16-2	36.81	5.14	12.38	19.15	0.12	12.57	0.00	0.56	9.56	0.02	96.31	54
BT-3B	BTE 16-3	36.76	5.11	12.39	19.07	0.12	12.58	0.00	0.57	9.53	0.16	96.29	54
BT-3B	BTE 16-4	36.55	5.28	12.66	18.88	0.11	12.38	0.04	0.51	9.37	0.51	96.28	54
BT-3B	BTE 16-5	36.68	5.22	12.19	19.21	0.12	12.48	0.00	0.57	9.55	0.24	96.27	54
BT-3B	BTE 16-6	36.64	5.26	12.25	19.23	0.12	12.47	0.00	0.56	9.66	0.06	96.26	54
BT-3B	BTE 16-7	36.81	5.08	12.44	19.21	0.13	12.49	0.03	0.51	9.51	0.04	96.25	54
BT-3B	BTE 16-8	36.71	5.13	12.47	18.95	0.13	12.58	0.05	0.59	9.44	0.20	96.24	54
BT-3B	BTE 16-9	36.78	5.12	12.29	19.12	0.10	12.57	0.00	0.55	9.52	0.18	96.23	54
BT-3B	BTE 16-10	36.93	5.11	12.55	19.19	0.12	12.44	0.01	0.59	9.41	0.04	96.38	54
BT-3B	BTE 16-11	36.09	5.32	12.96	19.13	0.14	12.01	0.00	0.53	9.37	0.82	96.38	53
BT-3B	BTE 16-12	36.95	5.25	12.35	19.14	0.12	12.48	0.00	0.55	9.47	0.06	96.36	54
BT-3B	BTE 16-13	36.87	5.09	12.48	19.17	0.13	12.54	0.00	0.56	9.43	0.08	96.34	54
BT-3B	BTE 16-14	36.83	5.19	12.38	19.00	0.13	12.55	0.02	0.56	9.47	0.22	96.34	54
BT-3B	BTE 16-15	37.22	5.18	12.46	18.91	0.12	12.56	0.03	0.53	9.27	0.04	96.32	54
BT-3B	BTE 17-1	36.96	4.96	12.52	19.00	0.12	12.53	0.01	0.55	9.51	0.06	96.22	54
BT-3B	BTE 17-2	36.62	5.23	12.33	19.22	0.09	12.59	0.02	0.56	9.50	0.05	96.21	54
BT-3B	BTE 17-3	36.72	5.24	12.26	19.37	0.12	12.35	0.00	0.54	9.56	0.04	96.20	53
BT-3B	BTE 17-4	37.23	4.92	12.74	18.41	0.11	12.72	0.07	0.61	9.38	0.00	96.18	55
BT-3B	BTE 17-5	36.65	5.25	12.19	19.28	0.11	12.49	0.01	0.56	9.49	0.14	96.17	54
BT-3B	BTE 18-1	36.77	5.16	12.43	18.99	0.12	12.64	0.01	0.52	9.48	0.04	96.16	54
BT-3B	BTE 18-2	36.82	5.12	12.45	18.94	0.11	12.55	0.02	0.57	9.53	0.03	96.13	54
BT-3B	BTE 18-3	36.82	5.13	12.40	18.97	0.09	12.42	0.00	0.55	9.63	0.13	96.13	54
BT-3B	BTE 18-4	36.95	5.09	12.46	18.68	0.12	12.68	0.04	0.51	9.48	0.11	96.11	55
BT-3B	BTE 18-5	36.57	5.26	12.24	19.27	0.12	12.49	0.01	0.58	9.52	0.02	96.08	54
BT-3B	BTE 18-6	36.73	5.15	12.34	19.02	0.12	12.48	0.01	0.52	9.46	0.19	96.03	54
BT-3B	BTE 18-7	36.61	5.05	12.35	19.37	0.12	12.36	0.04	0.59	9.51	0.03	96.02	53
BT-3B	BTE 18-8	36.67	5.24	12.40	19.02	0.10	12.36	0.03	0.56	9.55	0.07	96.00	54
BT-3B	BTE 18-9	36.80	5.15	12.38	18.80	0.13	12.52	0.01	0.52	9.62	0.07	96.00	54
BT-3B	BTE 18-10	36.66	5.31	12.21	19.27	0.11	12.38	0.00	0.55	9.58	0.05	96.14	53
BT-3B	BTE 20-1	36.92	5.13	12.33	19.01	0.12	12.55	0.05	0.53	9.21	0.16	96.00	54
BT-3B	BTE 20-3	37.07	5.03	12.62	19.09	0.12	12.12	0.02	0.56	9.25	0.08	95.97	53
BT-3B	BTE 20-4	36.63	5.25	12.18	19.21	0.11	12.45	0.03	0.55	9.51	0.04	95.97	54
BT-3B	BTE 20-5	36.67	5.19	12.24	19.03	0.13	12.54	0.00	0.56	9.44	0.18	95.97	54
BT-3B	BTE 20-6	36.69	5.05	12.32	19.13	0.13	12.50	0.02	0.60	9.46	0.07	95.97	54
BT-3B	BTE 20-7	37.97	4.82	12.27	19.36	0.10	11.80	0.11	0.51	8.96	0.02	95.92	52
BT-3B	BTE 20-8	36.91	5.08	12.28	18.97	0.12	12.50	0.02	0.53	9.44	0.07	95.92	54
BT-3B	BTE 20-9	36.41	5.15	12.43	19.10	0.14	12.45	0.00	0.58	9.44	0.22	95.91	54
BT-3B	BTE 20-10	37.64	4.99	12.39	17.94	0.11	12.43	0.28	0.58	9.49	0.15	95.99	55
BT-3B	BTE 20-11	36.71	5.18	12.23	19.22	0.10	12.47	0.03	0.56	9.30	0.19	95.99	54
BT-3B	BTE 20-12	36.70	4.95	12.41	19.09	0.11	12.63	0.03	0.52	9.46	0.07	95.97	54
BT-3B	BTE 21-1	37.17	4.93	12.29	19.03	0.10	12.42	0.13	0.51	9.17	0.14	95.89	54
BT-3B	BTE 21-2	36.96	5.19	12.16	19.01	0.11	12.36	0.06	0.54	9.35	0.15	95.88	54
BT-3B	BTE 21-3	36.58	5.21	12.38	18.95	0.12	12.53	0.04	0.50	9.35	0.22	95.88	54
BT-3B	BTE 21-4	36.79	5.05	12.31	19.02	0.13	12.58	0.05	0.55	9.35	0.04	95.88	54
BT-3B	BTE 21-5	36.68	5.12	12.25	19.12	0.13	12.43	0.02	0.53	9.43	0.17	95.87	54

BT-3B	BTE 22-1	36.63	5.28	12.30	18.94	0.11	12.43	0.01	0.57	9.52	0.08	95.86	54
BT-3B	BTE 22-2	37.01	5.15	12.64	18.48	0.11	12.41	0.05	0.50	9.40	0.08	95.83	54
BT-3B	BTE 22-3	36.77	4.89	12.19	19.00	0.12	12.59	0.03	0.55	9.54	0.09	95.77	54
BT-3B	BTE 22-4	36.82	5.19	12.43	18.77	0.10	12.25	0.00	0.55	9.59	0.07	95.77	54
BT-3B	BTE 22-5	36.89	5.14	12.29	18.77	0.12	12.55	0.15	0.55	9.16	0.14	95.76	54
BT-3B	BTE 22-6	36.72	4.96	12.38	19.02	0.11	12.57	0.01	0.57	9.33	0.09	95.75	54
BT-3B	BTE 22-7	37.05	4.98	12.46	18.88	0.12	12.28	0.02	0.53	9.34	0.09	95.75	54
BT-3B	BTE 22-8	36.84	5.07	12.41	18.90	0.13	12.34	0.03	0.57	9.40	0.03	95.73	54
BT-3B	BTE 22-9	36.91	5.00	12.61	18.60	0.13	12.44	0.03	0.51	9.43	0.05	95.72	54
BT-3B	BTE 22-10	36.59	5.13	12.52	18.83	0.11	12.54	0.03	0.56	9.47	0.07	95.84	54
	Average	**36.83**	**5.13**	**12.38**	**19.06**	**0.12**	**12.48**	**0.02**	**0.55**	**9.46**	**0.15**	**96.18**	**54**
	Standard Deviation	**0.28**	**0.11**	**0.15**	**0.23**	**0.01**	**0.17**	**0.03**	**0.03**	**0.15**	**0.13**	**0.56**	**0**

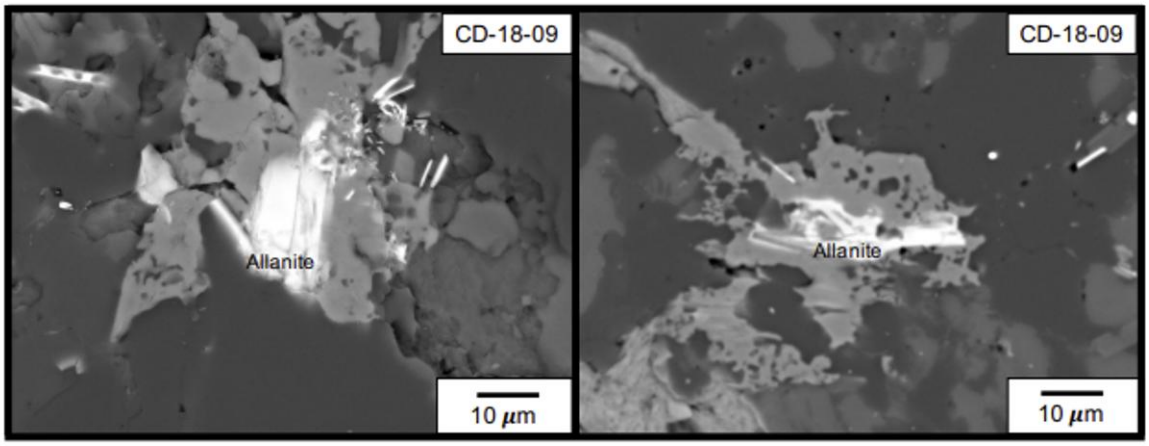
Table A-0-7 Average compositions (wt%) of titanomagnetite and ilmenite for previously published samples from Glass Mountain (Gordon, 2022)

Sample	GM-18	GM-01	GM-07	GM-20	GM-10
Eruptive Unit	OB	OC	OL	OT	YO
Study	This Study	This Study	This Study	This Study	This Study
TMTE, *N;n*	30;444	71;71	55;540	20;100	14;87
SiO_2	0.11	0.11	0.12	0.11	0.15
TiO_2	8.08	7.11	8.72	8.05	7.70
Al_2O_3	0.79	0.70	0.79	0.89	0.98
Fe_2O_3	52.13	54.19	51.10	52.33	52.48
V_2O_3	0.04	0.03	0.04	0.05	0.05
Cr_2O_3	0.00	0.00	0.00	0.00	0.00
FeO	36.83	34.45	36.97	37.03	36.86
MnO	1.37	2.68	1.85	1.13	0.91
MgO	0.22	0.25	0.23	0.31	0.31
CaO	0.00	0.00	0.00	0.00	0.00
Total	99.80	99.91	100.12	100.11	99.61
ln(XMg/XMn)	-0.55	-0.79	-0.66	-0.32	-0.22
ILMN, *N;n*	5;111	25;65	5;62	3;60	3;18
SiO_2	0.08	0.05	0.10	0.10	0.14
TiO_2	47.01	47.23	47.63	46.96	47.18
Al_2O_3	0.11	0.04	0.11	0.08	0.26
Fe_2O_3	10.20	9.98	9.69	11.14	10.99
V_2O_3	0.23	0.22	0.23	0.25	0.24
Cr_2O_3	0.00	0.00	0.00	0.00	0.00
FeO	37.06	33.52	36.62	37.40	37.31
MnO	3.10	6.94	4.07	2.45	2.01
MgO	0.59	0.66	0.60	0.79	0.81
CaO	0.01	0.00	0.02	0.01	0.03
Total	98.46	99.89	99.16	99.26	99.00
ln(XMg/XMn)	-0.48	-0.78	-0.59	-0.25	-0.15
[1]Fe-Ti T (°C)	698	660	700	716	695
ΔNNO	-0.3	-0.7	-0.6	-0.1	-0.2
[2]Activity TiO_2 (rutile)	0.487	0.378	0.431	0.536	0.528

Table A-0-8 Calculated values of D_{TiO2} (bte-liq) for previously published samples (Jolles and Lange, 2019; Bolte et al., 2015)

Sample	Avg Bte wt% TiO_2	± 1 SD	Avg Gl wt% TiO_2	± 1 SD	Calculated $D_{TiO_2}^{bte-liq}$	± 1 SD	$D_{TiO_2}^{bte-liq}$ Temperature (°C)	± 1 SD (model error)	Fe-Ti Oxide Temperature (°C)	Residuals
BT.22B	4.22	0.05	0.07	0.01	60	9	706	22	713	7
BT.22A	4.13	0.10	0.07	0.01	59	9	709	22	728	19
BT.8B	4.42	0.04	0.10	0.01	44	4	743	13	742	-1
BT-16B	4.17	0.02	0.07	0.01	60	9	708	22	706	-2
BT-13A	4.49	0.03	0.09	0.01	50	6	730	16	734	4
BT-19D	4.79	0.08	0.12	0.01	40	3	753	11	748	-5
BT-21F	4.87	0.05	0.19	0.01	26	1	787	8	781	-6
BT-19F	5.41	0.31	0.20	0.01	27	2	783	8	799	16
BT-19H	5.10	0.12	0.18	0.01	28	2	780	8	788	8
BT-19I	5.25	0.38	0.20	0.01	26	2	785	9	798	13
BT-3A	5.12	0.09	0.18	0.01	28	2	780	8	787	7
BT-3B	5.13	0.11	0.20	0.01	26	1	786	8	788	2
A18x	3.47	*1.03	0.25	0.02	14	4	814	12	825	11
A22	4.21	*1.03	0.19	0.02	22	6	795	15	800	5
A23	4.24	0.38	0.20	0.02	21	3	797	9	800	3

Figure A-0-1An SE image of allanite from a previously published sample from the Benton Range (Mesa, 2021)



Text A.1 Fe-Ti Two-Oxide thermometry and oxybarometry from Gordon (2022)

The Bacon and Hirschmann (1988) Mg/Mn equilibrium test, which is based on plots of molar $\log(Mg/Mn)^{titanomagnetite}$ versus molar $\log(Mg/Mn)^{ilmenite}$, was applied to the average ilmenite and titanomagnetite compositions reported for each Glass Mountain sample. The results are shown in Figure A-0-2 together with those obtained from the average analyses reported in Metz and Mahood (1991); all Fe-Ti oxide analyses pass the Bacon and Hirschmann (1988) test. Since the Fe-Ti oxides in all Glass Mountain samples pass this equilibrium test, the titanomagnetite and ilmenite pairs reported in Table 2-3 were used to calculate temperature and ΔNNO using the Fe-Ti two-oxide model of Ghiorso and Evans (2008).

Uncertainties in the calculated temperatures are based on the statistical model presented by Jolles and Lange (2019), which showed how many analyses of each oxide were required (assuming a single population in each sample and given the determined microprobe SD analytical uncertainty) to obtain an average TiO_2 and FeO^T concentration in each phase that is within ± 0.2 wt% of its true value. Based on the total number of ilmenite and titanomagnetite analyses obtained in this study, propagated analytical uncertainties in calculated temperature and ΔNNO are all < 10°C and < 0.05, respectively. The effect of a systematic error of <0.4 % relative in the wt% FeO^T analyses of the two Fe-Ti oxides leads to a < 1°C increase in calculated temperatures and is therefore considered negligible.

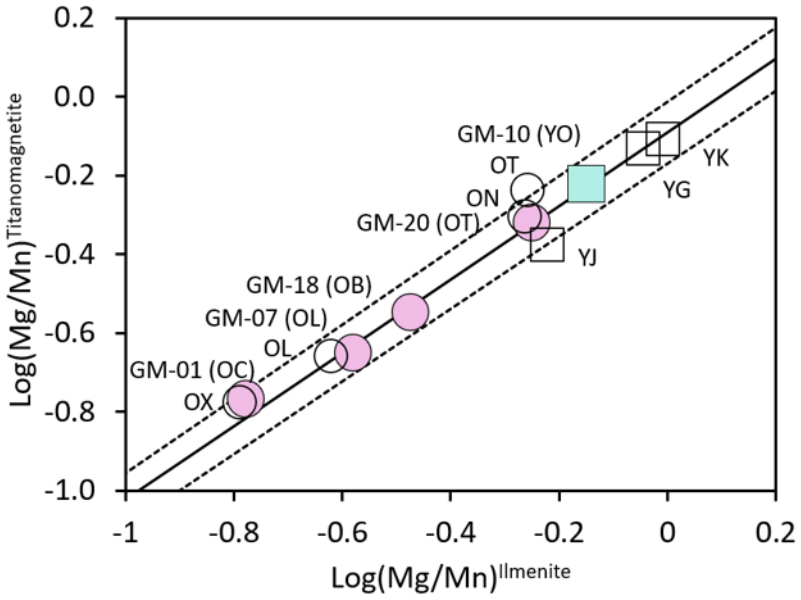
References:

Bacon CR, Hirschmann MM (1988) Mg/Mn partitioning as a test for equilibrium between coexisting Fe–Ti oxides. Am Mineral 73:57-61

Ghiorso, M.S. & Evans, B.W. (2008) Thermodynamics of rhombohedral oxide solutions and revision of the Fe–Ti two-oxide geothermometer and oxygen barometer. American Journal of Science, 308, 957-1039.

Jolles, J. S. R., & Lange, R. A. (2019). High-resolution Fe–Ti oxide thermometry applied to single-clast pumices from the Bishop Tuff: a re-examination of compositional variations in phenocryst phases with temperature. Contributions to Mineralogy and Petrology, 174(8). https://doi.org/10.1007/s00410-019-1597-z

Figure A-0-2 Plot of average $\log(Mg/Mn)^{titanomagnetite}$ versus $\log(Mg/Mn)^{ilmenite}$ obtained from Fe-Ti oxide analyses. Data from this study are shown in pink circles (Older GM) and green squares (Younger GM). Also shown are data from Metz and Mahood (1991) as open circles (Older GM) and open squares (Younger GM). The solid line is the Bacon and Hirschmann (1988) equilibrium relationship, and the dashed lines show the ±2 SD error envelope.



Appendix B: Supplemental Material for Chapter 3

Table B-0-9 Electron microprobe standards and conditions of analysis

Instrument:			
Cameca SX100, EMAL/University of Michigan			
Phases:			
Plagioclase/Sanidine			
Accelerating Voltage (kV)	**Beam Current (nA)**	**Beam Size (µm)**	**Peak Counting Time (s)**
15	20	2	20
Standard	**Elements Calibrated**		
Adularia (St. Gotthard)	Si, K		
Wollastonite	Ca		
Geikelite	Ti	3SD uncertainty based on counting statistics for plagioclase and sanidine: 0.67 wt% SiO_2, 0.02 wt% TiO_2, 0.38 wt% Al_2O_3, 0.04 wt% FeO^T, 0.03 wt% MnO, 0.02 wt% MgO, 0.05 wt% CaO, 0.15 wt% Na_2O, 0.15 wt%K_2O.	
Tanzanite	Al		
Ferrosilite (synthetic)	Fe		
Geikelite	Mg		
Albite (Tiburon)	Na		
Rhodonite (Broken Hill)	Mn		
Phase: biotite			
Accelerating Voltage (kV)	**Beam Current (nA)**	**Beam Size (µm)**	**Peak Counting Time (s)**
15	20	2	10-30
Standard	**Elements Calibrated**		
Ferrosilite (synthetic)	Si, Fe		
Geikelite (synthetic)	Ti, Mg		
Tanzanite	Al	3SD uncertainty based on counting statistics for biotite: 0.47 wt%SiO_2, 0.09 wt% TiO_2, 0.26 wt% Al_2O_3, 0.54 wt% FeO^T, 0.04 wt% MnO, 0.19 wt% MgO, 0.06 wt% BaO, 0.04 wt% CaO, 0.04 wt% Na_2O, 0.25 wt% K_2O.	
Rhodonite (Broken Hill)	Mn		
Wollastonite	Ca		
Albite (Tiburon)	Na		
Ba-Cl-Apatite	Ba		
Adularia (St. Gotthard)	K		

Table B-0-10 Natural individual plagioclase analyses (wt%)

Sample	Point	SiO_2	TiO_2	Al_2O_3	FeO	MnO	MgO	CaO	Na_2O	K_2O	Total	Or# (XOr *100)	An# (XAn *100)	Ab# (XAb *100)
GM-18 (OB)	GM-18_Feld_3-1	66.99	0.00	20.87	0.12	0.00	0.00	2.00	9.50	1.61	101.08	9.1	9.5	81.5
	GM-18_Feld_3-3	66.19	0.00	20.85	0.14	0.01	0.00	2.28	9.42	1.23	100.13	7.0	11.0	82.0
	GM-18_Feld_5-1	66.12	0.00	20.52	0.09	0.00	0.00	2.14	9.19	1.48	99.53	8.6	10.4	81.0
	GM-18_Feld_5-2	66.62	0.01	20.83	0.11	0.00	0.00	2.01	9.32	1.65	100.53	9.4	9.6	80.9
	GM-18_Feld_6-1	66.56	0.00	21.08	0.08	0.00	0.01	2.00	9.48	1.55	100.76	8.8	9.5	81.7
	GM-18_Feld_6-2	66.60	0.00	20.82	0.13	0.03	0.00	1.93	9.45	1.67	100.62	9.4	9.2	81.4
	GM-18_Feld_6-3	66.64	0.00	20.90	0.10	0.00	0.00	1.94	9.40	1.52	100.50	8.7	9.3	81.9
	GM-18_Feld_17-1	66.57	0.00	21.07	0.13	0.00	0.00	2.11	9.62	1.52	100.99	8.5	9.9	81.6
	GM-18_Feld_17-3	66.89	0.00	20.67	0.13	0.00	0.00	1.90	9.62	1.61	100.83	9.0	9.0	82.0
	GM-18_Feld_18-2	67.33	0.00	20.44	0.11	0.00	0.00	1.67	9.47	1.84	100.85	10.4	7.9	81.6
	GM-18_Feld_21-1	66.74	0.01	21.27	0.13	0.00	0.00	2.17	9.50	1.42	101.23	8.0	10.3	81.7
	GM-18_Feld_21-2	66.21	0.00	20.50	0.12	0.00	0.00	2.09	9.32	1.57	99.78	9.0	10.0	81.0
	GM-18_Feld_21-3	66.10	0.00	21.89	0.13	0.01	0.00	2.10	9.36	1.52	101.11	8.7	10.1	81.2
	GM-18_Feld_21-4	66.19	0.00	21.31	0.11	0.00	0.00	1.96	8.81	1.60	99.98	9.6	9.9	80.5
	GM-18_Feld_27-1	66.71	0.00	20.62	0.11	0.00	0.00	1.79	9.59	1.68	100.49	9.5	8.5	82.0
	GM-18_Feld_27-3	67.34	0.01	20.86	0.12	0.00	0.00	1.96	9.35	1.85	101.48	10.4	9.3	80.3
	GM-18_Feld_29-1	66.86	0.01	21.04	0.10	0.00	0.00	2.14	9.49	1.50	101.13	8.5	10.1	81.4
	GM-18_Feld_29-2	66.95	0.01	20.89	0.11	0.01	0.00	2.20	9.60	1.45	101.22	8.1	10.3	81.5
	GM-18_Feld_29-3	66.19	0.00	21.27	0.14	0.01	0.00	2.45	9.54	1.37	100.96	7.6	11.5	80.9
	GM-18_Feld_29-4	67.00	0.00	21.24	0.11	0.00	0.00	2.16	9.45	1.52	101.46	8.6	10.3	81.2
	Average	**66.64**	**0.00**	**20.95**	**0.12**	**0.00**	**0.00**	**2.05**	**9.42**	**1.56**	**100.73**	**8.9**	**9.8**	**81.4**
	Standard Deviation	**0.38**	**0.00**	**0.34**	**0.02**	**0.01**	**0.00**	**0.17**	**0.18**	**0.14**	**0.54**	**0.8**	**0.8**	**0.5**

GM-01 (OC)	GM-01_Feld_13-1	67.78	0.00	20.01	0.15	0.00	0.00	1.30	9.74	1.85	100.83	10.4	6.2	83.4
	GM-01_Feld_13-2	67.17	0.00	20.59	0.12	0.00	0.00	1.57	9.77	1.69	100.89	9.5	7.4	83.2
	GM-01_Feld_13-3	67.00	0.00	20.85	0.10	0.00	0.00	1.65	9.48	1.70	100.78	9.7	7.9	82.4
	GM-01_Feld_14-4 - dark	67.50	0.00	20.07	0.14	0.00	0.00	1.40	9.46	1.94	100.50	11.1	6.7	82.2
	GM-01_Feld_14-4 - dark	67.13	0.01	20.29	0.12	0.01	0.00	1.45	9.90	1.42	100.33	8.0	6.9	85.1
	GM-01_Feld_17-5 - dark	66.70	0.00	20.30	0.14	0.00	0.01	1.73	9.69	1.54	100.10	8.7	8.2	83.1
	GM-01_Feld_17-5 - dark	66.98	0.00	20.20	0.13	0.00	0.00	1.52	9.63	1.75	100.18	9.9	7.2	82.9
	GM-01_Feld_19-4 - dark	67.12	0.02	20.79	0.14	0.00	0.00	1.70	9.69	1.67	101.12	9.3	8.0	82.7
	GM-01_Feld_19-4 - dark	67.22	0.01	20.54	0.15	0.00	0.00	1.66	9.74	1.50	100.80	8.5	7.9	83.7
	GM-01_Feld_21-1	67.72	0.00	20.48	0.14	0.00	0.00	1.61	9.72	1.73	101.40	9.7	7.6	82.7
	GM-01_Feld_21-2	67.43	0.00	20.37	0.15	0.03	0.01	1.57	9.45	1.77	100.77	10.1	7.6	82.3
	GM-01_Feld_21-3	67.81	0.00	20.10	0.11	0.00	0.00	1.41	9.77	1.87	101.04	10.4	6.6	82.9
	GM-01_Feld_21-4	67.36	0.00	20.28	0.12	0.02	0.00	1.47	9.48	1.84	100.56	10.5	7.0	82.5
	GM-01_Feld_32-5 - dark	67.67	0.00	20.37	0.14	0.00	0.00	1.54	9.45	1.88	101.03	10.7	7.4	81.9
	GM-01_Feld_32-5 - dark	66.83	0.00	20.12	0.12	0.01	0.00	1.56	9.63	1.71	99.99	9.7	7.4	82.9
	GM-01_Feld_37-1	66.79	0.00	20.49	0.13	0.00	0.00	1.60	9.59	1.70	100.28	9.6	7.6	82.7
	GM-01_Feld_37-2	67.55	0.01	20.56	0.14	0.00	0.00	1.58	9.54	1.81	101.18	10.3	7.5	82.2
	GM-01_Feld_37-3	66.74	0.00	20.30	0.10	0.00	0.00	1.57	9.57	1.83	100.11	10.3	7.5	82.2
	GM-01_Feld_41-4	66.33	0.01	20.52	0.11	0.00	0.00	1.56	9.76	1.72	100.00	9.7	7.3	83.0

	GM-01_Feld_41-5	67.60	0.00	20.15	0.13	0.00	0.00	1.36	9.76	1.94	100.90	10.8	6.4	82.8
	GM-01_Feld_41-6	66.90	0.00	20.30	0.13	0.01	0.00	1.30	9.66	2.00	100.29	11.3	6.1	82.6
	GM-01_Feld_43-4 - dark	67.48	0.00	20.61	0.14	0.00	0.00	1.55	9.69	1.29	100.76	7.4	7.5	85.0
	GM-01_Feld_43-4 - dark	67.26	0.00	20.63	0.13	0.00	0.00	1.62	9.55	1.69	100.87	9.6	7.8	82.6
	GM-01_Feld_43-4 - dark	67.06	0.00	20.51	0.14	0.00	0.00	1.57	9.78	1.64	100.69	9.2	7.4	83.4
	GM-01_Feld_44-1	66.82	0.01	20.31	0.13	0.00	0.00	1.45	9.53	1.95	100.18	11.0	6.9	82.1
	GM-01_Feld_44-3	67.10	0.00	20.49	0.11	0.01	0.00	1.67	9.57	1.77	100.71	10.0	7.9	82.1
	GM-01_Feld_44-4	67.61	0.00	20.34	0.14	0.00	0.00	1.52	9.57	1.77	100.95	10.1	7.3	82.7
	GM-01_Feld_44-5	67.19	0.00	20.49	0.16	0.00	0.00	1.51	9.66	1.79	100.80	10.1	7.1	82.7
	GM-01_Feld_46-1	67.18	0.00	20.32	0.12	0.00	0.00	1.66	9.38	1.73	100.37	9.9	8.0	82.0
	GM-01_Feld_46-2	66.30	0.00	20.34	0.11	0.01	0.00	1.46	9.43	1.86	99.50	10.7	7.0	82.3
	GM-01_Feld_46-3	66.48	0.00	20.37	0.15	0.00	0.00	1.46	9.71	1.84	99.99	10.3	6.9	82.8
	GM-01_Feld_46-4	66.82	0.01	20.08	0.11	0.03	0.00	1.67	9.61	1.74	100.06	9.8	7.9	82.3
	GM-01_Feld_50-5 -dark	66.56	0.01	20.45	0.12	0.01	0.00	1.64	9.73	1.58	100.08	8.9	7.8	83.3
	GM-01_Feld_50-5 -dark	67.05	0.00	20.51	0.13	0.01	0.00	1.62	10.06	1.27	100.64	7.1	7.6	85.3
	GM-01_Feld_50-5 -dark	67.59	0.00	20.66	0.15	0.00	0.00	1.58	9.88	1.48	101.34	8.3	7.5	84.2
	Average	**67.14**	**0.00**	**20.39**	**0.13**	**0.00**	**0.00**	**1.55**	**9.65**	**1.72**	**100.57**	**9.7**	**7.3**	**82.9**
	Standard Deviation	**0.41**	**0.00**	**0.20**	**0.02**	**0.01**	**0.00**	**0.11**	**0.15**	**0.17**	**0.45**	**1.0**	**0.5**	**0.8**
GM-JJ-10 (OD) Plagioclase	GM-JJ-10A PLAG4	66.00	0.00	20.94	0.09	0.00	0.00	2.12	9.61	1.26	99.95	7.1	10.1	82.7
	GM-JJ-10A PLAG5	66.40	0.00	20.85	0.14	0.00	0.00	1.97	9.85	1.37	100.54	7.6	9.2	83.2
	GM-JJ-10A PLAG6	66.10	0.02	20.92	0.10	0.00	0.00	1.87	9.64	1.48	100.10	8.4	8.9	82.8

GM-JJ-10A PLAG7	66.53	0.00	20.36	0.11	0.00	0.00	1.78	9.63	1.49	99.89	8.5	8.5	83.1
GM-JJ-10A PLAG8	65.62	0.02	20.49	0.11	0.01	0.00	2.08	9.51	0.78	98.62	4.6	10.3	85.1
GM-JJ-10A PLAG9	66.12	0.00	20.64	0.11	0.04	0.00	2.00	9.46	1.42	99.79	8.1	9.6	82.2
GM-JJ-10A PLAG10	66.34	0.04	20.99	0.14	0.00	0.01	2.07	9.50	1.40	100.48	8.0	9.9	82.2
GM-JJ-10A PLAG11	66.67	0.01	20.72	0.16	0.01	0.00	1.65	9.70	1.60	100.50	9.0	7.8	83.1
GM-JJ-10A SAN 1 incl	66.62	0.00	21.18	0.10	0.02	0.00	2.07	9.66	1.43	101.05	8.0	9.7	82.3
GM-JJ-10A SAN 1 incl	66.88	0.00	20.90	0.11	0.02	0.01	1.69	9.79	1.50	100.92	8.4	8.0	83.6
GM-JJ-10A SAN 3 incl maybe	66.71	0.00	20.64	0.11	0.22	0.00	1.64	9.68	1.65	100.66	9.3	7.7	83.0
GM-JJ-10A SAN 3 incl maybe	65.46	0.02	20.58	0.11	0.02	0.00	1.75	9.65	1.20	98.77	6.9	8.5	84.6
GM-JJ-10A SAN 4 plag incl	66.80	0.00	20.75	0.08	0.01	0.00	1.71	9.74	1.48	100.57	8.4	8.1	83.5
GM-JJ-10A SAN 4 plag incl	65.91	0.00	20.86	0.10	0.01	0.00	1.83	9.60	1.55	99.84	8.8	8.7	82.5
GM-JJ-10A SAN 4 plag incl	66.12	0.00	20.78	0.10	0.00	0.00	1.90	9.77	1.22	99.91	6.9	9.0	84.1
GM-JJ-10A SAN 4 plag incl	66.53	0.01	20.88	0.13	0.00	0.00	1.78	9.68	1.49	100.46	8.4	8.5	83.1
GM-JJ-10A SAN 4 plag incl	66.03	0.00	21.06	0.09	0.00	0.00	2.01	9.74	1.10	100.03	6.2	9.6	84.1
GM-JJ-10A SAN 4 plag incl	66.29	0.02	20.74	0.13	0.00	0.00	1.85	9.71	1.49	100.23	8.4	8.7	82.9
GM-JJ-10A SAN 4 plag incl	67.34	0.01	20.66	0.13	0.01	0.00	1.81	9.71	1.47	101.14	8.3	8.5	83.2
GM-JJ-10A SAN 4 plag incl	66.39	0.01	20.79	0.12	0.07	0.00	1.96	9.69	1.40	100.39	7.9	9.3	82.9
GM-JJ-10A SAN 5 incl TR	66.59	0.00	20.91	0.10	0.05	0.00	1.85	9.70	1.46	100.65	8.2	8.8	83.0
GM-JJ-10A SAN 5 incl TR	65.95	0.00	20.97	0.12	0.07	0.00	1.99	9.72	1.36	100.13	7.6	9.4	83.0
GM-JJ-10A SAN 5 incl BR	66.02	0.01	21.00	0.11	0.03	0.00	1.90	9.64	1.44	100.15	8.2	9.0	82.8
GM-JJ-10A SAN 5 incl BR	66.03	0.00	20.92	0.11	0.01	0.00	1.83	9.65	1.54	100.07	8.7	8.7	82.7
GM-JJ-10A SAN 5 incl BR	66.81	0.00	20.56	0.12	0.02	0.00	1.62	9.68	1.60	100.36	9.1	7.7	83.3

GM-JJ-10A SAN 5 incl BR	66.69	0.02	20.85	0.11	0.02	0.01	1.76	9.49	1.52	100.47	8.7	8.5	82.8
GM-JJ-10A SAN 5 incl BR	66.07	0.00	20.95	0.11	0.01	0.00	1.96	9.60	1.43	100.11	8.1	9.3	82.6
GM-JJ-10A SAN 6 incl BR	65.64	0.00	20.95	0.10	0.02	0.00	2.10	9.71	1.34	99.84	7.5	9.9	82.6
GM-JJ-10A SAN 6 incl BR	65.50	0.00	20.97	0.11	0.00	0.00	2.09	9.65	1.33	99.59	7.5	9.9	82.6
GM-JJ-10A SAN 6 incl BR	66.49	0.00	20.86	0.08	0.00	0.00	1.84	9.65	1.42	100.30	8.0	8.7	83.2
GM-JJ-10A SAN 6 incl BC	66.37	0.00	20.99	0.10	0.00	0.00	2.00	9.62	1.40	100.47	7.9	9.5	82.6
GM-JJ-10A SAN 6 incl BC	65.96	0.00	21.04	0.10	0.01	0.00	2.00	9.73	1.29	100.12	7.3	9.5	83.3
GM-JJ-10A SAN 6 incl LoBC	66.26	0.00	21.05	0.12	0.01	0.00	2.09	9.59	1.39	100.50	7.8	9.9	82.2
GM-JJ-10A SAN 6 incl LoBC	66.78	0.00	21.04	0.08	0.02	0.00	1.92	9.61	1.45	100.87	8.2	9.1	82.6
GM-JJ-10A SAN 6 incl BL	65.94	0.01	20.79	0.10	0.01	0.00	1.91	9.60	1.40	99.76	8.0	9.1	82.9
GM-JJ-10A SAN 6 incl BL	66.20	0.00	20.90	0.08	0.01	0.01	1.90	9.61	1.46	100.11	8.2	9.0	82.7
GM-JJ-10A SAN 6 incl TL	66.40	0.01	20.83	0.08	0.01	0.00	1.78	9.62	1.49	100.18	8.5	8.5	83.0
GM-JJ-10A SAN 6 incl TL	66.38	0.00	20.91	0.11	0.00	0.00	1.85	9.57	1.52	100.34	8.6	8.8	82.5
GM-JJ-10A SAN 6 incl TL	66.03	0.01	20.93	0.11	0.00	0.00	2.00	9.65	1.37	100.10	7.7	9.5	82.8
GM-JJ-10A SAN 6 incl TR	65.67	0.01	21.04	0.13	0.00	0.00	2.10	9.63	1.32	99.92	7.4	10.0	82.6
GM-JJ-10A SAN 6 incl TR	66.62	0.00	20.94	0.11	0.03	0.00	1.99	9.61	1.41	100.70	8.0	9.4	82.6
GM-JJ-10A SAN 19 incl	66.51	0.00	20.72	0.10	0.00	0.00	1.75	9.66	1.46	100.17	8.3	8.3	83.4
GM-JJ-10A SAN 19 incl	66.00	0.00	21.22	0.10	0.01	0.00	2.14	9.52	1.36	100.32	7.7	10.2	82.1
GM-JJ-10A SAN 19 incl	66.23	0.00	20.93	0.11	0.02	0.00	2.04	9.79	1.20	100.30	6.8	9.6	83.6
GM-JJ-10A SAN 19 incl	66.55	0.00	20.85	0.09	0.00	0.00	1.95	9.59	1.33	100.37	7.6	9.3	83.1
GM-JJ-10A SAN 19 incl	66.33	0.00	20.70	0.11	0.00	0.00	1.78	9.60	1.54	100.04	8.7	8.5	82.8
Average	**66.28**	**0.00**	**20.86**	**0.11**	**0.02**	**0.00**	**1.91**	**9.65**	**1.40**	**100.21**	**7.9**	**9.1**	**83.0**
Standard Deviation	**0.39**	**0.01**	**0.17**	**0.02**	**0.04**	**0.00**	**0.14**	**0.08**	**0.15**	**0.47**	**0.8**	**0.7**	**0.6**

GM-07 (OL) Plagioclase	GM-07_Feld_30-1	67.48	0.00	20.94	0.13	0.00	0.00	1.76	9.62	1.84	101.74	10.3	8.2	81.5
	GM-07_Feld_30-2	66.54	0.01	21.35	0.13	0.01	0.01	1.86	9.29	1.78	100.97	10.2	8.9	80.9
	GM-07_Feld_30-3	67.24	0.00	20.56	0.13	0.01	0.00	1.84	9.60	1.72	101.09	9.6	8.7	81.7
	GM-07_Feld_30-4	67.37	0.00	20.79	0.14	0.00	0.00	1.84	9.62	1.73	101.48	9.6	8.6	81.7
	Average	**67.16**	**0.00**	**20.91**	**0.13**	**0.00**	**0.00**	**1.82**	**9.53**	**1.76**	**101.32**	**9.9**	**8.6**	**81.5**
	Standard Deviation	**0.42**	**0.00**	**0.33**	**0.01**	**0.00**	**0.00**	**0.04**	**0.16**	**0.06**	**0.35**	**0.3**	**0.3**	**0.4**
GM-20 (OT) Plagioclase	GM_20_Plag_1_1	65.37		21.36	0.15	0.01	0.00	2.57	9.40	1.35	100.23	7.6	12.1	80.3
	GM_20_Plag_1_2	64.77		21.12	0.11	0.01	0.00	2.50	9.35	1.47	99.33	8.3	11.8	79.9
	GM_20_Plag_1_3	64.96		21.09	0.13	0.00	0.00	2.50	9.34	1.53	99.53	8.6	11.8	79.6
	GM_20_Plag_1_4	65.03		20.99	0.08	0.01	0.00	2.53	9.34	1.51	99.49	8.5	11.9	79.6
	GM_20_Plag_1_5	65.03		21.12	0.13	0.01	0.00	2.54	9.35	1.50	99.67	8.4	11.9	79.7
	GM_20_Plag_1_6	65.45		21.03	0.11	0.00	0.00	2.52	9.37	1.48	99.93	8.3	11.9	79.8
	GM_20_Plag_1_7	65.67		21.35	0.12	0.00	0.00	2.52	9.47	1.52	100.66	8.4	11.7	79.8
	GM_20_Plag_1_8	65.27		21.16	0.13	0.00	0.00	2.51	9.38	1.51	99.94	8.5	11.8	79.8
	GM_20_Plag_1_9	64.91		21.00	0.13	0.01	0.00	2.52	9.35	1.49	99.40	8.4	11.9	79.7
	GM_20_Plag_1_10	65.28		21.26	0.15	0.00	0.00	2.54	9.27	1.53	100.01	8.6	12.0	79.4
	GM_20_Plag_1_11	65.05		21.30	0.13	0.00	0.00	2.54	9.36	1.52	99.89	8.5	11.9	79.5
	GM_20_Plag_1_12	65.59		21.20	0.11	0.01	0.00	2.52	9.35	1.53	100.31	8.6	11.8	79.6
	GM_20_Plag_1_13	65.33		21.04	0.13	0.00	0.00	2.49	9.45	1.51	99.95	8.4	11.6	79.9
	GM_20_Plag_1_14	65.30		21.35	0.11	0.00	0.00	2.54	9.31	1.53	100.14	8.6	12.0	79.4
	GM_20_Plag_1_15	65.09		21.25	0.11	0.00	0.00	2.53	9.29	1.53	99.79	8.6	12.0	79.4
	GM_20_Plag_1_16	64.80		20.97	0.12	0.00	0.00	2.56	9.33	1.49	99.26	8.4	12.1	79.5
	GM_20_Plag_1_17	65.09		21.08	0.15	0.00	0.00	2.57	9.40	1.51	99.78	8.4	12.0	79.6
	GM_20_Plag_1_18	64.87		21.07	0.10	0.00	0.00	2.58	9.38	1.54	99.53	8.6	12.0	79.4
	GM_20_Plag_1_19	64.92		21.19	0.14	0.01	0.01	2.52	9.36	1.49	99.64	8.3	11.9	79.8
	GM_20_Plag_1_20	64.93		20.94	0.14	0.00	0.01	2.58	9.29	1.50	99.38	8.4	12.2	79.4
	GM_20_Plag_1_21	64.86		21.09	0.12	0.01	0.00	2.54	9.37	1.14	99.11	6.5	12.2	81.3
	GM_20_Plag_1_22	65.05		21.39	0.12	0.00	0.00	2.60	9.28	1.50	99.93	8.4	12.3	79.3

GM_20_Plag_1_23	65.19	21.19	0.13	0.00	0.00	2.49	9.39	1.52	99.90	8.5	11.7	79.8
GM_20_Plag_1_24	65.04	21.08	0.11	0.00	0.00	2.55	9.22	1.52	99.51	8.6	12.1	79.3
GM_20_Plag_1_25	65.45	21.22	0.13	0.01	0.01	2.55	9.23	1.52	100.11	8.6	12.1	79.3
GM_20_Plag_1_26	65.34	21.28	0.14	0.02	0.00	2.55	9.17	1.55	100.04	8.8	12.2	79.1
GM_20_Plag_1_27	65.94	21.22	0.11	0.00	0.00	2.44	9.37	1.42	100.49	8.0	11.6	80.4
GM_20_Plag_1_28	64.77	20.66	0.13	0.01	0.00	2.43	9.38	1.52	98.88	8.5	11.5	80.0
GM_20_Plag_1_29	65.56	21.51	0.13	0.00	0.00	2.49	9.29	1.48	100.46	8.4	11.8	79.8
GM_20_Plag_1_30	64.67	20.89	0.11	0.01	0.00	2.62	9.15	1.48	98.94	8.4	12.5	79.1
GM_20_Plag_1_31	65.14	21.01	0.13	0.00	0.00	2.51	9.30	1.52	99.60	8.6	11.9	79.6
GM_20_Plag_1_32	65.02	21.34	0.11	0.00	0.00	2.58	9.18	1.59	99.82	9.0	12.2	78.8
GM_20_Plag_1_33	65.41	21.56	0.15	0.00	0.00	2.52	9.35	1.54	100.54	8.6	11.9	79.5
GM_20_Plag_2_1	65.50	20.62	0.11	0.00	0.00	2.07	9.47	1.84	99.59	10.2	9.7	80.1
GM_20_Plag_2_2	65.38	20.93	0.15	0.01	0.00	2.49	9.34	1.59	99.89	8.9	11.7	79.4
GM_20_Plag_2_3	65.21	21.11	0.11	0.00	0.00	2.53	9.33	1.55	99.83	8.7	11.9	79.4
GM_20_Plag_2_4	65.50	21.29	0.10	0.00	0.00	2.51	9.37	1.46	100.24	8.2	11.8	79.9
GM_20_Plag_2_5	65.58	21.13	0.14	0.00	0.00	2.38	9.40	1.62	100.23	9.1	11.2	79.8
GM_20_Plag_2_6	65.28	21.16	0.14	0.00	0.01	2.46	9.28	1.55	99.87	8.7	11.6	79.6
GM_20_Plag_2_7	65.32	21.05	0.11	0.00	0.00	2.48	9.32	1.59	99.88	8.9	11.7	79.4
GM_20_Plag_2_8	65.79	20.88	0.14	0.00	0.00	2.12	9.41	1.78	100.11	10.0	10.0	80.1
GM_20_Plag_2_9	65.33	20.69	0.11	0.00	0.00	2.18	9.37	1.79	99.46	10.0	10.3	79.7
GM_20_Plag_2_10	65.30	20.98	0.13	0.00	0.01	2.26	9.27	1.75	99.70	9.9	10.7	79.4
GM_20_Plag_2_11	65.31	20.99	0.13	0.00	0.00	2.40	9.51	1.37	99.71	7.7	11.3	81.0
GM_20_Plag_2_12	66.17	21.71	0.14	0.01	0.00	2.48	9.97	0.81	101.29	4.5	11.5	84.0
GM_20_Plag_2_13	65.24	21.17	0.12	0.00	0.00	2.47	9.28	1.54	99.81	8.7	11.7	79.6
GM_20_Plag_2_14	65.58	20.97	0.11	0.01	0.00	2.41	9.80	1.13	100.02	6.3	11.2	82.5
GM_20_Plag_2_15	65.80	20.72	0.12	0.00	0.01	2.13	9.51	1.56	99.83	8.7	10.0	81.2
GM_20_Plag_2_16	65.57	20.80	0.12	0.00	0.00	2.12	9.45	1.78	99.82	9.9	9.9	80.2
GM_20_Plag_2_17	65.68	21.06	0.09	0.00	0.00	2.19	9.44	1.74	100.21	9.7	10.3	80.0
GM_20_Plag_2_18	65.84	20.83	0.11	0.00	0.01	2.10	9.43	1.82	100.14	10.2	9.8	80.0
GM_20_Plag_2_19	65.45	20.88	0.13	0.00	0.01	2.17	9.38	1.76	99.78	9.9	10.2	79.9
GM_20_Plag_2_20	65.94	21.04	0.11	0.02	0.00	2.11	9.64	1.54	100.39	8.6	9.9	81.5
GM_20_Plag_2_21	65.33	21.11	0.12	0.00	0.00	2.47	9.40	1.56	99.99	8.7	11.6	79.7
GM_20_Plag_2_22	65.18	20.99	0.14	0.00	0.00	2.41	9.33	1.57	99.60	8.8	11.4	79.8
GM_20_Plag_2_23	65.00	21.07	0.12	0.00	0.00	2.45	9.37	1.58	99.59	8.8	11.5	79.7
GM_20_Plag_2_24	65.45	21.12	0.10	0.00	0.00	2.34	9.57	1.46	100.05	8.1	10.9	80.9

GM_20_Plag_2_25	65.52	20.74	0.12	0.01	0.00	2.16	9.37	1.77	99.71	9.9	10.2	79.9
GM_20_Plag_2_26	65.15	21.11	0.12	0.00	0.00	2.56	9.31	1.56	99.81	8.7	12.1	79.2
GM_20_Plag_2_27	64.76	21.28	0.11	0.00	0.00	2.65	9.20	1.52	99.48	8.6	12.5	78.9
GM_20_Plag_2_28	65.14	20.94	0.12	0.01	0.00	2.33	9.43	1.68	99.65	9.3	10.9	79.7
GM_20_Plag_2_29	65.05	21.11	0.14	0.00	0.00	2.42	9.47	1.31	99.49	7.4	11.5	81.1
GM_20_Plag_2_30	65.30	21.00	0.15	0.00	0.00	2.37	9.41	1.47	99.70	8.3	11.2	80.5
GM_20_Plag_2_31	65.20	21.11	0.11	0.01	0.00	2.39	9.36	1.59	99.76	8.9	11.2	79.8
GM_20_Plag_3_1	65.54	21.12	0.14	0.00	0.00	2.44	9.55	1.11	99.89	6.3	11.6	82.1
GM_20_Plag_3_2	65.82	20.95	0.11	0.00	0.00	2.15	9.41	1.63	100.06	9.2	10.2	80.6
GM_20_Plag_3_3	65.23	21.16	0.14	0.00	0.00	2.56	9.39	1.29	99.77	7.3	12.1	80.6
GM_20_Plag_3_4	65.47	21.30	0.13	0.00	0.00	2.51	9.49	1.24	100.13	7.0	11.8	81.2
GM_20_Plag_3_5	65.51	21.24	0.12	0.00	0.01	2.52	9.32	1.64	100.34	9.1	11.8	79.0
GM_20_Plag_3_6	66.04	20.76	0.12	0.00	0.00	2.04	9.47	1.81	100.25	10.1	9.6	80.3
GM_20_Plag_3_7	65.16	21.37	0.12	0.00	0.00	2.54	9.30	1.60	100.09	8.9	12.0	79.1
GM_20_Plag_3_8	65.67	20.58	0.13	0.00	0.00	2.02	9.46	1.87	99.74	10.4	9.5	80.1
GM_20_Plag_3_9	65.74	20.73	0.15	0.00	0.00	2.01	9.45	1.82	99.89	10.2	9.4	80.4
GM_20_Plag_3_10	65.96	20.60	0.15	0.00	0.00	2.04	9.39	1.88	100.01	10.5	9.6	79.9
GM_20_Plag_3_11	64.90	21.32	0.16	0.00	0.01	2.68	9.28	1.51	99.87	8.5	12.6	78.9
GM_20_Plag_3_12	65.13	21.46	0.16	0.01	0.00	2.64	9.25	1.53	100.19	8.6	12.5	78.9
GM_20_Plag_3_13	65.57	20.93	0.13	0.00	0.00	2.34	9.46	1.66	100.10	9.2	10.9	79.9
GM_20_Plag_3_14	65.51	20.88	0.11	0.00	0.00	2.36	9.37	1.67	99.87	9.3	11.1	79.6
GM_20_Plag_3_15	65.30	20.84	0.13	0.00	0.00	2.28	9.41	1.73	99.68	9.7	10.7	79.7
GM_20_Plag_3_16	65.07	20.95	0.13	0.02	0.00	2.48	9.45	1.38	99.46	7.7	11.7	80.6
GM_20_Plag_3_17	65.57	21.15	0.13	0.00	0.00	2.42	9.42	1.60	100.29	8.9	11.3	79.8
GM_20_Plag_3_18	65.51	21.11	0.13	0.00	0.00	2.46	9.37	1.61	100.20	9.0	11.5	79.5
GM_20_Plag_3_19	65.07	21.00	0.14	0.00	0.00	2.39	9.44	1.59	99.63	8.9	11.2	79.9
GM_20_Plag_3_20	65.39	20.79	0.10	0.01	0.00	2.40	9.43	1.58	99.70	8.8	11.2	80.0
GM_20_Plag_3_21	65.43	21.06	0.14	0.00	0.00	2.35	9.53	1.67	100.18	9.2	10.9	79.9
GM_20_Plag_3_22	65.12	20.59	0.13	0.00	0.00	2.23	9.42	1.69	99.18	9.4	10.5	80.1
GM_20_Plag_3_23	64.45	21.14	0.15	0.00	0.01	2.58	9.29	1.52	99.14	8.5	12.2	79.3
GM_20_Plag_3_24	65.48	21.04	0.12	0.00	0.00	2.40	9.31	1.65	100.00	9.3	11.3	79.4
GM_20_Plag_3_25	65.38	20.87	0.13	0.01	0.00	2.26	9.35	1.70	99.72	9.6	10.7	79.8
GM_20_Plag_3_26	65.60	20.61	0.13	0.00	0.00	2.17	9.49	1.74	99.71	9.7	10.1	80.2
GM_20_Plag_3_27	65.42	20.79	0.15	0.01	0.00	2.20	9.41	1.75	99.72	9.8	10.3	79.9
GM_20_Plag_3_28	65.18	21.02	0.11	0.00	0.00	2.35	9.41	1.66	99.74	9.3	11.0	79.7

	GM_20_Plag_3_29	65.91		20.78	0.14	0.00	0.00	2.21	9.41	1.75	100.19	9.8	10.3	79.9
	GM_20_Plag_3_30	64.88		21.46	0.12	0.01	0.00	2.36	9.17	1.67	99.66	9.5	11.3	79.2
	GM_20_Plag_3_31	65.22		20.97	0.14	0.00	0.00	2.42	9.29	1.65	99.69	9.3	11.4	79.3
	GM_20_Plag_3_32	64.98		20.89	0.15	0.00	0.00	2.38	9.39	1.63	99.40	9.1	11.2	79.7
	GM_20_Plag_3_33	65.23		21.03	0.11	0.00	0.01	2.41	9.39	1.68	99.83	9.3	11.3	79.4
	GM_20_Plag_3_34	65.33		20.97	0.14	0.00	0.00	2.31	9.36	1.69	99.80	9.5	10.9	79.6
	GM_20_Plag_3_35	65.65		21.19	0.13	0.01	0.01	2.39	9.34	1.64	100.36	9.2	11.2	79.6
	Average	**65.32**	**#DIV/0!**	**21.06**	**0.13**	**0.00**	**0.00**	**2.41**	**9.38**	**1.56**	**99.85**	**8.76**	**11.34**	**79.90**
	Standard Deviation	**0.33**	**#DIV/0!**	**0.22**	**0.02**	**0.01**	**0.00**	**0.16**	**0.11**	**0.17**	**0.37**	**0.92**	**0.79**	**0.76**
GM-16(YE) Plagioclase	GM_16_Plag_1_1	63.32		21.71	0.13	0.00	0.00	3.68	8.94	1.19	98.94	6.6	17.3	76.1
	GM_16_Plag_1_2	63.54		21.91	0.16	0.02	0.00	3.56	8.91	1.21	99.31	6.8	16.8	76.3
	GM_16_Plag_1_3	63.65		22.09	0.14	0.00	0.01	3.63	8.84	1.24	99.61	7.0	17.2	75.8
	GM_16_Plag_1_4	63.27		21.62	0.14	0.00	0.01	3.51	8.87	1.22	98.61	6.9	16.7	76.4
	GM_16_Plag_1_5	63.63		21.79	0.14	0.00	0.00	3.50	8.92	1.28	99.27	7.2	16.6	76.2
	GM_16_Plag_1_7	63.60		21.99	0.14	0.00	0.01	3.60	8.88	1.24	99.44	7.0	17.0	76.0
	GM_16_Plag_1_8	63.48		21.77	0.12	0.00	0.00	3.61	8.90	1.22	99.10	6.9	17.1	76.1
	GM_16_Plag_1_9	63.52		21.94	0.14	0.00	0.00	3.61	8.93	1.25	99.39	7.0	17.0	76.0
	GM_16_Plag_1_10	63.64		22.03	0.14	0.00	0.01	3.56	8.87	1.25	99.50	7.1	16.9	76.1
	GM_16_Plag_1_11	64.15		22.26	0.13	0.00	0.00	3.67	8.87	1.22	100.30	6.9	17.3	75.8
	GM_16_Plag_1_12	63.92		22.02	0.14	0.00	0.00	3.64	8.92	1.23	99.87	6.9	17.1	76.0
	GM_16_Plag_1_13	63.76		21.52	0.14	0.00	0.01	3.42	8.88	1.27	98.98	7.2	16.3	76.5
	GM_16_Plag_1_14	63.90		21.97	0.14	0.01	0.00	3.50	8.99	1.23	99.74	6.9	16.5	76.6
	GM_16_Plag_1_15	64.43		21.67	0.13	0.01	0.00	3.41	9.04	1.28	99.97	7.2	16.0	76.8
	GM_16_Plag_1_16	63.97		22.22	0.16	0.00	0.00	3.61	8.95	1.21	100.10	6.8	17.0	76.2
	GM_16_Plag_1_17	64.14		22.18	0.14	0.00	0.00	3.61	8.98	1.21	100.27	6.8	17.0	76.3
	GM_16_Plag_1_18	63.62		21.81	0.13	0.01	0.00	3.55	8.76	1.23	99.12	7.0	17.0	76.0
	GM_16_Plag_1_19	63.32		22.00	0.16	0.00	0.01	3.68	8.89	1.19	99.23	6.7	17.4	75.9
	GM_16_Plag_1_20	63.46		21.99	0.10	0.00	0.01	3.72	8.99	1.13	99.39	6.3	17.4	76.2
	GM_16_Plag_1_21	63.44		21.87	0.14	0.01	0.01	3.69	8.94	1.09	99.19	6.1	17.4	76.4
	GM_16_Plag_1_22	63.55		21.85	0.12	0.01	0.00	3.52	8.87	1.24	99.16	7.0	16.7	76.3
	GM_16_Plag_1_23	63.45		21.92	0.14	0.00	0.00	3.63	8.84	1.24	99.23	7.0	17.2	75.8

GM_16_Plag_1_24	63.65	21.76	0.17	0.00	0.00	3.53	8.87	1.26	99.23	7.1	16.7	76.2
GM_16_Plag_1_25	63.50	21.84	0.15	0.02	0.00	3.55	8.85	1.25	99.16	7.1	16.9	76.1
GM_16_Plag_1_26	63.72	21.81	0.16	0.02	0.00	3.59	9.02	1.24	99.56	6.9	16.8	76.3
GM_16_Plag_1_27	63.68	21.78	0.12	0.01	0.00	3.47	8.95	1.25	99.26	7.1	16.4	76.5
GM_16_Plag_1_28	63.56	22.02	0.16	0.01	0.00	3.57	8.89	1.30	99.50	7.3	16.8	75.9
GM_16_Plag_1_29	64.02	22.15	0.15	0.01	0.00	3.72	8.92	1.19	100.16	6.7	17.5	75.9
GM_16_Plag_1_30	63.85	21.95	0.11	0.00	0.00	3.57	8.90	1.24	99.62	7.0	16.9	76.2
GM_16_Plag_2_1	64.15	21.75	0.16	0.00	0.00	3.37	8.96	1.24	99.62	7.0	16.0	77.0
GM_16_Plag_2_2	64.00	21.91	0.15	0.00	0.01	3.52	8.93	1.25	99.75	7.0	16.6	76.3
GM_16_Plag_2_3	63.49	22.22	0.13	0.00	0.00	3.68	8.87	1.15	99.55	6.5	17.4	76.1
GM_16_Plag_2_4	64.40	22.10	0.15	0.01	0.00	3.49	9.03	1.26	100.44	7.0	16.4	76.6
GM_16_Plag_2_5	63.84	21.79	0.15	0.00	0.00	3.42	8.91	1.11	99.23	6.3	16.4	77.3
GM_16_Plag_2_6	63.71	21.79	0.14	0.00	0.00	3.43	8.91	1.21	99.18	6.9	16.3	76.8
GM_16_Plag_2_7	64.06	21.92	0.16	0.01	0.00	3.48	9.01	1.10	99.75	6.2	16.5	77.3
GM_16_Plag_2_8	63.67	22.04	0.14	0.00	0.00	3.48	8.95	1.30	99.58	7.3	16.4	76.3
GM_16_Plag_2_9	63.68	22.01	0.14	0.00	0.00	3.75	8.82	1.22	99.61	6.8	17.7	75.4
GM_16_Plag_2_10	63.46	22.01	0.13	0.00	0.00	3.56	8.94	1.23	99.33	6.9	16.8	76.3
GM_16_Plag_2_11	63.51	22.07	0.11	0.00	0.00	3.66	8.99	1.11	99.43	6.2	17.2	76.6
GM_16_Plag_2_13	63.75	21.86	0.15	0.00	0.01	3.43	8.86	1.26	99.31	7.1	16.4	76.5
GM_16_Plag_2_14	63.44	21.84	0.14	0.01	0.00	3.45	8.89	1.29	99.04	7.3	16.4	76.4
GM_16_Plag_2_16	63.84	21.67	0.13	0.00	0.00	3.45	8.87	1.17	99.13	6.7	16.5	76.8
GM_16_Plag_2_17	63.04	21.68	0.12	0.01	0.01	3.65	8.99	1.04	98.54	5.8	17.2	76.9
GM_16_Plag_2_18	63.16	21.82	0.14	0.01	0.01	3.63	8.89	1.22	98.88	6.8	17.2	76.0
GM_16_Plag_2_19	63.37	21.65	0.14	0.00	0.01	3.62	8.81	1.21	98.80	6.8	17.2	75.9
GM_16_Plag_2_20	63.46	22.32	0.12	0.00	0.01	3.66	8.91	1.13	99.61	6.4	17.3	76.3
GM_16_Plag_2_21	63.38	21.89	0.14	0.00	0.00	3.62	8.91	1.17	99.10	6.6	17.1	76.3
GM_16_Plag_2_22	63.61	22.06	0.12	0.00	0.00	3.65	8.90	1.19	99.53	6.7	17.2	76.0
GM_16_Plag_2_23	63.92	22.27	0.14	0.01	0.00	3.62	8.92	1.13	100.00	6.4	17.1	76.5
GM_16_Plag_2_24	63.91	21.90	0.14	0.00	0.00	3.59	8.89	1.20	99.62	6.8	17.0	76.2
GM_16_Plag_2_25	63.62	22.00	0.16	0.02	0.00	3.49	8.90	1.26	99.45	7.1	16.6	76.3
GM_16_Plag_2_26	63.66	22.14	0.12	0.00	0.01	3.65	8.93	1.18	99.67	6.6	17.2	76.2
GM_16_Plag_2_27	63.71	21.73	0.14	0.00	0.00	3.52	9.08	0.80	98.98	4.5	16.8	78.6
GM_16_Plag_2_28	63.91	22.02	0.15	0.01	0.00	3.58	9.17	0.84	99.66	4.7	16.9	78.4
GM_16_Plag_2_29	64.17	21.94	0.14	0.00	0.00	3.44	9.00	1.26	99.94	7.1	16.2	76.7
GM_16_Plag_3_1	63.73	22.02	0.17	0.01	0.01	3.54	8.94	1.21	99.63	6.8	16.7	76.4

	GM_16_P lag_3_2	63.69	22.66	0.15	0.00	0.01	3.78	8.73	1.22	100.24	6.9	18.0	75.1
	GM_16_P lag_3_3	63.68	21.95	0.12	0.02	0.00	3.55	8.92	1.25	99.49	7.0	16.8	76.2
	GM_16_P lag_3_4	63.70	21.71	0.16	0.01	0.01	3.46	8.92	1.29	99.27	7.3	16.4	76.4
	GM_16_P lag_3_5	63.30	22.06	0.15	0.00	0.00	3.70	8.88	1.22	99.32	6.9	17.4	75.7
	GM_16_P lag_3_6	63.56	22.09	0.13	0.00	0.00	3.58	8.99	1.29	99.62	7.2	16.8	76.1
	GM_16_P lag_3_7	63.65	22.03	0.14	0.00	0.01	3.52	8.97	1.29	99.59	7.2	16.5	76.3
	GM_16_P lag_3_9	63.79	21.94	0.12	0.00	0.01	3.53	9.15	1.24	99.77	6.8	16.4	76.8
	GM_16_P lag_3_10	64.15	22.19	0.14	0.00	0.01	3.58	9.11	1.19	100.37	6.6	16.7	76.7
	GM_16_P lag_3_11	64.07	22.08	0.13	0.00	0.01	3.55	8.90	1.26	100.00	7.1	16.8	76.1
	GM_16_P lag_3_12	63.68	22.15	0.15	0.00	0.00	3.67	8.86	1.21	99.73	6.8	17.4	75.8
	GM_16_P lag_3_13	63.47	21.92	0.17	0.00	0.01	3.56	8.92	1.26	99.31	7.1	16.8	76.1
	GM_16_P lag_3_14	63.73	22.13	0.15	0.01	0.00	3.64	8.89	1.20	99.76	6.8	17.2	76.1
	GM_16_P lag_3_15	63.63	21.98	0.14	0.00	0.00	3.70	8.86	1.24	99.54	6.9	17.5	75.6
	GM_16_P lag_3_16	63.40	21.97	0.14	0.01	0.00	3.61	8.90	1.20	99.23	6.8	17.1	76.1
	GM_16_P lag_3_17	63.89	22.16	0.15	0.00	0.00	3.63	8.90	1.26	99.99	7.1	17.1	75.8
	GM_16_P lag_3_18	63.76	21.95	0.17	0.00	0.00	3.43	8.94	1.30	99.56	7.3	16.2	76.5
	GM_16_P lag_3_19	63.56	22.05	0.17	0.01	0.01	3.63	8.82	1.27	99.53	7.2	17.2	75.6
	GM_16_P lag_3_20	63.70	21.84	0.14	0.02	0.00	3.53	8.91	1.24	99.39	7.0	16.7	76.3
	GM_16_P lag_3_21	63.52	21.88	0.13	0.00	0.00	3.48	8.84	1.27	99.11	7.2	16.6	76.2
	GM_16_P lag_3_22	63.87	21.82	0.13	0.01	0.01	3.64	8.90	1.23	99.61	6.9	17.2	75.9
	GM_16_P lag_3_23	63.64	22.05	0.14	0.00	0.00	3.69	8.86	1.24	99.62	6.9	17.4	75.6
	GM_16_P lag_3_24	63.74	22.21	0.15	0.01	0.00	3.65	8.88	1.23	99.87	6.9	17.2	75.9
	GM_16_P lag_3_25	63.92	22.07	0.18	0.00	0.01	3.69	8.90	1.24	100.00	6.9	17.4	75.7
	GM_16_P lag_3_26	63.38	22.00	0.14	0.00	0.00	3.69	8.96	1.20	99.35	6.7	17.3	76.0
	GM_16_P lag_3_27	63.26	21.82	0.13	0.01	0.00	3.70	8.90	1.20	99.02	6.8	17.4	75.8
	GM_16_P lag_3_28	63.34	21.66	0.14	0.02	0.01	3.66	8.99	1.22	99.04	6.8	17.1	76.1
	GM_16_P lag_3_29	63.43	21.59	0.14	0.01	0.00	3.40	8.86	1.27	98.71	7.2	16.2	76.5
	GM_16_P lag_3_30	63.41	22.08	0.15	0.00	0.00	3.66	8.88	1.21	99.40	6.8	17.3	75.9
	GM_16_P lag_3_31	63.15	21.97	0.15	0.01	0.01	3.61	9.08	1.22	99.20	6.7	16.8	76.4
	Average	**63.67**	**21.95**	**0.14**	**0.00**	**0.00**	**3.58**	**8.92**	**1.21**	**99.48**	**6.8**	**16.9**	**76.3**
	Standard Deviation	**0.27**	**0.19**	**0.01**	**0.01**	**0.00**	**0.09**	**0.07**	**0.08**	**0.39**	**0.4**	**0.4**	**0.5**
GM-13 (YG)	GM_13_P lag_1_1	64.32	22.06	0.16	0.00	0.01	3.35	8.92	1.34	100.16	7.6	15.9	76.5

Plagioclase	GM_13_Plag_1_2	64.46	22.09	0.17	0.02	0.00	3.50	8.85	1.30	100.38	7.4	16.6	76.0
	GM_13_Plag_1_3	64.09	22.27	0.13	0.00	0.00	3.63	8.66	1.22	100.00	7.0	17.5	75.5
	GM_13_Plag_1_4	64.12	22.30	0.17	0.00	0.00	3.63	8.60	1.28	100.08	7.3	17.5	75.1
	GM_13_Plag_1_5	64.04	21.96	0.15	0.00	0.00	3.62	8.74	1.25	99.75	7.1	17.3	75.6
	GM_13_Plag_1_6	63.61	21.91	0.15	0.00	0.00	3.61	8.67	1.24	99.17	7.1	17.4	75.5
	GM_13_Plag_1_7	63.85	21.83	0.15	0.00	0.01	3.50	8.75	1.28	99.38	7.3	16.8	75.9
	GM_13_Plag_1_8	63.30	21.94	0.15	0.00	0.01	3.54	8.61	1.29	98.83	7.4	17.1	75.4
	GM_13_Plag_1_9	63.79	21.39	0.15	0.01	0.01	3.59	8.68	1.27	99.38	7.3	17.3	75.4
	GM_13_Plag_1_11	64.59	21.38	0.12	0.00	0.00	2.87	8.89	1.55	99.38	8.8	13.8	77.4
	GM_13_Plag_1_12	64.52	21.34	0.16	0.00	0.00	2.99	8.86	1.58	99.45	9.0	14.3	76.7
	GM_13_Plag_1_13	64.34	21.64	0.16	0.01	0.00	3.20	8.92	1.45	99.73	8.2	15.2	76.6
	GM_13_Plag_1_14	64.26	21.93	0.16	0.00	0.00	3.35	8.91	1.32	99.92	7.5	15.9	76.6
	GM_13_Plag_1_15	64.51	22.08	0.15	0.00	0.00	3.44	8.86	1.28	100.30	7.3	16.4	76.4
	GM_13_Plag_1_16	63.89	21.93	0.14	0.00	0.00	3.37	8.84	1.32	99.48	7.5	16.1	76.4
	GM_13_Plag_1_17	64.23	21.90	0.14	0.02	0.00	3.42	8.82	1.33	99.86	7.5	16.3	76.1
	GM_13_Plag_1_18	64.08	21.96	0.15	0.00	0.01	3.53	8.79	1.26	99.77	7.2	16.8	76.0
	GM_13_Plag_1_19	64.23	22.33	0.15	0.00	0.00	3.54	8.63	1.28	100.16	7.4	17.1	75.5
	GM_13_Plag_1_20	64.36	21.89	0.15	0.00	0.01	3.33	8.91	1.34	99.98	7.6	15.8	76.6
	GM_13_Plag_1_21	64.33	22.23	0.15	0.01	0.00	3.48	8.79	1.34	100.33	7.6	16.6	75.8
	GM_13_Plag_1_22	64.75	21.96	0.15	0.01	0.00	3.31	9.03	1.34	100.55	7.5	15.6	76.9
	GM_13_Plag_1_23	64.22	21.94	0.17	0.00	0.01	3.43	8.83	1.31	99.90	7.4	16.4	76.2
	GM_13_Plag_1_24	64.21	21.98	0.13	0.01	0.01	3.47	8.75	1.28	99.83	7.3	16.7	76.0
	GM_13_Plag_1_25	64.23	21.75	0.12	0.02	0.00	3.30	8.84	1.38	99.61	7.8	15.8	76.4
	GM_13_Plag_1_26	63.93	21.89	0.15	0.01	0.00	3.53	8.69	1.32	99.51	7.5	17.0	75.5
	GM_13_Plag_1_27	64.22	21.95	0.13	0.01	0.01	3.44	8.76	1.32	99.83	7.6	16.5	76.0
	GM_13_Plag_1_28	64.87	21.79	0.13	0.00	0.01	3.28	9.04	1.38	100.48	7.7	15.4	76.9
	GM_13_Plag_1_29	64.57	21.77	0.12	0.00	0.00	3.21	8.93	1.41	100.00	8.0	15.2	76.8
	GM_13_Plag_1_30	64.51	21.64	0.13	0.00	0.00	3.08	8.81	1.45	99.61	8.3	14.8	76.8
	GM_13_Plag_1_31	63.95	21.73	0.11	0.00	0.01	3.33	8.70	1.37	99.20	7.9	16.1	76.0
	GM_13_Plag_1_32	64.44	22.06	0.13	0.01	0.00	3.40	8.94	1.33	100.31	7.5	16.1	76.4
	GM_13_Plag_1_33	64.67	21.90	0.12	0.00	0.00	3.46	9.10	1.31	100.56	7.2	16.1	76.6
	GM_13_Plag_1_34	64.62	22.28	0.14	0.01	0.00	3.50	9.01	1.27	100.83	7.1	16.4	76.5
	GM_13_Plag_1_35	63.96	22.13	0.16	0.00	0.01	3.64	8.79	0.95	99.64	5.5	17.6	76.9
	GM_13_Plag_1_36	63.61	22.14	0.17	0.00	0.01	3.74	8.64	1.16	99.46	6.6	18.0	75.3
	GM_13_Plag_1_37	64.29	22.15	0.14	0.01	0.01	3.59	8.75	1.27	100.20	7.2	17.1	75.6

GM_13_P lag_1_38	64.08	21.84	0.14	0.00	0.00	3.34	8.74	1.32	99.46	7.6	16.1	76.3
GM_13_P lag_1_39	64.49	22.08	0.13	0.00	0.00	3.39	8.91	1.31	100.29	7.4	16.1	76.5
GM_13_P lag_1_40	65.12	21.73	0.14	0.00	0.00	2.96	8.96	1.50	100.41	8.5	14.1	77.4
GM_13_P lag_1_41	64.55	22.09	0.16	0.00	0.01	3.45	8.80	1.32	100.37	7.5	16.5	76.0
GM_13_P lag_1_42	64.20	22.01	0.16	0.01	0.00	3.31	8.90	1.35	99.93	7.7	15.7	76.6
GM_13_P lag_1_43	64.79	22.17	0.13	0.00	0.00	3.39	8.86	1.36	100.70	7.7	16.1	76.2
GM_13_P lag_1_44	64.60	21.95	0.15	0.02	0.01	3.34	8.91	1.32	100.29	7.5	15.9	76.7
GM_13_P lag_1_45	63.90	22.05	0.17	0.02	0.00	3.58	8.74	1.26	99.70	7.2	17.2	75.7
GM_13_P lag_1_46	63.60	21.90	0.13	0.00	0.00	3.60	8.55	1.28	99.07	7.4	17.5	75.1
GM_13_P lag_1_47	64.65	21.73	0.16	0.00	0.01	3.07	8.91	1.45	99.97	8.3	14.7	77.1
GM_13_P lag_1_48	64.46	22.03	0.14	0.00	0.00	3.41	8.95	1.35	100.34	7.6	16.1	76.3
GM_13_P lag_1_49	63.83	21.55	0.17	0.00	0.01	3.23	8.81	1.45	99.05	8.3	15.5	76.3
GM_13_P lag_1_50	64.29	21.88	0.13	0.00	0.01	3.37	8.88	1.34	99.91	7.6	16.0	76.4
GM_13_P lag_2_1	64.53	21.65	0.13	0.00	0.00	3.00	8.90	1.55	99.76	8.8	14.3	76.9
GM_13_P lag_2_2	64.62	21.78	0.15	0.00	0.01	3.21	8.90	1.43	100.09	8.1	15.3	76.6
GM_13_P lag_2_3	64.21	21.88	0.15	0.00	0.00	3.39	8.85	1.37	99.81	7.7	16.1	76.2
GM_13_P lag_2_4	63.69	21.53	0.14	0.00	0.00	3.37	8.91	1.30	98.93	7.3	16.0	76.6
GM_13_P lag_2_5	64.04	21.41	0.14	0.02	0.00	3.17	8.88	1.40	99.05	8.0	15.2	76.8
GM_13_P lag_2_7	64.44	21.54	0.12	0.00	0.00	3.01	8.95	1.46	99.50	8.3	14.4	77.3
GM_13_P lag_2_8	64.23	21.52	0.15	0.00	0.00	3.07	8.94	1.45	99.34	8.2	14.6	77.1
GM_13_P lag_2_9	64.70	21.62	0.15	0.01	0.00	3.10	8.88	1.42	99.87	8.1	14.9	77.0
GM_13_P lag_2_10	64.55	21.52	0.13	0.00	0.00	3.03	8.85	1.52	99.59	8.7	14.5	76.8
GM_13_P lag_2_11	63.98	21.54	0.14	0.00	0.00	3.32	8.96	1.24	99.18	7.0	15.8	77.2
GM_13_P lag_2_12	65.09	21.24	0.16	0.00	0.00	3.01	8.73	1.64	99.88	9.4	14.5	76.1
GM_13_P lag_2_13	64.68	21.66	0.14	0.00	0.00	3.02	8.99	1.57	100.05	8.9	14.3	76.9
GM_13_P lag_2_14	64.25	21.25	0.16	0.00	0.01	3.02	8.96	1.53	99.17	8.7	14.3	77.0
GM_13_P lag_2_15	64.12	21.88	0.16	0.00	0.00	3.33	9.13	1.07	99.68	6.0	15.8	78.2
GM_13_P lag_2_16	64.39	21.34	0.14	0.00	0.00	3.05	8.94	1.48	99.33	8.4	14.5	77.1
GM_13_P lag_2_17	64.40	21.30	0.16	0.00	0.00	2.99	8.98	1.44	99.27	8.2	14.3	77.5
GM_13_P lag_2_18	64.06	21.80	0.16	0.00	0.00	3.11	8.78	1.38	99.28	8.0	15.1	77.0
GM_13_P lag_2_19	64.52	21.58	0.13	0.00	0.00	3.31	8.88	1.43	99.83	8.1	15.7	76.2
GM_13_P lag_2_20	64.03	21.73	0.14	0.00	0.00	3.31	8.87	1.36	99.41	7.7	15.8	76.5
GM_13_P lag_2_21	64.25	21.94	0.14	0.00	0.00	3.33	8.94	1.36	99.96	7.7	15.7	76.6
GM_13_P lag_2_22	63.99	21.74	0.14	0.01	0.01	3.40	8.85	1.33	99.47	7.5	16.2	76.3
GM_13_P lag_2_23	63.81	21.89	0.16	0.00	0.00	3.43	8.94	1.26	99.46	7.1	16.2	76.6

	GM_13_Plag_2_24	64.31		21.57	0.15	0.00	0.00	3.27	8.92	1.34	99.55	7.6	15.6	76.8
	GM_13_Plag_2_25	63.85		21.70	0.13	0.00	0.00	3.29	8.96	1.38	99.30	7.8	15.5	76.7
	GM_13_Plag_3_1	63.97		22.12	0.13	0.00	0.00	3.56	8.95	1.28	100.00	7.2	16.7	76.1
	GM_13_Plag_3_2	64.00		22.30	0.12	0.00	0.01	3.73	8.92	1.18	100.23	6.6	17.5	75.9
	GM_13_Plag_3_3	64.09		22.13	0.13	0.00	0.00	3.66	8.77	1.29	100.07	7.3	17.4	75.3
	GM_13_Plag_3_4	64.13		21.89	0.12	0.00	0.00	3.44	8.92	1.44	99.94	8.0	16.1	75.8
	GM_13_Plag_3_5	64.29		21.89	0.16	0.00	0.00	3.33	8.98	1.51	100.15	8.4	15.6	76.0
	GM_13_Plag_3_6	64.19		21.90	0.14	0.00	0.00	3.37	8.90	1.42	99.91	8.0	15.9	76.1
	GM_13_Plag_3_7	64.11		21.85	0.16	0.00	0.01	3.56	8.93	1.31	99.92	7.3	16.7	76.0
	GM_13_Plag_3_8	63.65		22.04	0.15	0.01	0.01	3.57	8.88	1.33	99.64	7.5	16.8	75.7
	GM_13_Plag_3_9	64.67		21.75	0.14	0.01	0.01	3.11	9.01	1.61	100.31	9.0	14.6	76.4
	GM_13_Plag_3_10	63.79		21.88	0.17	0.00	0.00	3.09	8.89	1.48	99.28	8.4	14.7	76.8
	GM_13_Plag_3_11	63.92		22.02	0.15	0.00	0.00	3.52	8.88	1.36	99.84	7.6	16.6	75.8
	GM_13_Plag_3_12	64.54		21.90	0.13	0.00	0.01	3.19	9.02	1.46	100.24	8.2	15.0	76.8
	GM_13_Plag_3_13	64.09		22.02	0.14	0.00	0.00	3.44	8.94	1.38	100.01	7.7	16.2	76.1
	GM_13_Plag_3_14	64.56		21.85	0.14	0.01	0.01	3.29	8.98	1.47	100.30	8.2	15.4	76.3
	GM_13_Plag_3_15	63.93		21.71	0.17	0.01	0.00	3.44	8.89	1.36	99.49	7.7	16.3	76.1
	GM_13_Plag_3_16	64.02		22.02	0.21	0.00	0.00	3.54	8.91	1.31	100.02	7.4	16.7	75.9
	GM_13_Plag_3_17	63.88		21.65	0.12	0.02	0.00	3.33	8.88	1.38	99.27	7.8	15.8	76.4
	GM_13_Plag_3_18	63.82		21.80	0.15	0.00	0.00	3.41	8.91	1.38	99.47	7.8	16.1	76.1
	GM_13_Plag_3_20	64.23		21.46	0.15	0.01	0.01	3.17	9.05	1.45	99.53	8.1	14.9	77.0
	GM_13_Plag_3_22	64.01		21.58	0.14	0.01	0.00	3.33	8.98	1.38	99.42	7.7	15.7	76.6
	GM_13_Plag_3_23	64.13		21.73	0.13	0.00	0.00	3.34	9.00	1.39	99.72	7.8	15.7	76.5
	GM_13_Plag_3_24	64.10		21.95	0.13	0.00	0.00	3.41	8.88	1.34	99.80	7.6	16.2	76.2
	GM_13_Plag_3_25	64.03		21.97	0.14	0.00	0.00	3.44	8.95	1.38	99.90	7.7	16.2	76.1
	GM_13_Plag_3_26	64.19		21.99	0.16	0.00	0.00	3.46	9.03	1.38	100.20	7.6	16.1	76.2
	GM_13_Plag_3_27	63.85		21.91	0.11	0.02	0.00	3.43	8.97	1.37	99.66	7.7	16.1	76.2
	GM_13_Plag_3_28	64.33		22.42	0.13	0.01	0.00	3.52	8.90	1.34	100.64	7.5	16.6	75.9
	GM_13_Plag_3_29	64.00		22.10	0.14	0.01	0.00	3.62	8.84	1.32	100.02	7.4	17.1	75.5
	Average	**64.22**		**21.85**	**0.14**	**0.00**	**0.00**	**3.35**	**8.87**	**1.36**	**99.80**	**7.7**	**16.0**	**76.3**
	Standard Deviation	**0.33**		**0.25**	**0.02**	**0.01**	**0.00**	**0.19**	**0.11**	**0.10**	**0.43**	**0.6**	**0.9**	**0.6**
GM-10(YO)	GM-10-2 Plag 3-1	64.62	0.00	21.51	0.13	0.00	0.00	3.07	8.89	1.35	99.56	7.7	14.8	77.5

Plagioclase	GM-10-2 Plag 3-2	65.32	0.00	21.34	0.12	0.00	0.00	2.56	9.07	1.57	100.00	9.0	12.3	78.7
	GM-10-2 Plag 3-3	64.32	0.00	21.59	0.13	0.00	0.00	3.11	8.87	1.34	99.34	7.7	15.0	77.3
	GM-10-2 Plag 3-4	64.40	0.00	21.47	0.15	0.01	0.00	3.00	8.80	1.47	99.30	8.4	14.5	77.0
	GM-10-2 Plag 5-1	64.42	0.00	21.61	0.14	0.00	0.00	2.99	8.97	1.36	99.49	7.8	14.4	77.8
	GM-10-2 Plag 5-2	65.01	0.00	21.75	0.14	0.00	0.00	3.00	8.99	1.37	100.23	7.8	14.3	77.9
	GM-10-2 Plag 5-3	64.46	0.01	21.74	0.17	0.00	0.00	3.07	8.92	1.34	99.71	7.7	14.8	77.6
	GM-10_Feld_1-1	64.80	0.00	22.13	0.14	0.00	0.00	3.49	8.90	1.37	100.81	7.7	16.4	75.9
	GM-10_Feld_1-2	65.70	0.00	21.65	0.14	0.00	0.00	3.02	8.93	1.46	100.89	8.3	14.4	77.2
	GM-10_Feld_3-1	65.47	0.00	22.01	0.12	0.00	0.00	3.15	8.92	1.37	101.02	7.8	15.1	77.1
	GM-10_Feld_3-2	65.63	0.00	21.77	0.11	0.00	0.00	3.07	9.12	1.45	101.15	8.1	14.4	77.5
	GM-10_Feld_3-4	65.38	0.00	22.03	0.14	0.01	0.00	3.25	8.86	1.38	101.03	7.8	15.5	76.6
	GM-10_Feld_4-1	65.28	0.00	21.97	0.15	0.02	0.00	3.12	9.08	1.38	101.01	7.8	14.7	77.5
	GM-10_Feld_4-2	65.08	0.00	21.80	0.13	0.01	0.01	3.01	8.91	1.47	100.42	8.4	14.4	77.2
	GM-10_Feld_4-3	65.37	0.00	22.01	0.16	0.00	0.00	3.21	8.98	1.32	101.05	7.4	15.3	77.3
	GM-10_Feld_5-1	65.03	0.00	22.02	0.13	0.00	0.00	3.24	8.94	1.28	100.62	7.3	15.5	77.3
	GM-10_Feld_5-2	65.05	0.01	22.27	0.18	0.00	0.00	3.40	8.97	1.37	101.25	7.7	16.0	76.3
	GM-10_Feld_5-3	65.64	0.00	21.65	0.11	0.00	0.02	2.97	9.09	1.42	100.89	8.0	14.1	77.9
	GM-10_Feld_5-4	64.99	0.00	21.58	0.13	0.00	0.00	3.00	9.03	1.41	100.13	8.0	14.3	77.8
	GM-10_Feld_7-1	65.92	0.00	21.62	0.15	0.00	0.00	2.85	9.02	1.54	101.08	8.7	13.6	77.7
	GM-10_Feld_7-2	65.19	0.00	21.86	0.18	0.00	0.00	3.13	8.93	1.34	100.61	7.6	15.0	77.4
	GM-10_Feld_7-3	65.57	0.00	22.19	0.13	0.00	0.00	3.25	8.96	1.28	101.36	7.2	15.5	77.3
	GM-10_Feld_7-4	65.85	0.01	21.58	0.13	0.01	0.00	2.96	9.04	1.52	101.10	8.6	14.0	77.4
	GM-10_Feld_10-1	65.56	0.00	21.89	0.13	0.01	0.01	2.98	9.08	1.40	101.05	7.9	14.1	77.9
	GM-10_Feld_10-2	65.46	0.00	21.46	0.13	0.00	0.00	2.96	8.97	1.43	100.42	8.2	14.2	77.7
	GM-10_Feld_10-3	65.36	0.00	21.77	0.15	0.00	0.00	3.21	8.98	1.37	100.82	7.7	15.2	77.0

	GM-10_Feld_10-4	65.43	0.00	21.72	0.12	0.02	0.00	3.00	8.94	1.46	100.68	8.3	14.3	77.3
	GM-10_Feld_20-2	65.48	0.01	21.59	0.14	0.00	0.00	3.14	9.08	1.37	100.81	7.7	14.8	77.5
	GM-10_Feld_20-3	65.46	0.00	21.76	0.13	0.01	0.00	2.91	9.22	1.47	100.94	8.2	13.6	78.2
	GM-10_Feld_21-1	65.53	0.00	21.86	0.09	0.00	0.01	2.90	9.00	1.46	100.85	8.3	13.9	77.9
	GM-10_Feld_21-2	66.17	0.00	21.81	0.15	0.00	0.00	2.93	8.99	1.40	101.43	8.0	14.0	77.9
	GM-10_Feld_21-3	65.65	0.01	21.78	0.12	0.00	0.00	2.72	8.99	1.48	100.73	8.5	13.1	78.4
	GM-10_Feld_22-1	64.90	0.00	22.13	0.11	0.03	0.00	2.88	8.76	1.49	100.29	8.7	14.1	77.3
	GM-10_Feld_22-2	65.40	0.00	21.96	0.13	0.00	0.00	3.23	9.02	1.33	101.06	7.5	15.3	77.2
	GM-10_Feld_22-3	65.31	0.02	22.24	0.13	0.01	0.01	2.95	8.83	1.44	100.93	8.3	14.3	77.4
	GM-10_Feld_23-2	65.09	0.00	22.30	0.13	0.01	0.00	3.19	8.89	1.37	100.98	7.8	15.3	76.9
	GM-10_Feld_23-3	66.35	0.01	21.26	0.13	0.01	0.00	2.47	9.19	1.48	100.89	8.5	11.9	79.7
	GM-10_Feld_28-1	65.53	0.01	21.90	0.14	0.00	0.00	3.13	9.07	1.43	101.19	8.0	14.7	77.3
	GM-10_Feld_28-2	65.30	0.00	21.58	0.10	0.00	0.00	3.01	9.01	1.36	100.35	7.8	14.4	77.9
	GM-10_Feld_28-3	64.90	0.00	21.84	0.11	0.01	0.01	3.18	8.99	1.35	100.37	7.6	15.1	77.3
	GM-10_Feld_30-1	65.87	0.01	21.41	0.13	0.00	0.00	2.65	9.21	1.58	100.86	8.9	12.5	78.6
	GM-10_Feld_30-2	65.35	0.00	21.55	0.13	0.00	0.00	2.88	9.18	1.38	100.47	7.7	13.6	78.6
	GM-10_Feld_30-3	65.82	0.01	21.65	0.14	0.00	0.01	2.78	9.19	1.55	101.14	8.7	13.1	78.2
	Average	**65.31**	**0.00**	**21.78**	**0.13**	**0.00**	**0.00**	**3.02**	**9.00**	**1.41**	**100.66**	**8.0**	**14.4**	**77.6**
	Standard Deviation	**0.46**	**0.00**	**0.25**	**0.02**	**0.01**	**0.00**	**0.20**	**0.11**	**0.07**	**0.54**	**0.4**	**0.9**	**0.7**
GM-09(YO) Plagioclase	GM-09-1 Plag 1-1	64.50	0.00	21.66	0.11	0.01	0.01	3.08	8.92	1.29	99.59	7.4	14.8	77.8
	GM-09-1 Plag 1-2	65.09	0.02	21.79	0.12	0.00	0.00	3.04	8.95	1.39	100.39	7.9	14.6	77.5
	GM-09-1 Plag 1-3	64.85	0.01	21.93	0.14	0.00	0.00	3.27	8.89	1.28	100.36	7.3	15.6	77.0
	GM-09-1 Plag 1-4	65.22	0.00	21.51	0.12	0.00	0.00	2.90	9.07	1.49	100.31	8.4	13.7	77.9

GM-09-1 Plag 4-1	64.95	0.01	21.75	0.13	0.00	0.00	3.01	8.94	1.43	100.22	8.1	14.4	77.4
GM-09-1 Plag 4-2	65.08	0.00	21.66	0.14	0.00	0.00	3.01	9.02	1.45	100.33	8.2	14.3	77.5
GM-09-1 Plag 4-3	65.01	0.00	21.61	0.17	0.00	0.01	3.06	8.98	1.35	100.17	7.7	14.6	77.7
GM-09-1 Plag 5-1	64.78	0.01	21.70	0.15	0.00	0.00	3.08	8.92	1.42	100.04	8.1	14.7	77.2
GM-09-1 Plag 5-2	65.05	0.00	21.81	0.12	0.01	0.00	3.02	9.09	1.40	100.50	7.9	14.3	77.8
GM-09-1 Plag 5-3	64.84	0.00	21.90	0.13	0.00	0.01	3.15	9.02	1.48	100.52	8.3	14.8	76.9
GM-09-1 Plag 5-4	64.96	0.00	21.44	0.13	0.00	0.00	2.98	9.07	1.48	100.04	8.3	14.1	77.6
GM-09-1 Plag 6-1	64.60	0.00	21.88	0.14	0.00	0.00	3.27	8.92	1.37	100.16	7.7	15.5	76.7
GM-09-1 Plag 6-2	64.58	0.00	21.96	0.14	0.02	0.00	3.21	8.93	1.30	100.13	7.4	15.4	77.2
GM-09-1 Plag 6-3	64.77	0.00	21.65	0.14	0.00	0.00	2.91	9.01	1.50	99.96	8.5	13.9	77.6
GM-09-1 Plag 6-4	65.31	0.00	21.43	0.13	0.02	0.00	2.77	9.06	1.45	100.16	8.3	13.2	78.5
GM-09-1 Plag 6-5	65.03	0.00	21.79	0.15	0.01	0.00	3.02	9.07	1.41	100.47	7.9	14.3	77.8
GM-09-1 Plag 6-6	64.89	0.01	21.75	0.13	0.00	0.00	3.21	8.96	1.41	100.36	7.9	15.2	76.8
GM-09-1 Plag 7-1	65.09	0.00	21.57	0.14	0.01	0.00	2.95	9.05	1.46	100.26	8.3	14.0	77.8
GM-09-1 Plag 7-2	64.84	0.00	21.66	0.15	0.01	0.00	3.04	9.07	1.40	100.18	7.9	14.4	77.7
GM-09-1 Plag 7-3	64.65	0.01	21.74	0.13	0.00	0.01	2.98	9.10	1.40	100.01	7.9	14.1	78.0
GM-09-1 Plag 7-4	64.39	0.00	21.77	0.17	0.01	0.01	3.11	9.02	1.34	99.81	7.6	14.8	77.6
GM-09-1 Plag 7-5	65.03	0.00	21.57	0.15	0.00	0.00	2.97	9.01	1.46	100.19	8.3	14.1	77.6
GM-09-1 Plag 9-1	65.07	0.00	22.15	0.13	0.00	0.00	3.25	9.01	1.34	100.95	7.6	15.3	77.1
GM-09-1 Plag 9-2	64.83	0.00	21.89	0.15	0.00	0.00	3.17	8.98	1.27	100.30	7.2	15.1	77.6
GM-09-1 Plag 9-3	64.41	0.00	22.02	0.15	0.00	0.00	3.34	8.97	1.23	100.13	7.0	15.9	77.1
GM-09-1 Plag 9-4	64.72	0.01	22.10	0.12	0.02	0.00	3.25	8.91	1.32	100.45	7.5	15.5	77.0
GM-09-1 Plag 10-1	65.36	0.00	21.84	0.11	0.00	0.00	3.26	8.96	1.34	100.84	7.6	15.5	77.0
GM-09-1 Plag 10-2	65.16	0.00	22.15	0.12	0.00	0.00	3.27	9.04	1.34	101.06	7.5	15.4	77.1
GM-09-1 Plag 10-3	65.29	0.01	21.93	0.12	0.01	0.00	3.18	8.93	1.37	100.82	7.8	15.2	77.0
GM-09-1 Plag 10-4	65.26	0.00	21.73	0.12	0.00	0.02	3.13	9.03	1.37	100.64	7.7	14.8	77.4
GM-09-1 Plag 11-1	64.90	0.00	22.05	0.15	0.00	0.01	3.27	8.95	1.38	100.71	7.8	15.5	76.7
GM-09-1 Plag 11-2	65.01	0.00	21.91	0.15	0.00	0.00	3.17	9.03	1.37	100.64	7.7	15.0	77.3
GM-09-1 Plag 11-3	64.97	0.00	21.66	0.13	0.00	0.01	3.23	9.07	1.37	100.42	7.7	15.2	77.1
GM-09-1 Plag 11-4	65.01	0.01	21.92	0.13	0.00	0.00	3.21	8.96	1.34	100.56	7.6	15.3	77.1
GM-09-1 Plag 11-5	64.64	0.00	22.03	0.13	0.00	0.00	3.37	9.01	1.20	100.36	6.8	16.0	77.2
GM-09-1 Plag 11-6	64.73	0.01	21.91	0.16	0.00	0.00	3.31	9.00	1.28	100.40	7.2	15.7	77.1
GM-09-1 Plag 11-7	64.42	0.01	22.00	0.16	0.01	0.00	3.31	8.96	1.28	100.16	7.2	15.7	77.1
GM-09-1 Plag 12-1	64.54	0.00	21.63	0.14	0.00	0.00	3.04	9.07	1.36	99.76	7.7	14.4	77.9
GM-09-1 Plag 12-2	65.17	0.01	21.80	0.14	0.00	0.01	3.12	9.09	1.34	100.68	7.5	14.7	77.7

GM-09-1 Plag 12-3	64.83	0.00	21.84	0.13	0.01	0.00	3.10	8.94	1.37	100.21	7.8	14.8	77.3
GM-09-1 Plag 12-4	64.77	0.00	21.85	0.14	0.01	0.00	3.19	9.08	1.36	100.42	7.6	15.0	77.3
GM-09-1 Plag 12-5	64.33	0.00	21.62	0.12	0.01	0.00	3.22	9.01	1.34	99.66	7.5	15.3	77.2
GM-09-1 Plag 12-6	64.27	0.00	21.60	0.13	0.00	0.01	3.43	8.90	1.27	99.59	7.2	16.3	76.5
GM-09-1 Plag13-1	64.90	0.01	21.70	0.14	0.00	0.00	3.11	9.00	1.34	100.17	7.6	14.8	77.6
GM-09-1 Plag13-2	64.55	0.01	21.69	0.14	0.00	0.00	3.05	8.98	1.39	99.79	7.9	14.5	77.6
GM-09-1 Plag13-3	65.14	0.01	21.53	0.11	0.00	0.00	2.94	9.04	1.48	100.25	8.4	14.0	77.7
GM-09-1 Plag13-4	64.95	0.00	21.95	0.15	0.01	0.00	3.16	9.04	1.29	100.55	7.3	15.0	77.7
GM-09-1 Plag13-5	65.09	0.00	21.68	0.11	0.00	0.00	3.03	9.06	1.41	100.38	8.0	14.4	77.7
GM-09-1 Plag13-6	64.79	0.01	21.69	0.14	0.00	0.00	3.19	8.97	1.31	100.08	7.5	15.2	77.3
Average	**64.87**	**0.00**	**21.78**	**0.13**	**0.00**	**0.00**	**3.13**	**9.00**	**1.37**	**100.29**	**7.7**	**14.9**	**77.4**
Standard Deviation	**0.27**	**0.00**	**0.18**	**0.01**	**0.01**	**0.00**	**0.14**	**0.06**	**0.07**	**0.33**	**0.4**	**0.6**	**0.4**

Table B-0-11 Natural individual sanidine analyses (wt%)

Sample	Point	SiO_2	TiO_2	Al_2O_3	FeO	MnO	MgO	CaO	Na_2O	K_2O	Total	Or#(XOr*100)	An#(XAn*100)	Ab#(XAb*100)
GM-18 (OB) Sanidine	GM-18_Feld_1-1	66.78	0.00	18.74	0.09	0.00	0.00	0.14	4.51	10.93	101.15	61.0	0.7	38.3
	GM-18_Feld_1-3	66.50	0.00	18.81	0.09	0.01	0.00	0.14	4.45	11.09	101.08	61.7	0.7	37.7
	GM-18_Feld_7-1	66.74	0.00	18.65	0.08	0.00	0.00	0.15	4.59	10.94	101.12	60.6	0.7	38.7
	GM-18_Feld_7-2	66.74	0.00	18.83	0.08	0.00	0.00	0.17	4.55	11.06	101.41	61.0	0.8	38.2
	GM-18_Feld_7-3	66.88	0.00	18.77	0.08	0.00	0.00	0.16	4.56	10.71	101.14	60.3	0.7	39.0
	GM-18_Feld_9-1	66.84	0.00	18.89	0.09	0.02	0.01	0.19	4.73	10.61	101.36	59.1	0.9	40.0
	GM-18_Feld_9-2	66.76	0.00	18.86	0.06	0.00	0.00	0.18	4.52	10.93	101.28	60.9	0.8	38.3
	GM-18_Feld_9-3	66.50	0.00	18.77	0.08	0.00	0.00	0.17	4.64	10.89	101.05	60.2	0.8	39.0
	GM-18_Feld_12-1	66.84	0.00	18.93	0.07	0.00	0.00	0.14	4.70	10.79	101.45	59.8	0.7	39.5
	GM-18_Feld_12-2	66.49	0.01	18.84	0.09	0.00	0.00	0.18	4.57	10.79	100.96	60.3	0.9	38.8
	GM-18_Feld_12-3	66.73	0.00	18.90	0.07	0.00	0.00	0.19	4.68	10.81	101.38	59.8	0.9	39.4
	GM-18_Feld_15-2	66.96	0.00	18.83	0.09	0.00	0.00	0.18	4.58	10.86	101.47	60.5	0.8	38.7
	GM-18_Feld_16-1	66.61	0.01	18.54	0.09	0.00	0.00	0.17	4.48	10.83	100.72	60.9	0.8	38.3
	GM-18_Feld_16-2	66.74	0.01	18.70	0.08	0.00	0.00	0.17	4.53	10.95	101.15	61.0	0.8	38.3
	GM-18_Feld_16-3	66.84	0.01	18.76	0.10	0.00	0.00	0.16	4.50	10.99	101.36	61.2	0.7	38.0
	GM-18_Feld_16-4	66.50	0.00	18.65	0.10	0.01	0.00	0.15	4.52	11.00	100.92	61.1	0.7	38.2
	GM-18_Feld_20-1	66.56	0.00	18.73	0.10	0.01	0.00	0.14	4.62	10.98	101.12	60.6	0.7	38.8
	GM-18_Feld_20-2	66.52	0.01	18.80	0.09	0.02	0.00	0.14	4.74	10.58	100.89	59.1	0.6	40.3
	GM-18_Feld_20-3	66.58	0.00	18.66	0.10	0.00	0.00	0.16	4.75	10.54	100.78	58.9	0.8	40.4
	GM-18_Feld_23-2	66.68	0.00	18.94	0.09	0.00	0.00	0.16	4.58	10.99	101.41	60.8	0.7	38.5
	GM-18_Feld_23-3	66.69	0.00	18.91	0.08	0.02	0.00	0.15	4.61	10.95	101.41	60.5	0.7	38.8

	GM-18_Feld_26-1	66.64	0.01	18.78	0.11	0.00	0.00	0.16	4.61	10.71	101.03	60.0	0.8	39.3
	GM-18_Feld_26-3	66.75	0.00	18.88	0.09	0.00	0.00	0.17	4.60	10.81	101.30	60.3	0.8	38.9
	GM-18_Feld_30-4 - middle	66.62	0.01	18.91	0.11	0.00	0.00	0.18	4.68	10.66	101.16	59.5	0.8	39.7
	GM-18_Feld_30-4 - middle	66.46	0.00	18.68	0.12	0.00	0.00	0.16	4.58	10.97	100.97	60.7	0.8	38.5
	Average	**66.68**	**0.00**	**18.79**	**0.09**	**0.00**	**0.00**	**0.16**	**4.60**	**10.86**	**101.16**	**60.4**	**0.8**	**38.9**
	Standard Deviation	**0.14**	**0.00**	**0.10**	**0.01**	**0.01**	**0.00**	**0.02**	**0.08**	**0.15**	**0.22**	**0.72**	**0.1**	**0.7**
GM-01 (OC) Sanidine	GM-01_Feld_1-1	66.58	0.00	18.77	0.09	0.02	0.00	0.20	4.94	10.13	100.71	56.9	0.9	42.2
	GM-01_Feld_1-2	65.95	0.00	18.70	0.09	0.00	0.00	0.16	4.93	10.28	100.07	57.4	0.8	41.8
	GM-01_Feld_1-3	66.65	0.01	18.85	0.10	0.00	0.00	0.14	4.96	10.27	100.94	57.3	0.6	42.1
	GM-01_Feld_1-4	66.64	0.01	18.86	0.11	0.00	0.00	0.16	5.04	10.32	101.12	57.0	0.7	42.3
	GM-01_Feld_2-1	66.76	0.00	18.99	0.10	0.00	0.00	0.20	5.26	9.81	101.11	54.6	0.9	44.5
	GM-01_Feld_2-2	66.32	0.00	19.05	0.10	0.00	0.00	0.19	5.13	10.06	100.83	55.9	0.9	43.3
	GM-01_Feld_2-3	66.83	0.00	18.96	0.11	0.01	0.00	0.12	4.92	10.36	101.29	57.8	0.6	41.7
	GM-01_Feld_2-4	66.31	0.01	18.67	0.09	0.00	0.00	0.20	5.29	9.83	100.40	54.5	0.9	44.5
	GM-01_Feld_2-5	66.07	0.00	18.70	0.08	0.00	0.00	0.22	4.91	10.04	100.00	56.7	1.0	42.2
	GM-01_Feld_3-1	66.08	0.00	18.66	0.09	0.00	0.00	0.17	4.91	10.21	100.09	57.3	0.8	41.9
	GM-01_Feld_3-2	66.74	0.00	18.89	0.07	0.01	0.00	0.14	4.96	10.36	101.17	57.5	0.6	41.8
	GM-01_Feld_3-3	66.49	0.00	18.90	0.08	0.00	0.00	0.17	4.93	10.19	100.77	57.2	0.8	42.0
	GM-01_Feld_3-4	66.53	0.00	18.81	0.10	0.00	0.00	0.16	5.06	10.18	100.83	56.6	0.7	42.7
	GM-01_Feld_4-1	66.52	0.00	18.85	0.14	0.01	0.00	0.18	5.09	10.14	100.90	56.3	0.8	42.9
	GM-01_Feld_4-2	66.82	0.00	19.00	0.09	0.00	0.00	0.18	5.12	10.05	101.25	55.9	0.8	43.3

GM-01_Feld_4-3	66.49	0.00	18.62	0.08	0.00	0.00	0.18	4.95	10.17	100.46	57.0	0.8	42.2
GM-01_Feld_5-1	66.34	0.00	18.85	0.09	0.00	0.00	0.15	4.98	10.16	100.55	56.9	0.7	42.4
GM-01_Feld_5-2	65.73	0.01	18.88	0.09	0.00	0.00	0.15	4.96	9.99	99.82	56.6	0.7	42.7
GM-01_Feld_5-3	65.81	0.00	18.60	0.08	0.00	0.00	0.20	5.02	10.07	99.77	56.4	1.0	42.7
GM-01_Feld_5-4	66.54	0.00	18.65	0.08	0.00	0.00	0.18	4.99	10.03	100.46	56.4	0.9	42.7
GM-01_Feld_6-3	66.77	0.00	18.92	0.10	0.00	0.01	0.17	5.05	10.06	101.06	56.3	0.8	42.9
GM-01_Feld_7-1	66.43	0.00	18.89	0.10	0.02	0.00	0.19	5.22	9.99	100.84	55.2	0.9	43.9
GM-01_Feld_7-2	66.63	0.01	18.98	0.10	0.01	0.00	0.18	5.20	10.09	101.20	55.6	0.8	43.6
GM-01_Feld_7-3	65.92	0.00	19.13	0.11	0.00	0.00	0.18	5.14	9.96	100.42	55.6	0.8	43.6
GM-01_Feld_10-1	66.05	0.00	18.95	0.08	0.00	0.00	0.16	4.92	10.36	100.49	57.7	0.8	41.6
GM-01_Feld_10-2	66.24	0.01	18.84	0.11	0.00	0.00	0.18	4.97	10.34	100.67	57.3	0.8	41.9
GM-01_Feld_10-3	66.54	0.00	18.77	0.09	0.01	0.00	0.16	4.88	10.31	100.76	57.7	0.7	41.5
GM-01_Feld_10-4	66.32	0.00	18.56	0.10	0.02	0.00	0.18	4.93	10.22	100.30	57.2	0.8	41.9
GM-01_Feld_11-1	66.32	0.00	18.51	0.09	0.00	0.00	0.15	4.97	10.26	100.29	57.2	0.7	42.1
GM-01_Feld_11-2	66.81	0.00	18.82	0.12	0.02	0.00	0.19	4.91	10.17	101.04	57.1	0.9	41.9
GM-01_Feld_11-3	66.56	0.00	18.89	0.08	0.02	0.00	0.16	5.13	9.91	100.73	55.5	0.7	43.7
GM-01_Feld_11-4	66.71	0.00	18.88	0.09	0.00	0.00	0.16	5.00	10.19	101.01	56.9	0.8	42.4
GM-01_Feld_12-1	66.75	0.00	18.86	0.11	0.00	0.00	0.15	4.86	10.35	101.05	57.9	0.7	41.4
GM-01_Feld_12-2	66.40	0.00	18.59	0.12	0.01	0.00	0.16	4.94	10.31	100.53	57.4	0.8	41.8
GM-01_Feld_12-3	66.89	0.00	18.87	0.11	0.00	0.00	0.14	4.85	10.48	101.33	58.3	0.7	41.0
GM-01_Feld_14-1	65.65	0.01	19.22	0.08	0.01	0.00	0.18	4.90	9.99	100.03	56.8	0.9	42.3
GM-01_Feld_14-3	66.89	0.01	18.96	0.09	0.00	0.00	0.17	5.10	10.10	101.32	56.1	0.8	43.1
GM-01_Feld_15-6 - light	65.63	0.01	19.77	0.09	0.00	0.00	0.19	4.78	10.17	100.63	57.8	0.9	41.3

GM-01_Feld_15-6 - light	66.58	0.00	18.94	0.08	0.02	0.00	0.16	5.00	10.25	101.02	57.0	0.7	42.3
GM-01_Feld_16-1	66.63	0.00	18.98	0.10	0.00	0.00	0.18	5.15	9.88	100.92	55.3	0.9	43.8
GM-01_Feld_17-1	66.06	0.00	18.71	0.11	0.03	0.00	0.18	5.15	10.05	100.29	55.8	0.9	43.4
GM-01_Feld_17-2	66.61	0.00	18.71	0.11	0.00	0.00	0.16	5.13	10.11	100.82	56.0	0.8	43.2
GM-01_Feld_17-3	65.67	0.00	18.62	0.11	0.00	0.00	0.17	4.70	10.20	99.45	58.3	0.8	40.8
GM-01_Feld_17-4	66.33	0.00	19.08	0.10	0.01	0.00	0.16	5.02	9.97	100.64	56.2	0.8	43.0
GM-01_Feld_19-1	66.58	0.00	18.84	0.11	0.02	0.00	0.18	5.13	10.00	100.82	55.7	0.8	43.4
GM-01_Feld_19-2	66.74	0.00	18.83	0.10	0.00	0.00	0.14	4.77	10.59	101.16	59.0	0.6	40.4
GM-01_Feld_19-3	65.94	0.00	18.80	0.13	0.00	0.00	0.19	5.11	9.80	99.97	55.3	0.9	43.8
GM-01_Feld_20-1	66.10	0.00	18.83	0.10	0.01	0.00	0.15	4.96	10.24	100.37	57.2	0.7	42.1
GM-01_Feld_20-2	66.74	0.01	18.81	0.10	0.00	0.00	0.17	5.07	10.09	100.98	56.3	0.8	42.9
GM-01_Feld_20-3	66.67	0.02	18.38	0.10	0.00	0.00	0.10	4.88	10.37	100.51	58.0	0.5	41.5
GM-01_Feld_20-4	66.17	0.01	18.76	0.09	0.00	0.00	0.17	4.99	10.27	100.43	57.1	0.8	42.2
GM-01_Feld_23-2	66.44	0.01	18.58	0.10	0.00	0.00	0.17	4.96	10.08	100.33	56.8	0.8	42.4
GM-01_Feld_25-1	66.75	0.00	18.84	0.11	0.00	0.00	0.18	5.15	10.10	101.11	55.9	0.8	43.3
GM-01_Feld_25-2	66.09	0.00	19.65	0.11	0.01	0.00	0.16	5.22	9.96	101.18	55.3	0.8	44.0
GM-01_Feld_25-3	66.62	0.00	18.83	0.12	0.01	0.00	0.16	5.16	9.95	100.83	55.5	0.7	43.8
GM-01_Feld_25-4	65.69	0.00	18.52	0.11	0.01	0.00	0.19	4.89	10.02	99.42	56.9	0.9	42.2
GM-01_Feld_26-1	66.53	0.01	18.89	0.12	0.01	0.00	0.16	4.93	10.46	101.10	57.8	0.7	41.4
GM-01_Feld_26-2	66.53	0.00	18.77	0.09	0.00	0.00	0.14	4.90	10.40	100.83	57.9	0.7	41.5
GM-01_Feld_26-3	65.84	0.00	18.34	0.11	0.00	0.00	0.13	4.86	10.26	99.52	57.8	0.6	41.6
GM-01_Feld_26-4	66.85	0.00	18.96	0.09	0.00	0.00	0.18	5.04	10.09	101.18	56.4	0.8	42.8
GM-01_Feld_29-2	66.42	0.01	18.54	0.08	0.00	0.00	0.16	4.94	10.30	100.43	57.4	0.7	41.8

GM-01_Feld_29-4	66.89	0.00	18.78	0.10	0.00	0.00	0.18	5.05	10.35	101.34	57.0	0.8	42.2
GM-01_Feld_30-1	67.00	0.00	18.88	0.10	0.02	0.00	0.20	5.25	9.94	101.39	55.0	0.9	44.1
GM-01_Feld_31-1	66.02	0.01	18.79	0.10	0.01	0.00	0.17	4.92	10.23	100.24	57.3	0.8	41.9
GM-01_Feld_31-3	66.37	0.01	18.68	0.11	0.00	0.00	0.16	5.02	10.15	100.50	56.6	0.8	42.6
GM-01_Feld_31-4	66.73	0.00	18.97	0.10	0.00	0.00	0.18	5.13	10.05	101.15	55.9	0.8	43.3
GM-01_Feld_32-1	65.84	0.02	18.53	0.12	0.02	0.00	0.18	4.89	10.16	99.76	57.3	0.8	41.9
GM-01_Feld_32-2	66.24	0.00	18.71	0.09	0.00	0.00	0.18	5.12	10.03	100.35	55.8	0.8	43.3
GM-01_Feld_33-1	66.68	0.01	18.88	0.12	0.02	0.00	0.17	4.99	10.18	101.05	56.9	0.8	42.4
GM-01_Feld_33-2	66.75	0.00	18.87	0.09	0.00	0.00	0.16	5.02	10.23	101.09	56.9	0.8	42.4
GM-01_Feld_33-4	66.45	0.00	18.78	0.10	0.00	0.00	0.16	4.91	10.27	100.66	57.5	0.7	41.8
GM-01_Feld_35-1	66.62	0.00	18.70	0.10	0.00	0.00	0.15	4.92	10.29	100.75	57.5	0.7	41.8
GM-01_Feld_35-2	66.76	0.01	18.80	0.11	0.01	0.00	0.17	5.03	10.25	101.12	56.9	0.8	42.4
GM-01_Feld_35-3	66.66	0.01	18.82	0.11	0.00	0.00	0.15	4.92	10.20	100.86	57.3	0.7	42.0
GM-01_Feld_38-1	66.37	0.00	18.68	0.14	0.01	0.00	0.15	4.81	10.38	100.54	58.3	0.7	41.0
GM-01_Feld_40-1	66.29	0.00	18.59	0.10	0.00	0.00	0.14	4.88	10.36	100.34	57.9	0.6	41.5
GM-01_Feld_40-2	66.14	0.00	18.61	0.09	0.01	0.00	0.15	4.84	10.31	100.14	58.0	0.7	41.3
GM-01_Feld_40-3	66.40	0.00	18.73	0.10	0.02	0.00	0.18	4.95	10.26	100.63	57.2	0.8	41.9
GM-01_Feld_40-4	66.64	0.01	18.79	0.11	0.00	0.00	0.18	4.99	10.31	101.04	57.1	0.8	42.0
GM-01_Feld_42-1	66.35	0.00	18.78	0.11	0.02	0.00	0.17	5.00	10.13	100.55	56.7	0.8	42.5
GM-01_Feld_42-2	66.03	0.00	18.54	0.11	0.00	0.00	0.17	4.79	10.36	99.99	58.3	0.8	40.9
GM-01_Feld_42-3	66.41	0.00	18.58	0.07	0.00	0.00	0.21	5.02	10.17	100.45	56.6	1.0	42.5
GM-01_Feld_42-4	66.59	0.00	18.82	0.11	0.00	0.00	0.17	5.12	10.15	100.93	56.2	0.8	43.1
GM-01_Feld_45-2	66.47	0.01	18.84	0.11	0.00	0.00	0.17	5.08	10.06	100.72	56.2	0.8	43.1

	GM-01_Feld_47-1	66.90	0.00	19.05	0.10	0.00	0.00	0.19	5.10	9.97	101.29	55.8	0.9	43.3
	GM-01_Feld_47-2	66.46	0.01	18.83	0.10	0.00	0.00	0.18	4.89	10.24	100.69	57.5	0.9	41.7
	GM-01_Feld_47-3	66.79	0.00	18.77	0.09	0.00	0.00	0.15	4.91	10.19	100.85	57.3	0.7	42.0
	GM-01_Feld_47-4	66.59	0.00	18.72	0.10	0.01	0.00	0.16	5.00	10.36	100.94	57.3	0.8	42.0
	GM-01_Feld_47-5	66.50	0.00	19.00	0.08	0.00	0.00	0.16	4.98	10.33	101.05	57.3	0.7	42.0
	GM-01_Feld_49-1	66.07	0.00	18.64	0.09	0.00	0.00	0.21	5.13	9.99	100.11	55.6	1.0	43.4
	GM-01_Feld_49-2	66.56	0.01	18.65	0.08	0.00	0.00	0.16	5.02	10.34	100.82	57.1	0.8	42.1
	GM-01_Feld_49-3	66.57	0.00	18.80	0.10	0.01	0.00	0.17	4.97	10.31	100.91	57.3	0.8	41.9
	GM-01_Feld_49-4	66.81	0.00	18.74	0.10	0.00	0.00	0.15	5.00	10.16	100.93	56.8	0.7	42.5
	GM-01_Feld_50-4	66.41	0.01	18.73	0.10	0.00	0.00	0.18	5.08	9.98	100.48	55.9	0.9	43.2
	Average	**66.43**	**0.00**	**18.81**	**0.10**	**0.00**	**0.00**	**0.17**	**5.00**	**10.17**	**100.67**	**56.8**	**0.8**	**42.4**
	Standard Deviation	**0.33**	**0.01**	**0.21**	**0.01**	**0.01**	**0.00**	**0.02**	**0.12**	**0.16**	**0.45**	**0.90**	**0.1**	**0.9**
GM-JJ-10 (OD) Sanidine	GM-JJ-10A SAN 4 test	66.22	0.00	18.97	0.10	0.00	0.00	0.13	4.46	10.88	100.76	61.2	0.6	38.2
	GM-JJ-10A SAN 1	66.20	0.00	18.99	0.08	0.00	0.00	0.12	4.82	10.70	100.89	59.0	0.6	40.4
	GM-JJ-10A SAN 1	66.28	0.00	18.99	0.08	0.05	0.01	0.12	4.35	11.10	101.01	62.3	0.6	37.1
	GM-JJ-10A SAN 1	66.24	0.00	18.92	0.08	0.02	0.00	0.15	4.60	10.79	100.76	60.2	0.7	39.1
	GM-JJ-10A SAN 1	65.94	0.00	18.98	0.09	0.03	0.00	0.17	4.63	10.82	100.66	60.1	0.8	39.1
	GM-JJ-10A SAN 1	65.92	0.00	18.78	0.09	0.06	0.00	0.15	4.44	11.03	100.49	61.6	0.7	37.7
	GM-JJ-10A SAN 2	66.06	0.00	18.97	0.06	0.18	0.00	0.12	4.47	11.00	100.83	61.5	0.6	38.0
	GM-JJ-10A SAN 2	65.76	0.00	18.81	0.08	0.00	0.00	0.14	4.50	10.89	100.19	61.0	0.7	38.3
	GM-JJ-10A SAN 2	65.94	0.00	18.85	0.07	0.03	0.00	0.14	4.50	11.01	100.57	61.3	0.7	38.1
	GM-JJ-10A SAN 2	65.98	0.01	19.02	0.08	0.02	0.00	0.12	4.61	10.84	100.70	60.4	0.6	39.0

GM-JJ-10A SAN 2	66.06	0.00	18.87	0.06	0.00	0.00	0.17	4.60	10.98	100.74	60.6	0.8	38.6
GM-JJ-10A SAN 2	65.91	0.00	19.06	0.09	0.08	0.00	0.15	4.52	10.99	100.78	61.1	0.7	38.2
GM-JJ-10A SAN 2	65.68	0.00	18.98	0.06	0.03	0.00	0.15	4.48	10.90	100.32	61.1	0.7	38.2
GM-JJ-10A SAN 2	66.16	0.00	18.78	0.08	0.02	0.00	0.14	4.47	10.93	100.58	61.3	0.6	38.1
GM-JJ-10A SAN 2	66.11	0.01	18.83	0.07	0.29	0.00	0.15	4.52	10.86	100.87	60.8	0.7	38.5
GM-JJ-10A SAN 2	66.11	0.00	18.80	0.08	0.00	0.00	0.13	4.45	10.97	100.57	61.5	0.6	37.9
GM-JJ-10A SAN 2	65.57	0.00	18.83	0.08	0.09	0.00	0.13	4.49	10.92	100.08	61.2	0.6	38.2
GM-JJ-10A SAN 2	65.58	0.02	18.70	0.08	0.09	0.00	0.14	4.51	10.87	99.97	60.9	0.6	38.4
GM-JJ-10A SAN 3	65.64	0.00	18.79	0.07	0.04	0.00	0.13	4.55	10.72	99.95	60.4	0.6	39.0
GM-JJ-10A SAN 3	65.62	0.00	18.87	0.08	0.05	0.00	0.14	4.53	11.05	100.34	61.2	0.7	38.2
GM-JJ-10A SAN 3	65.67	0.00	18.79	0.06	0.02	0.00	0.16	4.70	10.60	99.97	59.3	0.7	40.0
GM-JJ-10A SAN 3	66.04	0.01	18.78	0.08	0.01	0.00	0.14	4.73	10.61	100.39	59.2	0.7	40.1
GM-JJ-10A SAN 3	65.78	0.00	18.65	0.06	0.00	0.00	0.15	4.33	11.10	100.02	62.3	0.7	37.0
GM-JJ-10A SAN 3	66.05	0.00	18.71	0.06	0.03	0.01	0.15	4.41	11.05	100.48	61.8	0.7	37.5
GM-JJ-10A SAN 3	66.15	0.01	18.86	0.09	0.02	0.00	0.16	4.47	10.92	100.69	61.2	0.8	38.0
GM-JJ-10A SAN 4	66.10	0.00	18.89	0.08	0.02	0.00	0.14	4.43	11.01	100.67	61.6	0.7	37.7
GM-JJ-10A SAN 4	65.94	0.00	18.94	0.05	0.03	0.00	0.15	4.45	10.83	100.38	61.1	0.7	38.2
GM-JJ-10A SAN 4	66.05	0.00	18.80	0.07	0.00	0.00	0.13	4.42	11.03	100.51	61.8	0.6	37.6
GM-JJ-10A SAN 4	65.84	0.01	18.69	0.08	0.01	0.00	0.11	4.41	11.04	100.15	61.9	0.5	37.6
GM-JJ-10A SAN 4	66.03	0.00	18.76	0.07	0.01	0.00	0.12	4.40	11.12	100.50	62.1	0.5	37.3
GM-JJ-10A SAN 4	65.87	0.00	18.92	0.06	0.02	0.00	0.13	4.48	10.92	100.41	61.2	0.6	38.2
GM-JJ-10A SAN 4	65.70	0.01	18.79	0.08	0.03	0.00	0.16	4.53	10.86	100.15	60.8	0.7	38.5
GM-JJ-10A SAN 4	66.11	0.00	18.90	0.08	0.05	0.00	0.14	4.58	10.95	100.83	60.7	0.7	38.6

GM-JJ-10A SAN4	65.80	0.00	18.88	0.08	0.04	0.00	0.12	4.58	10.75	100.24	60.4	0.6	39.1
GM-JJ-10A SAN4	65.80	0.00	18.86	0.07	0.04	0.00	0.13	4.38	11.03	100.29	62.0	0.6	37.4
GM-JJ-10A SAN4	65.72	0.01	18.84	0.06	0.00	0.00	0.15	4.59	10.86	100.24	60.4	0.7	38.9
GM-JJ-10A SAN4	65.78	0.00	18.85	0.06	0.01	0.01	0.11	4.52	10.80	100.13	60.8	0.5	38.7
GM-JJ-10A SAN4	65.77	0.00	18.66	0.11	0.01	0.00	0.12	4.40	11.06	100.08	62.0	0.6	37.4
GM-JJ-10A SAN4	65.79	0.00	18.75	0.10	0.01	0.00	0.13	4.55	10.93	100.26	60.9	0.6	38.5
GM-JJ-10A SAN4	66.08	0.01	18.80	0.07	0.02	0.00	0.13	4.58	10.84	100.52	60.5	0.6	38.9
GM-JJ-10A SAN4	65.70	0.00	18.87	0.06	0.02	0.00	0.14	4.54	10.89	100.21	60.8	0.7	38.5
GM-JJ-10A SAN4	66.41	0.00	18.85	0.08	0.01	0.00	0.16	4.59	10.82	100.87	60.4	0.7	38.9
GM-JJ-10A SAN4	66.01	0.00	18.93	0.07	0.02	0.01	0.13	4.48	10.96	100.61	61.3	0.6	38.1
GM-JJ-10A SAN4	66.15	0.00	18.78	0.07	0.01	0.00	0.16	4.81	10.36	100.31	58.2	0.7	41.1
GM-JJ-10A SAN4	66.07	0.01	18.92	0.08	0.01	0.00	0.13	4.66	10.61	100.50	59.6	0.6	39.8
GM-JJ-10A SAN5	65.69	0.00	18.75	0.07	0.00	0.00	0.15	4.48	10.95	100.09	61.2	0.7	38.1
GM-JJ-10A SAN5	65.94	0.01	18.68	0.09	0.02	0.00	0.16	4.71	10.52	100.14	59.1	0.8	40.2
GM-JJ-10A SAN5	65.75	0.00	18.85	0.07	0.01	0.00	0.15	4.52	10.85	100.16	60.8	0.7	38.5
GM-JJ-10A SAN5	65.64	0.00	18.85	0.07	0.07	0.00	0.14	4.62	10.68	100.09	59.9	0.6	39.4
GM-JJ-10A SAN5	65.44	0.00	18.69	0.08	0.02	0.00	0.13	4.49	10.85	99.67	61.0	0.6	38.4
GM-JJ-10A SAN5	65.49	0.00	18.89	0.06	0.00	0.00	0.15	4.49	10.82	99.89	60.9	0.7	38.4
GM-JJ-10A SAN5	65.34	0.00	18.86	0.06	0.00	0.00	0.11	4.41	11.04	99.82	61.9	0.5	37.6
GM-JJ-10A SAN5	65.72	0.00	18.62	0.07	0.01	0.00	0.17	4.64	10.56	99.79	59.5	0.8	39.7
GM-JJ-10A SAN5	65.99	0.01	18.92	0.08	0.01	0.00	0.13	4.64	10.73	100.51	59.9	0.6	39.4
GM-JJ-10A SAN5	66.15	0.00	18.95	0.09	0.01	0.00	0.15	4.60	10.84	100.76	60.4	0.7	38.9
GM-JJ-10A SAN5	65.84	0.00	18.85	0.07	0.03	0.00	0.16	4.56	10.75	100.23	60.3	0.8	38.9

GM-JJ-10A SAN5	65.94	0.01	18.89	0.08	0.00	0.00	0.15	4.51	10.97	100.53	61.1	0.7	38.2
GM-JJ-10A SAN5	65.59	0.00	18.81	0.07	0.00	0.00	0.15	4.53	10.88	100.00	60.8	0.7	38.5
GM-JJ-10A SAN5	65.84	0.01	18.69	0.07	0.01	0.00	0.15	4.51	10.86	100.12	60.9	0.7	38.4
GM-JJ-10A SAN5	65.66	0.00	18.80	0.05	0.01	0.00	0.14	4.58	10.91	100.15	60.6	0.7	38.7
GM-JJ-10A SAN5	65.90	0.02	19.02	0.10	0.05	0.00	0.19	4.73	10.65	100.65	59.2	0.9	39.9
GM-JJ-10A SAN5	66.33	0.00	19.03	0.09	0.02	0.00	0.17	4.57	10.93	101.11	60.6	0.8	38.5
GM-JJ-10A SAN6	65.96	0.00	18.87	0.08	0.03	0.00	0.12	4.42	10.94	100.42	61.6	0.6	37.8
GM-JJ-10A SAN6	65.49	0.00	18.90	0.07	0.14	0.00	0.12	4.33	11.10	100.17	62.4	0.6	37.0
GM-JJ-10A SAN6	66.06	0.00	18.91	0.07	0.01	0.00	0.14	4.50	10.97	100.64	61.2	0.7	38.1
GM-JJ-10A SAN6	65.66	0.00	18.80	0.07	0.00	0.00	0.16	4.68	10.67	100.05	59.6	0.7	39.7
GM-JJ-10A SAN6	65.58	0.01	18.75	0.07	0.00	0.00	0.13	4.46	11.04	100.05	61.6	0.6	37.8
GM-JJ-10A SAN6	65.66	0.00	18.74	0.07	0.01	0.01	0.15	4.49	10.82	99.94	60.9	0.7	38.4
GM-JJ-10A SAN6	65.70	0.01	18.79	0.09	0.02	0.00	0.15	4.49	10.87	100.14	61.0	0.7	38.3
GM-JJ-10A SAN6	65.87	0.01	18.83	0.07	0.01	0.00	0.15	4.48	10.77	100.18	60.8	0.7	38.5
GM-JJ-10A SAN6	65.75	0.00	18.78	0.09	0.00	0.00	0.15	4.51	10.98	100.27	61.1	0.7	38.2
GM-JJ-10A SAN6	65.48	0.00	18.72	0.08	0.02	0.01	0.15	4.39	10.95	99.79	61.7	0.7	37.6
GM-JJ-10A SAN6	65.37	0.00	18.71	0.08	0.00	0.00	0.15	4.50	10.86	99.66	60.9	0.7	38.4
GM-JJ-10A SAN6	65.27	0.00	18.72	0.08	0.01	0.00	0.16	4.52	10.88	99.66	60.8	0.8	38.4
GM-JJ-10A SAN6	65.35	0.00	18.72	0.06	0.00	0.00	0.15	4.47	10.92	99.67	61.2	0.7	38.1
GM-JJ-10A SAN6	66.13	0.00	18.85	0.08	0.01	0.00	0.14	4.49	10.80	100.50	60.8	0.7	38.5
GM-JJ-10A SAN6	65.85	0.00	18.77	0.08	0.01	0.00	0.17	4.53	10.87	100.29	60.8	0.8	38.5
GM-JJ-10A SAN6	65.62	0.00	18.84	0.08	0.03	0.00	0.12	4.50	10.99	100.18	61.3	0.6	38.1
GM-JJ-10A SAN6	66.18	0.00	18.87	0.10	0.04	0.00	0.14	4.53	11.04	100.91	61.2	0.6	38.1

GM-JJ-10A SAN6	65.74	0.00	18.71	0.08	0.01	0.00	0.14	4.53	10.86	100.07	60.8	0.7	38.6
GM-JJ-10A SAN6	65.66	0.00	18.74	0.09	0.00	0.00	0.15	4.49	10.81	99.95	60.9	0.7	38.4
GM-JJ-10A SAN6	65.99	0.00	18.81	0.09	0.01	0.00	0.15	4.52	10.98	100.56	61.1	0.7	38.2
GM-JJ-10A SAN6	65.60	0.00	18.82	0.07	0.04	0.00	0.17	4.53	10.84	100.04	60.7	0.8	38.5
GM-JJ-10A SAN6	65.94	0.00	18.66	0.09	0.03	0.00	0.14	4.50	10.83	100.18	60.9	0.7	38.5
GM-JJ-10A SAN6	65.91	0.00	18.84	0.05	0.06	0.00	0.14	4.48	11.06	100.59	61.5	0.6	37.9
GM-JJ-10A SAN6	65.40	0.00	18.61	0.07	0.01	0.01	0.16	4.47	10.93	99.65	61.2	0.8	38.0
GM-JJ-10A SAN6	65.78	0.00	18.77	0.07	0.00	0.00	0.12	4.51	10.99	100.22	61.3	0.6	38.2
GM-JJ-10A SAN7	65.62	0.00	18.73	0.08	0.00	0.00	0.13	4.39	10.93	99.84	61.7	0.6	37.7
GM-JJ-10A SAN7	65.50	0.00	18.79	0.05	0.02	0.00	0.14	4.46	10.93	99.85	61.3	0.7	38.0
GM-JJ-10A SAN7	65.74	0.00	18.81	0.07	0.00	0.00	0.15	4.52	10.94	100.19	61.0	0.7	38.3
GM-JJ-10A SAN7	65.46	0.00	18.81	0.09	0.00	0.00	0.14	4.31	11.01	99.80	62.3	0.7	37.1
GM-JJ-10A SAN7	65.62	0.00	18.70	0.07	0.01	0.00	0.12	4.49	11.07	100.02	61.5	0.5	37.9
GM-JJ-10A SAN7	65.84	0.00	18.75	0.10	0.03	0.00	0.12	4.52	10.97	100.35	61.2	0.6	38.3
GM-JJ-10A SAN7	65.84	0.01	18.75	0.06	0.00	0.00	0.15	4.49	10.87	100.15	61.0	0.7	38.3
GM-JJ-10A SAN7	65.89	0.00	18.75	0.07	0.00	0.00	0.13	4.47	11.02	100.30	61.5	0.6	37.9
GM-JJ-10A SAN7	65.53	0.00	18.84	0.08	0.03	0.00	0.12	4.55	10.86	100.01	60.7	0.6	38.7
GM-JJ-10A SAN7	66.01	0.00	18.78	0.08	0.00	0.00	0.14	4.43	11.08	100.48	61.8	0.6	37.6
GM-JJ-10A SAN7	66.21	0.00	18.76	0.08	0.00	0.00	0.13	4.45	10.97	100.62	61.5	0.6	37.9
GM-JJ-10A SAN7	65.75	0.01	18.86	0.10	0.00	0.00	0.15	4.49	10.88	100.23	61.0	0.7	38.3
GM-JJ-10A SAN7	65.96	0.01	18.89	0.08	0.01	0.00	0.16	4.48	10.85	100.44	60.9	0.8	38.3
GM-JJ-10A SAN7	65.80	0.01	18.80	0.07	0.00	0.00	0.16	4.55	10.85	100.21	60.6	0.7	38.6
GM-JJ-10A SAN8	65.94	0.00	18.77	0.08	0.00	0.00	0.15	4.51	10.81	100.25	60.8	0.7	38.5

GM-JJ-10A SAN8	65.94	0.00	18.78	0.10	0.00	0.01	0.16	4.53	10.92	100.44	60.9	0.8	38.4
GM-JJ-10A SAN8	66.10	0.00	18.60	0.08	0.00	0.00	0.15	4.49	10.84	100.29	61.0	0.7	38.3
GM-JJ-10A SAN8	66.27	0.00	18.65	0.07	0.04	0.00	0.15	4.45	10.97	100.58	61.4	0.7	37.9
GM-JJ-10A SAN8	66.50	0.01	19.01	0.07	0.00	0.00	0.14	4.80	10.91	101.39	59.5	0.7	39.8
GM-JJ-10A SAN8	65.87	0.00	19.01	0.06	0.02	0.01	0.18	4.40	10.73	100.26	61.1	0.9	38.0
GM-JJ-10A SAN8	65.76	0.00	18.80	0.09	0.02	0.00	0.16	4.56	10.91	100.27	60.7	0.7	38.6
GM-JJ-10A SAN8	65.94	0.00	18.92	0.07	0.09	0.00	0.14	4.53	10.89	100.55	60.9	0.6	38.5
GM-JJ-10A SAN8	65.89	0.00	18.71	0.06	0.00	0.00	0.12	4.44	11.01	100.24	61.7	0.5	37.8
GM-JJ-10A SAN8	66.03	0.00	18.64	0.06	0.00	0.00	0.13	4.47	10.89	100.19	61.2	0.6	38.1
GM-JJ-10A SAN8	66.36	0.00	18.88	0.08	0.06	0.00	0.15	4.43	11.01	100.96	61.6	0.7	37.7
GM-JJ-10A SAN9	65.80	0.00	18.67	0.07	0.00	0.00	0.12	4.43	10.95	100.04	61.6	0.6	37.8
GM-JJ-10A SAN9	65.70	0.00	18.57	0.09	0.00	0.00	0.12	4.45	10.95	99.86	61.5	0.6	37.9
GM-JJ-10A SAN9	65.49	0.00	18.69	0.08	0.01	0.00	0.15	4.50	11.02	99.92	61.3	0.7	38.0
GM-JJ-10A SAN9	65.81	0.00	18.83	0.06	0.01	0.00	0.16	4.51	10.85	100.23	60.8	0.8	38.4
GM-JJ-10A SAN9	65.90	0.00	18.84	0.09	0.00	0.00	0.13	4.45	10.85	100.22	61.2	0.6	38.2
GM-JJ-10A SAN9	66.12	0.00	18.82	0.09	0.01	0.00	0.17	4.48	10.89	100.60	61.0	0.8	38.2
GM-JJ-10A SAN9	66.11	0.00	18.85	0.06	0.00	0.00	0.15	4.51	10.78	100.49	60.7	0.7	38.6
GM-JJ-10A SAN9	66.40	0.00	18.82	0.08	0.04	0.00	0.14	4.51	10.95	100.97	61.1	0.7	38.2
GM-JJ-10A SAN9	66.15	0.00	18.80	0.06	0.00	0.00	0.14	4.46	10.92	100.50	61.3	0.7	38.0
GM-JJ-10A SAN9	65.94	0.00	18.78	0.08	0.00	0.00	0.13	4.75	10.43	100.11	58.7	0.6	40.7
GM-JJ-10A SAN9	65.91	0.00	18.76	0.08	0.00	0.00	0.15	4.51	10.87	100.23	60.9	0.7	38.4
GM-JJ-10A SAN9	66.12	0.00	18.82	0.07	0.00	0.00	0.15	4.48	10.99	100.58	61.3	0.7	38.0
GM-JJ-10A SAN9	65.99	0.00	18.90	0.10	0.00	0.00	0.15	4.50	10.92	100.48	61.1	0.7	38.2

GM-JJ-10A SAN 10	65.77	0.00	18.79	0.06	0.00	0.00	0.15	4.60	10.80	100.15	60.3	0.7	39.0
GM-JJ-10A SAN 10	65.98	0.00	18.81	0.09	0.00	0.00	0.14	4.47	10.83	100.25	61.1	0.6	38.3
GM-JJ-10A SAN 10	65.73	0.01	18.88	0.08	0.00	0.00	0.16	4.51	10.91	100.27	60.9	0.7	38.3
GM-JJ-10A SAN 10	65.88	0.00	18.72	0.06	0.01	0.01	0.14	4.45	11.08	100.33	61.7	0.7	37.7
GM-JJ-10A SAN 10	65.77	0.00	18.82	0.07	0.00	0.00	0.13	4.48	10.86	100.09	61.1	0.6	38.3
GM-JJ-10A SAN 10	65.99	0.01	18.86	0.06	0.01	0.00	0.15	4.50	10.80	100.41	60.8	0.7	38.5
GM-JJ-10A SAN 10	65.98	0.00	18.87	0.08	0.01	0.02	0.13	4.42	10.95	100.44	61.6	0.6	37.8
GM-JJ-10A SAN 10	66.18	0.00	18.80	0.05	0.00	0.00	0.14	4.54	10.74	100.41	60.5	0.7	38.9
GM-JJ-10A SAN 11	65.49	0.01	18.65	0.07	0.00	0.00	0.14	4.45	10.94	99.77	61.4	0.7	37.9
GM-JJ-10A SAN 11	65.89	0.00	18.71	0.08	0.02	0.00	0.15	4.50	10.83	100.15	60.9	0.7	38.4
GM-JJ-10A SAN 11	66.20	0.00	18.79	0.09	0.10	0.00	0.14	4.55	10.79	100.61	60.6	0.6	38.8
GM-JJ-10A SAN 11	65.10	0.00	18.60	0.05	0.00	0.00	0.16	4.48	10.78	99.10	60.9	0.7	38.4
GM-JJ-10A SAN 11	65.32	0.00	18.63	0.07	0.00	0.00	0.15	4.47	10.75	99.39	60.8	0.7	38.5
GM-JJ-10A SAN 11	66.34	0.00	18.87	0.05	0.01	0.00	0.16	4.53	10.89	100.83	60.8	0.7	38.5
GM-JJ-10A SAN 11	65.46	0.01	18.88	0.07	0.00	0.01	0.15	4.49	10.88	99.96	61.0	0.7	38.3
GM-JJ-10A SAN 11	65.39	0.00	18.71	0.08	0.01	0.00	0.13	4.44	11.05	99.81	61.7	0.6	37.7
GM-JJ-10A SAN 11	65.54	0.00	18.67	0.06	0.00	0.00	0.14	4.50	10.92	99.80	61.1	0.7	38.3
GM-JJ-10A SAN 11	65.78	0.00	18.66	0.06	0.02	0.00	0.15	4.44	10.95	100.05	61.5	0.7	37.8
GM-JJ-10A SAN 11	65.60	0.00	18.82	0.08	0.00	0.00	0.12	4.38	10.98	99.93	61.9	0.6	37.5
GM-JJ-10A SAN 11	65.78	0.00	18.70	0.06	0.00	0.00	0.15	4.44	11.00	100.09	61.6	0.7	37.7
GM-JJ-10A SAN 11	65.82	0.00	18.90	0.07	0.00	0.00	0.17	4.53	10.95	100.41	60.9	0.8	38.3
GM-JJ-10A SAN 11	66.46	0.01	18.87	0.07	0.01	0.00	0.14	4.47	11.04	101.08	61.5	0.6	37.9
GM-JJ-10A SAN 12	65.40	0.00	18.73	0.06	0.00	0.00	0.13	4.44	10.91	99.68	61.4	0.6	38.0

GM-JJ-10A SAN 12	65.34	0.01	18.60	0.09	0.00	0.00	0.15	4.50	11.06	99.74	61.4	0.7	37.9
GM-JJ-10A SAN 12	65.64	0.00	18.63	0.07	0.00	0.00	0.13	4.47	10.88	99.80	61.2	0.6	38.2
GM-JJ-10A SAN 12	65.52	0.00	18.72	0.08	0.00	0.00	0.16	4.52	10.79	99.79	60.6	0.8	38.6
GM-JJ-10A SAN 12	65.72	0.00	18.81	0.08	0.01	0.00	0.16	4.61	10.76	100.14	60.1	0.8	39.1
GM-JJ-10A SAN 12	65.46	0.00	18.73	0.06	0.02	0.00	0.15	4.46	10.92	99.80	61.3	0.7	38.0
GM-JJ-10A SAN 12	65.25	0.00	18.70	0.05	0.00	0.00	0.15	4.46	10.96	99.50	61.4	0.7	37.9
GM-JJ-10A SAN 12	65.37	0.00	18.72	0.08	0.00	0.00	0.16	4.52	10.96	99.76	61.0	0.7	38.2
GM-JJ-10A SAN 12	65.65	0.00	18.76	0.10	0.00	0.00	0.14	4.56	10.73	99.88	60.4	0.6	39.0
GM-JJ-10A SAN 12	65.57	0.00	18.84	0.09	0.02	0.00	0.15	4.60	10.70	99.97	60.1	0.7	39.2
GM-JJ-10A SAN 12	65.44	0.00	18.90	0.09	0.01	0.00	0.16	4.50	10.84	99.93	60.8	0.7	38.4
GM-JJ-10A SAN 12	65.48	0.00	18.76	0.08	0.01	0.01	0.12	4.45	11.01	99.91	61.6	0.6	37.9
GM-JJ-10A SAN 13	66.02	0.00	18.80	0.07	0.01	0.00	0.15	4.49	10.94	100.49	61.1	0.7	38.1
GM-JJ-10A SAN 13	65.93	0.00	18.85	0.07	0.00	0.00	0.15	4.49	10.79	100.24	60.8	0.7	38.5
GM-JJ-10A SAN 13	65.92	0.00	18.78	0.07	0.00	0.00	0.10	4.38	11.02	100.26	62.1	0.5	37.5
GM-JJ-10A SAN 13	65.82	0.00	18.64	0.07	0.01	0.00	0.16	4.48	10.90	100.07	61.1	0.8	38.2
GM-JJ-10A SAN 13	65.73	0.00	18.80	0.07	0.00	0.00	0.15	4.49	10.88	100.05	61.0	0.7	38.2
GM-JJ-10A SAN 13	65.71	0.00	18.95	0.09	0.01	0.01	0.13	4.53	10.97	100.39	61.1	0.6	38.3
GM-JJ-10A SAN 13	65.56	0.00	18.76	0.08	0.00	0.00	0.14	4.42	10.96	99.93	61.6	0.7	37.8
GM-JJ-10A SAN 13	65.53	0.00	18.75	0.07	0.00	0.01	0.15	4.51	10.88	99.86	60.9	0.7	38.4
GM-JJ-10A SAN 13	65.26	0.00	18.67	0.07	0.00	0.00	0.16	4.42	10.82	99.38	61.2	0.8	38.0
GM-JJ-10A SAN 13	65.43	0.00	18.80	0.07	0.00	0.00	0.17	4.46	10.75	99.63	60.9	0.8	38.4
GM-JJ-10A SAN 13	65.19	0.00	18.62	0.07	0.00	0.00	0.16	4.53	10.69	99.22	60.4	0.7	38.9
GM-JJ-10A SAN 13	65.37	0.01	18.68	0.08	0.00	0.00	0.15	4.46	10.88	99.63	61.2	0.7	38.1

GM-JJ-10A SAN 13	65.01	0.00	18.65	0.08	0.02	0.00	0.15	4.47	10.95	99.33	61.3	0.7	38.0
GM-JJ-10A SAN 13	65.43	0.00	18.71	0.09	0.02	0.01	0.11	4.43	10.85	99.60	61.4	0.5	38.1
GM-JJ-10A SAN 13	65.40	0.00	18.77	0.07	0.01	0.00	0.15	4.49	10.95	99.85	61.1	0.7	38.1
GM-JJ-10A SAN 13	65.55	0.02	18.62	0.09	0.00	0.00	0.12	4.46	10.93	99.75	61.4	0.6	38.1
GM-JJ-10A SAN 13	65.31	0.00	18.68	0.07	0.03	0.00	0.12	4.38	10.95	99.56	61.8	0.6	37.6
GM-JJ-10A SAN 13	65.74	0.00	18.66	0.06	0.14	0.00	0.14	4.40	10.89	100.02	61.5	0.6	37.8
GM-JJ-10A SAN 13	65.11	0.01	18.66	0.08	0.00	0.00	0.15	4.41	10.82	99.20	61.3	0.7	38.0
GM-JJ-10A SAN 14	65.87	0.00	18.59	0.08	0.00	0.00	0.13	4.43	10.87	99.94	61.3	0.6	38.0
GM-JJ-10A SAN 14	65.34	0.00	18.62	0.08	0.00	0.00	0.18	4.46	10.78	99.41	60.9	0.9	38.3
GM-JJ-10A SAN 14	65.75	0.00	18.97	0.09	0.00	0.00	0.21	4.68	10.45	100.17	58.9	1.0	40.1
GM-JJ-10A SAN 14	65.77	0.01	18.78	0.10	0.00	0.00	0.17	4.61	10.62	100.05	59.7	0.8	39.5
GM-JJ-10A SAN 14	66.12	0.00	18.89	0.08	0.00	0.00	0.16	4.51	10.79	100.51	60.7	0.7	38.6
GM-JJ-10A SAN 15	65.36	0.00	18.64	0.08	0.02	0.01	0.16	4.47	10.72	99.43	60.7	0.8	38.5
GM-JJ-10A SAN 15	65.42	0.00	18.65	0.08	0.01	0.00	0.15	4.51	10.84	99.64	60.9	0.7	38.4
GM-JJ-10A SAN 15	65.10	0.00	18.72	0.07	0.00	0.00	0.13	4.44	11.01	99.48	61.6	0.6	37.8
GM-JJ-10A SAN 15	65.35	0.00	18.69	0.07	0.01	0.00	0.12	4.31	11.11	99.62	62.6	0.6	36.9
GM-JJ-10A SAN 15	65.50	0.00	18.79	0.05	0.02	0.00	0.16	4.38	10.94	99.81	61.7	0.7	37.6
GM-JJ-10A SAN 15	65.69	0.00	18.72	0.06	0.01	0.00	0.16	4.45	10.81	99.88	61.1	0.8	38.2
GM-JJ-10A SAN 15	65.36	0.00	18.76	0.08	0.01	0.00	0.13	4.48	10.93	99.76	61.2	0.6	38.1
GM-JJ-10A SAN 15	65.93	0.00	18.73	0.07	0.00	0.00	0.12	4.47	10.89	100.14	61.2	0.5	38.2
GM-JJ-10A SAN 15	65.74	0.00	18.86	0.07	0.03	0.00	0.13	4.51	10.89	100.24	61.0	0.6	38.4
GM-JJ-10A SAN 15	66.18	0.00	18.80	0.08	0.00	0.00	0.17	4.49	10.95	100.62	61.1	0.8	38.1
GM-JJ-10A SAN 15	65.97	0.00	18.93	0.09	0.00	0.00	0.15	4.55	10.87	100.52	60.7	0.7	38.6

GM-JJ-10A SAN 15	65.93	0.01	18.82	0.09	0.00	0.00	0.13	4.74	10.69	100.35	59.4	0.6	40.0
GM-JJ-10A SAN 15	65.86	0.00	18.67	0.08	0.01	0.00	0.15	4.47	10.92	100.13	61.2	0.7	38.1
GM-JJ-10A SAN 15	66.27	0.00	18.73	0.06	0.00	0.00	0.12	4.51	10.86	100.56	61.0	0.6	38.4
GM-JJ-10A SAN 15-2	65.95	0.00	18.79	0.08	0.02	0.00	0.14	4.72	10.37	100.08	58.7	0.7	40.6
GM-JJ-10A SAN 15-2	65.96	0.00	18.74	0.08	0.00	0.00	0.14	4.73	10.51	100.10	59.0	0.7	40.3
GM-JJ-10A SAN 15-2	65.71	0.00	18.85	0.09	0.01	0.01	0.14	4.64	10.67	100.11	59.8	0.7	39.6
GM-JJ-10A SAN 15-2	65.91	0.00	18.76	0.08	0.01	0.00	0.13	4.44	10.95	100.24	61.5	0.6	37.9
GM-JJ-10A SAN 15-2	65.82	0.00	18.66	0.07	0.01	0.00	0.16	4.44	10.92	100.03	61.4	0.7	37.9
GM-JJ-10A SAN 15-2	66.04	0.00	18.78	0.07	0.02	0.00	0.14	4.37	11.13	100.53	62.3	0.6	37.1
GM-JJ-10A SAN 15-2	65.74	0.01	18.72	0.07	0.02	0.00	0.17	4.57	10.76	100.05	60.3	0.8	38.9
GM-JJ-10A SAN 15-2	66.00	0.01	18.57	0.10	0.00	0.00	0.14	4.29	11.22	100.29	62.8	0.7	36.5
GM-JJ-10A SAN 15-2	65.71	0.01	18.73	0.10	0.00	0.00	0.15	4.44	11.11	100.24	61.8	0.7	37.5
GM-JJ-10A SAN 15-2	66.08	0.00	18.82	0.09	0.02	0.00	0.16	4.47	10.88	100.51	61.1	0.7	38.2
GM-JJ-10A SAN 15-2	65.88	0.00	18.87	0.05	0.01	0.00	0.12	4.46	10.95	100.33	61.4	0.5	38.0
GM-JJ-10A SAN 16	66.06	0.00	18.79	0.07	0.00	0.00	0.14	4.60	10.75	100.42	60.2	0.6	39.2
GM-JJ-10A SAN 16	65.85	0.00	18.77	0.07	0.00	0.00	0.18	4.48	10.83	100.17	60.9	0.8	38.3
GM-JJ-10A SAN 16	65.94	0.01	18.89	0.09	0.00	0.00	0.14	4.47	10.99	100.47	61.4	0.7	38.0
GM-JJ-10A SAN 16	66.35	0.00	18.83	0.08	0.02	0.00	0.14	4.50	10.98	100.86	61.2	0.6	38.1
GM-JJ-10A SAN 16	65.97	0.00	18.87	0.05	0.00	0.00	0.14	4.40	10.86	100.24	61.5	0.7	37.8
GM-JJ-10A SAN 16	66.35	0.01	18.78	0.06	0.03	0.00	0.14	4.42	10.95	100.72	61.6	0.7	37.8
GM-JJ-10A SAN 16	65.78	0.00	18.85	0.08	0.02	0.01	0.14	4.51	10.94	100.35	61.1	0.6	38.2
GM-JJ-10A SAN 16	65.74	0.00	18.75	0.10	0.00	0.00	0.15	4.47	10.81	99.98	61.0	0.7	38.3
GM-JJ-10A SAN 16	65.82	0.00	18.74	0.08	0.00	0.00	0.14	4.53	10.88	100.14	60.8	0.7	38.5

GM-JJ-10A SAN16	65.98	0.00	18.86	0.09	0.01	0.00	0.14	4.54	10.98	100.60	61.0	0.7	38.4
GM-JJ-10A SAN16	66.14	0.00	18.78	0.06	0.00	0.00	0.12	4.55	10.88	100.51	60.8	0.6	38.7
GM-JJ-10A SAN17	65.90	0.00	18.72	0.08	0.00	0.00	0.14	4.47	10.89	100.22	61.2	0.7	38.2
GM-JJ-10A SAN17	65.86	0.01	18.79	0.10	0.01	0.01	0.20	4.73	10.52	100.24	58.9	0.9	40.2
GM-JJ-10A SAN17	65.96	0.00	18.77	0.09	0.00	0.00	0.15	4.51	10.95	100.28	61.1	0.7	38.2
GM-JJ-10A SAN17	65.86	0.02	18.78	0.08	0.00	0.00	0.12	4.40	10.92	100.16	61.7	0.6	37.8
GM-JJ-10A SAN17	65.84	0.00	18.67	0.09	0.01	0.00	0.09	4.43	10.91	99.99	61.6	0.4	38.0
GM-JJ-10A SAN17	65.84	0.00	18.68	0.07	0.00	0.00	0.13	4.50	10.92	100.14	61.1	0.6	38.3
GM-JJ-10A SAN17	65.59	0.00	18.68	0.10	0.00	0.00	0.16	4.45	11.03	100.00	61.5	0.8	37.7
GM-JJ-10A SAN17	65.72	0.00	18.80	0.05	0.00	0.00	0.14	4.62	10.68	100.00	59.9	0.6	39.4
GM-JJ-10A SAN17	65.90	0.00	18.84	0.06	0.01	0.01	0.12	4.49	10.97	100.37	61.3	0.6	38.1
GM-JJ-10A SAN18	66.56	0.01	18.77	0.09	0.00	0.00	0.14	4.65	10.87	101.07	60.2	0.6	39.2
GM-JJ-10A SAN18	66.12	0.00	18.86	0.07	0.00	0.00	0.15	4.48	10.97	100.64	61.3	0.7	38.0
GM-JJ-10A SAN18	65.69	0.00	18.76	0.04	0.00	0.00	0.16	4.46	10.86	99.97	61.1	0.7	38.1
GM-JJ-10A SAN18	65.81	0.00	18.76	0.08	0.00	0.00	0.12	4.45	10.92	100.14	61.4	0.6	38.0
GM-JJ-10A SAN18	65.92	0.01	18.67	0.08	0.00	0.00	0.11	4.46	10.97	100.21	61.5	0.5	38.0
GM-JJ-10A SAN18	65.83	0.00	18.85	0.07	0.00	0.00	0.14	4.55	10.78	100.17	60.5	0.6	38.8
GM-JJ-10A SAN18	65.69	0.00	18.85	0.10	0.02	0.00	0.15	4.58	10.84	100.20	60.4	0.7	38.9
GM-JJ-10A SAN18	65.70	0.01	18.82	0.09	0.00	0.00	0.15	4.44	10.80	100.00	61.1	0.7	38.2
GM-JJ-10A SAN18	66.10	0.00	18.78	0.07	0.00	0.00	0.15	4.52	10.92	100.54	61.0	0.7	38.3
GM-JJ-10A SAN18	65.80	0.01	18.66	0.08	0.01	0.00	0.15	4.46	10.97	100.08	61.4	0.7	37.9
GM-JJ-10A SAN19	65.54	0.00	18.71	0.07	0.00	0.00	0.14	4.46	11.04	99.97	61.6	0.6	37.8
GM-JJ-10A SAN19	65.52	0.00	18.73	0.07	0.00	0.00	0.13	4.36	11.02	99.82	62.1	0.6	37.3

GM-JJ-10A SAN 19	66.00	0.01	18.81	0.07	0.03	0.00	0.13	4.45	10.98	100.46	61.5	0.6	37.9
GM-JJ-10A SAN 19	65.57	0.00	18.70	0.07	0.03	0.00	0.18	4.69	10.71	99.96	59.5	0.8	39.7
GM-JJ-10A SAN 19	65.62	0.01	18.58	0.09	0.01	0.00	0.15	4.48	11.07	100.00	61.5	0.7	37.8
GM-JJ-10A SAN 19	66.17	0.01	18.75	0.06	0.08	0.00	0.12	4.47	10.88	100.52	61.2	0.5	38.2
GM-JJ-10A SAN 19	65.90	0.00	18.75	0.10	0.00	0.00	0.16	4.61	10.79	100.29	60.2	0.7	39.1
GM-JJ-10A SAN 19	65.57	0.01	18.85	0.10	0.00	0.00	0.16	4.60	10.82	100.14	60.3	0.8	38.9
GM-JJ-10A SAN 19	65.76	0.00	18.85	0.08	0.00	0.00	0.17	4.57	10.77	100.16	60.3	0.8	38.9
GM-JJ-10A SAN 19	65.93	0.01	18.70	0.07	0.00	0.00	0.14	4.55	10.75	100.14	60.4	0.7	38.9
GM-JJ-10A SAN 19	66.04	0.00	18.81	0.05	0.00	0.00	0.14	4.51	10.89	100.43	61.0	0.7	38.4
GM-JJ-10A SAN 19	65.94	0.01	18.76	0.07	0.01	0.00	0.15	4.45	10.91	100.28	61.3	0.7	38.0
GM-JJ-10A SAN 19	66.23	0.00	18.82	0.11	0.00	0.00	0.13	4.48	10.91	100.66	61.2	0.6	38.2
GM-JJ-10A SAN 19	66.27	0.00	18.97	0.09	0.00	0.00	0.13	4.53	10.85	100.81	60.8	0.6	38.6
GM-JJ-10A SAN 19	66.32	0.00	18.97	0.09	0.00	0.00	0.13	4.49	10.83	100.83	61.0	0.6	38.4
GM-JJ-10A SAN 19	66.06	0.00	18.89	0.09	0.00	0.00	0.13	4.47	11.02	100.64	61.5	0.6	37.9
GM-JJ-10A SAN 20	65.92	0.02	18.53	0.09	0.00	0.00	0.13	4.55	10.75	99.99	60.5	0.6	38.9
GM-JJ-10A SAN 20	66.03	0.00	18.76	0.07	0.00	0.00	0.14	4.56	10.79	100.37	60.5	0.7	38.9
GM-JJ-10A SAN 20	65.92	0.00	18.91	0.09	0.01	0.00	0.16	4.46	10.93	100.46	61.3	0.8	38.0
GM-JJ-10A SAN 20	65.66	0.00	18.73	0.09	0.00	0.00	0.16	4.48	10.92	100.04	61.1	0.8	38.1
GM-JJ-10A SAN 20	65.72	0.01	18.82	0.11	0.00	0.00	0.17	4.58	10.67	100.12	60.0	0.8	39.2
GM-JJ-10A SAN 20	65.59	0.00	18.76	0.09	0.00	0.00	0.10	4.45	10.97	99.97	61.6	0.5	37.9
GM-JJ-10A SAN 20	65.74	0.00	18.70	0.09	0.01	0.00	0.16	4.58	10.75	100.06	60.3	0.7	39.0
GM-JJ-10A SAN 20	65.84	0.00	18.78	0.10	0.00	0.00	0.16	4.62	10.65	100.13	59.8	0.8	39.4
GM-JJ-10A SAN 20	65.46	0.01	18.72	0.08	0.00	0.00	0.18	4.58	10.68	99.68	60.0	0.9	39.1

GM-JJ-10A SAN 20	65.71	0.01	18.86	0.08	0.00	0.00	0.16	4.62	10.63	100.11	59.8	0.8	39.5
GM-JJ-10A SAN 20	65.59	0.00	18.71	0.08	0.00	0.00	0.13	4.49	11.04	100.05	61.4	0.6	38.0
GM-JJ-10A SAN 20	65.92	0.00	18.70	0.08	0.01	0.00	0.14	4.42	11.06	100.31	61.8	0.6	37.5
GM-JJ-10A SAN 21	66.09	0.00	18.74	0.05	0.00	0.00	0.15	4.58	10.84	100.43	60.5	0.7	38.8
GM-JJ-10A SAN 21	66.03	0.00	18.81	0.07	0.00	0.00	0.17	4.54	10.79	100.39	60.5	0.8	38.7
GM-JJ-10A SAN 21	66.08	0.00	18.85	0.09	0.00	0.00	0.15	4.56	10.87	100.54	60.7	0.7	38.6
GM-JJ-10A SAN 21	65.81	0.00	18.80	0.09	0.00	0.00	0.14	4.52	10.79	100.11	60.7	0.6	38.7
GM-JJ-10A SAN 21	65.57	0.00	18.73	0.07	0.00	0.00	0.15	4.62	10.82	99.97	60.3	0.7	39.1
GM-JJ-10A SAN 21	65.70	0.00	18.84	0.08	0.00	0.00	0.16	4.55	10.85	100.19	60.6	0.8	38.6
GM-JJ-10A SAN 21	65.68	0.00	18.86	0.09	0.00	0.00	0.15	4.52	10.88	100.16	60.8	0.7	38.4
GM-JJ-10A SAN 21	65.79	0.00	18.77	0.09	0.00	0.00	0.15	4.61	10.83	100.27	60.3	0.7	39.0
GM-JJ-10A SAN 21	65.81	0.00	18.77	0.08	0.01	0.01	0.13	4.51	10.86	100.16	60.9	0.6	38.4
GM-JJ-10A SAN 21	65.69	0.00	18.71	0.08	0.02	0.00	0.16	4.52	10.83	99.95	60.7	0.7	38.5
GM-JJ-10A SAN 21	65.63	0.00	18.87	0.05	0.00	0.00	0.13	4.47	10.76	99.90	60.9	0.6	38.5
GM-JJ-10A SAN 21	65.75	0.00	18.94	0.09	0.00	0.00	0.17	4.54	10.92	100.39	60.8	0.8	38.5
GM-JJ-10A SAN 21	66.01	0.00	18.83	0.09	0.01	0.00	0.16	4.53	10.86	100.44	60.7	0.8	38.5
GM-JJ-10A SAN 21	65.89	0.00	18.80	0.08	0.00	0.00	0.14	4.52	10.96	100.35	61.1	0.6	38.3
GM-JJ-10A SAN 21	65.92	0.00	18.79	0.07	0.00	0.00	0.15	4.53	10.82	100.26	60.7	0.7	38.6
GM-JJ-10A SAN 21	65.90	0.00	18.76	0.08	0.00	0.00	0.13	4.50	10.88	100.24	61.0	0.6	38.4
GM-JJ-10A SAN 21	66.19	0.00	18.92	0.07	0.00	0.00	0.15	4.46	10.99	100.74	61.4	0.7	37.9
GM-JJ-10A SAN 21	65.97	0.00	18.83	0.08	0.02	0.01	0.12	4.48	11.00	100.51	61.4	0.5	38.0
GM-JJ-10A SAN 21	66.06	0.00	18.93	0.07	0.00	0.00	0.14	4.48	10.95	100.63	61.3	0.6	38.1
GM-JJ-10A SAN 21	66.26	0.00	18.99	0.09	0.01	0.00	0.15	4.54	10.97	101.02	61.0	0.7	38.3

	GM-JJ-10A SAN 22	65.59	0.00	18.77	0.08	0.00	0.00	0.14	4.49	10.90	99.95	61.1	0.7	38.2
	GM-JJ-10A SAN 22	65.72	0.00	18.84	0.09	0.02	0.00	0.15	4.48	10.79	100.07	60.9	0.7	38.4
	GM-JJ-10A SAN 22	65.73	0.00	18.83	0.06	0.00	0.00	0.15	4.58	10.87	100.17	60.6	0.7	38.7
	GM-JJ-10A SAN 22	66.03	0.01	18.86	0.08	0.00	0.00	0.15	4.50	10.79	100.39	60.8	0.7	38.5
	GM-JJ-10A SAN 22	65.74	0.00	18.89	0.09	0.00	0.00	0.14	4.49	10.87	100.16	61.1	0.7	38.3
	GM-JJ-10A SAN 22	65.49	0.01	18.70	0.07	0.03	0.00	0.14	4.48	10.79	99.70	60.9	0.7	38.4
	GM-JJ-10A SAN 22	65.66	0.00	18.71	0.07	0.00	0.00	0.15	4.56	10.84	99.99	60.6	0.7	38.7
	GM-JJ-10A SAN 22	65.93	0.00	18.86	0.09	0.00	0.00	0.15	4.55	10.86	100.43	60.7	0.7	38.6
	GM-JJ-10A SAN 22	65.82	0.00	18.67	0.09	0.01	0.00	0.15	4.46	10.79	99.98	61.0	0.7	38.3
	GM-JJ-10A SAN 22	66.07	0.01	18.87	0.06	0.00	0.00	0.14	4.44	10.92	100.48	61.4	0.7	37.9
	GM-JJ-10A SAN 22	66.18	0.00	18.69	0.05	0.00	0.00	0.16	4.50	10.92	100.51	61.0	0.8	38.2
	GM-JJ-10A SAN 22	65.91	0.00	18.77	0.10	0.02	0.00	0.13	4.42	10.97	100.30	61.6	0.6	37.7
	GM-JJ-10A SAN 22	65.66	0.01	18.93	0.07	0.01	0.00	0.14	4.43	10.98	100.25	61.6	0.7	37.7
	GM-JJ-10A SAN 22	66.30	0.01	18.73	0.05	0.00	0.00	0.12	4.49	10.88	100.57	61.1	0.6	38.3
	GM-JJ-10A SAN 22	65.54	0.00	18.76	0.07	0.00	0.00	0.20	4.58	10.79	99.93	60.2	0.9	38.9
	GM-JJ-10A SAN 22	65.87	0.00	18.85	0.11	0.00	0.00	0.14	4.54	10.88	100.34	60.8	0.7	38.5
	GM-JJ-10A SAN 22	66.40	0.00	18.82	0.08	0.01	0.00	0.13	4.48	11.09	101.03	61.6	0.6	37.8
	Average	**65.82**	**0.00**	**18.79**	**0.08**	**0.01**	**0.00**	**0.14**	**4.51**	**10.88**	**100.22**	**61.0**	**0.7**	**38.4**
	Standard Deviation	**0.27**	**0.00**	**0.10**	**0.01**	**0.03**	**0.00**	**0.02**	**0.08**	**0.13**	**0.36**	**0.67**	**0.1**	**0.6**
GM-07 (OL) Sanidine	GM-07_Feld_1-2	66.63	0.00	18.80	0.09	0.00	0.00	0.14	4.87	10.34	100.83	57.9	0.7	41.4
	GM-07_Feld_1-3	66.49	0.01	18.77	0.09	0.00	0.00	0.19	4.95	10.26	100.74	57.2	0.9	41.9
	GM-07_Feld_4-1	66.84	0.02	18.57	0.08	0.00	0.00	0.17	4.81	10.42	100.90	58.3	0.8	40.9

GM-07_Feld_4-2	66.54	0.00	18.92	0.09	0.00	0.00	0.17	4.88	10.50	101.08	58.1	0.8	41.1
GM-07_Feld_4-3	66.47	0.00	18.76	0.08	0.00	0.00	0.18	4.81	10.56	100.83	58.6	0.9	40.6
GM-07_Feld_5-1	66.08	0.01	18.58	0.11	0.00	0.00	0.13	4.61	10.46	99.96	59.5	0.6	39.8
GM-07_Feld_5-2	66.58	0.01	18.97	0.09	0.00	0.00	0.19	4.81	10.45	101.09	58.3	0.9	40.8
GM-07_Feld_5-3	66.92	0.00	18.96	0.10	0.01	0.00	0.11	4.76	10.62	101.47	59.2	0.5	40.3
GM-07_Feld_6-1	66.63	0.00	18.89	0.07	0.00	0.00	0.16	4.81	10.57	101.13	58.6	0.8	40.6
GM-07_Feld_6-3	66.17	0.00	18.59	0.08	0.01	0.00	0.13	4.61	10.79	100.37	60.3	0.6	39.1
GM-07_Feld_6-4	66.60	0.01	18.77	0.08	0.00	0.00	0.21	4.89	10.38	100.93	57.7	1.0	41.3
GM-07_Feld_7-1	66.71	0.02	18.96	0.07	0.00	0.00	0.19	4.71	10.68	101.34	59.3	0.9	39.8
GM-07_Feld_7-2	66.46	0.00	18.88	0.08	0.00	0.00	0.17	4.95	10.16	100.69	57.0	0.8	42.2
GM-07_Feld_7-3	66.20	0.00	18.90	0.08	0.00	0.00	0.15	4.78	10.50	100.59	58.7	0.7	40.6
GM-07_Feld_16-1	66.36	0.00	18.75	0.09	0.02	0.00	0.15	4.62	10.80	100.77	60.2	0.7	39.2
GM-07_Feld_16-2	66.42	0.00	18.78	0.12	0.01	0.00	0.14	4.80	10.59	100.84	58.8	0.7	40.5
GM-07_Feld_19-1	66.59	0.01	18.83	0.11	0.00	0.00	0.17	4.86	10.47	101.03	58.2	0.8	41.0
GM-07_Feld_19-2	65.96	0.00	18.71	0.09	0.00	0.01	0.16	4.72	10.64	100.29	59.3	0.7	40.0
GM-07_Feld_19-3	66.63	0.00	18.66	0.07	0.00	0.00	0.15	4.83	10.38	100.70	58.2	0.7	41.1
GM-07_Feld_21-3	65.88	0.00	19.70	0.07	0.00	0.00	0.14	4.49	10.48	100.75	60.1	0.7	39.2
GM-07_Feld_22-1	66.47	0.00	18.91	0.08	0.01	0.00	0.18	4.95	10.47	101.06	57.7	0.8	41.5
GM-07_Feld_22-2	65.37	0.01	18.69	0.09	0.00	0.00	0.16	4.53	10.64	99.44	60.3	0.7	39.0
GM-07_Feld_23-2	66.76	0.00	18.74	0.08	0.02	0.00	0.18	4.83	10.48	101.09	58.3	0.9	40.9
GM-07_Feld_23-3	66.47	0.00	18.84	0.10	0.00	0.00	0.17	4.78	10.54	100.90	58.7	0.8	40.5
GM-07_Feld_23-4	66.33	0.00	18.91	0.08	0.00	0.00	0.17	4.70	10.58	100.75	59.2	0.8	40.0
GM-07_Feld_26-1	66.34	0.01	18.60	0.11	0.02	0.00	0.19	4.76	10.58	100.60	58.9	0.9	40.2

	GM-07_Feld_26-2	66.65	0.01	18.72	0.09	0.01	0.00	0.16	4.74	10.52	100.89	58.9	0.7	40.4
	GM-07_Feld_26-3	65.86	0.00	18.70	0.11	0.00	0.00	0.17	4.67	10.46	99.95	59.1	0.8	40.1
	GM-07_Feld_26-4	66.08	0.00	19.05	0.09	0.02	0.01	0.17	4.70	10.43	100.55	58.9	0.8	40.3
	GM-07_Feld_27-1	66.50	0.00	18.80	0.07	0.01	0.00	0.16	4.79	10.49	100.80	58.6	0.7	40.7
	GM-07_Feld_27-2	64.19	0.00	19.87	0.08	0.01	0.00	0.17	4.35	10.30	98.96	60.4	0.8	38.8
	GM-07_Feld_27-3	66.33	0.00	18.77	0.10	0.00	0.00	0.16	4.74	10.63	100.72	59.2	0.7	40.1
	GM-07_Feld_28-2	66.70	0.00	18.82	0.09	0.00	0.00	0.17	4.91	10.57	101.24	58.2	0.8	41.0
	GM-07_Feld_28-3	66.87	0.00	18.75	0.08	0.01	0.00	0.16	4.74	10.68	101.28	59.3	0.7	40.0
	GM-07_Feld_29-1	66.49	0.00	19.01	0.07	0.00	0.00	0.17	4.76	10.47	100.96	58.7	0.8	40.5
	GM-07_Feld_29-2	66.59	0.00	18.69	0.09	0.00	0.01	0.18	4.86	10.55	100.96	58.3	0.8	40.8
	Average	**66.36**	**0.00**	**18.85**	**0.09**	**0.00**	**0.00**	**0.16**	**4.76**	**10.51**	**100.74**	**58.8**	**0.8**	**40.5**
	Standard Deviation	**0.49**	**0.01**	**0.26**	**0.01**	**0.01**	**0.00**	**0.02**	**0.13**	**0.13**	**0.50**	**0.83**	**0.1**	**0.8**
GM-20 (OT) Sanidine	GM_20_San_2_1	65.14		18.35	0.09	0.00	0.00	0.18	4.11	11.57	99.43	64.4	0.8	34.8
	GM_20_San_2_2	64.77		18.35	0.08	0.01	0.00	0.18	4.25	11.48	99.10	63.5	0.8	35.7
	GM_20_San_2_3	65.39		18.51	0.07	0.01	0.00	0.18	4.28	11.46	99.89	63.3	0.8	35.9
	GM_20_San_2_4	65.59		18.54	0.08	0.00	0.00	0.16	4.33	11.44	100.12	63.0	0.7	36.2
	GM_20_San_2_5	65.75		18.52	0.07	0.00	0.00	0.16	4.30	11.53	100.34	63.4	0.8	35.9
	GM_20_San_2_6	65.51		18.65	0.09	0.00	0.00	0.16	4.46	11.21	100.08	61.9	0.8	37.4
	GM_20_San_2_8	65.07		18.46	0.07	0.00	0.00	0.17	4.42	11.26	99.45	62.1	0.8	37.1
	GM_20_San_2_12	65.74		18.52	0.09	0.00	0.00	0.17	4.27	11.43	100.22	63.3	0.8	35.9
	GM_20_San_2_13	65.78		18.78	0.10	0.00	0.00	0.21	4.38	11.39	100.64	62.5	1.0	36.5
	GM_20_San_2_14	65.81		18.66	0.10	0.00	0.00	0.18	4.23	11.52	100.51	63.6	0.8	35.5
	GM_20_San_2_18	65.81		18.61	0.10	0.00	0.00	0.16	4.26	11.42	100.35	63.4	0.7	35.9
	GM_20_San_2_19	65.60		18.70	0.11	0.02	0.00	0.19	4.31	11.24	100.17	62.6	0.9	36.5
	GM_20_San_2_20	65.93		18.69	0.10	0.00	0.00	0.14	4.25	11.48	100.59	63.6	0.7	35.8
	GM_20_San_2_21	65.76		18.59	0.10	0.01	0.00	0.16	4.30	11.29	100.21	62.9	0.7	36.4
	GM_20_San_2_22	65.67		18.55	0.12	0.00	0.00	0.15	4.14	11.68	100.29	64.6	0.7	34.8

	GM_20_San_2_23	65.73	18.54	0.10	0.02	0.00	0.16	4.19	11.60	100.32	64.1	0.7	35.2
	GM_20_San_2_24	65.66	18.50	0.09	0.00	0.00	0.17	4.46	11.22	100.07	61.9	0.8	37.3
	GM_20_San_2_25	65.37	18.59	0.08	0.00	0.00	0.15	4.61	10.91	99.69	60.5	0.7	38.8
	GM_20_San_2_30	65.11	18.28	0.10	0.00	0.00	0.17	4.48	10.93	99.06	61.1	0.8	38.1
	GM_20_San_2_32	65.36	18.62	0.08	0.00	0.00	0.18	4.33	11.26	99.82	62.6	0.8	36.6
	GM_20_San_2_33	65.48	18.65	0.09	0.02	0.00	0.18	4.31	11.38	100.12	62.9	0.9	36.2
	GM_20_San_2_34	65.04	18.41	0.08	0.00	0.00	0.18	4.20	11.41	99.33	63.6	0.8	35.6
	GM_20_San_2_35	65.14	18.33	0.10	0.00	0.00	0.18	4.20	11.38	99.32	63.5	0.9	35.6
	GM_20_San_2_36	65.45	18.60	0.10	0.00	0.00	0.18	4.20	11.47	99.98	63.7	0.8	35.4
	GM_20_San_2_37	65.58	18.64	0.08	0.01	0.00	0.16	4.57	10.87	99.90	60.6	0.7	38.7
	GM_20_San_2_38	65.21	18.62	0.09	0.00	0.00	0.18	4.19	11.58	99.83	64.0	0.8	35.2
	GM_20_San_2_39	65.82	18.64	0.08	0.00	0.00	0.17	4.23	11.37	100.32	63.3	0.8	35.8
	GM_20_San_2_40	65.46	18.60	0.08	0.00	0.00	0.17	4.34	11.20	99.86	62.4	0.8	36.8
	GM_20_San_2_43	65.86	18.77	0.09	0.00	0.00	0.19	4.38	11.29	100.58	62.3	0.9	36.8
	GM_20_San_2_44	65.53	18.62	0.10	0.02	0.00	0.20	4.32	11.13	99.91	62.3	0.9	36.7
	GM_20_San_2_45	65.43	18.72	0.09	0.00	0.00	0.20	4.43	11.14	99.99	61.8	0.9	37.3
	GM_20_San_2_46	65.51	18.78	0.10	0.00	0.00	0.15	4.56	11.03	100.12	61.0	0.7	38.3
	GM_20_San_2_47	65.31	18.45	0.08	0.00	0.00	0.17	4.62	10.79	99.42	60.1	0.8	39.1
	GM_20_San_2_48	65.40	18.56	0.09	0.00	0.01	0.16	4.53	10.95	99.68	61.0	0.7	38.3
	GM_20_San_2_49	65.06	18.49	0.10	0.00	0.01	0.19	4.19	11.39	99.43	63.6	0.9	35.5
	Average	**65.48**	**18.57**	**0.09**	**0.00**	**0.00**	**0.17**	**4.33**	**11.31**	**99.95**	**62.7**	**0.8**	**36.5**
	Standard Deviation	**0.28**	**0.13**	**0.01**	**0.01**	**0.00**	**0.02**	**0.14**	**0.22**	**0.43**	**1.15**	**0.1**	**1.2**
GM-16(YE) Sanidine	GM_16_San_1_1	65.09	18.47	0.08	0.00	0.00	0.16	3.92	11.83	99.56	66.0	0.8	33.2
	GM_16_San_1_2	65.20	18.45	0.08	0.00	0.00	0.17	3.82	11.99	99.71	66.8	0.8	32.4
	GM_16_San_1_3	65.71	18.82	0.07	0.01	0.00	0.17	3.74	12.26	100.78	67.8	0.8	31.4
	GM_16_San_1_4	65.22	18.61	0.11	0.01	0.00	0.19	3.78	12.16	100.08	67.4	0.9	31.8
	GM_16_San_1_5	64.94	18.48	0.09	0.00	0.00	0.17	3.85	12.08	99.60	66.9	0.8	32.3
	GM_16_San_1_6	65.42	18.41	0.07	0.01	0.00	0.18	3.73	12.10	99.91	67.5	0.9	31.6
	GM_16_San_1_7	65.38	18.62	0.08	0.00	0.00	0.17	3.80	12.08	100.15	67.1	0.8	32.1
	GM_16_San_1_8	65.09	18.74	0.11	0.00	0.00	0.19	3.80	12.10	100.02	67.1	0.9	32.0
	GM_16_San_1_9	65.46	18.56	0.09	0.00	0.00	0.18	3.83	12.09	100.20	67.0	0.8	32.2
	GM_16_San_1_10	65.90	18.71	0.06	0.01	0.01	0.17	3.83	12.08	100.77	66.9	0.8	32.3

GM_16_San_1_12	65.47	18.61	0.07	0.01	0.00	0.17	3.88	11.99	100.20	66.5	0.8	32.7
GM_16_San_1_14	65.07	18.45	0.08	0.00	0.00	0.16	3.83	11.87	99.46	66.6	0.8	32.6
GM_16_San_1_15	64.98	18.41	0.09	0.00	0.00	0.17	3.83	11.94	99.40	66.7	0.8	32.5
GM_16_San_1_16	65.51	18.63	0.09	0.02	0.01	0.18	3.84	11.98	100.26	66.7	0.8	32.5
GM_16_San_1_17	65.23	18.52	0.10	0.00	0.00	0.19	3.90	11.92	99.83	66.2	0.9	32.9
GM_16_San_1_18	65.41	18.64	0.10	0.00	0.00	0.18	3.82	12.06	100.21	67.0	0.9	32.2
GM_16_San_1_19	65.13	18.40	0.10	0.01	0.00	0.19	3.81	12.10	99.74	67.0	0.9	32.1
GM_16_San_1_20	65.22	18.69	0.06	0.01	0.00	0.18	3.83	11.97	99.96	66.7	0.8	32.4
GM_16_San_1_21	64.72	18.29	0.07	0.01	0.00	0.19	3.87	11.91	99.06	66.3	0.9	32.8
GM_16_San_1_22	64.72	18.06	0.08	0.01	0.01	0.17	3.84	11.68	98.57	66.1	0.8	33.1
GM_16_San_1_23	64.99	18.18	0.08	0.01	0.00	0.15	3.81	11.93	99.14	66.9	0.7	32.4
GM_16_San_1_24	65.33	18.65	0.10	0.00	0.00	0.17	3.83	12.11	100.21	67.0	0.8	32.2
GM_16_San_1_25	65.57	18.49	0.10	0.00	0.00	0.18	3.87	12.00	100.20	66.5	0.8	32.6
GM_16_San_1_26	65.57	18.66	0.08	0.00	0.00	0.18	3.84	12.16	100.48	67.0	0.8	32.2
GM_16_San_1_27	65.22	18.38	0.09	0.00	0.00	0.17	3.81	12.05	99.71	67.0	0.8	32.2
GM_16_San_1_28	65.30	18.45	0.09	0.00	0.00	0.18	3.82	12.03	99.83	66.9	0.8	32.3
GM_16_San_1_29	65.55	18.54	0.07	0.00	0.00	0.17	3.81	12.06	100.18	67.1	0.8	32.2
GM_16_San_1_30	65.07	18.46	0.07	0.00	0.00	0.17	3.80	11.97	99.53	66.9	0.8	32.3
GM_16_San_1_1	65.50	18.45	0.07	0.00	0.00	0.18	3.89	11.90	99.96	66.3	0.8	32.9
GM_16_San_1_2	65.44	18.43	0.10	0.01	0.00	0.17	3.82	11.88	99.85	66.6	0.8	32.6
GM_16_San_1_3	65.83	18.58	0.07	0.01	0.00	0.18	4.03	11.83	100.52	65.3	0.8	33.8
GM_16_San_1_5	65.09	18.33	0.07	0.00	0.00	0.16	3.94	11.68	99.26	65.6	0.8	33.6
GM_16_San_1_6	65.49	18.30	0.09	0.00	0.00	0.19	4.03	11.56	99.63	64.7	0.9	34.4
GM_16_San_1_7	64.51	18.20	0.07	0.00	0.01	0.17	3.84	11.75	98.53	66.3	0.8	32.9
GM_16_San_1_8	65.15	18.37	0.08	0.00	0.00	0.19	3.89	11.86	99.53	66.1	0.9	33.0
GM_16_San_1_9	65.10	18.47	0.08	0.00	0.00	0.20	3.99	11.72	99.56	65.3	0.9	33.8
GM_16_San_1_10	65.37	18.48	0.06	0.00	0.00	0.17	3.88	11.81	99.76	66.2	0.8	33.0
GM_16_San_1_11	65.41	18.79	0.06	0.00	0.00	0.17	4.11	11.63	100.15	64.5	0.8	34.7
GM_16_San_1_12	65.37	18.55	0.07	0.00	0.01	0.16	3.96	11.88	99.99	65.9	0.8	33.4
GM_16_San_1_13	65.30	18.46	0.09	0.02	0.00	0.18	3.89	11.79	99.73	66.0	0.8	33.1
GM_16_San_1_14	65.42	18.48	0.06	0.01	0.00	0.17	3.96	11.75	99.83	65.6	0.8	33.6
GM_16_San_1_15	65.39	18.45	0.10	0.02	0.00	0.17	3.84	11.99	99.95	66.7	0.8	32.5
GM_16_San_1_16	65.32	18.46	0.08	0.00	0.00	0.17	3.79	11.98	99.78	67.0	0.8	32.2
GM_16_San_1_17	65.44	18.59	0.09	0.01	0.00	0.17	4.04	11.82	100.15	65.3	0.8	33.9
GM_16_San_1_18	65.46	18.59	0.09	0.00	0.00	0.16	3.96	11.81	100.05	65.7	0.8	33.5

	GM_16_San_1_19	65.74	18.72	0.10	0.00	0.00	0.19	4.03	11.92	100.68	65.5	0.9	33.7
	GM_16_San_1_21	65.45	18.52	0.10	0.00	0.00	0.18	3.94	11.96	100.14	66.1	0.8	33.1
	GM_16_San_1_22	65.01	18.49	0.07	0.00	0.00	0.16	3.85	12.09	99.67	66.9	0.7	32.4
	GM_16_San_1_23	65.57	18.49	0.08	0.00	0.00	0.17	3.76	12.11	100.17	67.4	0.8	31.8
	GM_16_San_1_24	65.56	18.48	0.07	0.00	0.00	0.18	3.82	12.08	100.19	67.0	0.8	32.2
	GM_16_San_1_25	65.96	18.81	0.07	0.00	0.00	0.17	3.79	12.18	100.98	67.4	0.8	31.8
	GM_16_San_1_26	65.29	18.62	0.07	0.00	0.01	0.16	3.88	12.09	100.11	66.7	0.8	32.5
	GM_16_San_1_29	65.61	18.62	0.07	0.00	0.00	0.18	3.86	12.07	100.38	66.7	0.8	32.5
	GM_16_San_1_30	65.45	18.57	0.08	0.02	0.00	0.17	4.01	11.77	100.06	65.4	0.8	33.8
	GM_16_San_1_32	65.41	18.41	0.11	0.00	0.00	0.15	4.02	11.59	99.68	65.0	0.7	34.3
	Average	**65.33**	**18.51**	**0.08**	**0.00**	**0.00**	**0.17**	**3.87**	**11.95**	**99.91**	**66.5**	**0.8**	**32.7**
	Standard Deviation	**0.28**	**0.15**	**0.01**	**0.01**	**0.00**	**0.01**	**0.08**	**0.16**	**0.47**	**0.73**	**0.0**	**0.7**
GM-13 (YG) Sanidine	GM_13_San_1_14	65.73	18.75	0.10	0.02	0.00	0.18	4.04	11.52	100.35	64.6	0.9	34.5
	GM_13_San_1_15	65.45	18.82	0.07	0.00	0.00	0.21	4.08	11.50	100.11	64.3	1.0	34.7
	GM_13_San_1_40	66.07	18.67	0.09	0.01	0.00	0.16	4.12	11.37	100.48	64.0	0.8	35.2
	GM_13_San_1_42	65.99	18.81	0.08	0.02	0.00	0.16	4.02	11.49	100.55	64.8	0.8	34.4
	GM_13_San_1_43	65.87	18.57	0.12	0.00	0.00	0.17	3.85	11.62	100.18	66.0	0.8	33.2
	GM_13_San_1_44	65.49	18.30	0.07	0.00	0.00	0.21	3.84	11.78	99.68	66.2	1.0	32.8
	GM_13_San_1_45	65.83	18.52	0.10	0.02	0.01	0.21	3.90	11.75	100.33	65.8	1.0	33.2
	GM_13_San_1_46	65.54	18.71	0.08	0.01	0.00	0.18	3.94	11.65	100.09	65.5	0.8	33.7
	GM_13_San_1_47	65.27	18.65	0.10	0.02	0.00	0.19	3.83	11.82	99.87	66.4	0.9	32.7
	GM_13_San_1_48	65.35	18.42	0.08	0.02	0.00	0.19	3.85	11.83	99.72	66.3	0.9	32.8
	GM_13_San_1_50	65.38	18.51	0.11	0.01	0.00	0.18	3.89	11.76	99.84	66.0	0.9	33.1
	GM_13_San_3_1	65.30	18.61	0.09	0.01	0.00	0.18	3.81	12.40	100.40	67.6	0.8	31.6
	GM_13_San_3_2	64.93	18.60	0.09	0.00	0.00	0.17	3.77	12.36	99.91	67.8	0.8	31.4
	GM_13_San_3_3	65.01	18.55	0.07	0.02	0.00	0.18	3.79	12.33	99.93	67.6	0.8	31.6
	GM_13_San_3_4	65.29	18.52	0.07	0.02	0.00	0.20	3.82	12.28	100.20	67.3	0.9	31.8
	GM_13_San_3_5	65.41	18.58	0.11	0.00	0.00	0.21	3.87	12.25	100.42	66.9	1.0	32.2
	GM_13_San_3_6	65.37	18.78	0.07	0.00	0.00	0.19	3.88	12.25	100.53	66.9	0.9	32.2
	GM_13_San_3_8	65.01	18.67	0.08	0.00	0.00	0.18	3.84	12.25	100.03	67.2	0.8	32.0
	GM_13_San_3_9	65.27	18.53	0.09	0.00	0.00	0.18	3.88	12.29	100.25	67.0	0.8	32.2
	GM_13_San_3_10	65.27	18.52	0.06	0.01	0.00	0.16	3.81	12.22	100.04	67.3	0.7	31.9

	GM_13_San_3_11	65.46		18.66	0.05	0.01	0.00	0.18	3.74	12.38	100.49	67.9	0.8	31.2
	GM_13_San_3_12	65.20		18.59	0.08	0.00	0.01	0.17	3.82	12.25	100.10	67.3	0.8	31.9
	GM_13_San_3_13	65.26		18.68	0.07	0.02	0.00	0.18	3.82	12.39	100.41	67.5	0.8	31.7
	GM_13_San_3_14	65.49		18.69	0.07	0.00	0.00	0.19	3.86	12.42	100.71	67.3	0.9	31.8
	GM_13_San_3_15	65.31		18.45	0.08	0.00	0.00	0.19	3.81	12.41	100.23	67.6	0.9	31.5
	GM_13_San_3_16	65.54		18.73	0.09	0.00	0.00	0.17	3.81	12.29	100.62	67.5	0.8	31.7
	GM_13_San_3_17	65.64		18.64	0.08	0.00	0.00	0.19	3.85	12.25	100.66	67.1	0.9	32.1
	GM_13_San_3_18	65.31		18.75	0.08	0.00	0.00	0.18	3.84	12.13	100.29	66.9	0.9	32.2
	GM_13_San_3_19	65.32		18.57	0.09	0.02	0.00	0.18	3.82	12.32	100.32	67.4	0.8	31.8
	GM_13_San_3_20	65.42		18.58	0.09	0.00	0.00	0.18	3.73	12.39	100.37	68.0	0.8	31.1
	GM_13_San_3_21	64.90		18.23	0.10	0.01	0.00	0.16	3.78	12.23	99.40	67.5	0.8	31.7
	GM_13_San_3_22	65.51		18.70	0.06	0.00	0.00	0.19	3.82	12.27	100.54	67.2	0.9	31.9
	GM_13_San_3_23	65.39		18.67	0.10	0.01	0.00	0.18	3.82	12.26	100.43	67.3	0.8	31.9
	GM_13_San_3_24	64.82		18.34	0.10	0.00	0.00	0.19	3.82	12.11	99.38	67.0	0.9	32.1
	GM_13_San_3_25	65.18		18.61	0.09	0.00	0.00	0.17	3.82	12.37	100.23	67.6	0.8	31.7
	Average	**65.39**		**18.60**	**0.08**	**0.01**	**0.00**	**0.18**	**3.86**	**12.09**	**100.20**	**66.8**	**0.8**	**32.4**
	Standard Deviation	**0.28**		**0.14**	**0.02**	**0.01**	**0.00**	**0.01**	**0.09**	**0.33**	**0.33**	**1.05**	**0.1**	**1.0**
GM-10(YO)	GM-10-2 San 1-1 Core	65.51	0.00	18.62	0.08	0.01	0.00	0.19	3.97	11.46	99.84	64.9	0.9	34.2
Sanidine	GM-10-2 san Core 1-2	65.45	0.00	18.47	0.09	0.00	0.00	0.19	3.91	11.44	99.53	65.2	0.9	33.9
	GM-10-2 san Core 1-3	65.63	0.00	18.62	0.08	0.00	0.00	0.18	3.98	11.54	100.04	65.1	0.9	34.1
	GM-10-2 san Core 1-4	65.53	0.01	18.52	0.06	0.01	0.00	0.23	3.91	11.58	99.84	65.4	1.1	33.5
	GM-10-2 san Core 1-5	65.53	0.02	18.61	0.10	0.00	0.00	0.19	3.96	11.50	99.90	65.1	0.9	34.0
	GM-10-2 san Core 4-1	65.53	0.00	18.53	0.04	0.02	0.00	0.20	3.93	11.46	99.71	65.1	0.9	33.9
	GM-10-2 san Core 4-2	65.70	0.01	18.46	0.08	0.00	0.00	0.18	3.94	11.54	99.91	65.3	0.9	33.9
	GM-10-2 san Core 4-3	65.64	0.01	18.47	0.07	0.01	0.00	0.19	3.94	11.37	99.69	64.9	0.9	34.2
	GM-10_Feld_6-3	66.22	0.00	18.76	0.11	0.00	0.00	0.21	4.12	11.82	101.24	64.8	0.9	34.3
	GM-10_Feld_6-4	66.13	0.01	18.64	0.07	0.01	0.00	0.18	3.97	11.72	100.73	65.5	0.8	33.7

GM-10_Feld_8-2	65.50	0.00	18.82	0.06	0.00	0.00	0.18	4.03	11.59	100.16	64.9	0.8	34.3
GM-10_Feld_8-3	66.31	0.00	18.59	0.09	0.00	0.00	0.21	3.96	11.84	100.99	65.6	1.0	33.4
GM-10_Feld_9-1	66.41	0.01	18.86	0.09	0.00	0.00	0.24	4.13	11.73	101.46	64.4	1.1	34.5
GM-10_Feld_9-2	66.22	0.02	18.77	0.09	0.01	0.00	0.21	4.07	11.52	100.90	64.5	1.0	34.6
GM-10_Feld_9-3	66.28	0.02	18.67	0.08	0.01	0.00	0.18	3.98	11.95	101.15	65.8	0.8	33.3
GM-10_Feld_11-1	66.12	0.00	18.78	0.09	0.00	0.00	0.19	4.03	11.66	100.87	64.9	0.9	34.2
GM-10_Feld_11-2	66.25	0.00	18.71	0.09	0.00	0.00	0.19	3.98	11.74	100.94	65.4	0.9	33.7
GM-10_Feld_11-3	66.36	0.00	18.96	0.09	0.01	0.00	0.24	4.03	11.46	101.14	64.4	1.1	34.4
GM-10_Feld_12-1	64.89	0.00	18.78	0.07	0.00	0.00	0.20	3.74	11.70	99.36	66.7	1.0	32.4
GM-10_Feld_13-2	66.18	0.00	18.73	0.09	0.00	0.00	0.18	3.91	11.87	100.91	66.1	0.8	33.1
GM-10_Feld_13-3	66.47	0.00	18.78	0.11	0.00	0.00	0.18	3.91	11.92	101.36	66.1	0.9	33.0
GM-10_Feld_15-1	66.34	0.00	18.66	0.07	0.00	0.00	0.17	4.11	11.60	100.94	64.5	0.8	34.7
GM-10_Feld_15-2	65.56	0.01	18.85	0.08	0.01	0.01	0.20	3.97	11.64	100.33	65.2	0.9	33.8
GM-10_Feld_15-3	66.01	0.00	18.84	0.08	0.00	0.00	0.18	3.95	11.55	100.59	65.2	0.9	33.9
GM-10_Feld_16-2	66.54	0.01	18.86	0.08	0.00	0.00	0.17	4.03	11.61	101.28	64.9	0.8	34.3
GM-10_Feld_16-3	66.15	0.01	18.75	0.09	0.01	0.00	0.20	4.01	11.71	100.92	65.1	0.9	33.9
GM-10_Feld_17-1	66.55	0.00	18.77	0.10	0.01	0.00	0.19	4.00	11.73	101.33	65.3	0.9	33.8
GM-10_Feld_17-3	66.69	0.00	18.99	0.09	0.01	0.00	0.20	3.80	11.72	101.48	66.4	0.9	32.7
GM-10_Feld_18-1	65.99	0.00	18.83	0.08	0.01	0.00	0.18	3.99	11.80	100.88	65.5	0.8	33.7
GM-10_Feld_18-3	66.25	0.00	18.76	0.08	0.01	0.00	0.19	3.99	11.79	101.07	65.4	0.9	33.7
GM-10_Feld_24-1	66.31	0.00	18.89	0.12	0.02	0.01	0.17	4.00	11.83	101.35	65.5	0.8	33.7
GM-10_Feld_24-2	66.35	0.00	19.01	0.10	0.00	0.00	0.19	3.99	11.79	101.42	65.5	0.9	33.6
GM-10_Feld_24-3	66.49	0.00	18.84	0.08	0.01	0.00	0.17	3.95	11.76	101.27	65.7	0.8	33.5

	GM-10_Feld_25-1	65.96	0.01	18.75	0.08	0.00	0.00	0.21	3.86	11.64	100.50	65.8	1.0	33.2
	GM-10_Feld_27-1	66.14	0.01	19.37	0.10	0.00	0.00	0.19	3.94	11.65	101.38	65.5	0.9	33.6
	GM-10_Feld_27-2	65.98	0.01	18.88	0.07	0.00	0.00	0.20	3.93	11.80	100.86	65.8	1.0	33.3
	GM-10_Feld_27-3	66.42	0.01	18.76	0.07	0.01	0.00	0.18	4.02	11.92	101.38	65.6	0.8	33.6
	GM-10_Feld_29-1	66.14	0.00	18.76	0.08	0.00	0.00	0.19	3.99	11.77	100.91	65.4	0.9	33.7
	GM-10_Feld_29-2	66.01	0.00	18.65	0.09	0.00	0.00	0.18	3.93	11.80	100.66	65.8	0.9	33.3
	GM-10_Feld_29-3	66.33	0.00	18.71	0.09	0.00	0.00	0.21	3.98	11.83	101.11	65.5	1.0	33.5
	Average	**66.05**	**0.00**	**18.75**	**0.08**	**0.00**	**0.00**	**0.19**	**3.97**	**11.68**	**100.73**	**65.3**	**0.9**	**33.8**
	Standard Deviation	**0.40**	**0.01**	**0.17**	**0.01**	**0.01**	**0.00**	**0.02**	**0.07**	**0.15**	**0.62**	**0.51**	**0.1**	**0.5**
GM-09(YO) Sanidine	GM-09-1san Core 8-1	65.68	0.01	18.64	0.08	0.00	0.00	0.19	3.99	11.55	100.12	65.0	0.9	34.1
	GM-09-1san Core 8-2	65.98	0.00	18.59	0.08	0.00	0.00	0.18	4.02	11.64	100.48	65.0	0.9	34.1
	GM-09-1san Core 8-3	65.89	0.00	18.64	0.07	0.00	0.00	0.17	4.05	11.73	100.53	65.1	0.8	34.1
	GM-09-1san Core 2-1	65.71	0.01	18.70	0.08	0.00	0.00	0.19	3.99	11.81	100.49	65.5	0.9	33.6
	GM-09-1san Core 2-2	65.83	0.01	18.59	0.08	0.00	0.00	0.18	3.94	11.75	100.36	65.7	0.8	33.5
	GM-09-1san Core 2-3	65.95	0.01	18.68	0.07	0.01	0.00	0.17	3.93	11.81	100.64	65.9	0.8	33.3
	GM-09-1san Core 2-4	65.92	0.02	18.70	0.08	0.02	0.00	0.18	3.99	11.52	100.42	65.0	0.9	34.2
	Average	**65.85**	**0.01**	**18.65**	**0.08**	**0.00**	**0.00**	**0.18**	**3.99**	**11.69**	**100.43**	**65.3**	**0.8**	**33.9**
	Standard Deviation	**0.12**	**0.01**	**0.05**	**0.01**	**0.01**	**0.00**	**0.01**	**0.04**	**0.12**	**0.16**	**0.38**	**0.0**	**0.4**

Table B-0-12 Natural individual biotite analysese (wt%)

Sample	Point	SiO_2	TiO_2	Al_2O_3	FeO	MnO	MgO	CaO	Na_2O	K_2O	BaO	$Total_{initial}$	Mg#
GM-18 (OB)	GM-18_BTE_2_2	34.34	3.54	11.86	28.82	0.60	8.45	0.01	0.52	8.82	0.01	96.96	34
	GM-18_BTE_2_3	36.27	3.68	12.37	25.12	0.55	8.58	0.00	0.53	9.21	0.05	96.35	38
	GM-18_BTE_2_5	36.10	3.85	12.26	25.23	0.56	8.65	0.00	0.55	9.17	0.03	96.37	38
	GM-18_BTE_3_1	36.20	3.86	12.77	25.88	0.52	7.40	0.00	0.53	9.06	0.05	96.25	34
	GM-18_BTE_4_2	35.71	4.04	12.10	25.06	0.57	8.41	0.00	0.51	9.35	0.08	95.81	37
	GM-18_BTE_4_3	35.93	4.03	12.34	25.16	0.56	8.48	0.02	0.51	9.31	0.04	96.37	38
	GM-18_BTE_4_4	36.32	3.74	12.14	25.25	0.56	8.67	0.00	0.50	9.21	0.02	96.40	38
	GM-18_BTE_4_5	36.54	3.87	12.16	24.85	0.54	8.67	0.01	0.52	9.23	0.05	96.45	38
	GM-18_BTE_4_6	36.18	3.78	11.99	25.05	0.56	8.56	0.00	0.51	9.28	0.07	95.97	38
	GM-18_BTE_4_7	36.79	3.83	12.41	25.12	0.56	8.63	0.00	0.51	9.17	0.04	97.07	38
	GM-18_BTE_4_8	36.62	3.73	12.38	24.79	0.54	8.62	0.01	0.52	9.38	0.05	96.64	38
	GM-18_BTE_4_9	35.67	3.88	12.40	25.27	0.55	8.27	0.01	0.52	9.21	0.03	95.81	37
	GM-18_BTE_5_2	34.99	3.84	11.88	26.55	0.54	7.84	0.00	0.57	9.30	0.03	95.55	34
	GM-18_BTE_5_3	34.90	3.80	11.96	26.23	0.55	8.06	0.00	0.55	9.14	0.01	95.17	35
	GM-18_BTE_5_4	35.28	3.79	11.88	26.24	0.56	8.12	0.00	0.53	9.23	0.01	95.64	36
	GM-18_BTE_5_6	35.42	3.80	11.94	25.67	0.57	8.11	0.01	0.54	9.29	0.01	95.36	36
	GM-18_BTE_7_7	35.93	4.02	12.29	25.17	0.54	8.23	0.01	0.49	9.36	0.04	96.08	37
	GM-18_BTE_8_1	35.39	4.06	12.36	25.15	0.58	8.32	0.00	0.53	9.26	0.01	95.64	37
	GM-18_BTE_8_2	35.15	4.07	12.12	25.39	0.55	8.23	0.00	0.50	9.28	0.02	95.31	37
	GM-18_BTE_8_3	35.95	4.01	12.49	25.26	0.55	8.48	0.02	0.54	9.18	0.03	96.50	37
	GM-18_BTE_8_4	35.07	4.06	12.30	25.09	0.54	8.34	0.00	0.52	9.40	0.02	95.35	37
	GM-18_BTE_8_5	35.99	3.96	12.38	25.13	0.56	8.24	0.00	0.50	9.25	0.01	96.03	37
	GM-18_BTE_8_6	35.74	3.55	12.53	24.96	0.53	8.59	0.00	0.54	9.20	0.01	95.65	38
	GM-18_BTE_9_1	35.54	3.21	11.71	26.18	0.59	9.00	0.00	0.53	9.36	0.06	96.17	38
	GM-18_BTE_9_2	36.21	3.12	12.28	25.85	0.54	8.78	0.01	0.57	9.30	0.00	96.63	38
	GM-18_BTE_9_7	35.17	3.78	12.26	27.87	0.62	7.30	0.01	0.50	9.12	0.01	96.63	32
	GM-18_BTE_10_2	36.01	3.83	12.41	25.58	0.55	8.37	0.00	0.53	9.38	0.03	96.69	37
	GM-18_BTE_10_3	36.38	3.69	12.51	25.43	0.58	8.52	0.02	0.50	9.28	0.04	96.96	37
	GM-18_BTE_10_5	35.97	3.82	12.19	26.38	0.55	8.21	0.01	0.52	9.31	0.02	96.98	36
	GM-18_BTE_10_6	35.72	3.80	12.21	25.49	0.54	8.25	0.00	0.50	9.35	0.00	95.86	37
	GM-18_BTE_10_7	36.13	3.87	12.41	25.66	0.53	8.48	0.00	0.52	9.38	0.08	97.06	37
	GM-18_BTE_10_8	36.67	3.63	12.46	25.49	0.56	8.62	0.01	0.51	9.37	0.02	97.33	38
	GM-18_BTE_11_0	36.44	3.51	12.33	24.98	0.54	8.79	0.00	0.54	9.26	0.00	96.39	39
	GM-18_BTE_11_1	35.59	3.63	12.29	25.46	0.53	8.31	0.00	0.52	9.24	0.05	95.61	37
	GM-18_BTE_11_2	35.77	3.67	12.33	25.48	0.53	8.27	0.00	0.54	9.29	0.06	95.94	37
	GM-18_BTE_11_3	36.31	4.06	12.39	25.81	0.54	8.30	0.01	0.51	9.37	0.02	97.33	36
	GM-18_BTE_11_4	35.38	3.71	12.50	25.26	0.56	8.33	0.00	0.52	9.31	0.01	95.58	37
	GM-18_BTE_11_5	36.72	3.55	12.42	24.86	0.55	8.87	0.00	0.51	9.28	0.01	96.78	39
	GM-18_BTE_11_6	36.72	3.53	12.44	24.93	0.54	8.89	0.01	0.55	9.25	0.00	96.87	39

	GM-18_BTE_11_7	36.84	3.50	12.28	24.85	0.54	8.91	0.00	0.50	9.15	0.00	96.57	39
	GM-18_BTE_11_9	36.12	3.57	12.72	24.70	0.54	8.70	0.01	0.54	9.28	0.03	96.18	39
	GM-18_BTE_11_10	35.90	3.88	12.51	25.96	0.56	8.29	0.00	0.53	9.49	0.02	97.15	36
	GM-18_BTE_11_11	36.83	3.46	12.18	25.00	0.57	8.85	0.00	0.55	9.13	0.04	96.60	39
	GM-18_BTE_11_12	36.79	3.53	12.23	24.72	0.55	8.89	0.00	0.54	9.23	0.03	96.52	39
	GM-18_BTE_11_13	36.46	3.51	12.12	25.25	0.55	8.65	0.00	0.50	9.26	0.07	96.35	38
	GM-18_BTE_11_14	36.52	3.50	12.28	24.83	0.55	8.86	0.00	0.52	9.30	0.04	96.39	39
	Average	**35.97**	**3.74**	**12.28**	**25.49**	**0.55**	**8.44**	**0.00**	**0.52**	**9.26**	**0.03**	**96.29**	**37**
	Standard Deviation	**0.59**	**0.22**	**0.22**	**0.77**	**0.02**	**0.35**	**0.01**	**0.02**	**0.11**	**0.02**	**0.57**	**1**
GM-01(OC)	GM-01_BTE_15_7	35.68	4.54	12.94	28.59	0.29	5.31	0.00	0.37	9.10	0.07	96.87	25
	GM-01_BTE_15_8	34.97	4.52	12.48	28.61	0.30	5.35	0.00	0.41	9.06	0.12	95.80	25
	GM-01_BTE_15_9	35.52	4.64	12.80	28.70	0.29	5.35	0.01	0.42	9.24	0.08	97.05	25
	GM-01_BTE_15_10	35.09	4.62	12.63	28.28	0.31	5.26	0.00	0.43	9.16	0.09	95.83	25
	GM-01_BTE_15_11	35.15	4.59	12.49	29.00	0.30	5.27	0.00	0.41	9.23	0.08	96.53	24
	GM-01_BTE_15_12	36.14	4.47	12.81	28.14	0.30	5.12	0.00	0.39	9.10	0.08	96.53	24
	Average	**35.43**	**4.57**	**12.69**	**28.55**	**0.30**	**5.28**	**0.00**	**0.40**	**9.15**	**0.09**	**96.44**	**25**
	Standard Deviation	**0.44**	**0.06**	**0.19**	**0.31**	**0.01**	**0.09**	**0.00**	**0.02**	**0.07**	**0.02**	**0.52**	**0**
GM-JJ-10 (OD)	GM_JJ_10_BTE_1-1	34.93	3.99	12.17	27.57	0.88	6.39	0.04	0.49	9.53	0.03	96.02	29
	GM_JJ_10_BTE_1-2	34.80	3.96	12.19	28.68	0.90	6.62	0.00	0.49	9.36	0.01	97.01	29
	GM_JJ_10_BTE_1-3	35.36	3.91	12.25	27.98	0.90	6.59	0.02	0.48	9.36	0.05	96.90	30
	GM_JJ_10_BTE_1-4	34.77	3.85	12.41	26.86	0.97	5.84	0.27	0.45	9.34	0.03	94.79	28
	GM_JJ_10_BTE_1-5	36.14	3.66	12.76	26.84	0.89	6.14	0.12	0.87	8.91	0.03	96.37	29
	GM_JJ_10_BTE_1-6	34.58	3.88	11.99	27.44	0.92	6.29	0.09	0.47	9.21	0.03	94.89	29
	GM_JJ_10_BTE_1-8	35.19	3.97	12.29	28.08	0.93	6.73	0.19	0.52	9.39	0.04	97.33	30
	GM_JJ_10_BTE_1-9	35.01	3.94	12.14	27.91	0.90	6.74	0.03	0.50	9.42	0.03	96.61	30
	GM_JJ_10_BTE_1-11	35.33	3.86	12.55	27.84	0.86	6.20	0.08	0.38	9.52	0.07	96.68	28
	GM_JJ_10_BTE_1-12	35.62	4.00	12.29	27.94	0.88	6.55	0.01	0.47	9.58	0.04	97.39	29
	GM_JJ_10_BTE_1-13	35.70	3.91	12.56	27.44	0.97	6.57	0.09	0.45	9.40	0.02	97.10	30
	GM_JJ_10_BTE_1-14	35.46	3.99	12.38	28.10	0.88	6.55	0.00	0.51	9.41	0.02	97.28	29
	GM_JJ_10_BTE_1-18	34.90	3.82	12.20	27.10	0.89	5.97	0.31	0.45	9.27	0.07	94.96	28
	GM_JJ_10_BTE_1-19	35.36	3.86	12.72	27.24	0.89	6.25	0.20	0.44	9.31	0.03	96.29	29
	GM_JJ_10_BTE_1-20	35.62	4.00	12.32	28.08	0.88	6.29	0.01	0.47	9.68	0.00	97.35	29
	GM_JJ_10_BTE_1-21	34.77	3.94	12.09	27.91	0.92	6.57	0.19	0.50	9.42	0.05	96.36	30
	GM_JJ_10_BTE_1-22	35.14	4.00	12.21	28.33	0.89	6.69	0.00	0.51	9.50	0.03	97.30	30
	GM_JJ_10_BTE_1-23	34.64	3.87	12.19	27.47	0.88	6.45	0.08	0.50	9.24	0.05	95.36	30
	GM_JJ_10_BTE_2-1	35.12	3.80	12.37	27.73	0.96	6.38	0.01	0.48	9.12	0.01	95.98	29
	GM_JJ_10_BTE_2-2	34.48	3.87	12.23	27.96	0.87	6.25	0.00	0.48	9.31	0.05	95.49	28
	GM_JJ_10_BTE_2-4	35.63	3.75	13.40	27.07	0.89	5.84	0.01	0.35	9.09	0.00	96.04	28
	GM_JJ_10_BTE_2-5	35.23	3.88	12.32	28.04	0.91	6.27	0.04	0.48	9.43	0.02	96.60	29

GM_JJ_10_BTE_2-6	35.04	3.80	12.80	27.53	0.89	6.28	0.01	0.45	9.14	0.03	95.97	29
GM_JJ_10_BTE_2-7	34.85	3.93	12.12	29.55	0.87	5.72	0.00	0.39	9.48	0.04	96.96	26
GM_JJ_10_BTE_2-8	34.85	3.92	12.09	28.50	0.89	6.50	0.00	0.48	9.36	0.06	96.64	29
GM_JJ_10_BTE_2-9	35.45	3.74	13.18	27.34	0.84	5.75	0.03	0.41	9.16	0.05	95.95	27
GM_JJ_10_BTE_2-10	34.82	3.94	12.25	28.31	0.88	6.37	0.00	0.45	9.59	0.05	96.65	29
GM_JJ_10_BTE_2-11	34.36	3.86	12.12	27.78	0.87	6.18	0.02	0.46	9.23	0.07	94.94	28
GM_JJ_10_BTE_2-12	34.58	3.84	12.30	28.32	0.90	6.27	0.00	0.48	9.37	0.04	96.09	28
GM_JJ_10_BTE_2-13	35.18	3.79	12.79	27.34	0.89	6.25	0.07	0.42	9.39	0.01	96.13	29
GM_JJ_10_BTE_2-14	35.04	3.95	12.36	28.34	0.90	6.41	0.01	0.47	9.21	0.04	96.72	29
GM_JJ_10_BTE_2-16	35.31	3.88	12.90	28.25	0.89	6.13	0.01	0.41	9.17	0.00	96.96	28
GM_JJ_10_BTE_2-17	35.08	3.96	12.27	28.26	0.93	6.64	0.00	0.46	9.54	0.02	97.14	30
GM_JJ_10_BTE_2-18	35.40	3.78	13.62	27.18	0.79	5.23	0.06	0.28	8.94	0.06	95.33	26
GM_JJ_10_BTE_2-19	34.52	3.88	11.99	27.57	0.89	6.48	0.01	0.49	9.31	0.02	95.16	30
GM_JJ_10_BTE_2-20	34.75	3.88	12.25	28.29	0.89	6.48	0.00	0.46	9.37	0.00	96.36	29
GM_JJ_10_BTE_2-21	34.94	3.90	12.16	28.19	0.91	6.52	0.01	0.48	9.35	0.03	96.48	29
GM_JJ_10_BTE_2-22	35.18	3.87	12.83	27.60	0.91	6.04	0.02	0.46	9.32	0.08	96.30	28
GM_JJ_10_BTE_2-23	35.12	3.70	12.94	27.28	0.92	6.05	0.14	0.47	8.97	0.04	95.62	28
GM_JJ_10_BTE_3-1	34.85	3.94	12.34	28.16	0.89	6.60	0.00	0.48	9.46	0.02	96.75	29
GM_JJ_10_BTE_3-2	35.10	3.99	12.25	27.93	0.91	6.58	0.01	0.50	9.40	0.05	96.72	30
GM_JJ_10_BTE_3-3	35.03	3.93	12.17	28.05	0.88	6.56	0.03	0.48	9.43	0.03	96.59	29
GM_JJ_10_BTE_3-4	35.05	3.98	12.39	28.29	0.88	6.58	0.01	0.52	9.49	0.03	97.22	29
GM_JJ_10_BTE_3-5	35.10	4.00	12.25	28.22	0.87	6.63	0.00	0.48	9.39	0.02	96.95	30
GM_JJ_10_BTE_3-6	35.06	3.95	12.24	28.39	0.91	6.66	0.00	0.49	9.44	0.05	97.19	29
GM_JJ_10_BTE_3-7	34.73	3.93	12.16	28.99	0.88	5.94	0.02	0.50	9.45	0.00	96.60	27
GM_JJ_10_BTE_3-8	35.05	3.99	12.29	28.33	0.89	6.56	0.00	0.48	9.50	0.03	97.12	29
GM_JJ_10_BTE_3-9	35.75	3.97	12.34	26.56	0.89	6.81	0.01	0.53	9.49	0.04	96.39	31
GM_JJ_10_BTE_3-10	34.83	4.02	12.11	27.99	0.90	6.63	0.02	0.48	9.51	0.00	96.48	30
GM_JJ_10_BTE_3-11	35.11	4.00	12.22	28.40	0.89	6.63	0.01	0.52	9.42	0.07	97.25	29
GM_JJ_10_BTE_3-14	35.50	3.98	12.29	27.94	0.90	6.76	0.01	0.52	9.43	0.03	97.34	30
GM_JJ_10_BTE_3-15	34.34	3.91	12.01	28.86	0.94	7.03	0.01	0.46	9.22	0.06	96.85	30
GM_JJ_10_BTE_3-17	34.85	3.94	12.20	28.36	0.90	6.58	0.01	0.49	9.31	0.03	96.68	29
GM_JJ_10_BTE_3-18	35.05	4.04	12.31	28.37	0.93	6.61	0.00	0.49	9.56	0.03	97.38	29
GM_JJ_10_BTE_4-1	35.59	3.93	12.33	27.81	0.86	6.58	0.00	0.50	9.43	0.03	97.06	30
GM_JJ_10_BTE_4-2	35.51	3.66	13.04	25.96	0.84	5.76	0.21	0.46	8.90	0.08	94.43	28
GM_JJ_10_BTE_4-3	35.09	4.01	12.44	28.25	0.92	6.53	0.03	0.48	9.26	0.04	97.04	29
GM_JJ_10_BTE_4-4	35.21	3.92	12.01	28.20	0.91	6.70	0.03	0.53	9.32	0.04	96.87	30
GM_JJ_10_BTE_4-5	35.26	3.98	12.26	28.33	0.91	6.61	0.01	0.50	9.35	0.03	97.24	29
GM_JJ_10_BTE_4-6	35.18	3.98	12.44	28.14	0.90	6.70	0.03	0.50	9.34	0.02	97.24	30
GM_JJ_10_BTE_4-7	34.96	3.93	12.17	28.33	0.92	6.60	0.00	0.49	9.39	0.07	96.85	29

GM_JJ_10_BTE_4-8	35.36	4.01	12.17	27.92	0.89	6.63	0.00	0.52	9.41	0.03	96.92	30
GM_JJ_10_BTE_4-10	34.65	3.92	12.23	27.99	0.89	6.48	0.24	0.47	9.25	0.02	96.14	29
GM_JJ_10_BTE_4-11	35.00	3.90	12.05	28.21	0.91	6.64	0.03	0.46	9.38	0.05	96.64	30
GM_JJ_10_BTE_4-12	34.38	3.88	12.48	28.72	0.90	6.34	0.04	0.44	9.20	0.05	96.43	28
GM_JJ_10_BTE_5-1	35.53	3.82	11.77	27.93	0.93	6.90	0.00	0.55	9.40	0.05	96.87	31
GM_JJ_10_BTE_5-3	35.33	4.01	12.20	28.20	0.90	6.74	0.00	0.39	9.55	0.02	97.33	30
GM_JJ_10_BTE_5-4	35.60	3.74	13.26	27.53	0.87	6.28	0.01	0.45	9.09	0.06	96.89	29
GM_JJ_10_BTE_5-6	35.22	3.99	12.35	28.23	0.89	6.65	0.00	0.49	9.58	0.02	97.40	30
GM_JJ_10_BTE_5-7	35.30	4.00	12.45	27.99	0.91	6.65	0.01	0.48	9.50	0.02	97.32	30
GM_JJ_10_BTE_5-8	35.09	3.97	12.29	28.55	0.91	6.36	0.00	0.46	9.48	0.04	97.13	28
GM_JJ_10_BTE_5-9	35.13	3.90	12.17	28.26	0.90	6.68	0.00	0.50	9.43	0.03	96.98	30
GM_JJ_10_BTE_5-10	35.01	3.95	12.55	28.32	0.90	6.53	0.00	0.42	9.44	0.03	97.14	29
GM_JJ_10_BTE_5-11	35.47	3.99	12.32	28.05	0.86	6.66	0.00	0.48	9.47	0.01	97.31	30
GM_JJ_10_BTE_6-2	35.71	3.89	12.05	27.72	0.87	6.84	0.01	0.54	9.51	0.05	97.19	31
GM_JJ_10_BTE_6-3	35.25	3.83	12.38	27.25	0.86	6.75	0.09	0.48	9.34	0.00	96.22	31
GM_JJ_10_BTE_6-4	35.24	3.82	12.40	27.92	0.87	6.68	0.02	0.50	9.43	0.04	96.92	30
GM_JJ_10_BTE_6-5	34.50	3.69	12.04	26.60	0.85	6.55	1.35	0.46	8.93	0.05	95.03	30
GM_JJ_10_BTE_6-6	35.87	3.54	11.83	26.04	1.41	6.30	0.05	0.41	9.13	0.01	94.59	30
GM_JJ_10_BTE_6-7	34.96	3.95	12.08	28.25	0.86	6.71	0.00	0.47	9.43	0.05	96.75	30
GM_JJ_10_BTE_6-8	35.45	3.85	11.98	27.94	0.88	6.81	0.00	0.50	9.54	0.02	96.96	30
GM_JJ_10_BTE_6-9	34.98	3.93	12.30	28.23	0.88	6.49	0.01	0.43	9.34	0.07	96.67	29
GM_JJ_10_BTE_6-10	34.84	3.91	12.15	28.08	0.90	6.64	0.03	0.43	9.51	0.02	96.51	30
GM_JJ_10_BTE_6-11	34.71	3.77	12.50	27.39	0.86	6.42	0.15	0.41	9.20	0.04	95.45	29
GM_JJ_10_BTE_6-12	34.14	3.82	12.15	27.85	0.86	6.33	0.17	0.43	9.28	0.06	95.09	29
GM_JJ_10_BTE_7-1	33.96	3.81	12.42	27.44	0.84	6.09	0.01	0.41	9.25	0.07	94.30	28
GM_JJ_10_BTE_7-2	34.26	3.73	12.76	29.16	0.89	6.46	0.01	0.34	9.05	0.02	96.68	28
GM_JJ_10_BTE_7-4	34.69	3.87	12.66	27.51	0.87	6.50	0.01	0.42	9.36	0.02	95.92	30
GM_JJ_10_BTE_7-5	35.10	3.88	12.66	27.78	0.89	6.51	0.05	0.44	9.37	0.06	96.74	29
GM_JJ_10_BTE_7-6	33.90	3.79	12.28	27.70	0.89	6.34	0.22	0.43	9.24	0.01	94.80	29
GM_JJ_10_BTE_7-7	34.31	3.88	12.47	28.16	0.90	6.36	0.03	0.44	9.36	0.05	95.96	29
GM_JJ_10_BTE_7-8	34.71	3.83	12.58	27.68	0.86	6.36	0.00	0.46	9.12	0.05	95.66	29
GM_JJ_10_BTE_7-9	33.99	3.88	12.08	27.89	0.93	5.93	0.03	0.43	9.33	0.04	94.52	27
GM_JJ_10_BTE_7-10	35.78	3.85	13.30	27.60	0.75	5.09	0.03	0.28	9.37	0.04	96.09	25
GM_JJ_10_BTE_7-11	34.26	3.83	12.47	26.93	0.87	6.14	0.06	0.40	9.14	0.00	94.08	29
GM_JJ_10_BTE_7-13	34.89	3.84	12.56	27.74	0.89	6.44	0.00	0.46	9.37	0.02	96.21	29
GM_JJ_10_BTE_7-14	35.22	3.83	12.34	26.74	0.77	5.08	0.13	0.36	9.30	0.08	93.85	25
GM_JJ_10_BTE_8-1	36.06	3.95	12.84	27.55	0.83	5.92	0.00	0.50	9.51	0.02	97.17	28
GM_JJ_10_BTE_8-2	35.28	3.94	12.57	28.09	0.79	6.27	0.01	0.46	9.54	0.04	96.98	28
GM_JJ_10_BTE_8-3	34.74	3.89	11.91	27.87	0.88	6.60	0.00	0.50	9.36	0.06	95.81	30
GM_JJ_10_BTE_8-4	35.53	3.98	12.36	27.90	0.87	6.60	0.00	0.51	9.59	0.03	97.37	30
GM_JJ_10_BTE_8-5	35.17	3.93	12.27	28.08	0.88	6.47	0.00	0.46	9.53	0.01	96.78	29

GM_JJ_10_BTE_8-6	34.79	3.91	12.13	27.75	0.91	6.68	0.00	0.50	9.29	0.05	96.00	30
GM_JJ_10_BTE_8-7	34.24	3.83	12.02	28.58	0.94	6.35	0.00	0.44	9.15	0.03	95.59	28
GM_JJ_10_BTE_9-1	34.98	3.93	12.32	28.20	0.88	6.52	0.00	0.47	9.30	0.04	96.65	29
GM_JJ_10_BTE_9-2	34.96	3.95	12.21	28.33	0.90	6.59	0.00	0.46	9.45	0.05	96.90	29
GM_JJ_10_BTE_9-3	34.45	3.98	12.08	27.98	0.92	6.40	0.00	0.47	9.41	0.08	95.77	29
GM_JJ_10_BTE_9-4	34.88	3.95	12.30	28.33	0.88	6.33	0.00	0.47	9.58	0.06	96.77	28
GM_JJ_10_BTE_9-5	33.99	3.92	12.11	28.12	0.89	6.31	0.00	0.44	9.38	0.04	95.18	29
GM_JJ_10_BTE_9-6	34.59	3.94	12.20	28.25	0.90	6.35	0.00	0.47	9.42	0.02	96.13	29
GM_JJ_10_BTE_9-7	34.70	3.91	12.45	28.32	0.90	6.38	0.00	0.48	9.45	0.03	96.61	29
GM_JJ_10_BTE_9-8	34.80	3.95	12.55	28.04	0.89	6.34	0.01	0.49	9.41	0.00	96.48	29
GM_JJ_10_BTE_9-9	34.74	3.95	12.42	28.38	0.90	6.40	0.01	0.45	9.62	0.07	96.94	29
GM_JJ_10_BTE_9-10	34.92	3.94	12.39	28.19	0.88	6.39	0.00	0.48	9.53	0.05	96.76	29
GM_JJ_10_BTE_10-1	34.65	3.89	12.12	27.90	0.89	6.53	0.00	0.48	9.38	0.05	95.91	29
GM_JJ_10_BTE_10-2	34.80	3.92	12.24	28.28	0.88	5.92	0.07	0.45	9.15	0.05	95.75	27
GM_JJ_10_BTE_10-3	35.10	3.94	12.16	27.79	0.89	6.64	0.00	0.48	9.39	0.04	96.42	30
GM_JJ_10_BTE_10-4	34.48	3.77	12.12	27.15	0.90	6.49	0.00	0.49	9.22	0.02	94.63	30
GM_JJ_10_BTE_10-5	35.11	3.92	12.25	27.59	0.89	6.57	0.00	0.49	9.48	0.05	96.34	30
GM_JJ_10_BTE_10-6	35.29	3.73	13.03	26.41	0.88	6.32	0.08	0.46	8.95	0.00	95.15	30
GM_JJ_10_BTE_10-7	35.36	3.78	12.31	26.62	0.87	6.75	0.47	0.36	9.24	0.03	95.78	31
GM_JJ_10_BTE_10-8	34.94	3.92	12.21	27.87	0.88	6.61	0.00	0.49	9.40	0.05	96.35	30
GM_JJ_10_BTE_10-9	34.73	3.77	12.13	27.73	0.98	6.47	0.05	0.42	9.10	0.07	95.45	29
GM_JJ_10_BTE_10-10	35.00	3.96	12.26	28.28	0.90	6.57	0.01	0.50	9.30	0.03	96.82	29
GM_JJ_10_BTE_10-11	34.25	3.76	12.55	27.35	0.88	6.36	0.02	0.47	9.12	0.06	94.81	29
GM_JJ_10_BTE_10-12	34.98	3.97	12.25	27.78	0.91	6.65	0.01	0.53	9.37	0.04	96.49	30
GM_JJ_10_BTE_10-13	34.69	3.91	12.30	28.04	0.88	6.51	0.01	0.50	9.40	0.04	96.29	29
GM_JJ_10_BTE_10-14	35.24	3.92	12.33	28.25	0.86	6.48	0.01	0.46	9.42	0.02	97.00	29
GM_JJ_10_BTE_10-15	35.02	3.85	12.13	28.20	0.91	6.54	0.01	0.49	9.46	0.01	96.61	29
GM_JJ_10_BTE_11-1	34.30	3.80	12.49	29.26	0.96	6.12	0.01	0.48	9.12	0.02	96.55	27
GM_JJ_10_BTE_11-4	35.08	3.91	12.24	28.48	0.88	6.56	0.03	0.49	9.47	0.04	97.16	29
GM_JJ_10_BTE_11-5	35.11	3.90	12.19	28.94	0.88	6.18	0.00	0.51	9.41	0.03	97.12	28
GM_JJ_10_BTE_11-6	34.97	3.79	12.99	28.47	0.89	6.09	0.00	0.45	8.99	0.05	96.68	28
GM_JJ_10_BTE_11-8	35.37	3.76	12.49	27.87	0.87	6.25	0.01	0.49	9.15	0.04	96.30	29
GM_JJ_10_BTE_11-9	35.37	3.45	12.45	28.14	0.91	7.04	0.01	0.51	9.36	0.02	97.26	31
GM_JJ_10_BTE_11-10	35.21	3.88	12.13	28.08	0.92	6.69	0.00	0.50	9.46	0.03	96.90	30
GM_JJ_10_BTE_11-11	34.89	3.84	12.37	27.97	0.91	6.62	0.00	0.50	9.46	0.02	96.56	30
GM_JJ_10_BTE_11-12	34.97	3.94	12.45	27.30	0.95	7.06	0.01	0.49	9.56	0.04	96.78	32
GM_JJ_10_BTE_11-13	34.94	3.85	12.35	28.07	0.87	6.64	0.00	0.50	9.32	0.04	96.58	30

	GM_JJ_10_BTE_11-14	35.07	3.91	13.03	28.22	0.90	6.01	0.01	0.49	9.20	0.02	96.87	28
	GM_JJ_10_BTE_12-1	35.58	3.98	12.46	27.71	0.70	6.22	0.01	0.45	9.65	0.05	96.81	29
	GM_JJ_10_BTE_12-2	34.77	4.00	12.37	28.32	0.88	6.40	0.00	0.47	9.42	0.03	96.65	29
	GM_JJ_10_BTE_12-3	34.82	3.93	12.36	28.61	0.92	6.53	0.02	0.48	9.46	0.00	97.13	29
	GM_JJ_10_BTE_12-4	35.13	3.99	12.41	27.73	0.86	6.35	0.00	0.47	9.57	0.00	96.48	29
	GM_JJ_10_BTE_12-5	35.54	3.88	12.61	28.16	0.86	6.22	0.07	0.48	9.47	0.03	97.32	28
	GM_JJ_10_BTE_12-6	35.18	3.95	12.08	28.39	0.89	6.53	0.00	0.50	9.52	0.00	97.02	29
	GM_JJ_10_BTE_12-7	34.89	3.93	12.23	27.78	0.93	6.46	0.07	0.44	9.34	0.06	96.12	29
	GM_JJ_10_BTE_12-8	35.04	4.01	12.23	28.18	0.82	5.65	0.02	0.44	9.53	0.00	95.92	26
	GM_JJ_10_BTE_12-9	35.16	3.79	12.76	26.55	0.85	5.92	0.26	0.47	9.16	0.04	94.97	28
	GM_JJ_10_BTE_12-10	34.78	3.89	12.18	27.91	0.89	6.39	0.01	0.46	9.34	0.00	95.85	29
	GM_JJ_10_BTE_13-1	35.17	3.83	12.79	27.84	0.89	6.47	0.01	0.47	9.23	0.05	96.77	29
	GM_JJ_10_BTE_13-2	35.26	3.76	12.22	28.24	0.90	6.37	0.03	0.45	9.10	0.04	96.39	29
	GM_JJ_10_BTE_13-3	35.94	3.68	13.37	25.94	0.92	6.61	0.04	0.51	9.20	0.03	96.23	31
	GM_JJ_10_BTE_13-4	35.49	3.57	13.50	25.88	0.97	6.21	0.17	0.47	8.41	0.06	94.74	30
	GM_JJ_10_BTE_13-5	35.39	3.83	12.48	27.82	0.89	6.65	0.02	0.50	9.44	0.02	97.04	30
	GM_JJ_10_BTE_13-6	35.27	3.71	12.46	27.91	0.89	6.76	0.01	0.49	9.31	0.01	96.82	30
	GM_JJ_10_BTE_13-7	35.38	3.84	12.25	27.63	0.90	6.84	0.01	0.50	9.33	0.02	96.70	31
	GM_JJ_10_BTE_13-8	35.52	3.83	13.16	27.17	0.90	6.53	0.06	0.49	9.25	0.02	96.93	30
	GM_JJ_10_BTE_13-9	34.96	3.93	12.79	28.04	0.90	6.41	0.03	0.48	9.35	0.04	96.93	29
	GM_JJ_10_BTE_13-10	34.91	3.80	12.33	28.39	0.91	6.53	0.02	0.49	9.26	0.02	96.67	29
	GM_JJ_10_BTE_13-11	34.58	3.82	12.03	28.88	0.94	6.43	0.00	0.49	9.20	0.05	96.43	28
	GM_JJ_10_BTE_13-12	34.98	3.89	12.21	28.79	0.84	5.91	0.04	0.45	9.34	0.02	96.49	27
	GM_JJ_10_BTE_13-13	34.94	3.89	12.36	29.11	0.86	6.11	0.02	0.54	9.35	0.01	97.20	27
	GM_JJ_10_BTE_13-15	35.33	3.77	12.89	28.79	0.88	5.55	0.05	0.46	9.23	0.02	96.96	26
	Average	**35.02**	**3.88**	**12.39**	**27.92**	**0.89**	**6.41**	**0.04**	**0.47**	**9.34**	**0.03**	**96.40**	**29**
	Stadnard Deviation	**0.41**	**0.10**	**0.33**	**0.61**	**0.05**	**0.32**	**0.12**	**0.05**	**0.17**	**0.02**	**0.79**	**1**
GM-07(OL)	GM-07_BTE_1_2	37.20	3.85	12.37	21.74	0.71	10.23	0.00	0.57	9.26	0.06	95.99	46
	GM-07_BTE_1_3	36.93	3.14	12.45	24.85	0.74	8.91	0.00	0.54	9.13	0.04	96.74	39
	GM-07_BTE_1_5	35.90	3.85	12.30	24.67	0.71	9.01	0.02	0.54	9.08	0.03	96.13	39
	GM-07_BTE_1_7	36.07	3.88	11.99	24.17	0.71	8.70	0.00	0.53	9.12	0.03	95.18	39
	GM-07_BTE_1_9	37.52	3.98	12.56	20.61	0.73	10.72	0.00	0.60	9.39	0.01	96.10	48
	GM-07_BTE_1_10	36.49	3.24	12.48	25.51	0.76	9.05	0.00	0.54	9.15	0.03	97.24	39
	GM-07_BTE_1_11	36.79	3.17	12.32	25.59	0.77	8.91	0.01	0.56	9.00	0.05	97.16	38
	GM-07_BTE_1_12	36.70	3.05	12.29	25.11	0.74	8.60	0.01	0.56	8.95	0.04	96.05	38
	GM-07_BTE_2_1	36.61	3.64	12.25	25.10	0.66	8.54	0.01	0.59	9.03	0.07	96.50	38

GM-07_BTE_2_2	36.70	3.79	12.38	24.13	0.68	9.27	0.00	0.59	9.22	0.03	96.77	41
GM-07_BTE_2_5	36.68	3.78	12.25	24.13	0.68	9.40	0.01	0.58	9.18	0.03	96.71	41
GM-07_BTE_2_6	36.63	3.69	12.31	23.69	0.70	9.39	0.00	0.57	9.19	0.07	96.23	41
GM-07_BTE_2_7	39.53	3.53	12.64	23.37	0.65	8.24	0.02	0.52	9.00	0.00	97.47	39
GM-07_BTE_2_8	37.80	3.47	12.64	23.09	0.63	9.34	0.00	0.55	8.89	0.03	96.46	42
GM-07_BTE_4_1	35.77	3.83	12.37	25.14	0.76	9.20	0.00	0.55	9.35	0.06	97.00	39
GM-07_BTE_4_2	36.03	3.78	12.32	24.27	0.72	9.03	0.00	0.55	9.39	0.04	96.13	40
GM-07_BTE_4_3	36.73	3.79	11.97	23.68	0.69	8.91	0.00	0.51	9.20	0.02	95.48	40
GM-07_BTE_4_4	36.20	3.82	12.34	24.17	0.75	9.06	0.00	0.52	9.25	0.03	96.12	40
GM-07_BTE_4_5	36.71	3.84	12.52	24.28	0.70	9.10	0.00	0.53	9.39	0.05	97.11	40
GM-07_BTE_4_6	36.43	3.80	12.39	24.19	0.74	9.04	0.00	0.56	9.33	0.02	96.49	40
GM-07_BTE_4_7	35.87	3.81	12.18	25.89	0.70	7.77	0.00	0.55	9.27	0.00	96.03	35
GM-07_BTE_4_8	36.39	3.82	12.45	24.53	0.73	9.05	0.00	0.53	9.15	0.03	96.68	40
GM-07_BTE_4_9	36.13	3.80	12.45	24.27	0.71	8.95	0.00	0.54	9.40	0.02	96.27	40
GM-07_BTE_4_10	36.31	3.82	12.31	24.28	0.73	9.02	0.00	0.53	9.35	0.01	96.32	40
GM-07_BTE_4_13	36.76	3.78	12.27	23.88	0.70	8.99	0.00	0.51	9.14	0.03	96.04	40
GM-07_BTE_4_14	36.47	3.84	12.12	24.36	0.74	8.95	0.00	0.53	9.27	0.04	96.31	40
GM-07_BTE_5_1	36.46	3.65	12.35	24.71	0.71	9.27	0.00	0.53	9.24	0.02	96.95	40
GM-07_BTE_5_2	36.30	3.57	12.27	24.49	0.73	9.27	0.00	0.54	9.30	0.02	96.50	40
GM-07_BTE_5_3	36.42	3.58	12.28	24.91	0.70	8.94	0.01	0.55	9.22	0.03	96.64	39
GM-07_BTE_5_5	36.05	3.65	12.14	24.47	0.73	9.14	0.00	0.53	9.35	0.00	96.04	40
GM-07_BTE_5_6	36.43	3.55	12.29	24.45	0.72	9.09	0.00	0.53	9.19	0.04	96.28	40
GM-07_BTE_6_1	36.84	3.74	12.62	24.08	0.72	9.07	0.00	0.55	9.11	0.02	96.74	40
GM-07_BTE_6_3	36.65	3.75	12.42	23.96	0.70	8.87	0.00	0.53	9.11	0.02	96.01	40
GM-07_BTE_6_4	36.99	3.74	12.59	23.86	0.71	8.99	0.00	0.54	9.21	0.07	96.68	40
GM-07_BTE_6_5	36.90	3.65	12.69	23.51	0.70	8.88	0.00	0.53	8.92	0.02	95.80	40
GM-07_BTE_7_1	36.95	3.64	12.49	24.27	0.71	9.09	0.00	0.54	9.27	0.03	96.99	40
GM-07_BTE_7_2	36.11	3.82	11.91	24.49	0.74	8.57	0.00	0.50	9.28	0.04	95.44	38
GM-07_BTE_7_3	36.98	3.83	12.22	24.18	0.73	9.22	0.00	0.53	9.31	0.07	97.06	40
GM-07_BTE_7_4	36.79	3.69	12.20	24.31	0.72	9.06	0.00	0.53	9.28	0.03	96.59	40
GM-07_BTE_7_5	36.40	3.61	12.44	24.30	0.71	9.06	0.01	0.53	9.19	0.02	96.28	40
GM-07_BTE_7_8	36.24	3.65	12.17	24.23	0.70	8.88	0.00	0.52	9.21	0.04	95.64	40
GM-07_BTE_7_9	35.62	3.74	11.86	24.70	0.72	8.78	0.01	0.52	9.22	0.03	95.20	39
GM-07_BTE_7_11	36.55	3.87	12.19	24.71	0.71	8.74	0.00	0.54	9.24	0.02	96.56	39
GM-07_BTE_7_12	36.68	3.77	11.91	24.22	0.72	9.18	0.00	0.55	9.25	0.01	96.29	40
GM-07_BTE_8_1	36.79	3.70	11.70	23.29	0.71	9.31	0.01	0.56	9.17	0.05	95.28	42
GM-07_BTE_8_2	36.74	3.65	11.70	23.32	0.71	9.35	0.00	0.58	9.04	0.02	95.10	42
GM-07_BTE_8_3	36.79	3.66	11.71	23.55	0.68	9.33	0.00	0.56	9.12	0.04	95.44	41
GM-07_BTE_8_5	35.93	3.79	11.75	24.43	0.69	8.70	0.00	0.57	9.26	0.04	95.14	39
GM-07_BTE_8_6	36.04	3.79	12.43	24.28	0.72	8.62	0.00	0.53	9.13	0.05	95.57	39
GM-07_BTE_8_8	36.35	3.76	11.62	24.33	0.71	8.75	0.00	0.56	9.26	0.00	95.34	39
GM-07_BTE_9_1	36.10	3.93	12.43	24.40	0.53	8.80	0.00	0.50	9.21	0.03	95.91	39
GM-07_BTE_9_2	36.12	3.91	12.41	24.33	0.54	9.00	0.01	0.53	9.29	0.01	96.14	40
GM-07_BTE_9_3	35.90	3.91	12.47	24.60	0.55	8.82	0.00	0.48	9.37	0.02	96.12	39
GM-07_BTE_9_4	36.34	3.93	12.34	24.69	0.54	9.05	0.00	0.51	9.49	0.02	96.91	40

	GM-07_BTE_9_5	35.99	3.88	11.96	25.55	0.55	9.32	0.01	0.55	9.27	0.06	97.14	39
	GM-07_BTE_9_6	36.48	3.89	12.01	24.82	0.50	8.42	0.01	0.54	9.13	0.00	95.81	38
	Average	**36.54**	**3.72**	**12.26**	**24.25**	**0.69**	**9.02**	**0.00**	**0.54**	**9.21**	**0.03**	**96.26**	**40**
	Standard Deviation	**0.59**	**0.19**	**0.26**	**0.83**	**0.06**	**0.41**	**0.01**	**0.02**	**0.12**	**0.02**	**0.60**	**2**
GM-20 (OT)	GM-20_OT_BTE_1-18	35.77	4.03	13.46	22.62	0.39	9.65	0.00	0.55	9.01	0.01	95.47	43
	GM-20_OT_BTE_1-20	36.95	3.90	15.50	21.49	0.37	9.01	0.00	0.54	8.76	0.00	96.49	43
	GM-20_OT_BTE_1-21	36.58	3.92	13.52	23.09	0.37	10.11	0.01	0.65	8.83	0.02	97.10	44
	GM-20_OT_BTE_1-40	36.37	4.56	12.68	24.11	0.42	9.25	0.00	0.53	9.65	0.04	97.59	41
	GM-20_OT_BTE_1-43	36.19	4.47	12.69	24.10	0.43	9.60	0.00	0.55	9.49	0.01	97.51	42
	GM-20_OT_BTE_1-44	36.55	4.39	12.69	23.68	0.41	9.68	0.01	0.58	9.40	0.02	97.41	42
	GM-20_OT_BTE_1-48	36.14	4.39	12.63	24.20	0.39	9.60	0.00	0.55	9.58	0.02	97.46	41
	GM-20_OT_BTE_1-49	36.04	4.37	12.61	23.92	0.41	9.58	0.01	0.52	9.64	0.03	97.10	42
	GM-20_OT_BTE_1-50	36.11	4.36	12.59	24.16	0.40	9.68	0.00	0.54	9.62	0.04	97.49	42
	GM-20_OT_BTE_1-51	35.91	4.33	12.56	24.06	0.44	9.50	0.00	0.53	9.52	0.03	96.87	41
	GM-20_OT_BTE_1-53	36.11	4.31	12.61	24.01	0.40	9.77	0.02	0.55	9.65	0.03	97.45	42
	GM-20_OT_BTE_1-59	35.95	4.47	12.41	24.33	0.42	9.63	0.00	0.57	9.57	0.00	97.36	41
	GM-20_OT_BTE_1-62	35.89	4.54	12.44	23.91	0.42	9.39	0.00	0.51	9.45	0.00	96.54	41
	GM-20_OT_BTE_1-64	35.24	4.50	12.28	25.33	0.41	8.81	0.00	0.54	9.49	0.00	96.59	38
	GM-20_OT_BTE_1-65	35.59	4.48	12.29	24.72	0.41	9.03	0.00	0.54	9.42	0.03	96.51	39
	GM-20_OT_BTE_1-66	35.70	4.41	12.33	24.03	0.43	9.63	0.00	0.53	9.57	0.02	96.62	42
	GM-20_OT_BTE_1-70	36.15	4.37	12.66	24.05	0.43	9.47	0.00	0.56	9.55	0.00	97.22	41
	GM-20_OT_BTE_1-71	35.95	4.37	12.67	24.28	0.41	9.56	0.00	0.56	9.63	0.00	97.42	41
	GM-20_OT_BTE_1-73	36.04	4.37	12.49	24.05	0.39	9.56	0.00	0.51	9.55	0.01	96.98	41
	GM-20_OT_BTE_1-74	36.32	4.19	12.27	23.84	0.40	9.18	0.00	0.49	9.12	0.03	95.81	41
	GM-20_OT_BTE_1-77	35.91	4.42	12.45	24.40	0.38	9.46	0.01	0.54	9.66	0.02	97.25	41
	GM-20_OT_BTE_1-79	35.75	4.46	12.41	24.62	0.40	9.23	0.00	0.55	9.62	0.01	97.02	40
	GM-20_OT_BTE_4-1	35.62	4.41	12.16	25.20	0.43	8.81	0.00	0.55	9.48	0.03	96.67	38
	GM-20_OT_BTE_4-2	36.18	4.42	12.48	23.72	0.39	9.36	0.00	0.51	9.46	0.05	96.57	41
	GM-20_OT_BTE_4-3	35.61	4.44	12.22	24.15	0.40	9.25	0.00	0.52	9.45	0.03	96.09	41
	GM-20_OT_BTE_4-4	35.62	4.36	12.28	24.20	0.38	9.11	0.00	0.53	9.36	0.04	95.87	40
	GM-20_OT_BTE_4-5	36.27	4.41	12.70	23.83	0.38	9.18	0.00	0.52	9.69	0.03	97.00	41
	GM-20_OT_BTE_4-9	35.69	4.45	12.41	24.05	0.41	9.34	0.01	0.49	9.66	0.01	96.53	41
	GM-20_OT_BTE_4-10	36.10	4.45	12.64	23.89	0.42	9.57	0.00	0.56	9.55	0.03	97.19	42
	GM-20_OT_BTE_4-11	36.20	4.48	12.63	23.57	0.40	9.60	0.00	0.54	9.54	0.05	97.01	42
	GM-20_OT_BTE_4-12	35.65	4.45	12.39	23.63	0.43	9.57	0.00	0.54	9.43	0.01	96.11	42

GM-20_OT_BTE_4-13	36.22	4.39	12.59	23.81	0.40	9.49	0.01	0.56	9.59	0.05	97.11	42
GM-20_OT_BTE_4-17	36.42	4.49	12.61	23.67	0.42	9.69	0.01	0.57	9.48	0.05	97.40	42
GM-20_OT_BTE_4-18	36.15	4.44	12.70	23.61	0.40	9.61	0.00	0.52	9.53	0.04	97.00	42
GM-20_OT_BTE_4-19	36.15	4.41	12.63	23.55	0.41	9.52	0.02	0.54	9.53	0.04	96.79	42
GM-20_OT_BTE_4-20	35.87	4.41	12.55	23.88	0.41	9.57	0.00	0.57	9.57	0.03	96.86	42
GM-20_OT_BTE_4-21	36.05	4.44	12.66	23.86	0.41	9.52	0.00	0.51	9.63	0.00	97.05	42
GM-20_OT_BTE_4-22	36.20	4.43	12.63	23.79	0.39	9.48	0.00	0.53	9.70	0.06	97.22	42
GM-20_OT_BTE_4-23	36.39	4.33	12.75	25.03	0.40	8.59	0.00	0.56	9.45	0.04	97.54	38
GM-20_OT_BTE_4-24	35.46	4.27	12.84	24.35	0.41	8.74	0.00	0.54	9.36	0.02	95.98	39
GM-20_OT_BTE_4-25	36.30	4.40	12.81	23.94	0.39	9.39	0.01	0.54	9.46	0.05	97.27	41
GM-20_OT_BTE_4-26	36.29	4.42	12.70	23.81	0.41	9.57	0.00	0.53	9.56	0.00	97.24	42
GM-20_OT_BTE_4-27	36.13	4.44	12.71	23.93	0.42	9.55	0.01	0.52	9.61	0.03	97.36	42
GM-20_OT_BTE_4-28	36.65	4.58	12.61	23.71	0.41	9.73	0.10	0.80	8.97	0.01	97.55	42
GM-20_OT_BTE_4-29	36.20	4.40	12.55	23.99	0.36	9.58	0.00	0.55	9.56	0.04	97.21	42
GM-20_OT_BTE_4-30	36.40	4.44	12.71	23.61	0.40	9.83	0.00	0.55	9.57	0.01	97.50	43
GM-20_OT_BTE_4-34	36.54	4.42	12.69	23.89	0.41	9.38	0.00	0.52	9.52	0.03	97.39	41
GM-20_OT_BTE_4-36	36.21	4.42	12.80	23.63	0.38	9.77	0.00	0.53	9.46	0.06	97.25	42
GM-20_OT_BTE_4-39	36.21	4.43	12.74	23.64	0.42	9.56	0.00	0.53	9.65	0.04	97.19	42
GM-20_OT_BTE_4-40	36.25	4.37	12.69	23.97	0.42	9.68	0.02	0.55	9.59	0.03	97.57	42
GM-20_OT_BTE_4-41	36.36	4.41	12.86	23.80	0.41	9.53	0.00	0.54	9.49	0.00	97.40	42
GM-20_OT_BTE_4-42	35.83	4.33	12.57	24.65	0.41	8.64	0.00	0.52	9.49	0.00	96.42	38
GM-20_OT_BTE_4-43	36.01	4.37	12.72	24.07	0.39	8.99	0.00	0.55	9.51	0.01	96.62	40
GM-20_OT_BTE_4-44	36.08	4.58	12.74	21.44	0.40	10.37	0.00	0.57	9.55	0.00	95.70	46
GM-20_OT_BTE_4-46	36.04	4.37	12.75	24.46	0.41	9.09	0.00	0.54	9.60	0.00	97.25	40
GM-20_OT_BTE_4-48	36.37	4.47	12.89	22.74	0.39	10.13	0.03	0.57	9.59	0.00	97.19	44
GM-20_OT_BTE_4-49	35.86	4.41	12.47	23.70	0.36	9.47	0.02	0.57	9.55	0.03	96.43	42
GM-20_OT_BTE_4-50	36.14	4.42	12.69	23.27	0.39	9.80	0.00	0.57	9.59	0.02	96.89	43
GM-20_OT_BTE_4-52	36.32	4.41	12.60	23.72	0.40	9.76	0.01	0.54	9.45	0.00	97.20	42
GM-20_OT_BTE_4-53	36.15	4.40	12.53	24.12	0.40	9.38	0.00	0.57	9.61	0.04	97.18	41
GM-20_OT_BTE_4-54	36.13	4.42	12.54	24.51	0.40	9.19	0.01	0.52	9.49	0.05	97.26	40
GM-20_OT_BTE_4-57	36.15	4.43	12.55	23.82	0.42	9.70	0.00	0.52	9.62	0.02	97.24	42
GM-20_OT_BTE_4-58	36.41	4.42	12.72	23.58	0.39	9.83	0.01	0.54	9.60	0.02	97.51	43
GM-20_OT_BTE_4-59	36.23	4.44	12.48	23.83	0.38	9.46	0.00	0.53	9.45	0.03	96.85	41
GM-20_OT_BTE_4-60	36.60	4.50	13.00	21.84	0.34	10.67	0.00	0.64	9.55	0.00	97.13	47
GM-20_OT_BTE_4-61	36.46	4.43	12.59	23.76	0.38	9.66	0.00	0.54	9.62	0.04	97.45	42

	GM-20_OT_BTE_4-63	36.96	4.49	13.22	20.08	0.39	12.15	0.02	0.64	9.58	0.04	97.56	52
	GM-20_OT_BTE_4-66	36.30	4.41	12.74	23.42	0.39	9.79	0.01	0.53	9.60	0.04	97.23	43
	GM-20_OT_BTE_4-73	36.01	4.42	12.50	25.32	0.40	8.68	0.02	0.56	9.44	0.02	97.37	38
	GM-20_OT_BTE_4-76	36.24	4.36	12.58	24.54	0.36	9.18	0.01	0.55	9.47	0.07	97.35	40
	GM-20_OT_BTE_4-79	36.55	4.48	12.96	20.50	0.38	11.30	0.01	0.62	9.56	0.04	96.41	50
	GM-20_OT_BTE_4-80	35.77	4.36	12.49	24.59	0.38	8.72	0.00	0.57	9.45	0.02	96.33	39
	Average	**36.13**	**4.40**	**12.67**	**23.79**	**0.40**	**9.53**	**0.01**	**0.55**	**9.50**	**0.02**	**96.98**	**42**
	Standard Deviation	**0.32**	**0.11**	**0.41**	**0.91**	**0.02**	**0.53**	**0.01**	**0.04**	**0.18**	**0.02**	**0.50**	**2**
GM-16 (YE)													
	GM-16 BTE 1-1	35.85	4.07	12.81	22.63	0.28	10.46	0.01	0.53	9.40	0.04	95.53	45
	GM-16 BTE 1-2	35.88	4.25	12.82	23.34	0.31	10.34	0.00	0.52	9.38	0.05	96.08	44
	GM-16 BTE 1-3	35.78	4.43	12.73	23.17	0.28	10.03	0.00	0.51	9.59	0.05	96.87	44
	GM-16 BTE 2-1	36.30	4.19	12.71	21.96	0.25	10.12	0.00	0.54	9.29	0.03	96.58	45
	GM-16 BTE 2-2	36.10	4.00	12.77	22.36	0.26	10.40	0.02	0.56	9.41	0.00	95.39	45
	GM-16 BTE 2-3	36.21	4.21	12.67	22.19	0.26	10.06	0.00	0.55	9.43	0.06	95.90	45
	GM-16 BTE 3-1	36.17	4.35	12.76	22.61	0.29	10.03	0.00	0.54	9.42	0.05	95.61	44
	GM-16 BTE 3-2	36.19	4.37	12.75	22.75	0.25	10.12	0.00	0.54	9.51	0.03	96.19	44
	GM-16 BTE 3-3	36.17	4.38	12.75	22.99	0.28	10.08	0.00	0.53	9.52	0.03	96.51	44
	GM-16 BTE 4-1	35.95	4.30	12.67	22.45	0.26	10.16	0.01	0.55	9.44	0.02	96.71	45
	GM-16 BTE 4-2	36.10	4.31	12.61	22.84	0.29	10.13	0.01	0.52	9.36	0.03	95.81	44
	GM-16 BTE 4-3	35.85	4.35	12.70	22.57	0.28	10.08	0.00	0.55	9.41	0.04	96.20	44
	GM-16 BTE 5-1	35.99	4.30	12.72	22.50	0.29	10.19	0.00	0.54	9.42	0.05	95.81	45
	GM-16 BTE 5-2	36.04	4.33	12.73	22.64	0.28	10.03	0.00	0.52	9.45	0.02	96.00	44
	GM-16 BTE 5-3	36.35	4.37	12.85	23.02	0.28	10.21	0.00	0.56	9.64	0.01	96.02	44
	GM-16 BTE 6-1	36.19	4.44	12.75	23.33	0.29	10.31	0.01	0.55	9.60	0.00	97.29	44
	GM-16 BTE 6-2	36.47	4.37	12.87	23.24	0.31	10.27	0.00	0.53	9.54	0.06	97.46	44
	GM-16 BTE 7-1	36.11	4.31	12.75	22.58	0.29	10.16	0.01	0.55	9.51	0.07	97.26	45
	GM-16 BTE 7-2	35.78	4.32	12.68	22.44	0.28	10.18	0.00	0.53	9.30	0.03	96.36	45
	GM-16 BTE 7-3	35.59	4.32	12.62	22.64	0.27	10.47	0.00	0.54	9.34	0.04	95.53	45
	GM-16 BTE 8-1	35.97	4.09	12.76	22.28	0.27	10.30	0.00	0.54	9.43	0.08	95.80	45
	GM-16 BTE 8-2	36.12	3.82	12.75	22.30	0.28	10.51	0.01	0.55	9.43	0.06	95.71	46
	GM-16 BTE 8-3	35.90	4.02	12.77	22.40	0.28	10.33	0.00	0.53	9.23	0.04	95.84	45
	GM-16 BTE 9-2	36.02	4.40	12.80	22.43	0.29	10.14	0.00	0.54	9.36	0.05	95.50	45
	GM-16 BTE 9-3	36.08	4.36	12.54	22.56	0.25	10.23	0.01	0.53	9.38	0.06	96.03	45
	GM-16 BTE 9-1	36.70	4.58	12.94	20.83	0.27	10.36	0.00	0.61	9.46	0.05	96.00	47
	GM-16 BTE 10-1	35.98	4.30	12.76	22.32	0.27	10.11	0.00	0.53	9.44	0.06	95.81	45
	GM-16 BTE 10-2	36.10	4.28	12.65	22.09	0.27	10.23	0.01	0.56	9.30	0.03	95.78	45
	GM-16 BTE 10-3	36.05	4.27	12.85	22.72	0.27	10.00	0.00	0.53	9.53	0.04	95.52	44
	GM-16 BTE 11-1	35.80	4.37	12.57	22.97	0.30	10.17	0.00	0.52	9.43	0.06	96.26	44
	GM-16 BTE 11-2	36.04	4.21	12.60	23.68	0.29	10.29	0.00	0.56	9.41	0.03	96.19	44
	GM-16 BTE 11-3	35.93	4.37	12.77	22.48	0.29	10.04	0.01	0.55	9.41	0.06	97.09	44
	GM-16 BTE 11-4	36.10	4.28	12.60	22.58	0.28	10.25	0.01	0.54	9.45	0.02	95.91	45
	GM-16 BTE 12-1	36.06	4.31	12.64	22.40	0.27	10.36	0.00	0.55	9.31	0.03	96.10	45

GM-16 BTE 12-2	35.84	4.31	12.59	22.65	0.28	10.17	0.00	0.54	9.47	0.06	95.93	44
GM-16 BTE 12-3	35.83	4.28	12.62	22.21	0.26	10.31	0.00	0.56	9.35	0.02	95.91	45
GM-16 BTE 13-1	36.20	4.30	12.71	22.12	0.30	10.25	0.00	0.53	9.49	0.02	95.44	45
GM-16 BTE 13-2	35.85	4.23	12.63	24.52	0.31	9.86	0.01	0.55	9.30	0.06	95.90	42
GM-16 BTE 13-3	35.92	4.27	12.72	23.33	0.29	10.13	0.00	0.53	9.43	0.03	97.32	44
GM-16 BTE 14-1	35.61	4.32	12.62	23.11	0.27	9.67	0.00	0.55	9.38	0.01	96.64	43
GM-16 BTE 14-2	36.06	4.30	12.69	22.68	0.25	9.98	0.00	0.52	9.30	0.03	95.51	44
GM-16 BTE 14-3	35.84	4.30	12.72	22.19	0.28	10.07	0.00	0.53	9.54	0.00	95.81	45
GM-16 BTE 15-1	35.78	4.28	12.78	22.51	0.29	10.09	0.01	0.53	9.44	0.03	95.46	44
GM-16 BTE 15-2	36.01	4.30	12.85	22.63	0.29	10.26	0.00	0.55	9.37	0.05	95.73	45
GM-16 BTE 15-3	36.00	4.21	12.81	22.83	0.28	10.23	0.00	0.54	9.46	0.06	96.31	44
GM-16 BTE 15-4	35.99	4.22	12.76	22.42	0.27	10.20	0.00	0.57	9.45	0.00	96.41	45
GM-16 BTE 15-5	35.98	4.28	12.68	22.46	0.26	10.12	0.00	0.54	9.52	0.06	95.88	45
GM-16 BTE 16-1	36.00	4.42	12.88	23.09	0.28	10.17	0.00	0.53	9.47	0.04	95.90	44
GM-16 BTE 16-2	35.98	4.34	12.69	22.83	0.31	10.19	0.00	0.53	9.49	0.03	96.87	44
GM-16 BTE 16-3	35.88	4.38	12.68	22.83	0.27	10.20	0.00	0.53	9.32	0.03	96.40	44
GM-16 BTE 16-4	35.41	4.33	12.56	23.41	0.29	10.15	0.01	0.52	9.35	0.04	96.09	44
GM-16 BTE 17-1	36.20	4.40	12.68	22.65	0.27	10.19	0.01	0.53	9.50	0.01	96.07	45
GM-16 BTE 17-2	35.71	4.49	12.66	23.03	0.27	10.12	0.00	0.54	9.45	0.04	96.44	44
GM-16 BTE 17-3	35.95	4.39	12.78	22.98	0.29	10.13	0.00	0.55	9.40	0.02	96.32	44
GM-16 BTE 18-1	36.50	4.40	12.82	23.29	0.28	10.28	0.00	0.56	9.45	0.05	96.49	44
GM-16 BTE 18-3	36.10	4.37	12.79	22.78	0.29	10.38	0.00	0.55	9.49	0.07	97.50	45
GM-16 BTE 18-4	36.27	4.44	12.91	23.06	0.27	10.35	0.01	0.53	9.58	0.02	96.83	44
GM-16 BTE 18-5	36.05	4.36	12.60	23.75	0.29	10.27	0.00	0.57	9.37	0.03	97.43	44
GM-16 BTE 19-1	35.95	4.36	12.64	23.04	0.32	10.28	0.00	0.52	9.44	0.04	97.28	44
GM-16 BTE 19-2	36.04	4.36	12.67	22.95	0.29	10.31	0.00	0.53	9.51	0.03	96.60	44
GM-16 BTE 19-3	36.05	4.39	12.69	23.15	0.28	10.11	0.02	0.54	9.59	0.00	96.67	44
GM-16 BTE 20-1	36.32	4.35	12.79	22.49	0.27	10.19	0.00	0.53	9.42	0.04	96.80	45
GM-16 BTE 20-2	35.99	4.41	12.66	22.66	0.29	10.17	0.00	0.52	9.51	0.03	96.39	44
GM-16 BTE 20-3	36.31	4.42	12.70	23.14	0.28	10.26	0.01	0.51	9.50	0.03	96.25	44
GM-16 BTE 20-4	36.22	4.43	12.79	22.83	0.27	10.27	0.01	0.54	9.37	0.05	97.17	44
GM-16 BTE 21-1	36.00	4.36	12.82	22.59	0.29	10.22	0.00	0.54	9.35	0.03	96.77	45
GM-16 BTE 21-2	36.05	4.39	12.64	22.88	0.26	10.10	0.01	0.53	9.31	0.05	96.18	44
GM-16 BTE 21-3	35.68	4.37	12.55	22.72	0.27	10.20	0.01	0.51	9.16	0.04	96.23	44
GM-16 BTE 21-4	36.36	4.44	12.78	22.82	0.28	10.28	0.01	0.54	9.48	0.04	95.51	45
GM-16 BTE 22-1	36.18	4.38	12.63	23.13	0.28	10.19	0.00	0.54	9.38	0.07	97.04	44
GM-16 BTE 22-2	35.84	4.40	12.82	23.43	0.30	10.01	0.00	0.52	9.54	0.04	96.77	43
GM-16 BTE 22-3	35.92	4.37	12.67	22.79	0.28	10.21	0.00	0.52	9.42	0.05	96.90	44
GM-16 BTE 22-4	35.69	4.37	12.55	23.25	0.30	10.03	0.02	0.55	9.48	0.03	96.20	43
GM-16 BTE 22-5	36.01	4.44	12.74	22.91	0.28	10.16	0.00	0.57	9.54	0.06	96.26	44
GM-16 BTE 23-1	35.89	4.26	12.68	22.90	0.29	10.19	0.00	0.52	9.55	0.02	96.71	44
GM-16 BTE 23-2	36.12	4.28	12.73	22.90	0.26	10.31	0.00	0.54	9.54	0.02	96.31	45
GM-16 BTE 23-3	35.86	4.00	12.64	22.38	0.27	10.34	0.00	0.52	9.43	0.02	96.68	45
GM-16 BTE 23-4	35.83	4.18	12.55	22.39	0.28	10.26	0.00	0.52	9.28	0.05	95.46	45
GM-16 BTE 24-1	36.04	4.29	12.75	22.26	0.27	10.07	0.00	0.54	9.38	0.03	95.35	45

GM-16 BTE 24-2	35.93	4.32	12.72	22.10	0.31	10.10	0.00	0.55	9.45	0.03	95.63	45
GM-16 BTE 24-3	36.40	4.22	12.74	22.56	0.28	10.19	0.01	0.55	9.36	0.01	95.50	45
GM-16 BTE 24-4	35.71	4.19	12.75	22.19	0.27	10.19	0.01	0.53	9.51	0.02	96.33	45
GM-16 BTE 24-5	36.04	4.22	12.72	22.39	0.29	10.31	0.00	0.53	9.51	0.02	95.38	45
GM-16 BTE 25-1	36.32	4.23	12.65	22.17	0.28	10.28	0.00	0.54	9.40	0.06	96.02	45
GM-16 BTE 25-2	36.02	4.31	12.62	22.62	0.26	10.33	0.01	0.54	9.28	0.01	95.92	45
GM-16 BTE 25-3	35.85	4.42	12.76	22.67	0.28	10.17	0.01	0.52	9.40	0.05	96.01	44
GM-16 BTE 25-4	35.75	4.41	12.71	22.75	0.25	10.01	0.00	0.53	9.34	0.01	96.11	44
GM-16 BTE 26-1	35.86	4.38	12.65	23.06	0.25	10.22	0.00	0.53	9.42	0.03	95.76	44
GM-16 BTE 26-2	36.15	4.40	12.93	23.05	0.29	10.17	0.00	0.54	9.45	0.00	96.39	44
GM-16 BTE 26-3	35.97	4.33	12.86	22.68	0.26	10.08	0.01	0.57	9.39	0.04	96.95	44
GM-16 BTE 26-4	35.89	4.41	12.70	23.03	0.29	10.21	0.00	0.54	9.53	0.04	96.20	44
GM-16 BTE 27-1	36.20	4.38	12.51	24.54	0.30	9.82	0.00	0.58	9.51	0.05	96.64	42
GM-16 BTE 27-3	36.08	4.51	12.64	23.36	0.29	10.23	0.00	0.54	9.44	0.03	96.49	44
GM-16 BTE 28-1	35.95	4.36	12.82	22.80	0.27	10.26	0.00	0.53	9.45	0.04	97.10	45
GM-16 BTE 28-2	35.67	4.40	12.74	23.16	0.31	10.17	0.01	0.53	9.50	0.03	96.48	44
GM-16 BTE 28-3	35.88	4.45	12.74	23.91	0.28	9.83	0.00	0.55	9.54	0.04	96.50	42
GM-16 BTE 29-1	35.72	4.36	12.68	23.48	0.29	9.91	0.01	0.55	9.54	0.04	97.23	43
GM-16 BTE 29-2	36.12	4.43	12.75	23.49	0.29	10.16	0.01	0.54	9.50	0.04	96.57	44
GM-16 BTE 29-3	35.66	4.46	13.06	23.22	0.29	10.20	0.00	0.55	9.58	0.06	97.33	44
GM-16 BTE 29-4	36.01	4.36	12.78	23.03	0.30	10.17	0.00	0.51	9.59	0.03	97.08	44
GM-16 BTE 30-1	36.10	4.37	12.71	23.22	0.27	10.29	0.01	0.56	9.52	0.03	96.77	44
GM-16 BTE 30-2	35.90	4.32	12.67	22.65	0.27	10.17	0.00	0.53	9.48	0.07	97.08	44
GM-16 BTE 30-3	35.84	4.38	12.67	22.73	0.26	10.13	0.00	0.52	9.59	0.01	96.03	44
GM-16 BTE 30-4	36.12	4.30	12.60	22.74	0.27	10.27	0.00	0.52	9.49	0.02	96.11	45
GM-16 BTE 31-1	36.27	4.19	12.49	21.93	0.28	10.39	0.01	0.54	9.40	0.05	96.33	46
GM-16 BTE 31-2	36.00	4.23	12.61	23.40	0.28	9.52	0.00	0.54	9.38	0.05	95.54	42
GM-16 BTE 31-3	36.13	4.31	12.82	22.65	0.28	10.19	0.01	0.55	9.55	0.04	95.99	44
GM-16 BTE 31-4	35.87	4.30	12.74	22.57	0.25	10.13	0.00	0.54	9.47	0.01	96.54	44
GM-16 BTE 32-1	35.83	4.19	12.78	22.93	0.27	10.30	0.00	0.54	9.45	0.01	95.86	44
GM-16 BTE 32-2	35.39	4.20	12.40	22.72	0.28	10.18	0.00	0.53	9.32	0.00	96.30	44
GM-16 BTE 32-3	35.77	4.33	12.54	22.39	0.27	10.22	0.00	0.54	9.43	0.03	95.00	45
GM-16 BTE 32-4	35.69	4.17	12.56	22.33	0.28	10.26	0.00	0.54	9.39	0.04	95.52	45
GM-16 BTE 32-5	35.71	4.34	12.57	22.52	0.29	10.28	0.00	0.53	9.41	0.00	95.26	45
GM-16 BTE 32-6	36.00	3.67	12.43	22.02	0.26	10.69	0.00	0.56	9.28	0.06	95.65	46
GM-16 BTE 33-1	35.87	4.31	12.52	22.53	0.28	10.17	0.00	0.55	9.51	0.03	94.96	45
GM-16 BTE 33-2	35.88	4.18	12.62	22.78	0.29	10.36	0.00	0.52	9.44	0.00	95.76	45
GM-16 BTE 33-3	35.77	4.32	12.63	22.70	0.29	10.24	0.00	0.54	9.37	0.01	96.06	45
GM-16 BTE 33-4	35.93	4.29	12.81	22.76	0.29	10.25	0.00	0.56	9.56	0.04	95.87	45
GM-16 BTE 33-5	36.00	4.32	12.78	23.00	0.28	10.23	0.00	0.57	9.43	0.03	96.46	44
GM-16 BTE 33-6	36.00	4.24	12.74	22.78	0.26	10.29	0.00	0.56	9.49	0.02	96.65	45
Average	**35.99**	**4.31**	**12.71**	**22.77**	**0.28**	**10.19**	**0.00**	**0.54**	**9.44**	**0.03**	**96.23**	**44**
Standard Deviation	**0.21**	**0.12**	**0.11**	**0.49**	**0.01**	**0.15**	**0.01**	**0.02**	**0.09**	**0.02**	**0.57**	**1**

GM-13 (YG)	GM-13-1 BTE 1-1	36.48	4.32	13.01	22.31	0.26	10.09	0.01	0.54	9.54	0.04	96.61	45
	GM-13-1 BTE 1-2	36.45	4.37	12.92	22.45	0.29	10.02	0.01	0.56	9.55	0.01	96.62	44
	GM-13-1 BTE 1-3	36.54	4.34	13.01	22.65	0.28	10.04	0.00	0.55	9.42	0.05	96.89	44
	GM-13-1 BTE 1-4	36.71	4.35	12.89	22.50	0.28	10.18	0.01	0.56	9.48	0.04	97.00	45
	GM-13-1 BTE 1-5	36.65	4.42	12.93	22.69	0.28	10.07	0.00	0.53	9.63	0.00	97.18	44
	GM-13-1 BTE Core 1-1	36.48	4.32	12.76	22.53	0.26	10.04	0.00	0.54	9.45	0.09	96.47	44
	GM-13-1 BTE Rim 1-2	36.60	4.28	13.01	22.91	0.29	10.14	0.08	0.57	9.52	0.02	97.42	44
	GM-13-1 BTE Rim 1-3	35.92	4.29	12.61	24.73	0.29	9.29	0.02	0.54	9.49	0.04	97.23	40
	GM-13-1 BTE Rim 2-2	35.63	4.48	12.60	24.61	0.33	9.38	0.00	0.56	9.49	0.06	97.13	40
	GM-13-1 BTE Core 3-1	36.27	4.38	12.89	23.13	0.28	10.15	0.00	0.55	9.57	0.00	97.21	44
	GM-13-1 BTE Rim 4-3	36.33	4.39	12.70	23.21	0.27	10.11	0.00	0.55	9.52	0.02	97.09	44
	GM-13-1 BTE Rim 5-1	36.23	4.42	12.78	22.53	0.29	10.31	0.01	0.56	9.66	0.02	96.81	45
	GM-13-1 BTE 5-2	36.62	4.41	12.99	22.66	0.27	10.33	0.00	0.56	9.68	0.07	97.58	45
	GM-13-1 BTE 5-3	36.21	4.40	12.95	22.52	0.28	10.19	0.00	0.55	9.51	0.06	96.65	45
	GM-13-1 BTE 6-1	36.24	4.38	12.79	22.55	0.29	10.28	0.01	0.54	9.55	0.04	96.66	45
	GM-13-1 BTE 6-2	36.22	4.35	12.97	22.57	0.27	10.32	0.01	0.53	9.42	0.02	96.68	45
	GM-13-1 BTE 6-3	36.14	4.41	12.88	22.91	0.28	10.25	0.01	0.53	9.44	0.03	96.88	44
	GM-13-1 BTE 7-1	36.23	4.32	12.75	22.84	0.32	10.25	0.00	0.57	9.45	0.03	96.75	44
	GM-13-1 BTE 7-2	36.19	4.34	12.64	22.79	0.28	10.26	0.00	0.55	9.54	0.06	96.62	45
	GM-13-1 BTE 7-3	36.19	4.34	12.96	22.71	0.29	10.21	0.01	0.54	9.40	0.07	96.70	44
	GM-13-1 BTE 8-1	36.48	4.42	12.77	23.22	0.29	10.27	0.00	0.58	9.59	0.00	97.61	44
	GM-13-1 BTE 9-1	36.34	4.37	13.03	22.90	0.26	10.25	0.00	0.55	9.63	0.03	97.35	44
	GM-13-1 BTE 9-2	35.86	4.45	12.78	23.37	0.29	10.24	0.00	0.56	9.43	0.05	97.04	44
	GM-13-1 BTE 10-1	36.37	4.35	12.93	22.81	0.27	10.15	0.00	0.56	9.46	0.01	96.90	44
	GM-13-1 BTE 10-2	36.46	4.38	12.76	22.85	0.27	10.16	0.00	0.55	9.49	0.03	96.92	44
	GM-13-1 BTE 10-3	36.58	4.40	12.93	23.01	0.28	10.14	0.00	0.57	9.64	0.01	97.55	44
	GM-13-1 BTE 11-1	36.17	4.45	12.91	22.93	0.27	10.31	0.01	0.55	9.45	0.02	97.07	44
	GM-13-1 BTE 11-2	36.24	4.41	12.85	22.69	0.27	10.34	0.01	0.55	9.47	0.00	96.82	45
	GM-13-1 BTE 11-3	36.05	4.43	12.85	22.84	0.29	10.28	0.00	0.55	9.39	0.04	96.70	45
	GM-13-1 BTE 12-1	36.33	4.47	12.68	23.20	0.30	10.29	0.00	0.55	9.62	0.00	97.43	44
	GM-13-1 BTE 12-2	35.69	4.31	12.63	24.56	0.33	9.37	0.00	0.59	9.54	0.06	97.08	40
	GM-13-1 BTE 13-1	36.07	4.38	12.81	22.88	0.29	10.35	0.00	0.56	9.50	0.02	96.85	45
	GM-13-1 BTE 13-2	36.16	4.36	12.64	22.76	0.26	10.33	0.00	0.59	9.52	0.02	96.65	45
	GM-13-1 BTE 13-3	36.19	4.34	12.60	22.75	0.26	10.38	0.00	0.58	9.52	0.05	96.67	45
	GM-13-1 BTE 14-3	36.59	4.23	12.74	22.93	0.28	10.46	0.00	0.56	9.61	0.01	97.39	45
	GM-13-1 BTE 15-1	36.33	4.44	12.63	23.20	0.28	10.12	0.00	0.53	9.42	0.04	96.97	44
	GM-13-1 BTE 15-2	36.45	4.44	12.83	22.78	0.26	10.16	0.00	0.57	9.61	0.05	97.16	44
	GM-13-1 BTE 16-1	36.26	4.28	12.85	22.78	0.30	10.30	0.00	0.55	9.56	0.03	96.90	45
	GM-13-1 BTE 16-2	36.33	4.20	12.87	22.49	0.29	10.27	0.02	0.55	9.51	0.09	96.62	45
	GM-13-1 BTE 16-3	36.27	4.21	12.87	22.39	0.28	10.25	0.02	0.54	9.50	0.00	96.35	45
	GM-13-1 BTE 17-1	36.16	4.42	12.82	22.96	0.27	10.20	0.00	0.56	9.58	0.04	96.99	44

GM-13-1 BTE 17-2	36.28	4.42	12.70	22.82	0.29	10.32	0.00	0.55	9.51	0.00	96.86	45
GM-13-1 BTE 17-3	36.22	4.37	12.84	22.76	0.27	10.34	0.00	0.55	9.48	0.02	96.85	45
GM-13-1 BTE 18-3	36.41	4.44	12.86	23.06	0.28	10.23	0.00	0.54	9.63	0.03	97.47	44
GM-13-1 BTE 18-4	36.46	4.43	12.77	23.65	0.26	9.91	0.00	0.55	9.53	0.02	97.59	43
GM-13-1 BTE 19-1	36.18	4.42	12.74	22.68	0.28	10.21	0.00	0.55	9.52	0.04	96.60	45
GM-13-1 BTE 19-2	36.16	4.41	12.84	22.87	0.30	10.17	0.00	0.56	9.42	0.07	96.79	44
GM-13-1 BTE 19-3	36.23	4.40	12.72	23.35	0.28	10.21	0.00	0.54	9.57	0.03	97.32	44
GM-13-1 BTE 20-1	36.21	4.35	12.85	22.29	0.29	10.35	0.00	0.57	9.40	0.02	96.31	45
GM-13-1 BTE 20-2	36.10	4.43	12.79	22.69	0.27	10.37	0.00	0.55	9.44	0.02	96.65	45
GM-13-1 BTE 20-3	35.82	4.42	12.63	23.11	0.27	9.98	0.00	0.53	9.57	0.06	96.37	44
GM-13-1 BTE 21-1	36.47	4.25	12.80	22.71	0.30	10.51	0.00	0.57	9.47	0.00	97.08	45
GM-13-1 BTE 21-2	36.46	4.15	12.88	22.52	0.27	10.69	0.01	0.55	9.45	0.01	97.01	46
GM-13-1 BTE 21-3	36.84	4.10	12.84	22.74	0.29	10.56	0.00	0.57	9.49	0.02	97.46	45
GM-13-1 BTE 22-1	36.30	4.34	12.93	22.71	0.28	10.26	0.00	0.54	9.60	0.02	96.98	45
GM-13-1 BTE 22-2	36.47	4.40	12.95	22.82	0.26	10.34	0.00	0.56	9.44	0.02	97.25	45
GM-13-1 BTE 22-4	35.93	4.45	12.63	23.26	0.29	10.09	0.00	0.53	9.52	0.08	96.78	44
GM-13-1 BTE 23-1	36.65	3.73	12.95	22.24	0.26	10.50	0.00	0.57	9.47	0.03	96.39	46
GM-13-1 BTE 23-2	36.54	4.05	12.86	23.01	0.29	10.22	0.00	0.57	9.37	0.06	96.95	44
GM-13-1 BTE 23-3	36.47	3.81	12.95	22.48	0.28	10.41	0.01	0.51	9.45	0.03	96.39	45
GM-13-1 BTE 24-1	36.56	4.41	12.80	23.08	0.28	10.20	0.00	0.56	9.53	0.04	97.48	44
GM-13-1 BTE 24-2	36.53	4.33	12.74	22.77	0.29	10.13	0.00	0.56	9.45	0.03	96.84	44
GM-13-1 BTE 24-3	36.06	4.39	12.58	23.45	0.30	10.36	0.00	0.58	9.47	0.04	97.23	44
GM-13-1 BTE 25-1	35.67	4.16	12.71	24.72	0.34	9.53	0.02	0.54	9.34	0.01	97.05	41
GM-13-1 BTE 25-2	36.26	4.15	12.86	22.92	0.26	10.24	0.01	0.54	9.55	0.02	96.79	44
GM-13-1 BTE 25-3	36.08	4.34	12.86	23.22	0.27	10.11	0.02	0.55	9.63	0.01	97.10	44
GM-13-1 BTE 26-1	35.87	4.15	12.65	22.52	0.28	10.28	0.00	0.54	9.37	0.04	95.68	45
GM-13-1 BTE 26-2	36.14	4.14	12.72	22.78	0.27	10.32	0.00	0.55	9.46	0.02	96.36	45
GM-13-1 BTE 27-1	36.12	4.34	12.74	22.95	0.29	10.25	0.01	0.54	9.39	0.07	96.68	44
GM-13-1 BTE 27-2	36.08	4.39	12.55	22.74	0.27	10.22	0.00	0.54	9.47	0.04	96.30	44
GM-13-1 BTE 27-3	36.20	4.40	12.65	23.09	0.27	10.27	0.00	0.56	9.48	0.04	96.96	44
GM-13-1 BTE 28-1	36.19	4.32	12.98	19.46	0.31	12.19	0.01	0.42	9.37	0.22	95.47	53
2GM-13-1 BTE 28-2	36.51	4.26	13.12	19.15	0.28	12.10	0.01	0.41	9.36	0.18	95.39	53
2GM-13-1 BTE 28-3	36.50	4.33	12.97	19.22	0.29	12.10	0.00	0.40	9.48	0.21	95.51	53
2GM-13-1 BTE 28-4	36.39	4.32	13.08	19.20	0.29	12.18	0.00	0.41	9.33	0.23	95.43	53
2GM-13-1 BTE 29-1	36.24	4.41	12.71	23.54	0.28	10.11	0.02	0.55	9.56	0.06	97.48	43
2GM-13-1 BTE 29-2	36.02	4.38	12.73	22.83	0.27	10.16	0.01	0.54	9.55	0.00	96.47	44
2GM-13-1 BTE 29-3	38.52	4.75	13.13	18.49	0.27	11.48	0.03	0.59	9.55	0.02	96.83	53
2GM-13-1 BTE 30-1	36.34	4.38	12.64	22.86	0.28	10.27	0.00	0.58	9.61	0.07	97.04	44
2GM-13-1 BTE 30-3	36.58	4.39	12.58	22.78	0.27	10.28	0.00	0.56	9.64	0.05	97.14	45
2GM-13-1 BTE 31-1	36.48	4.35	12.82	22.92	0.30	10.26	0.01	0.55	9.57	0.04	97.30	44
2GM-13-1 BTE 31-2	36.43	4.27	12.72	23.88	0.28	9.72	0.00	0.55	9.53	0.01	97.36	42
2GM-13-1 BTE 31-3	36.64	4.37	12.70	22.81	0.29	10.37	0.00	0.58	9.60	0.04	97.38	45
2GM-13-1 BTE 32-1	35.88	4.22	12.64	22.48	0.28	10.35	0.00	0.53	9.49	0.08	95.95	45
2GM-13-1 BTE 32-2	36.28	4.43	12.63	23.29	0.30	10.13	0.00	0.55	9.58	0.03	97.21	44
2GM-13-1 BTE 32-3	35.55	4.28	12.65	23.61	0.30	10.42	0.01	0.54	9.55	0.01	96.92	44

	2GM-13-1 BTE 32-4	36.08	4.21	12.57	22.77	0.29	10.46	0.00	0.55	9.45	0.04	96.40	45
	2GM-13-1 BTE 32-5	35.87	4.19	12.55	22.88	0.29	10.28	0.00	0.52	9.40	0.04	96.01	44
	GM-13-1 BTE 33-1	36.07	4.39	12.78	22.87	0.28	10.22	0.00	0.57	9.53	0.04	96.71	44
	GM-13-1 BTE 33-2	35.93	4.38	12.70	22.73	0.28	10.17	0.00	0.57	9.53	0.04	96.31	44
	GM-13-1 BTE 33-3	36.14	4.38	12.63	23.50	0.28	9.87	0.00	0.56	9.52	0.05	96.92	43
	GM-13-1 BTE 33-4	35.91	4.42	12.56	22.84	0.29	10.01	0.00	0.57	9.48	0.02	96.10	44
	GM-13-1 BTE 34-1	36.32	4.37	12.73	23.13	0.29	10.22	0.00	0.56	9.45	0.06	97.15	44
	GM-13-1 BTE 34-2	36.27	4.41	12.77	22.92	0.27	10.19	0.01	0.57	9.52	0.04	96.98	44
	GM-13-1 BTE 34-3	36.14	4.43	12.75	23.06	0.28	10.09	0.00	0.54	9.49	0.02	96.80	44
	GM-13-1 BTE 35-1	36.39	4.40	12.68	24.04	0.30	9.64	0.00	0.59	9.49	0.03	97.56	42
	GM-13-1 BTE 35-3	36.15	4.43	12.79	23.11	0.28	10.29	0.00	0.55	9.43	0.04	97.06	44
	GM-13-1 BTE 36-1	36.03	4.41	12.77	22.69	0.27	10.16	0.00	0.56	9.52	0.05	96.45	44
	GM-13-1 BTE 36-2	35.99	4.44	12.78	22.96	0.28	10.17	0.00	0.55	9.48	0.02	96.67	44
	GM-13-1 BTE 36-3	37.14	4.51	13.17	19.94	0.26	11.68	0.00	0.61	9.59	0.04	96.94	51
	GM-13-1 BTE 36-4	36.19	4.43	12.86	22.60	0.29	10.21	0.01	0.56	9.61	0.02	96.77	45
	GM-13-1 BTE 37-1	36.62	3.75	12.81	22.38	0.28	10.51	0.00	0.55	9.43	0.06	96.38	46
	GM-13-1 BTE 37-2	36.00	4.15	12.82	22.63	0.29	10.37	0.00	0.53	9.41	0.01	96.19	45
	GM-13-1 BTE 37-3	36.10	4.13	12.82	22.74	0.28	10.28	0.01	0.56	9.60	0.05	96.57	45
	GM-13-1 BTE 38-1	36.31	4.30	12.74	23.14	0.28	10.37	0.00	0.53	9.60	0.00	97.26	44
	GM-13-1 BTE 38-2	36.16	4.38	12.70	23.34	0.27	10.30	0.02	0.56	9.53	0.03	97.29	44
	GM-13-1 BTE 38-3	36.18	4.25	12.62	22.74	0.30	10.33	0.00	0.54	9.48	0.02	96.43	45
	GM-13-1 BTE 38-4	36.17	4.34	12.86	23.35	0.28	10.28	0.00	0.55	9.56	0.03	97.40	44
	Average	**36.28**	**4.34**	**12.79**	**22.75**	**0.28**	**10.30**	**0.00**	**0.55**	**9.51**	**0.04**	**96.83**	**45**
	Standard Deviation	**0.34**	**0.14**	**0.14**	**0.98**	**0.02**	**0.46**	**0.01**	**0.03**	**0.08**	**0.04**	**0.48**	**2**
GM-10 (YO)	GM-10_BTE_1_1	36.21	4.29	12.54	24.11	0.34	9.07	0.01	0.51	9.54	0.02	96.63	40
	GM-10_BTE_1_2	36.41	4.28	12.61	24.79	0.35	9.13	0.00	0.57	9.36	0.02	97.51	40
	GM-10_BTE_1_3	36.10	4.31	12.62	23.57	0.36	9.58	0.01	0.53	9.41	0.06	96.53	42
	GM-10_BTE_1_4	36.01	4.28	12.32	23.04	0.36	9.62	0.01	0.54	9.21	0.05	95.43	43
	GM-10_BTE_1_5	35.94	4.30	12.55	23.84	0.36	9.53	0.00	0.54	9.46	0.04	96.56	42
	GM-10_BTE_1_6	35.89	4.31	12.59	23.52	0.31	9.59	0.00	0.52	9.37	0.00	96.10	42
	GM-10_BTE_1_7	36.32	4.30	12.62	23.42	0.36	9.54	0.00	0.52	9.34	0.04	96.45	42
	GM-10_BTE_1_8	36.35	4.30	12.57	23.84	0.30	9.61	0.00	0.56	9.44	0.04	97.00	42
	GM-10_BTE_1_9	36.20	4.28	12.51	23.48	0.35	9.40	0.00	0.53	9.35	0.06	96.15	42
	GM-10_BTE_1_10	36.02	4.24	12.41	23.45	0.34	9.53	0.00	0.50	9.27	0.05	95.81	42
	GM-10_BTE_2_1	36.23	4.27	12.42	23.40	0.32	9.53	0.00	0.50	9.36	0.02	96.03	42
	GM-10_BTE_2_2	36.03	4.24	12.59	23.66	0.33	9.69	0.01	0.52	9.49	0.02	96.58	42
	GM-10_BTE_2_3	37.26	4.23	12.52	23.35	0.32	9.64	0.00	0.54	9.42	0.03	97.31	42
	GM-10_BTE_2_4	36.26	4.18	12.52	24.01	0.35	9.21	0.01	0.56	9.37	0.04	96.50	41
	GM-10_BTE_2_5	36.55	4.20	12.53	23.60	0.34	9.73	0.00	0.56	9.36	0.04	96.91	42
	GM-10_BTE_2_8	35.90	4.11	12.34	23.54	0.33	9.18	0.00	0.54	9.23	0.02	95.20	41
	GM-10_BTE_3_1	35.50	4.31	12.30	23.71	0.36	9.74	0.00	0.54	9.49	0.01	95.97	42
	GM-10_BTE_3_2	36.09	4.34	12.51	23.50	0.33	9.63	0.00	0.54	9.30	0.07	96.31	42

GM-10_BTE_3_3	36.02	4.31	12.46	23.46	0.34	9.73	0.01	0.56	9.29	0.00	96.19	43
GM-10_BTE_3_4	36.16	4.20	12.66	23.80	0.31	9.54	0.00	0.54	9.31	0.01	96.52	42
GM-10_BTE_3_5	36.01	4.32	12.39	23.61	0.35	9.11	0.01	0.50	9.54	0.05	95.88	41
GM-10_BTE_4_1	35.54	4.35	12.15	23.83	0.35	8.96	0.00	0.49	9.49	0.01	95.16	40
GM-10_BTE_4_2	35.81	4.35	12.23	23.85	0.32	8.95	0.00	0.49	9.47	0.01	95.47	40
GM-10_BTE_4_3	36.60	4.29	12.59	23.41	0.32	9.48	0.00	0.51	9.55	0.03	96.77	42
GM-10_BTE_4_4	36.91	4.27	12.92	23.51	0.33	9.69	0.00	0.54	9.38	0.02	97.57	42
GM-10_BTE_4_6	36.61	4.30	12.58	23.23	0.32	9.72	0.01	0.55	9.40	0.03	96.75	43
GM-10_BTE_5_1	37.45	4.27	12.84	23.52	0.33	9.25	0.00	0.52	9.33	0.04	97.55	41
GM-10_BTE_5_3	36.23	4.25	12.58	23.70	0.31	9.54	0.00	0.51	9.24	0.01	96.36	42
GM-10_BTE_5_4	36.25	4.22	12.65	24.02	0.32	9.30	0.00	0.51	9.34	0.03	96.65	41
GM-10_BTE_5_5	36.51	4.22	12.41	24.51	0.33	8.79	0.02	0.51	9.37	0.01	96.69	39
GM-10_BTE_5_6	36.09	4.25	12.42	23.18	0.32	9.82	0.00	0.56	9.33	0.02	95.98	43
GM-10_BTE_5_7	36.45	4.26	12.42	23.35	0.31	9.62	0.00	0.53	9.41	0.03	96.39	42
GM-10_BTE_5_8	36.12	4.30	12.42	23.71	0.34	9.77	0.00	0.51	9.38	0.02	96.56	42
GM-10_BTE_6_1	36.56	4.23	12.47	22.87	0.34	9.56	0.00	0.53	9.29	0.01	95.84	43
GM-10_BTE_6_2	36.19	4.22	12.35	23.18	0.36	9.54	0.01	0.53	9.24	0.04	95.68	42
GM-10_BTE_6_3	36.32	4.34	12.37	23.49	0.34	9.59	0.01	0.55	9.44	0.03	96.49	42
GM-10_BTE_6_4	35.83	4.26	12.27	23.77	0.35	9.64	0.00	0.55	9.32	0.05	96.02	42
GM-10_BTE_6_5	38.07	4.55	12.89	20.40	0.32	9.95	0.02	0.58	9.43	0.06	96.27	47
GM-10_BTE_6_6	38.28	4.47	13.14	20.56	0.33	10.55	0.01	0.61	9.37	0.04	97.35	48
GM-10_BTE_6_7	36.19	4.25	12.36	23.01	0.32	9.59	0.00	0.55	9.16	0.03	95.47	43
GM-10_BTE_7_2	35.41	4.30	12.29	24.09	0.35	9.90	0.00	0.59	9.31	0.00	96.24	42
GM-10_BTE_7_4	35.86	4.33	12.36	23.58	0.34	9.54	0.00	0.52	9.50	0.03	96.04	42
GM-10_BTE_7_6	36.63	4.24	12.72	23.56	0.32	9.66	0.00	0.54	9.60	0.05	97.32	42
GM-10_BTE_8_1	37.30	4.28	12.92	23.16	0.33	9.72	0.00	0.55	9.30	0.01	97.57	43
GM-10_BTE_8_2	36.78	4.16	13.10	23.64	0.31	9.58	0.00	0.52	9.25	0.04	97.38	42
GM-10_BTE_8_3	36.71	4.30	12.65	23.30	0.35	9.72	0.00	0.56	9.32	0.07	96.98	43
GM-10_BTE_8_4	36.76	4.22	12.81	23.29	0.34	9.77	0.00	0.56	9.30	0.03	97.07	43
GM-10_BTE_8_5	37.06	4.27	12.91	23.29	0.35	9.74	0.00	0.55	9.22	0.05	97.43	43
GM-10_BTE_9_3	37.44	4.14	12.99	22.96	0.31	9.65	0.02	0.55	9.29	0.02	97.38	43
GM-10_BTE_9_4	37.06	4.21	12.85	23.19	0.33	9.66	0.00	0.53	9.38	0.00	97.19	43
GM-10_BTE_10_1	35.36	4.23	12.19	23.37	0.34	9.73	0.00	0.52	9.31	0.03	95.10	43
GM-10_BTE_10_2	36.12	4.21	12.50	23.17	0.33	9.68	0.00	0.56	9.17	0.01	95.75	43
GM-10_BTE_10_3	36.00	4.22	12.38	23.50	0.33	9.66	0.00	0.53	9.26	0.03	95.90	42
GM-10_BTE_10_5	35.82	4.20	12.25	23.22	0.36	9.60	0.00	0.53	9.17	0.03	95.17	42
GM-10_BTE_10_6	35.65	4.20	12.44	23.29	0.31	9.62	0.00	0.54	9.18	0.00	95.21	42
GM-10_BTE_10_7	35.71	4.17	12.23	23.38	0.32	9.69	0.00	0.50	9.31	0.04	95.37	42
GM-10_BTE_10_8	35.61	4.22	12.23	23.51	0.34	9.69	0.00	0.54	9.26	0.00	95.40	42
Average	**36.33**	**4.27**	**12.53**	**23.43**	**0.33**	**9.57**	**0.00**	**0.54**	**9.35**	**0.03**	**96.37**	**42**
Standard Deviation	**0.60**	**0.07**	**0.23**	**0.67**	**0.02**	**0.27**	**0.01**	**0.02**	**0.10**	**0.02**	**0.72**	**1**

Table B-0-13 Experimental individual plagioclase analyses (wt%)

Sample	Point	SiO_2	TiO_2	Al_2O_3	FeO	MnO	MgO	CaO	Na_2O	K_2O	Total	Or#(XOr*100)	An#(XAn*100)	Ab#(XAb*100)
Top Down 650 °C 200 Mpa	25MC-24_OX_07_Feld_2-3	67.20	0.01	21.09	0.20	0.00	0.00	1.17	9.88	1.92	101.48	10.71	5.50	83.80
	25MC-24_OX_07_Feld _2-5	66.92	0.00	21.12	0.14	0.00	0.00	1.52	10.24	1.10	101.03	6.16	7.11	86.73
	25MC-24_OX_07_Feld_4_9	64.98	0.01	21.31	0.18	0.00	0.00	2.09	8.48	2.67	99.73	15.44	10.13	74.43
	25MC-24_OX_07_Feld_4_13	64.73	0.01	20.89	0.38	0.01	0.00	2.28	9.97	0.98	99.26	5.44	10.62	83.94
	25MC-24_OX_07_Feld_4_15	66.88	0.00	20.62	0.16	0.00	0.00	1.84	9.23	1.71	100.44	9.90	8.92	81.18
	25MC-24_OX_07_Feld_4_17	67.80	0.01	20.24	0.25	0.02	0.07	1.76	8.99	1.34	100.47	8.12	8.97	82.91
	25MC-24_OX_07_Feld_5-3	66.62	0.01	21.31	0.20	0.00	0.00	1.62	9.65	1.77	101.17	9.95	7.65	82.40
	25MC-24_OX_07_Feld_5-7	67.35	0.00	20.73	0.14	0.00	0.00	1.24	10.12	1.71	101.28	9.44	5.75	84.81
	25MC-24_OX_07_Felds_6-17	67.25	0.00	20.21	0.19	0.02	0.00	1.75	9.27	1.50	100.17	8.80	8.60	82.59
	Average	**66.64**	**0.01**	**20.84**	**0.20**	**0.01**	**0.01**	**1.70**	**9.54**	**1.63**	**100.56**	**9.33**	**8.14**	**82.53**
	Standard Deviation	**1.06**	**0.01**	**0.42**	**0.07**	**0.01**	**0.02**	**0.36**	**0.58**	**0.50**	**0.75**	**2.89**	**1.79**	**3.43**
	25MC-24_OX_10_Feld_7-10	67.41	0.01	20.87	0.10	0.00	0.00	1.38	9.79	0.94	100.49	5.56	6.84	87.60
	25MC-24_OX_10_Feld_7-12	65.81	0.00	20.68	0.11	0.00	0.00	1.78	9.20	1.87	99.45	10.79	8.61	80.60
	25MC-24_OX_10_Feld_7-14	67.00	0.00	21.19	0.11	0.00	0.00	1.68	9.40	0.88	100.26	5.32	8.52	86.16
	25MC-24_OX_10_Feld_7-16	66.56	0.00	20.96	0.08	0.01	0.00	1.35	9.36	1.34	99.64	8.02	6.79	85.19
	Average	**66.70**	**0.00**	**20.92**	**0.10**	**0.00**	**0.00**	**1.55**	**9.44**	**1.26**	**99.96**	**7.42**	**7.69**	**84.89**
	Standard Deviation	**0.68**	**0.00**	**0.21**	**0.01**	**0.00**	**0.00**	**0.21**	**0.25**	**0.46**	**0.50**	**2.56**	**1.01**	**3.02**

Table B-0-14 Experimental individual sanidine analyses (wt%)

Sample	Point	SiO_2	TiO_2	Al_2O_3	FeO	MnO	MgO	CaO	Na_2O	K_2O	Total	Or#(XOr*100)	An#(XAn*100)	Ab#(XAb*100)
Top Down	25MC-24_OX_07_Feld_3-1	64.10	0.00	18.83	0.08	0.00	0.00	0.29	3.04	12.80	99.14	72.44	1.38	26.18
650 ℃	25MC-24_OX_07_Feld_3-2	64.71	0.01	18.59	0.08	0.00	0.00	0.22	2.75	13.41	99.74	75.45	1.02	23.52
200 Mpa	25MC-24_OX_07_Feld_3-3	65.04	0.00	18.57	0.14	0.00	0.00	0.18	2.61	13.70	100.22	76.90	0.84	22.27
	25MC-24_OX_07_Feld_3-4	64.44	0.00	18.35	0.10	0.00	0.00	0.19	2.52	13.76	99.35	77.50	0.91	21.59
	25MC-24_OX_07_Feld_3-5	65.73	0.00	17.77	0.09	0.00	0.00	0.02	2.16	13.89	99.65	80.82	0.12	19.06
	25MC-24_OX_07_Feld_3-6	64.08	0.00	18.13	0.10	0.00	0.00	0.17	2.39	13.91	98.77	78.66	0.82	20.52
	25MC-24_OX_07_Feld_3-7	66.55	0.00	18.18	0.12	0.01	0.00	0.01	2.37	13.90	101.13	79.37	0.04	20.60
	25MC-24_OX_07_Feld_4_1	65.41	0.01	19.22	0.12	0.02	0.00	0.06	3.41	12.25	100.48	70.10	0.28	29.62
	25MC-24_OX_07_Feld_4_3	65.71	0.00	18.03	0.15	0.00	0.00	0.09	3.37	12.23	99.56	70.18	0.42	29.40
	25MC-24_OX_07_Feld_light_5-8	65.77	0.00	18.43	0.13	0.00	0.00	0.00	2.73	13.44	100.50	76.39	0.00	23.61
	25MC-24_OX_07_Feld_light_5-10	65.21	0.00	18.49	0.11	0.00	0.00	0.05	3.39	12.53	99.76	70.69	0.24	29.07
	25MC-24_OX_07_Feld_light_5-11	64.86	0.00	18.01	0.09	0.00	0.00	0.06	3.24	12.70	98.95	71.85	0.27	27.88
	25MC-24_OX_07_Feld_light_5-12	65.15	0.00	18.00	0.08	0.01	0.00	0.06	3.52	12.35	99.16	69.58	0.27	30.15
	25MC-24_OX_07_Feld_light_5-13	64.57	0.01	18.10	0.17	0.01	0.00	0.04	3.46	12.47	98.83	70.19	0.20	29.61
	25MC-24_OX_07_Feld_light_5-15	65.74	0.00	18.14	0.11	0.01	0.00	0.01	3.07	12.91	99.98	73.39	0.06	26.55
	25MC-24_OX_07_Feld_light_5-16	64.48	0.00	17.99	0.07	0.00	0.00	0.08	3.37	12.65	98.59	70.90	0.36	28.74

25MC-24_OX_07_Felds_light_6-19	65.04	0.01	18.17	0.15	0.01	0.00	0.14	3.25	12.27	99.04	70.78	0.70	28.52
25MC-24_OX_07_Felds_light_6-20	66.37	0.02	17.88	0.15	0.01	0.00	0.04	2.83	12.71	100.01	74.54	0.21	25.25
25MC-24_OX_07_Felds_light_6-21	66.25	0.01	17.50	0.15	0.01	0.00	0.17	3.19	11.70	98.96	70.14	0.85	29.01
25MC-24_OX_07_Felds_light_6-22	64.80	0.01	17.93	0.22	0.00	0.00	0.07	2.31	13.82	99.14	79.46	0.35	20.20
25MC-24_OX_07_Felds_light_6-23	64.34	0.01	18.19	0.22	0.00	0.00	0.11	2.31	13.76	98.94	79.22	0.55	20.23
25MC-24_OX_07_Felds_light_6-25	64.72	0.00	18.34	0.18	0.00	0.00	0.07	3.19	12.18	98.65	71.28	0.35	28.37
25MC-24_OX_07_Felds_light_6-27	67.45	0.00	17.76	0.20	0.01	0.00	0.02	2.53	12.92	100.89	76.96	0.11	22.92
25MC-24_OX_07_Felds_light_6-28	64.75	0.00	18.04	0.22	0.00	0.00	0.07	2.41	13.74	99.21	78.67	0.34	20.99
25MC-24_OX_07_Felds_light_6-29	64.47	0.01	18.15	0.17	0.01	0.00	0.05	2.76	13.33	98.96	75.90	0.24	23.86
25MC-24_OX_07_Felds_light_6-30	65.10	0.00	18.31	0.21	0.00	0.00	0.07	2.38	13.83	99.89	79.01	0.35	20.63
25MC-24_OX_07_Felds_light_6-32	66.81	0.00	17.66	0.16	0.00	0.00	0.09	3.37	11.67	99.72	69.22	0.43	30.35
25MC-24_OX_07_Felds_light_6-33	65.25	0.00	18.01	0.19	0.00	0.00	0.10	2.76	13.12	99.41	75.41	0.48	24.10
25MC-24_OX_07_Felds_light_6-36	65.76	0.00	17.40	0.16	0.00	0.00	0.08	2.74	12.69	98.82	74.98	0.39	24.63
25MC-24_OX_07_Felds_light_6-37	64.15	0.01	18.24	0.18	0.01	0.00	0.29	2.99	12.65	98.53	72.56	1.40	26.04
25MC-24_OX_07_Felds_light_6-39	66.68	0.01	18.05	0.23	0.03	0.00	0.07	2.68	12.95	100.69	75.81	0.34	23.85
25MC-24_OX_07_Felds_light_6-40	66.07	0.00	17.84	0.17	0.00	0.00	0.01	2.72	13.04	99.85	75.86	0.07	24.07
25MC-24_OX_07_Felds_light_6-41	65.70	0.00	17.93	0.17	0.00	0.00	0.10	2.74	12.79	99.41	75.06	0.47	24.46
25MC-24_OX_0	64.66	0.01	18.69	0.18	0.00	0.00	0.36	2.93	12.85	99.68	72.95	1.74	25.31

	7_Felds_light_6-43											**69.22**		
												80.82		
25MC-24_OX_10	25MC-24_OX_10_Feld-3-1	65.49	0.00	17.98	0.21	0.00	0.00	0.07	2.28	12.76	98.78	78.31	0.39	21.30
Top Down	25MC-24_OX_10_Feld-3-2	65.09	0.00	18.31	0.16	0.00	0.00	0.03	2.38	13.87	99.83	79.17	0.16	20.66
650 ℃	25MC-24_OX_10_Feld-3-4	66.40	0.02	17.95	0.10	0.01	0.00	0.05	2.87	12.63	100.02	74.14	0.26	25.60
200 Mpa	25MC-24_OX_10_Feld-3-6	66.09	0.00	17.74	0.18	0.00	0.00	0.02	2.28	13.50	99.80	79.53	0.08	20.39
	25MC-24_OX_10_Feld-3-7	65.74	0.00	18.06	0.20	0.00	0.00	0.07	2.33	13.05	99.43	78.40	0.34	21.26
	25MC-24_OX_10_Feld-3-8	65.48	0.01	17.73	0.20	0.00	0.00	0.01	2.32	13.38	99.12	79.11	0.07	20.82
	25MC-24_OX_10_Feld-3-9	65.99	0.00	17.63	0.15	0.00	0.00	0.06	2.44	12.87	99.11	77.39	0.28	22.34
	25MC-24_OX_10_Feld-3-10	65.76	0.01	17.45	0.14	0.00	0.01	0.04	2.68	12.75	98.85	75.61	0.20	24.18
	25MC-24_OX_10_Feld-3-11	65.03	0.00	17.94	0.15	0.01	0.00	0.06	2.65	12.71	98.57	75.67	0.32	24.01
	25MC-24_OX_10_Feld-3-12	65.10	0.05	17.65	0.45	0.02	0.06	0.01	2.74	12.48	98.55	74.95	0.07	24.98
	25MC-24_OX_10_Feld-3-14	64.51	0.01	18.02	0.20	0.00	0.00	0.03	2.22	13.91	98.87	80.37	0.12	19.51
	25MC-24_OX_10_Feld-3-16	64.33	0.00	18.27	0.11	0.01	0.00	0.13	3.11	12.68	98.62	72.41	0.62	26.98
	25MC-24_OX_10_Feld-3-18	64.28	0.00	19.04	0.15	0.00	0.00	0.13	2.74	12.90	99.23	75.13	0.64	24.23
	25MC-24_OX_10_Feld-3-19	66.53	0.01	17.57	0.18	0.00	0.00	0.00	2.49	12.82	99.58	77.20	-0.04	22.83
	25MC-24_OX_10_Feld-3-20	65.03	0.00	18.88	0.18	0.00	0.00	0.03	2.53	12.61	99.25	76.49	0.16	23.36
	25MC-24_OX_1	65.28	0.01	18.13	0.14	0.02	0.00	0.10	2.74	12.91	99.31	75.22	0.47	24.31

0_Feld-3-22													
25MC-24_OX_10_Feld-3-24	64.91	0.01	18.10	0.20	0.01	0.00	0.09	2.61	13.03	98.94	76.31	0.42	23.26
25MC-24_OX_10_Feld_4-1	64.82	0.00	18.13	0.16	0.00	0.00	0.08	2.99	12.55	98.71	73.13	0.37	26.50
25MC-24_OX_10_Feld_4-2	66.99	0.00	17.92	0.13	0.00	0.00	0.08	3.28	11.64	100.02	69.75	0.41	29.83
25MC-24_OX_10_Feld_4-3	67.18	0.00	17.84	0.14	0.00	0.00	0.07	3.20	12.02	100.44	70.95	0.35	28.70
25MC-24_OX_10_Feld_5-1	65.60	0.00	17.84	0.21	0.00	0.00	0.04	2.25	13.35	99.28	79.40	0.22	20.38
25MC-24_OX_10_Feld_5-3	67.06	0.00	18.06	0.16	0.00	0.00	0.04	3.01	11.81	100.13	71.95	0.20	27.84
25MC-24_OX_10_Feld_5-4	65.36	0.00	18.15	0.24	0.01	0.00	0.05	2.27	13.70	99.78	79.67	0.23	20.10
25MC-24_OX_10_Feld_6-2	66.66	0.00	17.59	0.11	0.00	0.00	0.00	2.38	12.78	99.51	77.96	0.01	22.03
25MC-24_OX_10_Feld_6-3	66.35	0.00	17.63	0.13	0.01	0.00	0.02	2.27	13.32	99.72	79.32	0.11	20.57
25MC-24_OX_10_Feld_6-4	66.72	0.02	17.40	0.11	0.00	0.00	0.01	2.10	12.57	98.92	79.68	0.08	20.24
25MC-24_OX_10_Feld_6-5	65.44	0.01	18.15	0.10	0.01	0.00	0.05	2.41	13.71	99.88	78.73	0.25	21.02
25MC-24_OX_10_Feld_6-6	66.19	0.00	17.52	0.21	0.00	0.00	0.02	2.26	12.80	98.98	78.78	0.12	21.10
25MC-24_OX_10_Feld_6-7	65.44	0.00	18.63	0.10	0.01	0.01	0.07	2.70	12.86	99.80	75.55	0.33	24.13
25MC-24_OX_10_Feld_6-8	65.25	0.00	18.16	0.09	0.00	0.00	0.07	2.86	12.74	99.16	74.29	0.34	25.37
25MC-24_OX_10_Feld_6-9	65.39	0.00	18.26	0.09	0.00	0.00	0.04	2.42	13.52	99.72	78.43	0.21	21.36
25MC-24_OX_10_Feld_6-10	65.35	0.01	18.48	0.13	0.00	0.01	0.05	2.54	12.70	99.24	76.49	0.24	23.27
25MC-24_OX_10_Feld_6-11	65.72	0.01	18.34	0.17	0.00	0.00	0.06	2.82	12.88	99.99	74.80	0.28	24.92

25MC-24_OX_10_Feld_6-12	66.97	0.01	17.45	0.14	0.00	0.00	0.03	2.26	12.43	99.28	78.21	0.17	21.62
25MC-24_OX_10_Feld_6-13	65.24	0.00	18.13	0.10	0.03	0.00	0.06	2.51	13.38	99.44	77.59	0.31	22.10
25MC-24_OX_10_Feld_6-14	65.45	0.00	17.90	0.10	0.00	0.00	0.04	2.69	12.99	99.15	75.91	0.19	23.90
25MC-24_OX_10_Feld_7-1	66.91	0.00	17.87	0.13	0.00	0.00	0.07	3.15	11.98	100.11	71.15	0.37	28.48
25MC-24_OX_10_Feld_7-2	66.31	0.00	17.87	0.10	0.01	0.00	0.05	2.82	12.66	99.81	74.48	0.26	25.26
25MC-24_OX_10_Feld_7-3	66.69	0.00	17.34	0.11	0.00	0.00	0.02	2.29	12.62	99.06	78.29	0.09	21.62
25MC-24_OX_10_Feld_7-4	65.64	0.00	17.73	0.09	0.00	0.00	0.02	2.26	13.40	99.10	79.56	0.08	20.36
25MC-24_OX_10_Feld_7-5	66.16	0.00	17.84	0.10	0.00	0.00	0.04	2.27	12.83	99.23	78.66	0.19	21.15
25MC-24_OX_10_Feld_7-6	65.42	0.00	17.87	0.12	0.01	0.00	0.05	2.24	13.77	99.47	80.01	0.24	19.75
25MC-24_OX_10_Feld_7-7	66.04	0.01	17.64	0.07	0.00	0.00	0.04	2.44	12.90	99.12	77.55	0.19	22.26
25MC-24_OX_10_Feld_7-8	66.14	0.01	17.45	0.13	0.00	0.01	0.09	2.38	12.58	98.76	77.31	0.46	22.23
25MC-24_OX_10_Feld_8-1	64.59	0.00	18.93	0.15	0.00	0.00	0.36	2.63	12.97	99.65	75.07	1.77	23.16
25MC-24_OX_10_Feld_8-3	65.99	0.01	18.10	0.16	0.02	0.00	0.10	3.01	12.75	100.12	73.25	0.47	26.28
25MC-24_OX_10_Feld_8-4	65.38	0.01	18.23	0.14	0.00	0.00	0.08	2.48	13.41	99.71	77.74	0.38	21.88
25MC-24_OX_10_Feld_8-6	63.44	0.00	19.22	0.15	0.00	0.00	0.24	2.26	13.49	98.79	78.82	1.16	20.02
25MC-24_OX_10_Feld_8-7	64.66	0.00	18.43	0.13	0.00	0.00	0.30	2.47	13.33	99.33	76.87	1.46	21.67
25MC-24_OX_10_Feld_8-9	64.83	0.00	18.50	0.14	0.00	0.00	0.33	2.74	12.90	99.45	74.37	1.60	24.04
25MC-24_OX_1	63.55	0.01	19.52	0.15	0.01	0.00	0.32	2.52	13.09	99.17	76.14	1.55	22.31

	0_Feld_8-10													
	Average	**65.60**	**0.00**	**18.07**	**0.15**	**0.00**	**0.00**	**0.09**	**2.60**	**12.87**	**99.38**	**76.19**	**0.42**	**23.39**
	Standard Deviation	**0.85**	**0.01**	**0.49**	**0.06**	**0.01**	**0.01**	**0.11**	**0.42**	**0.64**	**0.46**	**3.78**	**0.53**	**3.49**
25MC-24_OX_2	25MC24_OX_2_san2-1	66.57	0.00	18.16	0.40	0.03	0.00	0.12	2.23	12.82	100.33	78.61	0.60	20.79
Top Down	25MC24_OX_2_san2-3	66.24	0.02	18.13	0.40	0.00	0.01	0.07	2.48	12.90	100.23	77.12	0.38	22.50
700°C	25MC24_OX_2_san2-4	66.53	0.01	18.35	0.49	0.01	0.00	0.16	2.58	12.62	100.75	75.72	0.79	23.49
200 Mpa	25MC24_OX_2_san2-5	67.32	0.05	17.80	0.41	0.00	0.00	0.04	2.17	12.82	100.61	79.39	0.19	20.42
	25MC24_OX_2_san2-9	67.15	0.02	18.47	0.48	0.01	0.00	0.13	2.57	12.83	101.66	76.17	0.64	23.19
	25MC24_OX_2_san2-12	67.33	0.03	18.19	0.47	0.01	0.00	0.02	2.26	13.02	101.35	79.06	0.11	20.83
	25MC24_OX_2_san2-13	67.25	0.01	18.28	0.47	0.00	0.00	0.02	2.62	13.01	101.67	76.50	0.09	23.41
	25MC24_OX_2_san2-15	67.56	0.03	18.07	0.46	0.00	0.00	0.04	2.39	12.91	101.44	77.85	0.22	21.93
	25MC24_OX_2_san2-16	67.38	0.03	18.35	0.56	0.02	0.01	0.14	2.42	12.53	101.45	76.71	0.73	22.56
	25MC24_OX_2_san2-18	67.18	0.01	18.60	0.34	0.02	0.01	0.07	2.38	13.04	101.65	78.00	0.37	21.63
	25MC24_OX_2_san2-19	66.67	0.00	18.65	0.44	0.00	0.01	0.12	2.38	12.71	100.96	77.37	0.62	22.01
	25MC24_OX_2_san2-21	65.38	0.01	17.95	0.43	0.00	0.01	0.19	2.54	12.62	99.15	75.87	0.95	23.18
	25MC24_OX_2_san2-23	65.52	0.05	17.80	0.39	0.00	0.00	0.15	2.51	12.82	99.22	76.50	0.73	22.77
	25MC24_OX_2_san2-26	64.93	0.03	18.94	0.37	0.02	0.01	0.12	2.46	12.69	99.57	76.82	0.59	22.59
	Average	**66.64**	**0.02**	**18.27**	**0.44**	**0.01**	**0.00**	**0.10**	**2.43**	**12.81**	**100.72**	**77.26**	**0.50**	**22.24**
	Standard Deviation	**0.84**	**0.02**	**0.33**	**0.06**	**0.01**	**0.01**	**0.05**	**0.14**	**0.16**	**0.90**	**1.17**	**0.27**	**1.01**

Appendix C: Supplemental Material for Chapter 4

Table C-0-15 Analytical settings for Laser ablation and ICP-MS

	LaserChron (University of Arizona)	**MI-Chron (University of Michigan)**
Standards:	FC-1, SL-F,R33	Z_91500, r33, peng16_2, nist612_2
Mount	1 inch epoxy mount	1 inch epoxy mount
CL Imaging	Hitachi 3400N SEM	JEOL JSM-7800FLV SEM
Laser ablation system		
Make, Model, and type	Teledyne Iridia (500) MLase	ESI NWR 193 EXCIMER
Ablation cell and volume	Cobalt ablation cell	TwoVo12 sample chamber
Energy density	~4 J/cm2	1.7 J/cm2
Repetition rate	8 Hz	50 Hz
Ablation duration	15 sec	4 second
Ablation pit depth	~12 microns	~ 20 microns
Spot diameter nominal/actual	15-20 microns	20 micron
Cleaning Shot	40 microns/ 3 burst per spot	20 microns/4 shots
Sampling mode/pattern	Spot	Spot
Carrier gas	Helium	Helium
Cell carrier gas flow	0.19 L/min He in cobalt cell, 0.17L/min He in z-prime cup	0.8 L/min He in cell, 3.5 mL/min He collision cell rate
ICP-MS instrument		
Make, Model, and type	Thermo Element2 HR ICPMS	Agilent 7900 ICP-MS
Sample introduction	Ablation aerosol	Ablation aerosol
RF power	1200 W	
Make-up gas flow	0.8 L/min Ar	1 L/min Ar
Detection system	Dual mode Secondary Electron Multiplier	
Masses measured	202Hg, 204(Hg+Pb), 206Pb, 207Pb, 208Pb, 232Th, 235U	Pb206,Pb207,Pb208,Th232,U235,U238
Settle times/Dwell times (ms)	Hg202=0.001/0.021, Pb204=0.001/0.031, Pb206=0.001/0.081, Pb207=0.001/0.150, Pb208=0.001/0.010, Th232=0.001/0.010, U235=0.001/0.150	20 milliseconds for Pb206, 30 milliseconds for Pb207 and 10 milliseconds for Pb208, Th232, U235, and U238

Table C-0-16 Individual zircon spot analyses for samples analyzed by LaserChron

Analysis Name	U (ppm)	Th/U	206Pb/ 207Pb	± 2 SE (%)	207Pb/ 235U	± 2 SE (%)	206Pb/ 238U	error corr.	**206Pb/ 238U age (Ma)**	± 2 SE (Ma)	Conc %	Discon %
CD-18-06 An 1	1206	1.52	19.6	3.7	0.188	4.6	0.027	0.59	**170.4**	4.6	72.3	3
CD-18-06 An 2	513	2.33	19.8	5	0.176	5.5	0.025	0.406	**161.2**	3.6	73.3	2
CD-18-06 An 3	636	0.61	19.8	4.4	0.180	5.2	0.026	0.523	**164.3**	4.4	75.2	2
CD-18-06 An 4	735	0.57	19.9	4	0.178	5	0.026	0.61	**163.6**	4.9	78.1	2
CD-18-06 An 5	654	0.44	20.0	4.2	0.175	5.8	0.025	0.687	**161.5**	6.3	84.3	1
CD-18-06 An 6	645	1.27	20.6	4.7	0.172	5.9	0.026	0.618	**163.2**	5.9	127.8	-1
CD-18-06 An 8	2283	0.02	19.9	2	0.177	3	0.026	0.741	**163**	3.6	81.3	2
CD-18-06 An 9	1598	2.38	20.1	2.4	0.187	3.9	0.027	0.785	**174**	5.3	96.4	0
CD-18-06 An 11	7122	1.28	19.2	2	0.195	2.7	0.027	0.666	**172.9**	3.1	59.5	5
CD-18-06 An 12	3922	1.20	18.5	2.9	0.207	3.6	0.028	0.593	**176.4**	3.7	47.4	7
CD-18-06 An 13	1231	0.93	20.3	3	0.176	3.9	0.026	0.654	**165.1**	4.2	101.4	0
CD-18-06 An 14	2980	0.76	19.6	1.8	0.183	4.3	0.026	0.911	**165.4**	6.3	67.4	3
CD-18-06 An 15	456	0.44	20.3	4.8	0.185	5.3	0.027	0.444	**173.7**	4.1	109.5	-1
CD-18-06 An 16	10961	0.92	18.9	4.3	0.181	6.4	0.025	0.734	**157.5**	7.3	47.8	7
CD-18-06 An 17	3729	1.25	20.3	1.5	0.187	2.1	0.028	0.692	**174.9**	2.5	106.8	0
CD-18-06 An 19	3347	1.27	19.5	1.9	0.179	2.8	0.025	0.73	**160.7**	3.3	63	4
CD-18-06 An 20	809	0.96	19.5	4.8	0.177	5.6	0.025	0.51	**159.4**	4.5	64.2	3
CD-18-06 An 22	4089	0.82	20.1	2	0.186	3.3	0.027	0.785	**172.3**	4.3	91.6	1
CD-18-06 An 23	907	0.67	20.5	4.5	0.170	5.9	0.025	0.644	**160.6**	6	119.2	-1
CD-18-06 An 24	1527	0.05	20.2	3.1	0.178	3.8	0.026	0.595	**166.3**	3.8	98.9	0
CD-18-06 An 25	5168	1.08	19.8	1.7	0.187	2.4	0.027	0.689	**171.1**	2.8	80.6	2
CD-18-06 An 26	7394	1.02	19.6	1.5	0.192	2.3	0.027	0.742	**172.9**	2.9	70.5	3
CD-18-06 An 27	669	0.78	20.1	4.2	0.180	4.7	0.026	0.45	**166.8**	3.5	92.2	1
CD-18-06 An 28	2748	1.16	19.9	1.9	0.192	3.1	0.028	0.778	**176.2**	4.1	86.4	1
CD-18-06 An 29	304	0.36	19.7	6.4	0.181	7.8	0.026	0.563	**164.6**	7.1	73.4	2
CD-18-06 An 30	9002	1.45	19.5	2	0.187	3.1	0.027	0.772	**168.8**	4	67.5	3
CD-18-09 An 1	879	0.97	20.4	3.1	0.175	4.8	0.026	0.754	**164.8**	5.9	116	-1
CD-18-09 An 2	563	0.76	20.1	4.9	0.174	6	0.025	0.589	**161.6**	5.7	87.6	1
CD-18-09 An 3	1231	1.08	20.7	2.9	0.172	3.9	0.026	0.65	**164.2**	4.1	140.7	-2
CD-18-09 An 4	762	0.74	20.5	4.1	0.171	4.8	0.025	0.528	**161.8**	4	114.7	-1
CD-18-09 An 5	550	0.68	19.9	5.1	0.180	5.6	0.026	0.402	**165.1**	3.7	79.1	2

CD-18-09 An 6	558	0.57	20.2	6.3	0.175	7.7	0.026	0.586	**163**	7.3	92.8	1
CD-18-09 An 7	491	1.09	20.4	4.8	0.171	6.2	0.025	0.636	**160.9**	6.3	108.5	0
CD-18-09 An 8	674	0.77	19.8	4.7	0.179	6	0.026	0.612	**164.5**	5.9	77.5	2
CD-18-09 An 9	513	0.88	19.4	5.8	0.178	7.4	0.025	0.629	**159.5**	7.4	59.7	4
CD-18-09 An 10	4142	0.42	19.7	4.5	0.177	4.8	0.025	0.352	**161.8**	2.7	72.2	2
CD-18-09 An 11	532	0.75	20.2	5.3	0.177	6.1	0.026	0.502	**164.8**	5	96.5	0
CD-18-09 An 13	670	0.76	20.3	5.3	0.176	6.8	0.026	0.634	**165.1**	7.1	104	0
CD-18-09 An 14	224	0.48	20.8	7.2	0.165	11.7	0.025	0.786	**158.3**	14.3	150	-2
CD-18-09 An 15	1015	0.99	21.0	6.5	0.168	9	0.026	0.692	**162.9**	10.1	210.5	-3
CD-18-09 An 17	2413	0.60	20.1	2.3	0.173	3	0.025	0.662	**160.4**	3.2	88.5	1
CD-18-09 An 18	965	1.00	20.2	3.5	0.172	4.5	0.025	0.618	**160.6**	4.4	92.4	0
CD-18-09 An 19	2556	0.54	19.2	2.5	0.184	3.6	0.026	0.729	**163.5**	4.2	56.6	5
CD-18-09 An 20	322	0.60	20.4	7.3	0.174	8.9	0.026	0.569	**163.9**	8.2	114	-1
CD-18-09 An 21	906	0.71	20.0	3	0.176	3.6	0.026	0.562	**163.1**	3.2	86.2	1
CD-18-09 An 22	1695	0.52	19.9	2.1	0.189	3.1	0.027	0.743	**173.5**	3.9	84.9	1
CD-18-09 An 23	901	1.06	20.1	3.6	0.176	4.8	0.026	0.665	**163.3**	5.1	90.7	1
CD-18-09 An 24	732	1.01	20.3	4.7	0.166	5.4	0.025	0.474	**156.3**	3.9	101.3	0
CD-18-09 An 25	629	0.93	20.2	4.5	0.177	5.1	0.026	0.502	**164.6**	4.2	94.9	0
CD-18-09 An 26	1011	0.58	18.4	4	0.191	4.8	0.026	0.558	**162.4**	4.3	42.2	9
CD-18-09 An 27	1173	0.48	20.3	3.2	0.171	4.1	0.025	0.64	**160.8**	4.2	104.8	0
CD-18-09 An 28	1866	1.28	20.5	2.5	0.181	3.9	0.027	0.776	**171.3**	5.2	124	-1
CD-18-09 An 29	784	0.82	20.1	3	0.173	4.3	0.025	0.717	**160.5**	4.9	89.6	1
CD-18-13 An 1	863	0.95	20.4	2.9	0.172	3.9	0.025	0.667	**162.2**	4.1	107.5	0
CD-18-13 An 2	1210	1.08	20.6	3.3	0.169	4	0.025	0.578	**161.2**	3.7	132.3	-2
CD-18-13 An 3	3074	0.61	20.0	1.6	0.180	3.1	0.026	0.859	**166.9**	4.3	87.8	1
CD-18-13 An 5	4651	0.47	20.1	1.8	0.179	3.1	0.026	0.816	**165.9**	4.1	88.9	1
CD-18-13 An 7	779	0.54	20.4	4.8	0.177	5.6	0.026	0.507	**166**	4.6	109.9	-1
CD-18-13 An 8	419	0.51	20.0	4.5	0.173	8.4	0.025	0.842	**159.2**	11.1	80.6	2
CD-18-13 An 9	1704	0.65	19.9	3.1	0.172	5.5	0.025	0.83	**158**	7.1	76.5	2
CD-18-13 An 10	571	0.79	20.1	4	0.173	5	0.025	0.609	**160.5**	4.8	86.1	1
CD-18-13 An 11	969	0.86	20.3	4.3	0.183	4.7	0.027	0.407	**170.8**	3.2	104.4	0
CD-18-13 An 12	1000	0.65	20.0	3	0.181	3.4	0.026	0.465	**166.6**	2.6	84.2	1
CD-18-13 An 13	2109	1.04	20.2	2.8	0.182	4.4	0.027	0.771	**169.2**	5.7	98.8	0
CD-18-13 An 14	329	0.54	20.4	5.8	0.176	6.7	0.026	0.523	**165.5**	5.8	110.7	-1

CD-18-13 An 15	416	0.57	19.8	5.4	0.181	6.8	0.026	0.609	**165.3**	6.8	76.8	2
CD-18-13 An 16	3333	0.68	20.1	2.2	0.183	3.7	0.027	0.808	**169.6**	5.1	92.6	1
CD-18-13 An 18	419	0.68	20.6	7	0.170	8.4	0.025	0.55	**162**	7.4	126.4	-1
CD-18-13 An 19	453	1.00	20.7	7.3	0.171	8	0.026	0.428	**162.8**	5.5	138.3	-2
CD-18-13 An 20	278	0.67	20.5	8.6	0.177	9.4	0.026	0.392	**167.8**	6.1	124.2	-1
CD-18-13 An 21	501	0.85	20.7	5.5	0.171	5.9	0.026	0.357	**162.9**	3.4	137.5	-2
CD-18-13 An 23	610	0.46	20.5	4.2	0.175	5.3	0.026	0.599	**165.5**	5.2	120.5	-1
CD-18-13 An 24	1667	0.53	20.2	2.3	0.176	2.9	0.026	0.595	**163.9**	2.8	97.2	0
CD-18-13 An 25	1127	0.92	20.0	2.9	0.174	4.1	0.025	0.717	**160.4**	4.7	81.5	1
CD-18-13 An 26	575	0.81	18.8	4.8	0.187	5.4	0.025	0.454	**162.3**	3.9	48.6	7
CD-18-13 An 27	1641	0.49	20.2	3.3	0.175	4.1	0.026	0.585	**163.3**	3.9	94.7	0
CD-18-13 An 28	667	0.54	20.2	3.9	0.176	5.7	0.026	0.728	**163.8**	6.7	95.1	0
CD-18-13 An 30	5221	0.56	19.2	2.9	0.190	3.7	0.027	0.611	**169**	3.8	59	5
CD-18-20 An 1	879	2.08	20.5	3.4	0.168	4.8	0.025	0.708	**159**	5.3	115.7	-1
CD-18-20 An 2	4024	1.56	20.1	2.7	0.187	3.6	0.027	0.672	**173.9**	4.2	97.7	0
CD-18-20 An 4	2678	1.45	20.0	2.5	0.191	3.4	0.028	0.688	**176.5**	4.1	91.2	1
CD-18-20 An 5	1085	0.68	20.2	2.7	0.179	3.4	0.026	0.608	**166.3**	3.4	95.7	0
CD-18-20 An 6	1659	1.72	20.4	2.9	0.188	4.4	0.028	0.743	**176.6**	5.7	120.1	-1
CD-18-20 An 7	781	0.97	20.5	4.6	0.170	6.3	0.025	0.672	**160.7**	6.7	120.1	-1
CD-18-20 An 8	1116	0.69	20.1	3.7	0.175	4.2	0.026	0.484	**162.7**	3.3	89.2	1
CD-18-20 An 9	635	0.68	20.4	4.2	0.165	11	0.024	0.923	**155.1**	15.6	102.7	0
CD-18-20 An 10	2494	1.56	20.2	2.3	0.187	3.3	0.027	0.722	**173.7**	4.1	98.6	0
CD-18-20 An 11	1834	1.39	20.2	2.2	0.193	3.6	0.028	0.782	**179.5**	4.9	102	0
CD-18-20 An 12	1282	1.22	20.4	2.9	0.173	3.5	0.026	0.55	**162.7**	3.1	109.8	-1
CD-18-20 An 13	562	0.75	20.7	5.1	0.172	6.1	0.026	0.543	**164.4**	5.4	152.4	-2
CD-18-20 An 14	2103	0.71	20.4	3	0.175	3.7	0.026	0.587	**164.7**	3.6	107.9	0
CD-18-20 An 15	1724	1.35	20.4	3.1	0.184	4.3	0.027	0.708	**173.1**	5.2	116.3	-1
CD-18-20 An 16	1102	1.30	19.9	3.9	0.179	5.1	0.026	0.642	**164.4**	5.4	78.7	2
CD-18-20 An 17	3544	1.28	20.2	2.2	0.187	3.4	0.027	0.769	**173.9**	4.4	101.1	0
CD-18-20 An 18	2519	1.75	20.3	2.2	0.192	3.3	0.028	0.733	**179.8**	4.2	111.4	-1
CD-18-20 An 19	482	1.23	20.0	4.1	0.170	5.2	0.025	0.629	**156.4**	5.1	78.4	2
CD-18-20 An 20	3533	1.35	20.2	2	0.186	2.9	0.027	0.724	**173.9**	3.6	103.8	0
CD-18-20 An 21	1034	0.89	20.0	3.9	0.182	5	0.026	0.629	**168.3**	5.2	89	1
CD-18-20 An 22	1523	0.92	20.3	2.8	0.178	3.5	0.026	0.61	**166.3**	3.5	101.5	0

CD-18-20 An 23	1742	0.85	20.5	2.1	0.172	2.9	0.026	0.681	**162.7**	3.2	114.9	-1
CD-18-20 An 24	1797	0.60	19.5	3.6	0.174	4.2	0.025	0.535	**156.6**	3.5	60.9	4
CD-18-20 An 25	2203	0.83	20.1	2.3	0.181	3	0.026	0.609	**167.6**	3	89.4	1
CD-18-20 An 26	822	1.35	20.2	3.2	0.173	3.9	0.025	0.546	**161.9**	3.4	95.2	0
CD-18-20 An 27	2393	1.45	20.1	1.7	0.190	2.9	0.028	0.801	**176.5**	4	96.2	0
CD-18-20 An 28	371	0.64	20.9	5.2	0.177	5.7	0.027	0.421	**170.4**	4	178.8	-3
CD-18-20 An 29	863	1.05	20.2	4.3	0.182	5.2	0.027	0.548	**169.2**	4.7	98.4	0
CD-18-20 An 30	923	0.78	20.4	3.1	0.174	4.4	0.026	0.714	**163.3**	5.1	107.1	0
CD-18-21 An 1	1071	0.94	19.5	3.8	0.178	5.3	0.025	0.712	**159.8**	6	62.6	4
CD-18-21 An 2	1597	0.72	20.2	3.8	0.174	5.6	0.025	0.728	**162.2**	6.5	94.8	0
CD-18-21 An 3	1586	0.74	20.6	3	0.172	4.5	0.026	0.743	**163.6**	5.4	127.5	-1
CD-18-21 An 4	2530	0.79	20.3	2.3	0.180	3.4	0.027	0.725	**168.7**	4.1	102.7	0
CD-18-21 An 5	1092	1.16	20.1	3	0.176	3.6	0.026	0.574	**163.7**	3.4	89.6	1
CD-18-21 An 6	1827	0.74	20.3	3.5	0.172	4.2	0.025	0.571	**160.9**	3.8	98.5	0
CD-18-21 An 7	1557	0.67	20.2	2.8	0.174	3.3	0.025	0.521	**162.1**	2.7	96.9	0
CD-18-21 An 8	1689	0.83	20.2	2.1	0.174	2.9	0.025	0.679	**162.3**	3.1	98	0
CD-18-21 An 10	3995	1.32	19.1	2.7	0.173	4.5	0.024	0.795	**152.4**	5.3	50.3	6
CD-18-21 An 11	2111	1.01	20.6	2.8	0.179	4.4	0.027	0.775	**169.7**	5.7	131.9	-2
CD-18-21 An 12	2295	0.72	20.1	2.5	0.182	3.8	0.027	0.748	**168.7**	4.7	91.3	1
CD-18-21 An 13	1206	0.51	20.1	4.3	0.168	7.1	0.025	0.8	**156.8**	8.8	88.6	1
CD-18-21 An 14	1309	0.53	20.3	2.9	0.175	3.6	0.026	0.597	**163.8**	3.4	100.6	0
CD-18-21 An 15	1970	1.12	20.4	1.9	0.183	3.9	0.027	0.867	**172.2**	5.7	115.8	-1
CD-18-21 An 16	1336	0.65	20.1	2.9	0.178	4.5	0.026	0.759	**165.6**	5.5	92.2	1
CD-18-21 An 17	953	0.68	20.0	3.6	0.183	4.1	0.027	0.481	**168.8**	3.3	88	1
CD-18-21 An 18	820	0.49	20.7	4.1	0.169	5.1	0.025	0.587	**161.7**	4.7	145	-2
CD-18-21 An 19	1124	0.52	20.6	3.2	0.168	4	0.025	0.615	**159.7**	3.9	127	-1
CD-18-21 An 20	756	1.00	20.0	3	0.174	4.3	0.025	0.709	**161.4**	4.8	85	1
CD-18-21 An 21	1262	0.50	20.3	3.1	0.175	6.2	0.026	0.871	**164.2**	8.8	106.8	0
CD-18-21 An 22	3102	0.88	20.1	1.9	0.182	2.9	0.027	0.772	**168.8**	3.8	93	0
CD-18-21 An 23	1124	0.74	20.4	3.3	0.169	3.7	0.025	0.474	**159.8**	2.8	110.7	-1
CD-18-21 An 24	1062	0.56	20.2	2.8	0.177	3.7	0.026	0.666	**165.2**	4.1	95.2	0
CD-18-21 An 25	1502	0.70	20.1	2.7	0.177	3.7	0.026	0.675	**164.3**	4.1	89.4	1
CD-18-21 An 26	1724	1.33	20.6	2.6	0.179	4.6	0.027	0.818	**170.2**	6.3	139.3	-2
CD-18-21 An 27	1797	1.23	20.1	2.5	0.186	4.3	0.027	0.808	**172.6**	5.9	97.3	0

CD-18-21 An 28	1522	0.79	20.5	2.7	0.175	3.4	0.026	0.604	**165.8**	3.4	123	-1
CD-18-21 An 29	1668	0.90	20.2	2.8	0.179	5	0.026	0.825	**166.6**	6.7	97.5	0
CD-18-21 An 30	2278	1.16	20.2	2	0.191	3.2	0.028	0.791	**177.4**	4.4	100.8	0

Outliers

Analysis Name	U (ppm)	Th/U	206Pb/ 207Pb	± 2 SE (%)	207Pb/ 235U	± 2 SE (%)	206Pb/ 238U	error corr.	206Pb/ 238U age (Ma)	± 2 SE (Ma)	Conc %	Discon %
CD-18-06 An 10	4171	2.04	14.7	5.9	0.243	6.5	0.026	0.417	164.7	4.4	18.9	25
CD-18-09 An 16	486	0.56	23.0	7.9	0.149	8.4	0.025	0.36	159	4.8	31.8	-12
CD-18-09 An 30	1008	0.83	17.6	9.6	0.202	9.8	0.026	0.214	164.3	3.4	34.1	12
CD-18-13 An 4	2837	0.76	16.3	12.9	0.236	13.5	0.028	0.285	177.6	6.7	27.5	17
CD-18-13 An 6	206	0.61	23.3	22	0.150	22.6	0.025	0.214	161.3	7.7	91.9	-14
CD-18-13 An 17	4577	0.62	17.5	2.6	0.197	3.7	0.025	0.708	159.3	4.1	32.2	13
CD-18-13 An 22	576	0.42	16.8	14.1	0.208	16.4	0.025	0.506	162.1	13.3	27.9	16
CD-18-13 An 29	3020	0.82	17.4	3.6	0.205	3.9	0.026	0.373	164.6	2.4	32.1	13
CD-18-06 An 7	237	5.56	11.2	19.3	0.136	26.5	0.011	0.685	70.7	12.8	5	45.45
CD-18-20 An 3	402	0.94	12.2	30.7	0.321	31.3	0.029	0.204	181.2	11.4	14.6	35.88
CD-18-21 An 9	4194	0.76	20.1	1.7	0.221	3	0.032	0.823	**204.1**	4.9	109.7	-1
CD-18-06 An 21	467	2.70	18.8	4.5	0.162	5.6	0.022	0.592	**141.1**	4.6	42	8
CD-18-06 An 18	1249	1.64	19.0	3.4	0.159	5.9	0.022	0.817	139.8	6.7	45	6.676
CD-18-09 An 12	1434	1.77	20.1	4.8	0.179	7.6	0.026	0.778	166.3	9.7	89.5	0.776

Table C-0-17 Individual zircon spot analyses for samples analyzed by MI-Chron

Analysis Name	207Pb/ 206Pb	± 2 SE	238U/2 06 Pb	± 2 SE	error corr.	**206Pb/238U age (Ma)**	± 2 SE (Ma)
CD-18-03a_ann_1	0.053	0.0020	39.78	1.21	-0.024	159.8	4.8
CD-18-03a_ann_10	0.048	0.0022	40.20	1.38	0.269	157.5	5.1
CD-18-03a_ann_11	0.051	0.0030	40.35	1.68	0.078	158.2	6.5
CD-18-03a_ann_12	0.048	0.0028	39.22	1.06	0.074	162.0	4.3
CD-18-03a_ann_13	0.047	0.0026	39.22	1.58	-0.273	163.3	6.3
CD-18-03a_ann_14	0.050	0.0029	39.59	1.39	0.336	161.0	5.2
CD-18-03a_ann_15	0.050	0.0016	39.81	1.37	0.436	160.7	4.8
CD-18-03a_ann_16	0.049	0.0017	39.55	1.28	0.221	161.0	4.9
CD-18-03a_ann_17	0.048	0.0016	39.98	1.66	0.155	158.2	6.3
CD-18-03a_ann_18	0.048	0.0015	38.77	1.25	0.322	162.4	4.8
CD-18-03a_ann_19	0.048	0.0019	39.06	1.37	0.271	161.6	5.3
CD-18-03a_ann_20	0.049	0.0015	40.37	1.14	0.026	157.6	4.4
CD-18-03a_ann_21	0.047	0.0016	38.35	1.27	0.611	160.9	4.0
CD-18-03a_ann_23	0.049	0.0011	39.00	0.99	0.164	162.7	4.0
CD-18-03a_ann_24	0.051	0.0016	41.29	1.28	-0.359	152.8	4.5
CD-18-03a_ann_25	0.050	0.0016	38.19	1.07	0.238	166.8	4.4
CD-18-03a_ann_26	0.050	0.0016	37.91	1.16	0.149	168.0	4.9
CD-18-03a_ann_3	0.050	0.0021	39.00	1.67	0.398	164.2	6.2
CD-18-03a_ann_4	0.050	0.0014	40.23	1.09	0.004	158.4	4.2
CD-18-03a_ann_5	0.049	0.0015	39.58	1.45	-0.077	160.8	5.8
CD-18-03a_ann_6	0.048	0.0015	39.29	1.17	0.224	160.9	4.5
CD-18-03a_ann_7	0.048	0.0017	38.42	1.08	0.227	164.9	4.4
CD-18-03a_ann_8	0.050	0.0017	38.86	1.03	0.144	164.1	4.2
CD-18-03a_ann_9	0.048	0.0011	40.50	0.98	0.163	156.4	3.6
Outliers							
CD-18-03a_ann_2	0.049	0.0033	36.03	1.41	0.053	176.3	6.8
CD-18-03a_ann_22	0.050	0.0020	36.63	1.30	0.306	174.0	5.7

Figure C-0-3 Scatter diagrams of 206Pb/238U age (Ma) vs U (ppm) concentration for samples analyzed by LaserChron

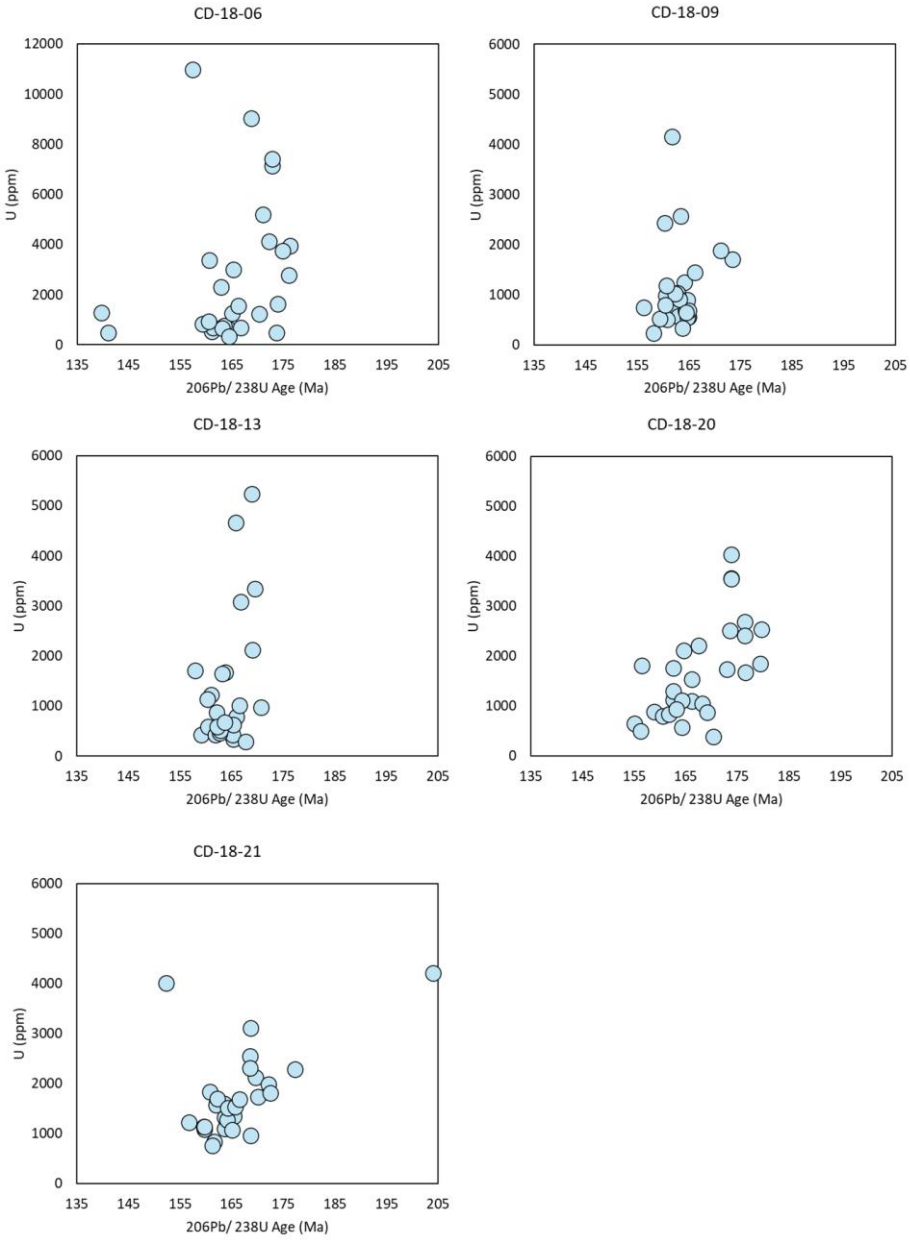


Figure C-0-4 Scatter diagrams of 206Pb/238U age (Ma) vs. Th/U for samples analyzed by LaserChron

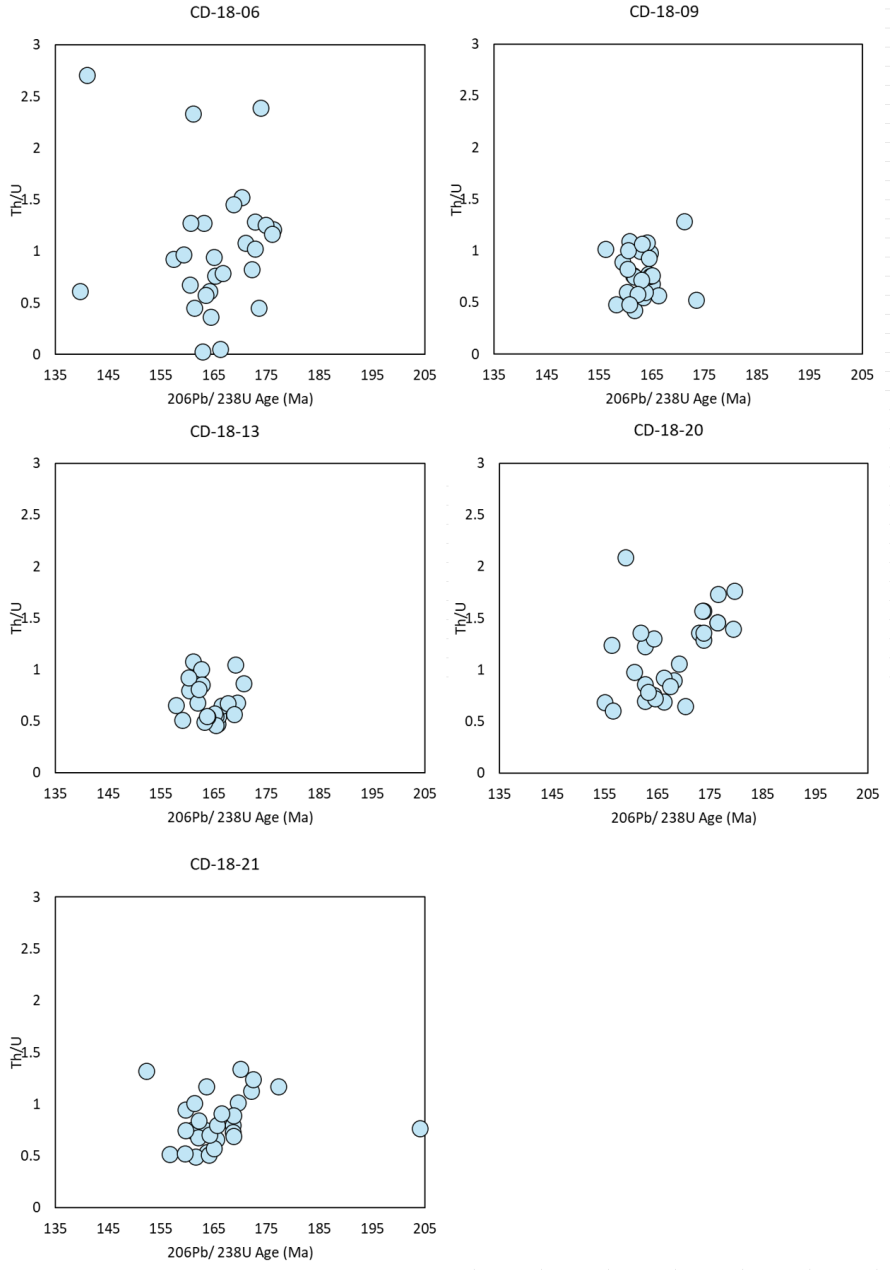
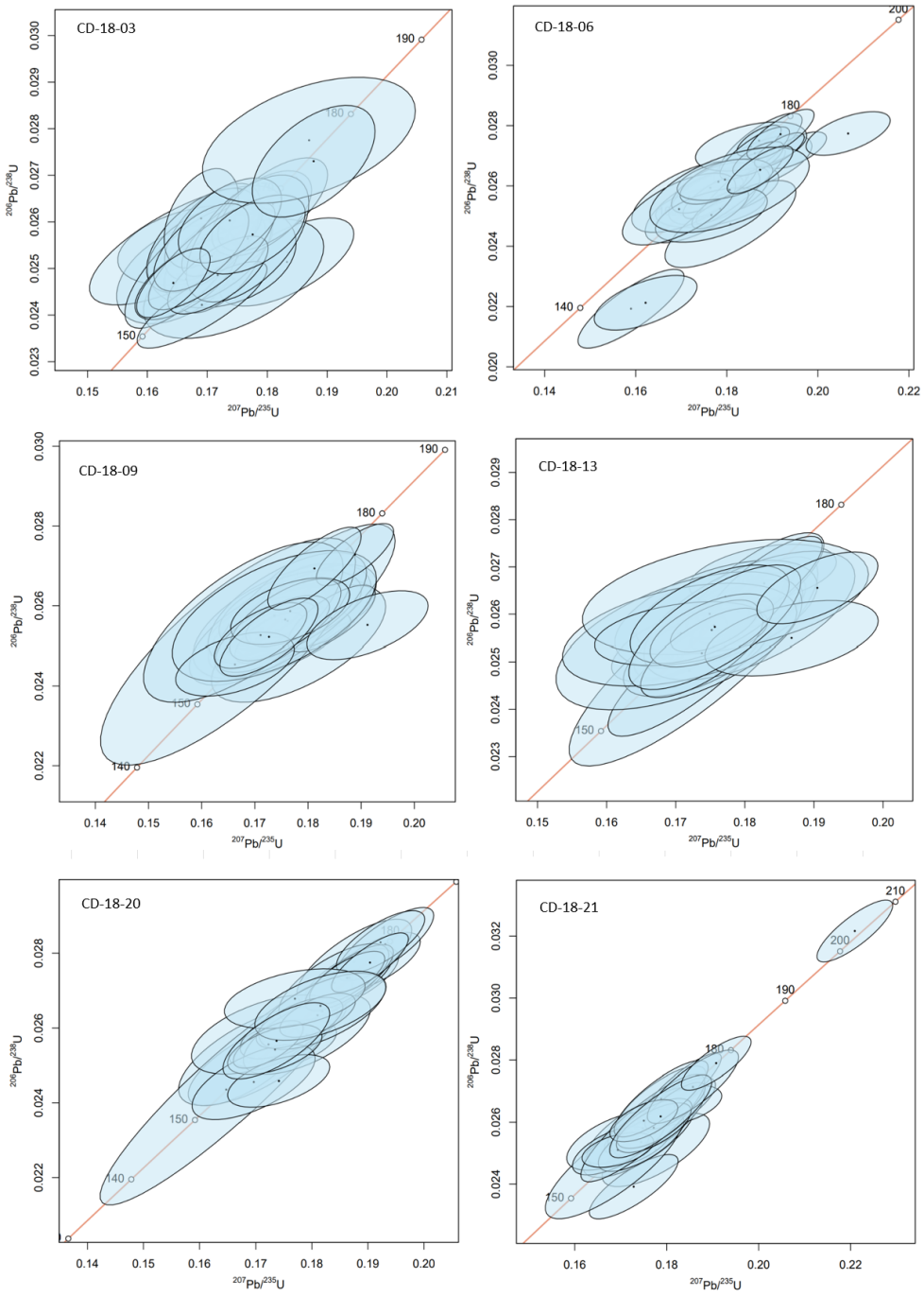


Figure C-0-5 Concordia diagrams for all samples plotted with IsoplotR



Reference:

Vermeesch, P., 2018, IsoplotR: a free and open toolbox for geochronology. Geoscience Frontiers, v.9, p.1479-1493, doi:10.1016/j.gsf.2018.04.001.